NASA TECHNICAL NOTE

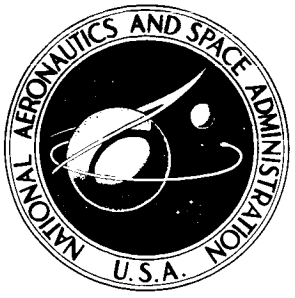


NASA TN D-6416

NASA TN D-6416



# RAPID ESTIMATION OF WIND-TUNNEL CORRECTIONS WITH APPLICATION TO WIND-TUNNEL AND MODEL DESIGN

*by Harry H. Heyson*

*Langley Research Center*
*Hampton, Va. 23365*

NATIONAL AERONAUTICS AND SPACE ADMINISTRATION • WASHINGTON, D. C. • SEPTEMBER 1971

| 1. Report No. | 2. Government Accession No. | 3. Recipient's Catalog No. |
|---|---|---|
| NASA TN D-6416 | | |

| 4. Title and Subtitle | 5. Report Date |
|---|---|
| RAPID ESTIMATION OF WIND-TUNNEL CORRECTIONS WITH APPLICATION TO WIND-TUNNEL AND MODEL DESIGN | September 1971 |
| | 6. Performing Organization Code |

| 7. Author(s) | 8. Performing Organization Report No. |
|---|---|
| Harry H. Heyson | L-7793 |
| | 10. Work Unit No. |
| | 760-72-01-05 |

| 9. Performing Organization Name and Address | 11. Contract or Grant No. |
|---|---|
| NASA Langley Research Center<br>Hampton, Va. 23365 | |
| | 13. Type of Report and Period Covered |
| | Technical Note |

| 12. Sponsoring Agency Name and Address | 14. Sponsoring Agency Code |
|---|---|
| National Aeronautics and Space Administration<br>Washington, D.C. 20546 | |

15. Supplementary Notes

16. Abstract

A chart method is developed for the rapid estimation of wind-tunnel interference in closed and closed-on-bottom-only tunnels. In addition, testing-limit charts, based on varying degrees of correction, are developed. Applications of these results indicate very powerful effects of wing sweep and the degree of correction on the usable testing range of wind tunnels.

| 17. Key Words (Suggested by Author(s)) | 18. Distribution Statement |
|---|---|
| Wind-tunnel corrections<br>V/STOL wind-tunnel design | Unclassified – Unlimited |

| 19. Security Classif. (of this report) | 20. Security Classif. (of this page) | 21. No. of Pages | 22. Price* |
|---|---|---|---|
| Unclassified | Unclassified | 369 | $6.00 |

*For sale by the National Technical Information Service, Springfield, Virginia 22151

# RAPID ESTIMATION OF WIND-TUNNEL CORRECTIONS WITH APPLICATION TO WIND-TUNNEL AND MODEL DESIGN

By Harry H. Heyson
Langley Research Center

## SUMMARY

A chart method is developed for the rapid estimation of wind-tunnel interference in closed and closed-on-bottom-only tunnels. In addition, testing-limit charts, based on varying degrees of correction, are developed. Applications of these results indicate very powerful effects of wing sweep and the degree of correction on the usable testing range of wind tunnels.

## INTRODUCTION

One of the most difficult choices involved in the design of a wind-tunnel experiment is the maximum allowable size of the model. Minimum allowable sizes are often required because of Reynolds number effects or, in powered-model testing, by the size of the available powerplants and actuator components. The maximum size is set by the estimated effects of the test-section boundaries on the flow near the model. The problem is compounded in the design of the wind tunnel itself, for the initial consideration is an estimate of the types and sizes of model which may be tested in the tunnel throughout its entire span of operation. Only then is it possible to attempt to estimate the optimum configuration for the test section. The eventual choices may vary greatly even for wind tunnels designed to do essentially the same type of work. (See ref. 1.)

The theoretical treatments of wall effects do not actually provide directly an estimate of the maximum relative sizes of model and tunnel but only the interference to be expected for a given combination of model and tunnel. The limiting values of this interference are often obtained by reference to "rules-of-thumb" developed over the course of many years of testing and of applying a given correction method to the results of the tests. Thus, for tests of relatively conventional wings at moderate lift coefficients, it has long been recognized (for example, ref. 2) that the corrected results will suffer in accuracy if classical theory (summarized in ref. 3) predicts an interference angle in excess of $2^{\circ}$, and that the span of the wing should be less than three-quarters of the test-section width. It must be observed that such rules have certain inherent limitations: they only apply to models similar to those for which they were developed (in this case to relatively unswept

wings); and they only apply in relationship to a specified theoretical treatment of wall interference. As examples, one recent paper (ref. 4) observes an equivalent limiting value of interference angle of about $3/4^{\circ}$ for highly swept or delta wings, and reference 1 has noted that interference angles on the order of $5^{\circ}$ or more may be acceptable if more complete theoretical treatments are employed.

The "rules" become even more complex when VTOL and STOL models are contemplated. For such models, with their associated large downward wake deflections, the available theory (refs. 5 to 8) indicates that the wall interferences are substantially modified by the wake deflection, which, in turn, is a complicated function (ref. 9) of the model operating conditions. Furthermore, it has been shown, both experimentally (refs. 10 to 13) and theoretically (refs. 14 and 15), that, under certain extreme conditions, tests of such models may so alter the flow within the walls of the tunnel that the measured results may be meaningless in terms of any equivalent free-air condition.

It is possible to use the theory of references 5 to 8 to correct data for a given specific operating condition if adequate information regarding the forces and their distribution over the model is obtained during the test. On the other hand, such information may be inadequately known during the preliminary planning of a particular test and, in any event, such information is much too specific to one model for the design of a wind tunnel. If attention is restricted to one broad class of vehicles for which the wake may be considered to exist as a single blended entity (for example, rotors, jet flaps, tilt wings, deflected slipstreams), it becomes possible to produce charts of generalized corrections which facilitate estimates of wall interference under extreme conditions. Indeed, a notable advance in this direction was made by Templin (ref. 16) during the design stages of one major wind tunnel.

Templin's analysis was limited to the tables of interference factors (for example, ref. 17) which were available at the time for a vanishingly small model. This work, of course, includes neither the subsequent discoveries of "flow-breakdown" limits in the tunnel (ref. 10) nor the later recognition that an effective wake angle (accounting for rollup) should be used in applying the theory of reference 7. Because of the use of the "vanishingly small" concept, the resulting chart is somewhat inconvenient to apply since the ultimate results are in terms of nondimensional interference velocities rather than directly in terms of correction angles and dynamic pressure ratios. A more severe restriction is that the vanishingly small concept eliminates the possibility of considering either the effect of relative model size on the interference factors or the nonuniformity of interference over the model. Reference 8 shows that both of these conditions introduce significant effects.

The present analysis originated in sizing studies of several current and proposed wind tunnels. It may be considered as a substantial expansion of the technique used by

Templin. The average interference, the interference at a standardized tail, and the nonuniformity of interference over the model span are computed for a wide range of wake deflections and drag-lift ratios. By means of certain momentum relationships derived in references 9 and 15, the operating conditions are converted to functions of two parameters, the lift coefficient and the induced drag-lift ratio. The results are then presented in terms of these relatively simple parameters directly as correction angles and dynamic-pressure ratios.

The present charts are based ultimately on the theory of reference 7 as implemented by the superposition techniques of reference 8 and the computer programs of reference 18. They cover closed wind tunnels having width-height ratios ranging from 3 to 1/2. The charts for tunnels closed only on the bottom are limited to two current examples of this configuration and certain variable-geometry versions (ref. 19) of this type of tunnel are considered even more briefly. The ratio of model span to tunnel width covers a wide range, from as small as 1/12 to as great as 5/6. Because sweep was found to have notable effects on the nonuniformity of corrections, sweep angles from $0^{\circ}$ to $45^{\circ}$ are considered. Except for the variable-geometry tunnels, the charts are limited to models centered in the wind-tunnel test section.

The equivalent correction angles have also been obtained from conventional interference theory for most of the configurations considered. These corrections are compared with those on the charts. The comparison indicates probable sources of the previously available rules limiting the magnitude of the correction angles.

Finally, the correction charts are converted into testing limits by the expedient of setting up somewhat arbitrary, but reasonably plausible, limits for the various effects imposed by the constraint of the test-section boundaries. These different levels of data correction range from considerably more rigorous techniques than now in use to no correction at all. Examples of comparisons between differing tunnel configurations are included.

## SYMBOLS

| | |
|---|---|
| $A$ | aspect ratio, $b^2/S$ |
| $A_m$ | momentum area of lifting system |
| $A_T$ | cross-sectional area of test section, $4BH$ |
| $B$ | semiwidth of test section |

| | |
|---|---|
| $b$ | full span of a wing, $2s$ |
| $C_D$ | induced drag coefficient, $D/qS$ |
| $C_L$ | lift coefficient, $L/qS$ |
| $D$ | induced drag |
| $H$ | semiheight of test section |
| $h$ | height of lifting system above test-section floor |
| $L$ | lift |
| $l_t$ | tail length, distance of tail behind aerodynamic center of lifting system |
| $m$ | an integer |
| $n$ | ratio of final induced velocity in wake to induced velocity at lifting system |
| $q$ | dynamic pressure, $\frac{1}{2}\rho V^2$ |
| $q_t$ | corrected dynamic pressure at tail |
| $R$ | resultant force |
| $r$ | rotor radius |
| $S$ | wing area or swept area of rotor disk |
| $s$ | semispan of wing |
| $u_0$ | momentum theory value of longitudinal induced velocity at lifting system |
| $V$ | flow velocity in test section |
| $w_h$ | induced velocity in hovering |
| $w_0$ | momentum theory value of vertical induced velocity at lifting system |

$x_f$ distance behind model at which theoretical wake impinges on test-section floor

$y$ lateral distance from plane of symmetry

$\alpha$ angle of attack, positive with nose up

$\gamma$ width-height ratio of test section, B/H

$\Delta H$ height of model above test-section center line

$\Delta i_t$ boundary-induced change in tail incidence, positive with nose up

$\Delta i_w$ maximum boundary-induced difference in local wing incidence across the span, positive in sense of wash-in

$\Delta q$ maximum boundary-induced difference in local dynamic pressure across the span, positive when greatest dynamic pressure is outboard of minimum dynamic pressure

$\Delta u$ total boundary-induced longitudinal interference velocity

$\Delta u_D$ boundary-induced longitudinal interference velocity resulting from model induced drag

$\Delta u_L$ boundary-induced longitudinal interference velocity resulting from model lift

$\Delta w$ total boundary-induced vertical interference velocity

$\Delta w_D$ boundary-induced vertical interference velocity resulting from model induced drag

$\Delta w_L$ boundary-induced vertical interference velocity resulting from model lift

$\Delta\alpha$ equivalent change in angle of attack caused by boundary interference

$\delta$ conventional boundary interference factor defined implicitly by $\Delta\alpha = \delta \frac{S}{A_T} C_L$

$\delta_{u,D}$ interference factor related to $\Delta u_D$ (see eq. (13d))

$\delta_{u,L}$ interference factor related to $\Delta u_L$ (see eq. (13b))

$\delta_{w,D}$ interference factor related to $\Delta w_D$ (see eq. (13c))

$\delta_{w,L}$ interference factor related to $\Delta w_L$ (see eq. (13a))

$\epsilon$ wake deflection angle at model from linearized theory, $C_L/\pi A$, positive downward

$\zeta$ semiheight of tunnel divided by height of model above floor, $H/h$

$\theta$ deflection of wake from horizontal, measured at model, and positive downward $(90^o - \chi)$

$\Lambda$ wing-sweep angle, measured positive rearward from lateral axis of model

$\rho$ mass density of test medium

$\sigma$ ratio of model span to tunnel width, $\frac{s}{B}$, $\frac{b}{2B}$, or $\frac{r}{B}$

$\chi$ wake skew angle, angle between wake and vertical axis of tunnel, measured at model, and positive rearward from vertical $(90^o - \theta)$

Subscripts:

av average

c corrected value

e effective value

max maximum value

min minimum value

## ANALYSIS

### MOMENTUM CONSIDERATIONS

Appendix A of reference 15 extends the momentum theory of reference 9 to the calculation of the lift coefficient in terms of the wake skew angle and the induced drag-lift ratio. Equation (A18) of reference 15 gives this result in the form

$$C_L = \frac{\pi A}{\left(\tan \chi + \frac{D}{L}\right)^2 \cos \chi} \tag{1}$$

Also, from equation (A6) of reference 15

$$\frac{V}{w_0} = - \left(\tan \chi + \frac{D}{L}\right) \tag{2}$$

Thus, equation (1) may be rewritten as

$$\frac{C_L}{A} = \frac{\pi}{\left(\tan \chi + \frac{D}{L}\right)^2 \cos \chi} = \frac{\pi}{\left(\frac{V}{w_0}\right)^2 \cos \chi} \tag{3}$$

Observe that when $V/w_0 = 0$, equations (1) and (3) become infinite. This result is to be expected since the lift coefficient is defined in terms of the free-stream dynamic pressure which is zero when $V$ is zero.

Now, if a series of values of $\chi$ and $D/L$ are substituted into equations (2) and (3), it is possible to crossplot the results and eventually to obtain the ideal performance of a V/STOL aircraft as in figure 1 where the results are in terms of $C_L/A$ and $D/L$. Lines of constant skew angle and lines of constant $V/w_0$ are indicated.

The theory of reference 9 was presented originally in terms of velocities nondimensionalized with respect to the hovering-induced velocity $w_h$ which is defined as

$$w_h = - \sqrt{\frac{L}{n \rho A_m}} \tag{4}$$

For lifting systems which have twice the induced velocity infinitely far behind the aircraft as at the aircraft (wings, rotors, etc.), $n = 2$ and equation (4) reduces to (eq. (A13) of ref. 15)

$$\frac{w_h}{V} = - \sqrt{\frac{C_L}{\pi A}} \tag{5}$$

Thus $V/w_h$ is independent of $D/L$ and is presented in figure 1 by means of an auxiliary scale on the right-hand side of the figure.

Similarly, the classical value of the downwash angle at the aircraft

$$\epsilon = \frac{C_L}{\pi A}$$

is independent of $D/L$ and is also represented by an auxiliary scale. It will be recognized that $\epsilon$ is merely the linearized version of the net wake deflection $\theta$ which, in turn, is merely the complement of the wake skew angle $\chi$. It is of interest to observe that for zero drag, $\epsilon$ is very close to $\theta$ for wake deflections as great as $20^o$, but that substantial differences occur, in either direction, if the drag significantly differs from zero.

In order to obtain a proper perspective, it is helpful to examine the path traced out on figure 1 by an unpowered wing. If the wake of the wing is assumed to be flat without rolling up, it is evident that the average induced velocity, and consequently the resultant force vector, must be perpendicular to the wake. Thus,

$$\frac{D}{L} = \cot \chi \tag{6}$$

Substitution of equation (6) into equation (3) yields, after some simplification

$$\frac{C_L}{A} = \pi \sin^2\chi \cos \chi \tag{7}$$

Equations (6) and (7), evaluated for various values of $\chi$, are sufficient to obtain the curve labeled "Unpowered wing" in figure 1. Observe that for the wing, large values of $C_L/A$ require significant values of $D/L$, and the difference between $\theta$ and $\epsilon$ is increased. Indeed, equation (7) has a maximum value of

$$\left.\begin{aligned} \frac{C_L}{A} &= \frac{2}{3}\sqrt{\frac{1}{3}}\,\pi \approx 1.21 \\ \frac{C_D}{A} &= \frac{1}{3}\sqrt{\frac{2}{3}}\,\pi \approx 0.855 \end{aligned}\right\} \tag{8}$$

at

$$\chi = \cos^{-1}\sqrt{\frac{1}{3}} \approx 54.74^o$$

The maximum lift coefficient found in this manner is identical with that obtained by use of other methods by McCormick (ref. 20) for the identical wake configuration.

It is interesting to note that the value of $V/w_0$ at the maximum lift coefficient is $-3/\sqrt{2}$. The maximum value of this parameter is $-2$ and occurs at a steeper wake angle of $45^o$.

## EFFECTIVE WAKE ANGLE

The wake angles $\chi$, $\theta$, and $\epsilon$ discussed prior to this point are all the direct product of momentum theory. The wake of a lifting system in forward flight is unstable and will not retain its original form or its original angular deflection as it passes rearward. Experimentally, this condition has been shown to be true for wings (ref. 21), rotors (ref. 22), and jets (ref. 23) and is presumably true for any lifting system; the eventual result is a pair of trailing vortices in the flow. During the process of rolling up, these vortices do not progress downward as rapidly as the central portions of the wake. The central portions of the wake involve almost all the momentum transfer induced by the lifting system. However, the actual location of these regions of the flow is constrained to be eventually within the legs of the trailing vortex pair which exists after rollup.

The actual downward deflection angle of the wake vorticity in the rolled-up wake is only approximately one-half that predicted by momentum theory. Indeed, reference 11 has already indicated that the use of a simple relationship such as

$$\theta_e = \frac{\theta}{2} \tag{9}$$

within the theory of reference 7 leads to a satisfactory correlation of data on the same model. A theoretical treatment for elliptic loading (ref. 24) yields only a slightly different result

$$\theta_e = \frac{4}{\pi 2}\theta \tag{10}$$

Equations (9) and (10) can both be obtained from rather linearized concepts of the actual flow. They suffer from at least one significant defect; namely, for the hovering case they do not indicate that the flow is indeed directly downward. This defect can be eliminated, at least formally, by observing the small angle origin of equation (10) and then extending the expression at large angles in a plausible manner by using the tangents of the angles rather than the angles themselves (ref. 11); that is,

$$\tan \theta_e = \frac{4}{\pi^2} \tan \theta \tag{11}$$

or, in terms of the skew angle

$$\tan \chi_e = \frac{\pi^2}{4} \tan \chi \tag{12}$$

These various relationships are displayed and compared in figure 2. It is obvious that there is no significant difference involved until the flow is directed downward by angles in excess of $50^o$ or $60^o$. In most cases, it will be found that it is not reasonable to test in a wind tunnel at conditions more severe than this. On the other hand, the present paper examines theoretical corrections when the deflections are as great as $\theta = 80^o$ even though such test conditions may not be meaningful. Under such conditions, the expression for $\chi_e$ given by equation (12) is the most reasonable and it has been used throughout the entire study.

It should be pointed out that the effective skew angle is used only for obtaining the interference factors. The values used for the induced velocities must be obtained directly from momentum theory. Any other procedure would lead to an inbalance between the forces and the induced velocities engendered by those forces.

## INTERFERENCE CALCULATIONS

The theory of reference 7 obtains the interference velocities in terms of four interference factors relating the vertical and horizontal interference velocities at a point within the test section to the momentum velocities caused by the lift and drag of the model. These factors define the interference velocities as

$$\Delta w_L = \delta_{w,L} \frac{A_m}{A_T} w_0 \tag{13a}$$

$$\Delta u_L = \delta_{u,L} \frac{A_m}{A_T} w_0 \tag{13b}$$

$$\Delta w_D = \delta_{w,D} \frac{A_m}{A_T} u_0 \tag{13c}$$

$$\Delta u_D = \delta_{u,D} \frac{A_m}{A_T} u_0 \tag{13d}$$

For the present purposes the momentum area of the lifting system may be taken as the area of a circle circumscribing the lateral extremities of the model; that is, $A_m = \pi b^2/4$. The cross-sectional area of the test section is $A_T = 4BH$. Thus

$$\frac{A_m}{A_T} = \frac{\pi b^2/4}{4BH} = \frac{\pi}{4}\left(\frac{s}{B}\right)\left(\frac{s}{B}\right)\frac{B}{H} = \frac{\pi}{4}\sigma^2\gamma \tag{14}$$

Furthermore, from reference 9,

$$\frac{u_0}{w_0} = \frac{D}{L} \tag{15}$$

Now the total interference in each direction is the sum of the individual interference velocities in that direction, or

$$\left.\begin{aligned} \Delta w &= \Delta w_L + \Delta w_D \\ \Delta u &= \Delta u_L + \Delta u_D \end{aligned}\right\} \tag{16}$$

Thus, dividing each side of equations (16) by V, and substituting equations (2), (13), (14), and (15) into equations (16) yields

$$\left.\begin{aligned} \frac{\Delta w}{V} &= \frac{-\pi\sigma^2\gamma}{4\left(\tan\chi + \frac{D}{L}\right)}\left(\delta_{w,L} + \frac{D}{L}\delta_{w,D}\right) \\ \frac{\Delta u}{V} &= \frac{-\pi\sigma^2\gamma}{4\left(\tan\chi + \frac{D}{L}\right)}\left(\delta_{u,L} + \frac{D}{L}\delta_{u,D}\right) \end{aligned}\right\} \tag{17}$$

For a given model configuration, tunnel configuration, skew angle, and drag-lift ratio, equations (17) are completely determinate. The interference factors for the configuration are most directly obtained from the computer programs of reference 18 by use of the effective value of $\chi$ given by equation (12).

Once the total interference velocities are known, they may be converted to a correction angle $\Delta\alpha$ and a corrected velocity or dynamic-pressure ratio (see fig. 3) by means of the relationships

$$\Delta\alpha = \tan^{-1}\left(\frac{\frac{\Delta w}{V}}{1 + \frac{\Delta u}{V}}\right) \tag{18}$$

$$\frac{V_c}{V} = \sqrt{\left(1 + \frac{\Delta u}{V}\right)^2 + \left(\frac{\Delta w}{V}\right)^2} \tag{19}$$

$$\frac{q_c}{q} = \left(1 + \frac{\Delta u}{V}\right)^2 + \left(\frac{\Delta w}{V}\right)^2 \tag{20}$$

The conditions under which the forces are measured in the tunnel are thus equivalent to a somewhat different condition in free air with a corrected forward speed given by equation (19) and a corrected angle of attack given by

$$\alpha_c = \alpha + \Delta\alpha \tag{21}$$

The final step is, of course, to resolve the resultant force R, which is totally unaltered by the wall interference, into lift and drag components perpendicular and parallel to the effective stream axis

$$\left.\begin{aligned} L_c &= L \cos \Delta\alpha - D \sin \Delta\alpha \\ D_c &= D \cos \Delta\alpha + L \sin \Delta\alpha \end{aligned}\right\} \tag{22}$$

If the results are to be presented in the form of coefficients based on free-stream dynamic pressure, the expression equivalent to equation (22) is

$$\left.\begin{aligned} C_{L,c} &= \frac{q}{q_c}\left(C_L \cos \Delta\alpha - C_D \sin \Delta\alpha\right) \\ C_{D,c} &= \frac{q}{q_c}\left(C_D \cos \Delta\alpha + C_D \sin \Delta\alpha\right) \end{aligned}\right\} \tag{23}$$

In general, the operations indicated by equations (22) and (23) are not attempted herein. The drag force in these equations and in figure 3 should quite properly be the entire drag force and not merely the induced part of the drag. These final operations would therefore require additional assumptions as to the magnitude of the profile or parasite drag involved in the tests. Consequently, other than one illustrative sample, no such generalized charts of corrected lift and drag are presented.

## FLOW BREAKDOWN IN THE TUNNEL

It has been known for some time (ref. 10) that sufficiently severe downwash angles may disrupt the basic flow in the tunnel to such an extent that the tunnel no longer provides any reasonable approximation to the essentially uniform flow that an aircraft experiences in flight. Wind-tunnel testing under such conditions is pointless; thus, the present correction charts will be invalid above some limiting value of the lift coefficient.

Reference 25 has correlated the data of reference 10, together with a few points from references 11 and 26, in a form which may be used to provide an indication of the upper limit of validity of the present charts. In this correlation it appears that the controlling parameter is $x_f/b$; where $x_f$ is the distance behind the model at which the theoretically straight wake impinges on the floor and $b$ is the full span of the model. From figure 4(a)

$$\frac{x_f}{b} = \frac{h \tan \chi}{b} = \frac{\tan \chi}{2\sigma\gamma\zeta} \tag{24}$$

Observe that if $h$ (or $\zeta$) is constant or varies only as a function of $\chi$, then $x_f/b$ will be constant along lines of constant skew angle $\chi$ such as those shown in figure 1. Such a behavior indicates that a constant limiting value of $x_f/b$ will limit testing far more severely when the model is producing a large drag that when it produces a large forward thrust. Certain contrary indications for $D/L < 0$ result from the tests of reference 27. This disagreement is discussed in reference 15.

The models considered herein are generally centered in the tunnel test section; however, the form of equation (24) indicates that the usable testing range of the tunnel will be increased if the model is located above the tunnel center line, and, correspondingly decreased if the model is located below the center line. This trend has recently been confirmed by the experimental results of reference 12. Such an alteration in model location will also alter the wind-tunnel interference and the charts presented herein will not be applicable.

The minimum allowable values of $x_f/b$ have been obtained from the correlation of experimental results presented in reference 25 and reproduced in figure 4(b). In view of the scatter involved in such measurements, the values used in the present paper are chosen only within increments of one-quarter span. The actual values used are given in the following table:

| $\gamma$ | $(x_f/b)_{min}$ |
|---|---|
| 3 to 4/3 | 1.25 |
| 1 | 1.75 |
| 2/3 | 1.25 |
| 1/2 | 1.5 |

It will be observed that the values used for the very wide tunnels do not follow the reciprocal relationship between $\gamma$ and $1/\gamma$ that is implied by the form of presentation in figure 4(b). The values used herein result from a preliminary examination of unpublished data for wide ($\gamma = 2$) tunnels which were made available through the courtesy of William H. Rae, Jr., and Shojiro Shindo of the University of Washington. The value used for $\gamma = 3$ is an extrapolation of this result based upon the supposition that for such a tunnel the walls are so much further from the model than the floor that their contribution to the phenomenon should be negligible.

The values in the foregoing table have been chosen to correspond to completely rectangular tunnels having no corner fillets. The allowable minimum value of $x_f/b$ may increase significantly if the test section has large fillets. The increase appears to be particularly large if the tunnel is square; however, the increase caused by fillets decreases with the width-height ratio, and appears, from the aforementioned unpublished data, to be negligible for very wide tunnels. This result appears to be reasonable because of the relatively large distance of the walls and their fillets from the model.

The fundamental cause of the flow breakdown phenomenon appears (refs. 13 to 15) to be a complete reversal of the flow near the point where the wake touches the floor. This reversal gives rise to powerful standing vortices in the tunnel which, in turn, influence the data. Since the initiation of the phenomenon is dependent almost solely upon the floor, the same phenomenon must exist for tunnels which are closed only on the bottom even though the location of the standing vortices and their consequent effect upon the data may be quite different. No comprehensive examination of such tunnels has yet been made; however, a few isolated unpublished data points indicate that essentially the same limits apply in this configuration as well. Thus, the values in the foregoing table have been used for <u>all</u> tunnels considered herein.

The actual procedure followed in obtaining the limiting lines on the present charts was first to solve equation (24) for $\chi$ to obtain

$$\chi = \tan^{-1}\left(2\sigma\gamma\zeta\frac{x_f}{b}\right) \tag{25}$$

This value of $\chi$, together with a range of values of $D/L$, may then be inserted in equation (3) to obtain the corresponding values of $C_L/A$.

It is recognized that the present knowledge of this phenomena is not yet in a totally satisfactory state and that future experiments may yield effects of model or tunnel configuration which are unrecognized at the present time. Later information on these effects can, of course, be used to update the present charts by following this procedure, or any necessary modification of it, as warranted by the then current state of knowledge.

## CONVENTIONAL CORRECTIONS

Wherever possible, the present results are compared with those which would be obtained by using conventional interference theory where the wake is assumed to pass directly downstream with no downward deflection whatever. This treatment is appropriate for a vanishingly small lift coefficient. The normal presentation of such corrections is in the form

$$\Delta\alpha = \delta \frac{S}{A_T} C_L \tag{26}$$

Since $A = \frac{b^2}{S}$ and $A_m = \frac{\pi}{4} b^2$, equation (26) may be rewritten as

$$\Delta\alpha = \delta \frac{S}{A_T} \frac{b^2}{S} \frac{C_L}{A} = \delta \frac{b^2}{A_T} \frac{C_L}{A} = \frac{4}{\pi} \delta \frac{A_m}{A_T} \frac{C_L}{A} \tag{27}$$

Thus, the conventional correction $\Delta\alpha$, being dependent only upon $C_L/A$, may be shown simply as an auxiliary scale when presented on the $C_L/A$ against $D/L$ plane of figure 1. Now the theory for deflected wakes has been shown (refs. 5, 7, and 11) to contain as a special case ($\chi = 90^o$) the results of conventional theory. The main difference lies in the definition of the interference factors which is such that

$$\delta = - \frac{\delta_{w,L}}{4} \Bigg|_{\chi=90^o} \tag{28}$$

Thus, equation (25) may be rewritten as

$$\Delta\alpha = - \frac{1}{\pi} \delta_{w,L} \Bigg|_{\chi=90^o} \frac{A_m}{A_T} \frac{C_L}{A} \tag{29}$$

Components of horizontal interference are generally neglected in the application of conventional corrections even though they may attain appreciable values if the model is mounted well above or below the center of the tunnel, or if the tunnel boundaries are dissimilar as in the tunnels closed only on the bottom. Components of interference caused by drag forces are also generally neglected.

It should be noted that conventional theory contains significant small-angle assumptions. These assumptions are entirely appropriate and in consonance with its representation of the wake as that of a model with a vanishingly small lift coefficient. Thus, conventionally, $\Delta w/V$ is obtained and converted to a correction angle by observing that for small angles,

$$\frac{\Delta w}{V} = \tan \Delta\alpha \approx \Delta\alpha \tag{30}$$

When equation (24) is applied to conditions involving very large lift coefficients, it will be observed that the effect of the small angle assumptions (eq. (30)) is to increase the calculated $\Delta\alpha$ significantly. As an example, consider a test condition with a lift coefficient approaching infinity. The direct use of equation (24) would yield a correction angle

which also approaches infinity; however, if the small angle assumptions had not been employed, the left-hand scale of equation (26) would have been $\tan \Delta\alpha$ and equation (26) would then indicate a correction angle approaching only $90^{\circ}$.

For the present purposes, whenever conventional corrections are displayed, it should be understood that these corrections are complete with small angle assumptions, that streamwise interference velocities are ignored, and that any interference velocities caused by drag forces are also ignored. This treatment is in complete conformity with the manner in which conventional corrections are employed in practice.

As a convenience and to insure complete conformity with the present results, conventional corrections, as presented herein, have been obtained directly from equation (29). A literature search to obtain published values of $\delta$ for use in equation (26) would have been excessively time consuming and, in addition, would most likely not have provided all the values required herein.

## TYPES OF CHARTS

The main differences between the various types of charts presented herein lies in the selected points at which the interference is calculated and in the subsequent treatment of the resulting interference angles and dynamic-pressure ratios. Three main types of charts are presented: first, the average corrections over the lifting system; second, the corrections at a standardized tail; and, finally, certain terms representing the nonuniformity of interference over the span of the model. These different types of charts are discussed separately in the following several sections of this paper.

## AVERAGE CORRECTIONS

Charts of average corrections are obtained basically from the computer program given as appendix B of reference 18. In this program interference factors are obtained which represent average interference factors along a lifting line representing an arbitrary wing. In the present paper, the wing generally is assumed to be centered in the tunnel and always is assumed to be unswept and uniformly loaded. For an unswept lifting line there is no relative displacement of any part of the line as the angle of attack changes so that the results are independent of angle of attack. If the angle of attack is zero and the load distribution is unaltered, the average interference over the wing in a rectangular tunnel will be independent of sweep angle when the wake is undeflected. (See the appendix of ref. 8.) When the wake is deflected from the horizontal, there will be some effect of sweep angle on the corrections; however, the numerical results presented

in reference 8 indicate that such effects are sufficiently small that they should not interfere with the intended usage of the present charts for preliminary design purposes.

For the present purposes the program of reference 18 was modified in several regards. First, the DO loops containing $\chi$ were altered to correspond to each of the 11 values of $\chi$ between $10^{\circ}$ and $88^{\circ}$ shown in figure 1. An additional value of $\chi = 90^{\circ}$ was used to obtain the values corresponding to classical theory for use in equation (29). The values of the interference factors were always computed by use of $\chi_e$ from equation (12). Subsequently, these interference factors were used to calculate $\Delta\alpha$ and $q_c/q$ (eqs. (17), (18), and (20)) for values of $D/L$ ranging from -1.0 to 1.0 in increments of 0.2. In addition, $C_L/A$ was computed simultaneously from equation (3). It is important to note that $\chi_e$ was used only in obtaining the interference factors (that is, in calling Subroutine DLTAS of ref. 18); all other computations involved $\chi$ but not $\chi_e$. The results of these calculations were then prepared as contours of equal value against the same coordinates which were used in figure 1.

The ultimate accuracy of the contours on charts such as these depends upon the accuracy of fairing contours through the assemblage of points at which the values were computed. The accuracy of fairing, in turn, depends upon the spacing of the points which is actually fairly nonuniform. For the spacing specified in the foregoing paragraph, figure 1 indicates that the spacing is fairly close for large positive $D/L$ and the spacing becomes considerably coarser as $D/L$ diminishes to -1. All the curves presented herein were faired by a single individual so that some consistency in the possible error is probably present. Although no exact tolerance can be specified, it is estimated that the contours are most likely within 5 percent of the correct value with possibly somewhat larger errors in regions of very large gradients.

In one case charts of the average corrections are presented for a lifting rotor. These charts were prepared in an analogous manner to those for the wing except that the basic program which was modified was that of appendix H of reference 18. An additional complication arises in this calculation in that the resultant induced-force vector of the rotor remains essentially normal to the disk; thus, the drag-lift ratio of the rotor is related to the rotor angle of attack as

$$D/L = \tan \alpha \tag{31}$$

The dependence of $D/L$ on $\alpha$ is a considerable complication since changing $\alpha$ changes the relative location of the various parts of the rotor within the tunnel boundaries and this effect, in turn, influences the interference factors. (See fig. 31 of ref. 8.) Thus, it is necessary to compute the interference factors independently for each combination of $\chi$ and $D/L$ rather than only for each value of $\chi$ as in the simpler case of a wing. It is noted that the aspect ratio of a single rotor is fixed; that is

$$A = \frac{b^2}{S} = \frac{(2r)^2}{\pi r^2} = \frac{4}{\pi} \tag{32}$$

Therefore, unlike wings where the aspect ratio may vary over wide limits, the results may be presented directly in terms of $C_L$.

Only comparatively simple modifications to the already available programs of reference 18 are required in order to produce the present results. Consequently, the actual modified programs are not presented herein.

## CORRECTIONS AT THE TAIL

Because the interference within the test section is typically nonuniformly distributed, a tail located behind a lifting system will experience a substantially different, and usually greater, interference than the average interference over the lifting system itself. The most powerful effects of this difference are generally related to the model pitching moment; however, certain lifting systems of large longitudinal extent, such as low-aspect-ratio wings or tandem rotors, may experience measurable alterations of lift or drag as well.

The application of corrections to pitching moments (for example, ref. 28) caused by the tail depends upon the difference in interference at the lifting system and at the tail. This difference, of course, depends upon the tail location. In a practical sense, it is impossible to produce charts for all possible tail locations; consequently, a single standardized tail is used herein. The tail length is chosen equal to three-quarters of the wing span; that is, in using the programs of references 8 and 18

$$\frac{l_t}{H} = \frac{3}{2}\sigma\gamma \tag{33}$$

The tail height (termed $h_t$ in ref. 8) is arbitrarily set to zero; that is, the wing and the tail are in the same plane. Because certain of the tunnels considered herein exhibit a pronounced dependence of the interference on the angle of attack, $\alpha$ has been arbitrarily maintained throughout the paper at $20^\circ$. This value should be reasonably representative of the maximum angles of attack at which models this long might be tested in typical wind-tunnel practice.

Other known effects of model configuration generally will be found to be small compared with accepting a standard tail location. Therefore, as an economy in computing time, the tail span has always been considered to be zero and only the unswept wing is considered.

Since differences between the wing and the tail are of interest, the programs of appendixes B and D of reference 18 were combined and subjected to modifications similar to those described in the section entitled "Average Corrections." At each combination of $\chi$ and D/L, the correction angles $\Delta\alpha$ and the dynamic-pressure ratios $q_c/q$ were calculated independently at the wing and at the tail. The results presented are in terms of

$$\Delta i_w = \Delta\alpha|_{tail} - \Delta\alpha|_{wing} \tag{34}$$

and

$$\frac{q_t}{q_c} = \frac{(q_c/q)|_{tail}}{(q_c/q)|_{wing}} \tag{35}$$

Observe that $\Delta i_w$ is equivalent to an increase in tail-plane incidence and that $q_t/q_c$ represents an alteration in the tail efficiency factor $(q_t/q$, sometimes denoted as $\eta_t)$.

The fact that $\Delta i_w$ and $q_t/q_c$ are not, in general, zero indicates the existence of a gradient of interference along the longitudinal axis of the model. This gradient, even in the absence of a tail, may have substantial effects on the model characteristics. As an example, such a gradient can be considered as an effective aerodynamically induced camber of a wing surface. (See ref. 25.) The gradients could be computed directly (for example, from ref. 29) and presented in some similar chart form. This computation has not been made, however, since large values of $\Delta i_w$ or $q_t/q_c$ should provide a reasonable index to the existence of large gradients along the longitudinal axis of the model.

The calculation of conventional corrections for comparison purposes follows the same general steps as those listed with the wake skew angle $\chi$ set to $90^\circ$, except that the interference factors are converted to correction angles in a manner analogous to equation (29). In practice, many wind-tunnel tests are corrected by use of only a known distribution of interference factors along the longitudinal axis of the tunnel. This procedure is equivalent to neglecting the lowered position of the tail in the tunnel or, otherwise stated, is equivalent to always assuming that $\alpha = 0^\circ$. Thus, the conventional corrections are presented twice herein, once with $\alpha = 20^\circ$ as in the main body of the chart, and once with $\alpha = 0^\circ$.

## NONUNIFORMITY OF CORRECTIONS

The actual distribution of interference is nonuniform across the span of the model as well as along its longitudinal axis. This nonuniformity can have significant effects on the observed stall angle, and, in the case of swept wings can have powerful effects on the pitching moment as well. A complete description of this nonuniformity would require a

complete graph of the interference against spanwise location at each point of the chart. Since this procedure is impractical, the results are presented in terms of three indices which only roughly indicate the degree of nonuniformity.

The first of these indices is the maximum difference in $\Delta\alpha$ across the span of the wing. This term is obtained by utilizing the program given as appendix C of reference 18. For greater accuracy the program was modified slightly to obtain the local interferences at intervals of 0.1 semispan rather than 0.2 semispan as in the original version of reference 18. The correction angle $\Delta\alpha$ and the dynamic-pressure ratio $q_c/q$ were computed at each spanwise station by using equations (17), (18), and (20). The resulting values of $\Delta\alpha$ are then searched to find the maximum $\Delta\alpha$ and the minimum $\Delta\alpha$. Then these values are used to obtain the maximum difference in effective wing incidence from the equation

$$\left|\Delta i_w\right| = \Delta\alpha_{max} - \Delta\alpha_{min} \tag{36}$$

The sign of $\Delta i_w$ is chosen according to the relative spanwise locations of the maximum and minimum points. If the maximum $\Delta\alpha$ occurs farther outboard than the minimum $\Delta\alpha$, $\Delta i_w$ is defined as positive. Thus, positive $\Delta i_w$ is in the sense of a wash-in, and negative $\Delta i_w$ is in the sense of a wash-out.

The second index relates to the effect of the boundary interference on the local spanwise dynamic pressure. The values of dynamic-pressure ratio which were computed together with the local $\Delta\alpha$ values in the preceding paragraph are searched for maximum and minimum values. Then

$$\left|\Delta\left(\frac{q_c}{q}\right)\right| = \left(\frac{q_c}{q}\right)_{max} - \left(\frac{q_c}{q}\right)_{min} \tag{37}$$

The sign of $\Delta\left(q_c/q\right)$ is chosen in the same manner as the sign of $\Delta i_w$; thus, positive values indicate a greater local dynamic pressure outboard of the minimum. It is desirable to reference this dynamic-pressure difference to that of the average corrected condition; thus, the value presented in the charts is

$$\frac{\Delta q}{q_c} = \frac{\Delta\left(\frac{q_c}{q}\right)}{\left(\frac{q_c}{q}\right)_{av}} \tag{38}$$

Now the differences calculated to this point are not linearly distributed over the span of the model. Thus, the final index used herein is the maximum local gradient of $\Delta\alpha$ across the span. This term is obtained by taking the previously calculated local values of $\Delta\alpha$ and searching for the maximum difference between adjacent spanwise stations. Thus, with the given 11 points running from $y/s = 0$ to $y/s = 1$

$$\frac{d\Delta i_w}{d(y/s)} = \text{Maximum of} \left\{ \left[ \frac{\Delta\alpha_{m+1} - \Delta\alpha_m}{(y/s)_{m+1} - (y/s)_m} \right] \Bigg|_{m=0}^{10} \right\} \tag{39}$$

In equation (39), m increases from the root to the tip of the wing, so that the resulting sign convention is identical to that of equation (36).

Because of the finite spacing between the spanwise stations, the values obtained by equation (39) are not the true local slopes. Instead, they represent an average local slope across 0.1 semispan intervals of the wing. This is just as well since it insures that a large value is not so localized as to have insignificant effects.

The actual interference distributions across the span are continuous; however, the indices described are not necessarily also continuous with changes in $\chi$ or D/L. It is possible to find, for example, peculiar kinked distributions for which $\Delta i_w$ may be positive but the maximum local slope may be negative. Similarly, for conditions in which the interference has a sharp maximum or minimum near the middle of the span, a small change in $\chi$ or D/L may alter the distribution so that the relative position of the maximum and minimum $\Delta\alpha$ values are altered. For such a set of conditions $\Delta i_w$ may actually change discontinuously from a large positive to a large negative value without ever passing through zero.

These conditions are indicated at times in the numerical values which were used to prepare the present charts. Examination of the numerical values indicates, however, that such behavior is generally confined either to regions where the values are so small as to be insignificant or to regions where the changes with $\chi$ and D/L are so sharp and severe that the charts cannot be read with significant accuracy. Consequently, no great violence is done to the results by fairing contours as if both $\Delta i_w$ and its local gradient were actually continuous. Therefore this convention was adopted in the preparation of the current charts; indeed, to do otherwise would have required a substantial expansion of the number of calculated points in order to obtain greater definition.

Wing sweep is found to have major effects on the nonuniformity of corrections as would be expected from the results of reference 8. Thus, it is necessary to consider a range of sweep angles encompassing current design practice.

In order to achieve lift coefficients (or, more properly $C_L/A$) of the order dealt with herein, a wing would most likely require a significant angle of attack. The angle of attack by itself may noticeably alter the distribution of interference over the span (ref. 8) if the wing is swept. However, in terms as general as those used herein, the angle of attack is indeterminate. It would depend not only on aspect ratio, but also upon the addition of power to increase lift as, for example, the use of a trailing-edge jet on a jet-flap

model or an array of propellers on a tilt-wing model. Consequently, the charts illustrating the nonuniformity of correction have all been prepared for $\alpha = 0^{o}$. This procedure also eliminates any concern about the point about which the model rotates as the angle of attack changes; such an effect has also been shown (ref. 8) to have a large influence on the interference.

As before, the conventional corrections of identical nature are obtained by the analogous treatment of the interference factors with $\chi$ set equal to $90^{o}$.

## NONRECTANGULAR TUNNELS

The theory of references 5 to 8 applies to rectangular tunnels. The full-scale tunnels at the Ames and Langley Research Centers do not fall into this category; thus, strictly speaking, they cannot be treated by this theory. Unfortunately, no theory comparable to that of references 5 to 8 exists at present to cover such configurations in which the sides of the test sections are in the form of circular arcs. Nevertheless, these two wind tunnels play such a prominent part in low-speed wind-tunnel testing that at least an approximate treatment is required in the present study.

For the present purposes it has been assumed that these tunnels should have about the same interference as a rectangular tunnel having the same cross-sectional area and the same average width. This treatment is analogous to that used for circular tunnels in reference 30.

The Ames Research Center tunnel has a width of 24.4 meters (80 ft) and a height of 12.2 meters (40 ft) for a nominal width-height ratio of 2. The average width divided by the height yields an effective width-height ratio of $\gamma_e = 1 + \pi/4$ which is approximately 11 percent less than the nominal width-height ratio.

The Langley Research Center tunnel is basically an open tunnel of the identical configuration with a width of 18.3 meters (60 ft) and a height of 9.1 meters (30 ft). However, a ground board is generally installed in the tunnel for high-lift testing. This ground board is not at the lower boundary of the open tunnel but is located 0.61 meter (2 ft) above the lower boundary. This is the configuration treated herein. The active or useful region of this closed-on-bottom-only configuration has a height of 8.5 meters (28 ft) so that the nominal width-height ratio is $\gamma = 30/14 \approx 2.1429$. The average width of the active region of the tunnel is found to be 16.6182 meters (54.5215 ft) so that the effective width-height ratio is $\gamma_e \approx 1.9472$. When a model is stated to be centered in this tunnel, it should be understood to be centered in the active region of the tunnel and not centered in the original open version of the tunnel. In actual use, the mounting arrangements of the tunnel are such that the model locations tend to approximate the central location as defined herein.

Since in each of these tunnels the effective width has been decreased from the nominal width, it would appear necessary to alter the ratio of the model span to the tunnel width to conform to the same average width; that is,

$$\sigma_e = \sigma \frac{\gamma}{\gamma_e} \tag{40}$$

The simultaneous use of both the effective $\gamma_e$ and the effective $\sigma_e$ will be found to yield the correct area ratio in equation (14).

These changes were made internally in the programs used to compute the numerical values upon which the charts are based. For simplicity and ease of application, the charts are referred to the nominal rather than to the effective values of $\gamma$ and $\sigma$.

It should be observed that the nominal values of width-height ratio $\gamma$ and span-width ratio $\sigma$ rather than the corresponding "effective" values, $\gamma_e$ and $\sigma_e$, are used in determining Rae's limit (eq. (24)). In the present formulation, any effect of changes in the side boundaries, such as fillets or semicircular sides, is considered to be included in the allowable values of $x_f/b$.

Although no appropriate theory exists for these tunnels when the model wake is sharply deflected, a theory appropriate to at least the Ames tunnel does exist (ref. 31) for models having a vanishingly small lift coefficient. Certain results from that treatment are compared with the present results for similar conditions at a later point in this paper.

## PRESENTATION OF RESULTS

The closed wind-tunnels treated herein cover a wide range of width-height ratios (fig. 5) from extremely wide tunnels ($\gamma = 3$) to extremely narrow tunnels ($\gamma = 1/2$). The closed-on-bottom-only configuration is encountered less frequently and its treatment herein is confined (fig. 5) to two examples representative of current practice. In each case, a range of span-width ratios $\sigma$ and a range of sweep angles are considered. The increments of span-width ratio vary for the different tunnel configurations. These increments were chosen to facilitate certain comparisons between present and proposed wind tunnels. In any event, these charts cannot necessarily be used on the basis of equal span-width ratios in comparing different tunnels. Several examples of their correct use are presented later in the discussion.

Reference 19 has indicated the possibility of designing certain tunnels with variable width-height ratio or variable model height in order to reduce the magnitude of wall interference. The variable width-height ratio type of tunnel has not yet been attempted; however, the new Langley V/STOL tunnel (ref. 32) is capable of variable model-height

operation. Therefore, charts appropriate to this configuration, with the model height adjusted according to $\chi$ (or both $\chi$ and D/L) have been prepared and are presented herein.

It should be observed that the height of each tunnel is implicitly assumed to be that dimension parallel to the lift-force vector and that the width is that dimension perpendicular to that vector. Thus, if for any reason it becomes desirable to mount the model with the lifting force toward the side, the width-height ratio of a given tunnel changes from $\gamma$ to $1/\gamma$. For example, in figure 6, if the initial tunnel has a width-height ratio of 3/2, rotating the model $90^{\circ}$ results in a tunnel having a width-height ratio of 2/3. A similar model rotation in a tunnel having a width-height ratio of 2 results in a tunnel having a width-height ratio of 1/2.

It is often desirable to test semispan models rather than complete models. Such tests are generally accomplished by mounting the model from either the tunnel wall or the tunnel floor and using that boundary as a reflection plane to simulate a complete model. Interference in such tunnels is treated by considering the image reflection of both the model and the tunnel across the surface on which the model is mounted. The width-height ratio of the tunnel may differ according to the boundary against which the model is mounted. For example, if the initial tunnel (fig. 6) has a width-height ratio of 3/2, mounting from the sidewall results in a tunnel having a width-height ratio of 3, and mounting from the floor results in a tunnel having a width-height ratio of 4/3. Similarly mounting a semispan model from the floor of a tunnel having a width-height ratio of 2 results in a square ($\gamma = 1$) tunnel. (Mounting from the sidewall in this tunnel would result in a tunnel with $\gamma = 4$; however, this width-height ratio is not included herein.) The possibilities are reduced in a square tunnel; the width-height ratio is 1 regardless of the orientation of the complete model and is 2 regardless of the boundary from which a semispan model is mounted.

The two NASA full-scale tunnels would be somewhat more difficult to treat on this basis because of the curved side boundaries. If these two tunnels are omitted from consideration, and if it is recognized that the one rectangular closed-on-bottom-only tunnel may be obtained simply by modifying a closed test section, it will be observed that the present set of charts, despite their number, do not even include all the possible mountings of centrally located models in only two basic test sections.

All the charts pertaining to each tunnel configuration are grouped together. The results for the closed tunnels, in order of decreasing effective width-height ratio, are presented in figures 7 to 43. The charts for the closed-on-bottom-only tunnels are presented in figures 44 to 55. The charts for the variable-model-height tunnels, together with the appropriate model-height schedules are presented in figures 56 to 67. Table I serves as an index to the individual figures.

## DISCUSSION

### CORRECTION CHARTS

Because of the large number of charts presented herein, no attempt will be made to discuss these correction charts in detail. Instead, only a few comments are offered concerning the general nature of the results, the degree to which they agree with conventional theory, and the degree to which these results indicate the reasons for the currently accepted limitations on wind-tunnel testing. The following discussion is divided according to the type of boundaries employed in the tunnel.

#### Closed Tunnels

Average corrections.- The average correction angles in the closed tunnels increase, as expected, with both model size and with lift. In addition, the contours of equal values of $\Delta\alpha$ have a decided negative slope; that is, for a constant value of $C_L/A$, an increase in $D/L$ increases the indicated correction angle. This result is anticipated since increasing the drag at constant lift not only decreases the wake angle $\chi$ (fig. 1) which increases the vertical interference due to lift, but it also increases the vertical interference due to drag which acts in the same sense.

There is a surprisingly good correlation between the conventional corrections and those of the more complete analysis (refs. 5 to 8) at zero drag even, at times, for $\Delta\alpha$ in excess of $10^o$ or $20^o$. This result may be surprising since, for high lift coefficients (low skew angle), these papers indicate vertical interference factors significantly greater in magnitude than the equivalent factors of conventional theory. On the other hand, examination of the behavior of $\delta_{w,L}$ in the figures of references 7 and 8 indicates that for $\chi_e$ greater than about $75^o$ to $80^o$, the magnitude of $\delta_{w,L}$ remains about constant at a value equivalent to that of conventional theory. Indeed, the magnitude of the values for $\chi_e$ on the order of $75^o$ or $80^o$ may even be slightly less than those at $90^o$. Now an effective wake skew angle of $75^o$ is equivalent (eq. (12)) to a momentum skew angle of about $50^o$, and it will be seen from figure 1 that a large region of these correction charts lies below this wake angle. (At zero drag, $\chi = 50^o$ occurs at $C_L/A \approx 3.5$.) Thus, the agreement between the conventional and the more complete theory is not surprising.

At more extreme conditions where the indicated average correction angles are very large, it will be observed that at zero drag, the corrections in these charts are significantly less than those that are predicted by conventional theory. This is true despite the fact that for these low wake skew angles, $\delta_{w,L}$ of references 5 to 8 is significantly greater in magnitude than the equivalent interference factor of conventional theory, and that the more complete theory also predicts a horizontal interference which generally

tends to increase (eq. (18)) the correction angle. The reason is simply the assumption of small angles in conventional theory. As previously discussed (eq. (30)), this assumption tends to increase the size of the indicated correction angle substantially over that which would be obtained without the small-angle assumptions.

The drag-lift ratio has a significant effect on the average corrections. For a centrally located model in a closed tunnel with the wake passing directly rearward ($\chi = 90^{o}$), such effects are zero; however, the effect of the drag terms increases rapidly as the wake is depressed downward. Because drag effects are zero for the undeflected wake, they are not obtained in conventional theory even though the result of these effects may be significant for wakes which are deflected only slightly downward.

Certain rules for acceptable wind-tunnel practice have been developed empirically over many years of testing models, generally of unpowered wings, in wind tunnels. Perhaps the most widely used of these rules (for example, ref. 2) is that the model should be sized in relation to the tunnel so that, when using conventional corrections, $\Delta\alpha$ does not exceed $2^{o}$ for the greatest lift coefficient at which the model is to be tested. (An alternate form of this limit, given in ref. 4, is essentially equivalent to the foregoing statement.) Since wings are normally tested to lifts corresponding to stall, such a limit generally results in estimating $\Delta\alpha$ at the maximum lift coefficient. However, the maximum lift is not obtained without a significant drag; the induced drag at such lift coefficients will fall to the right-hand (higher drag) side of the curve shown for an ideal unpowered wing in figure 1. Under such conditions the correction angle indicated on the charts is significantly greater than that predicted by conventional theory. Indeed this difference would appear to be at least one reason for the existence of such a restrictive limit. If so, it is reasonable to assume that such a limit should be far less restrictive than $2^{o}$ if applied to powered models (such as rotors, for example) where very large lifts are not necessarily associated with high drag. In such cases, if the drag were nearly zero, a more appropriate limit (when considering only the average correction) might be as much as an order of magnitude greater than $2^{o}$ even when applying corrections obtained by conventional theory.

The contours of dynamic-pressure ratio indicate that in the wide tunnels at moderate $C_L/A$, there will be some small decrement in the corrected dynamic pressures. As the width-height ratio $\gamma$ decreases, the magnitude of the decrement decreases until there is a small increase in the corrected dynamic pressure in the very deep, narrow tunnels.

The magnitude of the decrement of corrected dynamic pressure in the wide tunnels may seem to be small if only the longitudinal interference velocities are considered. However, the form of equations (19) and (20) shows that the vertical interference velocities $\Delta w$ will tend to compensate for the generally negative values of the longitudinal interference velocities $\Delta u$. Indeed, at extreme conditions, the increase in $\Delta w$ totally

overpowers the $\Delta u$ term to produce enormous increases in effective dynamic pressure. Such conditions are generally so severe that it would not be reasonable to consider performing wind-tunnel tests.

In the narrow tunnels $\Delta u_L$ is reduced significantly and $\Delta u_D$ actually reverses sign (ref. 5). Combined with the always positive effect of $\Delta w$ in equation (20), the overall result is the mild increase in dynamic pressure shown, for example, in figure 40.

In one case (fig. 22), the model has been taken to be a uniformly loaded rotor rather than a uniformly loaded wing. Although there are, of course, differences in the values presented in this figure and the equivalent figure (fig. 21) for the wing, in general, the values for the two configurations are quite similar. (In comparing these figures, note that the aspect ratio of the rotor is $4/\pi$ and that $\chi = 90^o$ the wake of the uniformly loaded rotor is equivalent to that of an elliptically loaded wing.)

Effect of corrections on data.- The overall effect of corrections on a given set of data is rather involved. In addition to the comparatively simple changes in dynamic pressure and angle of attack, the resultant total-force vector is rotated with respect to the stream axis; thus, its resolution into lift and drag components (eqs. (22) and (23)) is altered. As observed earlier in this paper, the calculation of such effects within the present analysis cannot be carried out rigorously because an unstated amount of profile drag must be present in the resultant-force vector as well as in the induced drag and lift. However, for illustrative purposes only, one such set of calculations has been carried out on the assumption of zero profile drag. (See fig. 68.)

Figure 68 shows that, as might be expected, the corrected lift coefficient is not significantly altered at modest lift coefficients although it is obtained at a significantly different corrected angle of attack. (See eq. (21) and fig. 21(c).) At higher lift coefficients $\left(C_L/A > 1\right)$ the lift coefficient is affected and because of the dynamic-pressure corrections, is generally increased. The effects on the drag-lift ratio are considerably more severe even at fairly low values of $C_L/A$, and the corrected drag-lift ratio may be as much as 20 percent greater than the observed drag-lift ratio for conditions less severe than Rae's flow-breakdown limit (ref. 10).

In the case of powered-lift testing, it is generally desired to set some equivalent steady-state flight condition with a given lift, with zero net horizontal force, and with some given value of an operating parameter which may, in turn, be defined in terms of either forward velocity (for example, tip-speed ratio for a helicopter) or dynamic pressure (for example, thrust coefficient for a tilt-wing aircraft). The alterations in $q_c$, $V_c$, $\alpha_c$, $C_{L_c}$ and $C_{D_c}$ implied by figures 21(c) and 68 combine to make it extraordinarily difficult to set such a predetermined condition as a single test point in a wind-tunnel investigation. It may be necessary to do considerable interpolation between a large

number of corrected test points in order to obtain the desired information. If the corrections are sufficiently large, the test engineer may even be embarrassed by finding that the conditions which he set in the tunnel were not sufficiently broad to cover the corrected flight condition for which he required experimental data.

Corrections at tail.- The corrections at the tail display the same general character as those at the wing when the lift coefficients are moderate, and are also generally greater for greater values of D/L. At the more extreme lift coefficients there is generally a tendency for the sign of $\Delta i_t$ to reverse; that is, $\Delta i_t$ tends to become negative for extreme conditions whereas it is always positive at low $C_L/A$.

Examination of the longitudinal distribution of interference factors in reference 7 indicates the reason for the behavior of $\Delta i_t$. For the hovering condition where $\chi = 0^o$, the peak vertical interference occurs at the model and as $\chi$ increases the location of the peak interference shifts to ever greater distances behind the model. Now $\Delta i_t$ is the difference between the interference at the location of the tail and the interference at the location of the wing. Thus, if the effective wake skew angle is large enough to place the maximum interference behind the tail, $\Delta i_t$ will be positive. Once the point of maximum interference moves forward in front of the tail, $\Delta i_t$ will decrease. Further forward movement of the point of maximum interference will eventually, at some small wake skew angle, lead to a condition where the interference at the tail is less than that at the wing and $\Delta i_t$ will become negative. When dealing with a tail length proportional to span, such effects become very predominantly a function of span. A somewhat altered effect might have been obtained if the tail corrections had been computed at a constant distance behind the wing. (See, for example, fig. 21 of ref. 8.) It will be noted that this change in sign of $\Delta i_t$ generally occurs for conditions above Rae's flow breakdown limit; thus, generally speaking, it will have no significant effect on valid V/STOL data for the classes of model considered herein.

The classical corrections in the closed tunnels appear to be a weak function of angle of attack for the tail length considered herein. Again at low $C_L/A$ the classical corrections correspond fairly well with the present results at $D/L = 0$. The correspondence is generally best in the wide tunnels and when the classical corrections are computed at the same angle of attack ($20^o$). It will be noted that, in general, this correspondence between classical corrections and the present work weakens at lower lift coefficients than in the case of the average corrections.

The dynamic-pressure ratios $q_t/q_c$ are a complex mixture of effects caused by lift and by drag and at the model and at the tail. At low lift there is generally a small decrease in effective tail efficiency; however, sufficiently large drags will reverse this effect. The indicated dynamic-pressure ratios well above Rae's breakdown limit show extreme increases in tail efficiency.

Corrections to tail-caused pitching moments have a general reputation of being inherently less accurate than corrections to the lift, drag, and angle of attack. There are many reasons why this should be so. First, there is a smaller region of correspondence between the usually used conventional corrections and those predicted by the more complete theory. The differences between the two theories increase significantly for the large drags which are associated with large lift coefficients for conventional unpowered models. The upwash created by the tunnel boundaries also influences the wing wake and displaces it to a higher position with respect to the wake in the tunnel than in free air. The direct effect of the altered wake location may be quite large. (See ref. 33.) Finally, the distribution of vorticity within the wake may be significantly altered by the distribution of interference across the span of the wing which will be discussed next.

Nonuniformity of corrections.- The distribution of interference over the span of the model is very nonuniform if the span of the model is a significant fraction of the tunnel width and this nonuniformity becomes even greater as the sweep angle of the wing increases.

The magnitude of this nonuniformity of interference is shown in a later section to be one of the most severe limits on the usable testing range of a given wind tunnel. It is also a significant limit on the validity of the present charts when applied to extreme conditions. The present charts are all obtained on the basis of an assumed uniform spanwise distribution of lift and induced drag. (The one sample of average corrections for a rotor differs in that it assumes a uniform distribution over the area of the disk.) Undoubtedly, some peculiar distribution of chord and twist could be obtained which for, at least one condition, would result in this uniform loading. On the other hand, the tunnel constraints impose an alteration of the local loading through the medium of nonuniformities in the wall effects. It is obvious that in the face of the extreme nonuniformities of wall effects indicated herein (for example, fig. 27(e), where $\Delta i_w$ ranges between $-50^o$ and $90^o$, and where $\Delta q/q_c$ ranges between -0.5 and 2.0) that the load distribution across the span will be altered violently. The altered load distribution would, in turn, change the interference distribution and the entire cycle would then repeat. Presumably, for some specified constant planform, such effects could be computed by some iterative cycle; however, the required computer time might be excessive for routine application and the resulting corrections to the load distribution might be large enough to overpower the measured data. In any event, even if desired, such calculations would be excluded from the present study in which the model can assume almost any form, powered or unpowered, subject only to specified relative size and sweep. The foregoing comments apply equally well to the previously discussed charts giving average corrections and corrections at the tail since a radically altered load distribution will affect such charts as well as the charts of nonuniformities.

In most cases, Rae's flow breakdown limit eliminates consideration of test conditions at which the worst nonuniformities are encountered. However, even below this limit,

clearly excessive nonuniformities may exist. For example, consider figure 27(e) where differences of $20^{o}$ in incidence with local gradients of $50^{o}$ per semispan are predicted at conditions less severe than Rae's limit.

A few basic concepts will help to explain the somewhat involved character of the nonuniformity of corrections. First consider an unswept wing. In hovering where the wind-tunnel interference is much the same as the ground effect (refs. 5 and 7), the interference is primarily caused by the floor of the wind tunnel if the tunnel width-height ratio is reasonably large. It is less true in narrow tunnels where the walls have stronger effects. The maximum vertical interference, at least for the uniform loadings considered herein, will occur under the center of the model and the interference will diminish as the lateral distance from the center of the model increases. Thus, for conditions at, and near, hovering $\Delta i_w$ should be negative at least for wider tunnels.

As the skew angle increases, the effect of the walls increases. When the wake passes directly rearward ($\chi = 90^{o}$), the effect of the walls will predominate if the span of the model is large or if the width-height ratio is small. (Observe, on page 193 of reference 34, that the effect of the walls at $\chi = 90^{o}$ will dominate the interference at a very small model if the width-height ratio is less than $\sqrt{2}$, but that the combined effect of floor and ceiling is greater than the effect of the walls for $\gamma > \sqrt{2}$. Increasing the span, of course, will bring parts of the model closer to the walls and increase the effect of the walls.) The presence of the walls at high skew angles results in a strong upwash which is stronger locally as the tips of the model approach the walls. Under these conditions the interference is greater at the extremities of the model and $\Delta i_w$ becomes positive.

These trends may be observed in the charts pertaining to unswept wings. For small models in wide tunnels, where the floor of the tunnel is always the predominant cause of interference, $\Delta i_w$ may always be negative. In the very deep narrow tunnels, where the walls tend to predominate, $\Delta i_w$ is often always positive. For large spans in moderately wide tunnels it is found that at high skew angles the walls have the larger effect and thus produce a positive $\Delta i_w$, but that as the lift coefficient increases, reducing the wake skew angle, $\Delta i_w$ changes in a relatively complex manner until it finally becomes negative. This balancing of effects can result in large regions of the chart in which the nonuniformity of correction is remarkably small for a straight wing (for example, fig. 24(d)) even though the span may be quite large relative to the wind-tunnel width.

For very large span-width ratios, the lateral tips of the model are very close to the walls. The strong local effect of the walls produces very large effects near the wing tips that result in a wall-induced kink in the interference distribution. In the charts this effect shows as large positive values of $d\Delta i_w/d(y/s)$ and it may achieve extremely large values even at relatively small lift coefficients. The existence of this local effect at the tip is,

of course, the reason why conventional wind-tunnel procedure is to limit model spans to less than three-quarters of the wind-tunnel width.

If the wing is swept back, the tips will be well behind the lift-producing regions at the center of the wing. Thus, the downstream growth of interference (discussed previously in relation to the tail) tends to assume great significance. This effect increases substantially the interference at the wing tip. Even for wing sweep angles as small as $15^{\circ}$, the downstream growth of interference is significant in the interference distributions. Thus, $\Delta i_w$ is almost always positive (wash-in) for the swept wings (except at extremely small $\chi$) and it is almost always much greater than that obtained for an unswept wing under the same circumstances.

If conditions are such that the range over which an unswept wing may be tested is limited by the nonuniformity of interference over the span, the present charts indicate that a swept wing of the same span should be confined to much more restrictive limits. This effect has been observed experimentally. In terms of $\Delta\alpha$, reference 4 has observed that tests of highly swept wings should be confined to a maximum $\Delta\alpha$ of about $3/4^{\circ}$ rather than $2^{\circ}$ when using conventional correction techniques. This markedly smaller value of $\Delta\alpha$ will confine testing to smaller $C_L/A$ and will result in a consequent reduction in the nonuniformity of interference.

The differences in dynamic pressure across the span also display different behavior with sweep. However, large values of $\Delta q/q_c$ do not usually seem to appear unless associated with large values of $\Delta i_w$ or its gradient. Thus, testing will seldom be limited by consideration of the interference effects on the distribution of dynamic pressure across the span.

The conventional corrections once more are found to lead to approximately the correct order of nonuniformity at $D/L = 0$ for small $C_L/A$. However, in certain cases, because of the varying importance of walls and floor, conventional corrections may lead to grossly different results at larger values of $C_L/A$.

Approximate treatment of nonrectangular tunnels.- As noted in an earlier section of this paper, the two NASA full-scale tunnels each have been treated herein on the basis of presenting results for a rectangular tunnel of equal average width. Since no theory equivalent to that of references 5 to 8 exists for these tunnel configurations, it is not possible to assess fully the effect of the approximation.

Reference 31, however, does present a method of treating such tunnels when the wake is undeflected ($\chi = 90^{\circ}$) as in conventional theory. In essence, this method consists of replacing the wind-tunnel boundaries by a grid of rectangular vortex lines of unknown strength lying on the actual contours of the tunnel. The resultant of the velocities induced by both the model and the walls is then computed in terms of the unknown vortex strengths

at an equal number of control points. These equations can be solved for the unknown strengths by using matrix techniques, and finally the interference factor is calculated by using the vortex strengths obtained from the matrix inversion.

The wind-tunnel configurations of interest in the present paper are not included in the numerical results represented in reference 31; however, Paul M. Reeves and Robert G. Joppa of the University of Washington have graciously provided the appropriate numerical results for the closed tunnel. These results are presented in figures 69 and 70 where they are compared with the equivalent interference factors of reference 8 for rectangular tunnels having width-height ratios of $1 + \pi/4$ and 2.

Figure 69 indicates that the quasi-elliptical shape of the round-sided tunnel results in a slightly lower interference factor than does either of the rectangular tunnels. The rectangular tunnel of the same average width provides a closer approximation to the desired result for spans of less than one-half the tunnel width ($\sigma < 0.5$), but the rectangular tunnel of equal width is closer for spans larger than this.

The reason that the tunnel of equal average width is less representative at large spans is evident in the spanwide distribution of figure 70. It is evident that the foreshortened width overestimates the interference near the tip, primarily because the "effective" side boundary is closer to the tip than the actual boundary is. Although not as evident in figure 70, close examination shows that the distributions for small spans are somewhat less nonuniform for the rectangular tunnel of equal width.

The results presented in figures 69 to 70 apply only to the case of vanishingly small lift and do not necessarily apply to large lift coefficients. It will be observed that when the floor is close to the model (large $\gamma$), only modest vertical deflection of the wake is required to produce large increases in interference. When the span of the wing is sufficiently great to overhang the curved sidewalls, the local distance to the "floor" is decreased. Thus, a round-sided tunnel such as this probably will show an exaggerated effect of wake deflection on the nonuniformity of corrections.

## Closed-on-Bottom-Only Tunnels

Average corrections.- The average corrections for the tunnels which are closed only on the bottom (figs. 44 and 50) display a totally different behavior than those of the equivalent closed tunnels (figs. 15 and 21). This type of tunnel configuration is one of the classical "zero-correction" tunnels when the width-height ratio is 2 and the model is vanishingly small and the wake is undeflected ($\chi = 90^{\circ}$). (See ref. 35.) For the tunnels considered herein, where the effective width-height ratios ($\gamma_e = 1.947$ and 1.5) are less than 2 and where the model span is finite, conventional theory predicts a mild downwash (ref. 35, and also ref. 5 when $\chi = 90^{\circ}$).

The theory of references 5 to 8 predicts that as the wake is depressed from the horizontal, these tunnels should indicate upwash as the influence of the floor becomes greater. Furthermore, significant effects of drag are predicted. Some of these trends are illustrated in figures 44 and 50. Because the vertical interference due to lift has such small values at small lift coefficients, the correction angles $\Delta\alpha$ tend to depend far more on the drag-lift ratio than on $C_L/A$. Negative drag (otherwise, forward thrust) results in an induced downwash. Positive drag, if sufficiently great, results in an upwash. This effect is not symmetric, however, because increases in span-width ratio or departures of the width-height ratio from 2 do result in a downwash contribution from the lift forces.

For large spans, there is some correlation between conventional corrections and the present results at $D/L = 0$ with small $C_L/A$. (Presumably, if contours of sufficiently small $\Delta\alpha$ were presented, there might also be some correlation when the span is small.) The change from downwash to upwash as the skew angle is decreased may lead to extreme disagreement at high $C_L/A$. It is further obvious that a model following the curve labeled "unpowered wing" in figure 1 will see correction angles which bear little or no relationship to those predicted by conventional theory.

The corrections to dynamic pressure generally result in a reduction in the corrected dynamic pressure. The effective reduction is substantially greater than that in the equivalent closed tunnels. (Compare figs. 21 and 50.) For some extreme conditions, well beyond Rae's limit, the corrected dynamic pressure is predicted to be near zero. Such a tremendous correction is not likely in practice since the model forces would, of course, be drastically altered by such a major change.

Corrections at tail.- As in the case of the closed tunnels, the angular corrections at the tail are generally positive except at extreme wake skew angles. This result occurs largely because of the assumption of a standard angle of attack of $20^\circ$. Positive angles of attack result in lowering the tail so that it is closer to the closed floor. The floor, being closed, produces an upwash interference which is greater as the distance from the floor decreases.

Because the upper and lower boundaries of these tunnels are of opposite character, it should be anticipated that the angular corrections should show a pronounced dependence on the angle of attack. This dependence is evident in the auxiliary scales which indicate the conventional corrections. The dependence of the corrections on angle of attack persists throughout the entire range of wake angles. (See, for example, fig. 23 of ref. 8.) Because the "upwash" interference increases with angle of attack, these tunnels will generate much larger corrections to static margin than will closed tunnels where the interference is almost independent of angle of attack.

Corrections to the dynamic pressure are mild for conditions below Rae's limit. In this region, there is often a small increase in the effective tail efficiency factor.

Nonuniformity of corrections.- The nonuniformity of the corrections over the span shows a strong dependence on the drag-lift ratio. The nonuniformity is generally in the nature of an induced washout; that is, $\Delta i_w$ is generally negative. Sufficient forward thrust, if the model is reasonably large, will actually reverse the sense of the nonuniformity because of the action of the interference due to drag.

In these tunnels the effect of the open sidewalls is that of an increased downwash. Thus, there is no balancing of the effects of the floor and the walls. These effects are generally additive. Thus, the nonuniformity over unswept wings does not display the peculiar behavior indicated in the closed tunnels which for that configuration, led to very small nonuniformities for unswept wings. In the present case, the nonuniformity becomes greater as the span becomes greater, and the nonuniformity over unswept wings is relatively worse than that in the corresponding closed tunnel.

The downstream growth of interference again results in greater nonuniformity as the wing sweep increases. However, the interference in the closed-on-bottom-only tunnels grows more slowly with distance downstream that in the closed tunnel. Thus, the nonuniformity does not increase as rapidly with wing sweep in these configurations.

Conventional corrections yield approximately the correct values at $D/L = 0$ if the lift coefficient is small enough. On the other hand, if the model span is small in relation to the tunnel width, this agreement may not be obvious, for the nonuniformity only becomes large enough to show for conditions of large $C_L/A$. Once again, however, the changes in nonuniformity with drag-lift ratio are sufficiently large to indicate that the use of conventional corrections could lead to rather optimistic results for a model such as the "Unpowered wing" of figure 1.

In general, the contours of $\Delta q/q_c$ do not achieve values large enough to be troublesome within the usable testing range of the tunnel. Large values of dynamic pressure nonuniformity are, in general, only encountered in the presence of prohibitive angular nonuniformities.

## Closed-on-Bottom-Only Tunnels With Variable Model Height

Reference 19 indicates the possibility of designing certain closed-on-bottom-only tunnels in which the corrections could be minimized by varying either the width-height ratio or the model height as a function of the wake skew angle. One recent tunnel, the Langley V/STOL tunnel has been designed so that such operation with variable model height is possible. Consequently, this configuration has been treated herein in a manner identical to that of the preceding configurations. The one alteration is that the model

height is now subjected to the schedule required by the computer programs of reference 19. These programs, in essence, are equivalent to the more general interference programs of reference 18 except that before computing the interference, the computer is first required to search at each $\chi_e$ for the model height which reduces $\delta_{w,L}$, and thus $\Delta w_L$, to zero.

Average corrections.- The required schedules of model height, shown in figure 56, result in the corrections shown in figure 57 for a tunnel having a width-height ratio of 3/2. The effect of the variable model height may be seen by comparing figure 57 with figure 50 which considers the same tunnel configuration with a centered model.

The result of the foregoing comparison is somewhat disappointing. The primary effect is, in essence, to straighten out the $\Delta\alpha = 0^o$ contour so that it lies along $D/L = 0$. Because of the corresponding changes in the drag components of interference, $\Delta\alpha$ and $q_c/q$ may actually increase for drag-lift ratios other than zero. Indeed, for a model following the "Unpowered wing" curve of figure 1, the interference may be increased substantially.

The more rapid decrease in $q_c/q$ is partially a result in the reduction of $\Delta w_L$ as may be seen from equations (16) and (20). When the span-width ratio is large, this effect can lead to an indicated complete reversal of the flow with a singular point of zero dynamic pressure. (See fig. 57(c), and particularly note the indicated singular point at $D/L = 0$ and $C_L/A \approx 7$.)

Although this technique may be of value if the drag-lift ratio is near zero, such as it might be for a lifting rotor, it is obviously not of general utility. Reference 19, however, suggests an alternate possibility of choosing the model height so that $\Delta w = 0$, that is, so that

$$\delta_{w,L} + \frac{D}{L}\delta_{w,D} = 0 \tag{41}$$

Under such conditions, with the total vertical interference velocity equal to zero, $\Delta\alpha$ must be zero, or if the horizontal interference is sufficiently great to reverse the flow at the model, $\Delta\alpha = 180^o$.

The required schedules for this type of operation are given in figure 61. At low lift coefficients the required model height is primarily a function of drag-lift ratio; however, at extreme lift coefficients the schedule tends to become more nearly a function of wake skew angle. (Compare fig. 61 with fig. 1.) This general trend would be expected from the average corrections when the model is centered. (See fig. 50.) The required schedule indicates the need for model heights very close to the tunnel floor when the drag-lift ratio

becomes negative. This restriction is a marked disadvantage in several respects. The most obvious of these disadvantages is with respect to Rae's limit, which is lowered substantially for such conditions.

If the drag-lift ratio is less than about -0.5, there is no model location which will satisfy equation (41). This observation is true for all span-width ratios. A brief examination of other width-height ratios (fig. 65) indicates the same result. Indeed, in some cases, values of $D/L$ in excess of about 0.8 lead to a similar problem (fig. 65(b)).

With $\Delta w = 0$, as noted earlier, and as shown in figures 62 and 66, $\Delta\alpha$ is indeed zero throughout the region below Rae's limit. At much higher lift coefficients, where the flow at the model becomes reversed, $\Delta\alpha$ discontinuously changes to $\pm 180^{\circ}$. The effect of interference on $q_c/q$ becomes even greater as might be expected from the complete elimination of $\Delta w$ in equation (20).

Corrections at tail.- Either form of variable-model-height tunnel leads to some reduction of $\Delta i_t$ for positive drag-lift ratios (compare figs. 51, 58, and 63); however, at negative drag-lift ratios, $\Delta i_t$ may be increased. This latter increase may be large when operation for $\Delta w = 0$ (fig. 63) is chosen because of the very low model heights required at negative drag-lift ratios. The increases in boundary-induced tail efficiency are notable.

Nonuniformity of corrections.- Examination of the charts related to the nonuniformity of corrections (figs. 59, 60, and 64) indicates that the effect of variable-geometry operation of these tunnels is relatively small. When compared with the same tunnel with a centered model (figs. 52 and 55), the nonuniformity is slightly reduced for positive drag-lift ratios and it is somewhat increased for negative drag-lift ratios.

## ESTIMATION OF LIMITING VALUES OF INTERFERENCE PARAMETERS

### General Considerations

Of all the terms herein relating to wind-tunnel boundary effects, the only one that appears explicitly as a limit is Rae's flow-breakdown limit. (See ref. 10.) Inherently, this limit is a statement that beyond this point extraneous influences present in the tunnel, but not in free air, will seriously affect the data. Actually all the other terms presented in the foregoing charts pose limits to testing equally as well as does Rae's limit. However, the actual limiting values can be chosen only after consideration of the consequences on different models of differing levels of each of the various parameters.

It is necessary in order to proceed further to choose some such set of limits. It is recognized that the particular values used may differ for different models; however, the present choices are based on values that might be appropriate to a wing or at least a "wing-like" model.

The basic principles involved in choosing limits are at least twofold. First, if it is desired to ignore a particular interference parameter in correcting the data, then the maximum value of that parameter must be chosen small enough to insure that it will not have a major influence on the final data. Second, the maximum allowable values of each parameter should be chosen to be sufficiently small to insure that the corrections for it will not be greater than the effect of reasonable variations in the model itself. To accept larger values would inherently make the corrected data more nearly a function of the theoretical calculations than the product of measurements. In cases where the experimenter possessed that great a level of confidence in theory, he would be well advised to save the time, trouble, and expense of wind-tunnel tests.

The actual values chosen under these guiding principles will depend ultimately on how much effort one is willing to put into correcting his data. The next several paragraphs will discuss possible plausible limiting values of the interference parameters at three different levels of applied corrections. These three levels are recognized as ranging from more rigorous to less rigorous than those typically employed as current wind-tunnel practice.

### Maximum Practical Corrections

Even when employing the maximum practical level of corrections, it will be found appropriate to accept some limit on the average corrections because excessive values will make it exceedingly difficult to set the desired flight conditions in the tunnel. Actually, experimental studies, such as those of references 11 to 13, seem to indicate that $\Delta\alpha$ values on the order of $5^{\circ}$ and dynamic-pressure corrections on the order of 10 percent of free-stream dynamic pressure are acceptable. These values are accepted here.

Once the maximum level of the average corrections is determined, one must then deal with different types of nonuniformity over the model. It has been observed earlier that large values of $\Delta i_t$ introduce uncertainty into moment corrections because of induced camber and wake relocation effects. Thus, a rather arbitrary limit of $5^{\circ}$ might be imposed on $\Delta i_t$. It is desirable not to mask the usual values of tail efficiency factor $\left(\text{on the order of } q_t/q = 0.9\right)$ so that $q_t/q_c$ should most likely be limited so that the effective dynamic pressure at the tail is altered from the corrected dynamic pressure by no more than 10 percent. Correction limits this large will undoubtedly require at least elementary estimation of the effect of interference on the actual wake location at the tail.

The span-load distribution over the wing and its consequent effect on pitching moment for swept wings could probably be corrected for by the application of known lifting-line or lifting-surface techniques. As an upper limit it would be desirable not to mask the built-in wing twist which is likely to be on the order of $2^{\circ}$. Local kinks of spanwise loading may be acceptable up to a larger value, a local gradient of, for example, $5^{\circ}$

per semispan. Certainly some limit, for example, 10 percent, should be imposed on the dynamic-pressure difference over the span since the local loading would be expected to vary almost linearly with the local dynamic pressure.

An excellent case could be made for imposing more stringent limitations on the nonuniformity for highly swept wings since their greater longitudinal extent will result in more significant effects on pitching moments. This procedure is not followed herein for the reason that there have been so few attempts actually to apply corrections to spanwise loading that the limits of application as affected by sweep angle are essentially indeterminate.

The foregoing limits are summarized in table II(a).

### Moderate Corrections

The degree of correction typically employed as current practice involves a much smaller emphasis on the nonuniformity of interference than is implied in the preceding discussion. Consequently, smaller limits on the interference parameters may be required.

The average interference factors may be taken as having about the same limiting values as before. These values are used primarily for ease of setting wind-tunnel conditions and the values used in the preceding discussion would be relatively unaffected.

Current practice in correcting pitching moments often neglects tail location as a function of angle of attack, often omits induced camber effects, and almost never considers wake relocation caused by the boundary interference. Thus, the tail-related interference parameters must be somewhat more restrictive. Values of $\Delta i_w$ of $2^\circ$ and dynamic-pressure differences of 5 percent are chosen somewhat arbitrarily herein.

At the present time the spanwise load distribution is hardly ever considered in correcting wind-tunnel data. Thus, the limiting values of those parameters must be greatly reduced so that their effects will not compromise the final data. Suggested values, used in the present study, reduce $\Delta i_w$ to a maximum of $1/2^\circ$ with a local spanwise gradient of $1^\circ$ per semispan. Concurrently, the maximum spanwise difference in dynamic pressure is reduced to 5 percent.

The foregoing values are summarized in table II(b).

### No Corrections

If the model is sufficiently small with respect to the test-section dimensions, the data may be satisfactory without applying corrections. Indeed, the data from certain wind tunnels which specialize in crude "first-look" studies may be uncorrected even when the model is relatively large. The absence of corrections, however, implies that testing

should be limited to maximum values of the interference parameters which are significantly smaller than those which are appropriate when corrections are applied.

The values chosen for the nonuniformity of corrections when using moderate corrections are sufficiently small so that they probably apply equally as well when no corrections are employed. However, it will be necessary to reduce significantly the tolerances on the average corrections and on corrections at the tail. For the present purposes both $\Delta\alpha$ and $\Delta i_t$ are chosen to have limiting values of $1/2^o$ and both $q_c/q$ and $q_t/q_c$ are chosen so that the corrected $q_c$ and $q_t$ will be within 5 percent on the nominal measured tunnel dynamic pressures. The use of limits this stringent will most likely be adequate if only the lift curve ($C_L$ plotted against $\alpha$) is considered; however, the accuracy of drag and moments will probably suffer when compared with corrected data.

The foregoing values are summarized in table II(c).

It will be observed that all the foregoing limits have been chosen on the basis that the model is "wing-like" or has "wing-like" characteristics. Many models do not possess this type of aerodynamic behavior. For example, centrally hinged helicopter rotors are essentially unaffected by longitudinal interference gradients (except for a small lateral tilt of the tip-path plane), and generally tend to average out lateral gradients to a marked degree. On the other hand, a so-called "rigid" (or hingeless) rotor might be so sensitive to longitudinal gradients that even more restrictive limits would be required for wind-tunnel tests. The present results are intended only to be illustrative of the general techniques. The actual limits for a given class of model can only be determined by a consideration of the effect of the different interference parameters on that particular class of model.

## TESTING LIMITS IN WIND TUNNELS

### Charts of Testing Limits

Once tolerances have been specified on the individual interference parameters it is possible to specify testing limits in terms of a maximum $C_L/A$ for a given value of $D/L$. These testing limits are found by superimposing the contours corresponding to the limiting values of each of the individual parameters on a single chart. Such a chart is specific, of course, to a given span of model, having a given wing sweep, in a test section of given size and proportions. A sample of such a chart is presented in figure 71 for wings of $0^o$ and $45^o$ sweep which span half the width of a tunnel having a width-height ratio of 2/3.

In all cases, the maximum lift coefficient at which the model can be tested is determined by a line which is defined at each value of $D/L$ by the smallest $C_L/A$ defined by the tolerances allowed by the degree of correction employed (in fig. 71, by table II).

The limiting parameter may vary according to the drag-lift ratio; for example, in figure 71 as the drag-lift ratio increases from -1.0 to 1.0, testing of an unswept wing is limited first by excessive values of $q_t/q$, then by excessive values of $\Delta\alpha$, and finally by Rae's limit $\left(x_f/b = 1.25\right)$. The testing limits may also be affected by sweep angle; for example, in figure 71 the testing limits for a wing with $45^o$ of sweep are defined by $\Delta i_w$ for $-1.0 \leqq D/L < 0.4$ instead of by $q_t/q_c$ and $\Delta\alpha$ as for the unswept wing.

It should be observed that testing limits defined in this manner are highly dependent on the previous choice of limiting values of each interference parameter. However, relaxing the tolerance on a single parameter may not produce a proportionate increase in testing limits. For example, in figure 71, even if Rae's limit $\left(x_f/b = 1.25\right)$ were totally ignored, the overall test limits would change only slightly. The limit at large $D/L$ would be replaced by a limit on $\Delta\alpha$ at almost the same values of $C_L/A$. Indeed, figure 71 is not typical of many of the test limits presented herein. This particular case was chosen primarily because the various limits were widely spaced on the chart and thus the sample could be more easily scanned. In general, the limiting lines corresponding to the individual interference parameters tend to group together more closely than in figure 71.

The presentation of testing limits is made considerably more compact by displaying only the lowermost limiting values rather than all the limiting values. This presentation has been made for the three levels of correction considered in table II. The results for the closed tunnels are presented in figures 72 to 74; those for the closed-on-bottom-only tunnels with centered models are presented in figures 75 to 77; and those for the variable-model-height tunnels are presented in figures 78 to 80. In each case, the particular interference parameter responsible for each segment of the limit is indicated by a symbol.

When the maximum practical corrections are applied, it will be observed that Rae's limit is the primary limitation on testing models of relatively small span-width ratio. As the model span increases, the longitudinal and lateral interference distributions tend to become far more restrictive and these latter terms overpower all else for the largest span-width ratios. The average correction angle $\Delta\alpha$ is notable by its absence as a limit except in the narrowest tunnels considered. When moderate corrections are applied, the increased emphasis on the lateral distribution produces significant reductions in the testing limits and markedly increases the effect of wing sweep on these limits. If no corrections are applied, the limits are found to be primarily determined by $\Delta\alpha$ and $\Delta i_t$.

### Effect of Correction Level on Testing Limits

Few effects shown herein, other than major changes in the relative model and tunnel sizes, are more significant than completeness of corrections in determining testing

limits. A sample comparison, for a model spanning half the width of a closed tunnel having a width-height ratio of 3/2, is shown in figure 81. Here it is seen that using the maximum practical corrections increases the allowable maximum lift coefficient by as much as a whole order of magnitude over tests with no corrections applied. This difference may be translated directly, although nonlinearily, into an increased model size. For example, the testing limit shown for no corrections in figure 81 for $\sigma = 1/2$ is of the same general level as that shown in figure 72(d) for the maximum practical corrections when $\sigma = 5/6$.

## APPLICATION TO MODEL DESIGN

The most difficult choice in the preliminary planning of a wind-tunnel test is the scale to which the model is to be built. Even for relatively conventional unpowered models, the effects of Reynolds number will dictate some minimum size of model. The effects of Reynolds number indicate the need, in general, for still larger models of powered aircraft since it will be necessary to maintain reasonable Reynolds numbers over items such as propeller and rotor blades and over various flow-turning devices such as control vanes. In addition, requirements of power and physical size on the drive systems of powered-lift models may set some severe physical restraints on the minimum size to which the model can be manufactured. These requirements are all related to the model itself, and the selection of minimum size may be dependent largely on the mechanical ingenuity of the model designer.

On the other hand, the maximum size of the model depends largely on the interference created by the boundaries of the test section in which the model is to be tested and upon the degree to which the data will be corrected. In some cases, the level of corrections applied to the data may be an option solely of the experimenter. More likely, however, this choice will depend upon the options available as standard data-reduction procedures in the possible tunnels in which the model might be tested. In such cases, it may turn out that the allowable maximum model size is more nearly a function of the diligence of the tunnel staff in correcting data than it is a function of the proportions or even the size of their wind tunnel.

Once the tunnels which might be available for a given test and their correction procedures are known, it is relatively simple to scan the test limit charts of figures 72 to 80 in order to determine whether any of the available tunnels are suitable for testing the model at minimum (or greater) scale over the anticipated range of lift and drag coefficients. Usually the total cost of the model and the test will be a minimum for the smallest practical model in the smallest and least sophisticated tunnel. In general, the test

should be planned for the minimum cost consistent with good data; however, it is recognized that cost may be dependent greatly upon who owns the tunnel and who is sponsoring the research. These last factors may have a substantial impact on the final choice.

If it turns out that none of the available tunnels is capable of testing the complete minimum model throughout the required range of lift and drag, it may still be possible to use one of these tunnels for tests of a semispan model of the equivalent same minimum model. It was noted earlier that such information for semispan models was present within these charts by considering both the real model and tunnel together with their reflection images as indicated in figure 6.

When mounting configurations other than the normal full-span arrangement are considered, the appropriate tunnel width-height ratio and span-width ratio vary according to the mounting configuration. In such cases, it is usually advantageous to work in dimensional terms rather than in the nondimensional terms used heretofore. Several sample cases, pertaining to models of constant full span in wind tunnels with test sections of $2 \times 3$ meters, $2 \times 4$ meters, and $2 \times 2$ meters are presented in figures 82 to 88. In general, it will be seen that semispan tests, particularly when the semispan is perpendicular to the floor, do permit an expanded test range, or, conversely, somewhat larger equivalent full spans. This observation is particularly true when considering models with highly swept planforms for which the data are corrected with "moderate" corrections.

Factors other than wall interference must be considered in choosing a semispan model. Such models cannot be tested in yaw or roll to obtain lateral-directional stability data. The boundary layer on the wall may affect the data since it is now in the plane of symmetry of the equivalent full-span model. On the other hand, the complexity and cost of powered-lift models can be approximately halved if it is necessary to build only a single semispan. On balance, however, the full-span model is generally preferable if considerations of model cost or available tunnel size do not intervene.

## APPLICATION TO WIND-TUNNEL DESIGN

The design of a wind tunnel is predicated on many factors, not all of which may be determined with any real degree of precision. The required speed range of the tunnel and its size may be determined by the need to fill voids in the testing capability of other existing facilities. These requirements in themselves may be modified to a great degree by limitations in cost or in available power. Within such bounds some estimate must be made as to the type, size, and performance range of the models that will be tested throughout the useful lifetime of the tunnel. Since this lifetime may, in some cases, exceed 40 years, the design must proceed on the basis of subjective extrapolations to the technology that will exist long after the designer has retired.

Within such bounds, there is no truly optimum test-section or wind-tunnel design; however, the design must at least proceed on some rational basis. The present system of charts and limits at least provides a means for a reasonable consistent comparison of differing test-section designs.

## Choice of Tunnel Size

The present charts can be used to provide some estimate of the minimum dimensions of the tunnel. This problem is recognized as the inverse of the problem just discussed, namely, that of determining the maximum dimensions of a model for a given wind-tunnel test. The difference is in the depth to which the study must be carried, for now a whole range of model sizes, model performances, tunnel-boundary configurations, and model mounting possibilities must be considered. The considerations discussed in both the preceding sections and those sections to follow adequately encompass the problems of choosing the overall tunnel size; thus, no additional discussion is presented at this point.

## Choice of Type of Boundaries

One of the early design decisions is the type of boundaries to be used in the test section. This choice will be influenced to some degree by practical considerations. It is generally simpler to arrange a tunnel for extensive flow-survey or flow-visualization studies if most of the boundaries are open, and access to the test section for model mounting is simplified. On the other hand, it is easier to obtain a smooth flow with no pulsations and an essentially zero longitudinal static-pressure gradient in a closed tunnel. Other things being equal, the power requirements of a closed tunnel will generally be somewhat less than those of an open tunnel.

As indicated in discussing the correction charts, the choice of boundaries will influence the wind-tunnel interference over the model. A good example of these effects may be obtained by examining the testing limits for one model in the new Langley V/STOL tunnel which has been arranged so that several different types of boundaries can be used. Among these configurations are both the closed and closed-on-bottom-only types treated herein. Furthermore, a variable-height string mount is available in the tunnel so that the closed-on-bottom-only configuration can be operated in the variable-model-height mode with the available equipment.

A comparison of the testing limits for a model spanning half the tunnel width when using these four options is presented in figure 89. All three levels of applied corrections are considered.

When the maximum practical corrections are applied (fig. 89(a)), the testing limits for centered models are about the same regardless of the type of boundary used. The use

of variable-model-height operation is contraindicated by the greatly reduced testing limits in this case. Reference to figure 78 indicates that the cause of this restriction is the large effect of the boundaries on $q_c/q$. This particular parameter could be compensated for in some degree by providing the tunnel operator with a precomputed table of approximate compensating velocities as a function of $C_L/A$. The use of such a table would increase the allowable testing range in this mode of operation; however, the procedure would substantially complicate the conduct of the test.

When moderate corrections are employed (fig. 89(b)), the comparison is quite different and depends largely on the degree to which the wings of the model are swept. For unswept wings, the limits are about the same regardless of the wall configuration; however, for highly swept planforms, the completely closed tunnel appears to have a more restricted region of testing than any of the four cases considered. The penalties for variable-model-height operation are relatively small in figure 89(b).

When no corrections are applied, as in figure 89(c), variable-model-height operation is superior provided that the drag-lift ratio is greater than about -0.2. Philosophically, figure 89 indicates that there is little point in trying to reduce corrections if one is willing to accept large corrections. The effort only pays dividends when one is not willing to apply corrections to his data.

Comparisons such as those of figure 89 imply that the design of the tunnel will depend upon the extent to which the data from the tunnel will be corrected. The initial design decision must be a commitment to a selected level of correction.

Another example of the effect of the type of boundary is provided by the Langley full-scale tunnel. Although the tunnel was originally built as a completely open tunnel, it is usually used at present in a closed-on-bottom-only mode for high-lift testing. This mode is obtained by the use of a ground board which was described in an earlier section of this paper. In the course of 40 years of operation, many modifications to the tunnel have been proposed informally. One frequent suggestion has been to close the test section. The effect of such a change is indicated for one span-width ratio in figure 90.

Figure 90 indicates that the testing range of this tunnel could be increased considerably by closing the tunnel provided that the models had small sweep. However, for modern planforms which tend toward $30^{\circ}$ or more wing sweep, there would be little or no gain despite the fact that the present tunnel has about 5 percent less useful area because of the raised location of the ground board.

## Choice of Test-Section Shape

The shape and proportions of the test section must also be chosen early in the design of the tunnel. The present charts of interference and testing limits can also be used to

provide guidance in this regard by comparison between various design alternatives. The comparison cannot be made on the basis of equal span-width ratio models. The required power and the cost of the tunnel will depend largely upon the cross-sectional area of the test section, whereas the models to be tested in the tunnel will remain fixed in span. As the proportions of the tunnel change, the tunnel width for a constant cross-sectional area also changes. Consequently, the span-width ratio for models of constant span will differ in the tunnels of differing proportions or shape. The technique used in comparing different test sections should be the same as that used earlier in comparing the different mounting possibilities of a wing in a given tunnel. (See figs. 82 to 88.) In general, it is simpler to work in dimensional terms rather than in terms of dimensionless ratios.

As an example, consider two different hypothetical test sections: the first has round sidewalls and is 7.5 meters high and 15 meters wide; the second is completely rectangular and is 8 meters high and 12 meters wide. Both tunnels are closed.

The cross-sectional areas of these two test sections are roughly equal; the area of the round-sided tunnel being only about 5 percent greater than that of the rectangular tunnel. Now consider a series of wings having constant spans in the sequence 2, 4, 6, . . . meters. In the 7.5- by 15-meter tunnel the corresponding width-height ratios from the sequence 2/15, 4/15, 6/15, . . . and in the 8- by 12-meter tunnel the corresponding sequence is 1/6, 2/6, 3/6, . . . The appropriate testing limits from figures 72 to 74 may then be traced to form the comparison shown in figures 91 to 93.

The comparison indicates that when the data are corrected (figs. 91 and 92), there is a small advantage in using the 8- by 12-meter configuration, but that there is a significant advantage in using the 7.5- by 15-meter configuration when the spans are large. As indicated by the results of the calculations from reference 31 (figs. 69 and 70), this effect is undoubtedly real despite the rather crude treatment of the nonrectangular tunnels in the present paper. There might be some doubt as to the adequacy of present theoretical treatments of interference in applying corrections to the spanwise distribution except for very low-lift cruising conditions; however, the extension of the technique of reference 31 to a linearized deflected wake would not appear to involve excessive difficulty.

The comparison is altered somewhat if no corrections are applied (fig. 93). In this case, the 8- by 12-meter tunnel is always at an advantage over the 7.5- by 15-meter tunnel. The reason is simply that the use of uncorrected data restricts the allowable test range so severely that it is not feasible to test the very large-span models.

In addition to the normal model mounting arrangements, the test sections should also be considered in regard to semispan arrangements. Such a comparison, which can readily be scaled to these dimensions, has already been made for the 8- by 12-meter section. (See figs. 82 to 84.) The correctly scaled values for the 7.5- by 15-meter tunnel

cannot be obtained without interpolation from the present charts, although figures 85 to 87 provide some rough indication of the relative effects. A few general comments are appropriate.

For semispan tests with the model mounted from the floor, the equivalent full tunnel (real tunnel plus image) will be 15 meters wide for the 7.5- by 15-meter tunnel and 16 meters wide for the 8- by 12-meter tunnel. For large span models, the effect of the difference in width on the width-height ratio should put the 7.5- by 15-meter tunnel at a disadvantage with respect to the 8- by 12-meter tunnel. Furthermore, for small-span models mounted in this manner, the equivalent full tunnel has a width-height ratio of about one and the round ends are at least the equivalent of large fillets. For these small spans, where Rae's limit is of paramount importance, this is about the worst possible configuration (refs. 10 and 25). Thus, the 8- by 12-meter tunnel would be expected to be a significantly better choice for semispan tests of this nature.

It is occasionally desirable for mechanical reasons to mount a semispan model from the tunnel sidewall. There is no inherent difficulty in this procedure in the 8- by 12-meter configuration; however, such tests in the round-sided tunnel present severe problems. Undoubtedly, such tests would require the erection of a false wall located several meters in from the tunnel extremity in order to simulate a reflection plane properly. One effect of such a wall is a substantial reduction in the active width and cross-sectional area of the tunnel. The division of the flow between the separate regions defined by the wall may also present problems in measuring the correct dynamic pressure in the active region of the wind tunnel. Such effects were found in reference 36, and were only eliminated (ref. 10) by extremely long walls and the extensive use of shielded pressure probes within the walls.

Although not discussed specifically herein, the tunnel with round ends also presents obvious problems when used to obtain ground-effect data. If the model has any significant span, it is obvious that the floor of the tunnel is not sufficiently flat to be used to represent the ground. Thus, it will be necessary to erect a false floor above the bottom of the tunnel. As in reflection-plane testing, this false floor reduces the effective area of the tunnel and presents difficulties in the measurement of the effective tunnel velocity. In addition, a circulation about the ground plane itself may be generated (ref. 37) and this circulation may result in the need for still further corrections.

In balancing these various effects, the 8- by 12-meter tunnel would appear to be the more versatile and desirable of the two test sections since the only real advantage accruing to the 7.5- by 15-meter tunnel involves models of extreme span at near-cruising lift coefficients. If the tunnel were to have two test sections, either in tandem or interchangeable, it might be desirable to use both geometric shapes. The round-ended tunnel

would be very suitable as a high-speed section intended primarily for the investigation of high-speed low-lift testing whereas a scaled-up version of the rectangular section could be utilized for low-speed high-lift testing. This type of combination would tend to emphasize the desirable features of both combinations.

## CONCLUDING REMARKS

This investigation has provided in chart form a means for rapidly estimating the magnitude of the boundary interference to be expected in a given wind-tunnel test in tunnels whose test sections are closed or closed only on the bottom. In addition, possible reasons for currently accepted limitations on wind-tunnel testing are indicated. Once plausible maximum values are chosen for the various effects of boundary interference, the charts may be used to define the range of lift and drag for which the wind tunnel may be expected to yield usable results. Such charts of testing limits have been developed herein. It is shown that models with significant wing sweep should be smaller than models with unswept wings. Numerous examples of the application of the present technique to model and tunnel design have been given. The degree to which the data will be corrected has extraordinary effects on testing limits. A decision in this regard should be made prior to the design of either a model or a wind tunnel.

Langley Research Center,
National Aeronautics and Space Administration,
Hampton, Va., July 1, 1971.

## REFERENCES


1. Templin, R. J.: Recent Trends in Low-Speed Wind-Tunnel Design and Techniques. International Congress on Subsonic Aeronautics, Ann. N.Y. Acad. Sci., vol. 154, art. 2, Nov. 22, 1968, pp. 1055-1073.

2. Anscombe, A.; and Williams, J.: Some Comments on High-Lift Testing in Wind Tunnels With Particular Reference to Jet-Blowing Models. Rep. 63, AGARD, North Atlantic Treaty Organization (Paris), Aug. 1956.

3. Garner, H. C.; Rogers, E. W. E.; Acum, W. E. A.; and Maskell, E. C.: Subsonic Wind Tunnel Wall Corrections. AGARDograph 109, 1966.

4. Vayssaire, J. C.: Nouvelle Méthode de Calcul de Correction des Résultats d'Essais en Soufflerie Basse-Vitesse. 1re Partie – Corrections de Blocage et Corrections de Parois. (New Method of Calculating Corrections of Test Results in a Low-Speed Wind Tunnel. 1st Part – Blockage Corrections and Wall Corrections.) L'Aeronautique et l'Astronautique, vol. 15, no. 8, 1969, pp. 55-67.

5. Heyson, Harry H.: Jet-Boundary Corrections for Lifting Rotors Centered in Rectangular Wind Tunnels. NASA TR R-71, 1960.

6. Heyson, Harry H.: Wind-Tunnel Wall Interference and Ground Effect for VTOL-STOL Aircraft. J. Amer. Helicopter Soc., vol. 6, no. 1, Jan. 1961, pp. 1-9.

7. Heyson, Harry H.: Linearized Theory of Wind-Tunnel Jet-Boundary Corrections and Ground Effect for VTOL-STOL Aircraft. NASA TR R-124, 1962.

8. Heyson, Harry H.: Use of Superposition in Digital Computers to Obtain Wind-Tunnel Interference Factors for Arbitrary Configurations, With Particular Reference to V/STOL Models. NASA TR R-302, 1969.

9. Heyson, Harry H.: Nomographic Solution of the Momentum Equation for VTOL-STOL Aircraft. NASA TN D-814, 1961. (Also available as: V/STOL Momentum Equation, Space/Aeronaut., vol. 38, no. 2, July 1962, pp. B-18 – B-20.)

10. Rae, William H., Jr.: Limits on Minimum-Speed V/STOL Wind-Tunnel Tests. J. Aircraft, vol. 4, no. 3, May-June 1967, pp. 249-254.

11. Heyson, Harry H.; and Grunwald, Kalman J.: Wind-Tunnel Boundary Interference for V/STOL Testing. Conference on V/STOL and STOL Aircraft, NASA SP-116, 1966, pp. 409-434.

12. Rae, William H., Jr.; and Shindo, Shojiro: Comments on V/STOL Wind Tunnel Data at Low Forward Speeds. Proceedings Third CAL/AVLABS Symposium, Aerodynamics of Rotary Wing and V/STOL Aircraft, vol. II, June 1969.

13. Lazzeroni, F. A.; and Carr, L. W.: Problems Associated With Wind Tunnel Tests of High Disk Loading Systems at Low Forward Speeds. Proceedings Third CAL/AVLABS Symposium, Aerodynamics of Rotary Wing and V/STOL Aircraft, vol. II, June 1969.

14. Heyson, Harry H.: The Flow Throughout a Wind Tunnel Containing a Rotor With a Sharply Deflected Wake. Proceedings Third CAL/AVLABS Symposium, Aerodynamics of Rotary Wing and V/STOL Aircraft, vol. II, June 1969.

15. Heyson, Harry H.: Theoretical Study of Conditions Limiting V/STOL Testing in Wind Tunnels With Solid Floor. NASA TN D-5819, 1970.

16. Templin, R. J.: The Choice of Working Section Size and Shape for V/STOL Wind Tunnels. Nat. Res. Counc. Can., Quart. Bull., no. 4, 1965, pp. 63-93.

17. Heyson, Harry H.: Tables of Interference Factors for Use in Wind-Tunnel and Ground-Effect Calculations for VTOL-STOL Aircraft. Part III.- Wind Tunnels Having Width-Height Ratio of 1.0. NASA TN D-935, 1962.

18. Heyson, Harry H.: Fortran Programs for Calculating Wind-Tunnel Boundary Interference. NASA TM X-1740, 1969.

19. Heyson, Harry H.: Theoretical Study of The Use of Variable Geometry in The Design of Minimal-Correction V/STOL Wind Tunnels. NASA TR R-318, 1969.

20. McCormick, Barnes W.: The Limiting Circulatory Lift of a Wing of Finite Aspect Ratio. J. Aero/Space Sci., vol. 26, no. 4, Apr., 1959, pp. 247-248.

21. Silverstein, Abe; Katzoff, S.; and Bullivant, W. Kenneth: Downwash and Wake Behind Plain and Flapped Airfoils. NACA Rep. 651, 1939.

22. Heyson, Harry H.; and Katzoff, S.: Induced Velocities Near a Lifting Rotor With Nonuniform Disk Loading. NACA Rep. 1319, 1957. (Supersedes NACA TN 3690 by Heyson and Katzoff and TN 3691 by Heyson.)

23. Margason, Richard J.: Jet-Induced Effects in Transition. Conference on V/STOL and STOL Aircraft. NASA SP-116, 1966, pp. 170-189.

24. Cone, Clarence D.: A Theoretical Investigation of Vortex-Sheet Deformation Behind a Highly Loaded Wing and Its Effect on Lift. NASA TN D-657, 1961.

25. Heyson, Harry H.: Wind-Tunnel Wall Effects at Extreme Force Coefficients. Ann. N.Y. Acad. Sci., vol. 154, art. 2, Nov. 22, 1968, pp. 1074-1093.

26. Grunwald, Kalman J.: Experimental Study of Wind-Tunnel Wall Effects and Wall Corrections for a General-Research V/STOL Tilt-Wing Model With Flap. NASA TN D-2887, 1965.

27. South, P.: Measurements of Flow Breakdown in Rectangular Wind Tunnel Working Sections. NRC-10616, Nat. Res. Counc. Can., Nov. 1968.

28. Heyson, Harry H.: Equations for the Application of Wind-Tunnel Wall Corrections to Pitching Moments Caused by the Tail of an Aircraft Model. NASA TN D-3738, 1966.

29. Heyson, Harry H.: General Theory of Wall Interference for Static Stability Tests in Closed Rectangular Test Sections and in Ground Effect. NASA TR R-364, 1971.

30. Heyson, Harry H.: Approximate Treatment of V/STOL Wall Interference for Closed Circular Tunnels. NASA TN D-6127, 1971.

31. Joppa, Robert G.: A Method of Calculating Wind Tunnel Interference Factors for Tunnels of Arbitrary Cross Section. NASA CR-845, 1967.

32. Hunter, George S.: V/STOL Push Requiring Tunnel Advances. Aviat. Week Space Technol., vol. 89, no. 2, July 8, 1968, pp. 39-51.

33. Joppa, Robert G.: Wall Interference Effects in Wind-Tunnel Testing of STOL Aircraft. J. Aircraft, vol. 6, no. 3, May-June 1969, pp. 209-214.

34. Glauert, H.: The Elements of Aerofoil and Airscrew Theory. Second ed., Cambridge Univ. Press, 1947.

35. Theodorsen, Theodore: The Theory of Wind-Tunnel Wall Interference. NACA Rep. 410, 1931.

36. Ganzer, Victor M.; and Rae, William H., Jr.: An Experimental Investigation of the Effect of Wind Tunnel Walls on the Aerodynamic Performance of a Helicopter Rotor. NASA TN D-415, 1960.

37. Hackett, J. E.; and Justice, J. L.: The Aerodynamics of a Fixed Ground Plane for a Powered STOL Wind-Tunnel Model. AIAA Paper No. 71-266, Mar. 1971.

TABLE I

GUIDE TO BASIC FIGURES GIVING CORRECTIONS

(a) Closed tunnels

| Width-height ratio | Average corrections | Tail corrections | Nonuniformity of corrections | | | |
|---|---|---|---|---|---|---|
| | | | $\Lambda = 0^o$ | $\Lambda = 15^o$ | $\Lambda = 30^o$ | $\Lambda = 45^o$ |
| 3 | 7 | 8 | 9 | --- | --- | 10 |
| 2 | 11 | 12 | 13 | --- | --- | 14 |
| 2* | 15 | 16 | 17 | 18 | 19 | 20 |
| 3/2 | 21, 22** | 23 | 24 | 25 | 26 | 27 |
| 4/3 | 28 | 29 | 30 | --- | --- | 31 |
| 1 | 32 | 33 | 34 | --- | --- | 35 |
| 2/3 | 36 | 37 | 38 | --- | --- | 39 |
| 1/2 | 40 | 41 | 42 | --- | --- | 43 |

*With semicircular sides.

**For a rotor.

(b) Closed-on-bottom-only tunnels

| Width-height ratio | Average corrections | Tail corrections | Nonuniformity of corrections | | | |
|---|---|---|---|---|---|---|
| | | | $\Lambda = 0^o$ | $\Lambda = 15^o$ | $\Lambda = 30^o$ | $\Lambda = 45^o$ |
| 2* | 44 | 45 | 46 | 47 | 48 | 49 |
| 3/2 | 50 | 51 | 52 | 53 | 54 | 55 |

*Langley full-scale tunnel.

(c) Tunnels with variable model height

| Width-height ratio | Operation for zero value of – | Schedule of model height | Average corrections | Tail corrections | Nonuniformity of corrections | |
|---|---|---|---|---|---|---|
| | | | | | $\Lambda = 0^o$ | $\Lambda = 45^o$ |
| 3/2 | $\Delta w_L$ | 56 | 57 | 58 | 59 | 60 |
| 3/2 | $\Delta w$ | 61 | 62 | 63 | 64 | --- |
| 1 and 2 | $\Delta w$ | 65 | 66 | 67 | --- | --- |

TABLE II

TESTING LIMITS FOR "WING-LIKE" MODELS

(a) Maximum practical corrections

| Parameter | Upper limit | Lower limit |
|---|---|---|
| Rae's limit | $x_f/b$ | ----- |
| $\Delta\alpha$, deg | 5 | -5 |
| $q_c/q$ | 1.1 | 0.9 |
| $\Delta i_t$, deg | 5 | -5 |
| $q_t/q_c$ | 1.1 | .9 |
| $\Delta i_w$, deg | 2 | -2 |
| $d(\Delta i_w)/d(y/s)$, deg/semispan | 5 | -5 |
| $\Delta q/q_c$ | .1 | -.1 |

(b) Moderate corrections

| Parameter | Upper limit | Lower limit |
|---|---|---|
| Rae's limit | $x_f/b$ | ----- |
| $\Delta\alpha$, deg | 5 | -5 |
| $q_c/q$ | 1.1 | 0.9 |
| $\Delta i_t$, deg | 2 | -2 |
| $q_t/q_c$ | 1.05 | .95 |
| $\Delta i_w$, deg | 1/2 | -1/2 |
| $d(\Delta i_w)/d(y/s)$, deg/semispan | 1 | -1 |
| $\Delta q/q_c$ | .05 | -.05 |

TABLE II.- Concluded.

TESTING LIMITS FOR "WING-LIKE" MODELS

(c) No corrections

| Parameter | Upper limit | Lower limit |
|---|---|---|
| Rae's limit | $x_f/b$ | ----- |
| $\Delta\alpha$, deg | 1/2 | -1/2 |
| $q_c/q$ | 1.05 | 0.95 |
| $\Delta i_t$, deg | 1/2 | -1/2 |
| $q_t/q_c$ | 1.05 | .95 |
| $\Delta i_w$, deg | 1/2 | -1/2 |
| $d(\Delta i_w)/d(y/s)$, deg/semispan | 1 | -1 |
| $\Delta q/q_c$ | .05 | -.05 |

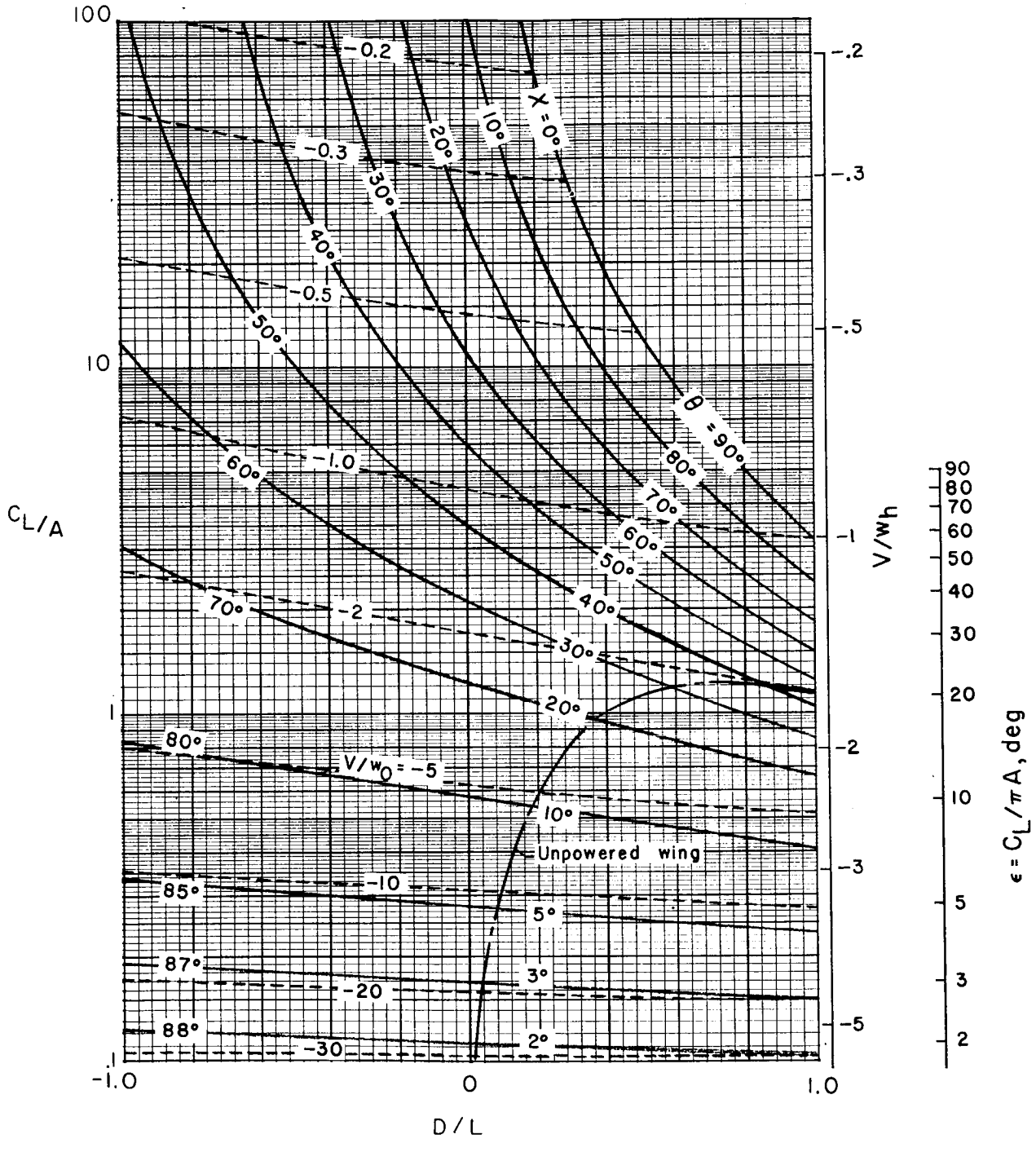


Figure 1.- Ideal performance of a V/STOL aircraft.

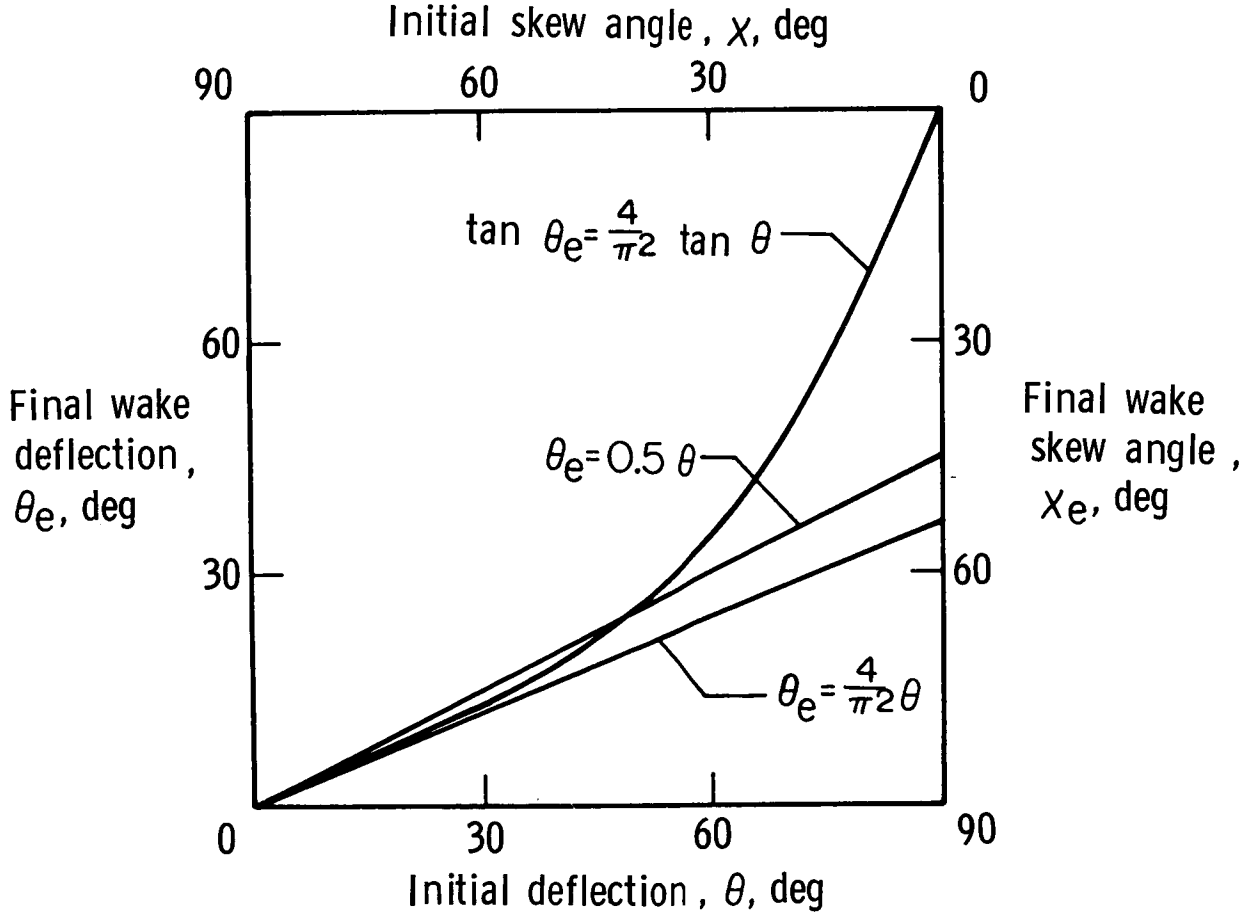


Figure 2.- Effect of wake rollup on final or effective wake inclination.

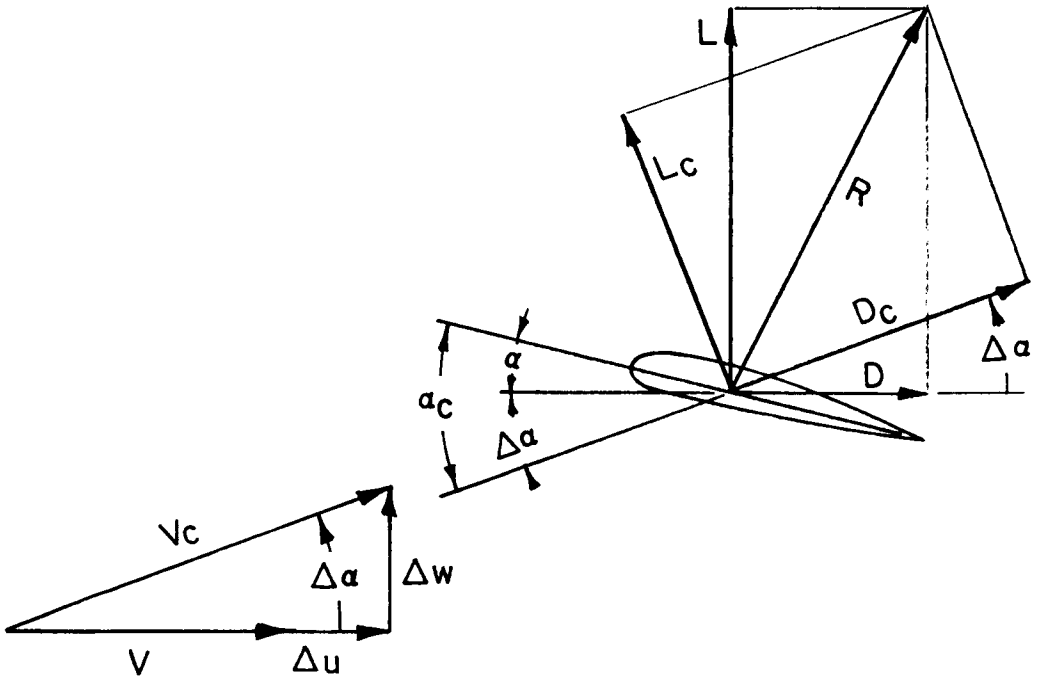


Figure 3.- Correction of lift, drag, and angle of attack.

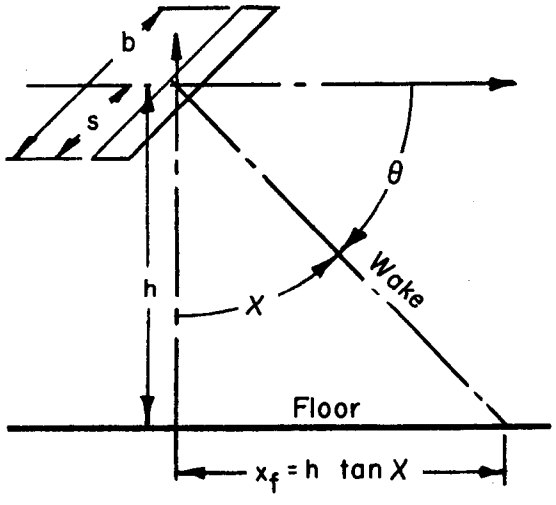


(a) Sketch for calculating $x_f/b$.

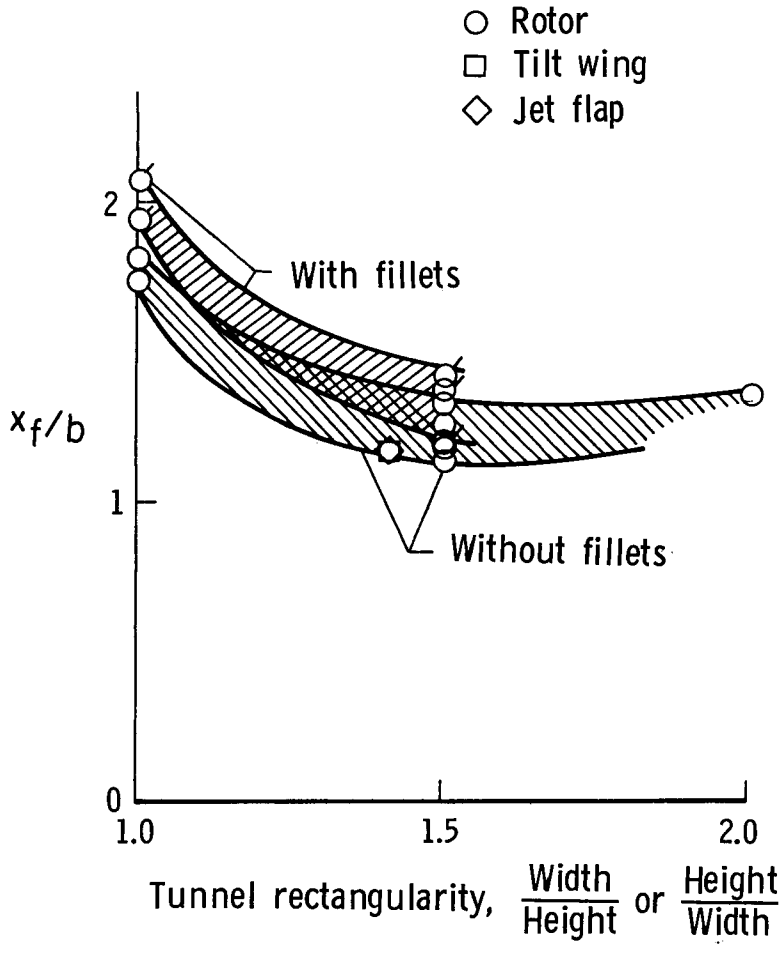


(b) Allowable values of $x_f/b$ based on data of reference 10.

Figure 4.- Rae's limit for flow breakdown in the tunnel as correlated according to wake-impingement distance.

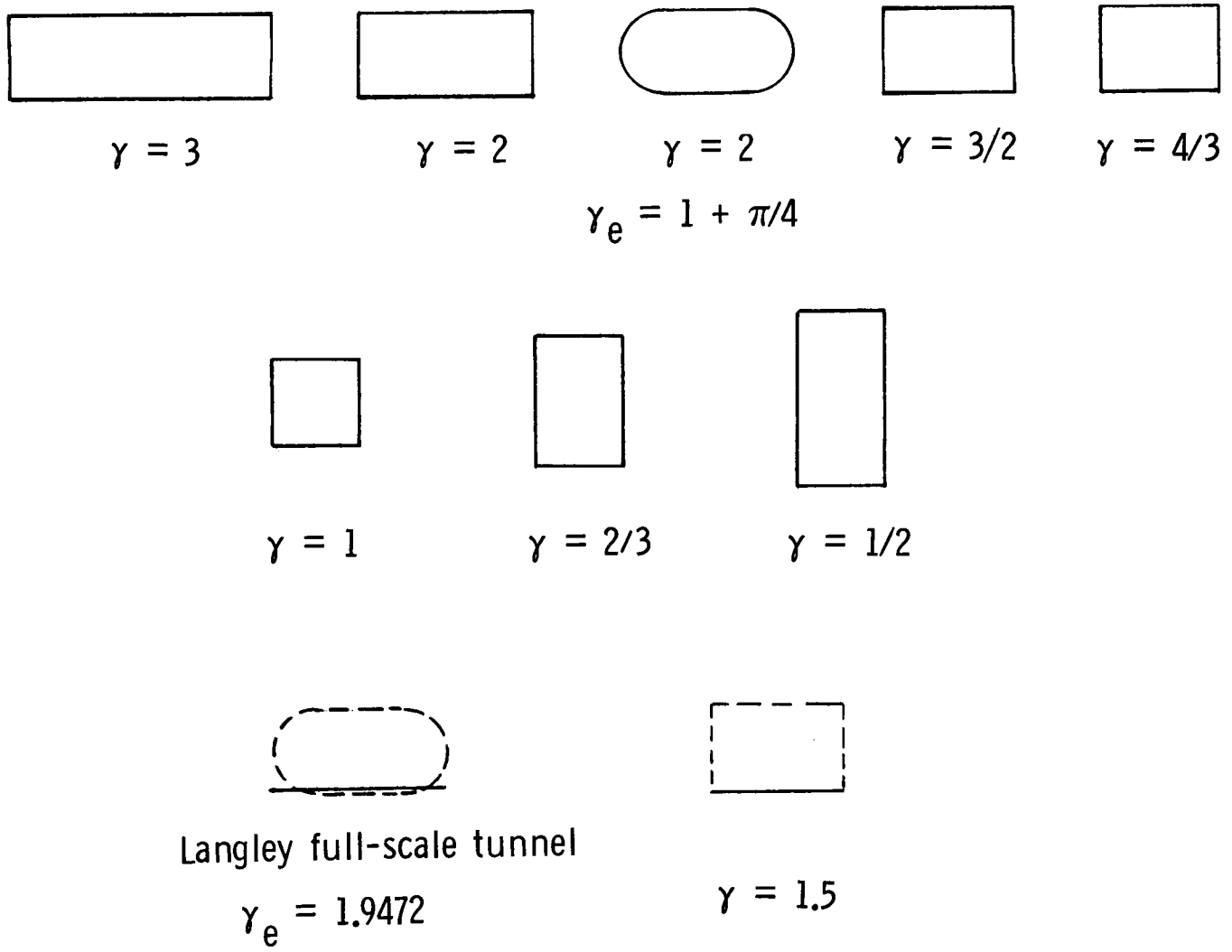


Figure 5.- Basic wind-tunnel configurations considered in this study.

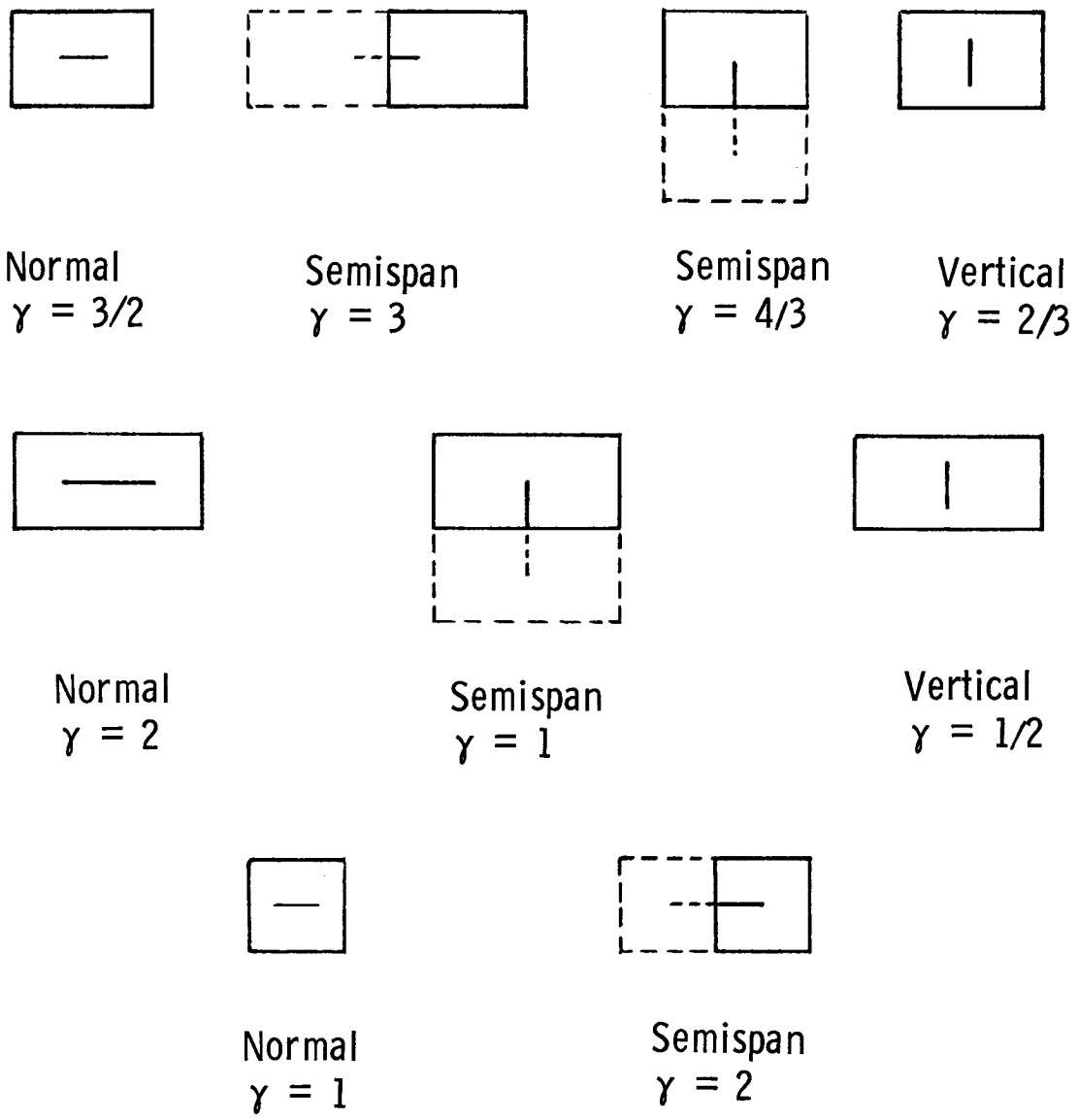


Figure 6.- Effect of model mounting on width-height ratio.

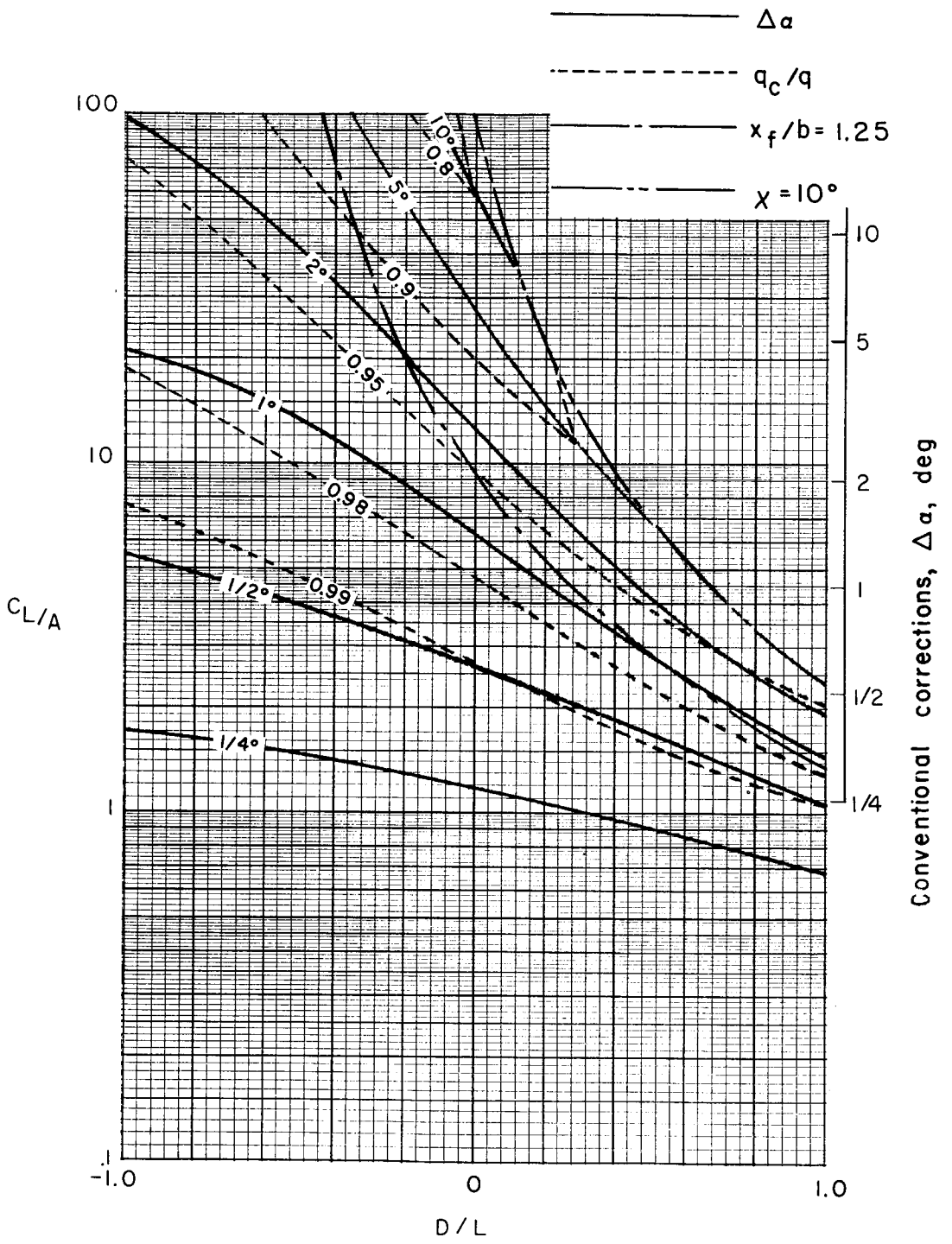


(a) σ = 1/12.

Figure 7.- Average corrections for a uniformly loaded wing centered in a closed rectangular tunnel. γ = 3.0; Λ = 0°.

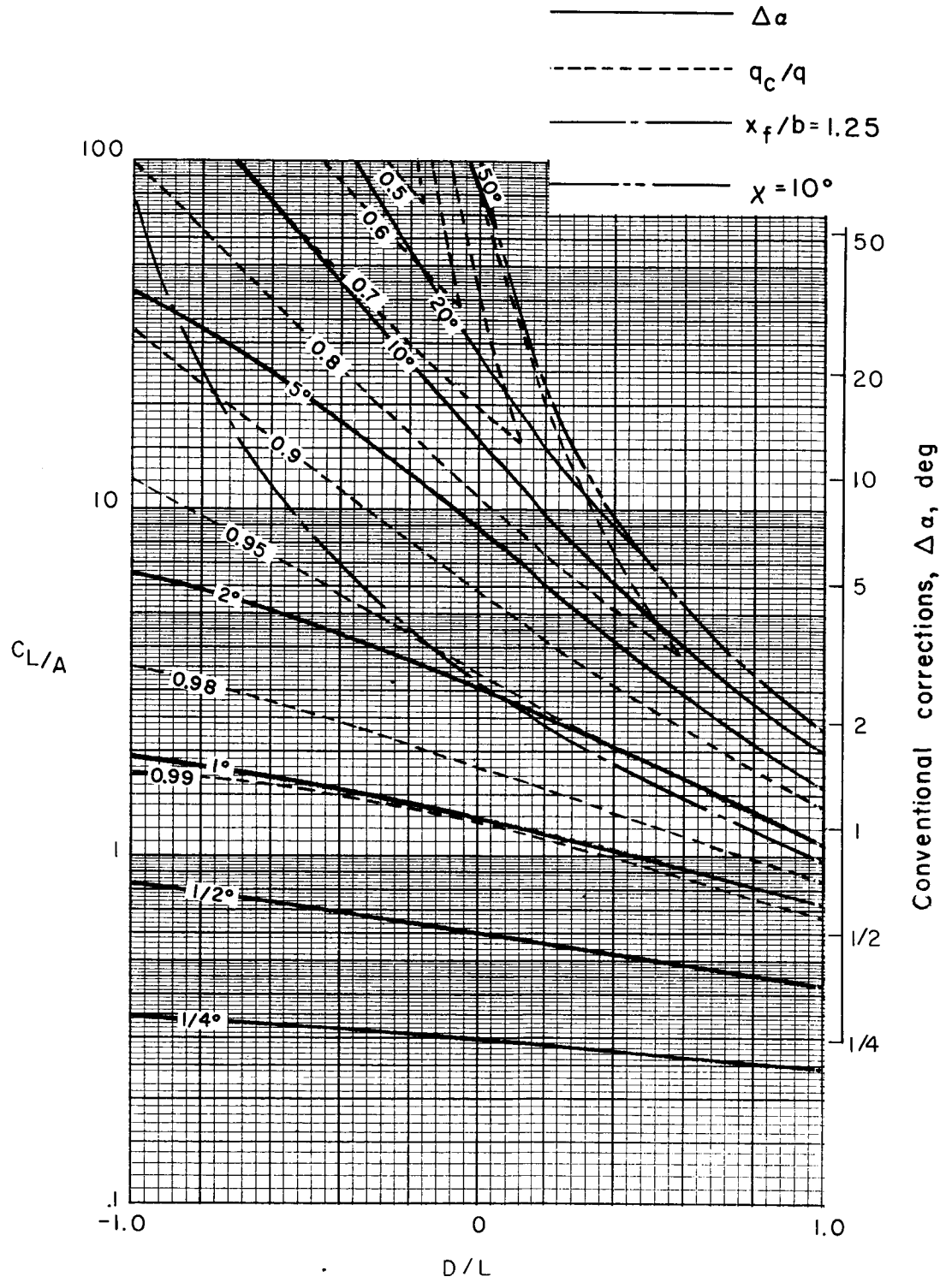


(b) $\sigma = 1/6$.

Figure 7.- Continued.

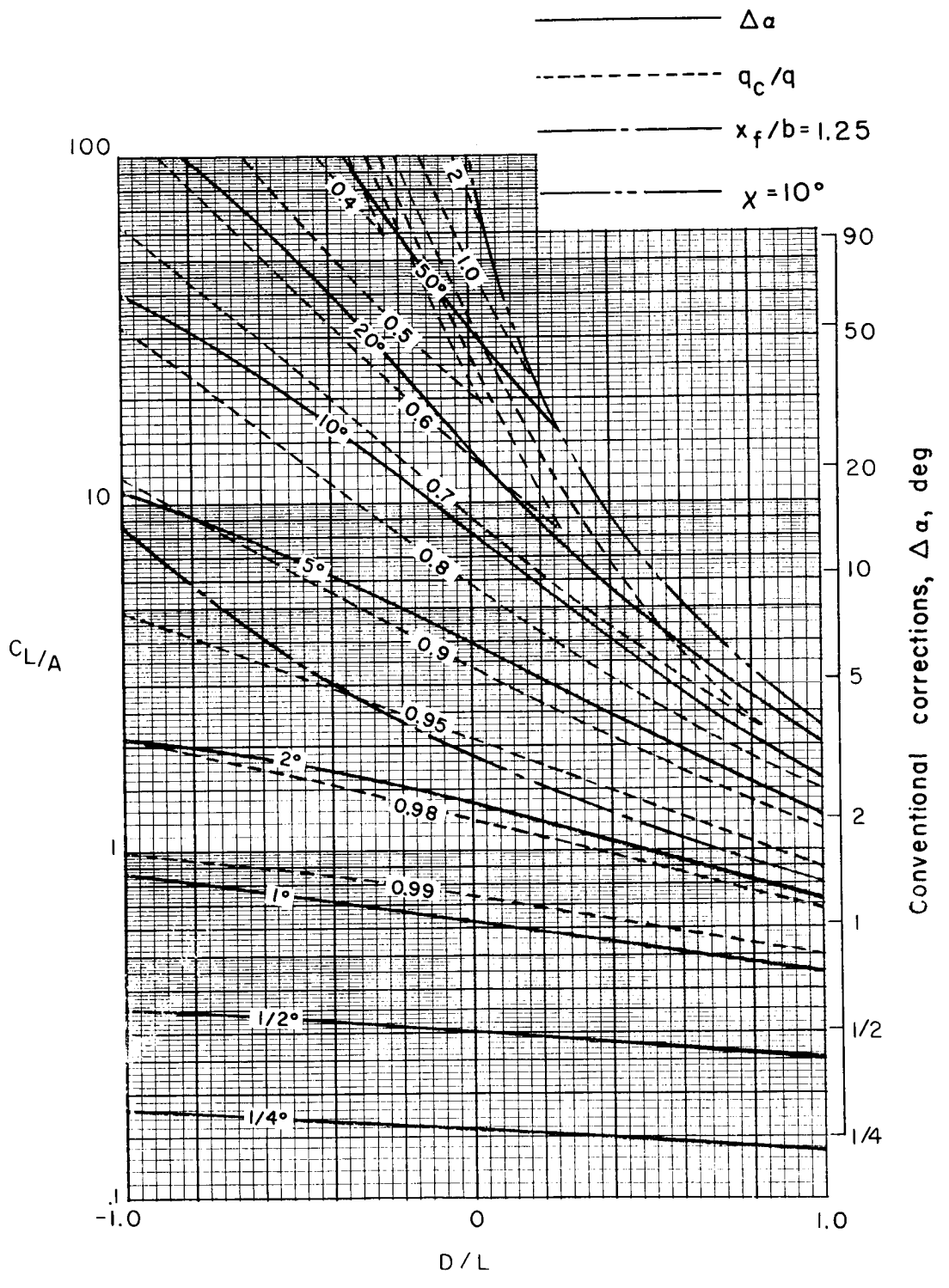


(c) σ = 1/4.

Figure 7.- Continued.

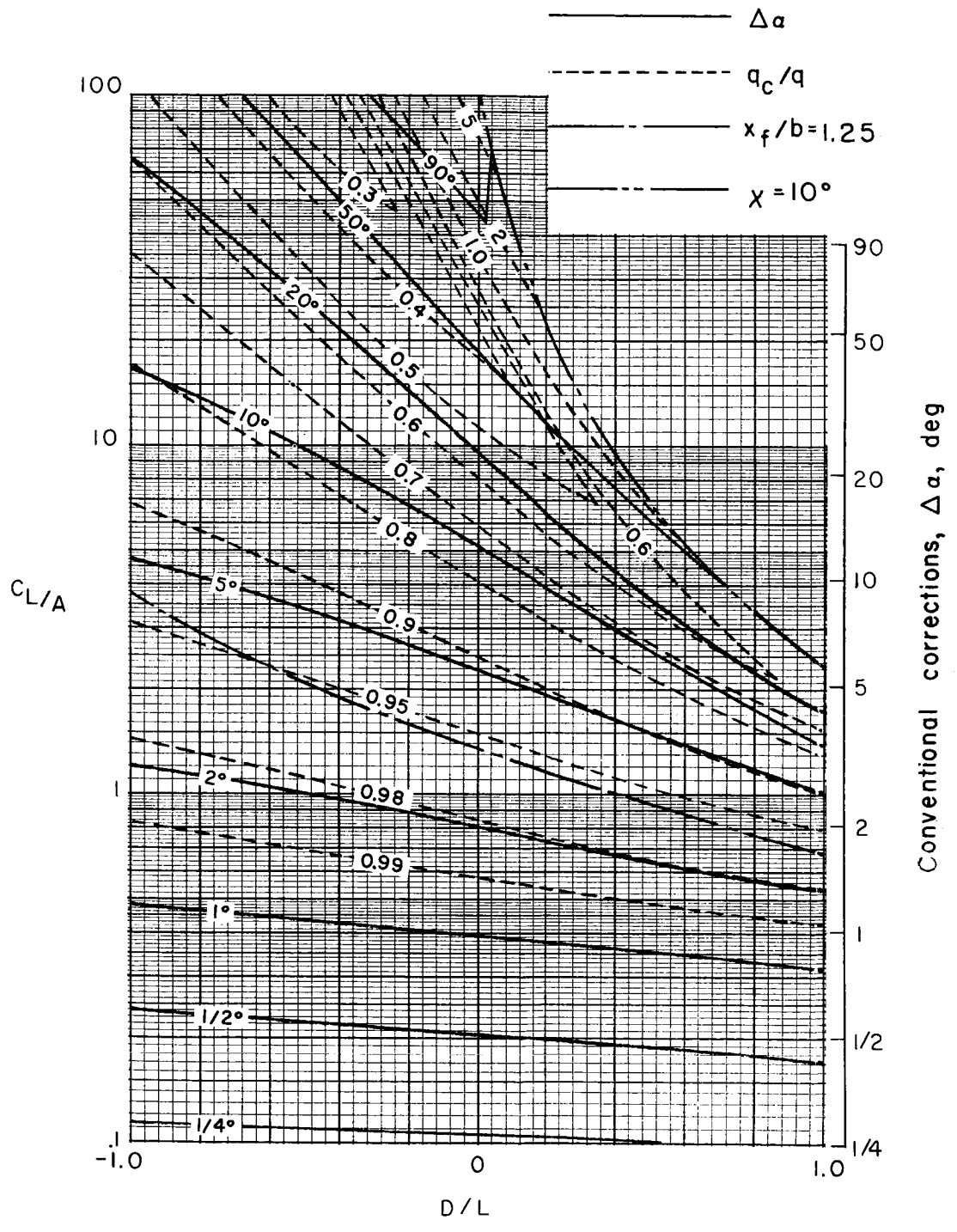


(d) $\sigma = 1/3$.

Figure 7.- Continued.

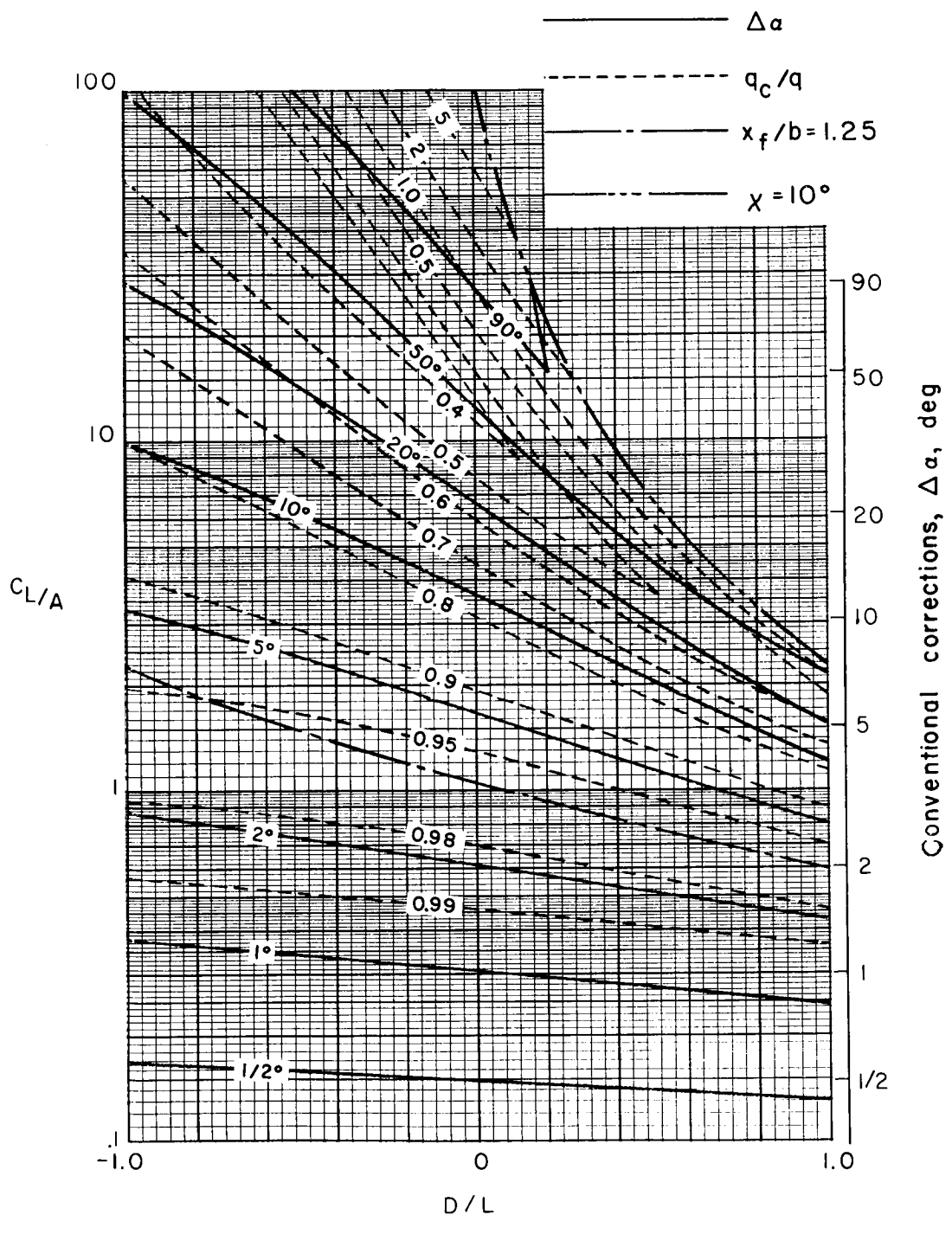


(e) σ = 5/12.

Figure 7.- Continued.

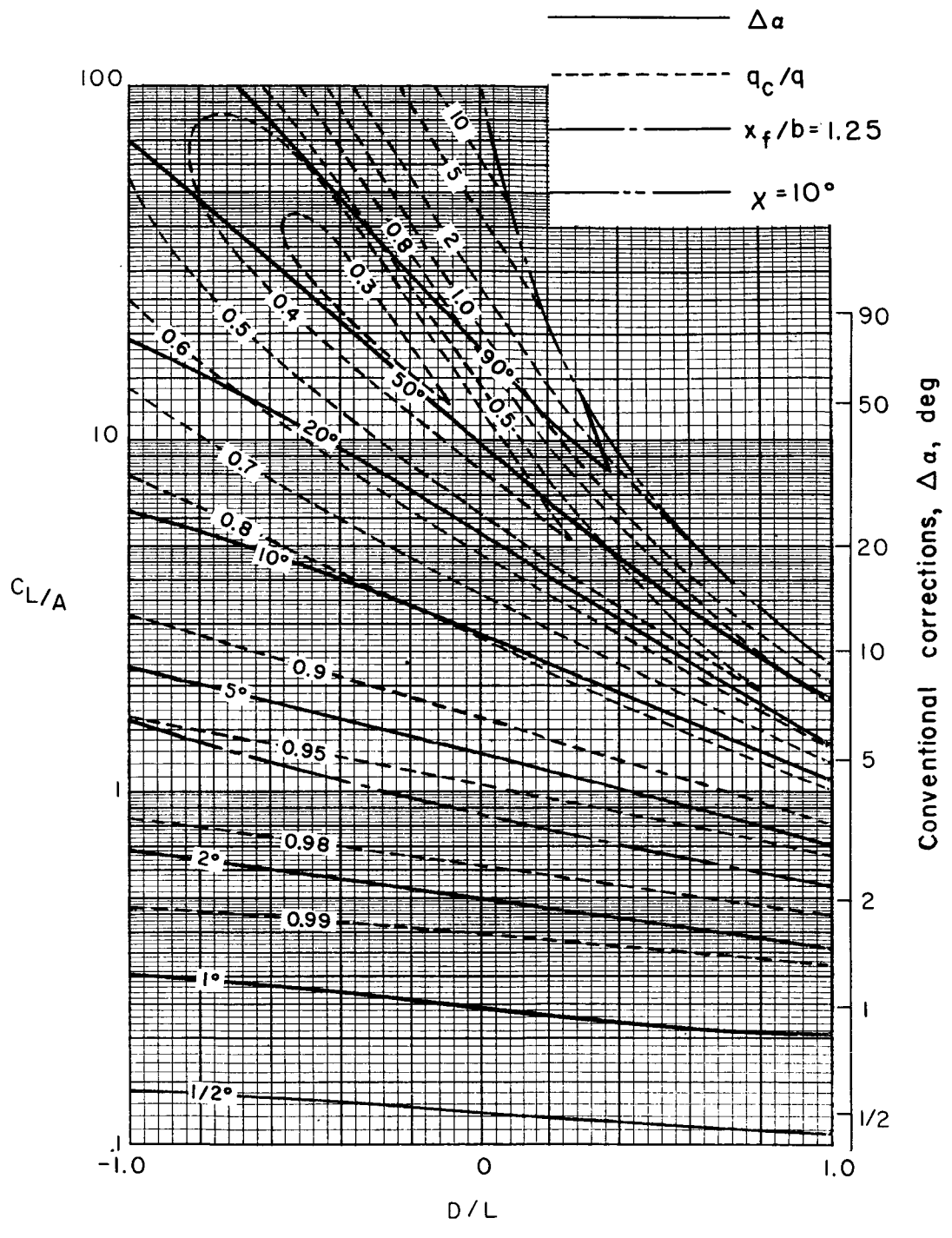


(f) σ = 1/2.

Figure 7.- Concluded.

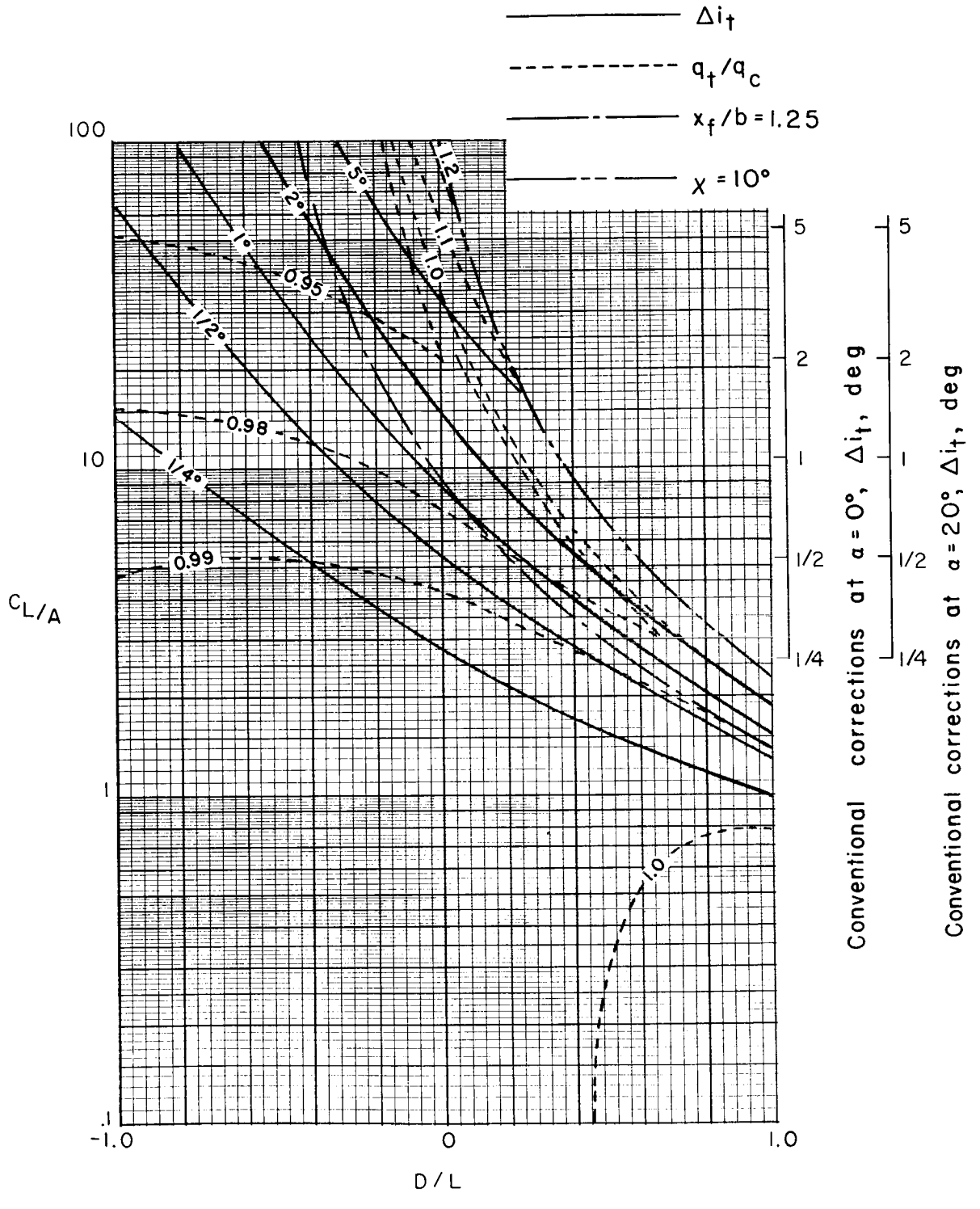


(a) $\sigma = 1/12$.

Figure 8.- Corrections at a zero-span tail behind a uniformly loaded wing centered in a closed rectangular tunnel. Tail length is three-fourths of wing span; tail height is zero; $\alpha = 20^0$; $\Lambda = 0^0$; $\gamma = 3$.

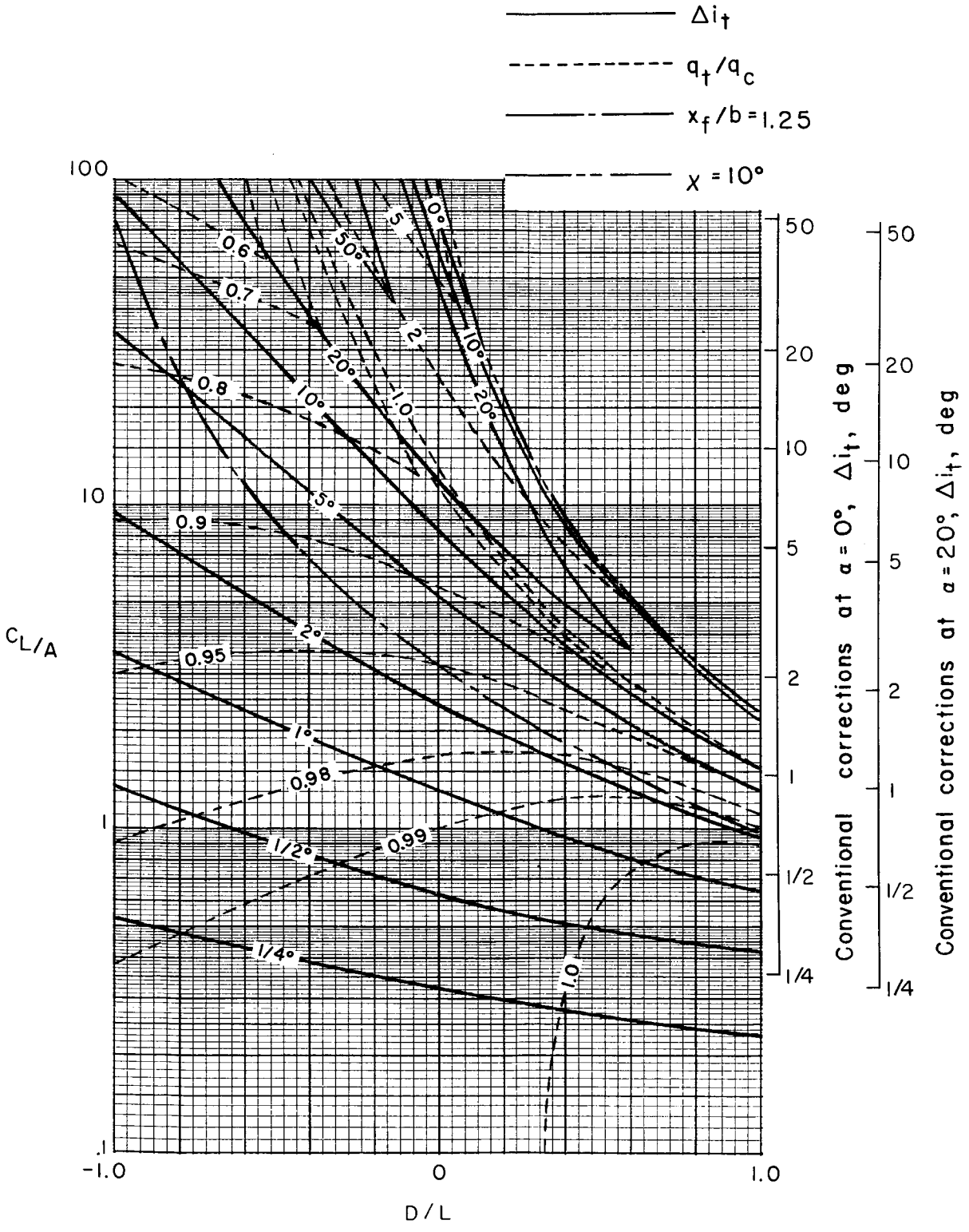


(b) $\sigma = 1/6$.

Figure 8.- Continued.

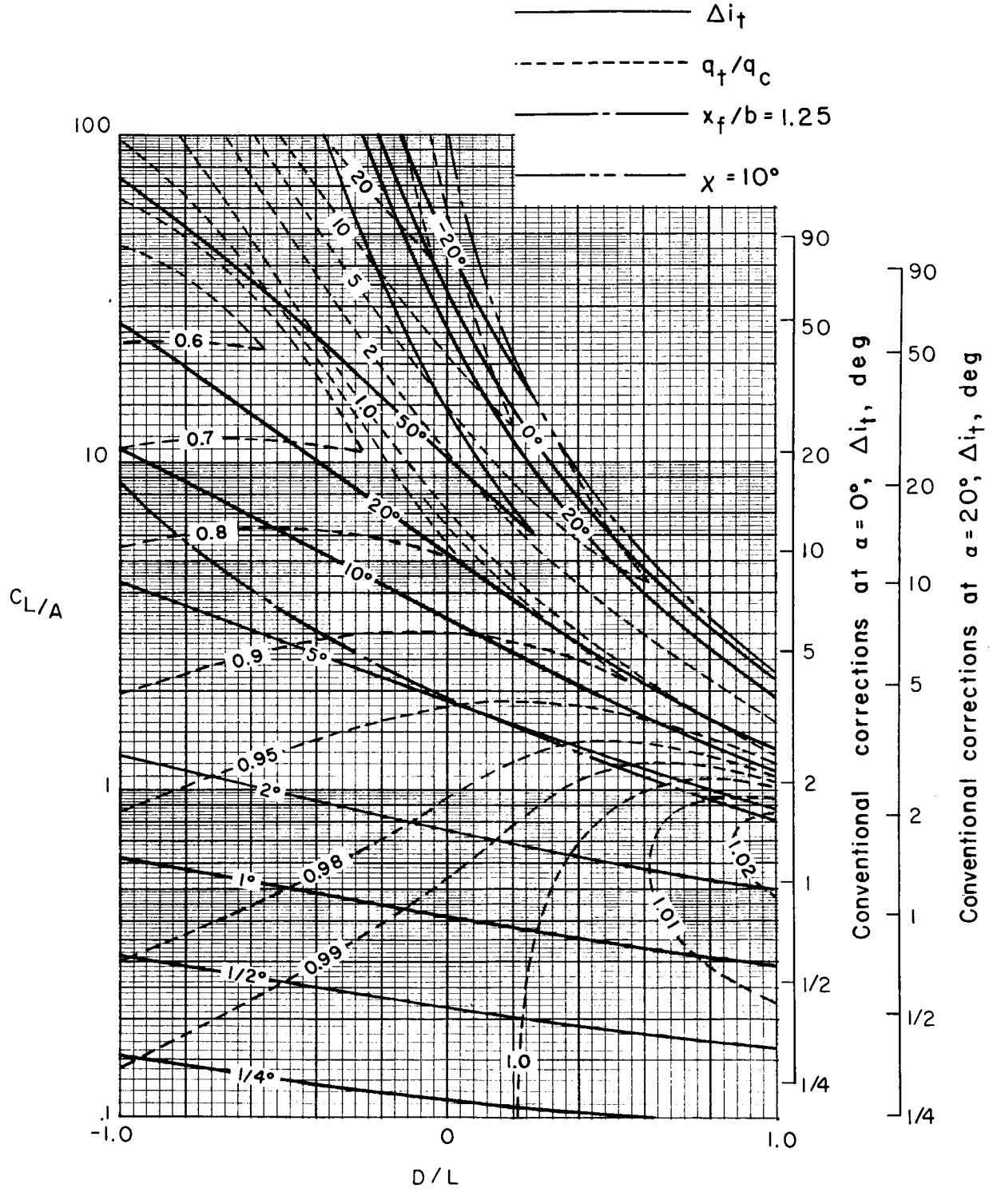


(c) $\sigma = 1/4$.

Figure 8.- Continued.

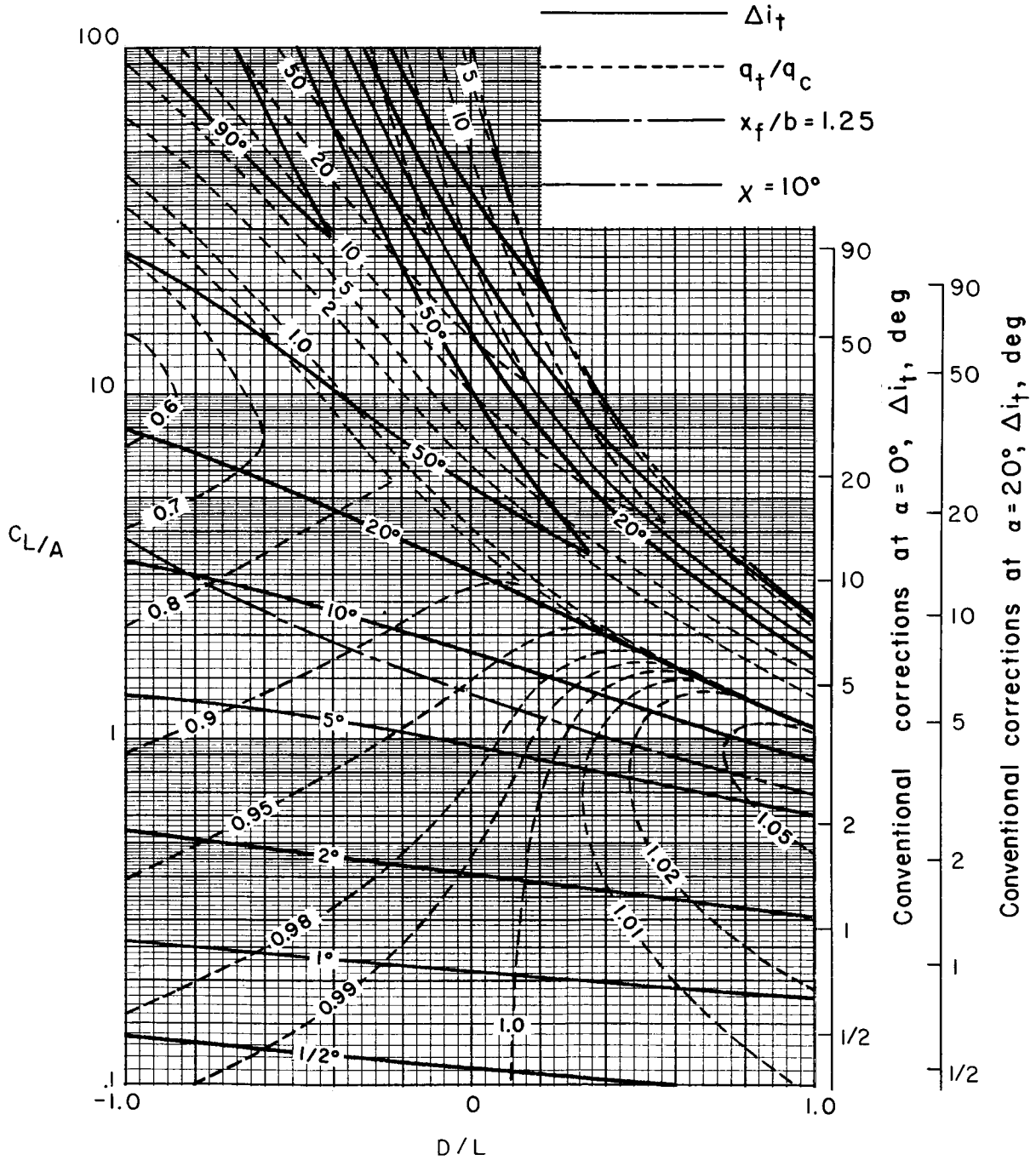


(d) $\sigma = 1/3$.

Figure 8.- Continued.

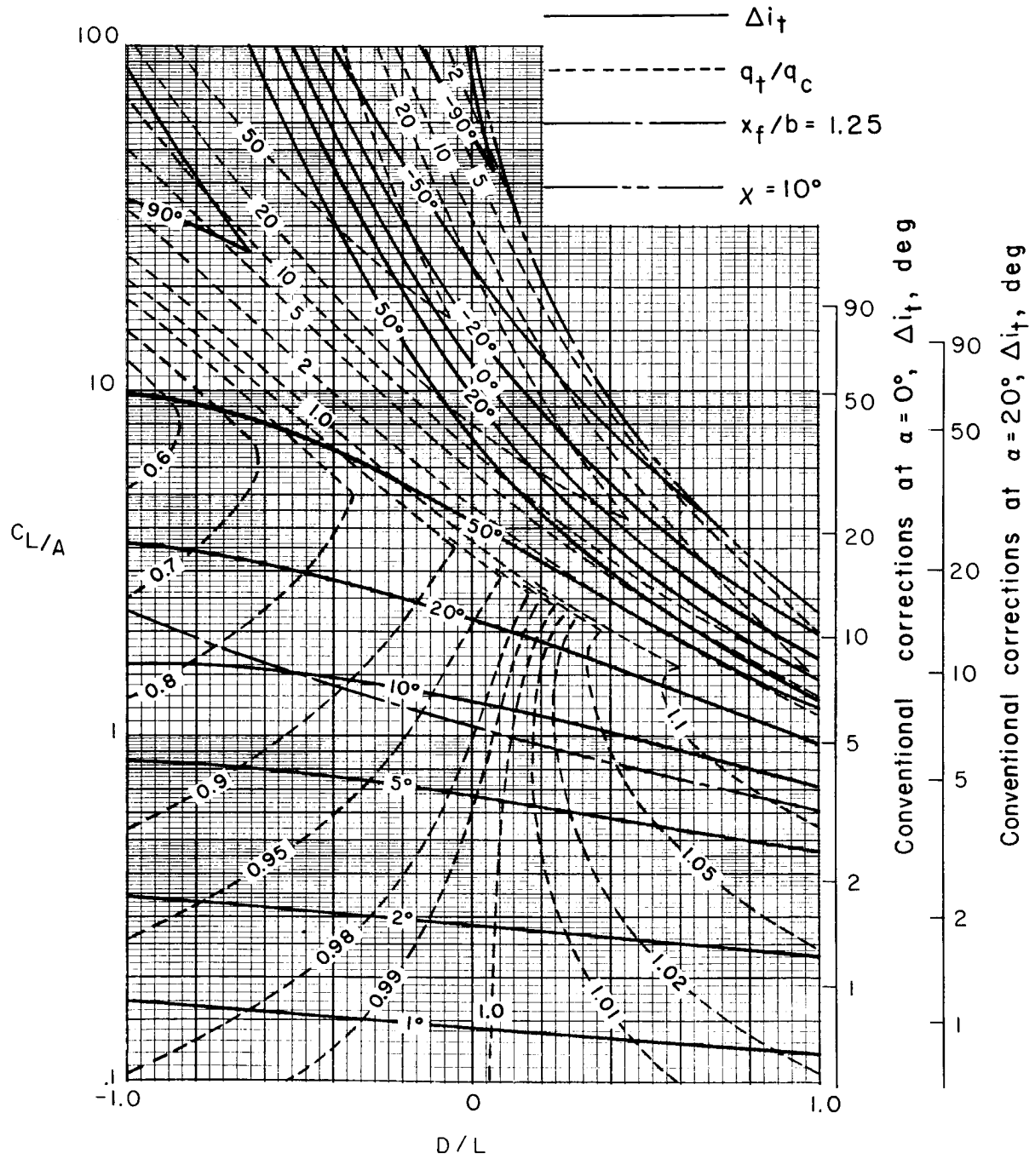


(e) σ = 5/12.

Figure 8.- Continued.

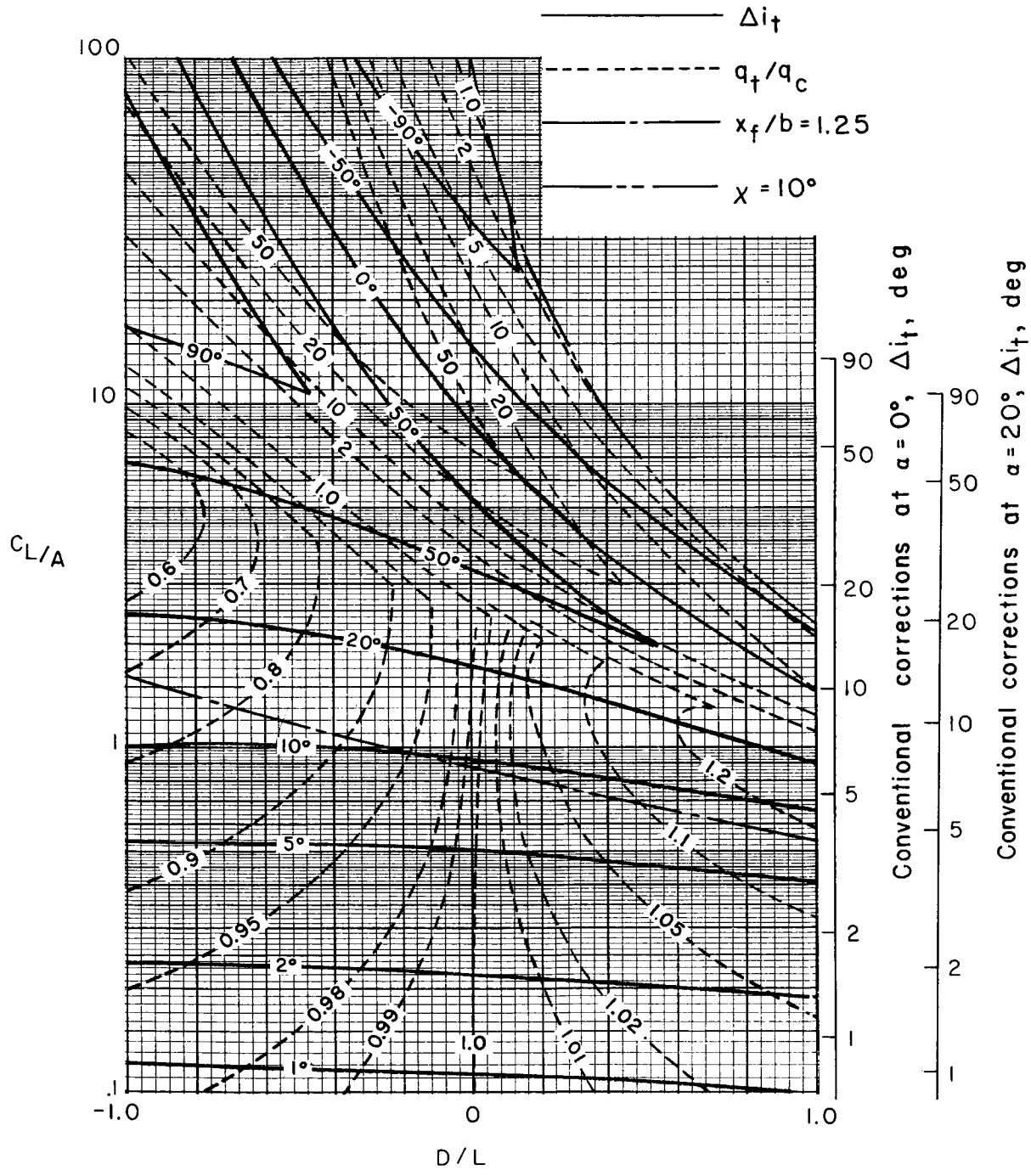


(f) $\sigma = 1/2$.

Figure 8.- Concluded.

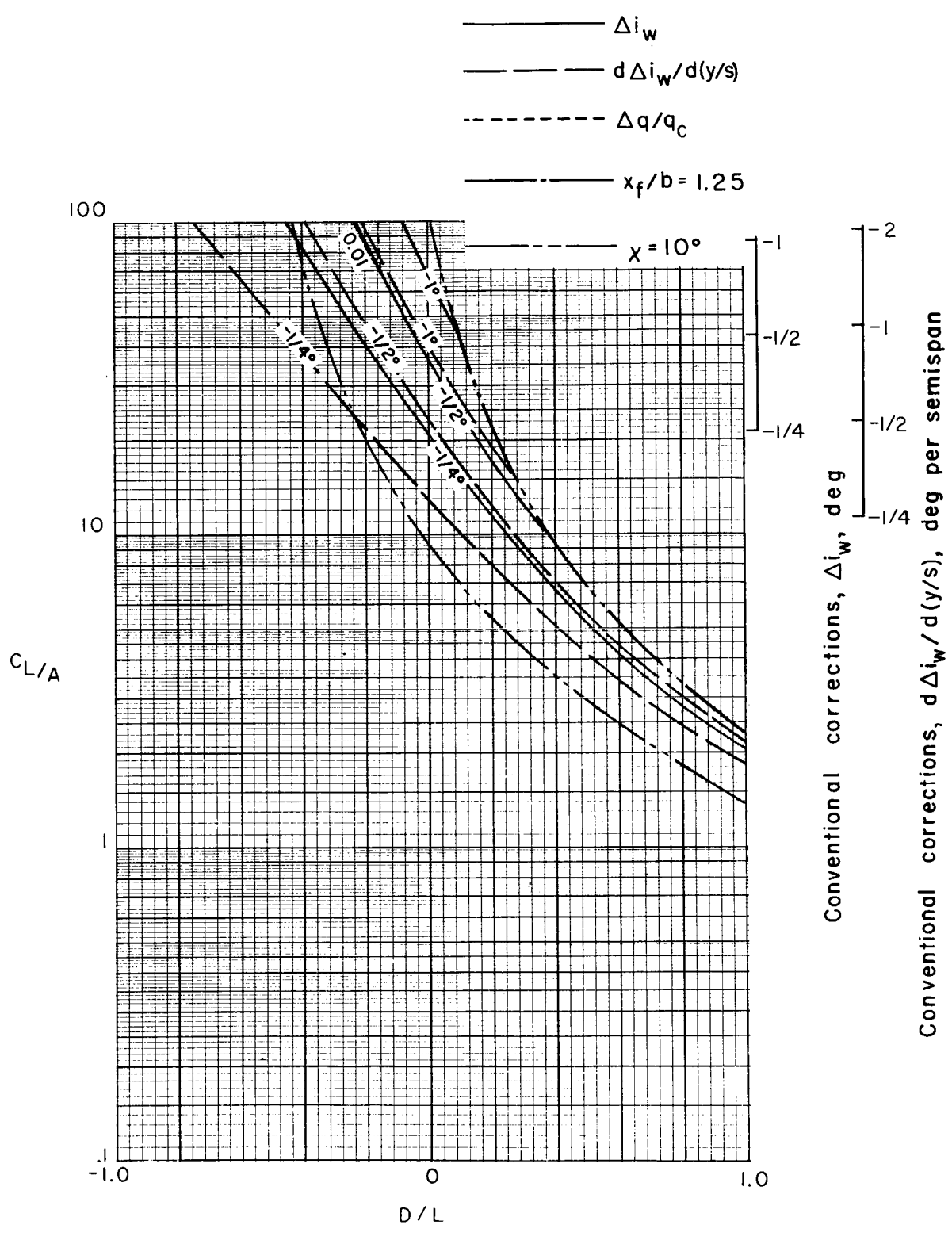


(a) $\sigma = 1/12$.

Figure 9.- Nonuniformity of corrections over a uniformly loaded wing centered in a closed rectangular tunnel. $\gamma = 3.0$; $\alpha = 0^0$; $\Lambda = 0^0$.

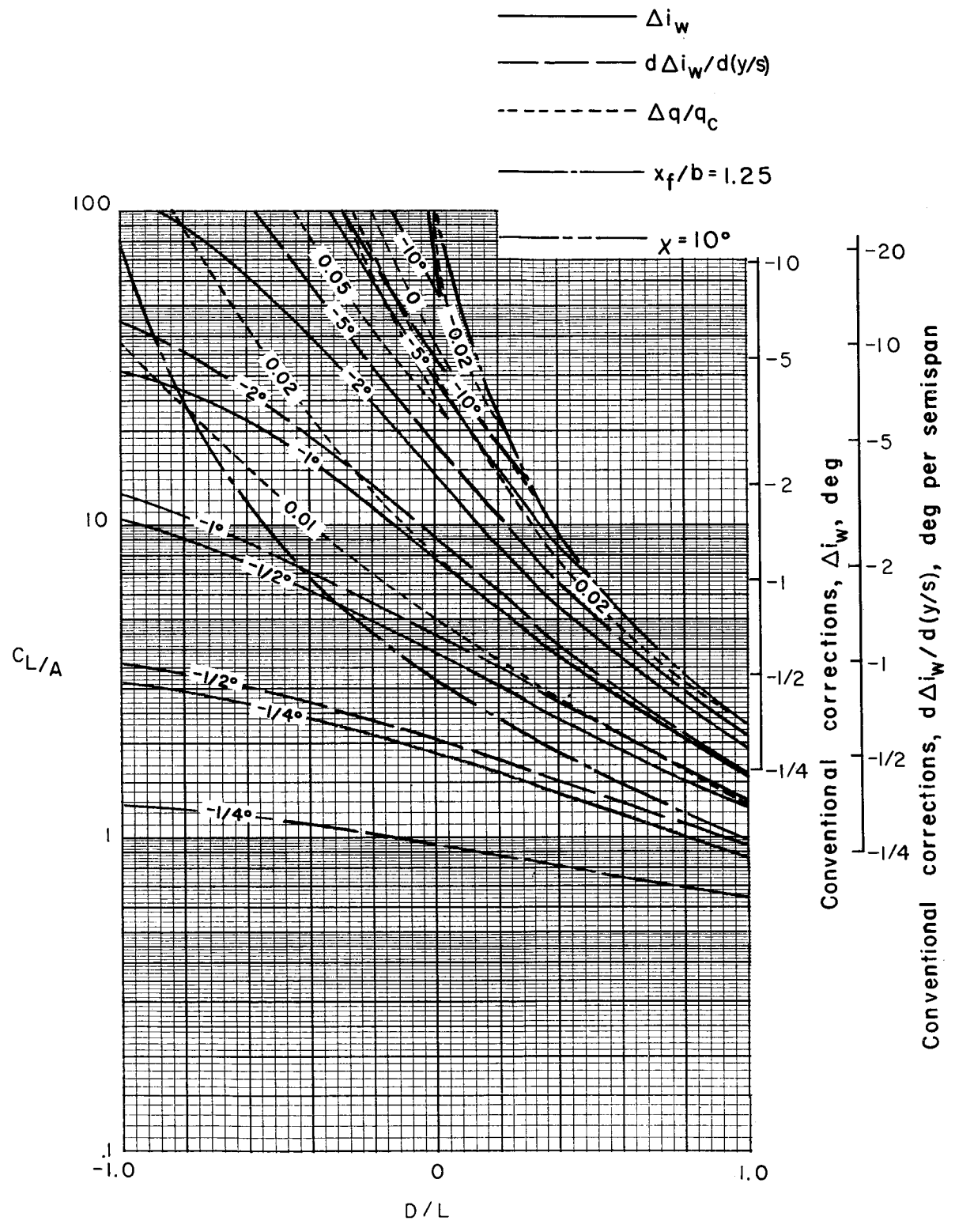


(b) $\sigma = 1/6$.

Figure 9.- Continued.

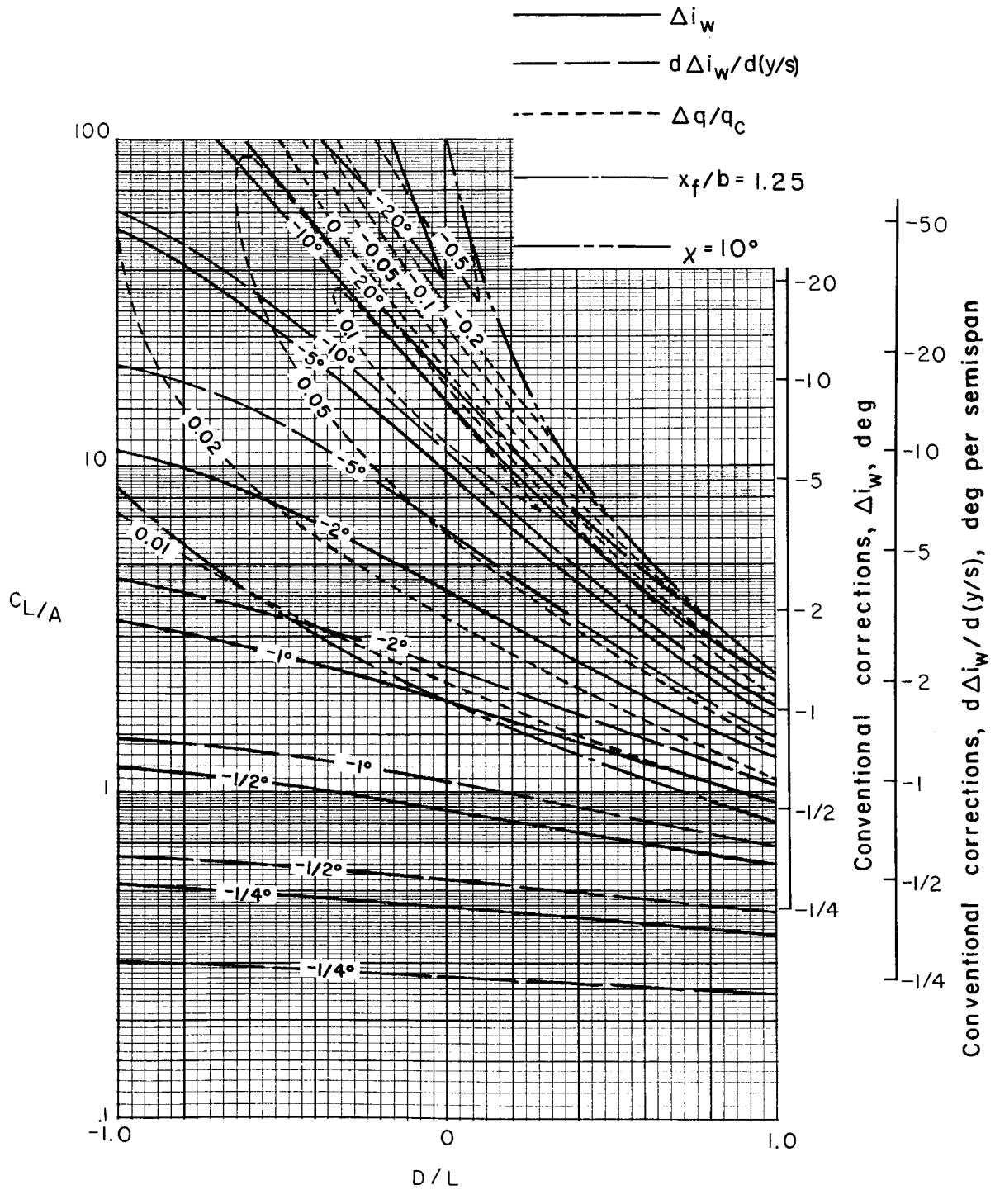


(c) $\sigma = 1/4$.

Figure 9.- Continued.

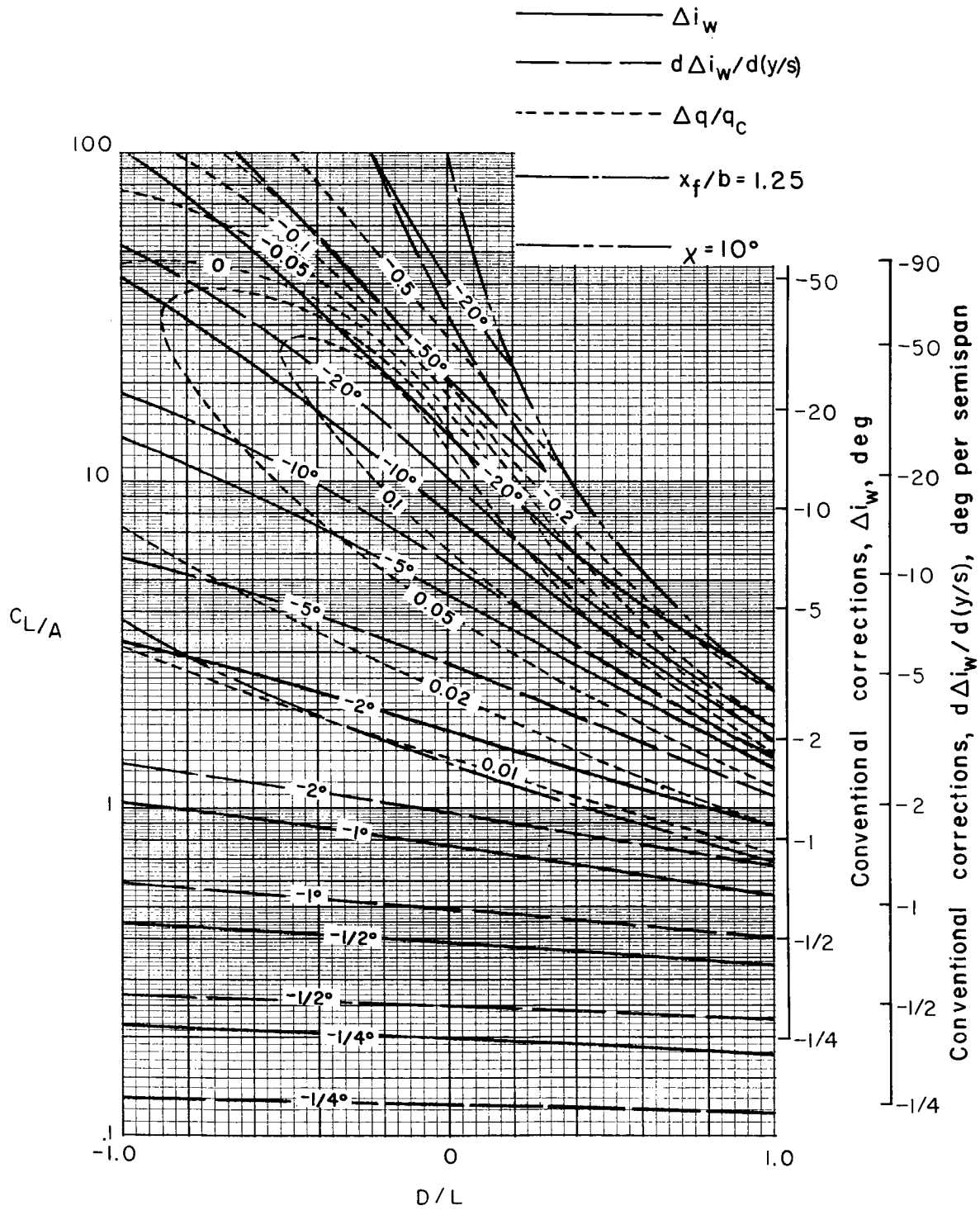


(d) $\sigma = 1/3$.

Figure 9.- Continued.

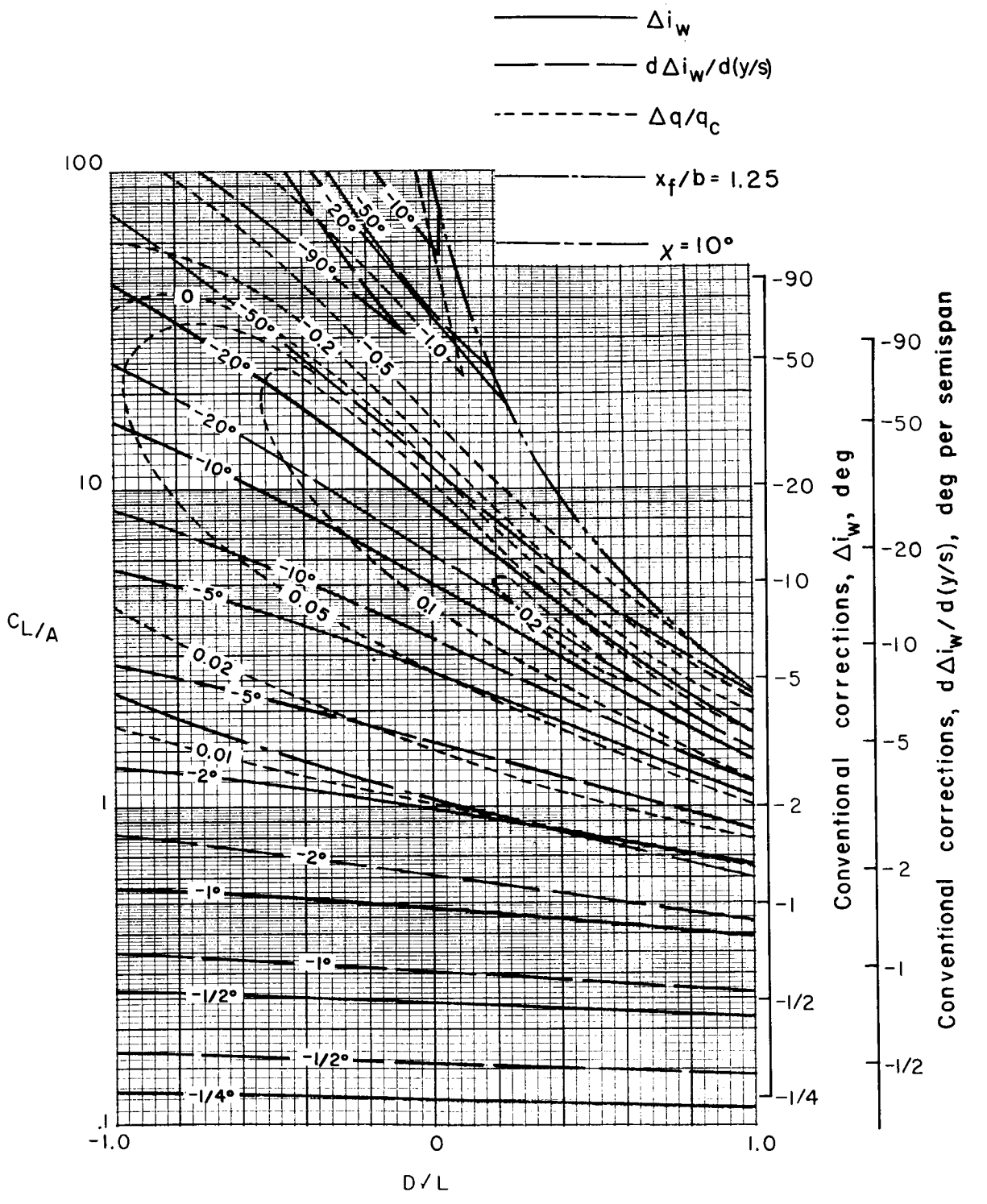


(e) $\sigma = 5/12$.

Figure 9.- Continued.

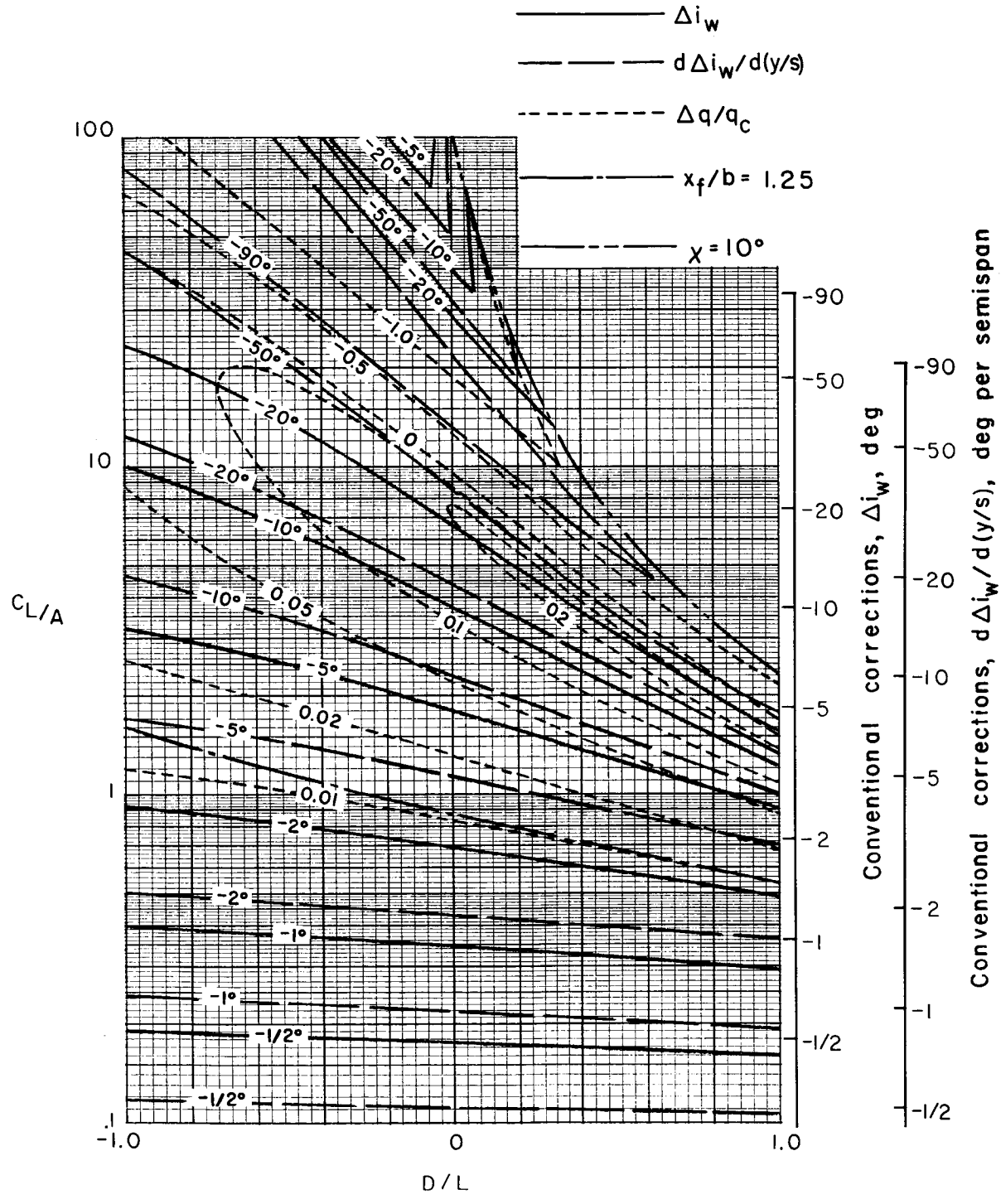


(f) $\sigma = 1/2$.

Figure 9.- Concluded.

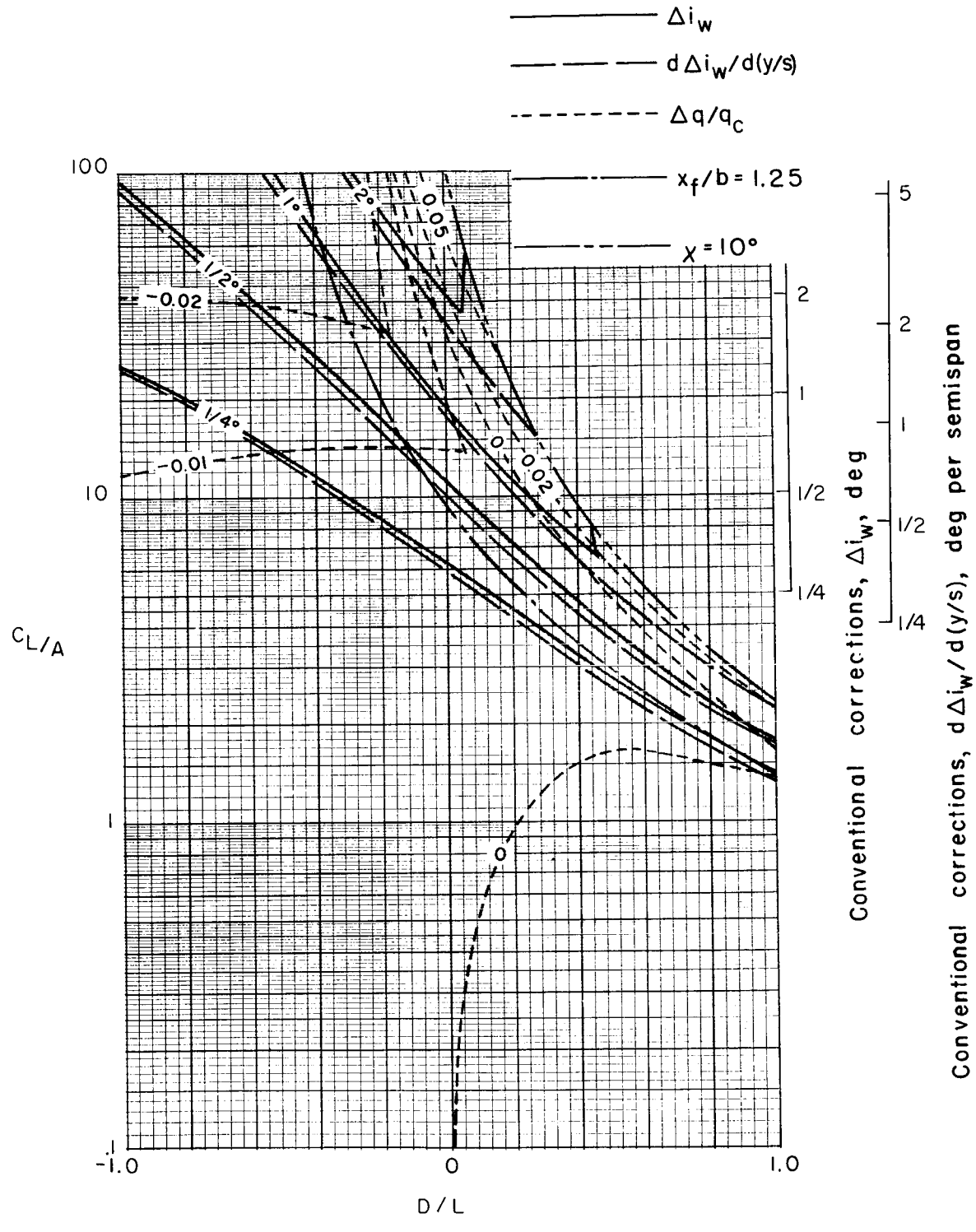


(a) $\sigma = 1/12$.

Figure 10.- Nonuniformity of corrections over a uniformly loaded wing centered in a closed rectangular tunnel. $\gamma = 3.0$; $\alpha = 0^0$; $\Lambda = 45^0$.

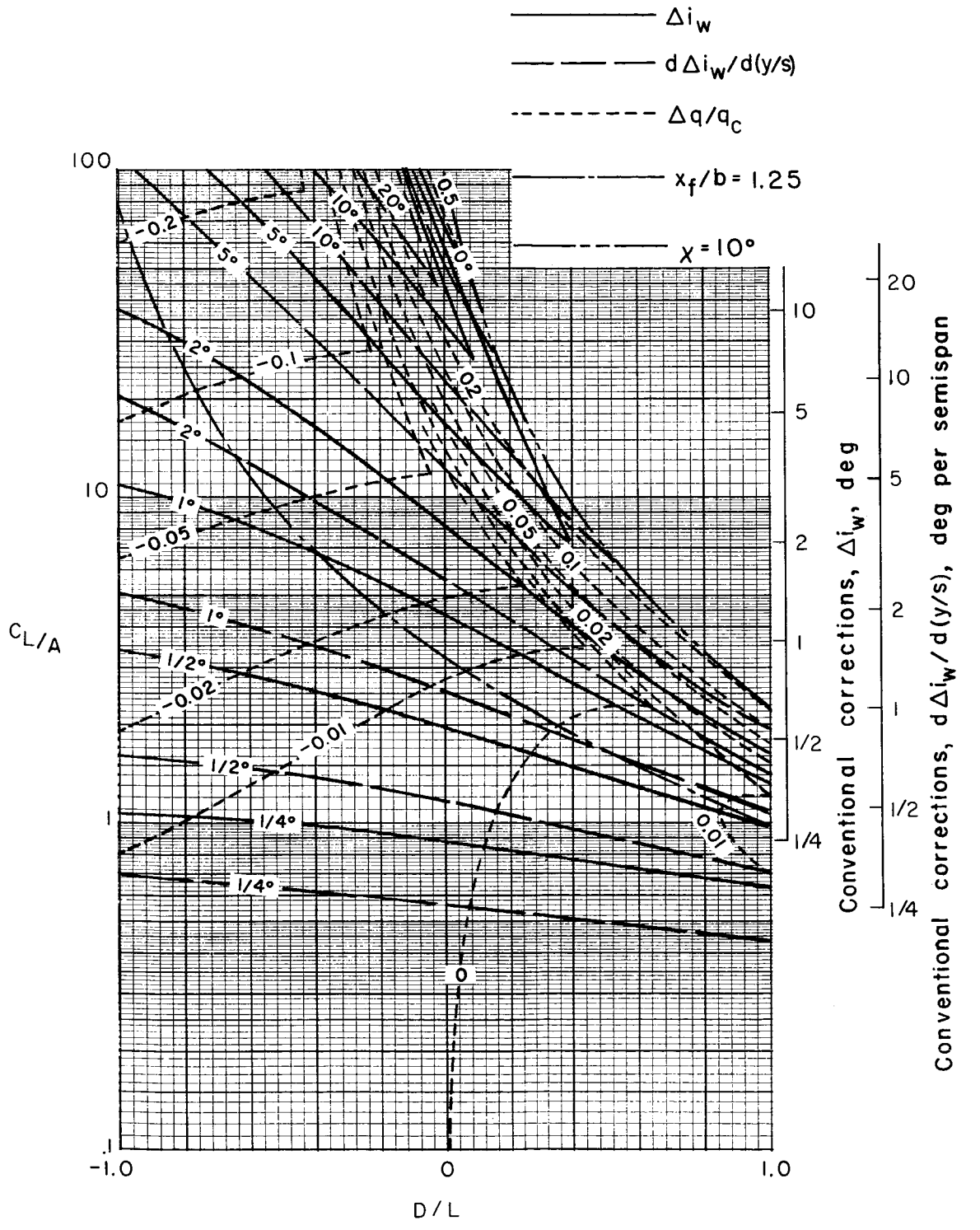


(b) $\sigma = 1/6$.

Figure 10.- Continued.

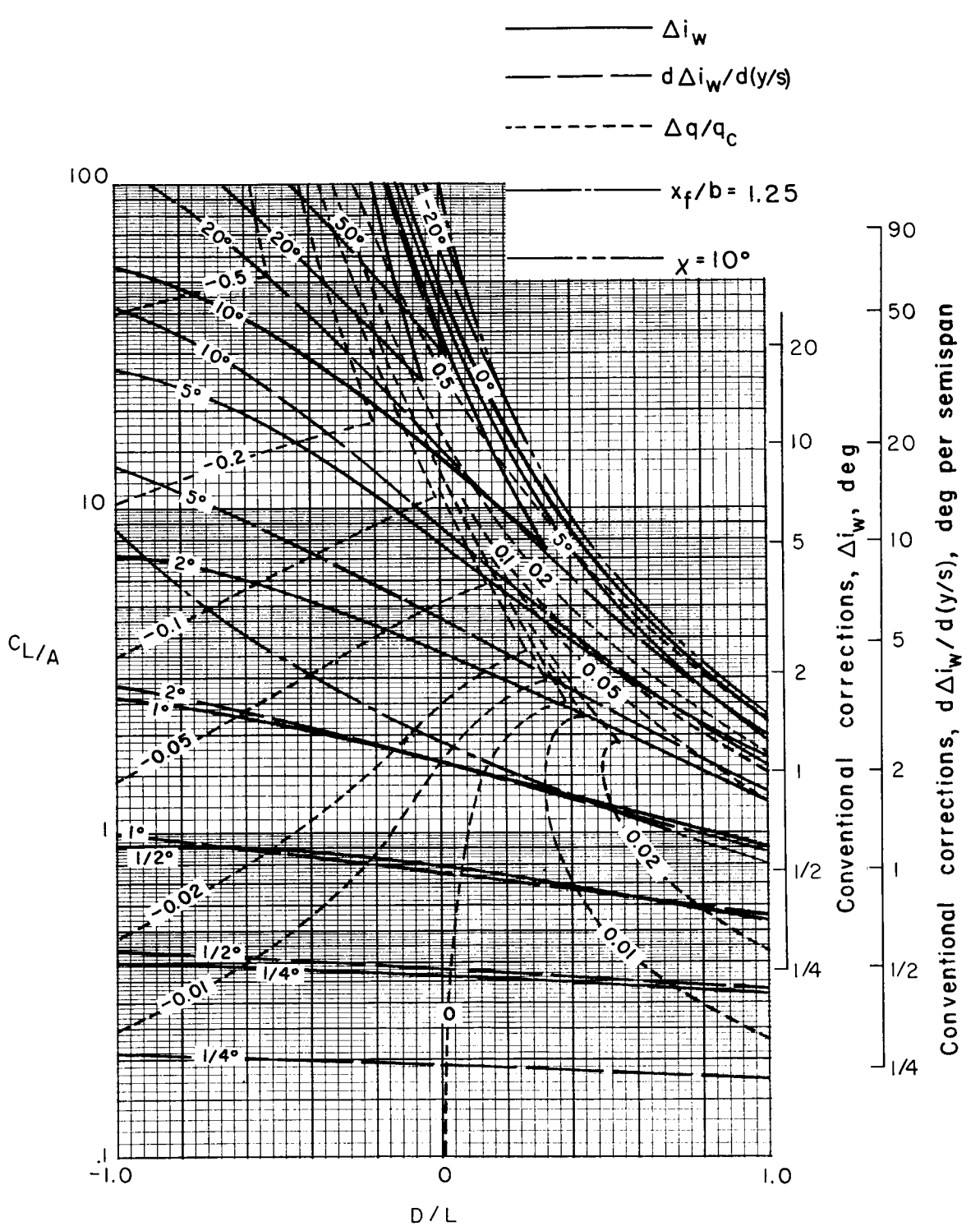


(c) $\sigma = 1/4$.

Figure 10.- Continued.

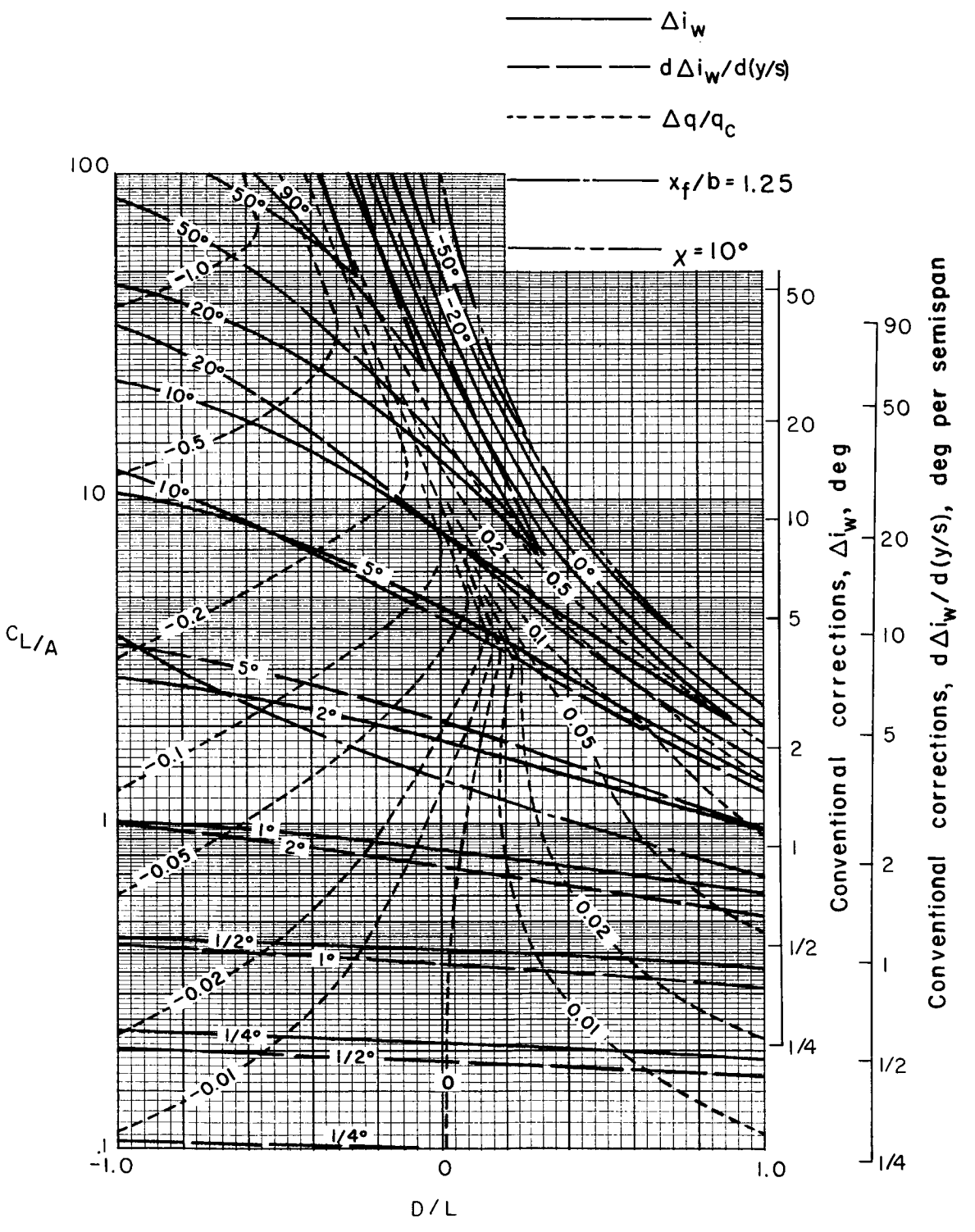


(d) $\sigma = 1/3$.

Figure 10.- Continued.

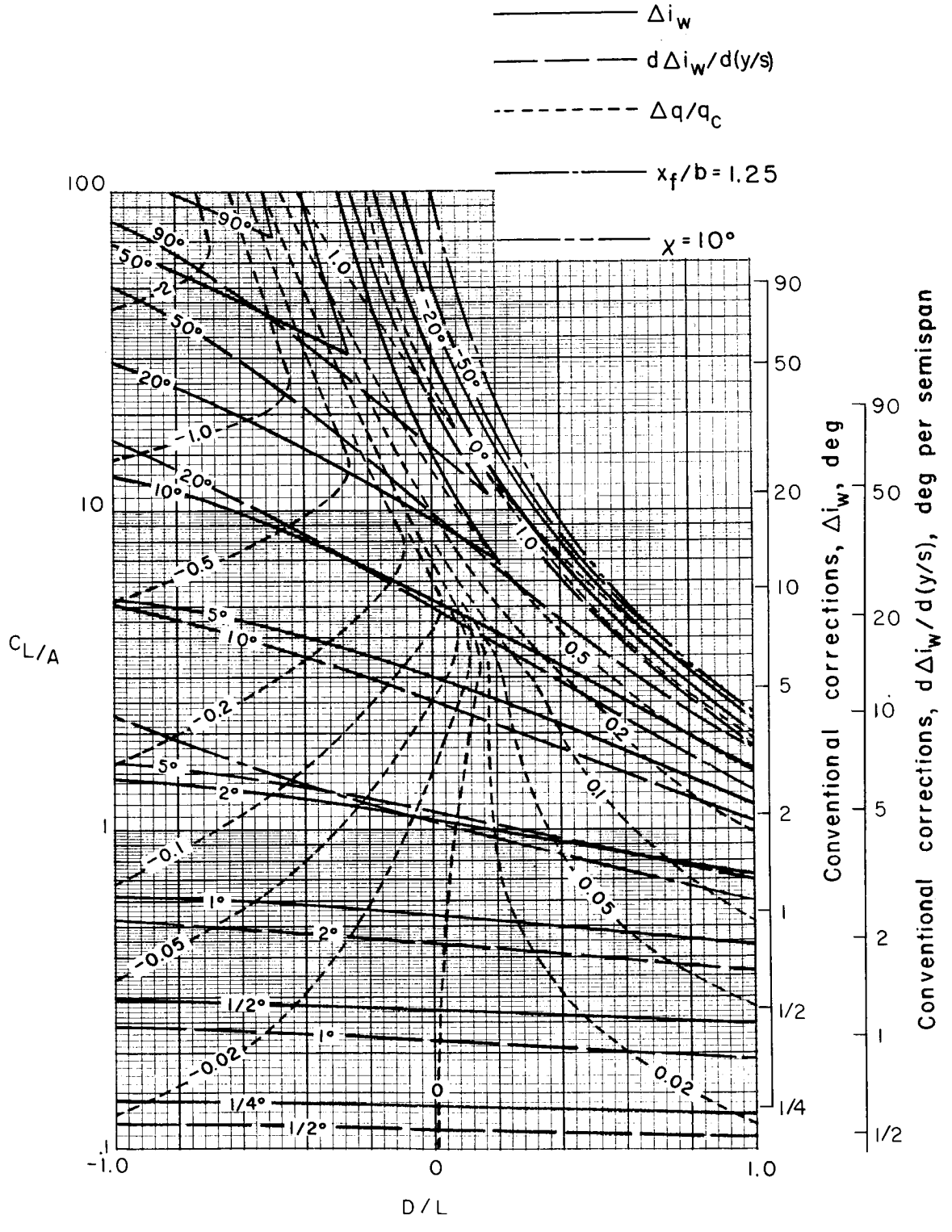


(e) $\sigma = 5/12$.

Figure 10.- Continued.

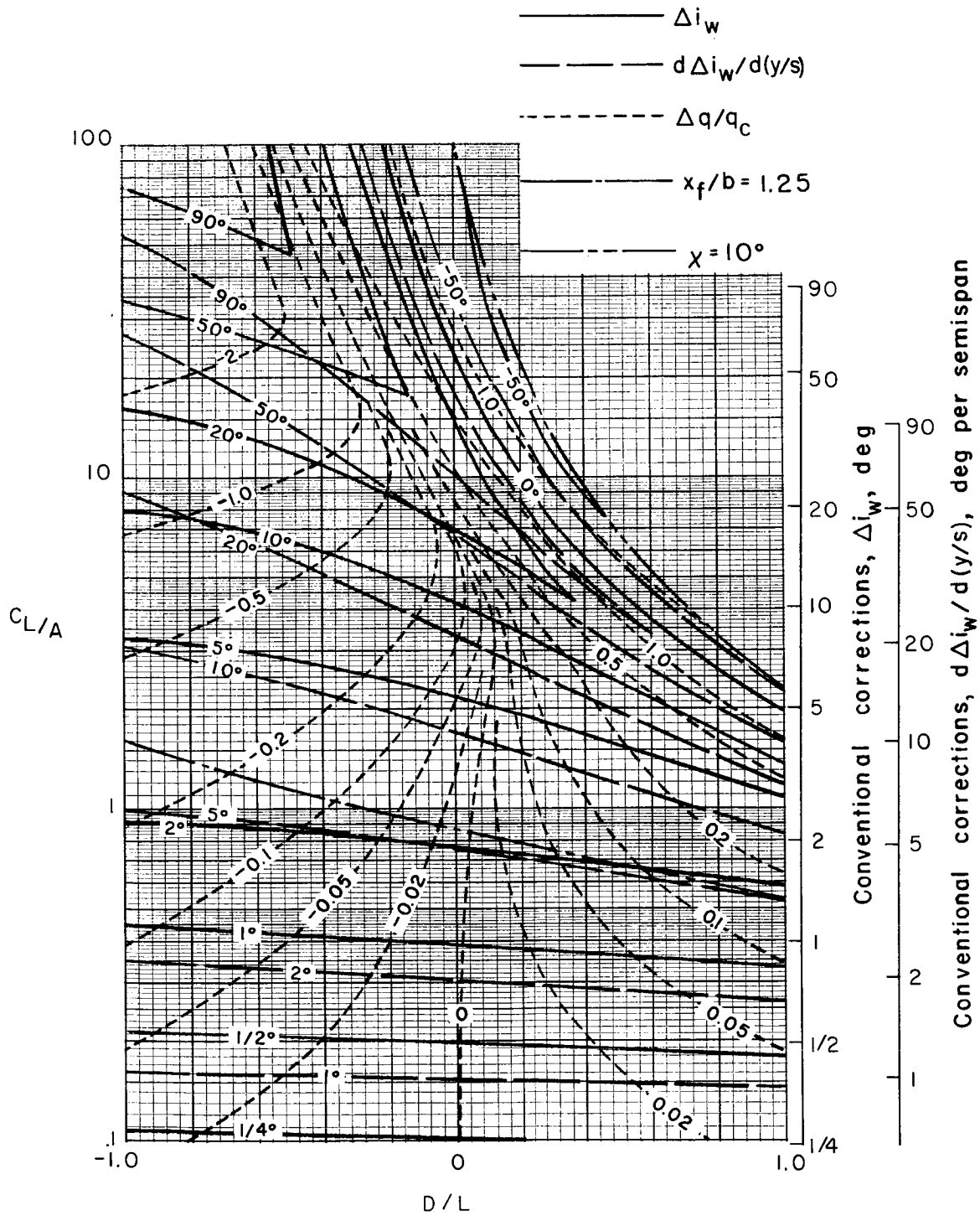


(f) $\sigma = 1/2$.

Figure 10.- Concluded.

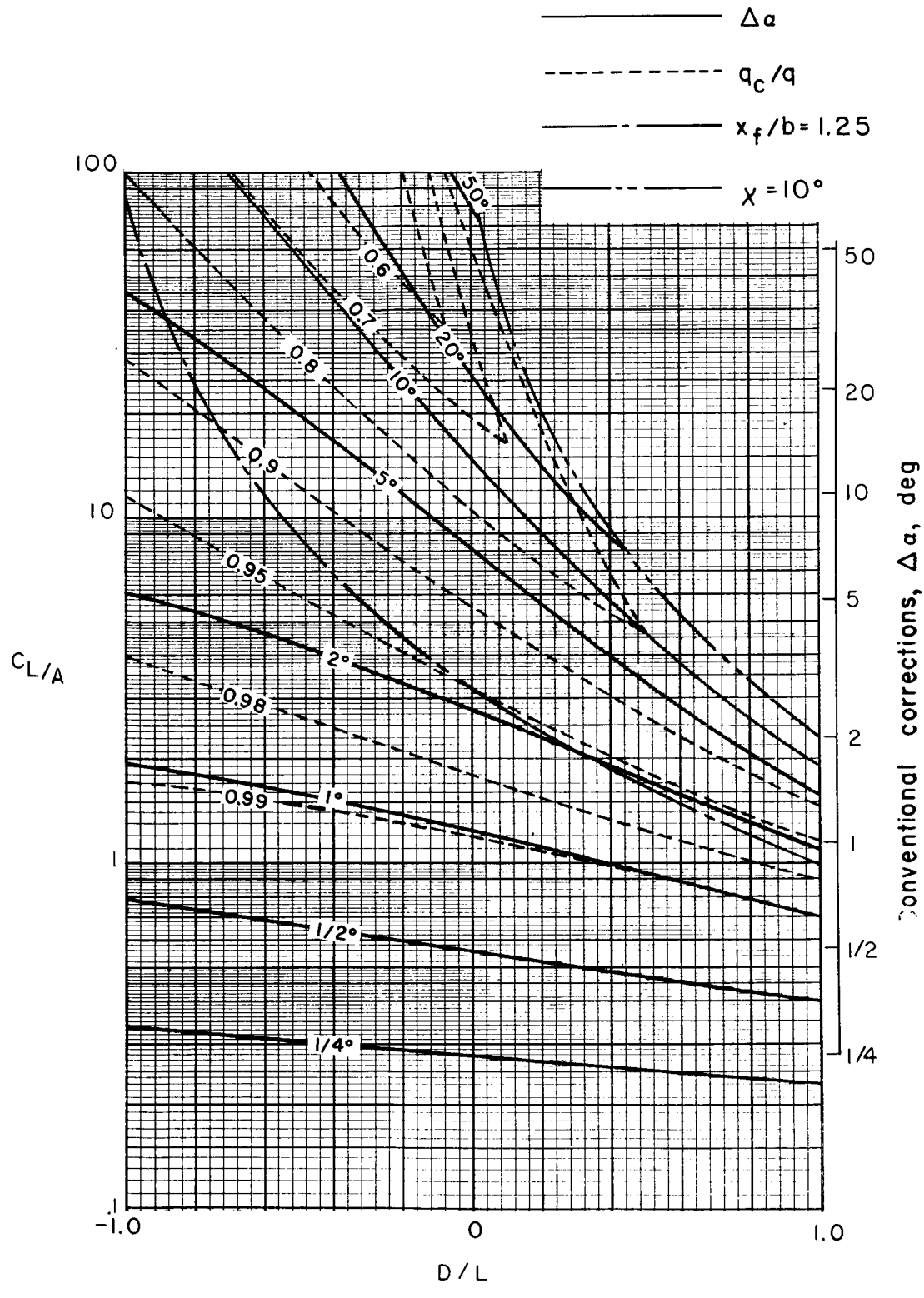


(a) σ = 1/4.

Figure 11.- Average corrections for a uniformly loaded wing centered in a closed rectangular tunnel. γ = 2; Λ = 0°.

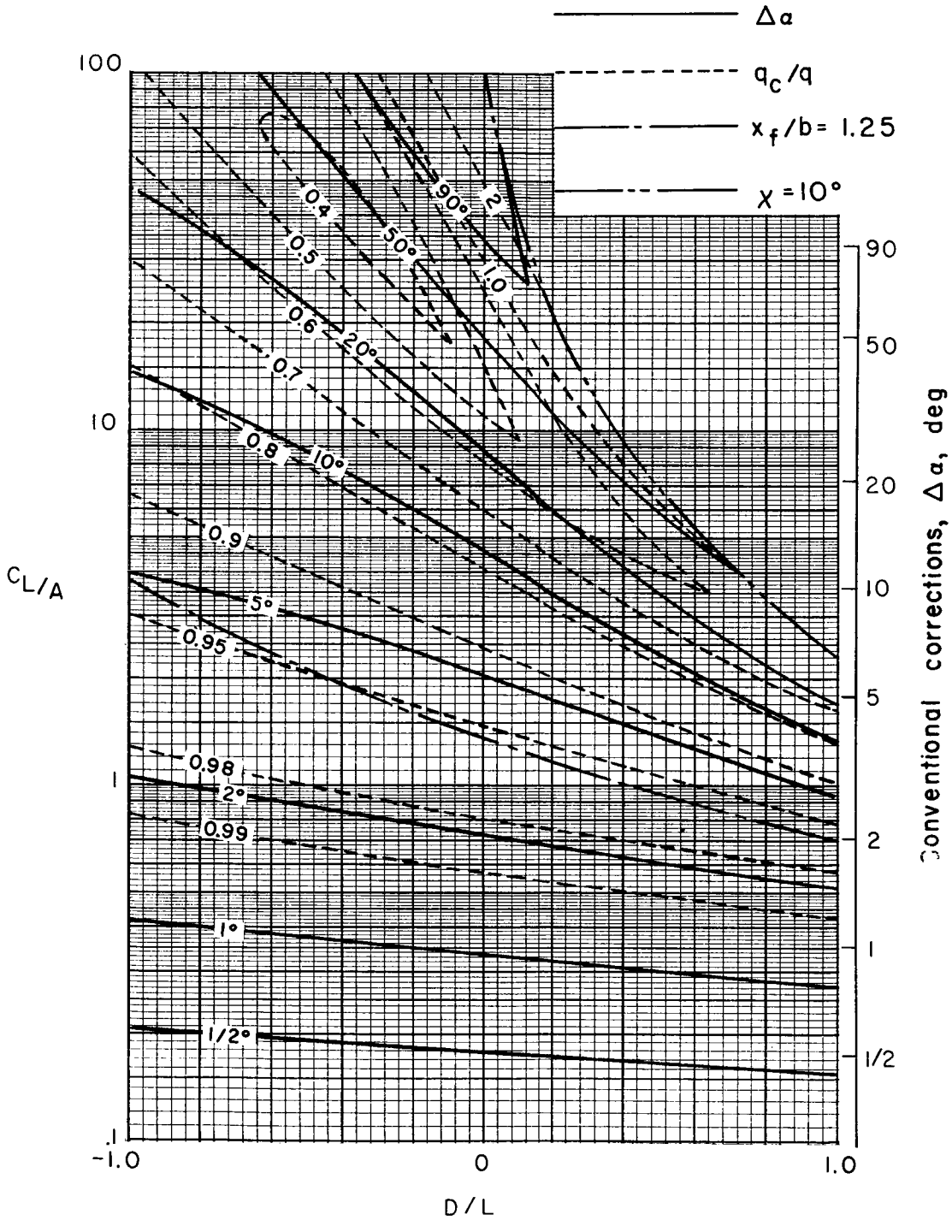


(b) $\sigma = 1/2$.

Figure 11.- Continued.

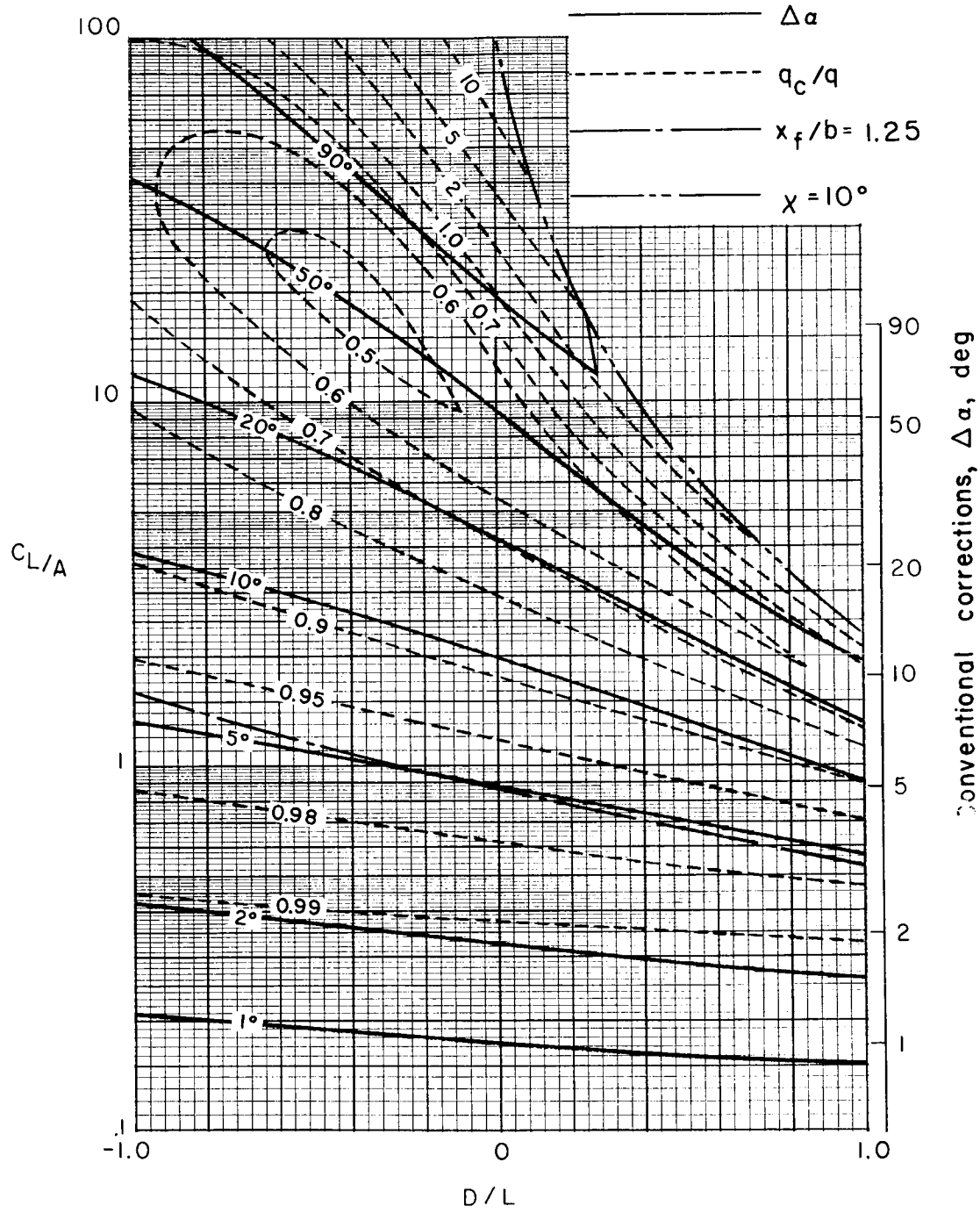


(c) σ = 3/4.

Figure 11.- Concluded.

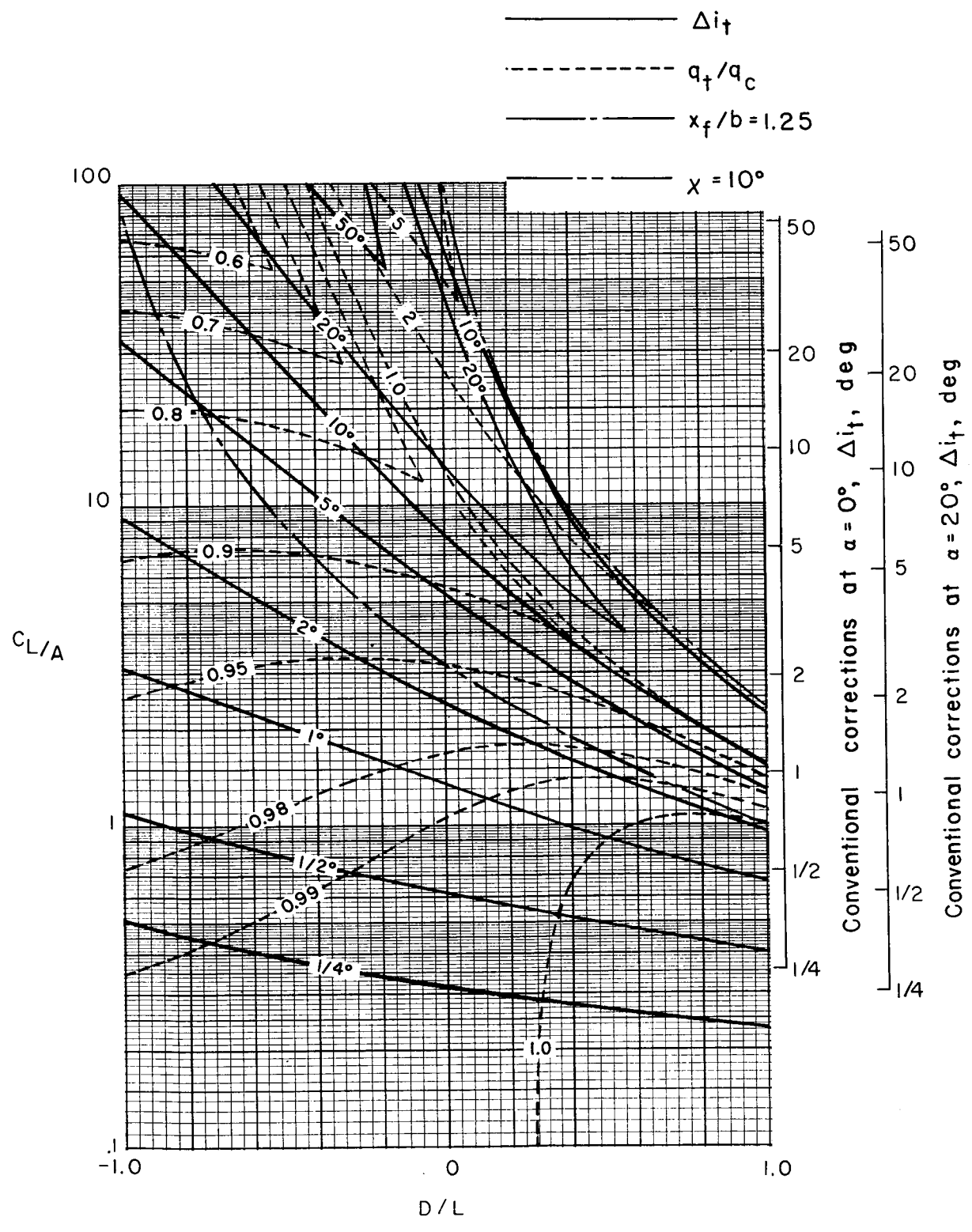


(a) $\sigma = 1/4$.

Figure 12.- Corrections at a zero-span tail behind a uniformly loaded wing centered in a closed rectangular tunnel. $\alpha = 20^0$; $\gamma = 2$; $\Lambda = 0^0$.

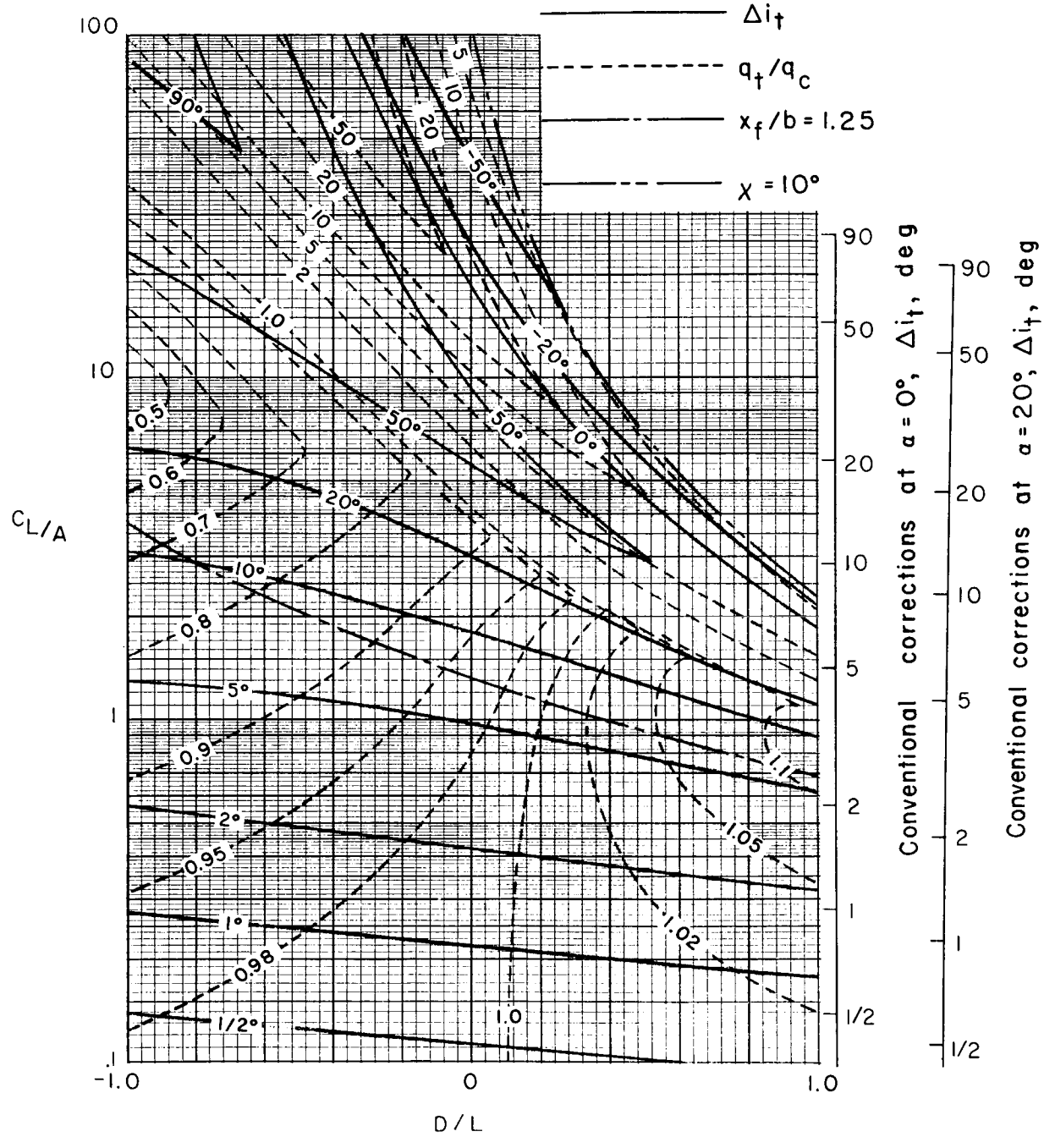


(b) $\sigma = 1/2$.

Figure 12.- Continued.

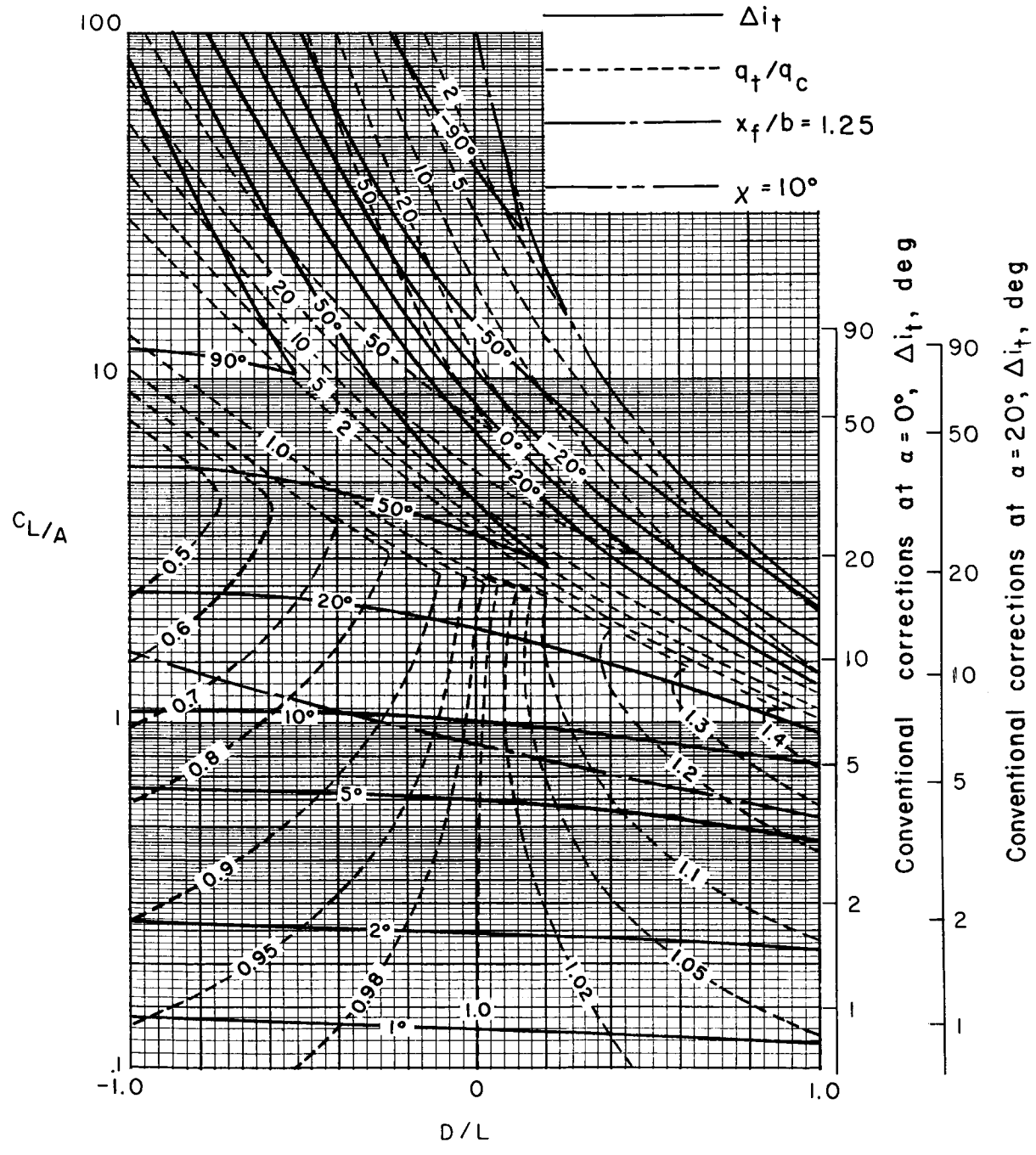


(c) σ = 3/4.

Figure 12.- Concluded.

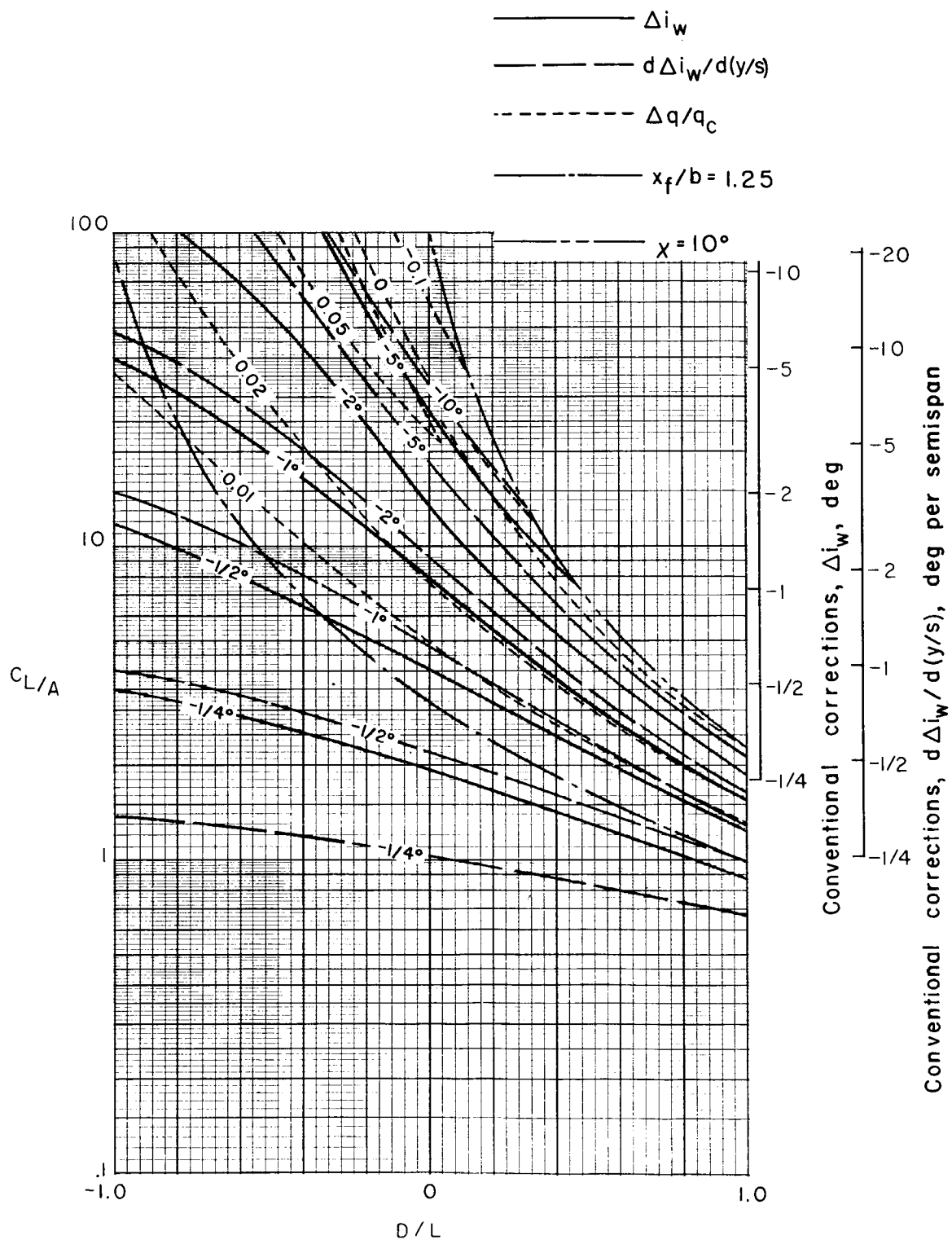


(a) $\sigma = 1/4$.

Figure 13.- Nonuniformity of corrections over a uniformly loaded wing centered in a closed rectangular tunnel. $\gamma = 2$; $\alpha = 0^0$; $\Lambda = 0^0$.

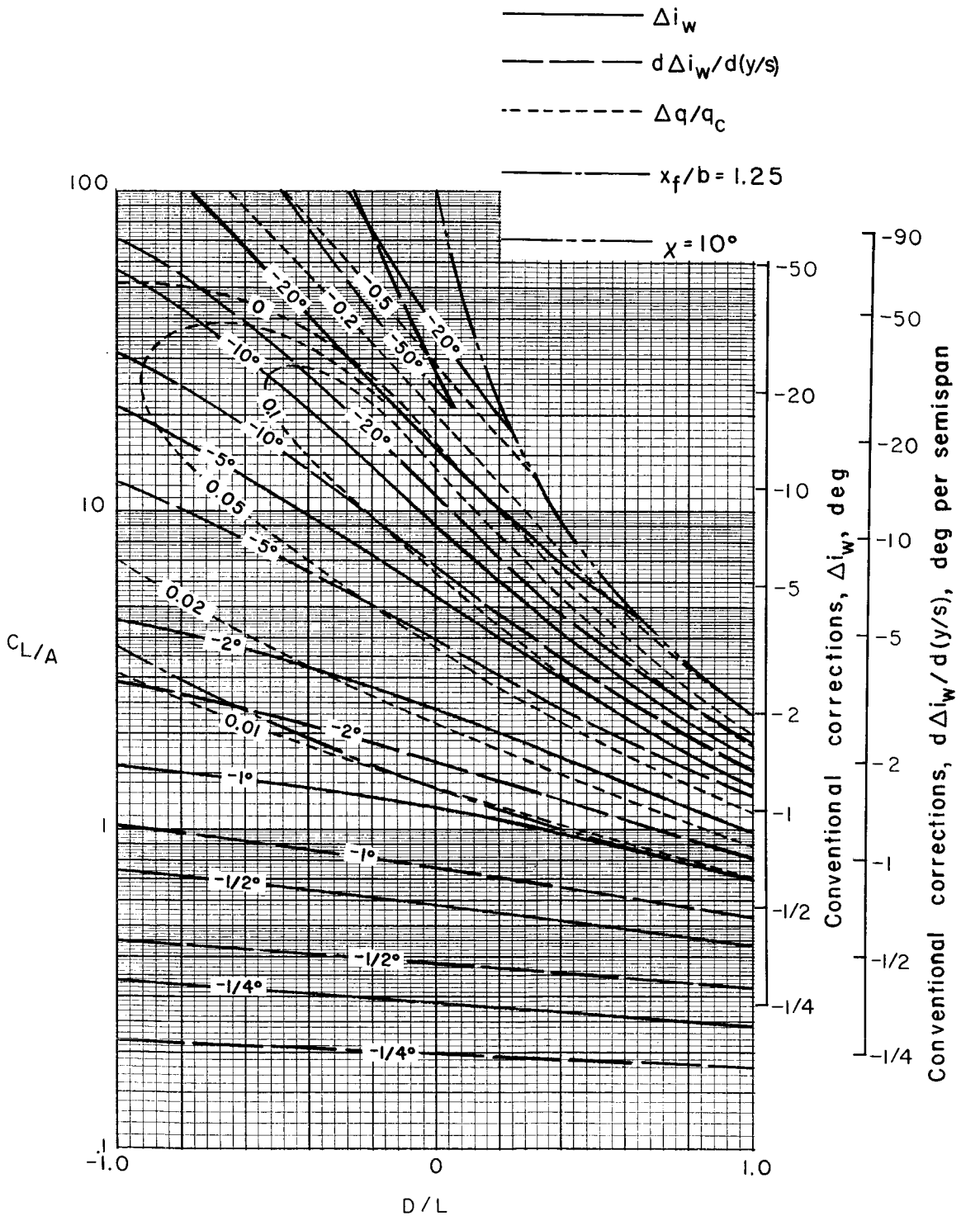


(b) $\sigma = 1/2$.

Figure 13.- Continued.

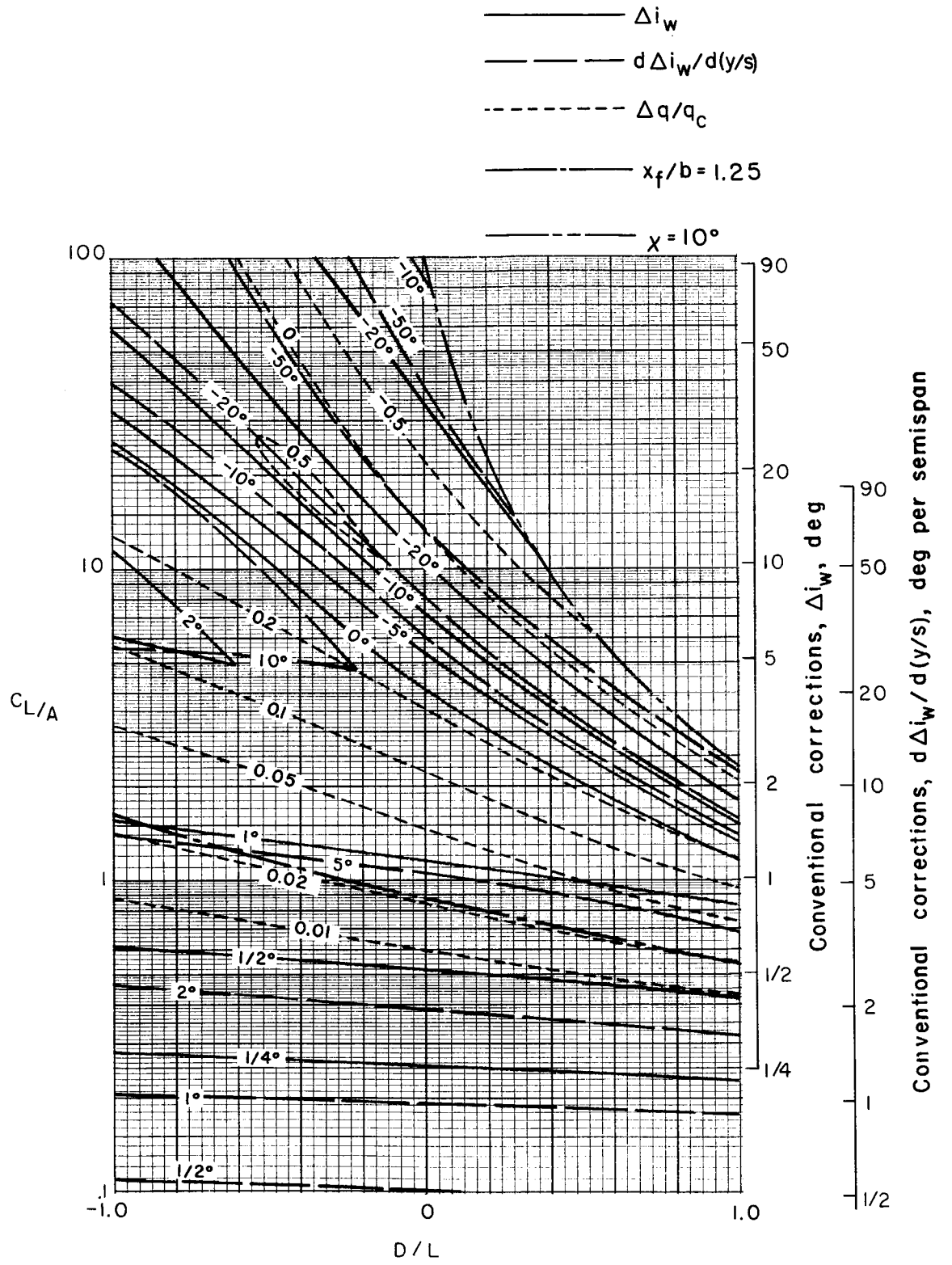


(c) $\sigma = 3/4$.

Figure 13.- Concluded.

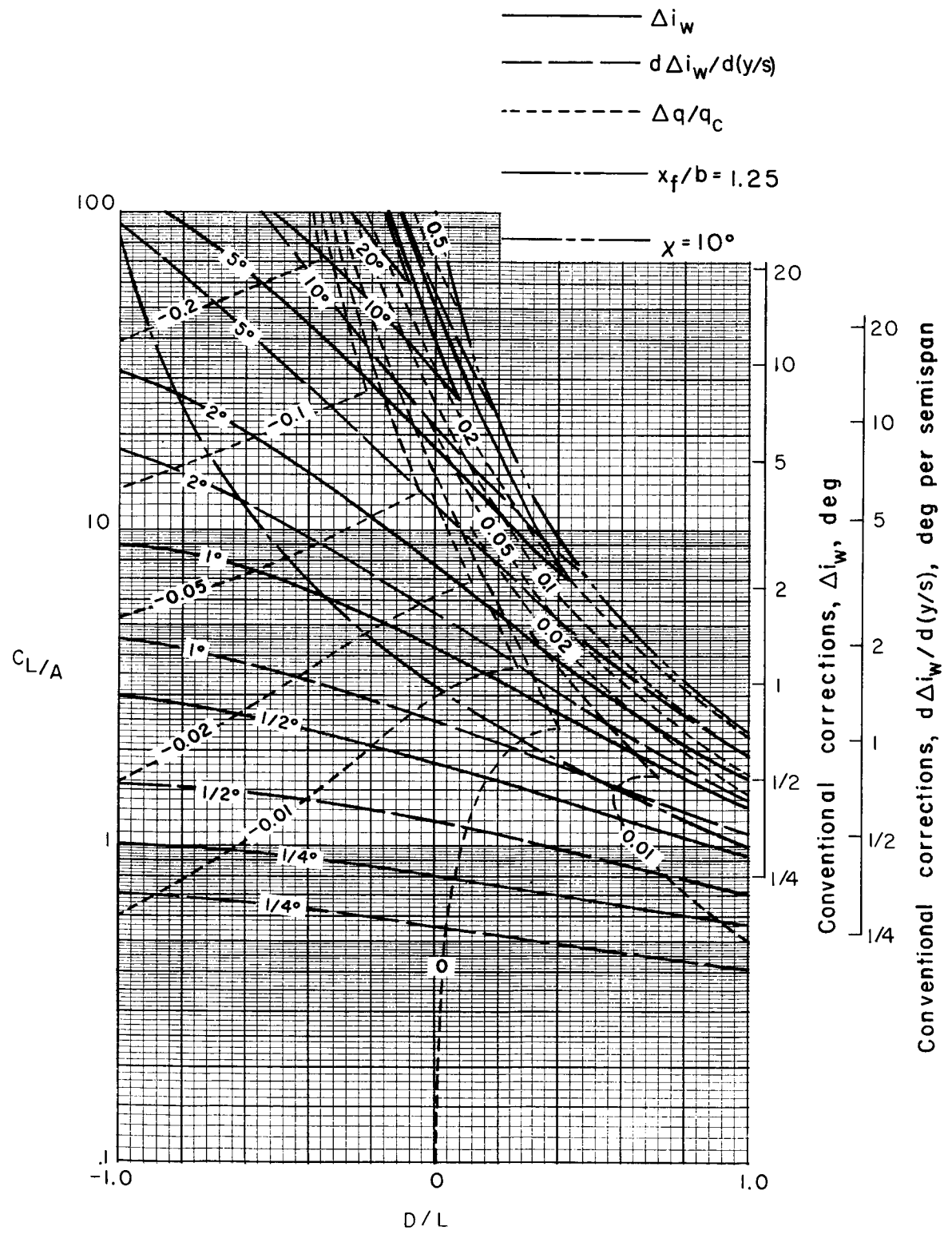


(a) $\sigma = 1/4$.

Figure 14.- Nonuniformity of corrections over a uniformly loaded wing centered in a closed rectangular tunnel. $\gamma = 2$; $\alpha = 0^0$; $\Lambda = 45^0$.

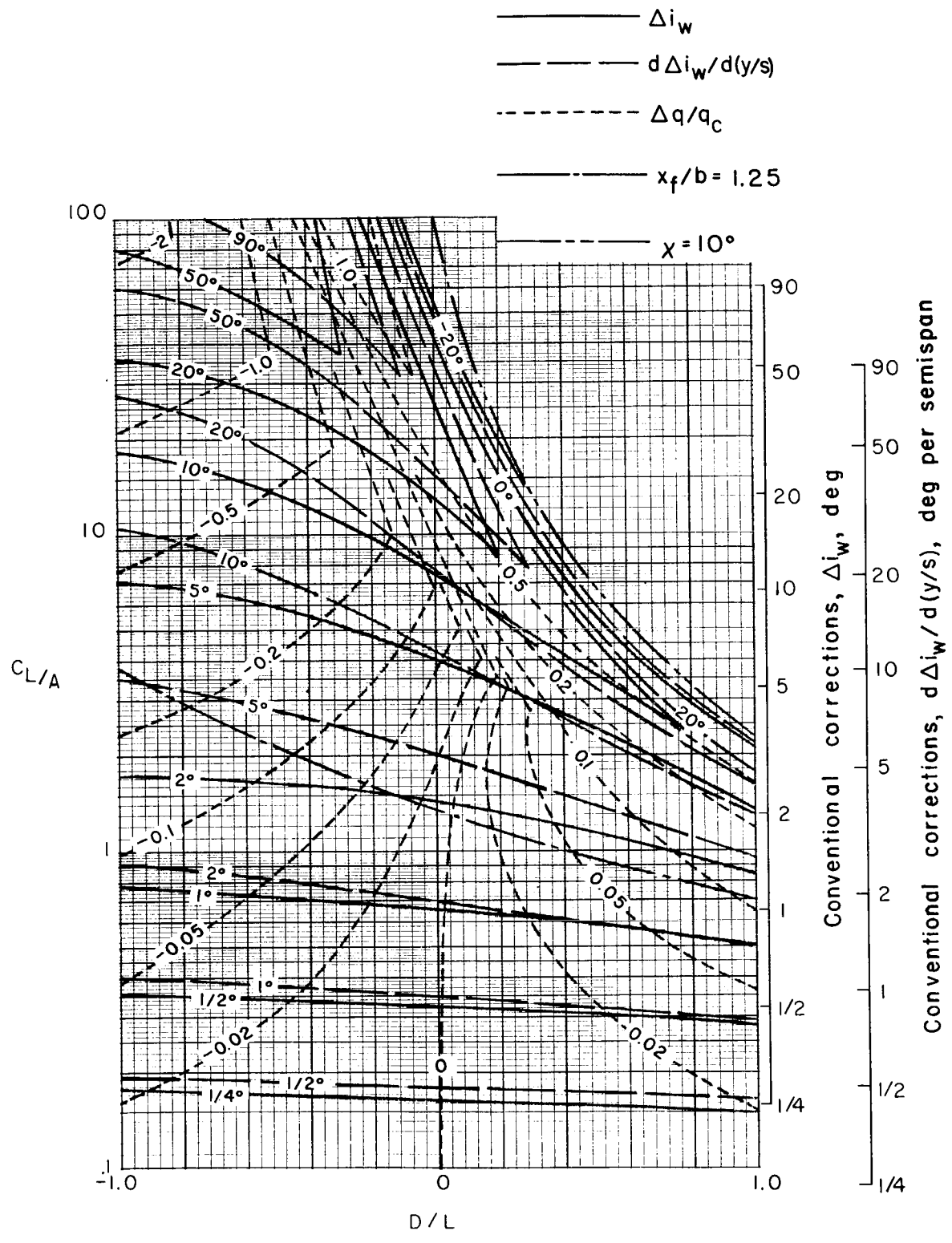


(b) $\sigma = 1/2$.

Figure 14.- Continued.

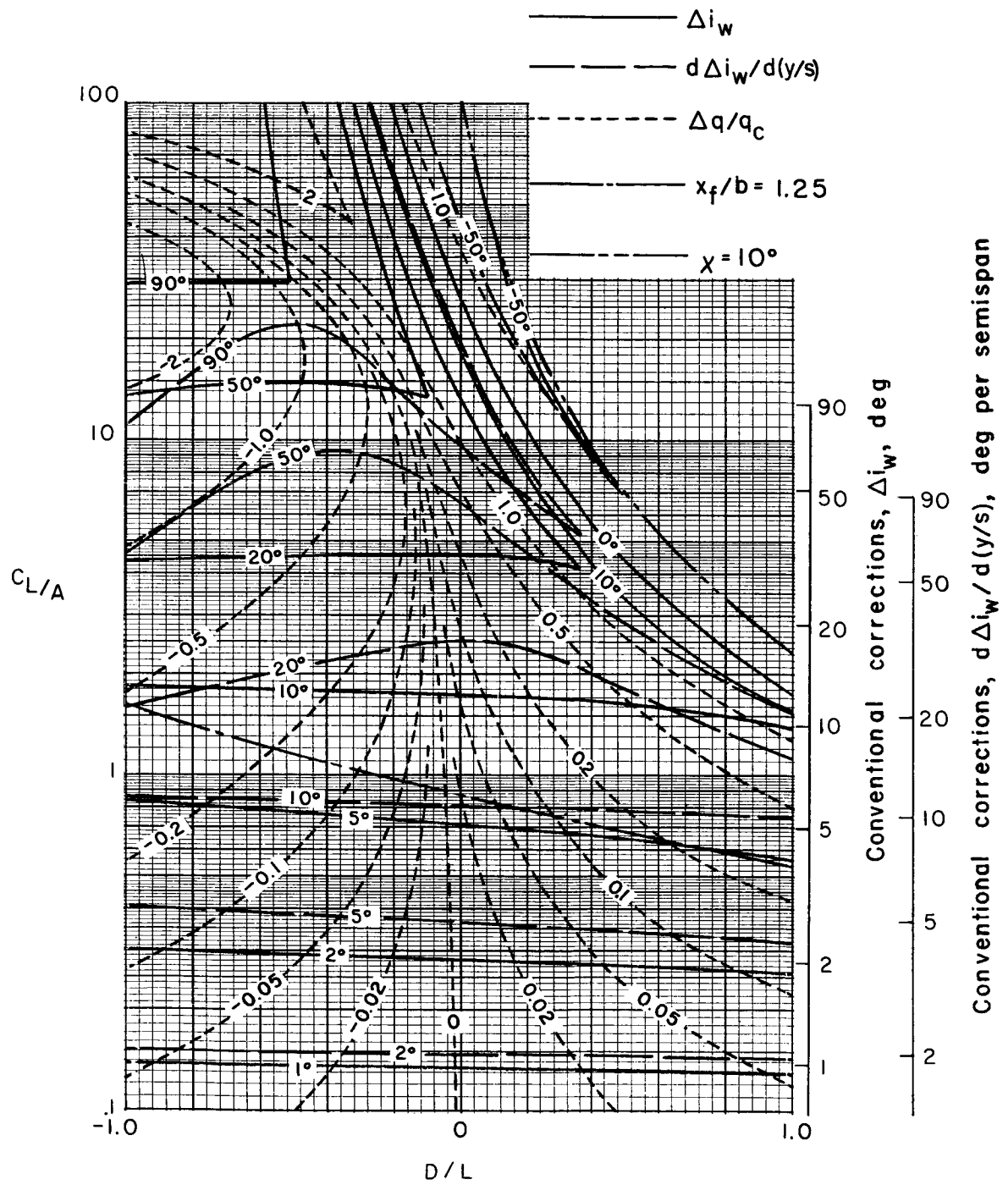


(c) $\sigma = 3/4$.

Figure 14.- Concluded.

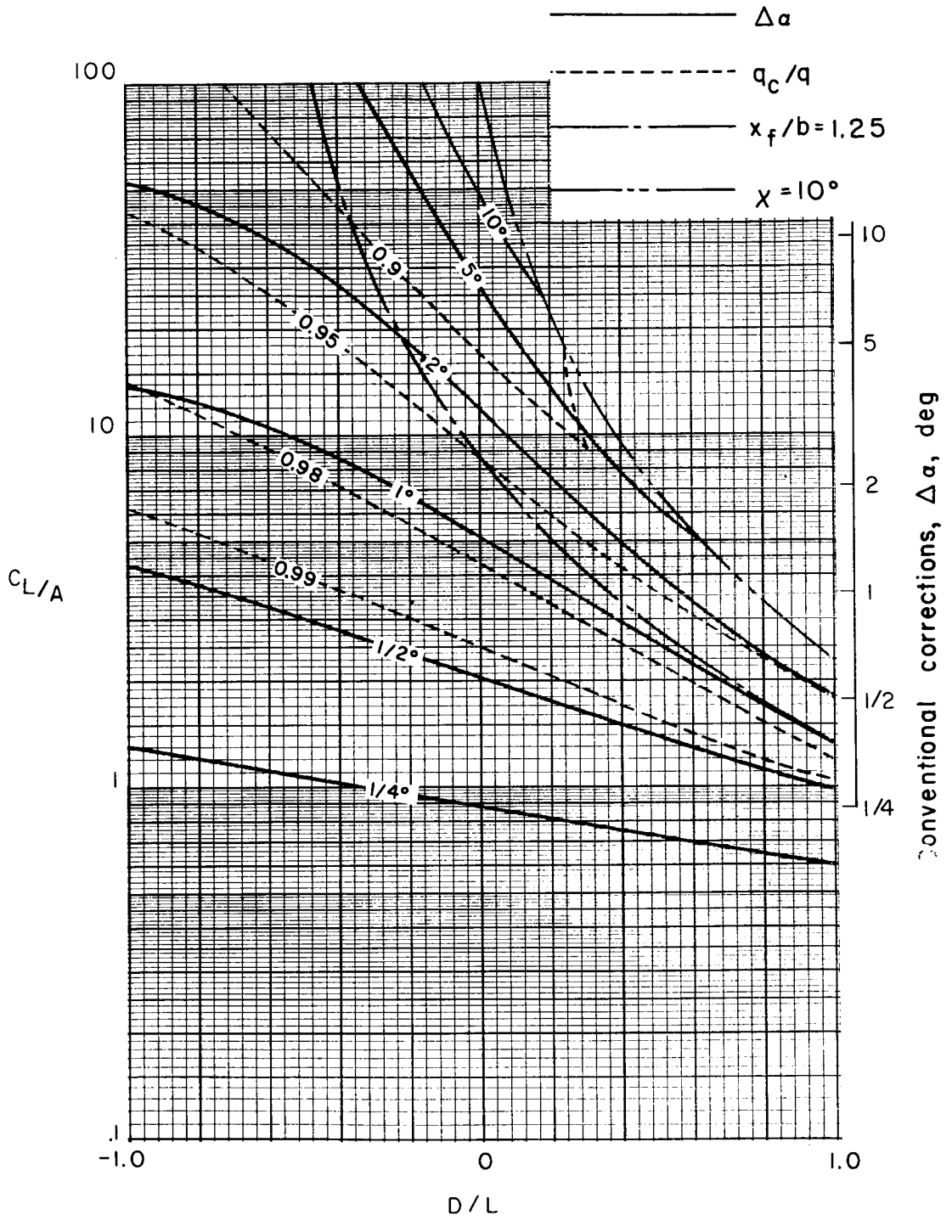


(a) σ = 2/15.

Figure 15.- Average corrections for a uniformly loaded wing centered in a closed tunnel with semicircular sides. γ = 2; Λ = 0°.

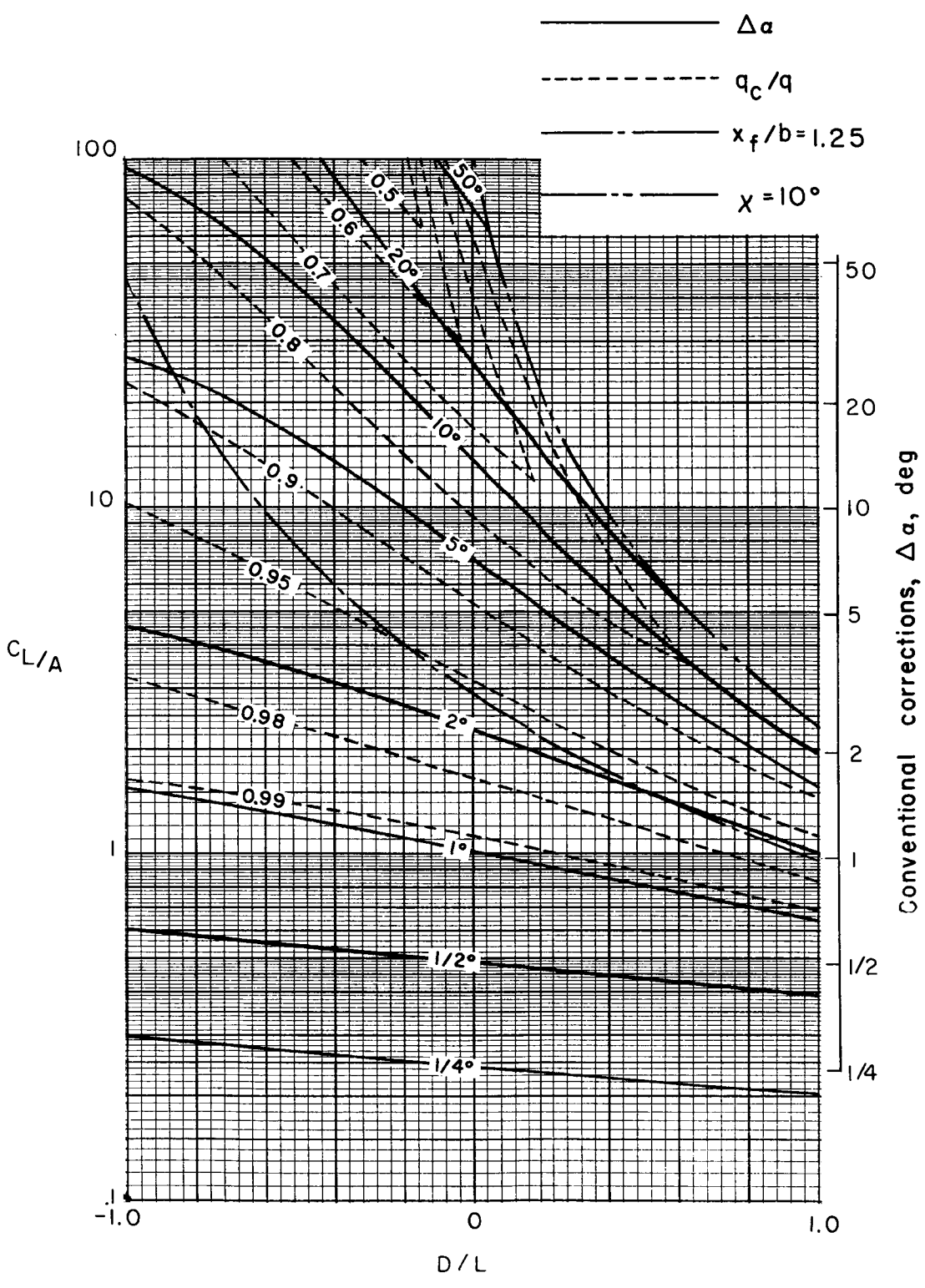


(b) σ = 4/15.

Figure 15.- Continued.

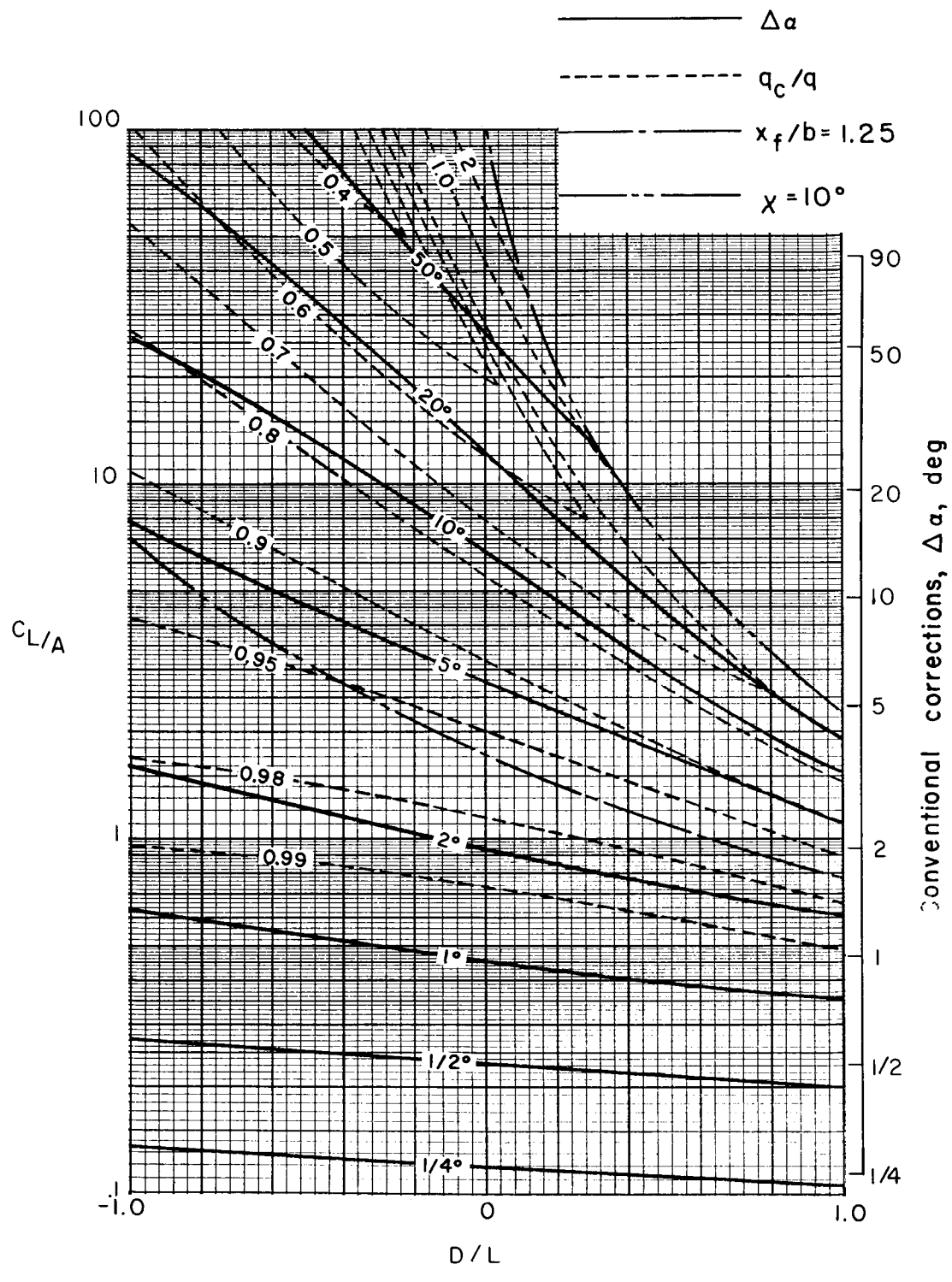


(c) $\sigma = 2/5$.

Figure 15.- Continued.

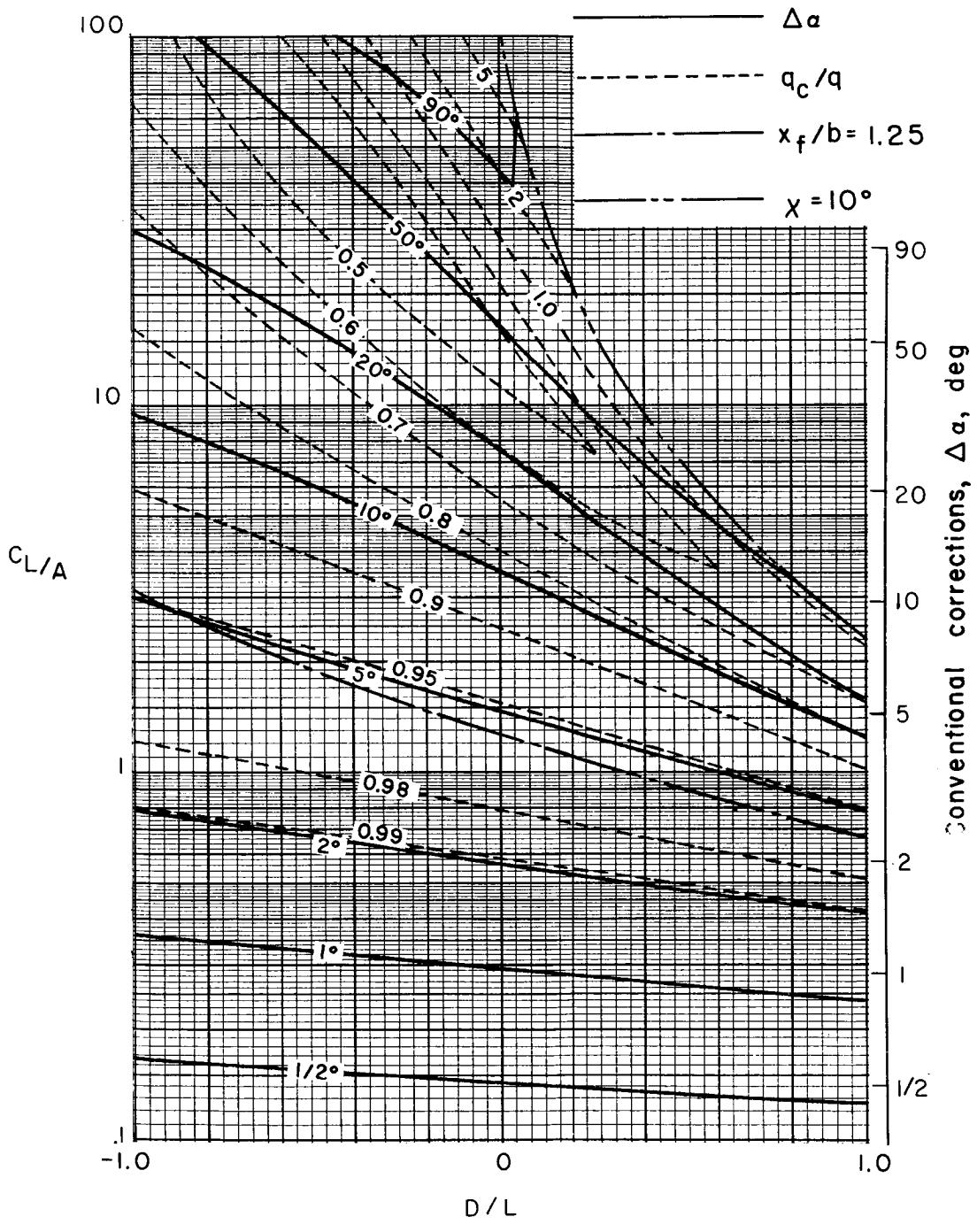


(d) σ = 8/15.

Figure 15.- Continued.

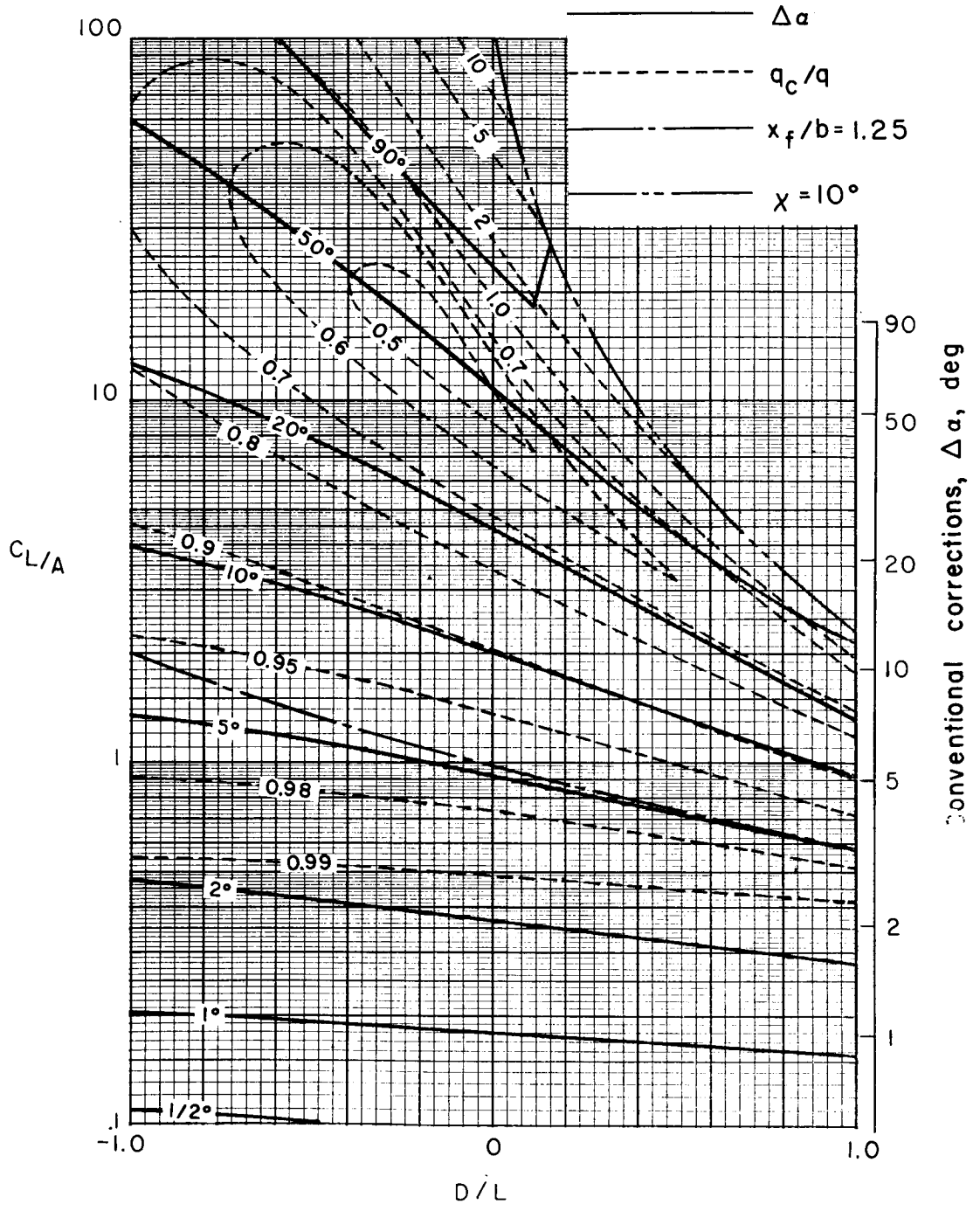


(e) σ = 2/3.

Figure 15.- Continued.

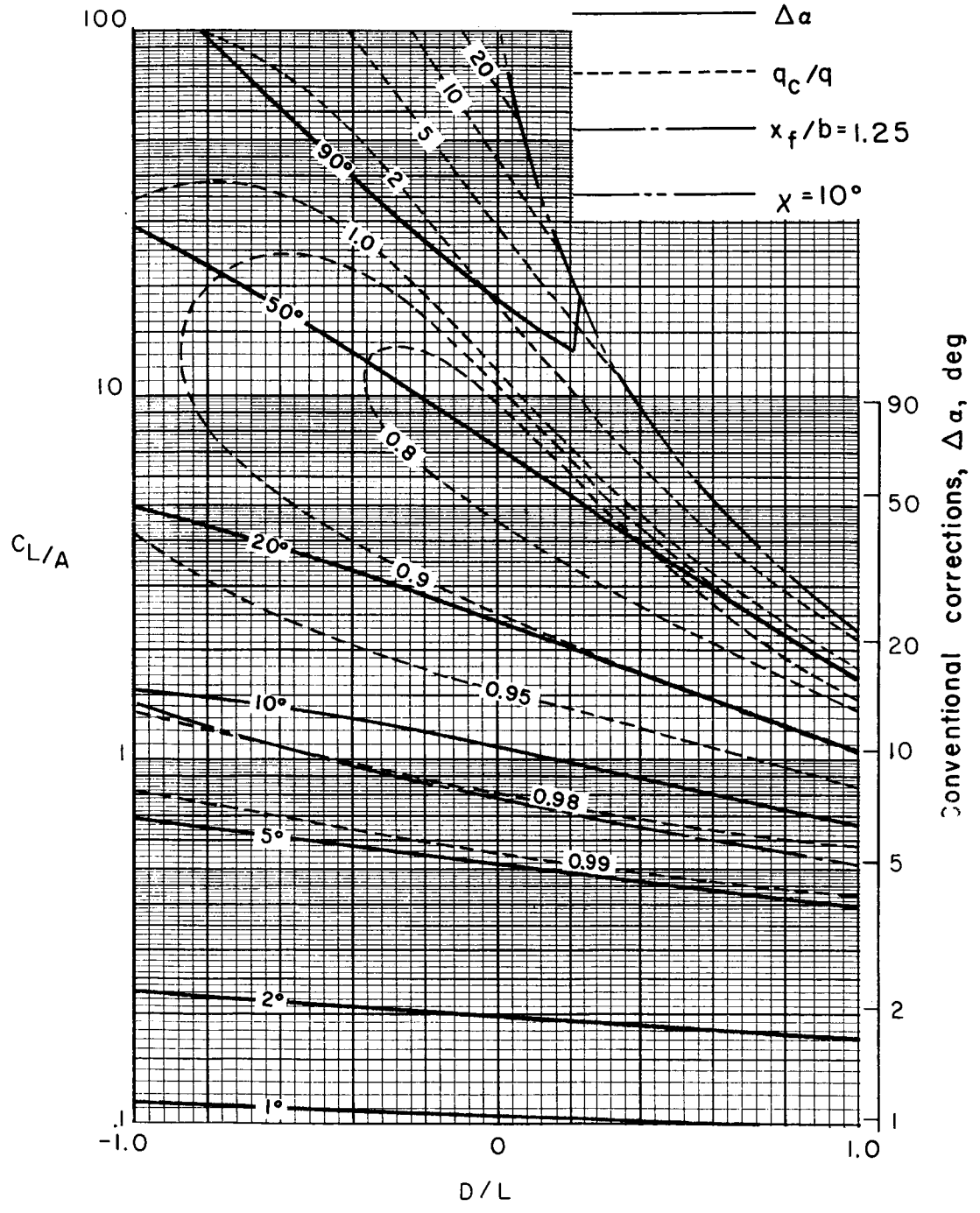


(f) σ = 4/5.

Figure 15.- Concluded.

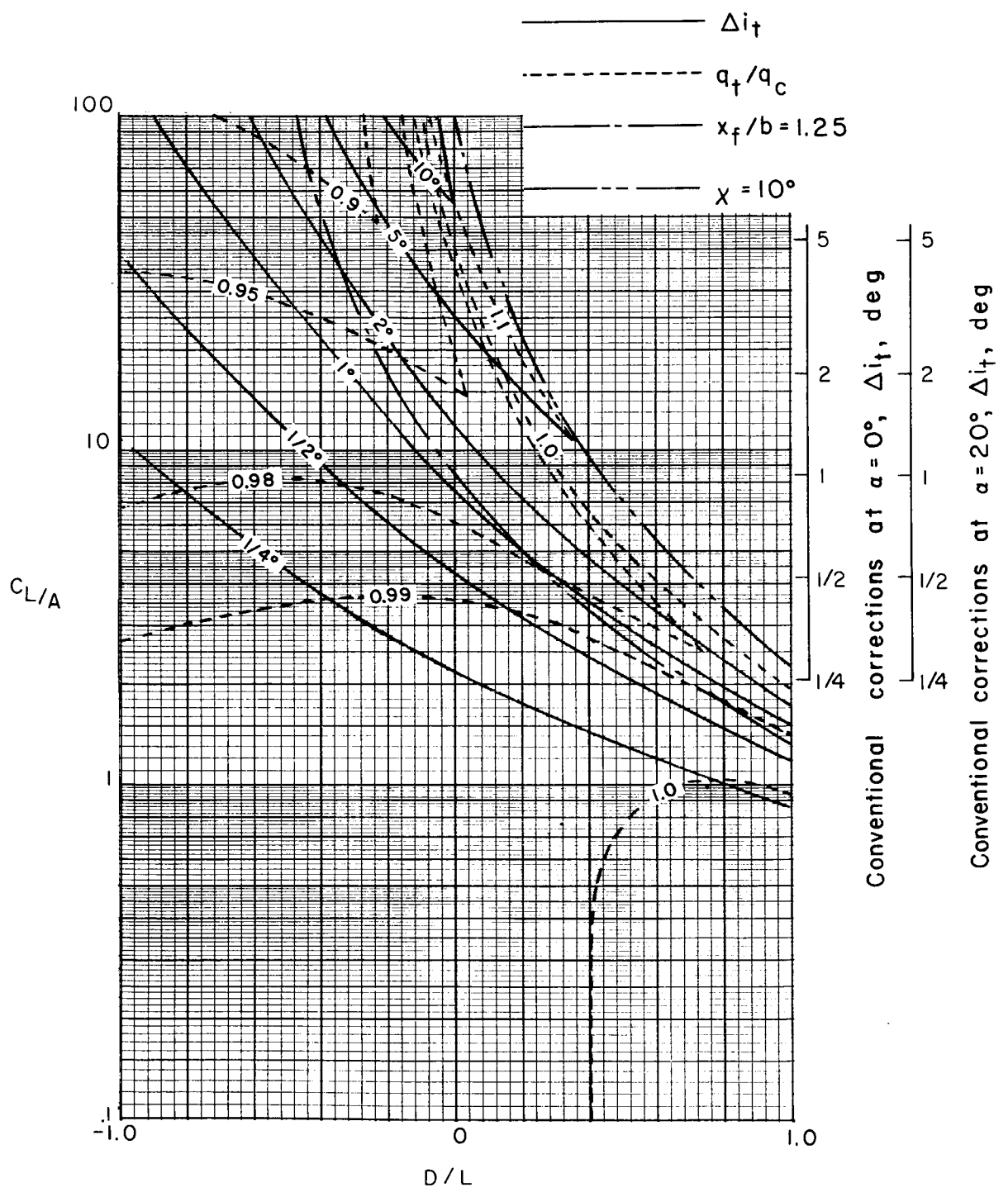


(a) $\sigma = 2/15$.

Figure 16.- Corrections at a zero-span tail behind a uniformly loaded wing centered in a closed tunnel with semicircular sides. Tail length is three-fourths of wing span; tail height is zero; $\alpha = 20^0$; $\Lambda = 0^0$; $\gamma = 2$.

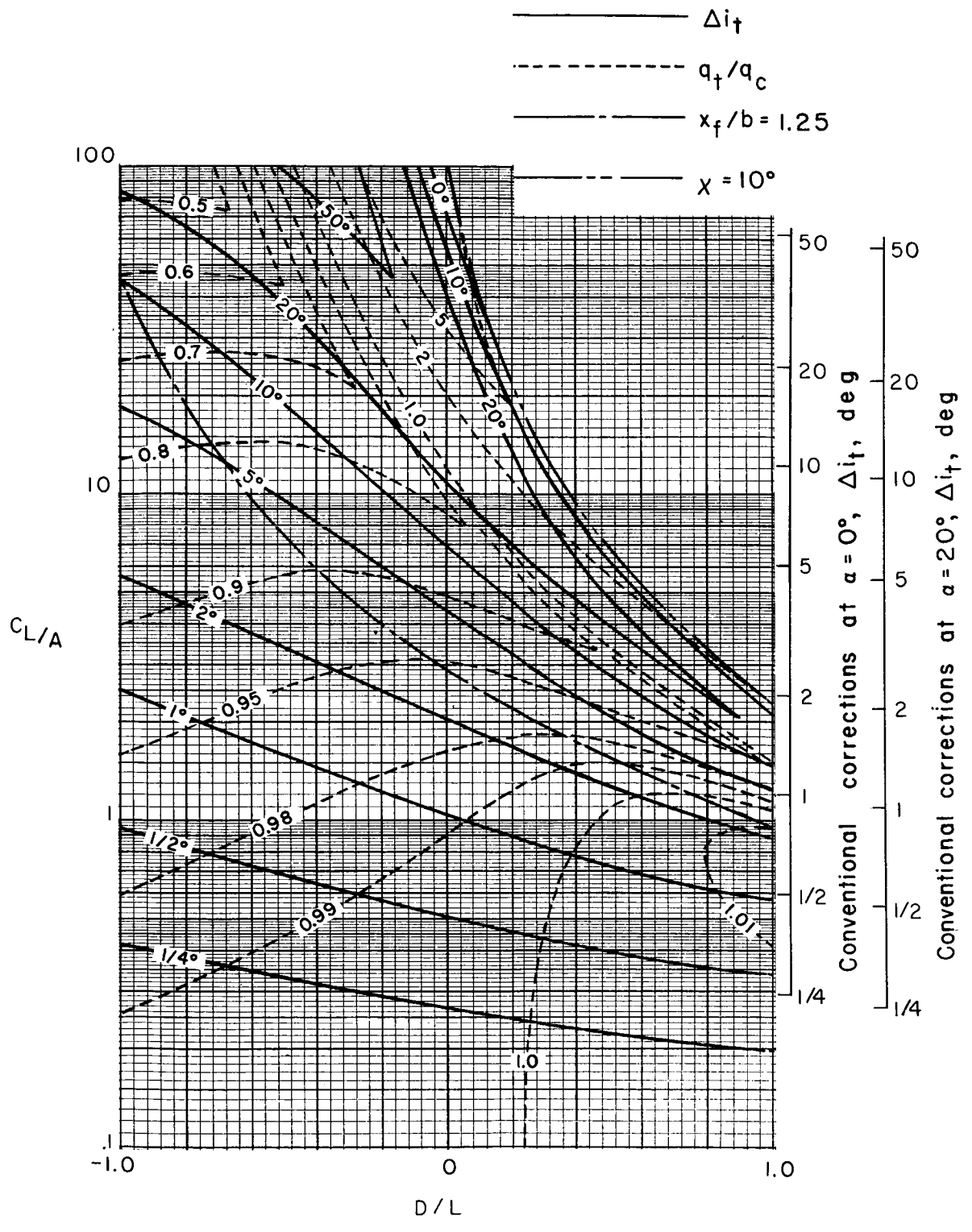


(b) $\sigma = 4/15$.

Figure 16.- Continued.

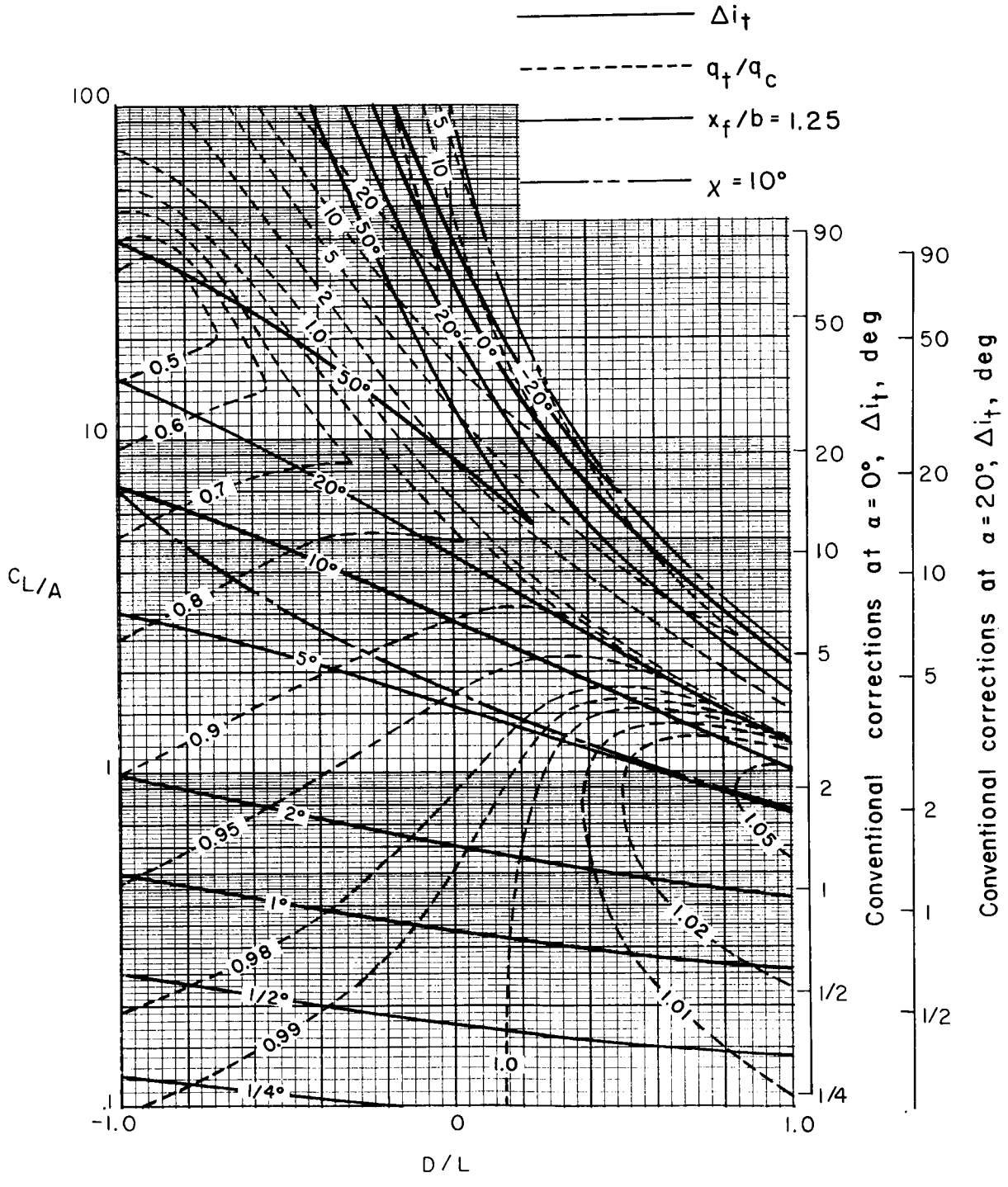


(c) $\sigma = 2/5$.

Figure 16.- Continued.

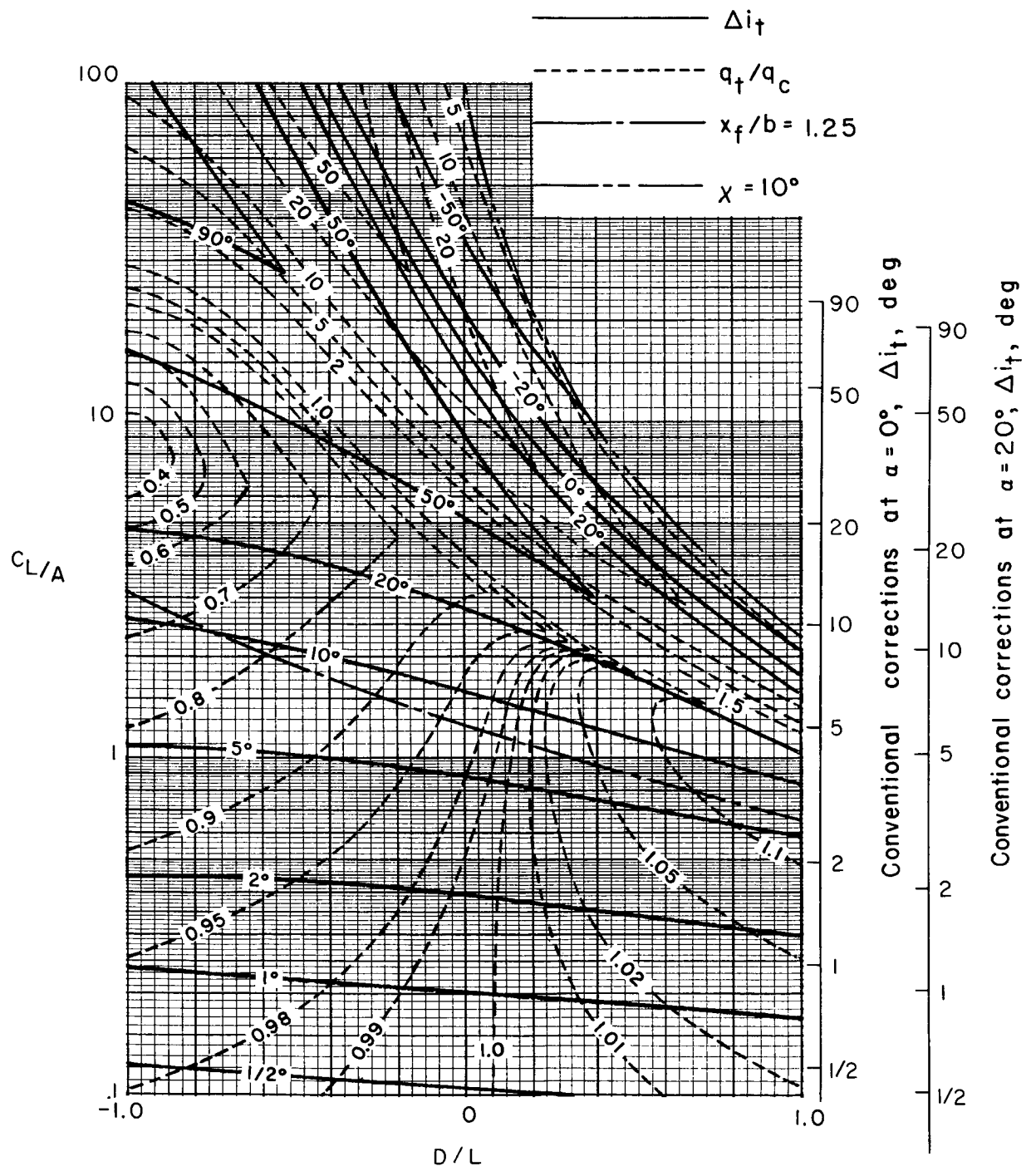


(d) σ = 8/15.

Figure 16.- Continued.

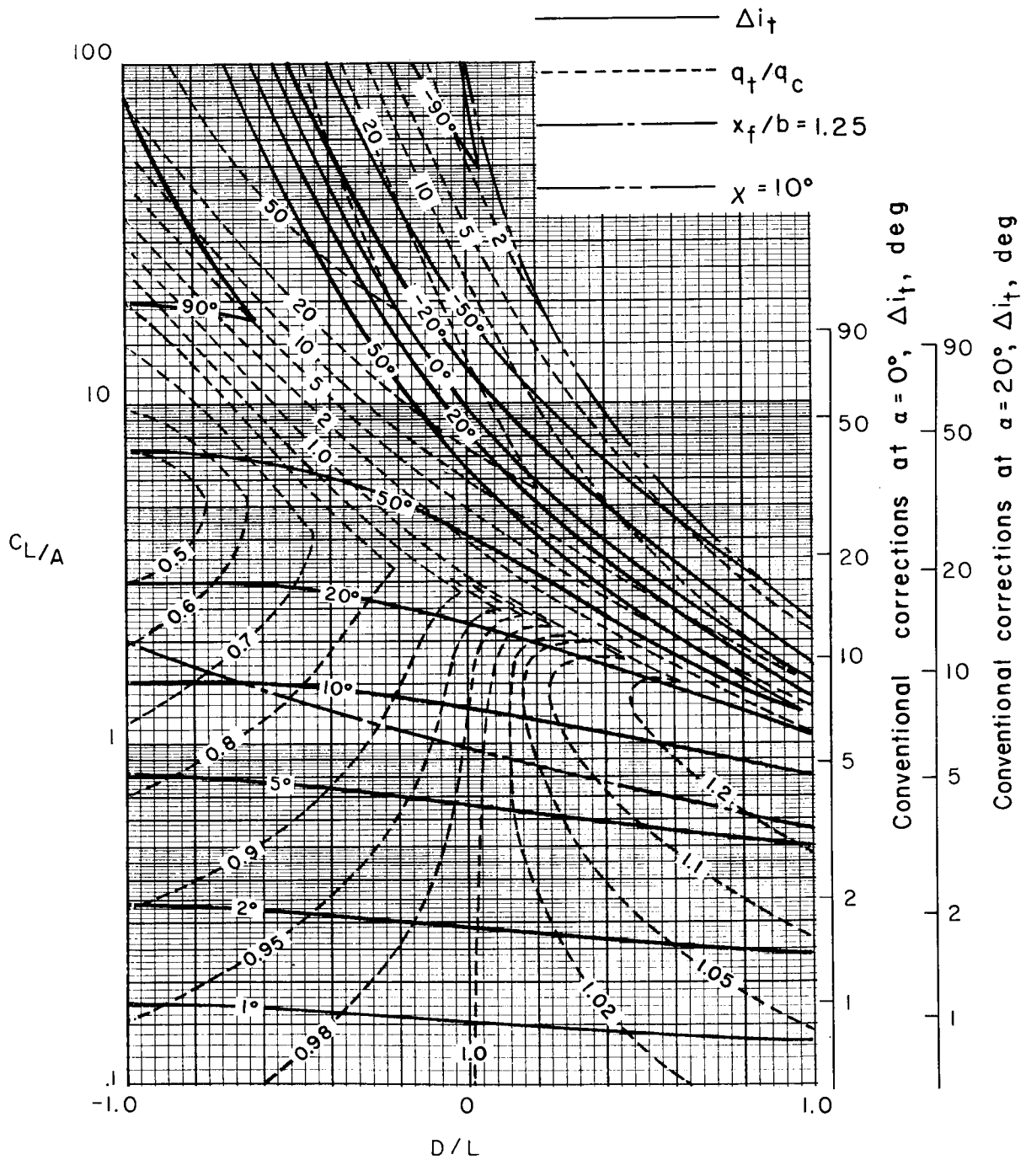


(e) $\sigma = 2/3$.

Figure 16.- Continued.

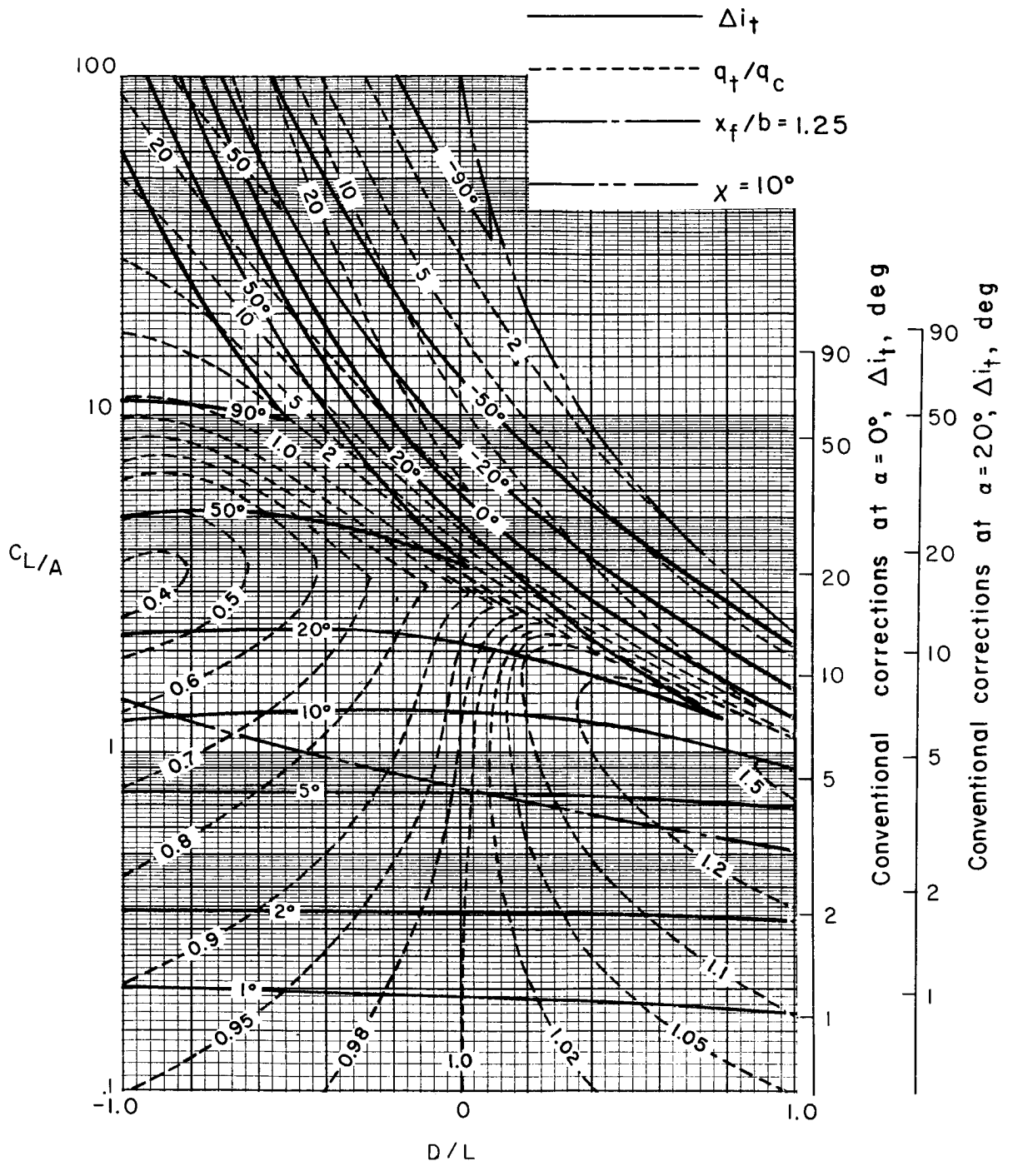


(f) σ = 4/5.

Figure 16.- Concluded.

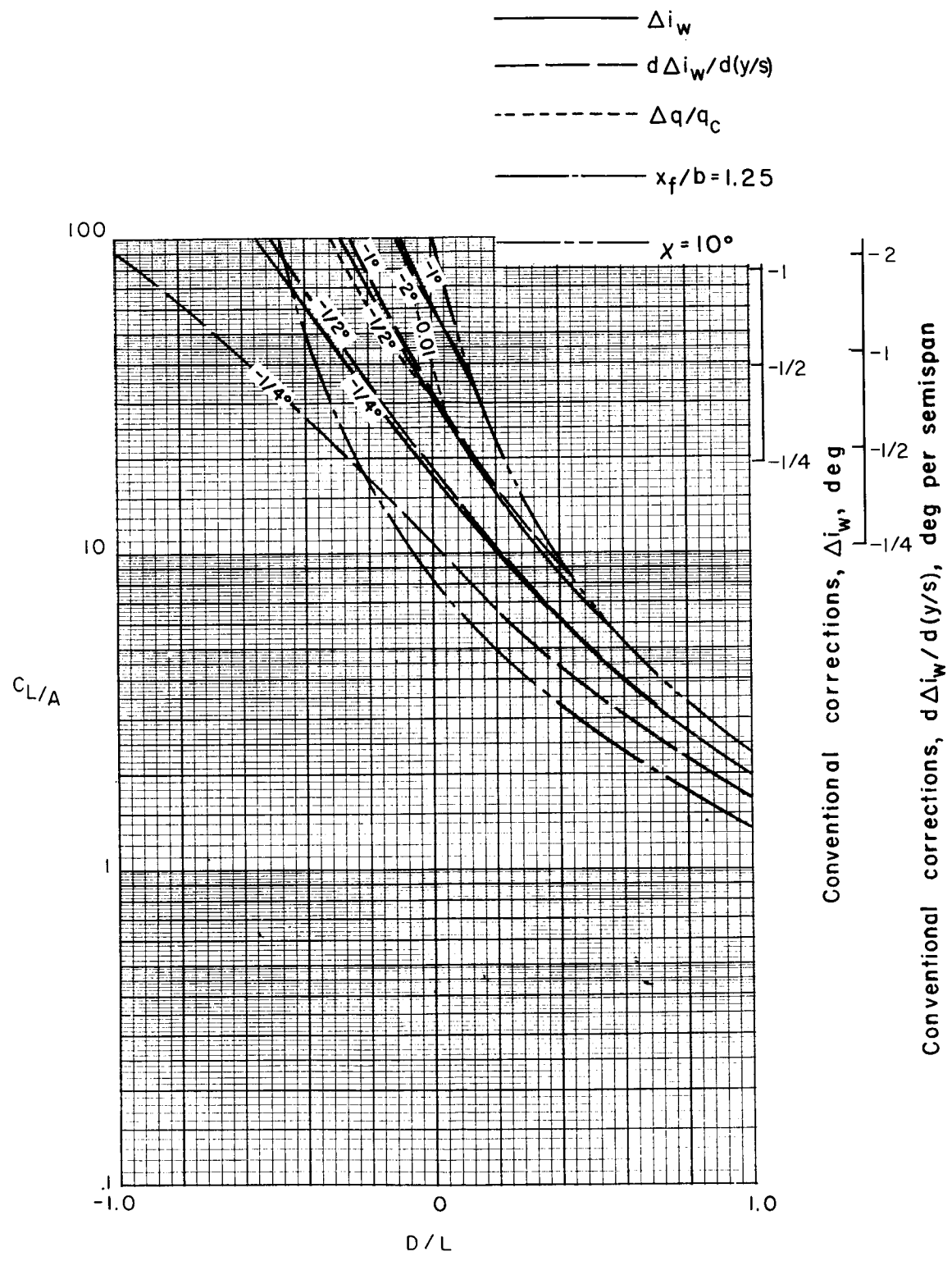


(a) $\sigma = 2/15$.

Figure 17.- Nonuniformity of corrections over a uniformly loaded wing centered in a closed tunnel with semicircular sides. $\gamma = 2$; $\Lambda = 0^0$; $\alpha = 0^0$.

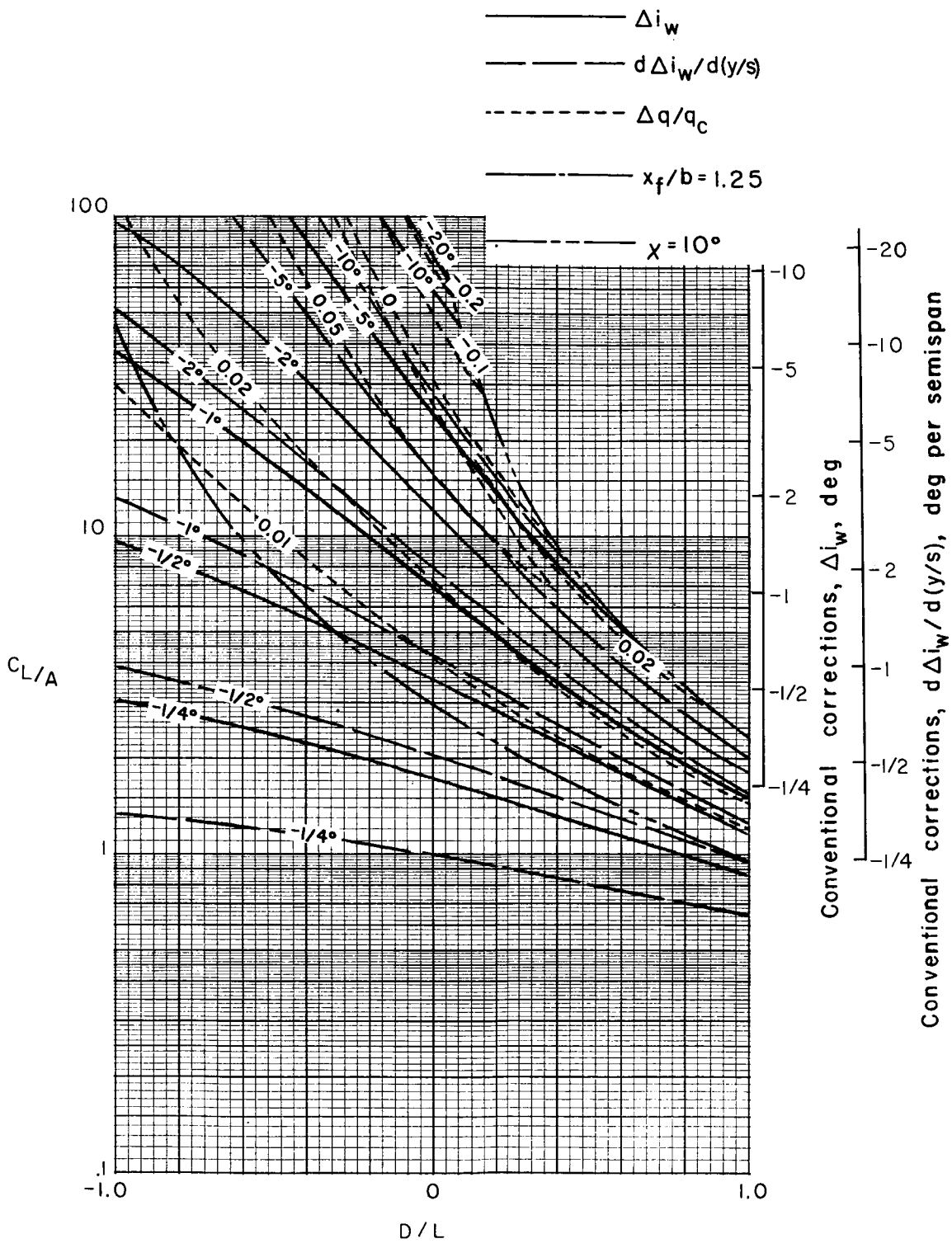


(b) $\sigma = 4/15$.

Figure 17.- Continued.

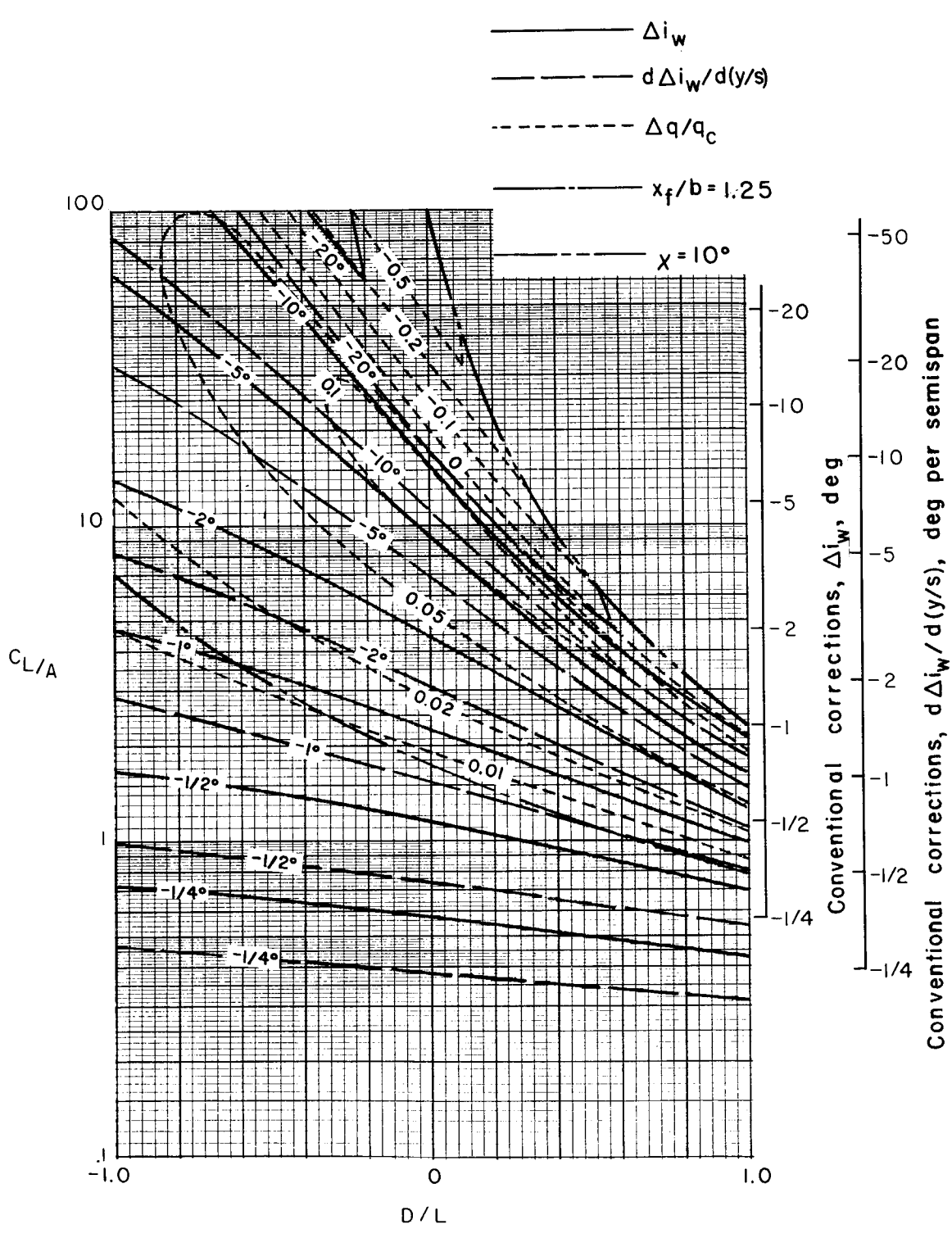


(c) $\sigma = 2/5$.

Figure 17.- Continued.

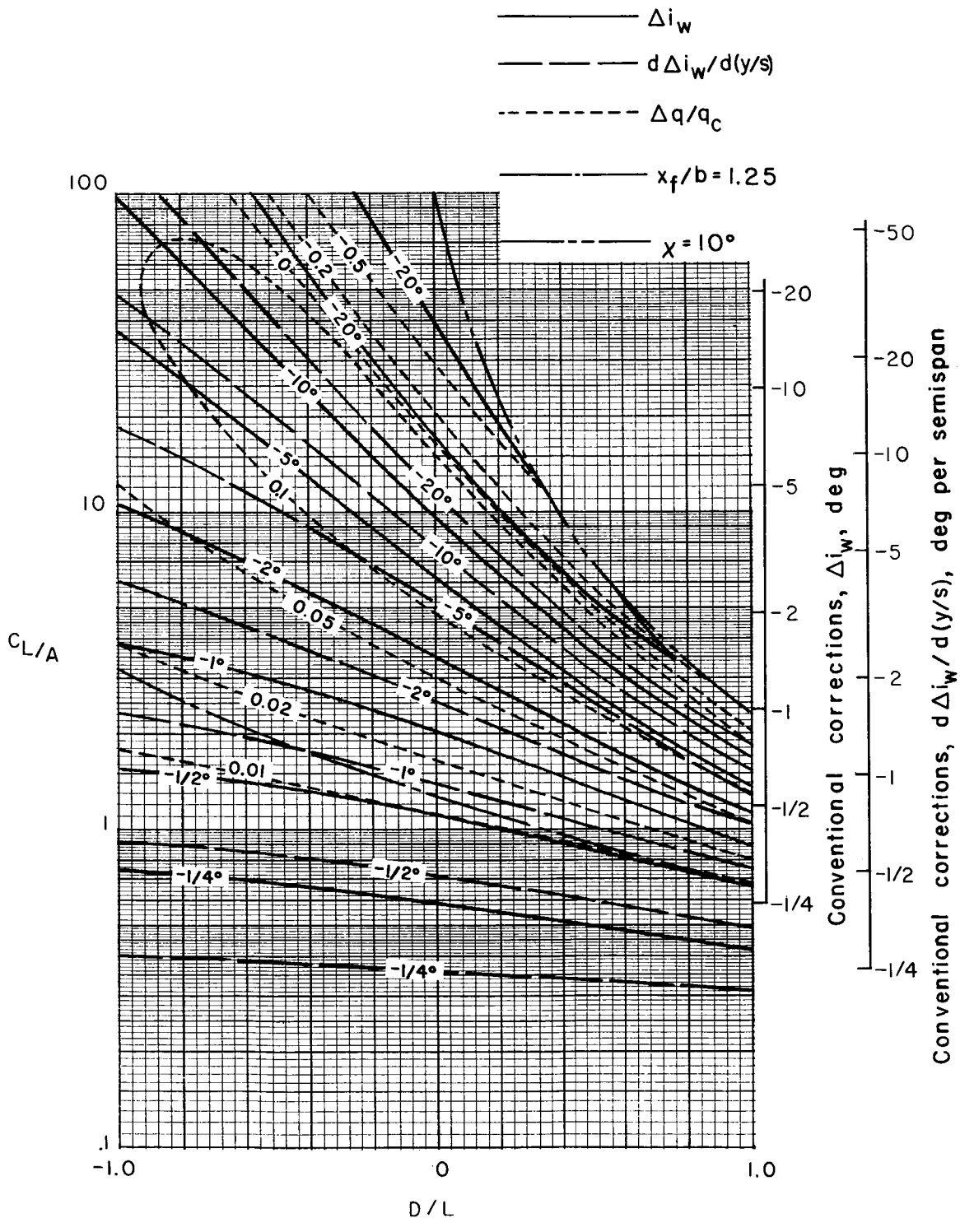


(d) $\sigma = 8/15$.

Figure 17.- Continued.

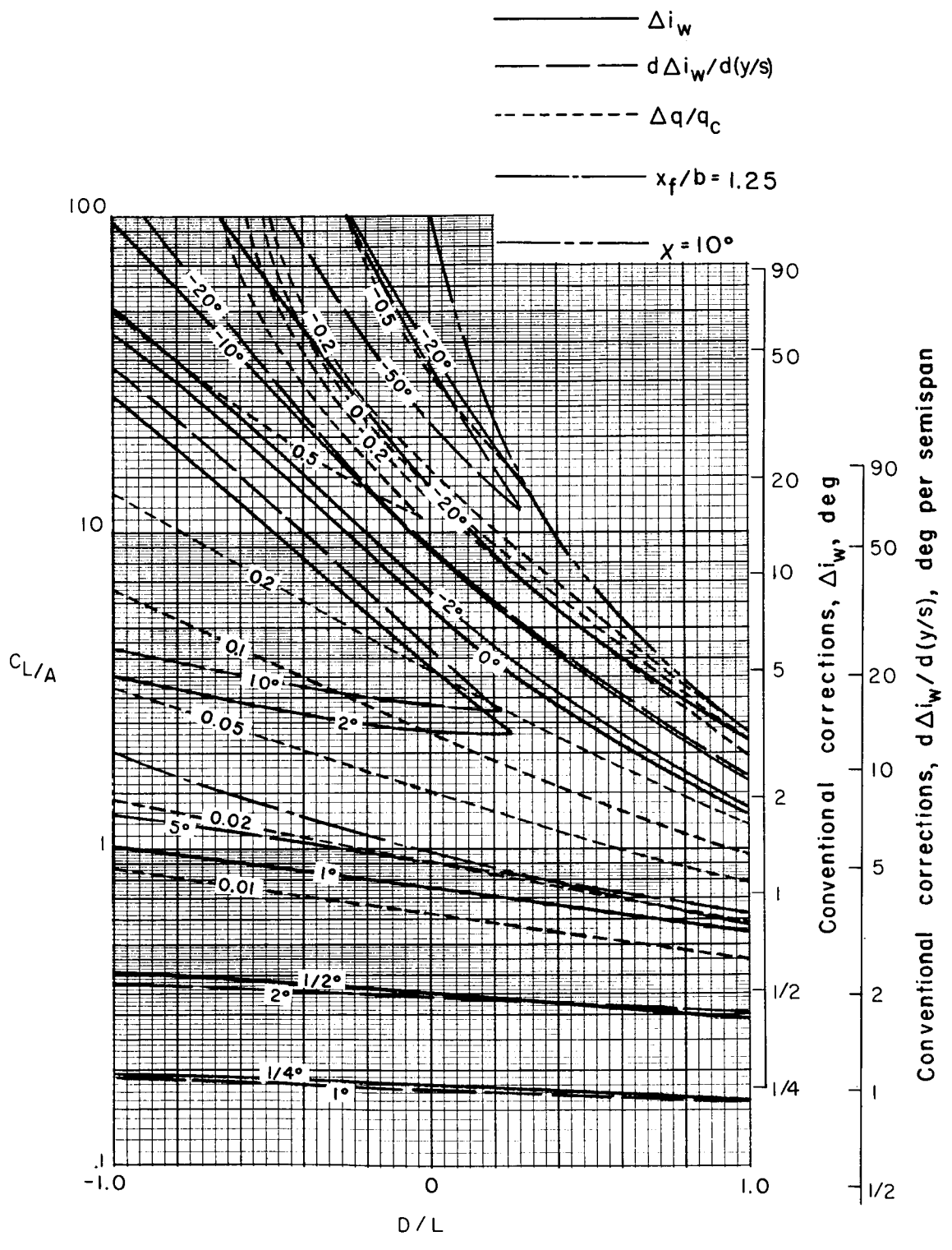


(e) $\sigma = 2/3$.

Figure 17.- Continued.

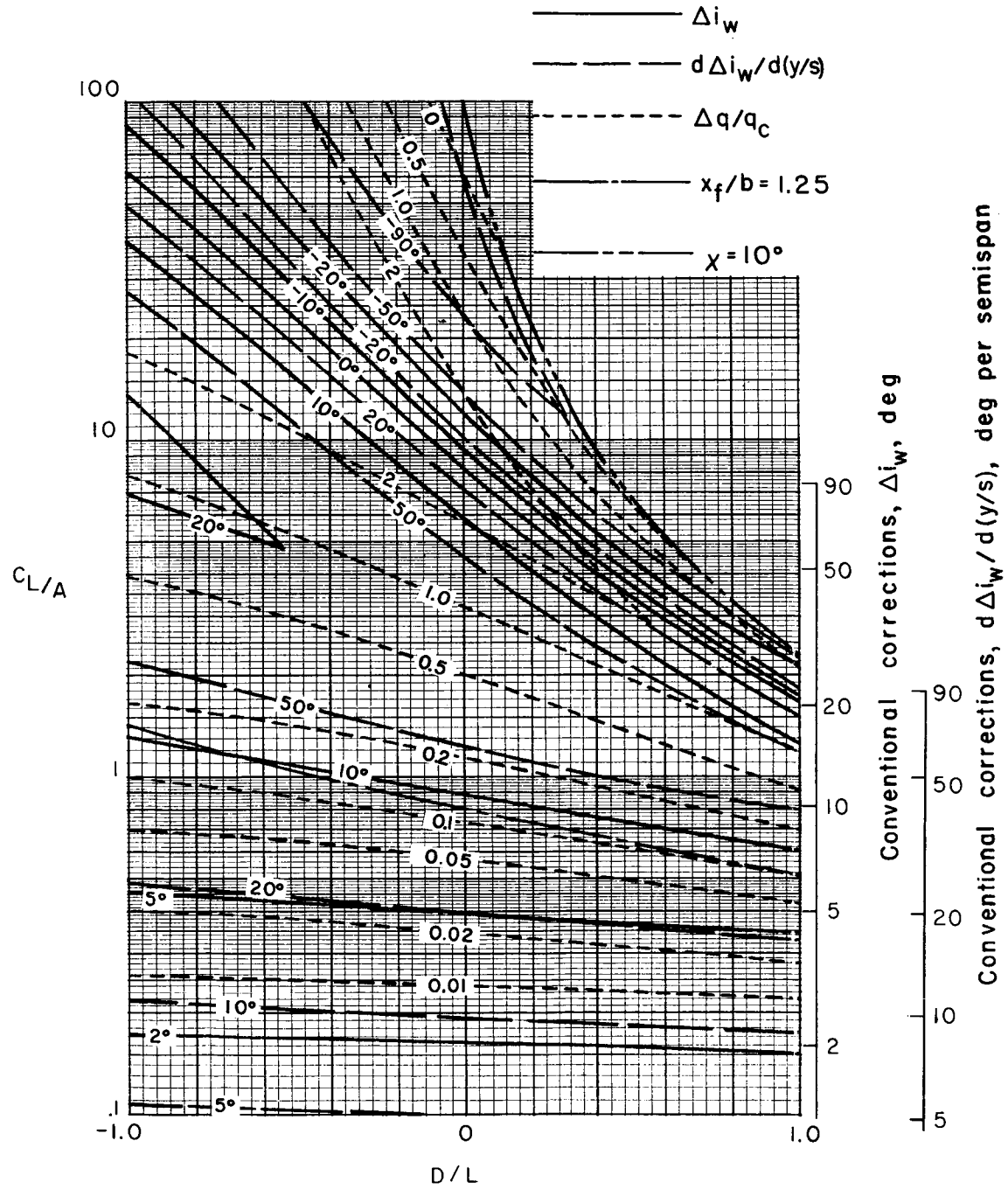


(f) $\sigma = 4/5$.

Figure 17.- Concluded.

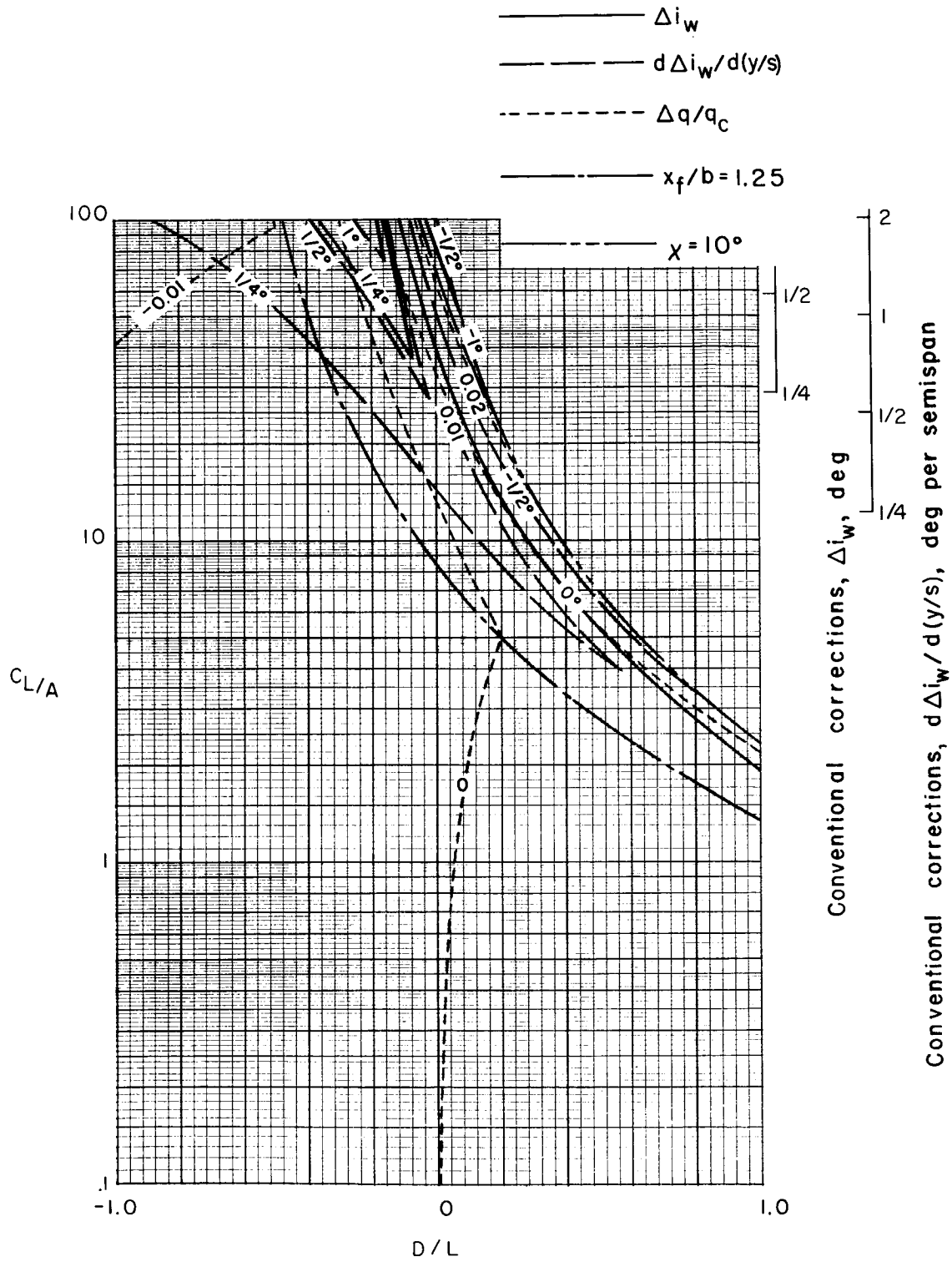


(a) $\sigma = 2/15$.

Figure 18.- Nonuniformity of corrections over a uniformly loaded wing centered in a closed tunnel with semicircular sides. $\gamma = 2$; $\Lambda = 15^0$; $\alpha = 0^0$.

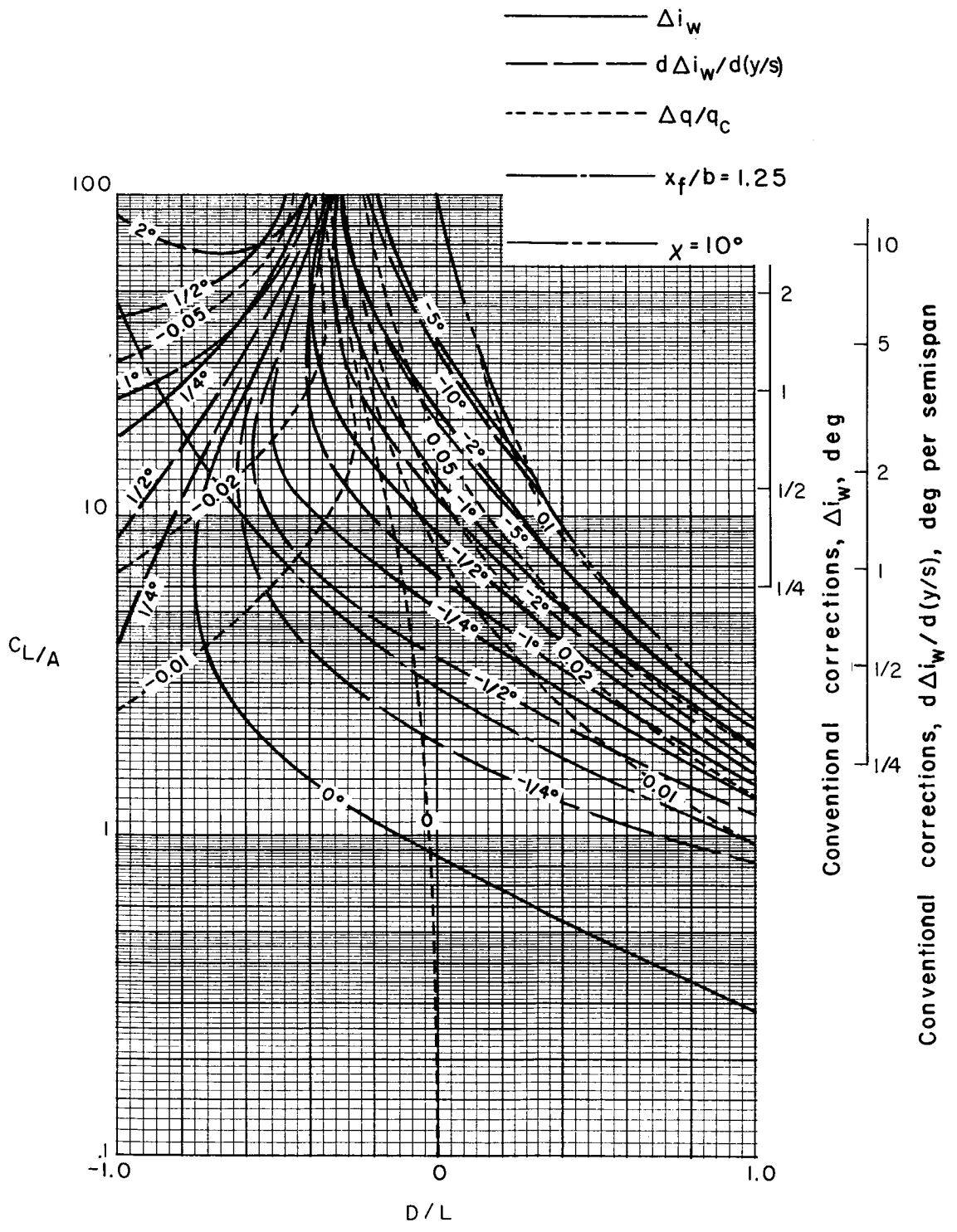


(b) $\sigma = 4/15$.

Figure 18.- Continued.

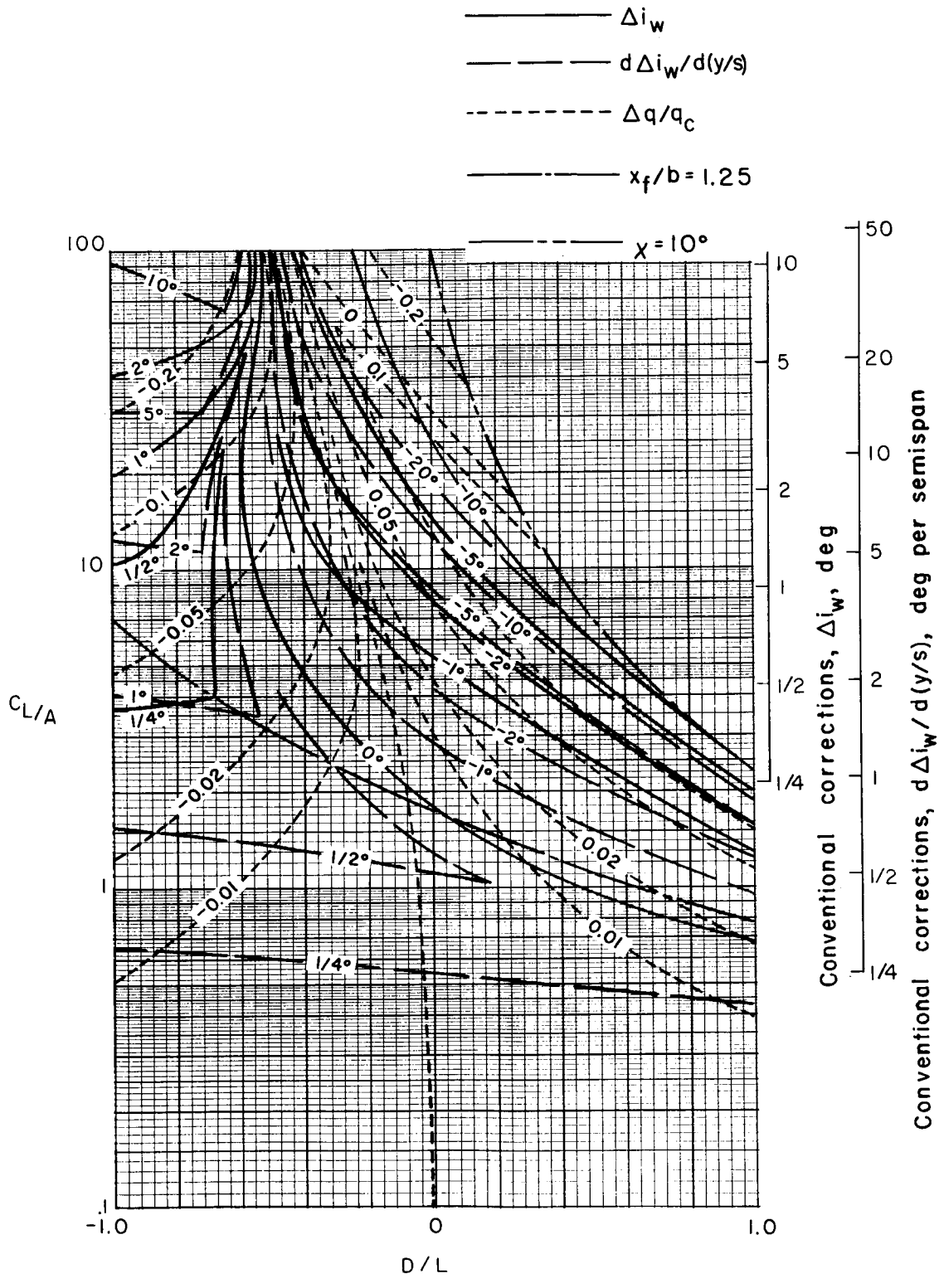


(c) $\sigma = 2/5$.

Figure 18.- Continued.

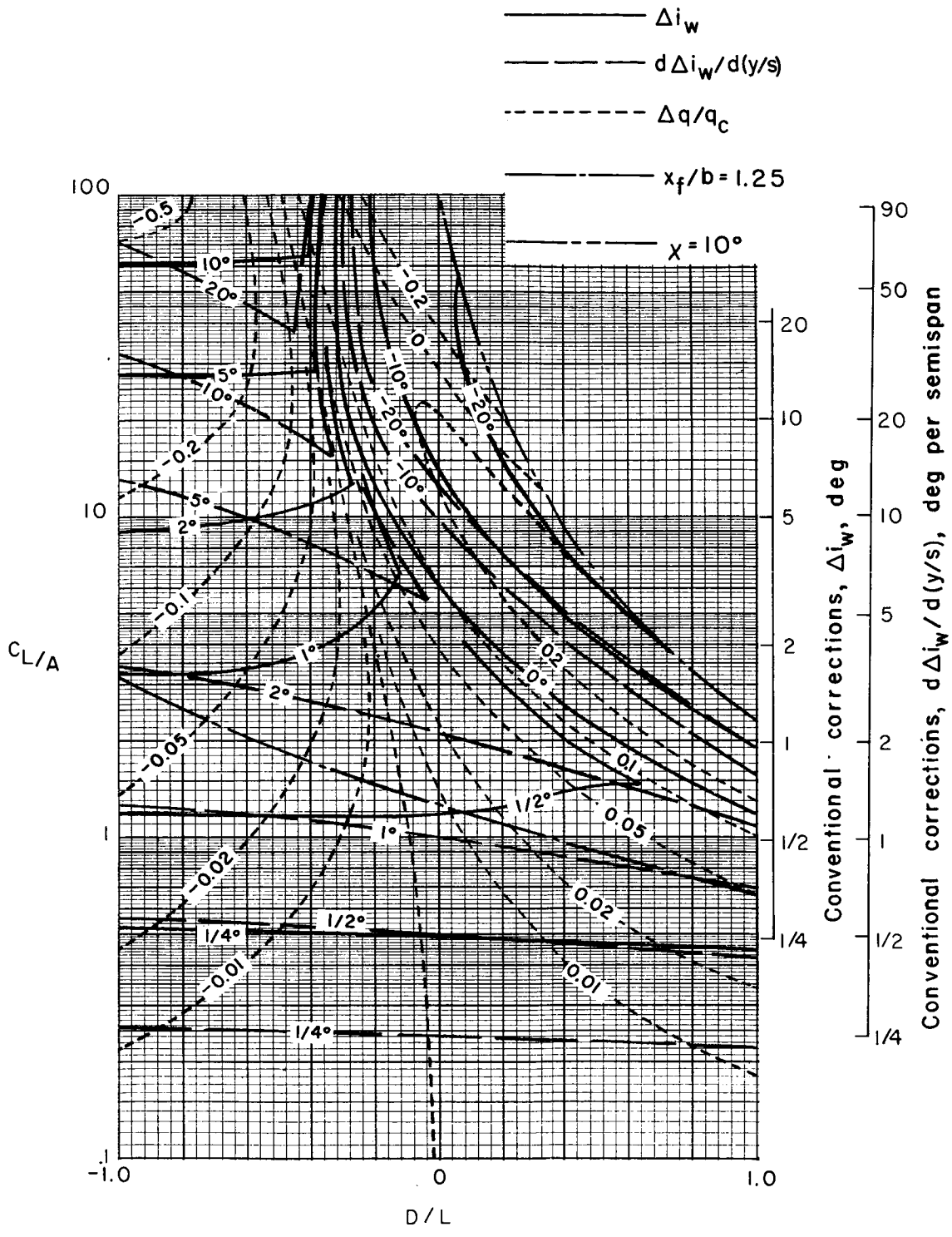


(d) $\sigma = 8/15$.

Figure 18.- Continued.

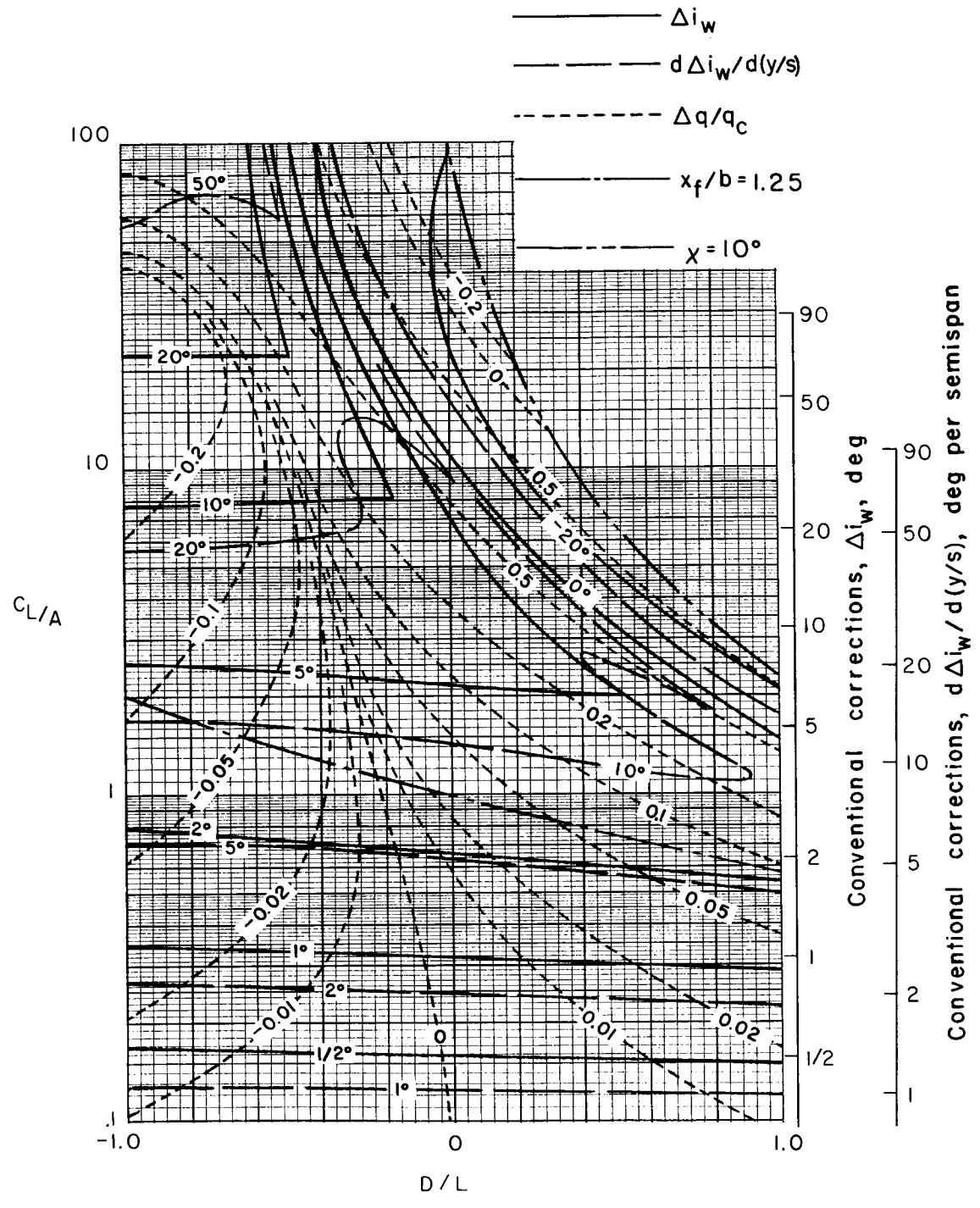


(e) $\sigma = 2/3$.

Figure 18.- Continued.

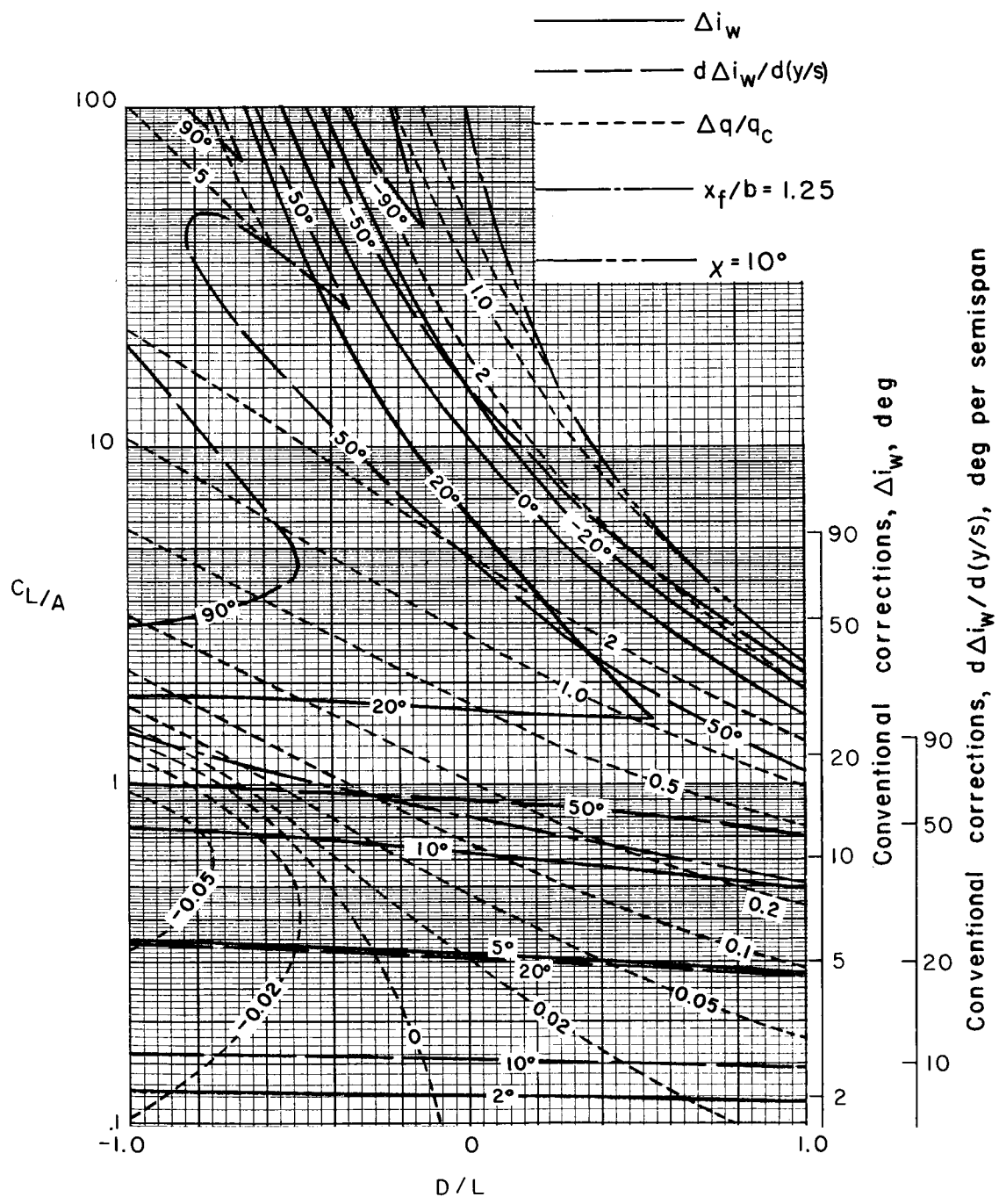


(f) $\sigma = 4/5$.

Figure 18.- Concluded.

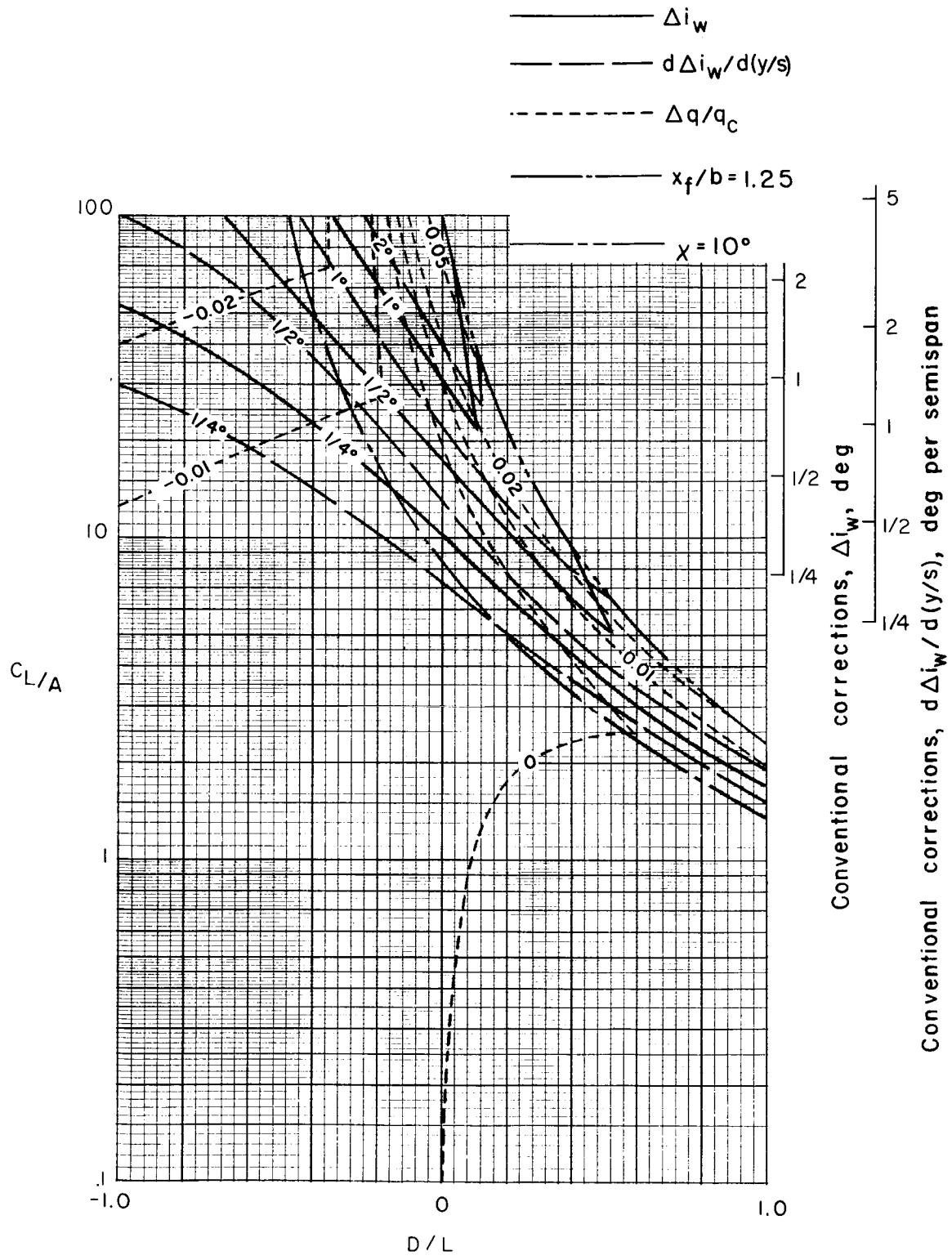


(a) $\sigma = 2/15$.

Figure 19.- Nonuniformity of corrections over a uniformly loaded wing centered in a closed tunnel with semicircular sides. $\gamma = 2$; $\Lambda = 30^0$; $\alpha = 0^0$.

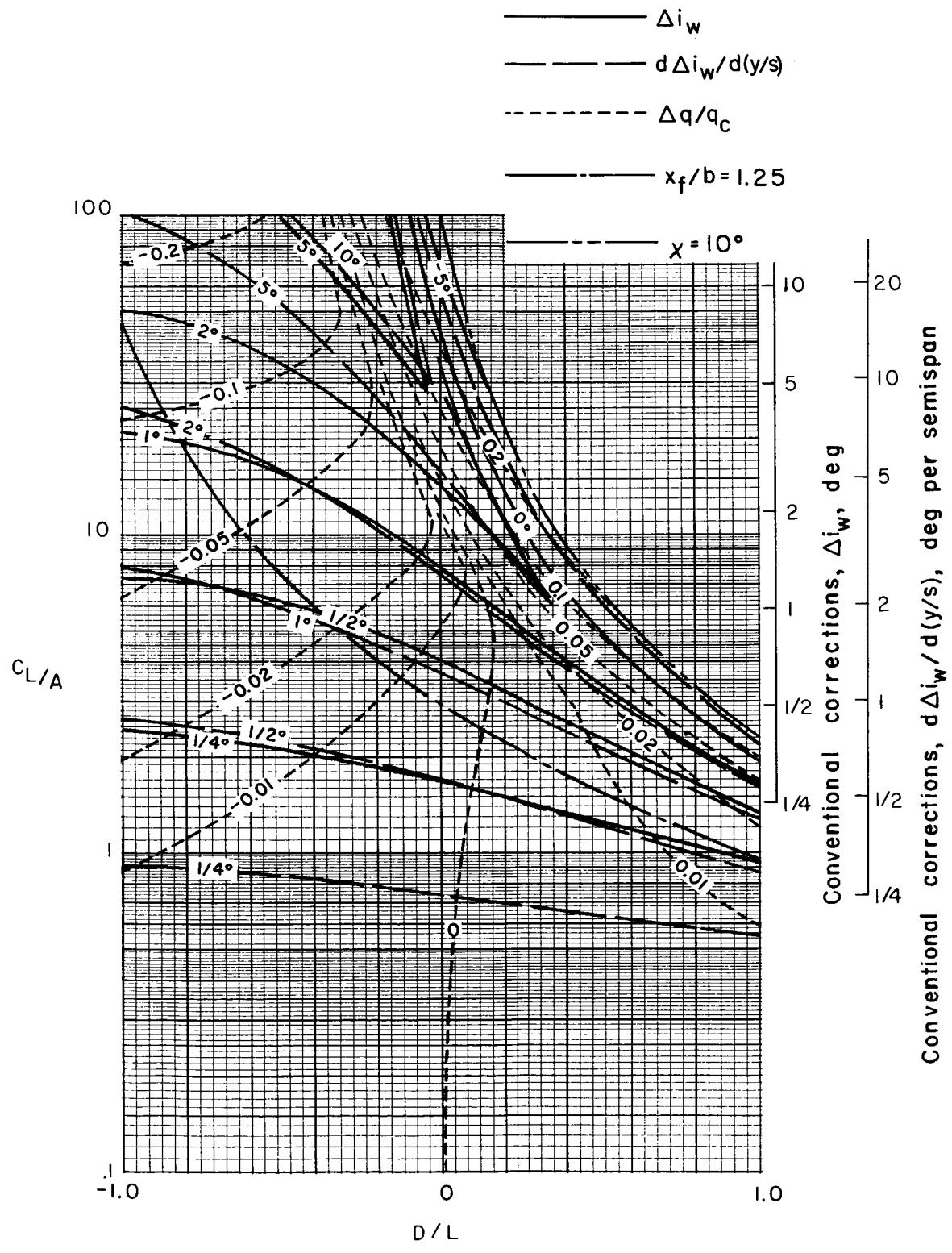


(b) $\sigma = 4/15$.

Figure 19.- Continued.

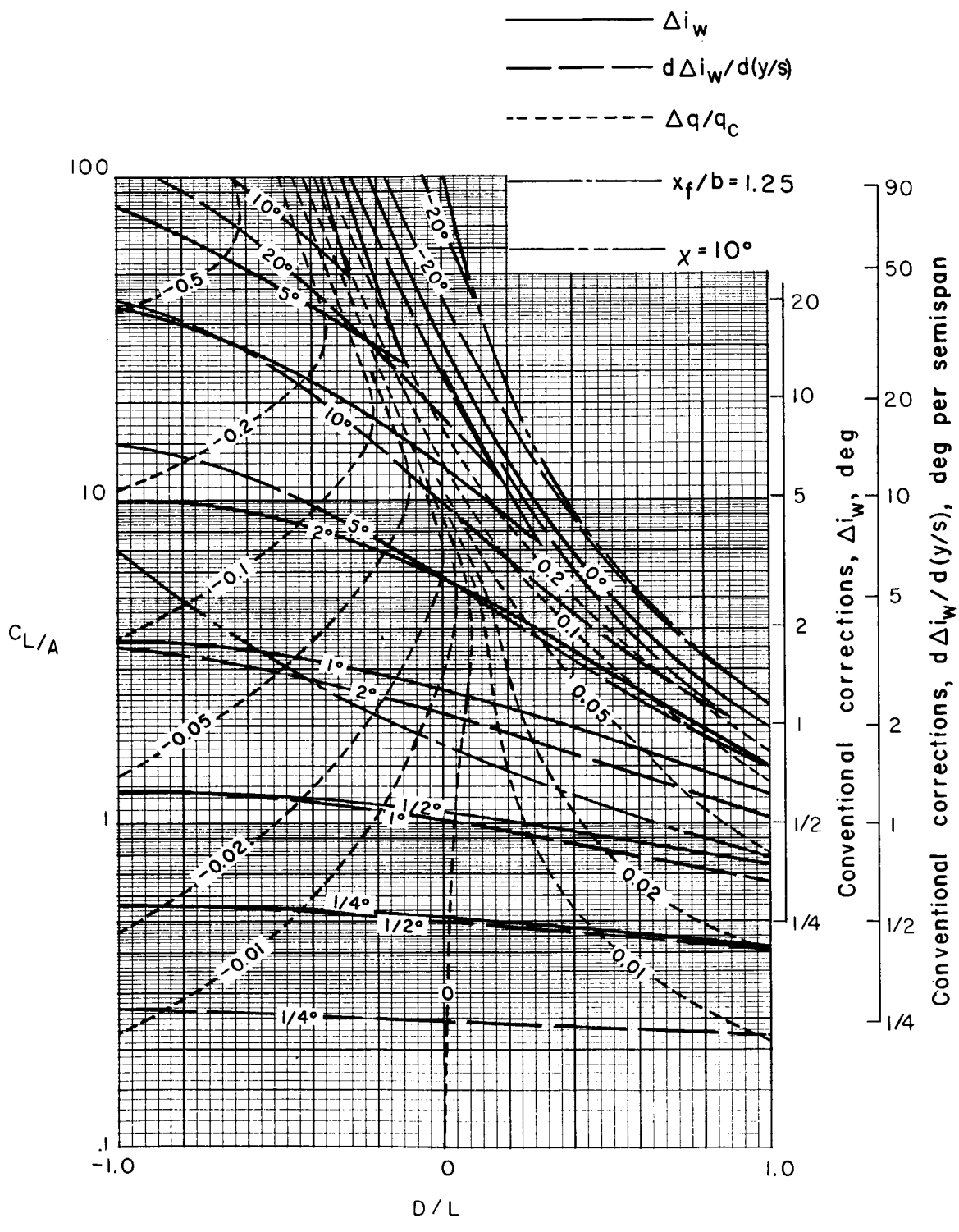


(c) $\sigma = 2/5$.

Figure 19.- Continued.

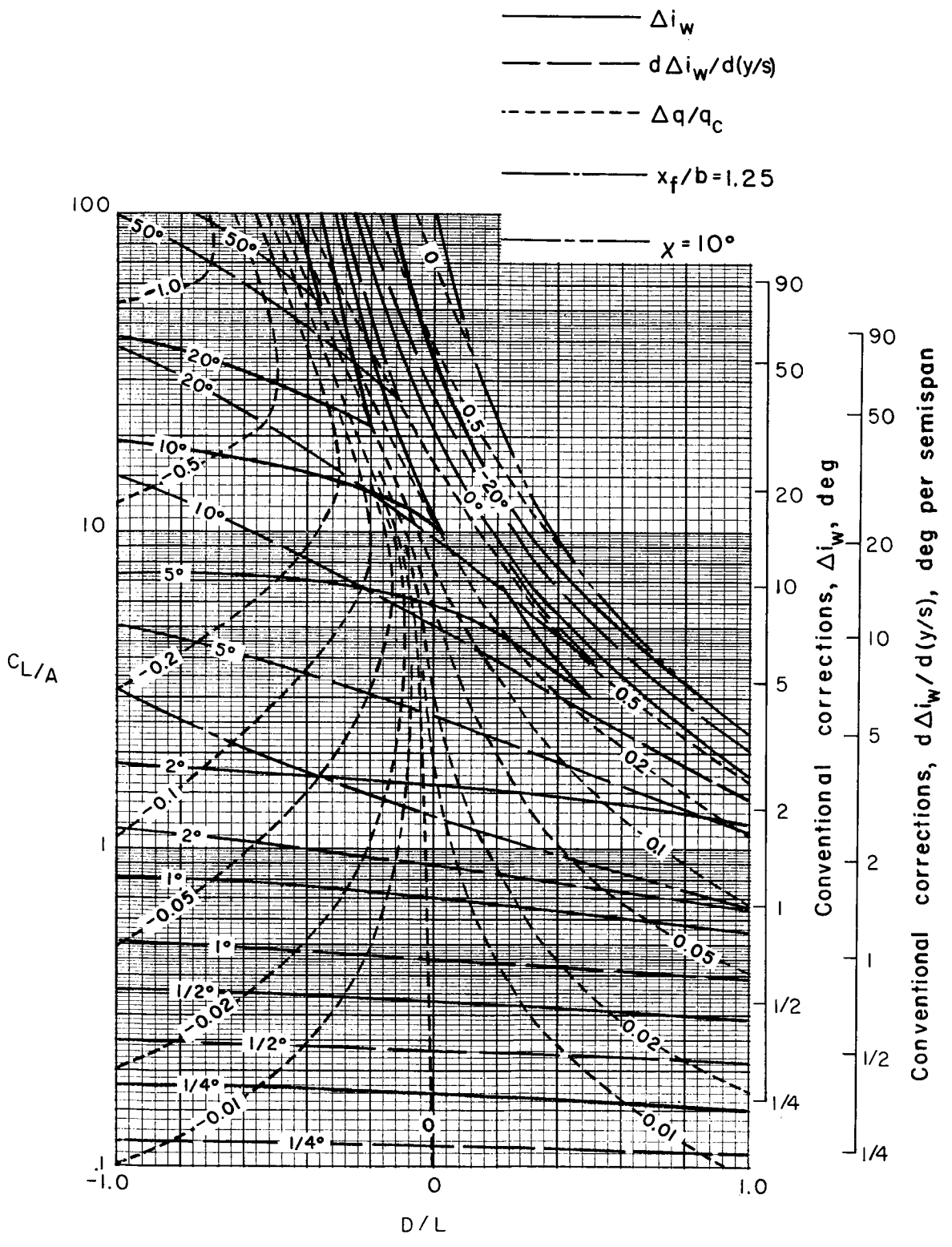


(d) $\sigma = 8/15$.

Figure 19.- Continued.

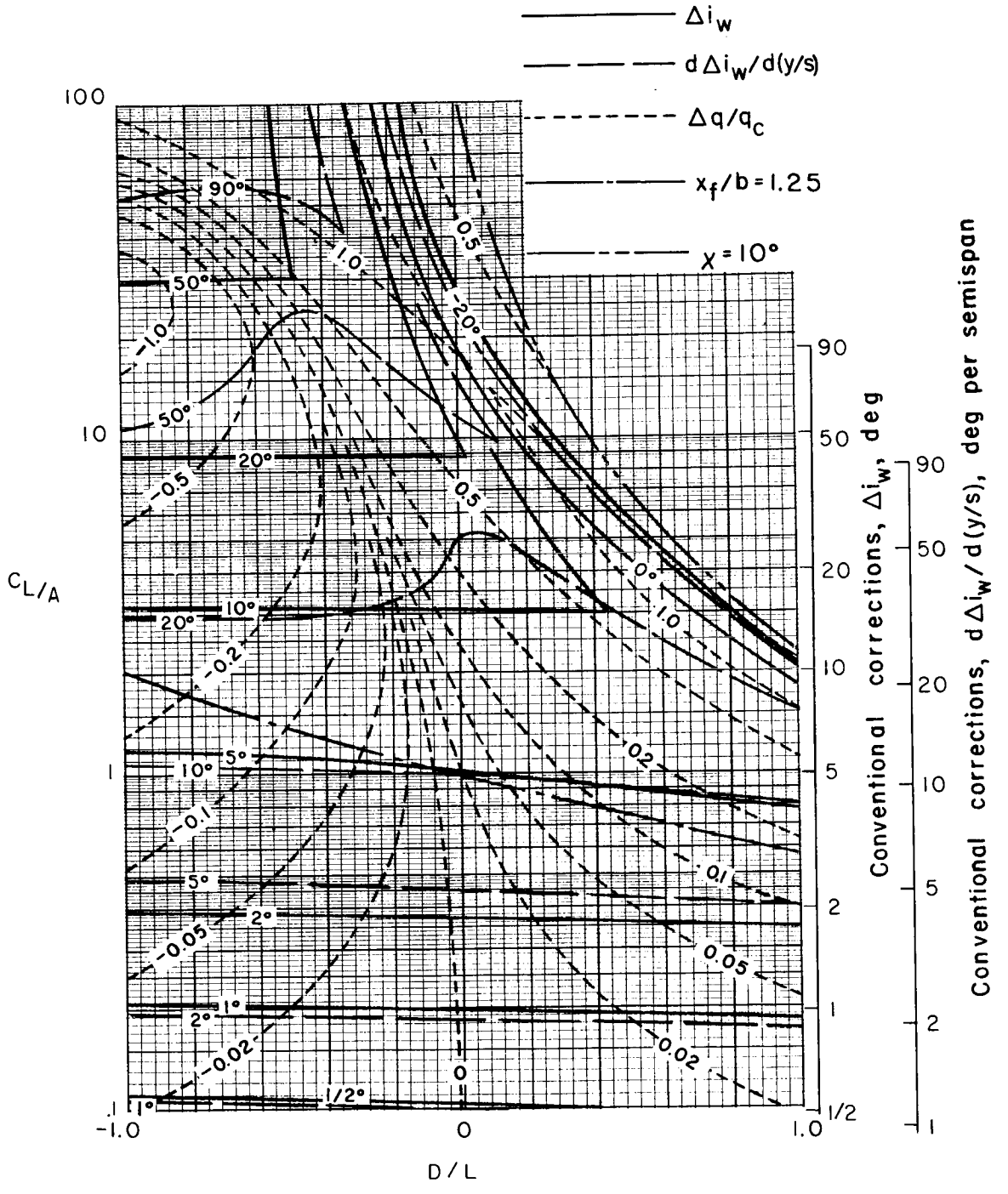


(e) $\sigma = 2/3$.

Figure 19.- Continued.

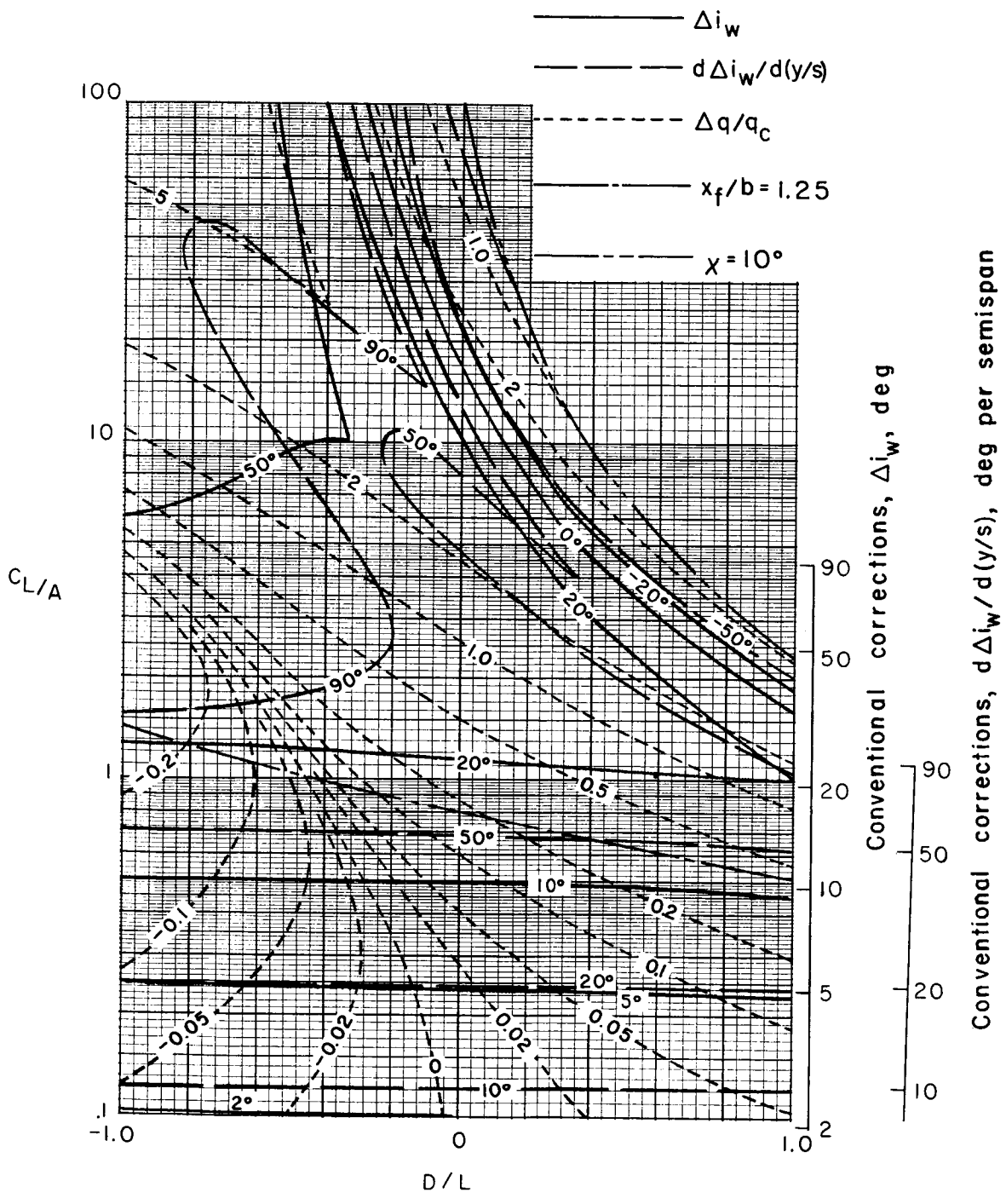


(f) $\sigma = 4/5$.

Figure 19.- Concluded.

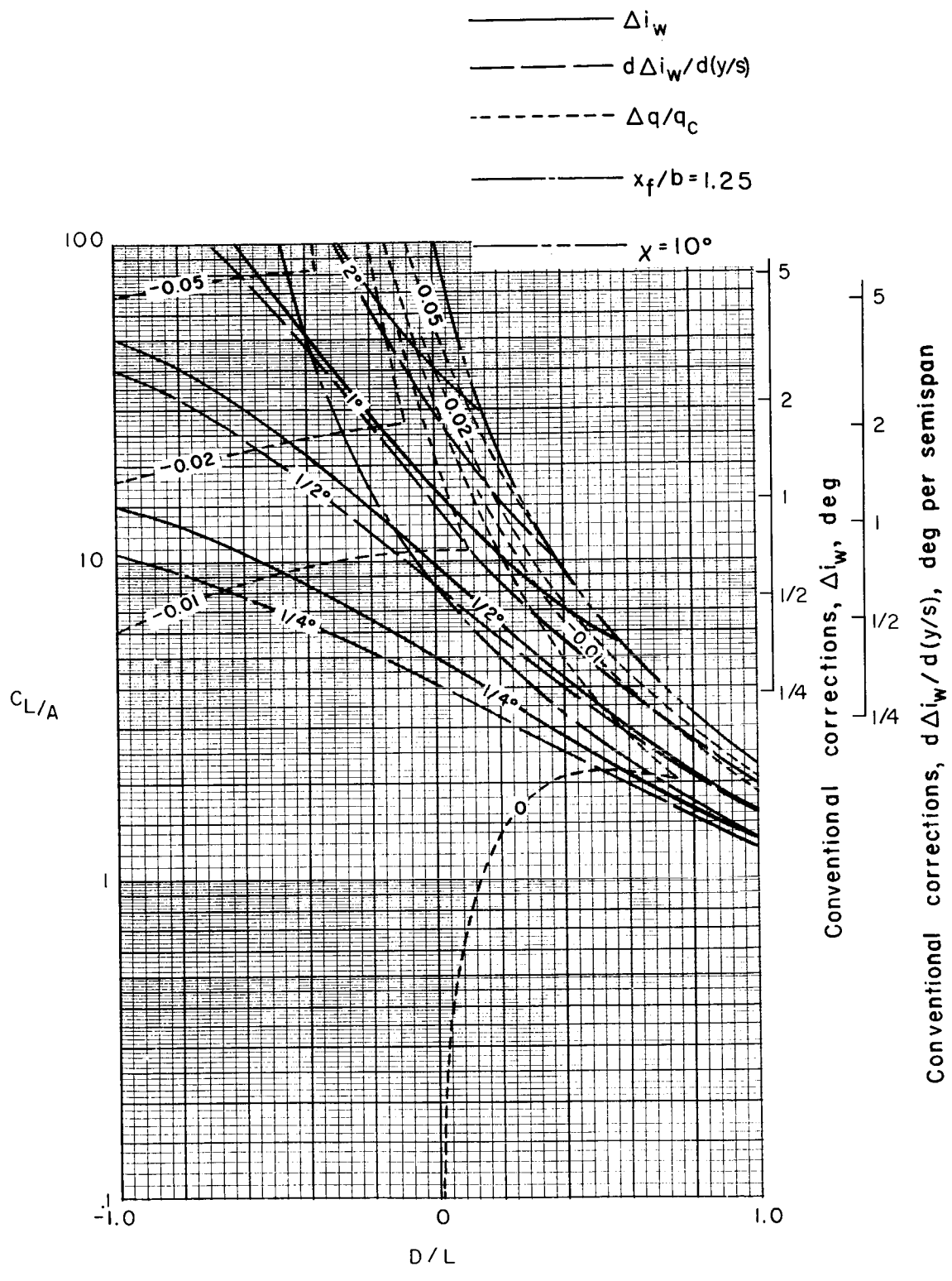


(a) $\sigma = 2/15$.

Figure 20.- Nonuniformity of corrections over a uniformly loaded wing centered in a closed tunnel with semicircular sides. $\gamma = 2$; $\Lambda = 45^0$; $\alpha = 0^0$.

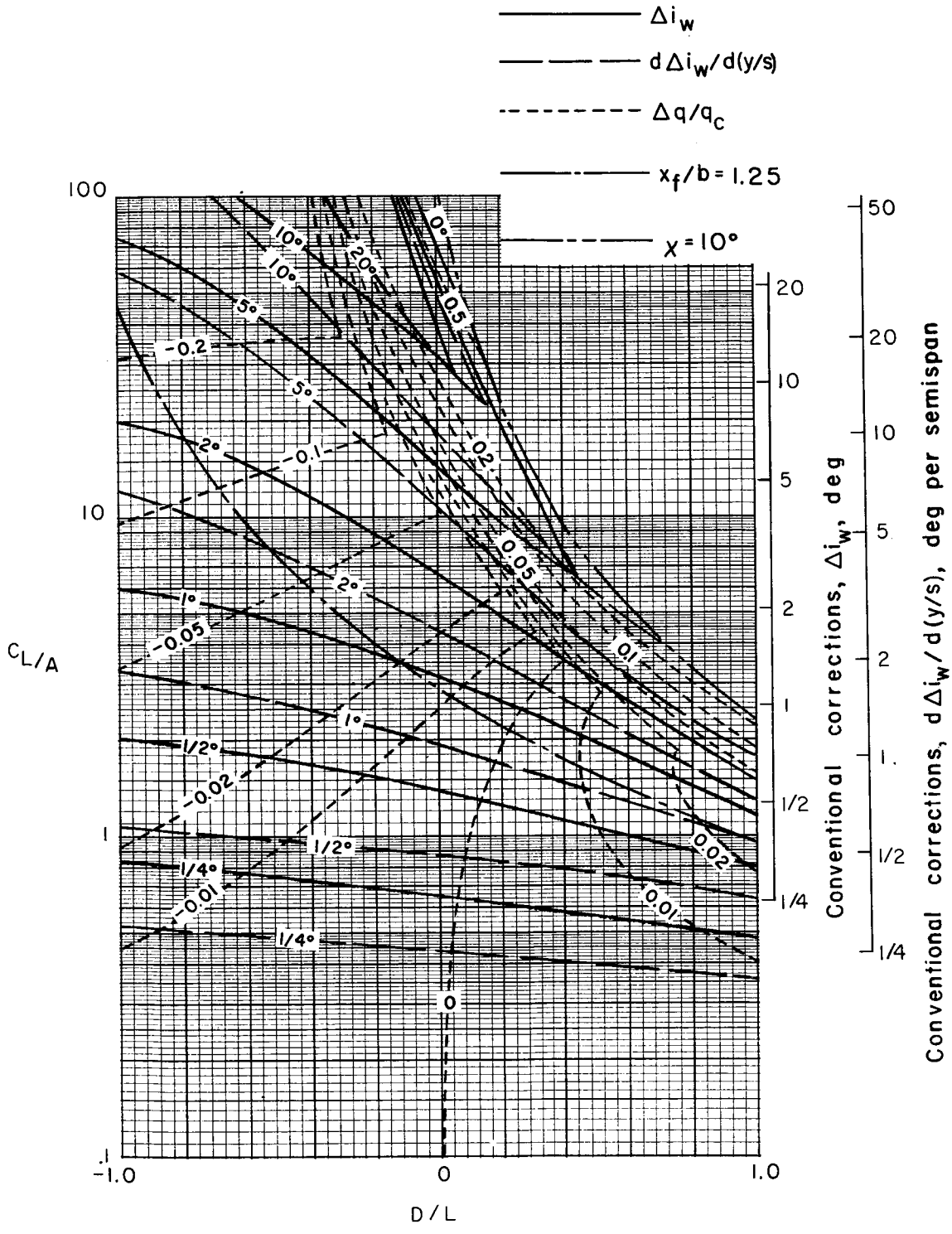


(b) $\sigma = 4/15$.

Figure 20.- Continued.

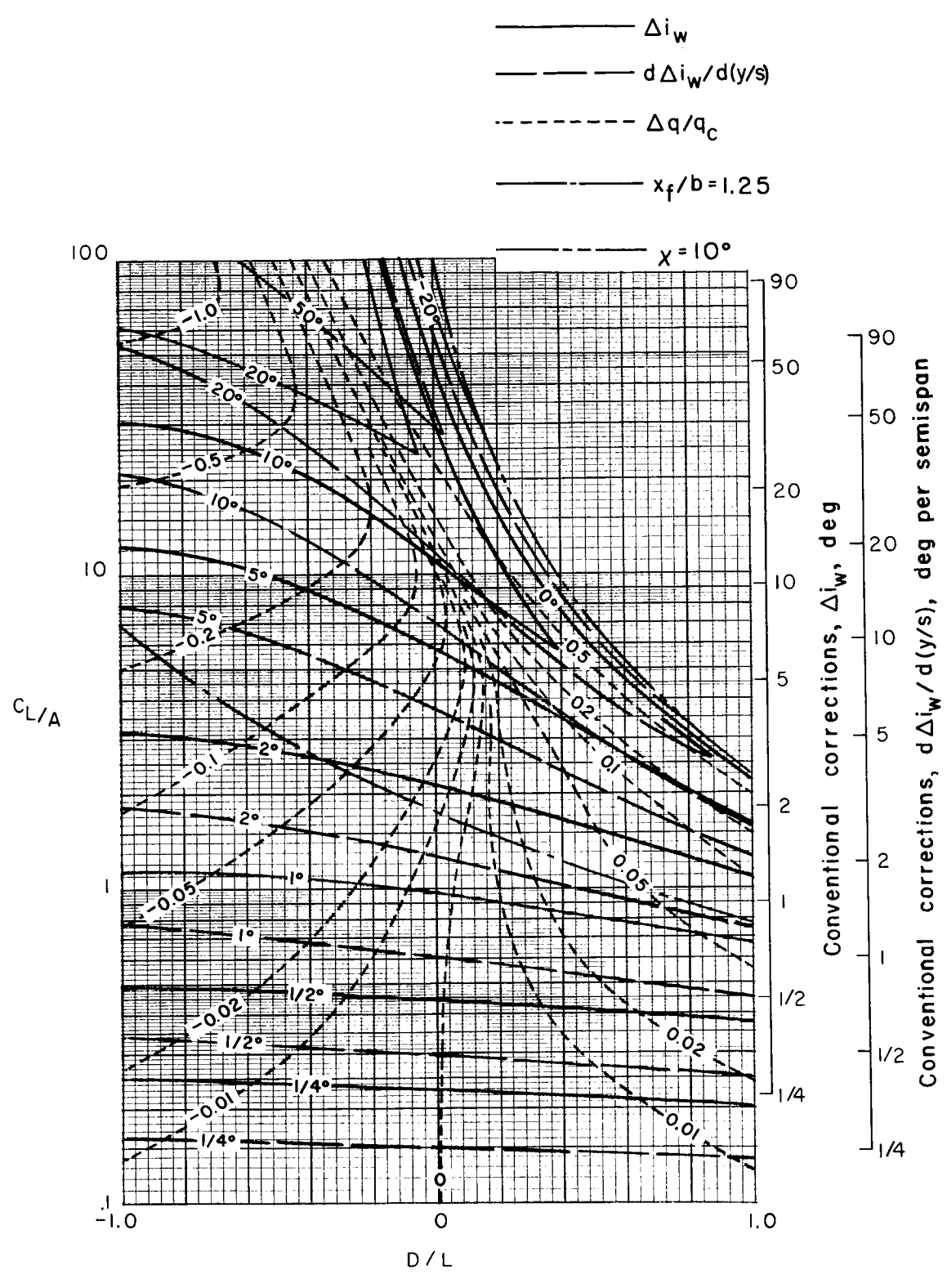


(c) $\sigma = 2/5$.

Figure 20.- Continued.

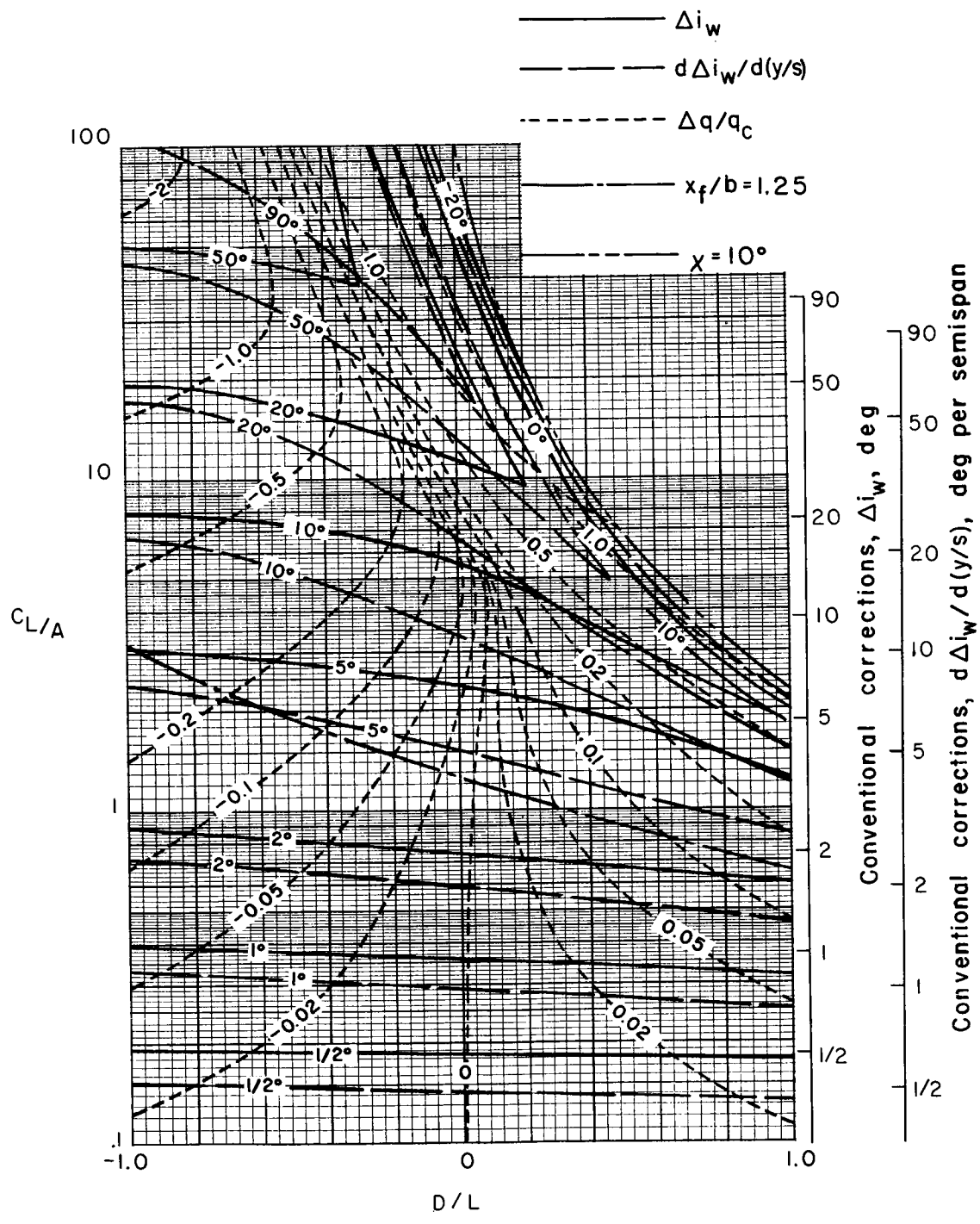


(d) $\sigma = 8/15$.

Figure 20.- Continued.

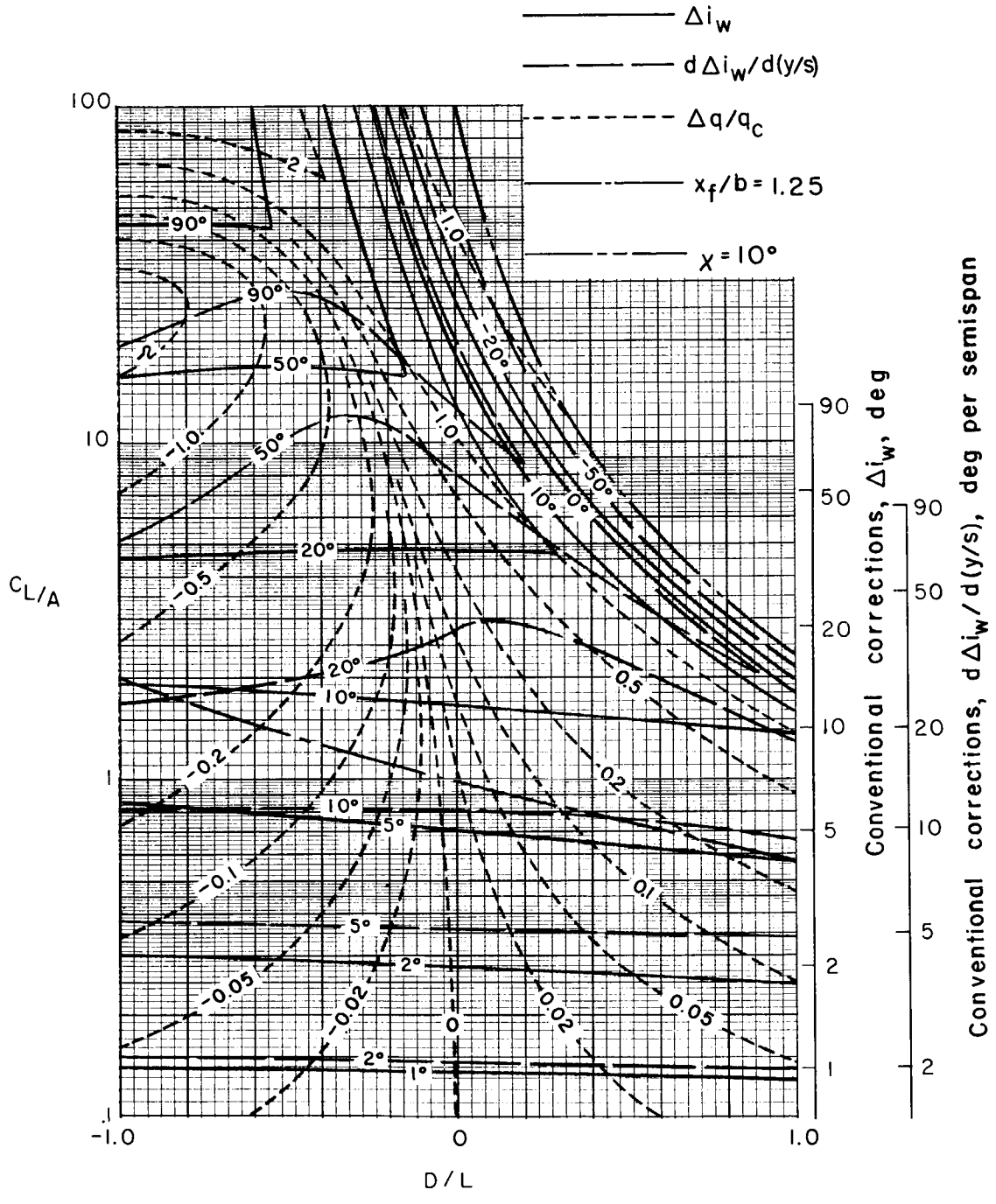


(e) $\sigma = 2/3$.

Figure 20.- Continued.

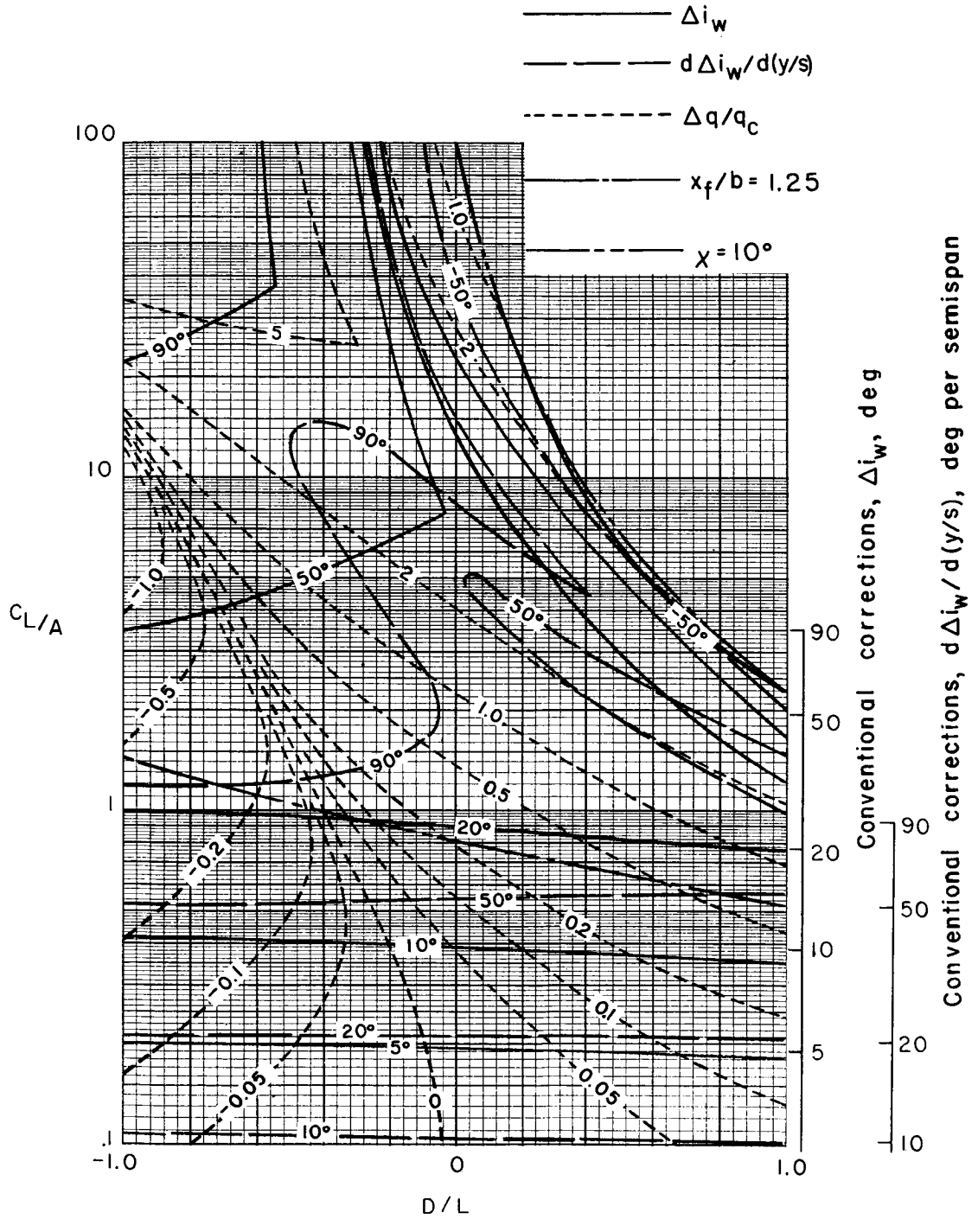


(f) $\sigma = 4/5$.

Figure 20.- Concluded.

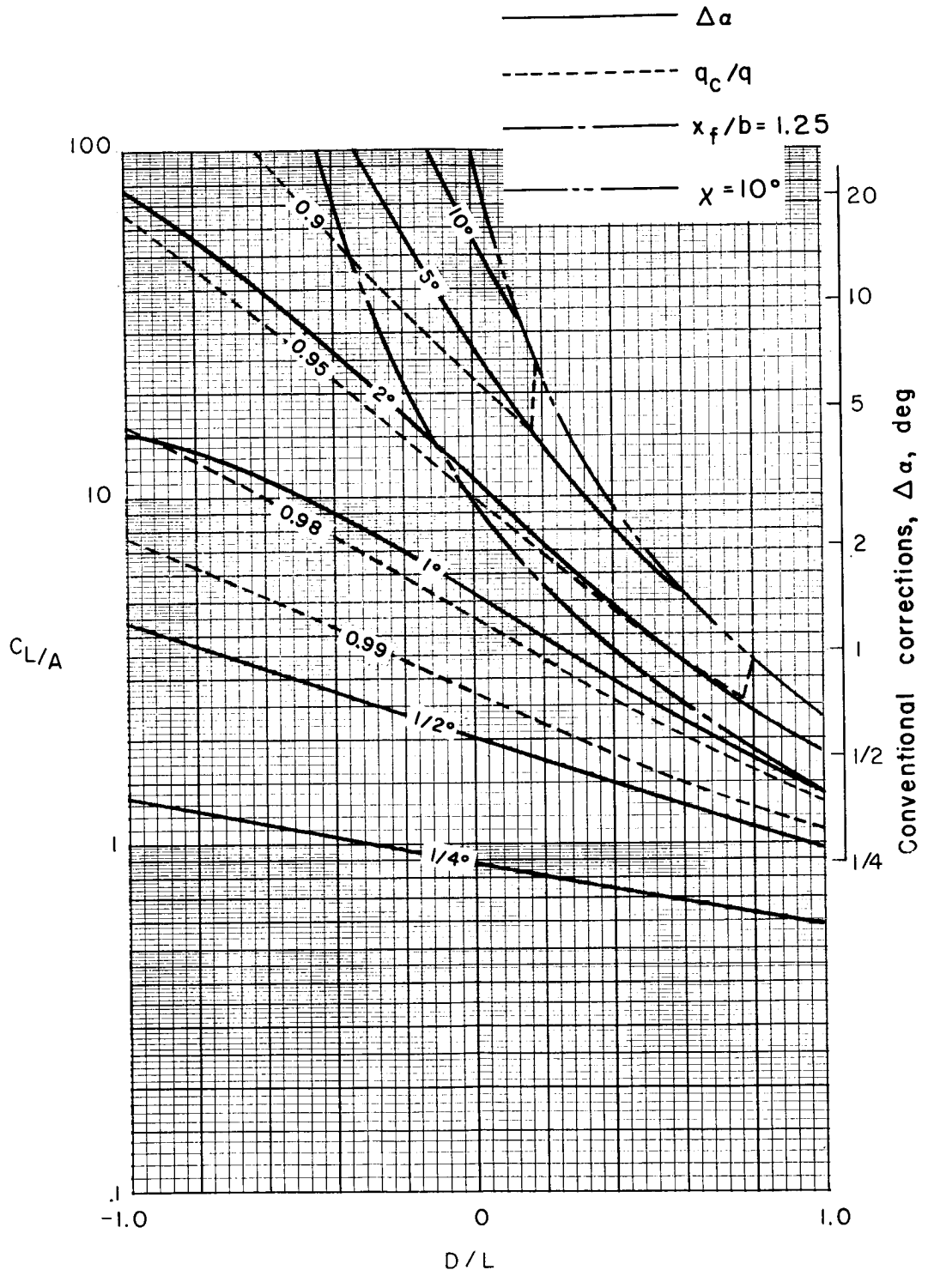


(a) σ = 1/6.

Figure 21.- Average corrections for a uniformly loaded wing centered in a closed rectangular tunnel. γ = 1.5; Λ = 0°.

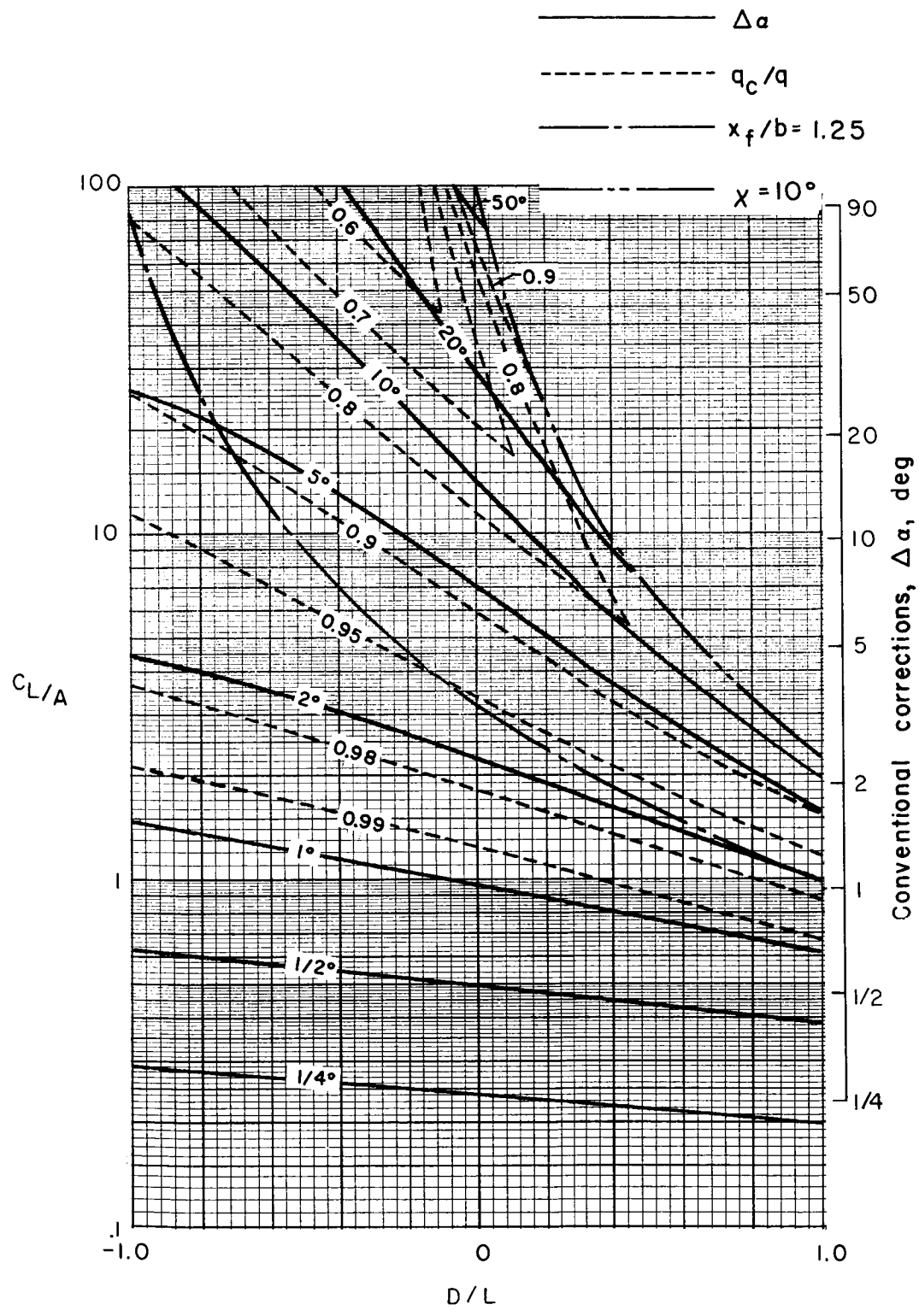


(b) σ = 1/3.

Figure 21.- Continued.

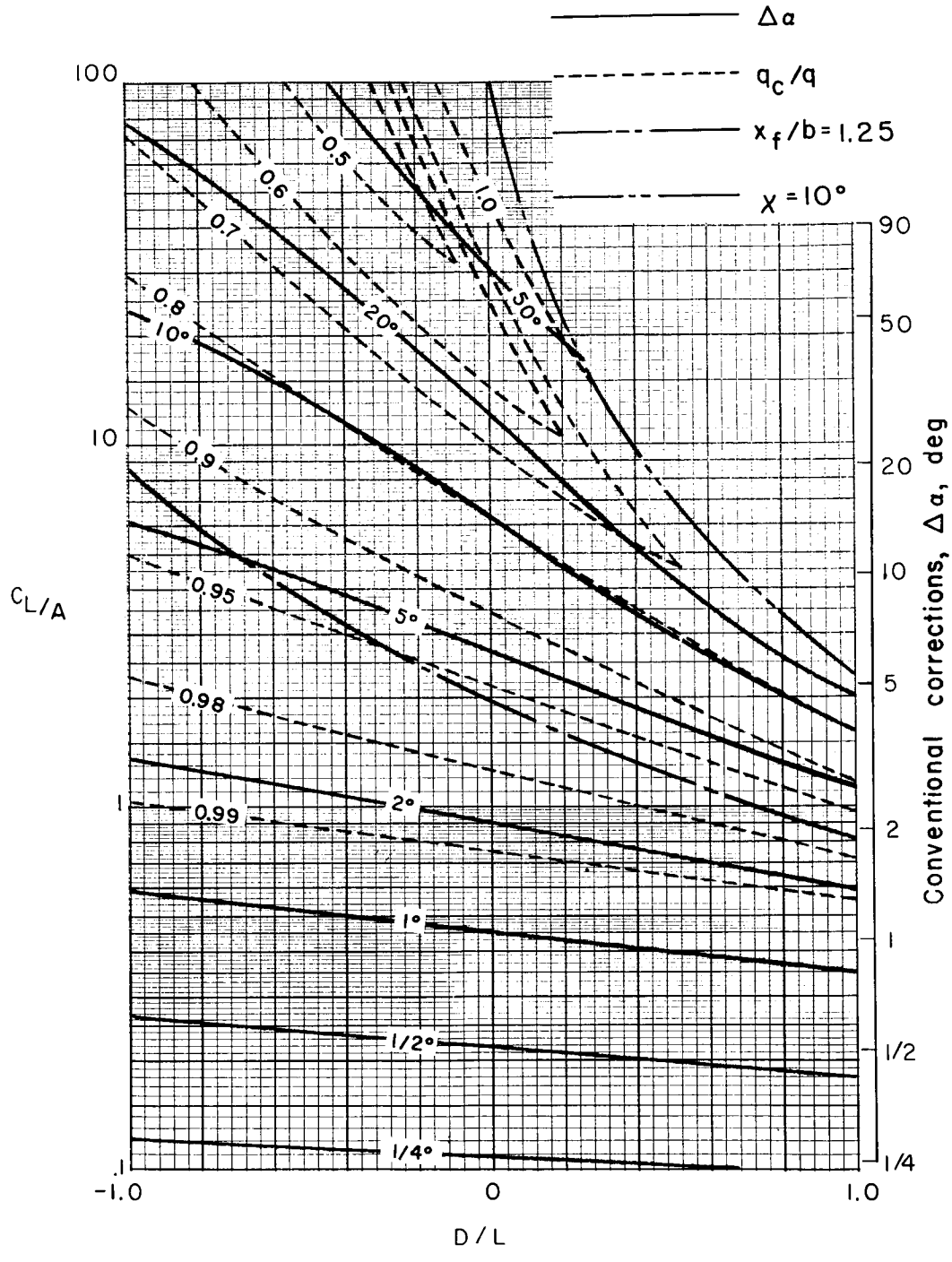


(c) $\sigma = 1/2$.

Figure 21.- Continued.

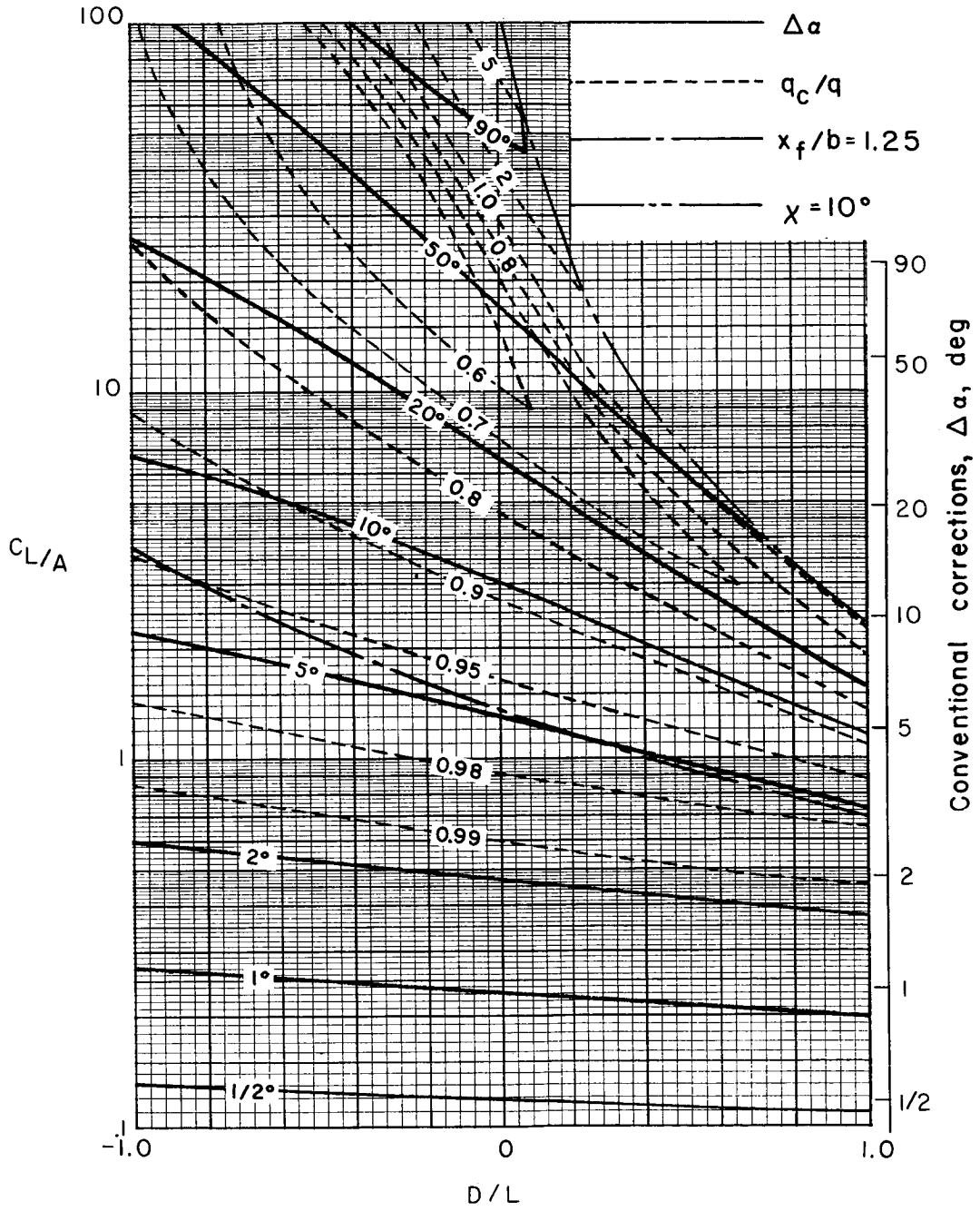


(d) σ = 2/3.

Figure 21.- Continued.

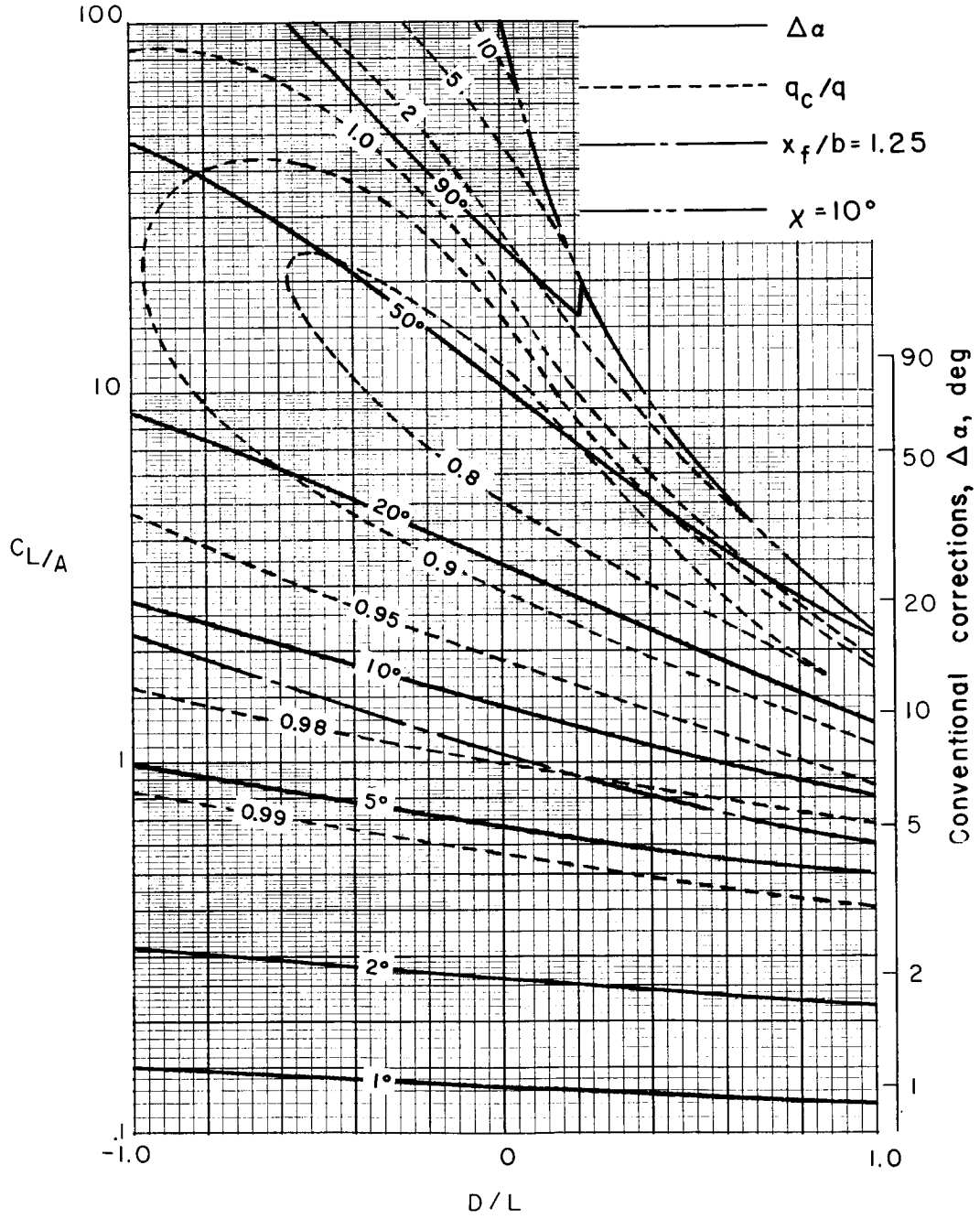


(e) $\sigma = 5/6$.

Figure 21.- Concluded.

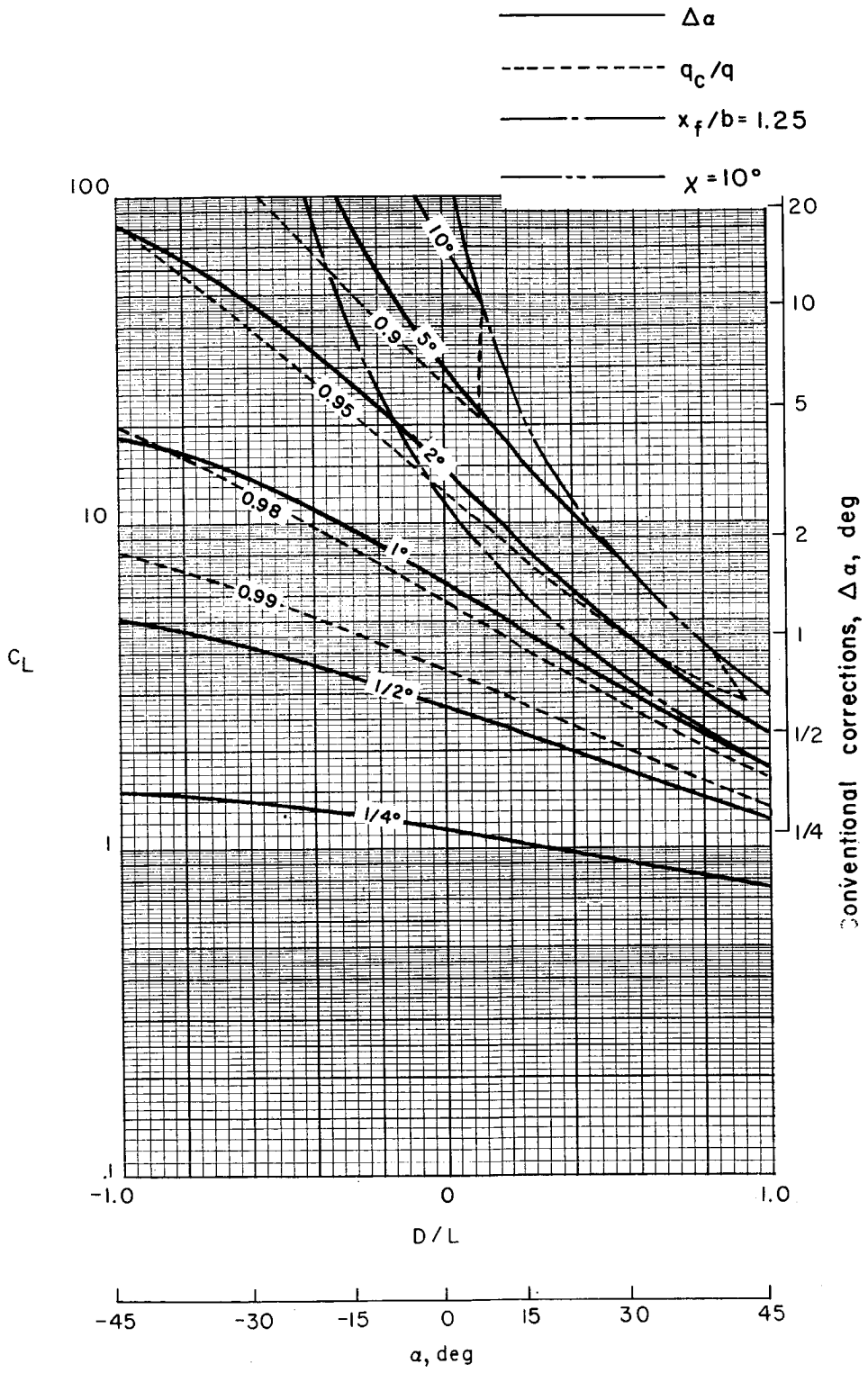


(a) σ = 1/6.

Figure 22.- Average corrections for a uniformly loaded rotor centered in a closed rectangular tunnel. γ = 1.5.

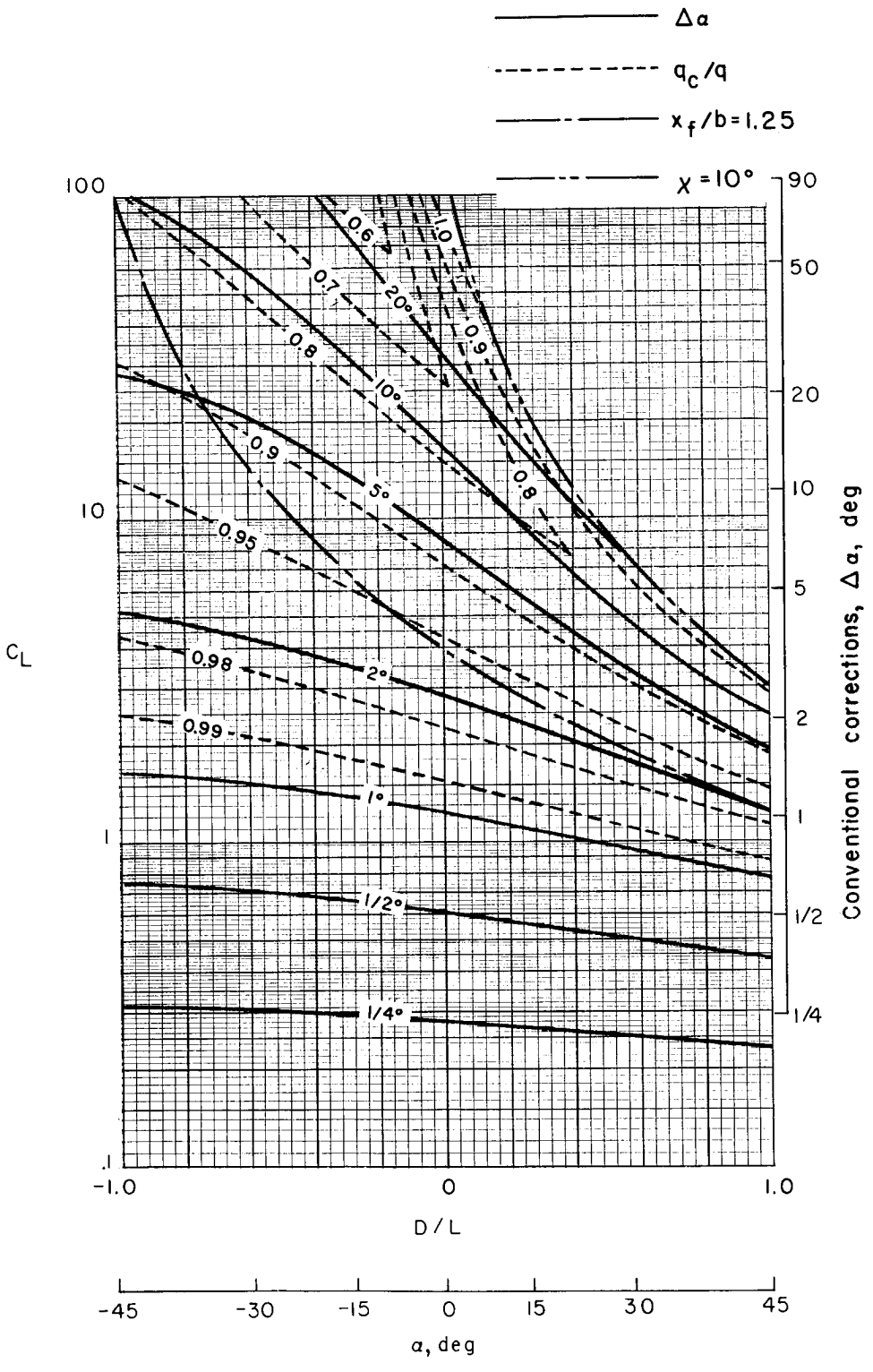


(b) σ = 1/3.

Figure 22.- Continued.

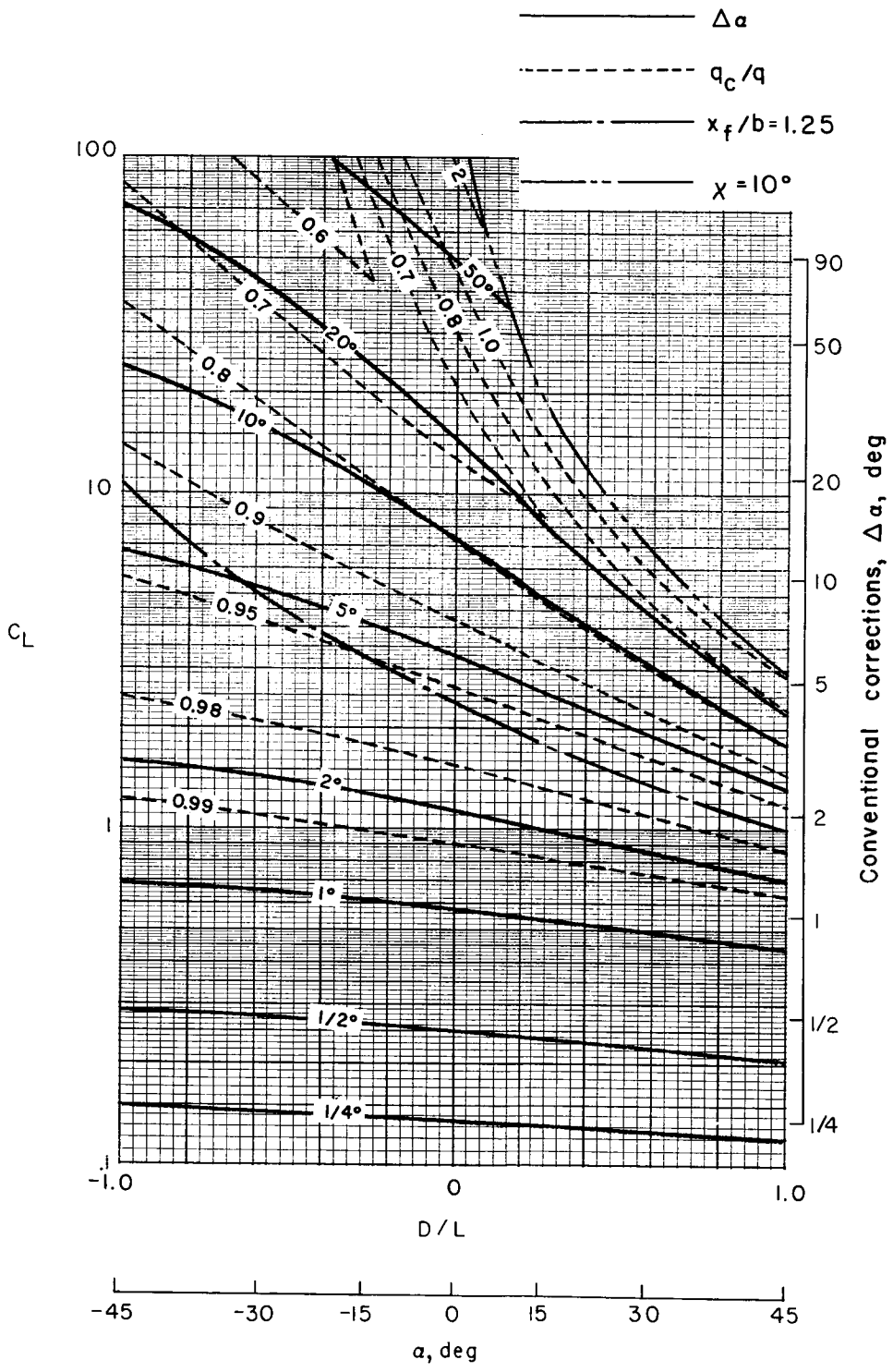


(c) σ = 1/2.

Figure 22.- Continued.

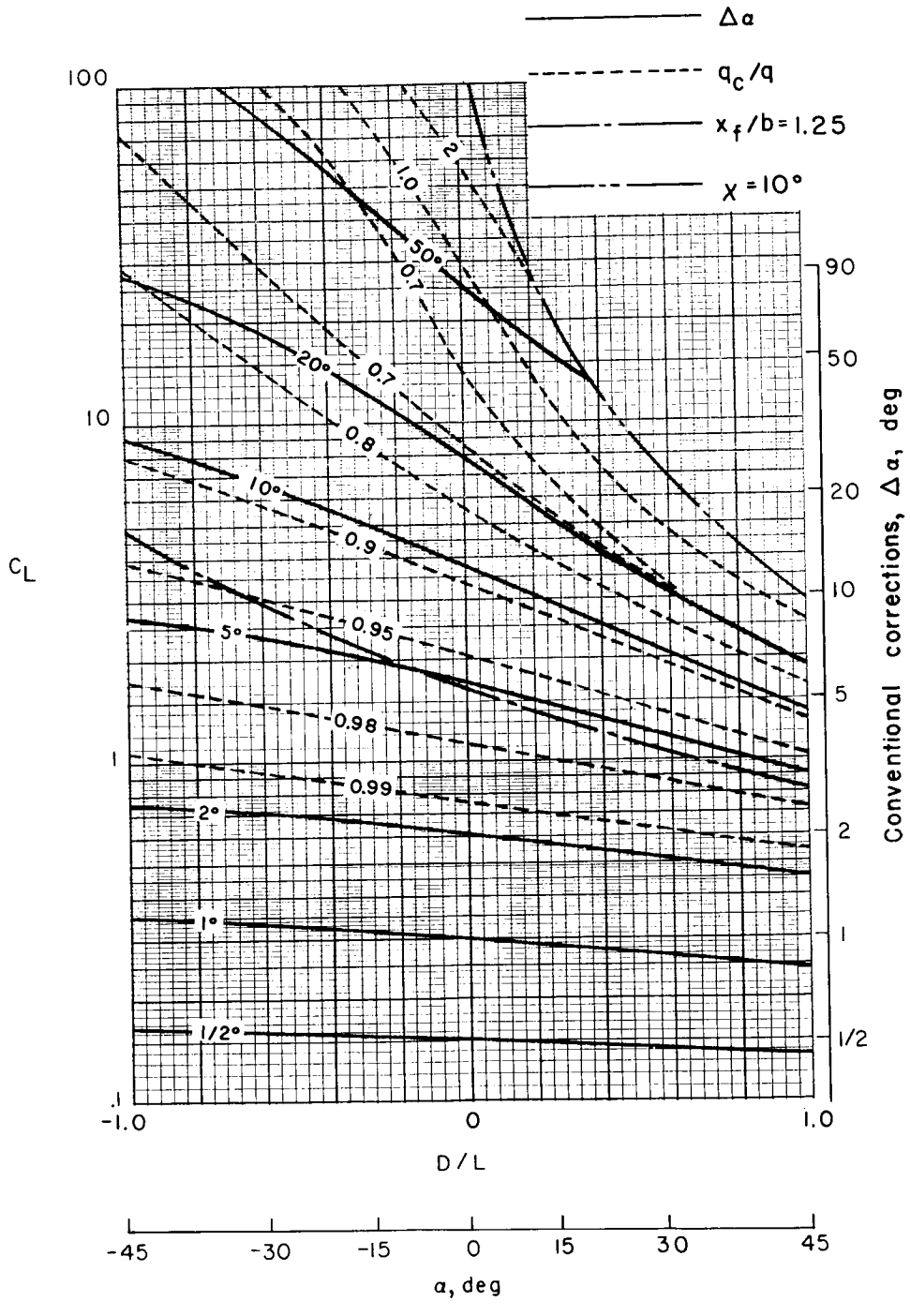


(d) σ = 2/3.

Figure 22.- Continued.

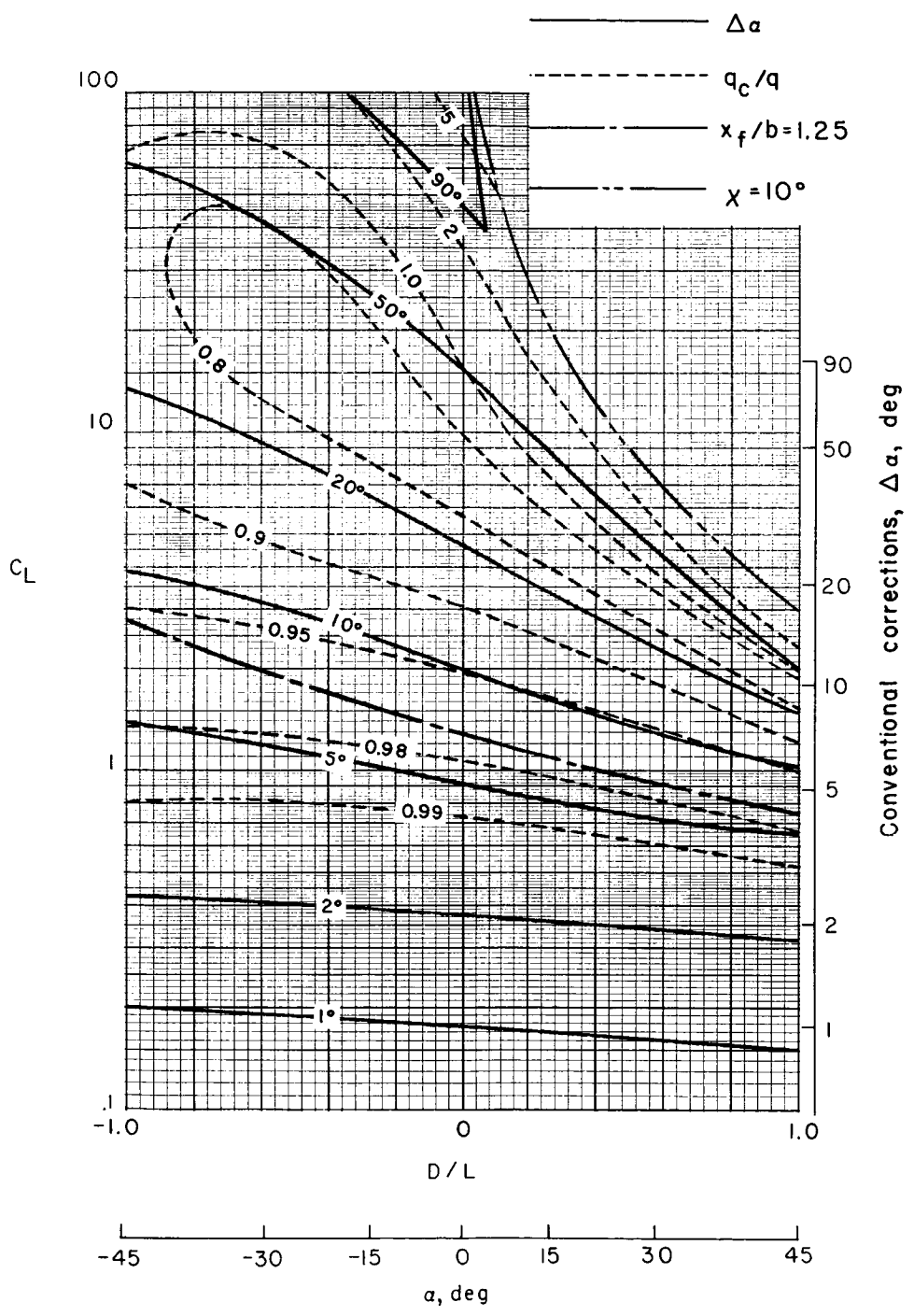


(e) σ = 5/6.

Figure 22.- Concluded.

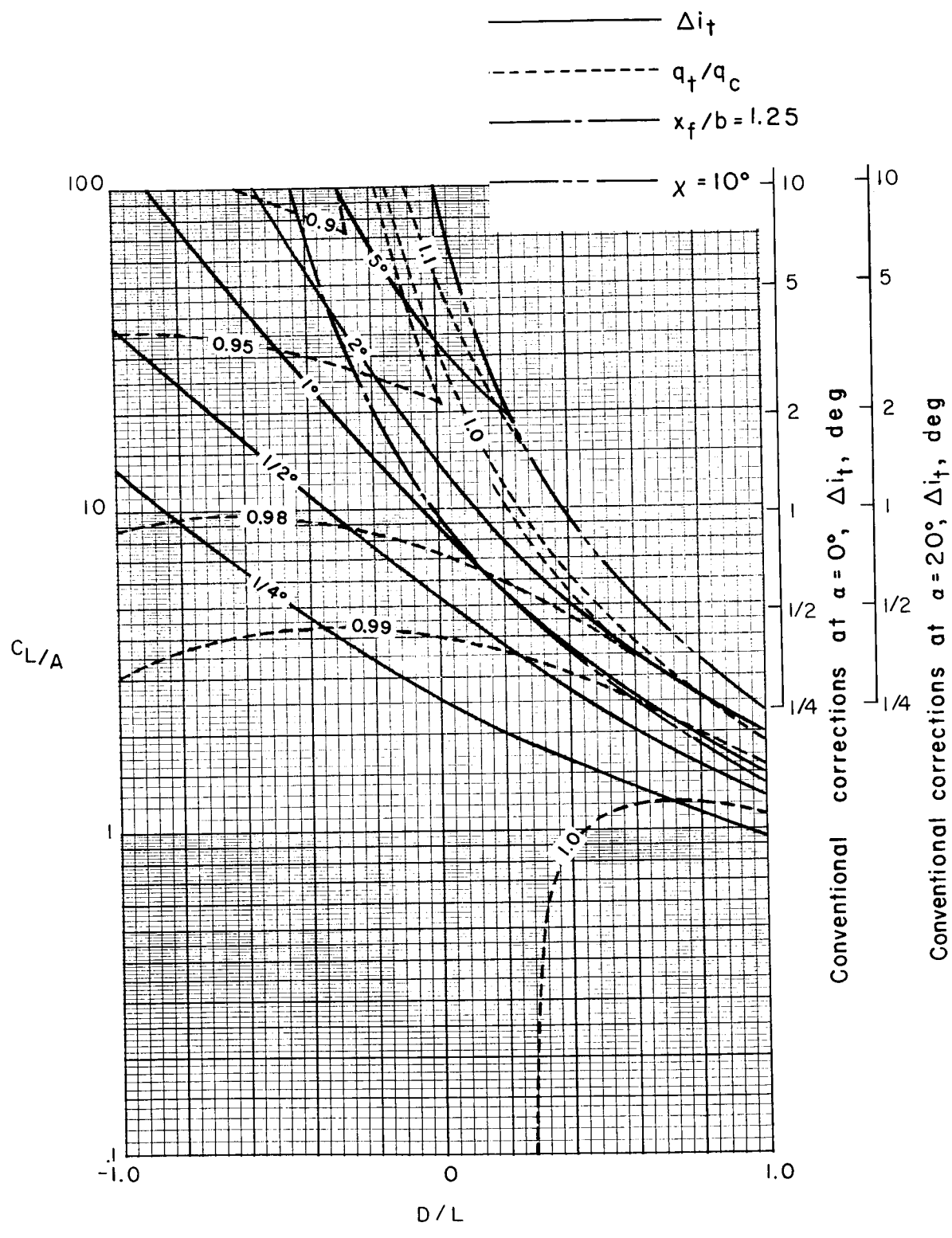


(a) $\sigma = 1/6$.

Figure 23.- Corrections at a zero-span tail behind a uniformly loaded wing centered in a closed rectangular tunnel. Tail length is three-fourths of wing span; tail height is zero; $\alpha = 20^0$; $\gamma = 1.5$.

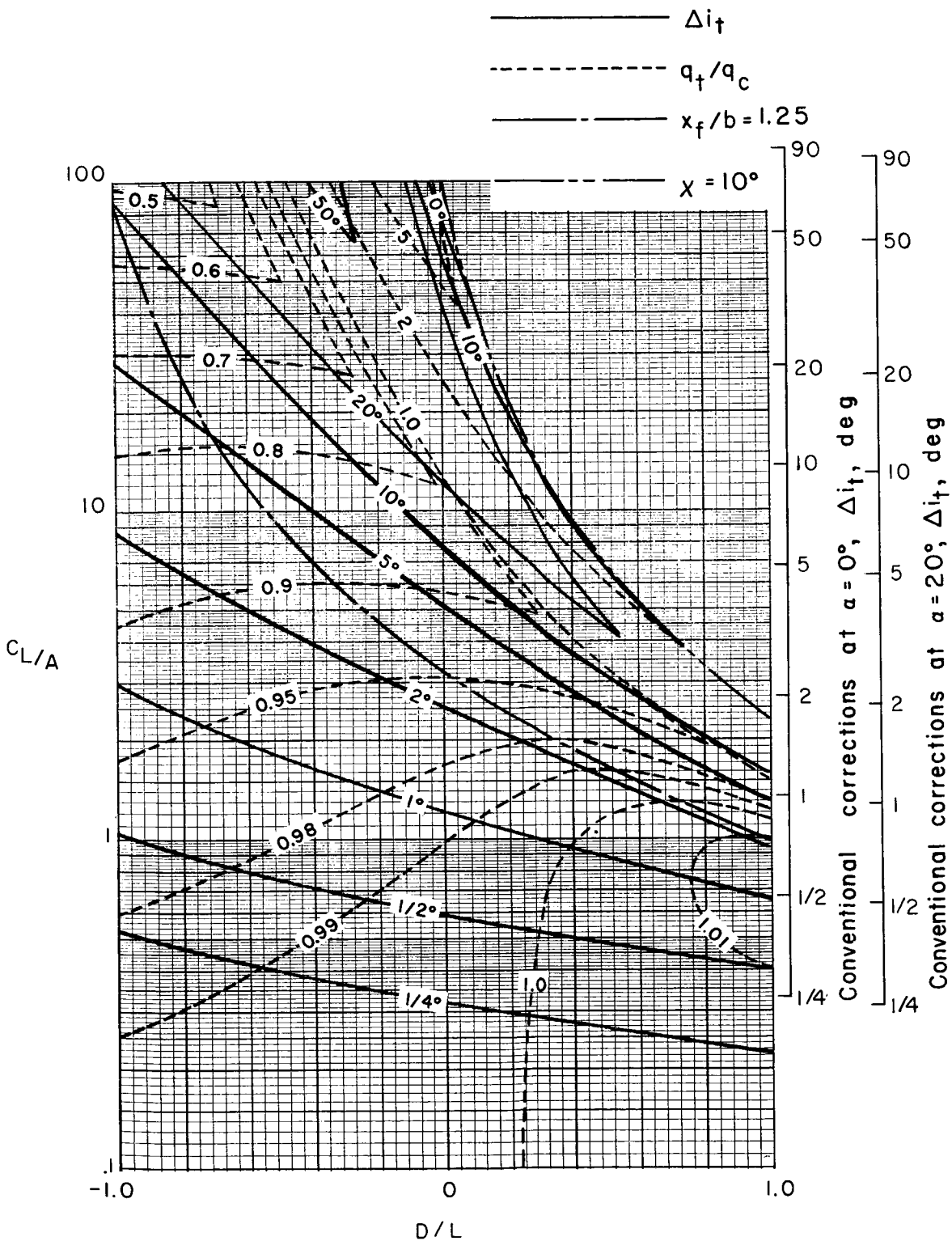


(b) $\sigma = 1/3$.

Figure 23.- Continued.

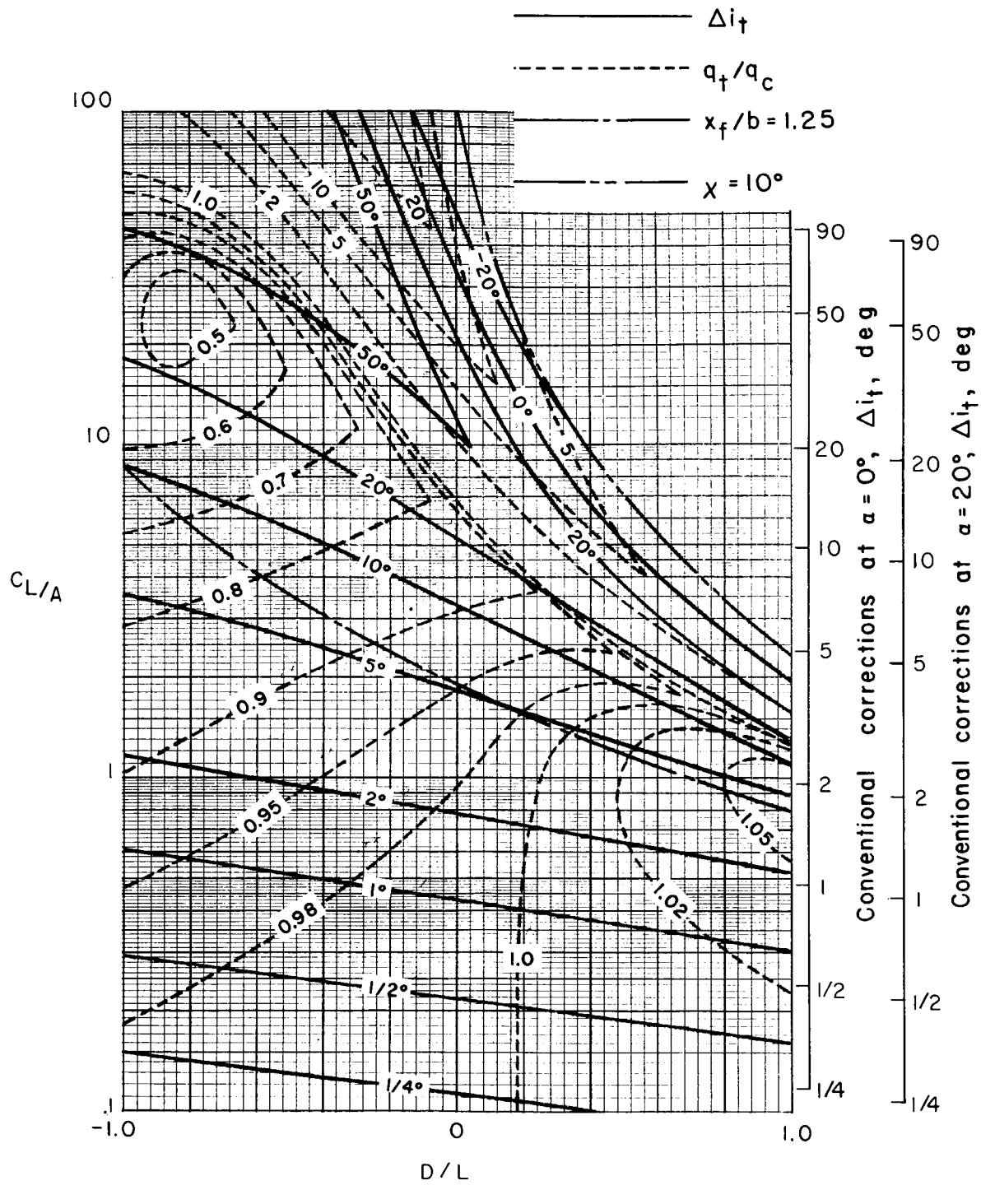


(c) σ = 1/2.

Figure 23.- Continued.

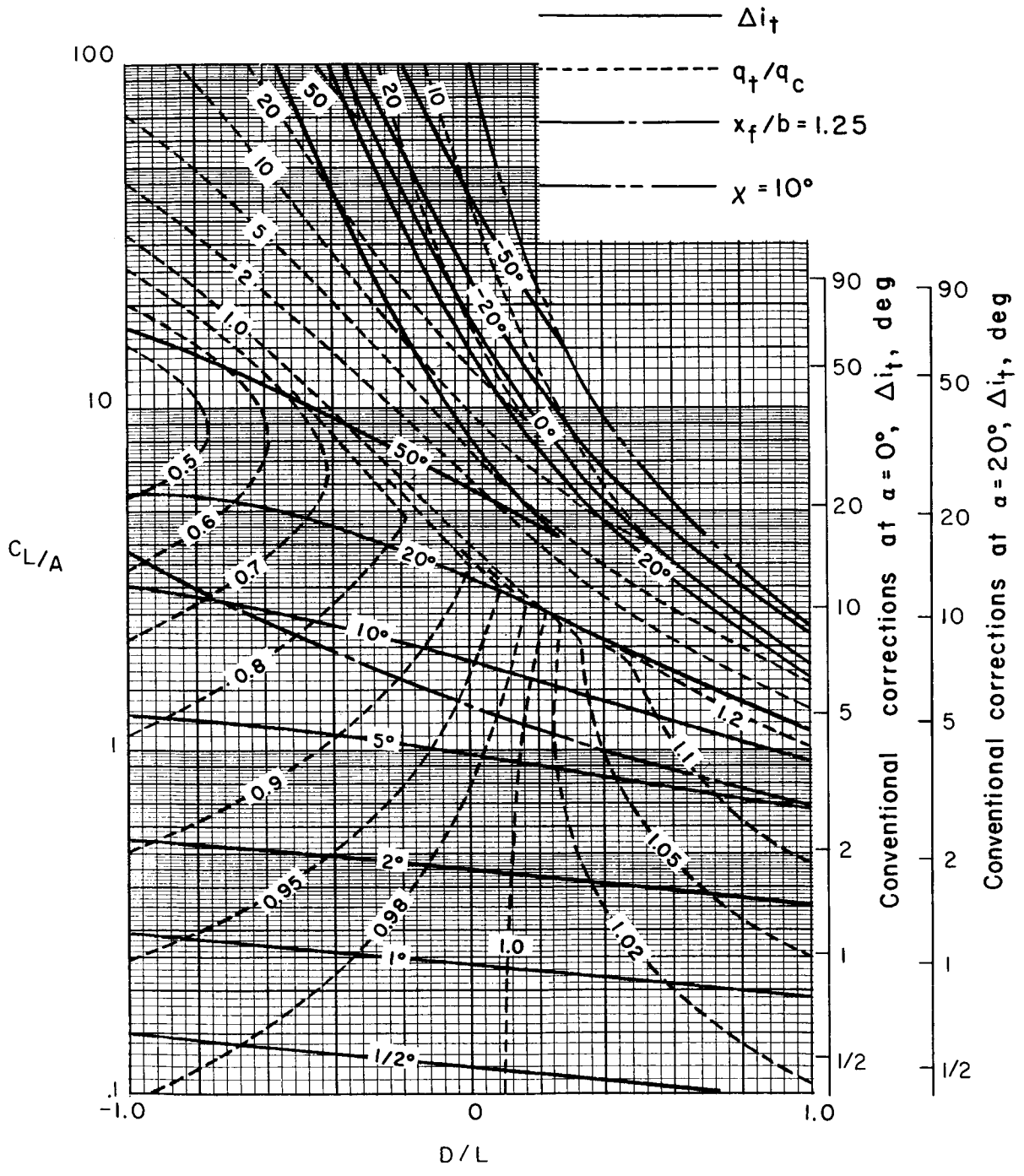


(d) $\sigma = 2/3$.

Figure 23.- Continued.

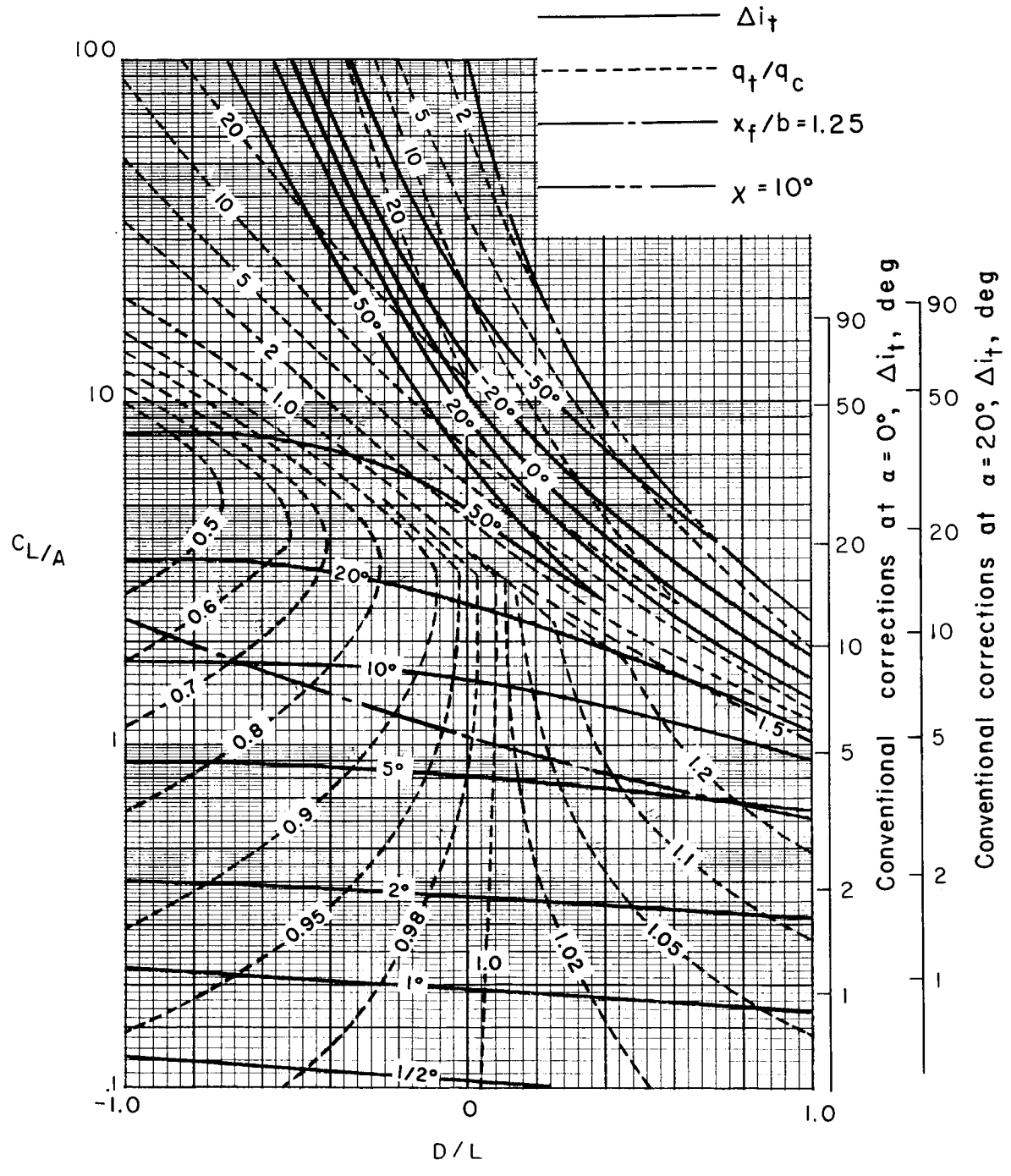


(e) σ = 5/6.

Figure 23.- Concluded.

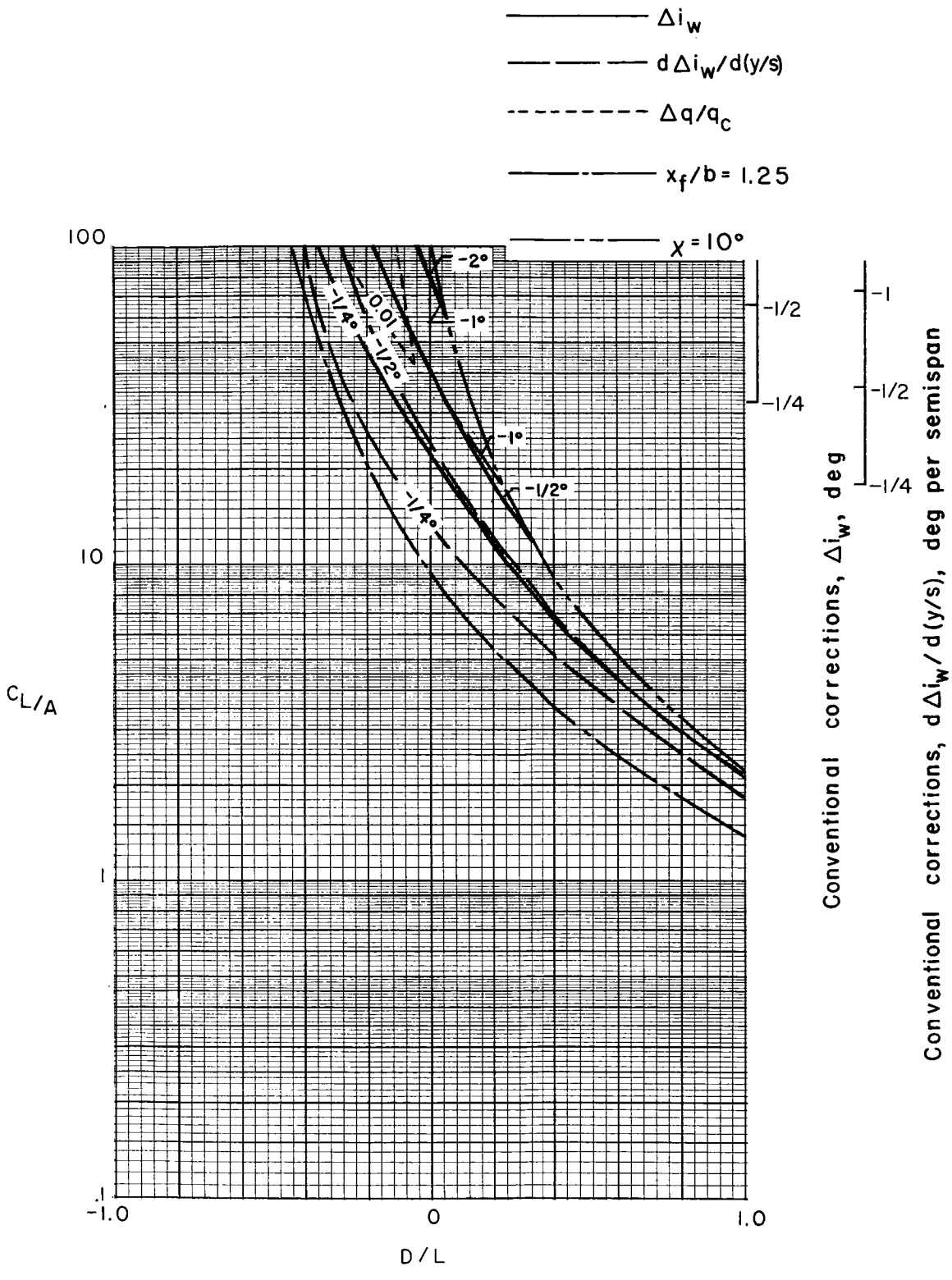


(a) $\sigma = 1/6$.

Figure 24.- Nonuniformity of corrections over a uniformly loaded wing centered in a closed rectangular tunnel. $\gamma = 1.5$; $\Lambda = 0^0$; $\alpha = 0^0$.

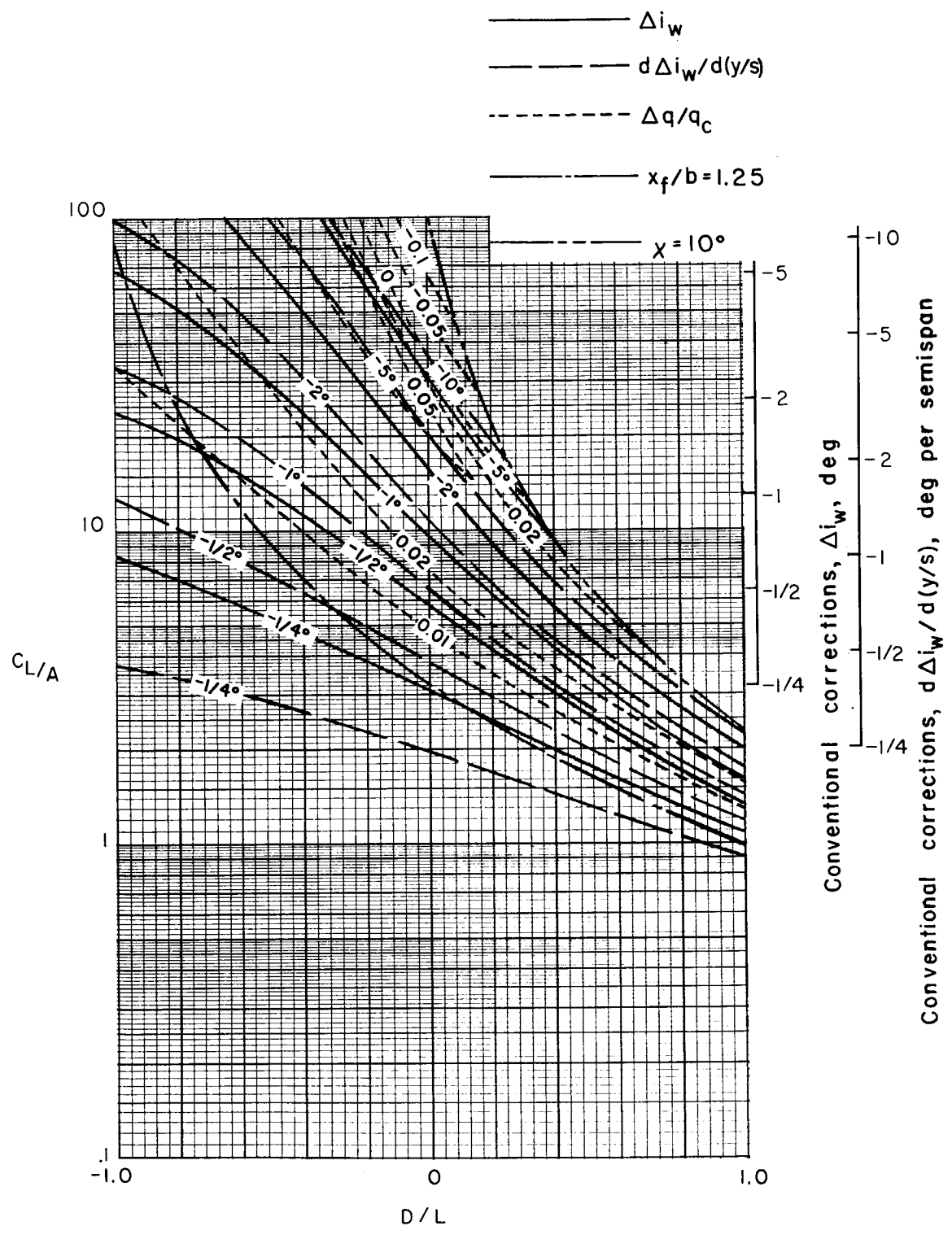


(b) $\sigma = 1/3$.

Figure 24.- Continued.

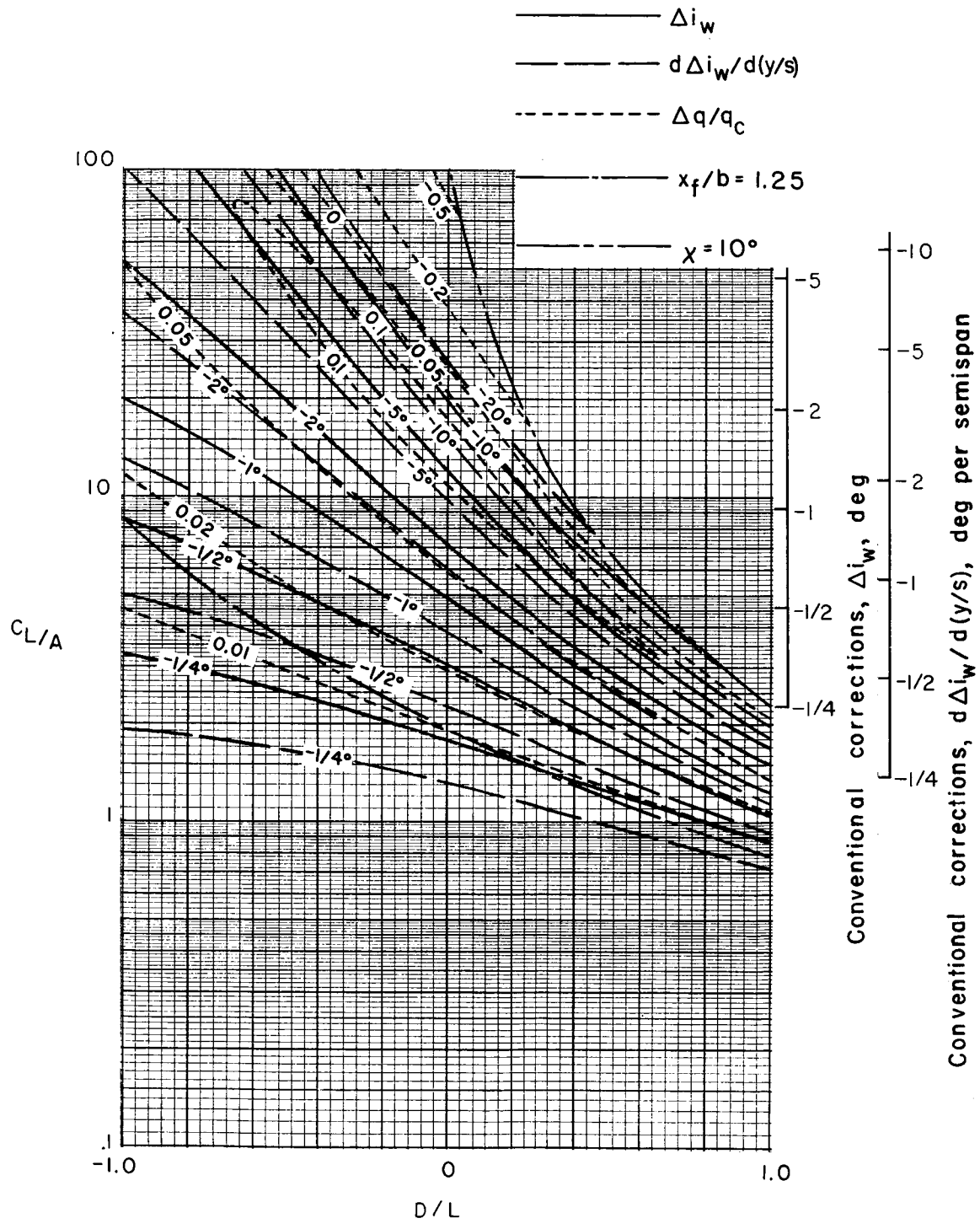


(c) $\sigma = 1/2$.

Figure 24.- Continued.

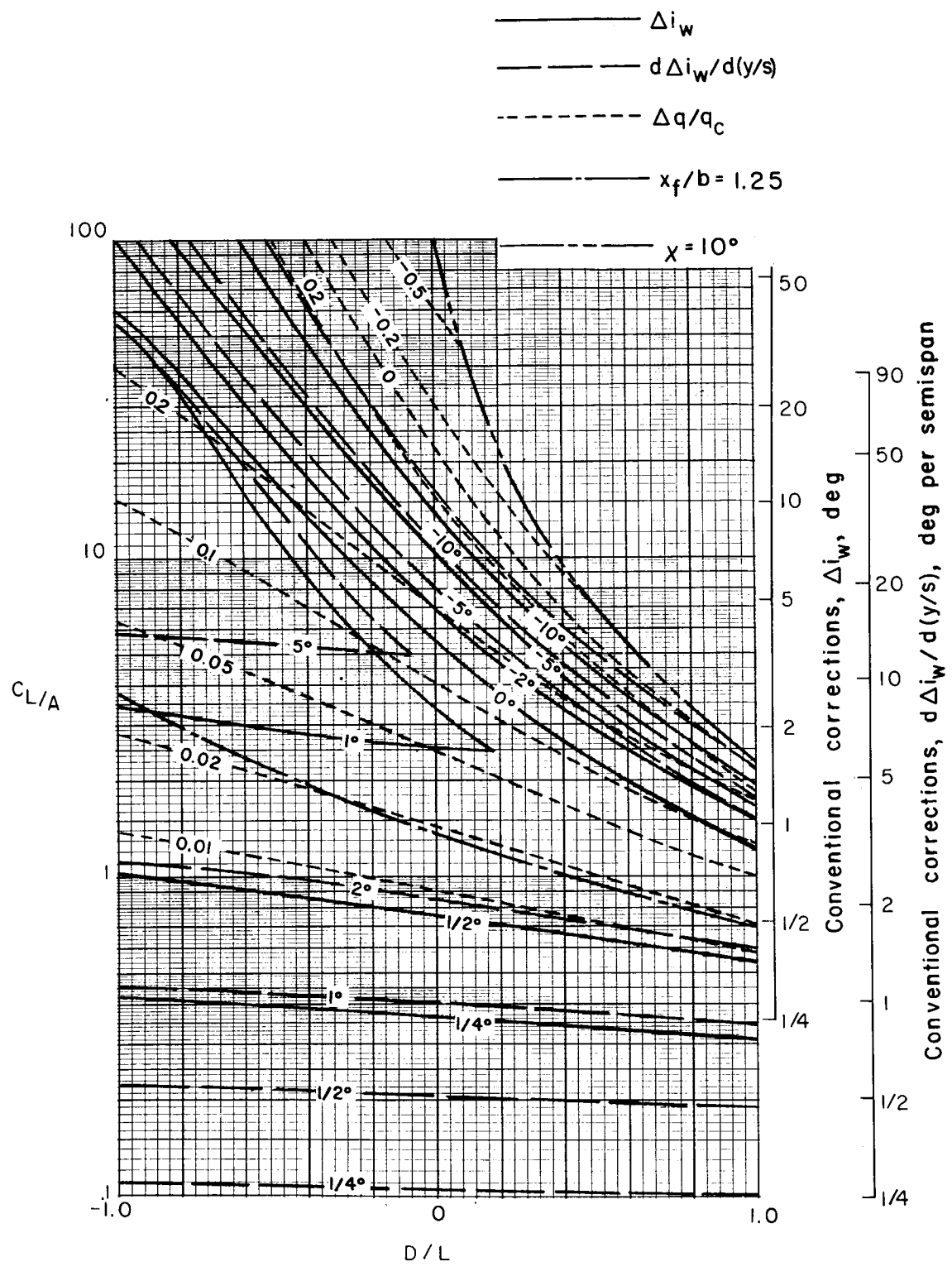


(d) $\sigma = 2/3$.

Figure 24.- Continued.

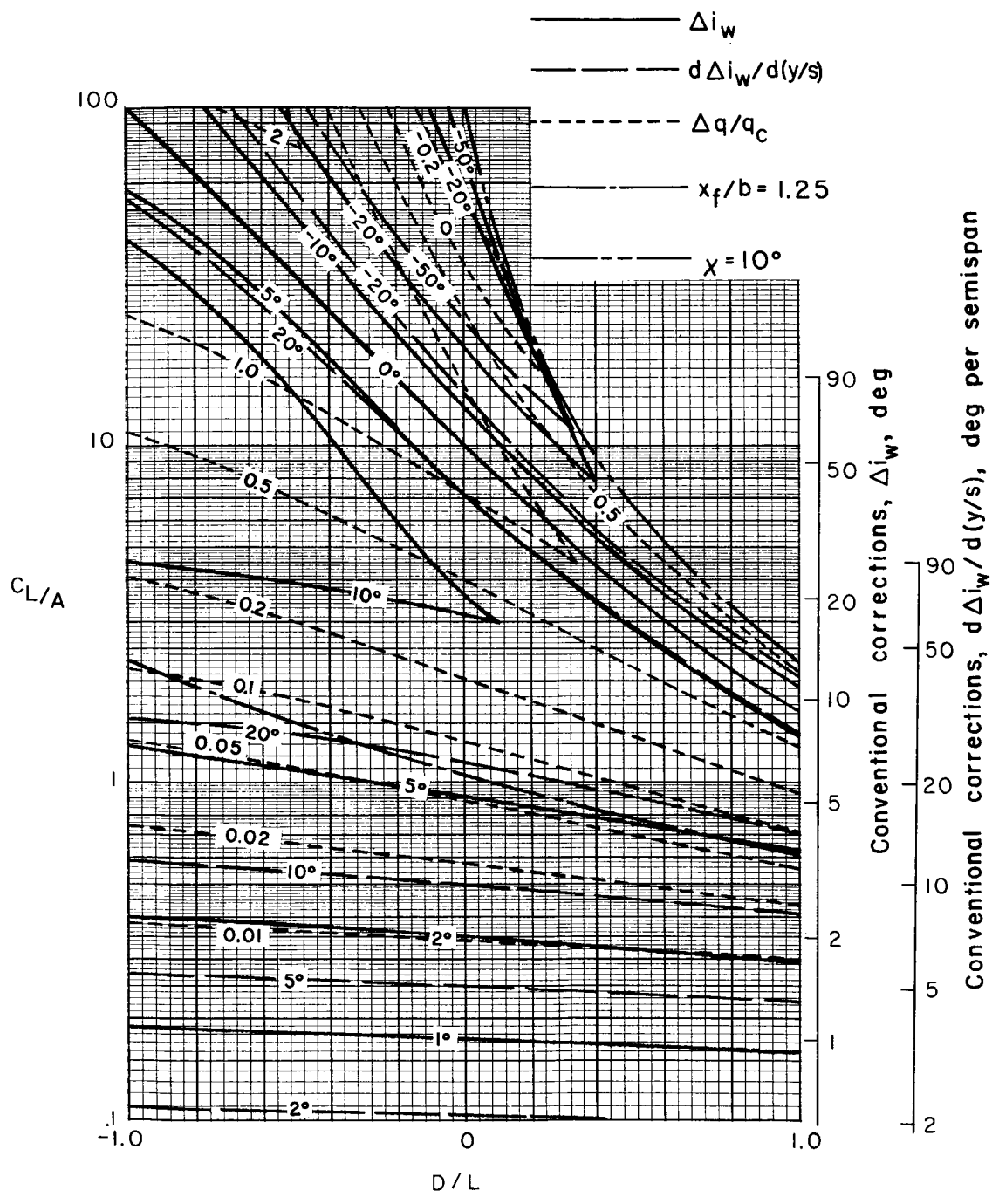


(e) $\sigma = 5/6$.

Figure 24.- Concluded.

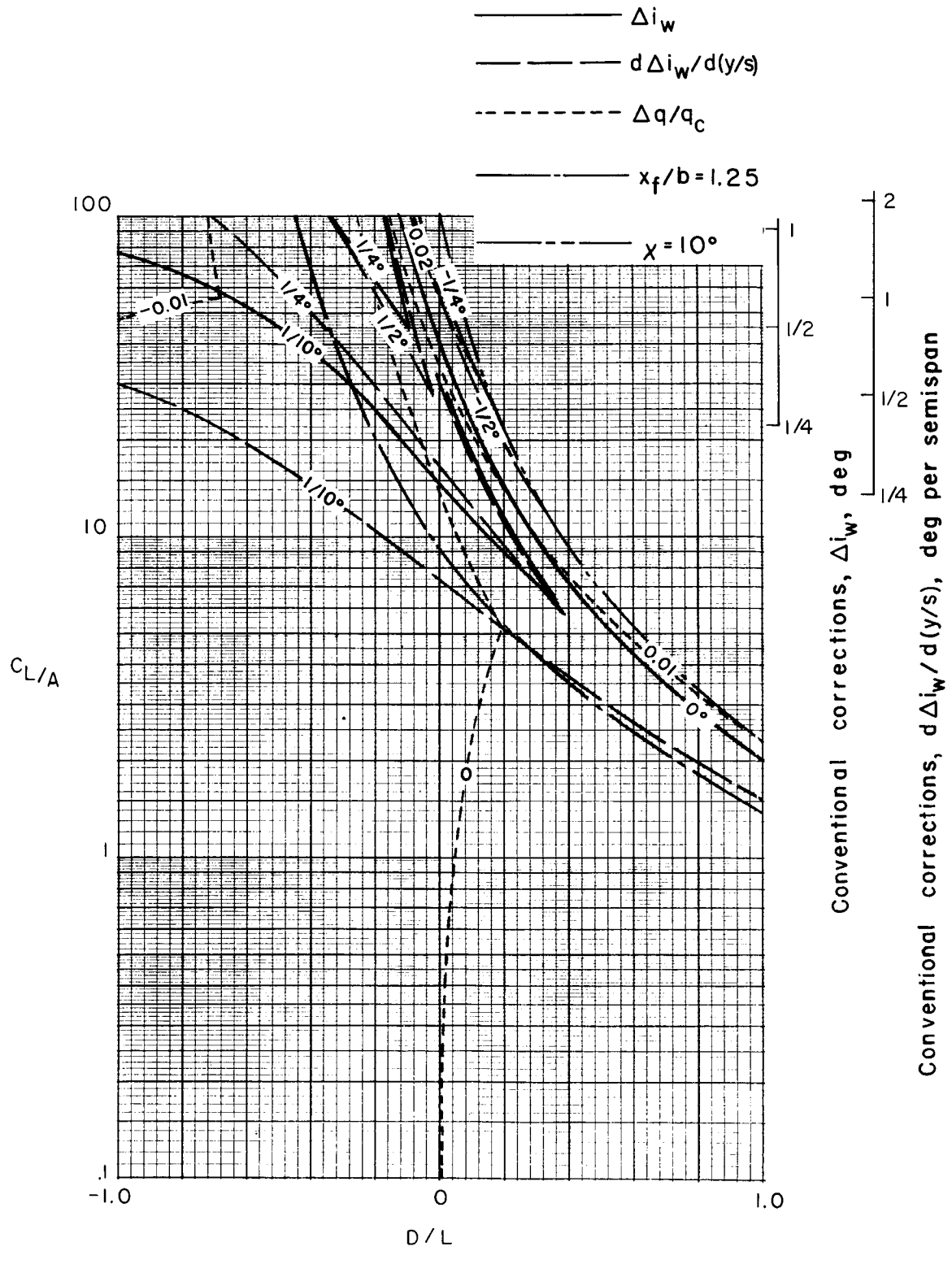


(a) $\sigma = 1/6$.

Figure 25.- Nonuniformity of corrections over a uniformly loaded wing centered in a closed rectangular tunnel. $\gamma = 1.5$; $\Lambda = 15^0$; $\alpha = 0^0$.

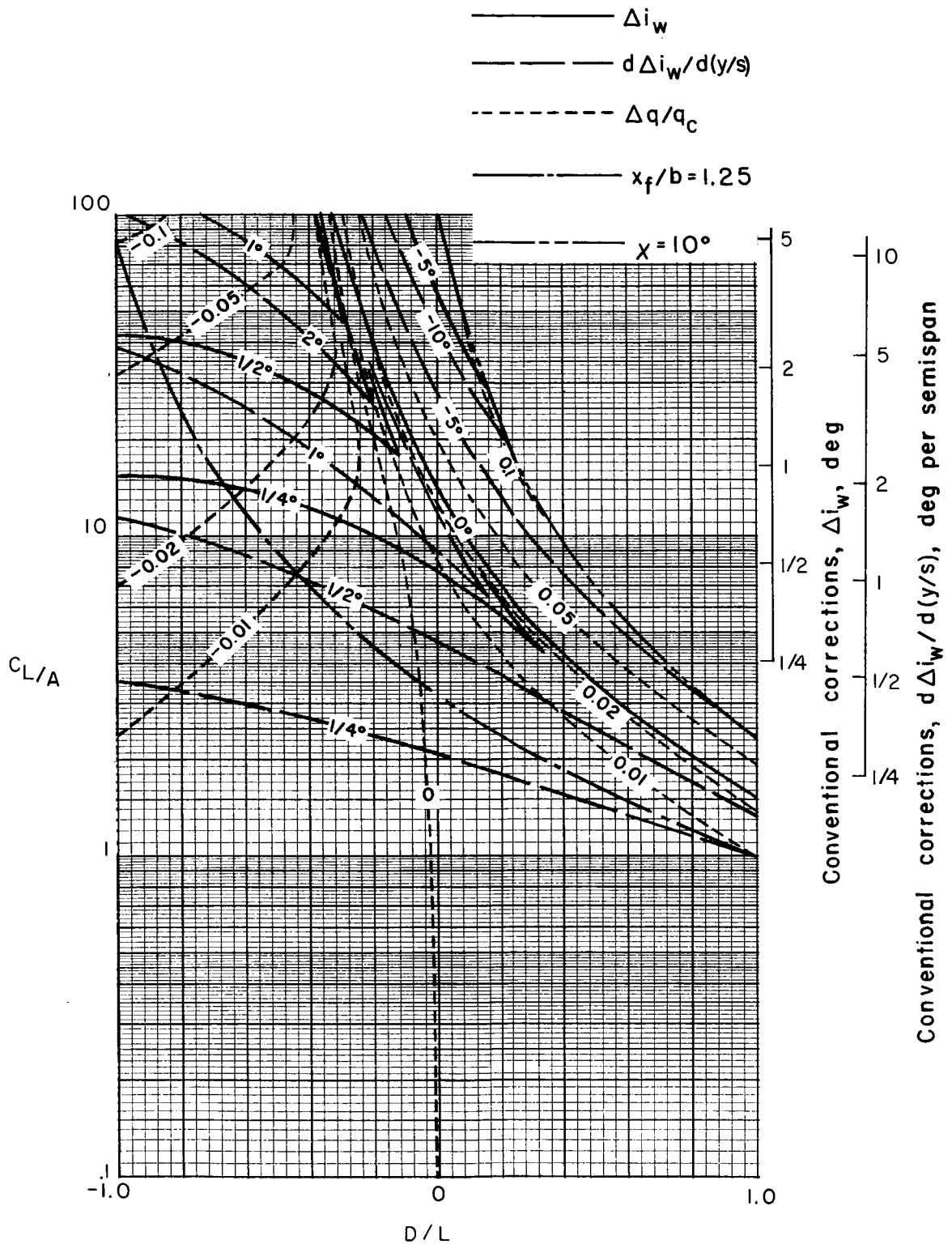


(b) $\sigma = 1/3$.

Figure 25.- Continued.

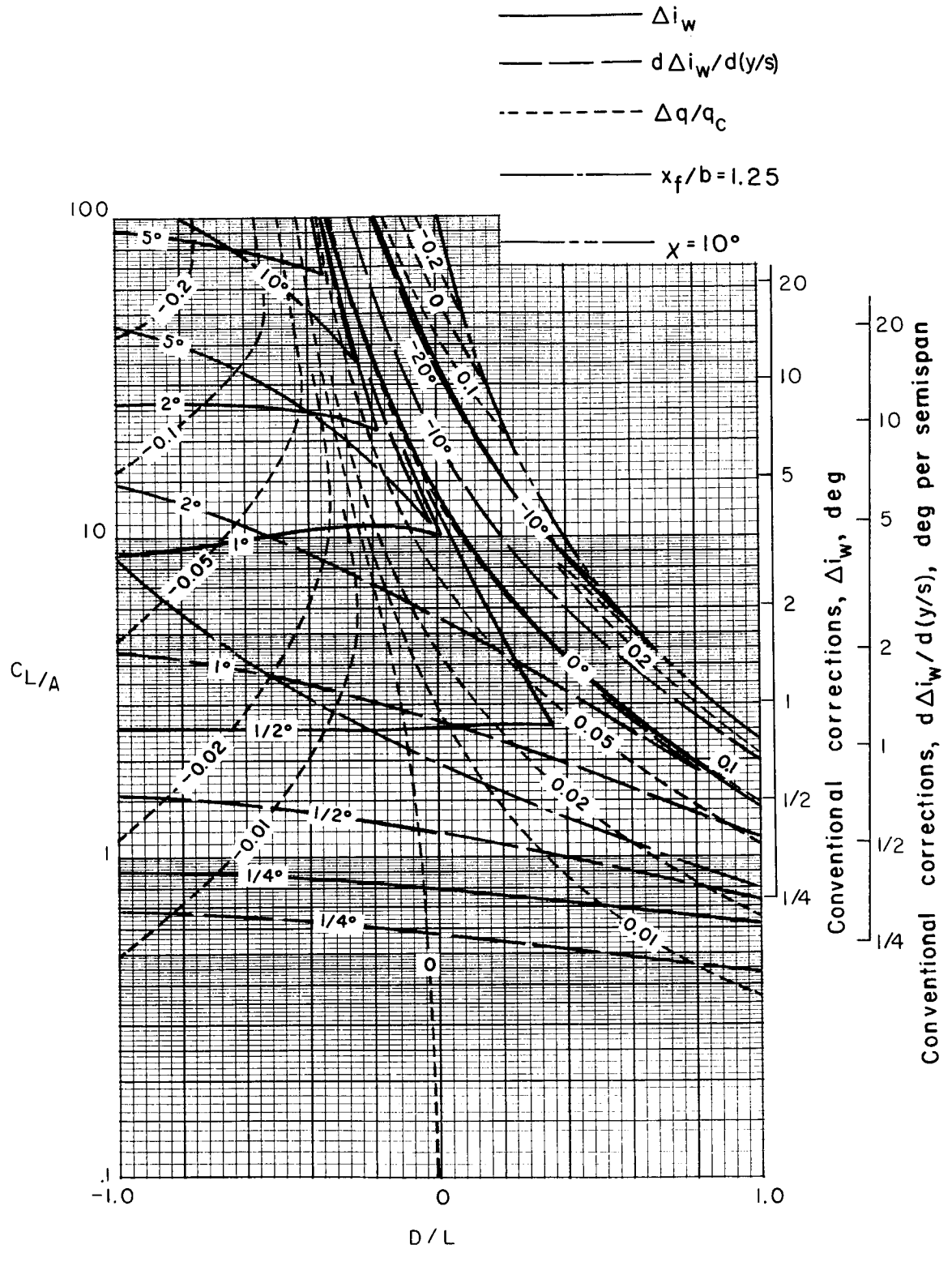


(c) $\sigma = 1/2$.

Figure 25.- Continued.

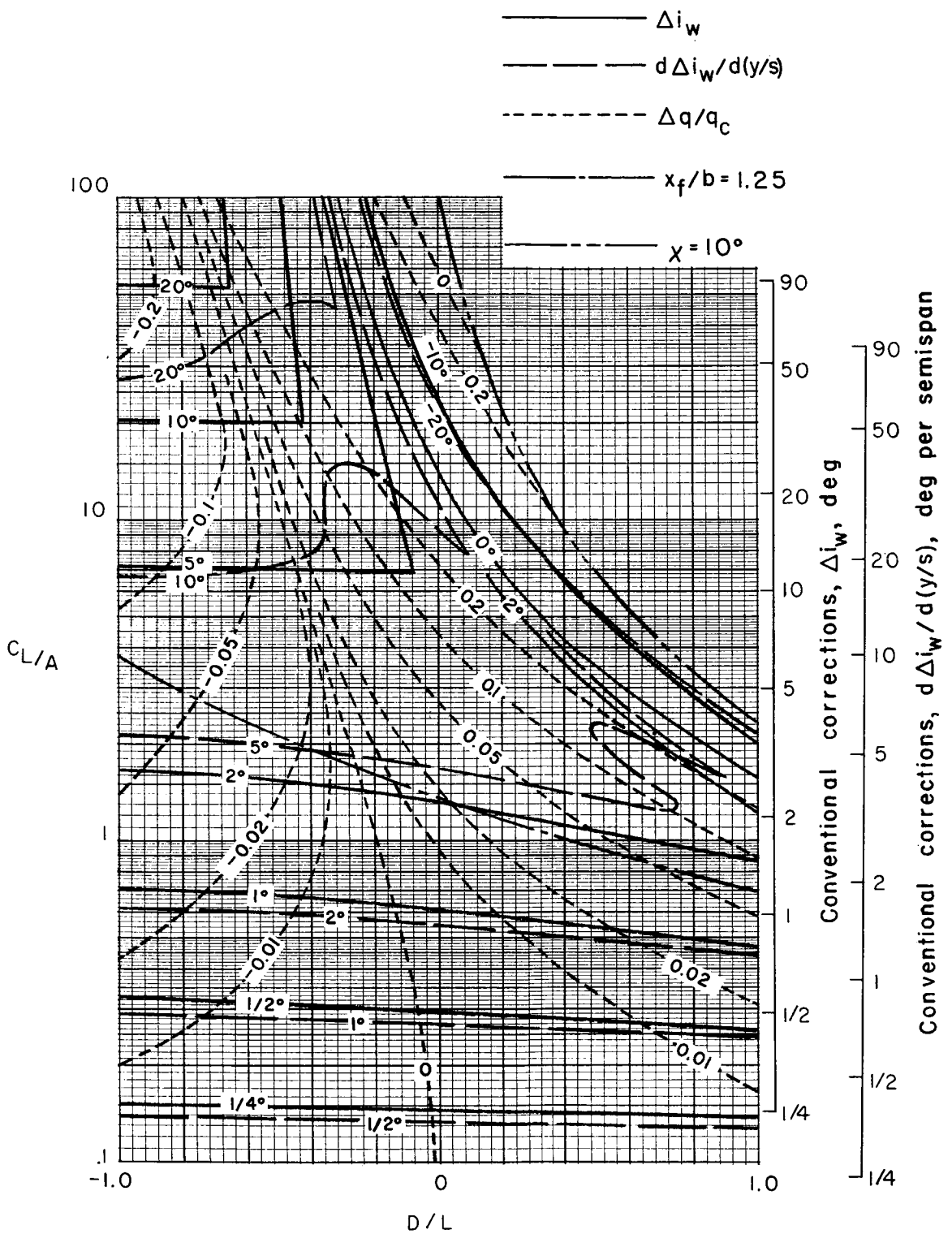


(d) $\sigma = 2/3$.

Figure 25.- Continued.

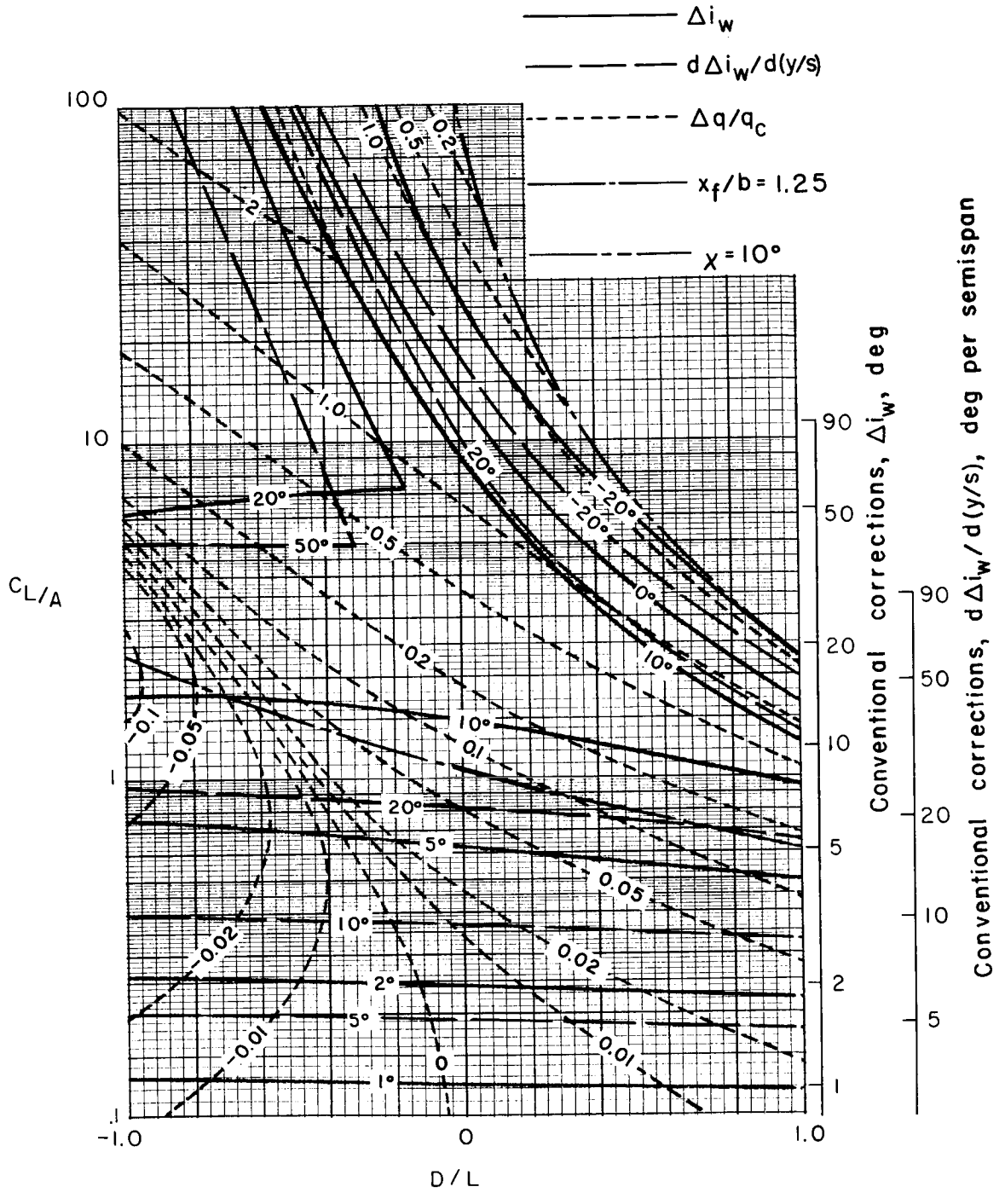


(e) $\sigma = 5/6$.

Figure 25.- Concluded.

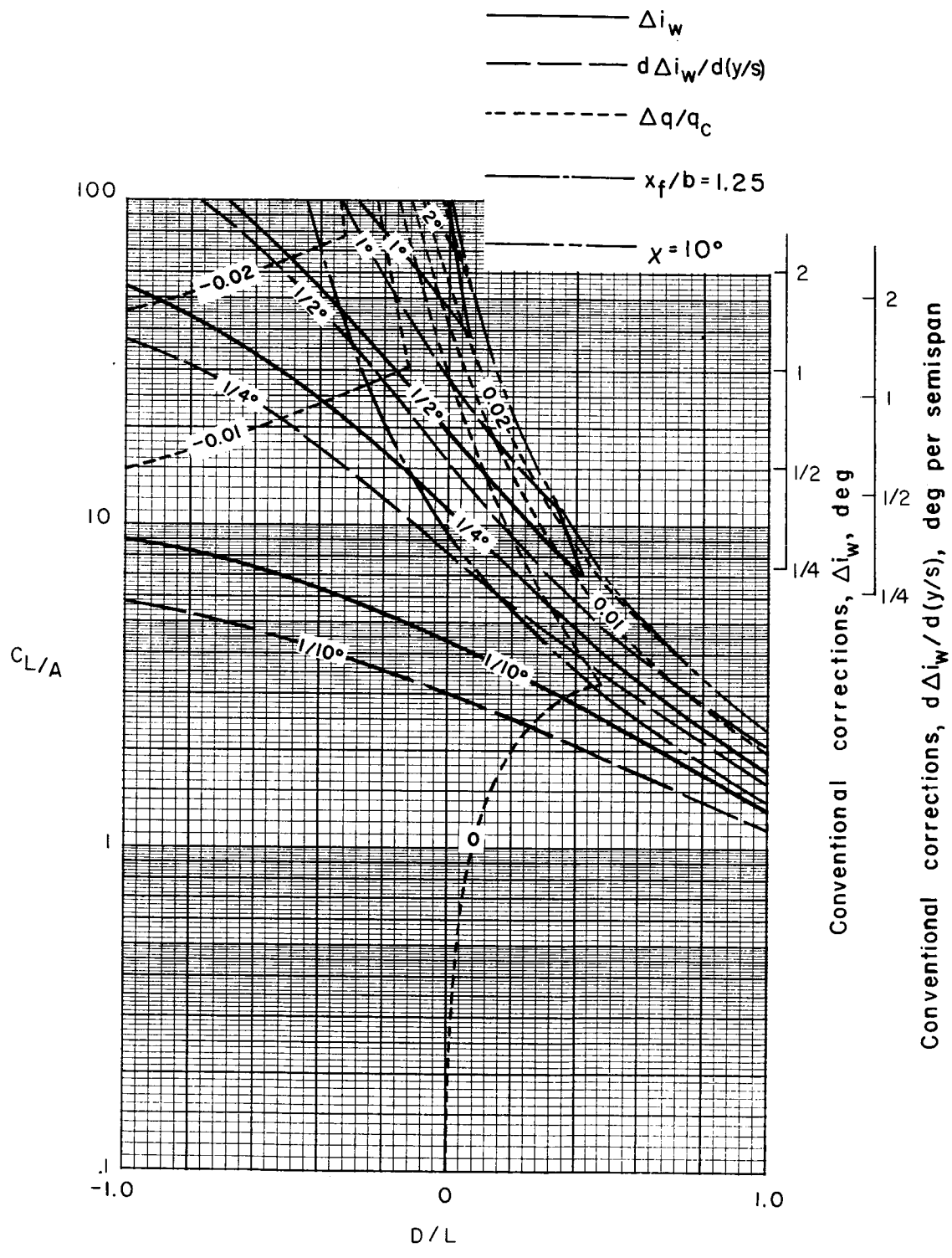


(a) $\sigma = 1/6$.

Figure 26.- Nonuniformity of corrections over a uniformly loaded wing centered in a closed rectangular tunnel. $\gamma = 1.5$; $\Lambda = 30^0$; $\alpha \doteq 0^0$.

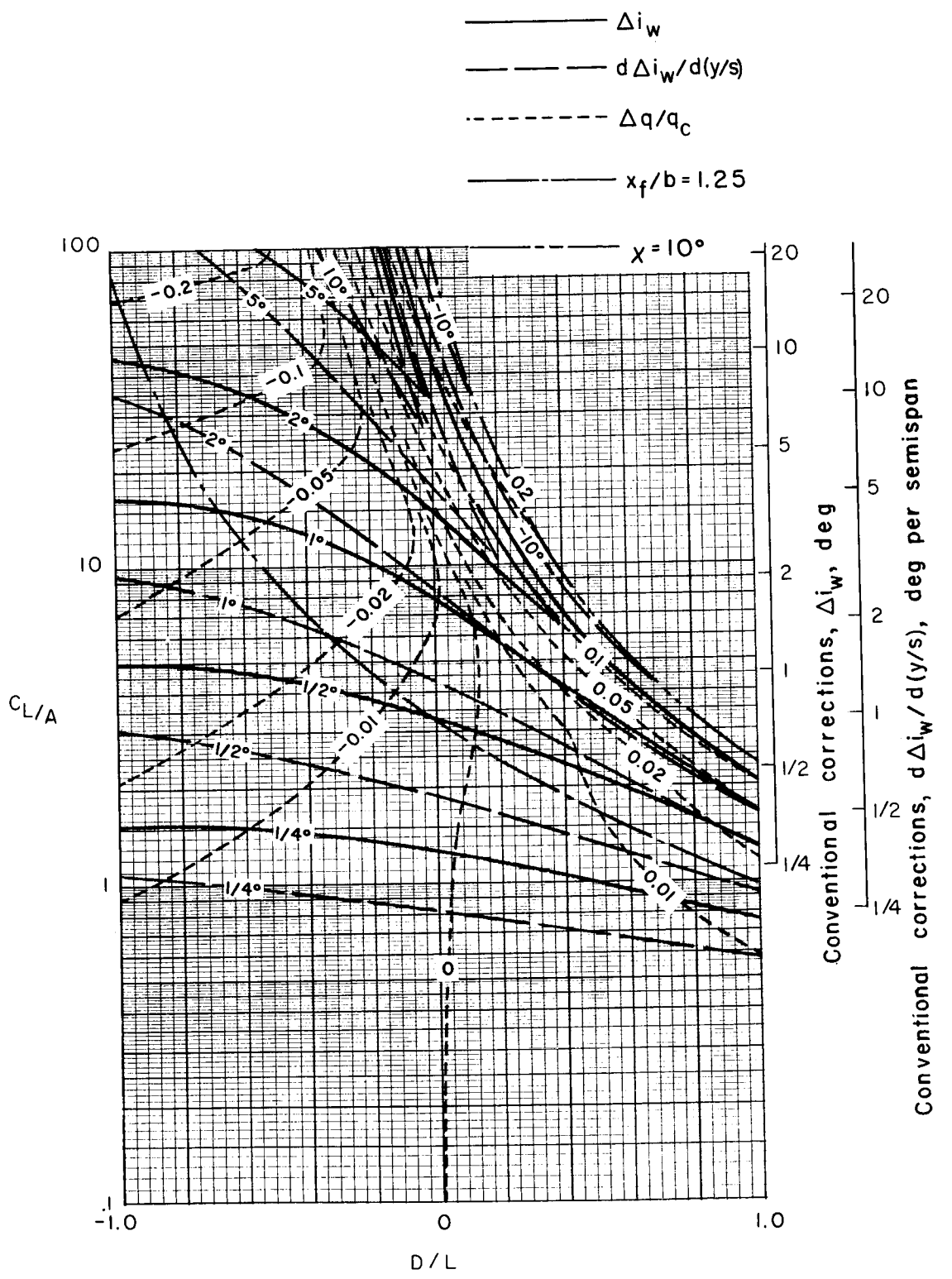


(b) $\sigma = 1/3$.

Figure 26.- Continued.

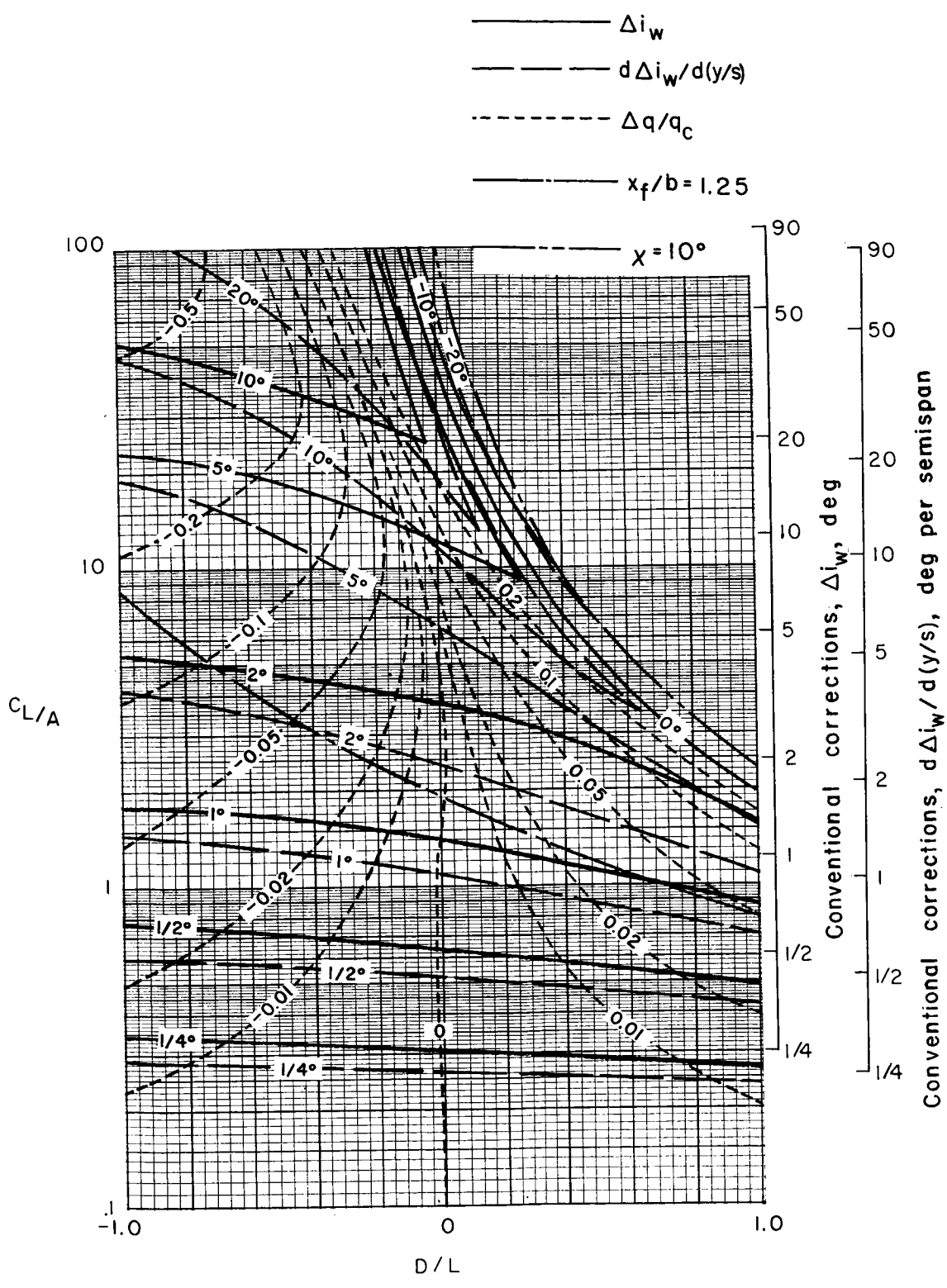


(c) $\sigma = 1/2$.

Figure 26.- Continued.

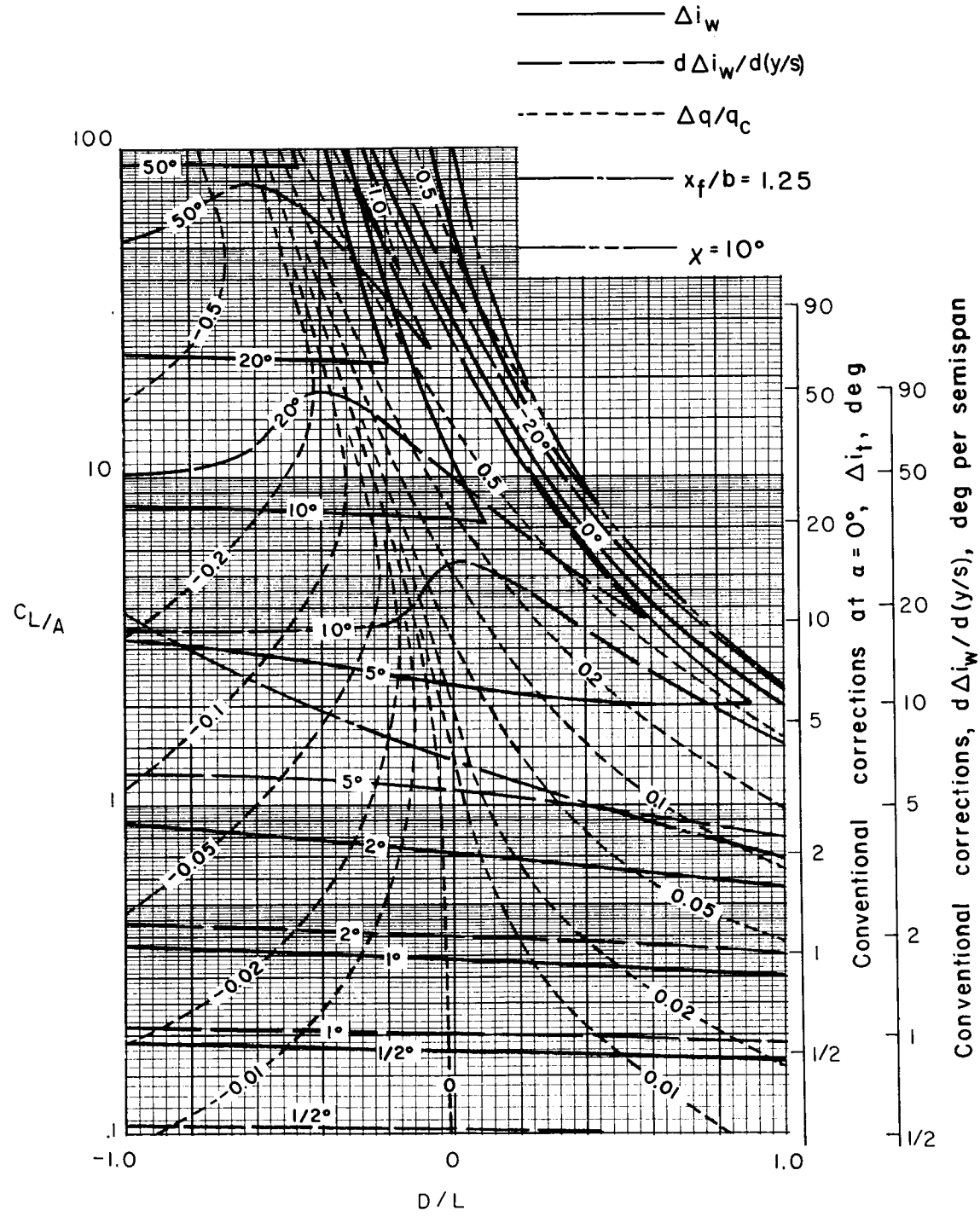


(d) σ = 2/3.

Figure 26.- Continued.

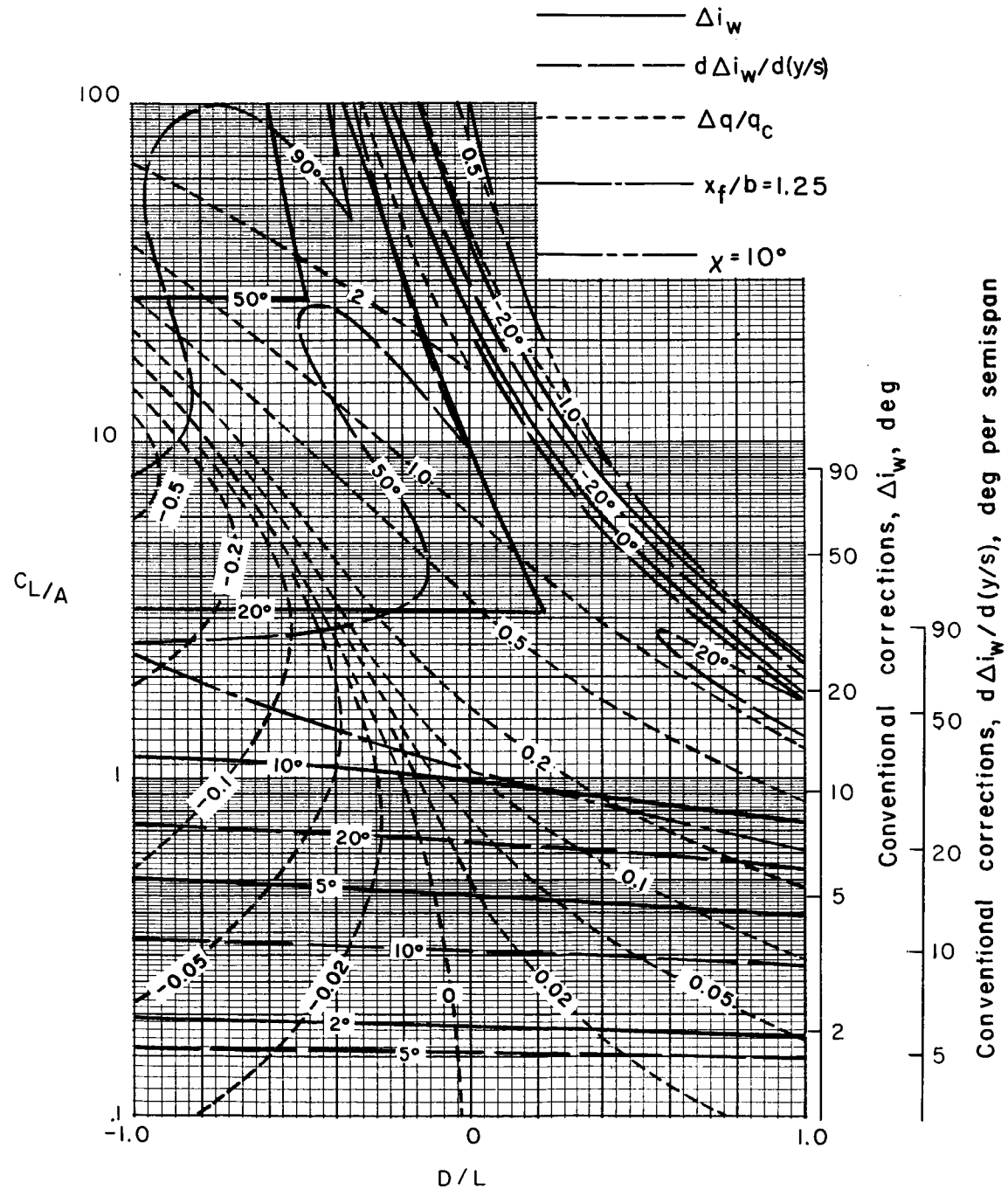


(e) $\sigma = 5/6$.

Figure 26.- Concluded.

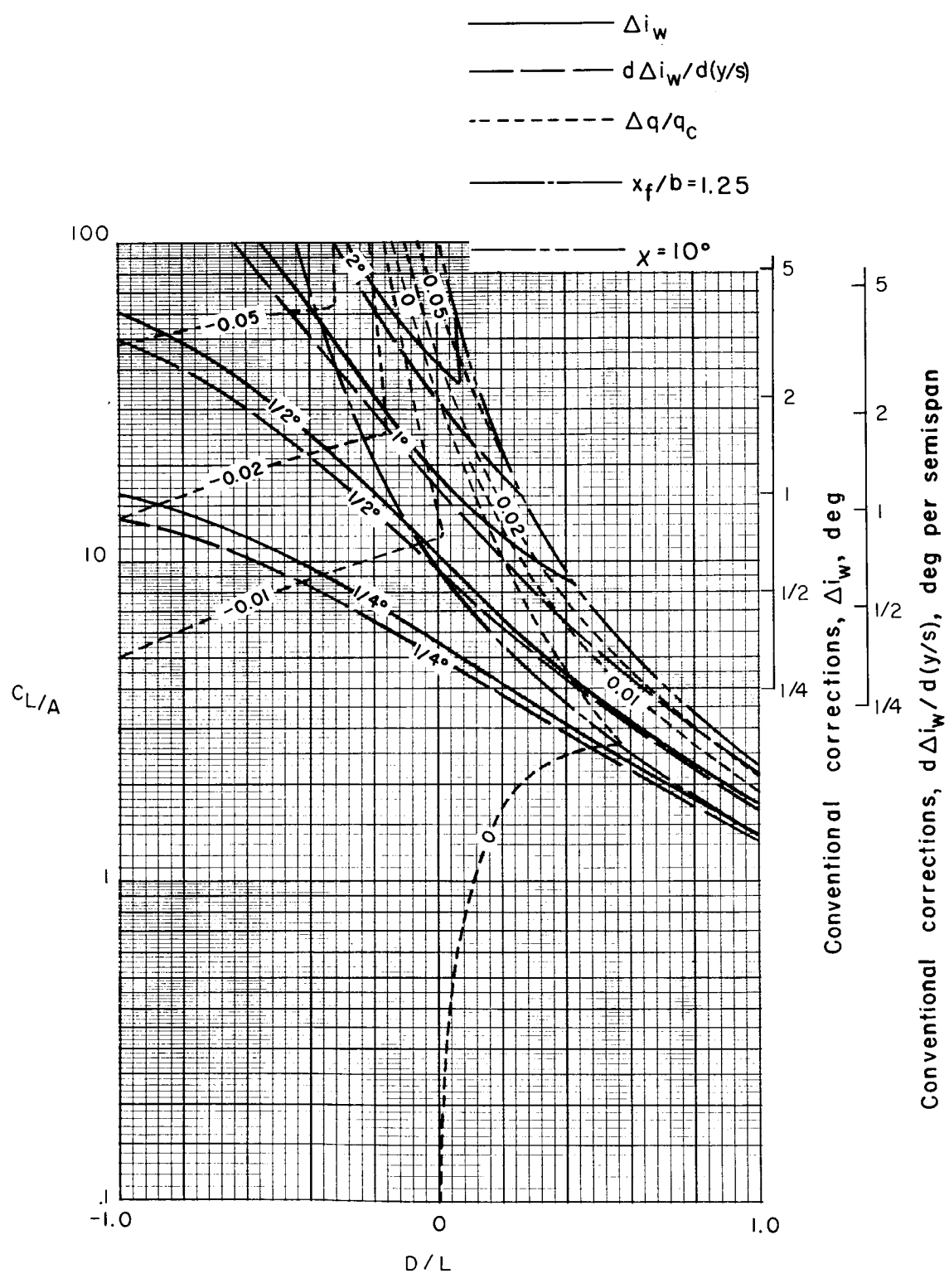


(a) $\sigma = 1/6$.

Figure 27.- Nonuniformity of corrections over a uniformly loaded wing centered in a closed rectangular tunnel. $\gamma = 1.5^0$; $\Lambda = 45^0$; $\alpha = 0^0$.

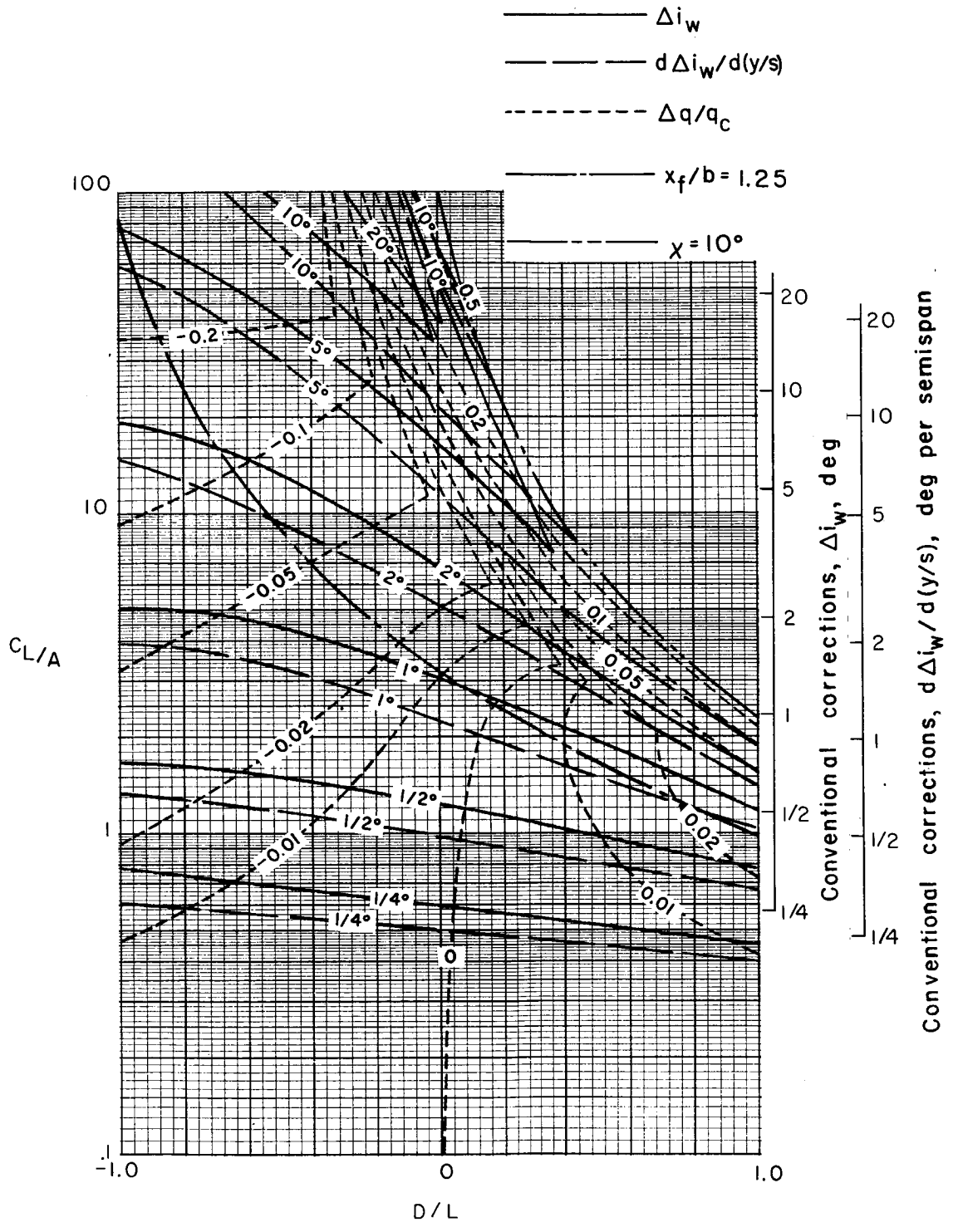


(b) $\sigma = 1/3$.

Figure 27.- Continued.

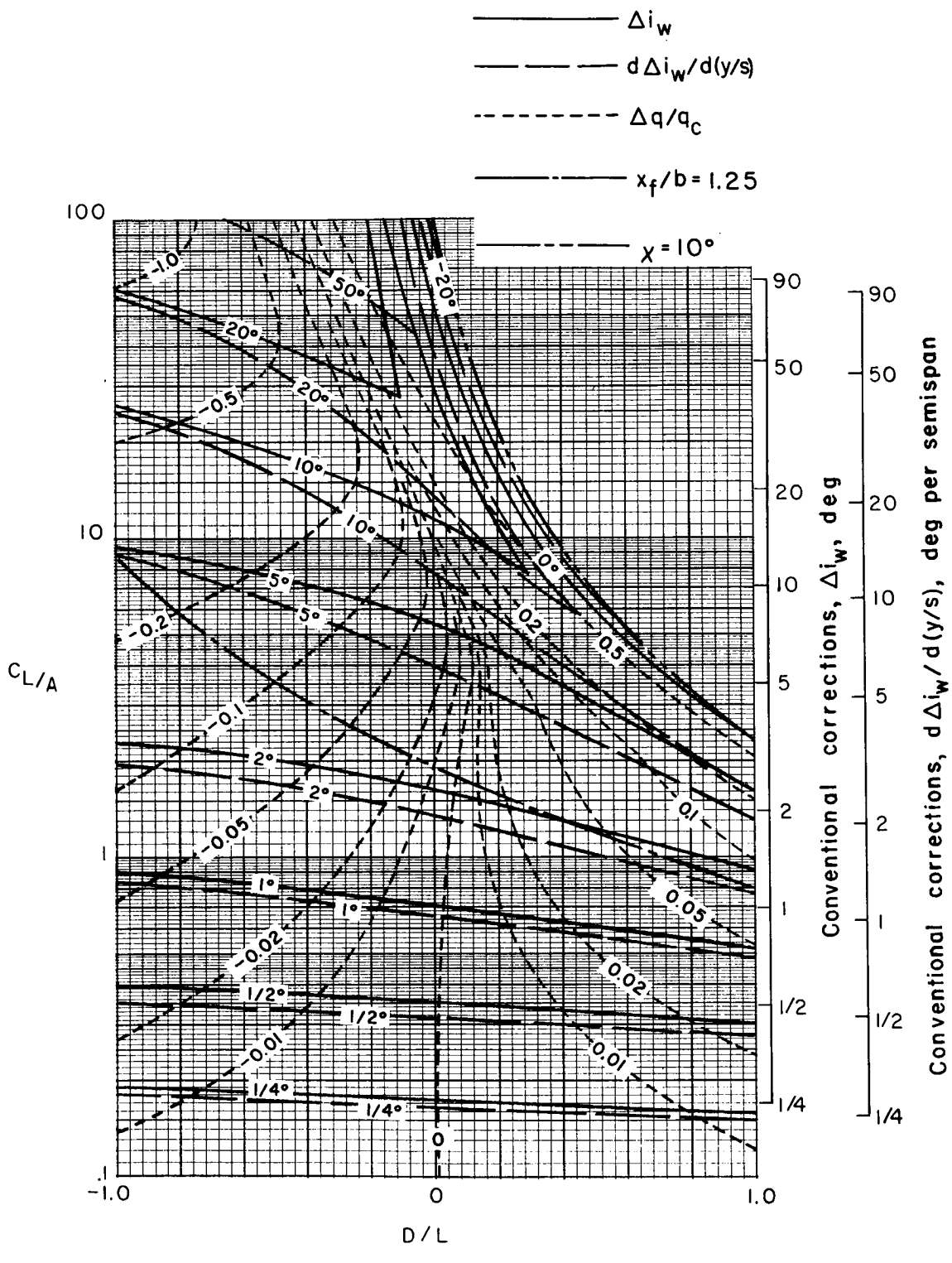


(c) $\sigma = 1/2$.

Figure 27.- Continued.

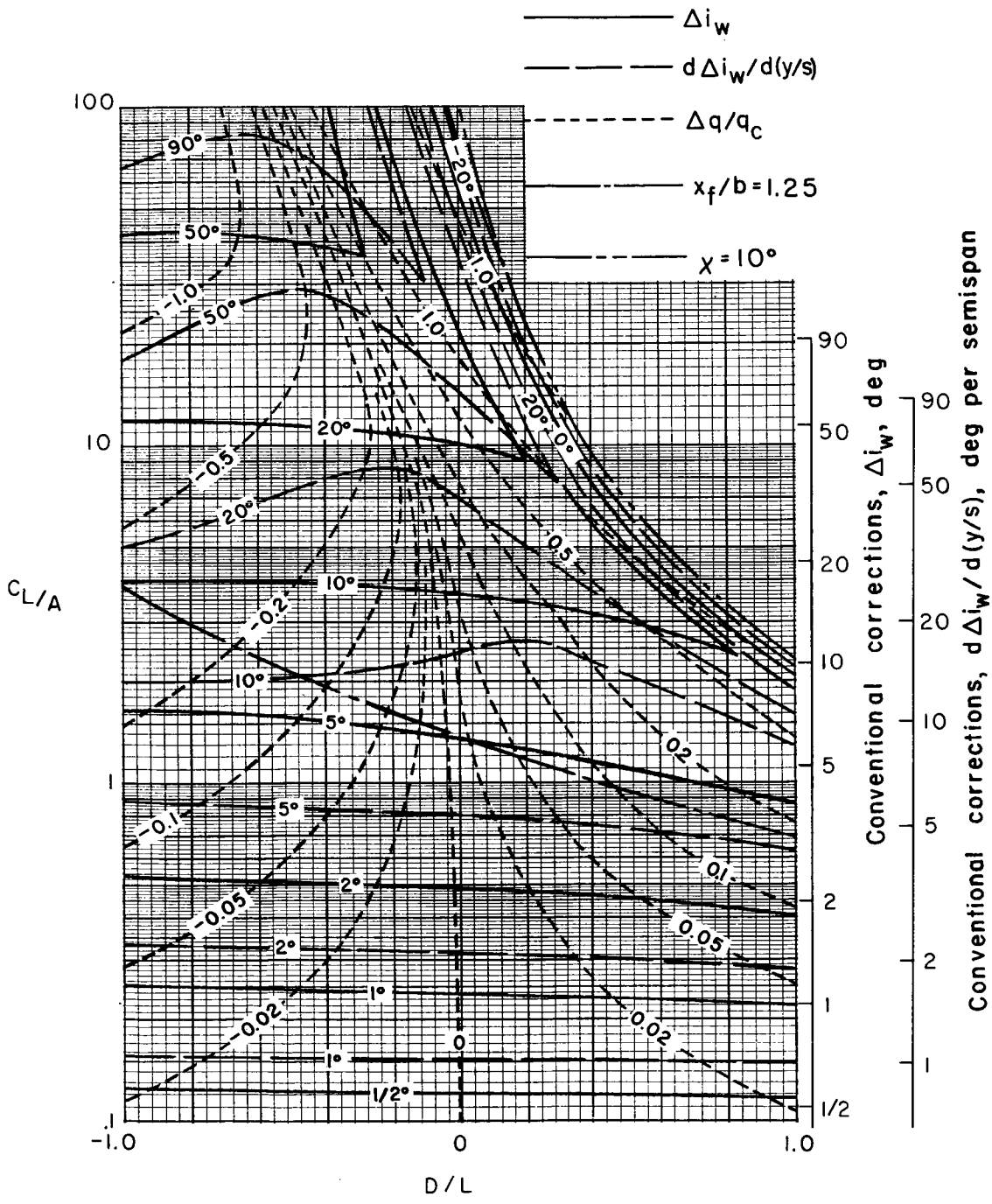


(d) $\sigma = 2/3$.

Figure 27.- Continued.

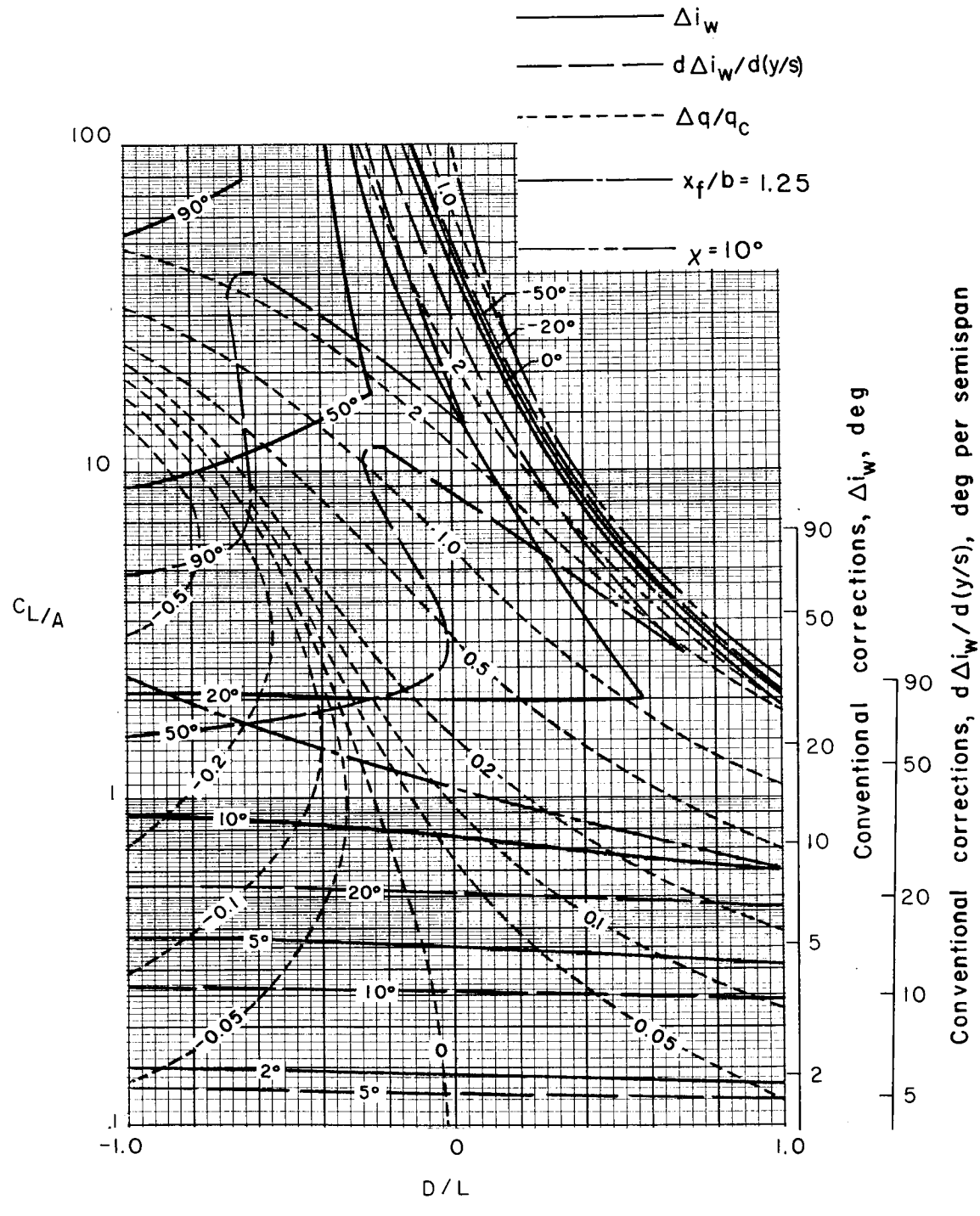


(e) $\sigma = 5/6$.

Figure 27.- Concluded.

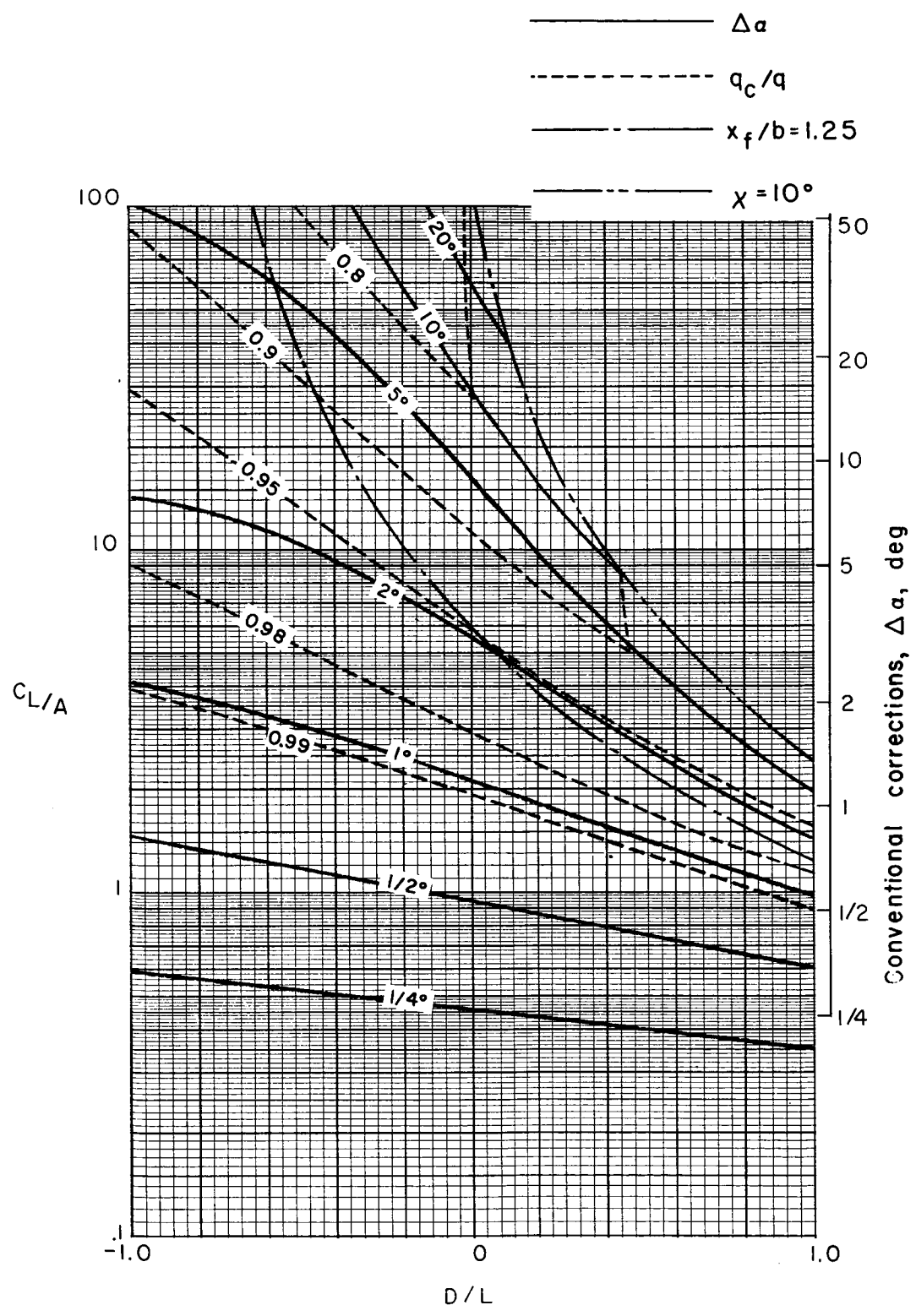


(a) σ = 1/4.

Figure 28.- Average corrections for a uniformly loaded wing centered in a closed rectangular tunnel. Λ = 0°; γ = 4/3.

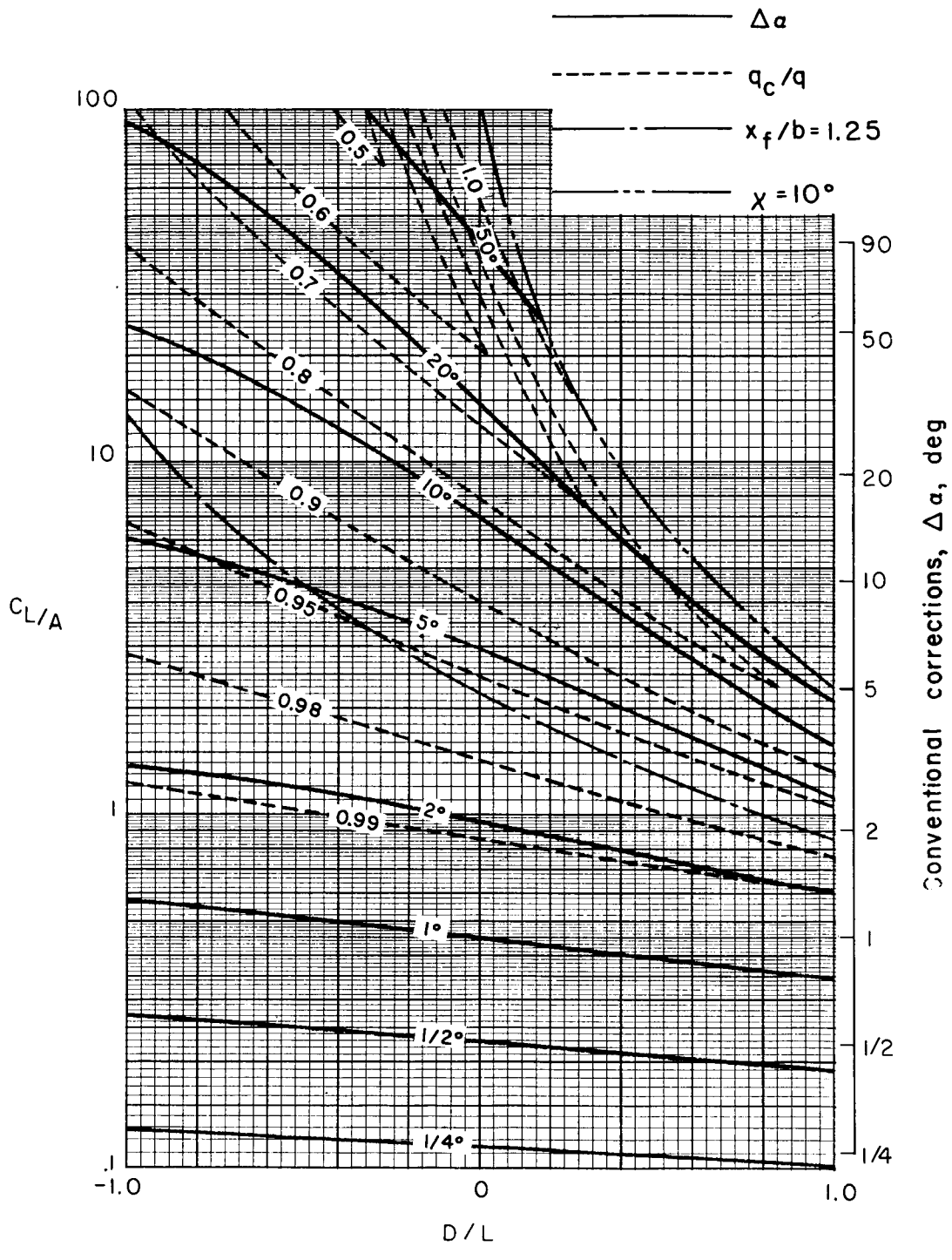


(b) σ = 1/2.

Figure 28.- Continued.

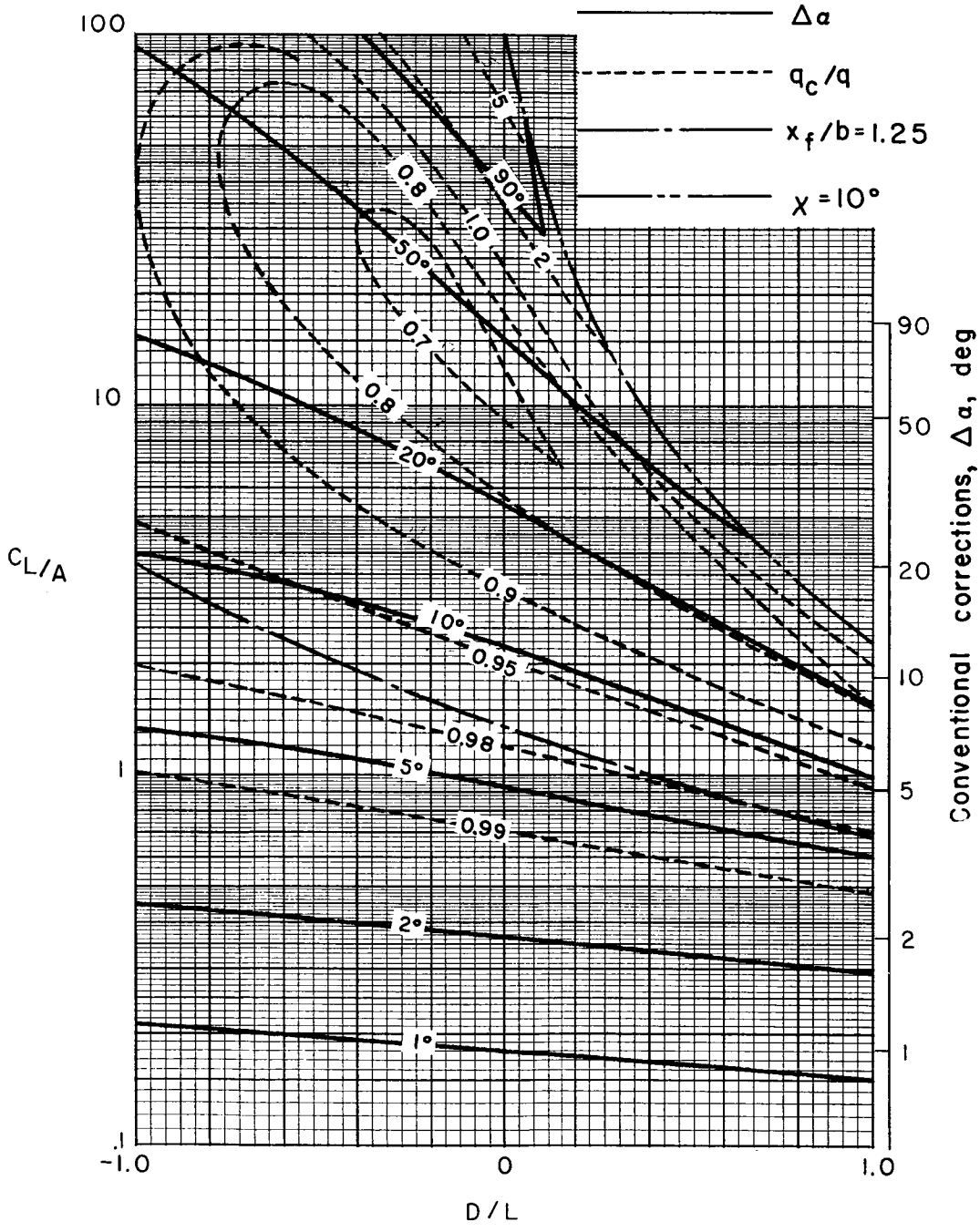


(c) σ = 3/4.

Figure 28.- Concluded.

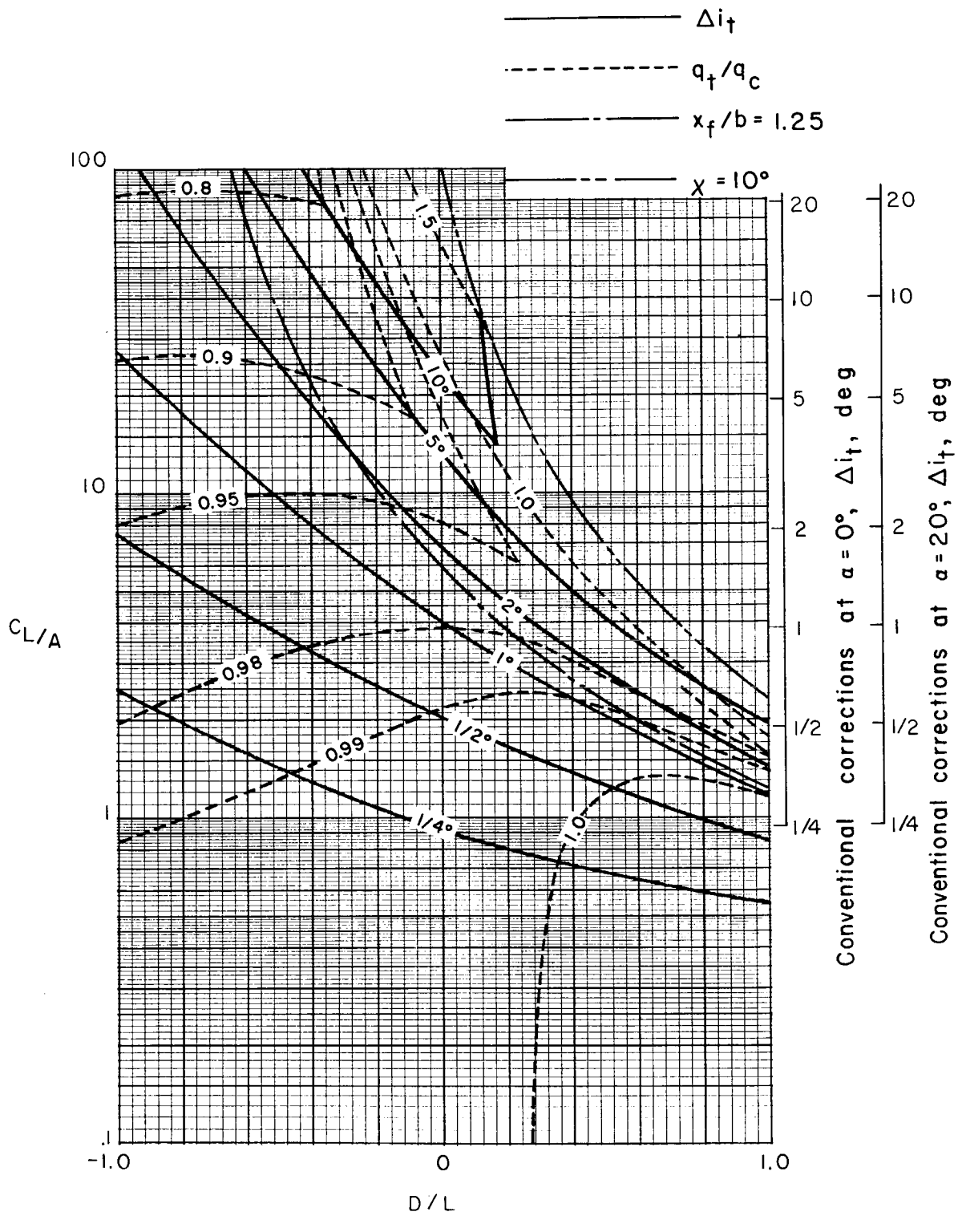


(a) $\sigma = 1/4$.

Figure 29.- Corrections at a zero-span tail behind a uniformly loaded wing centered in a closed rectangular tunnel. Tail length is three-fourths of wing span; tail height is zero; $\alpha = 20^0$; $\Lambda = 0^0$; $\gamma = 4/3$.

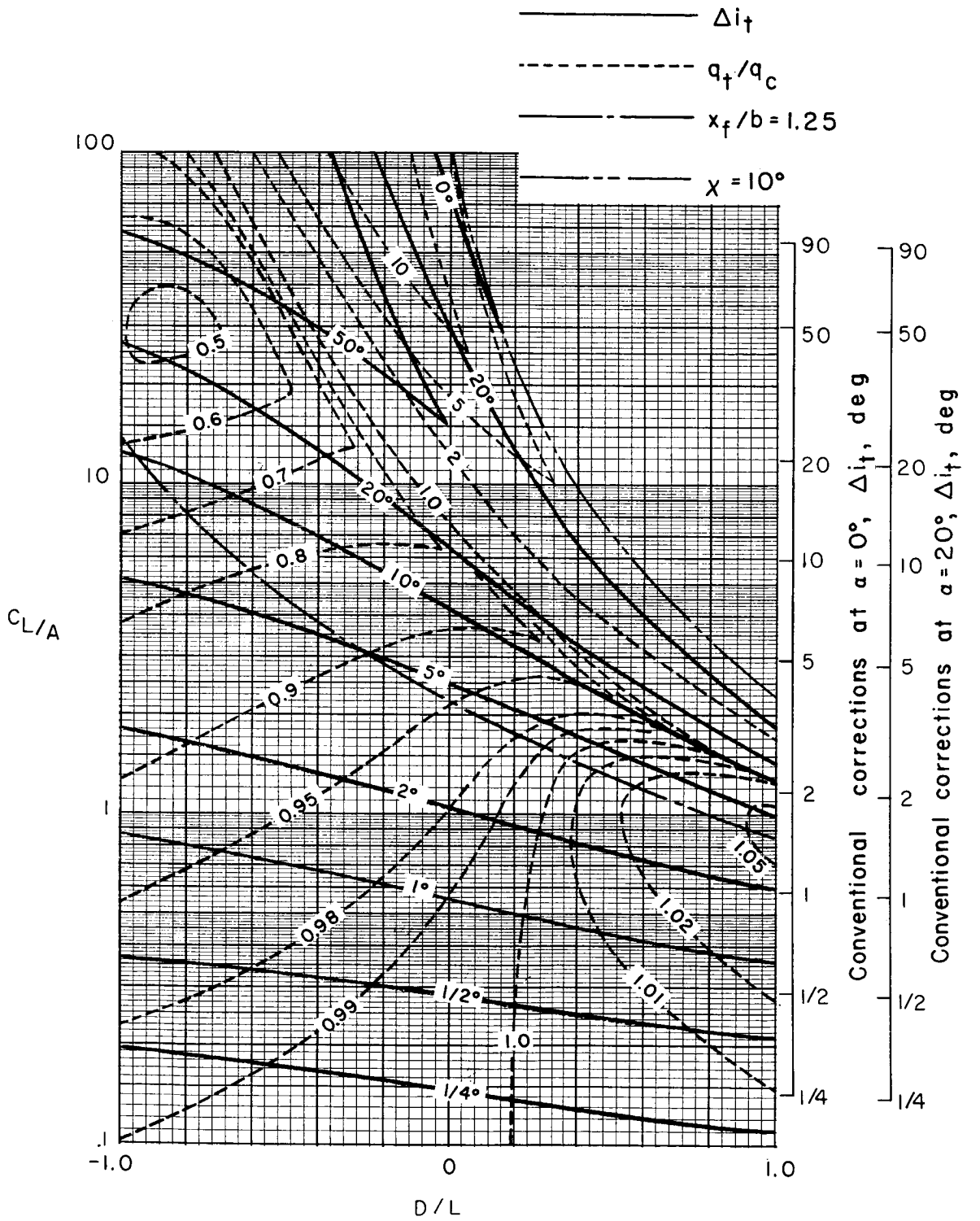


(b) $\sigma = 1/2$.

Figure 29.- Continued.

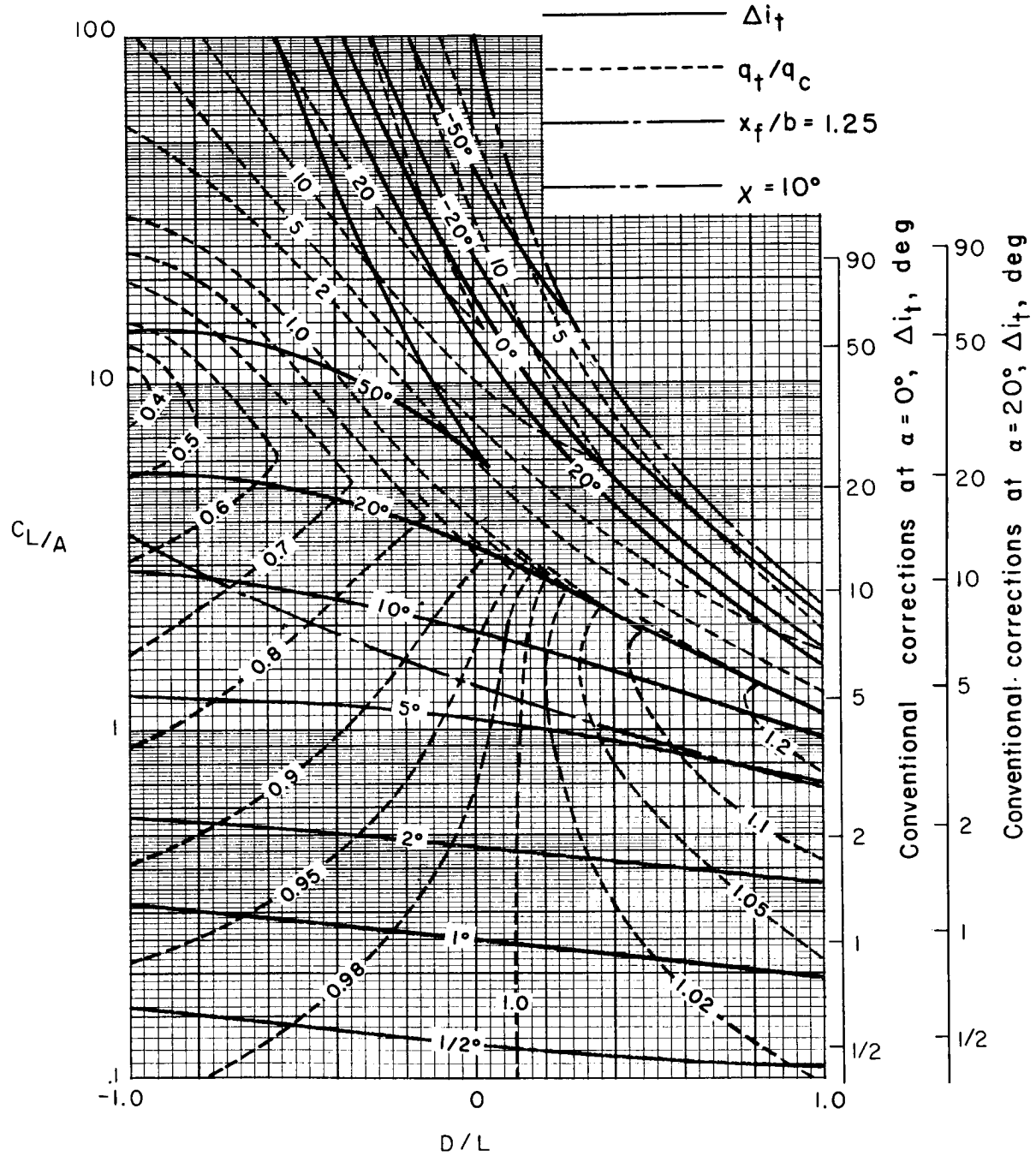


(c) $\sigma = 3/4$.

Figure 29.- Concluded.

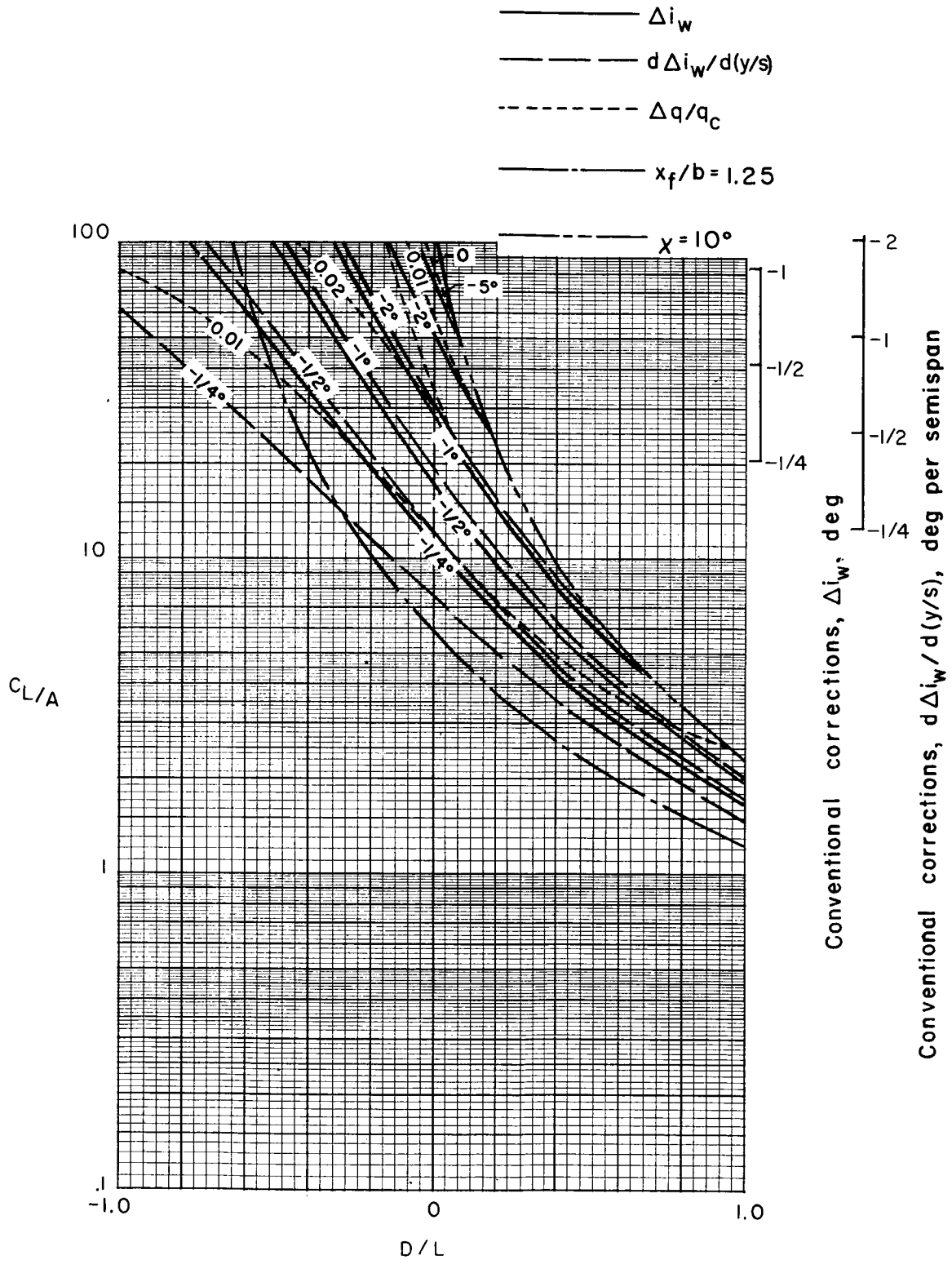


(a) $\sigma = 1/4$.

Figure 30.- Nonuniformity of corrections over a uniformly loaded wing centered in a closed rectangular tunnel. $\gamma = 4/3$; $\alpha = 0^0$; $\Lambda = 0^0$.

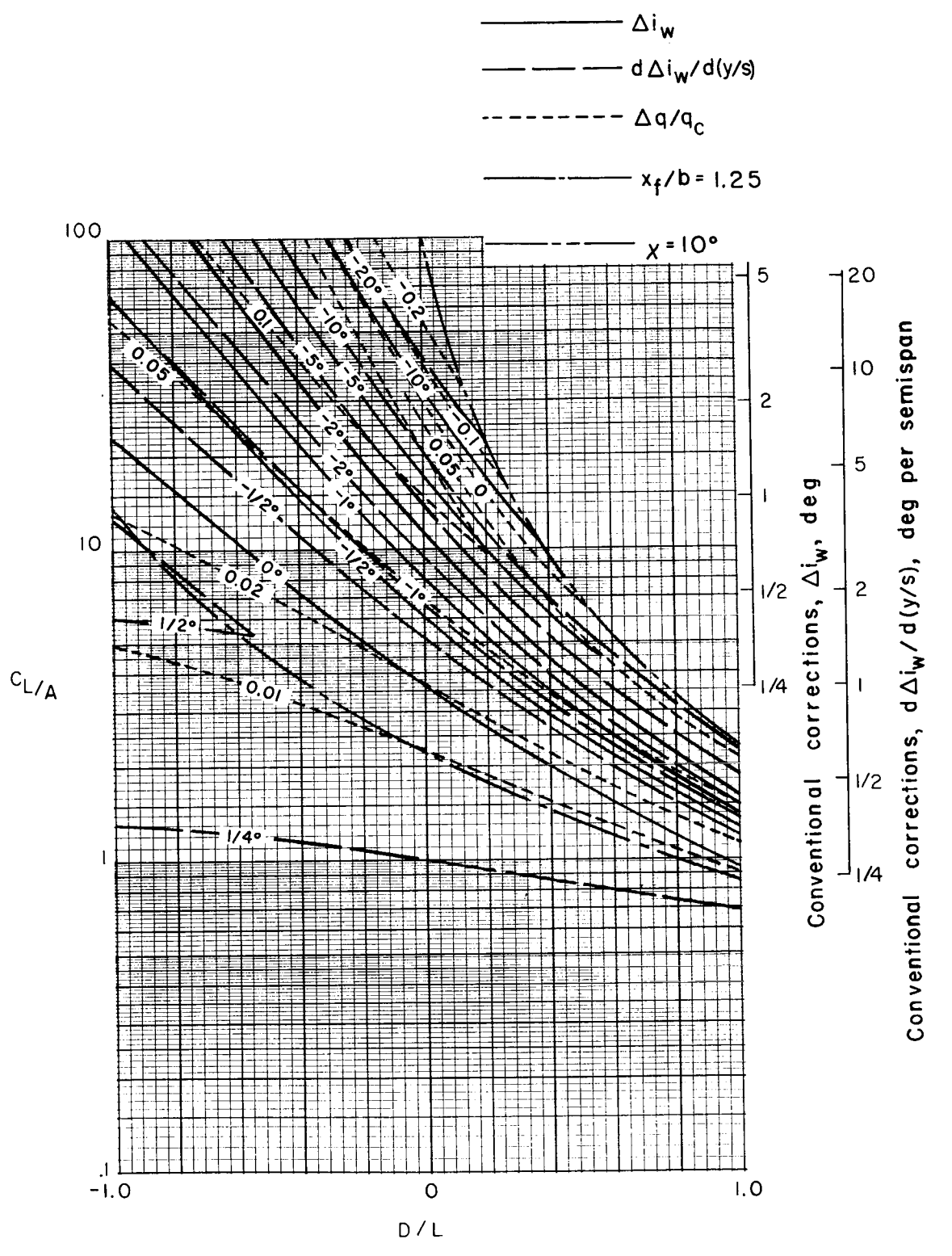


(b) $\sigma = 1/2$.

Figure 30.- Continued.

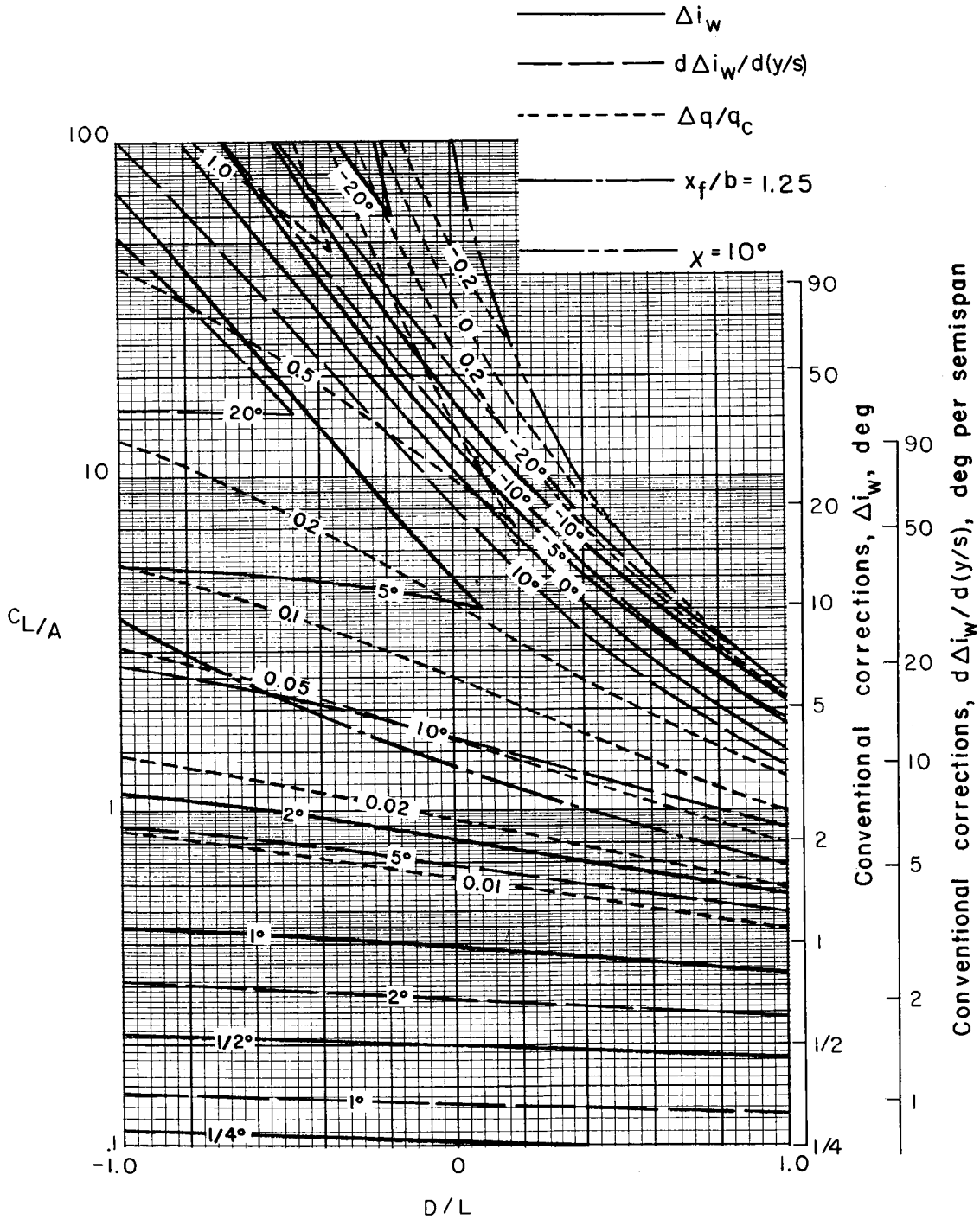


(c) $\sigma = 3/4$.

Figure 30.- Concluded.

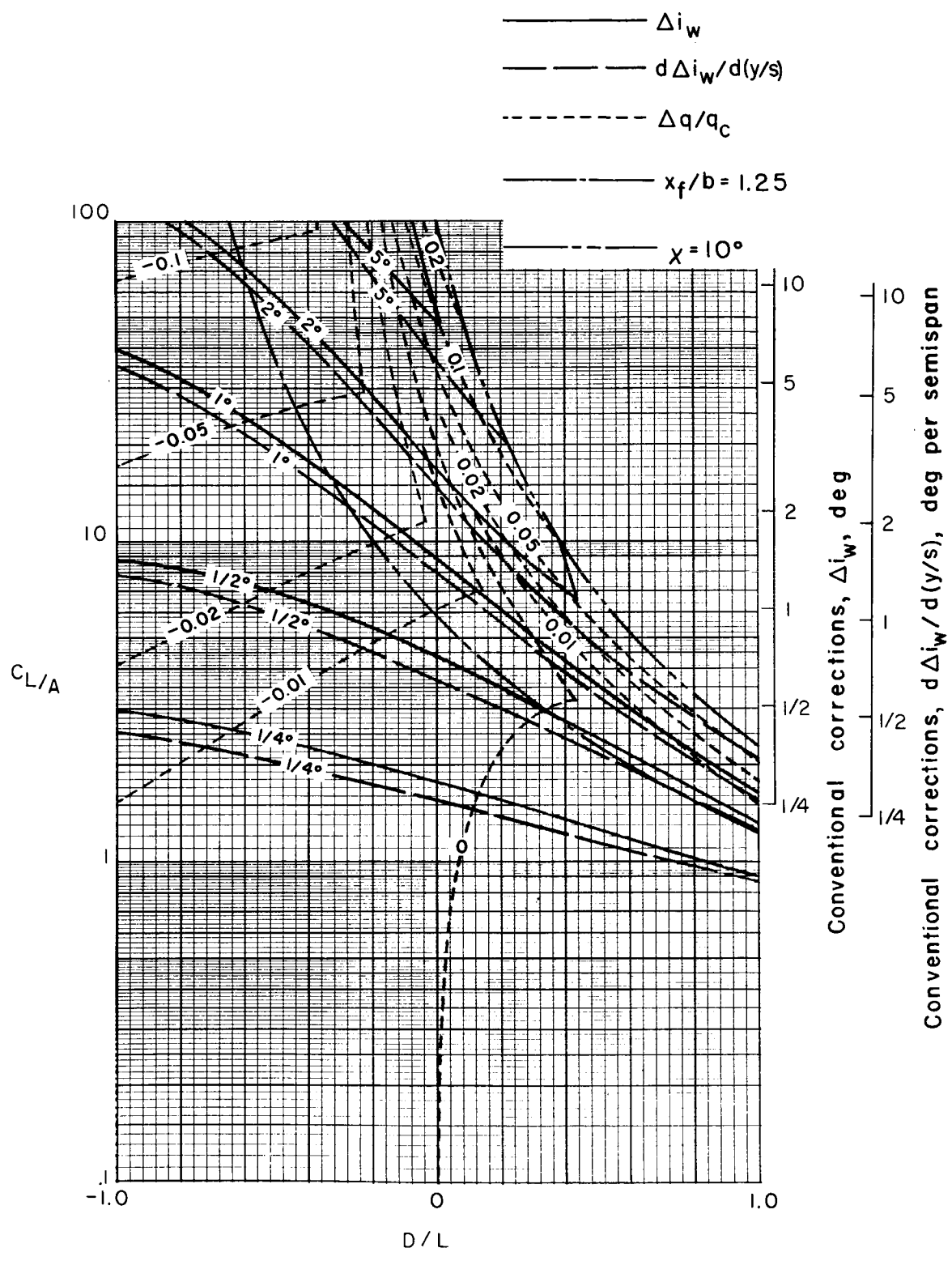


(a) $\sigma = 1/4$.

Figure 31.- Nonuniformity of corrections over a uniformly loaded wing centered in a closed rectangular tunnel. $\gamma = 4/3$; $\alpha = 0^0$; $\Lambda = 45^0$.

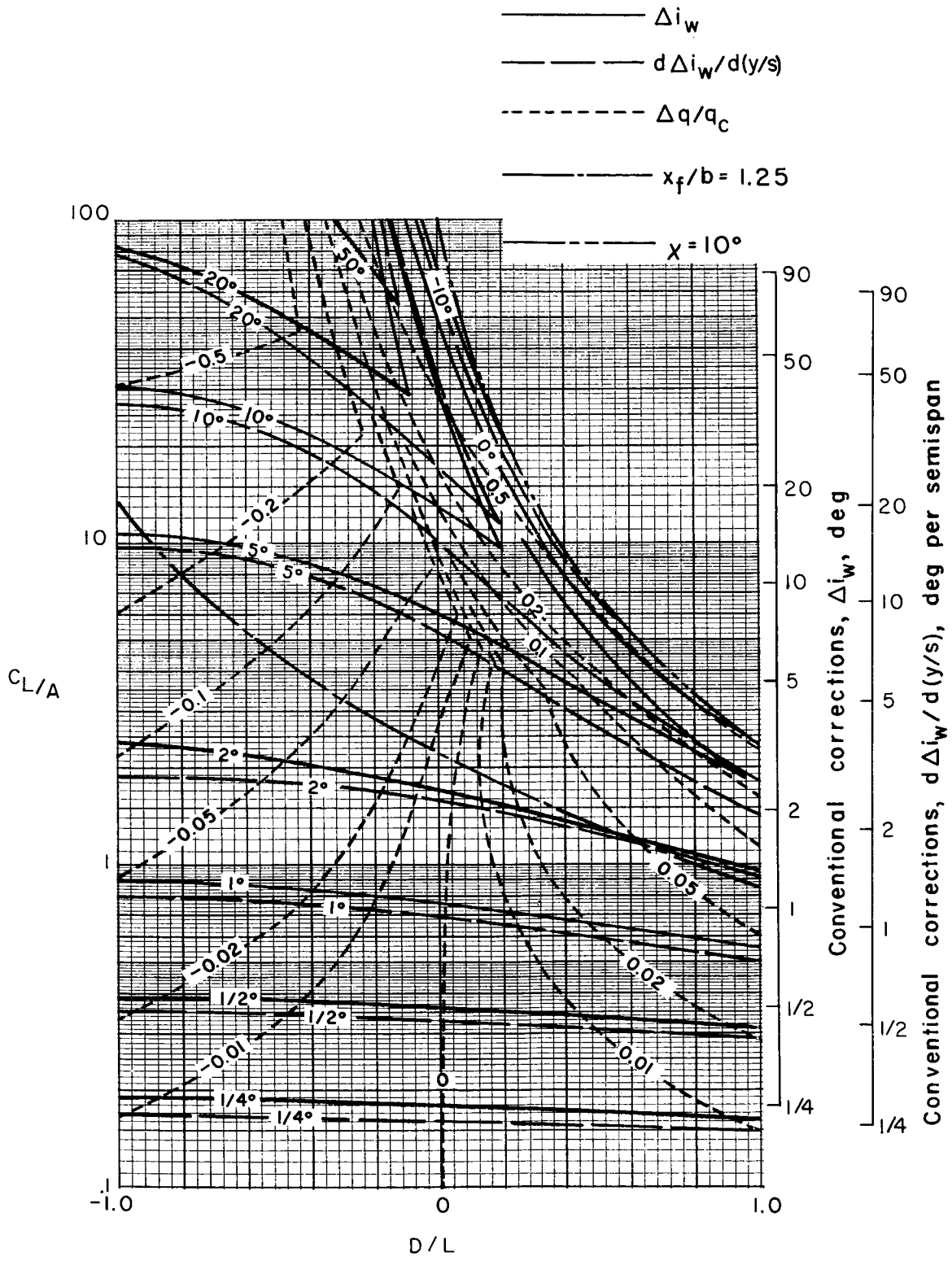


(b) $\sigma = 1/2$.

Figure 31.- Continued.

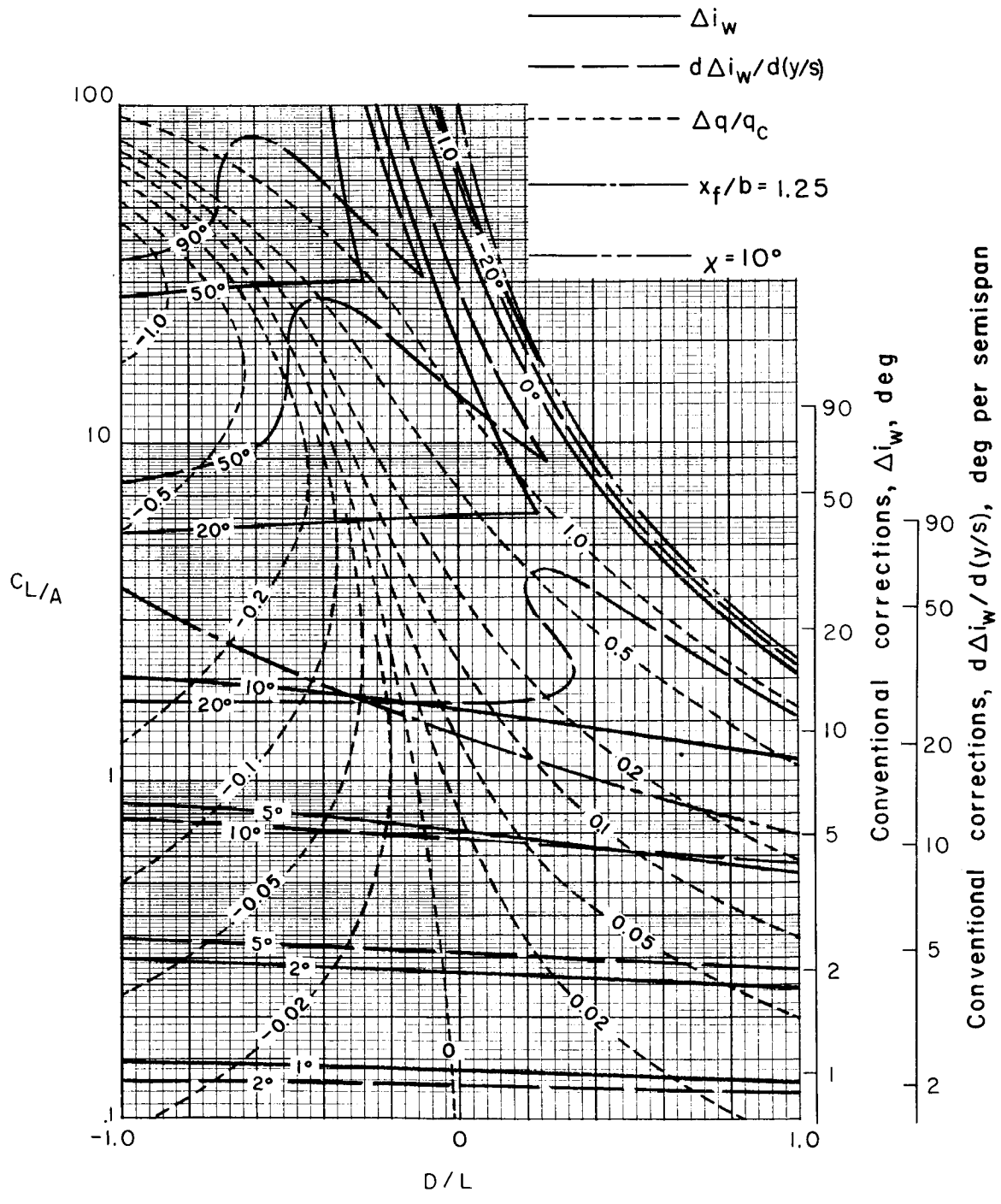


(c) $\sigma = 3/4$.

Figure 31.- Concluded.

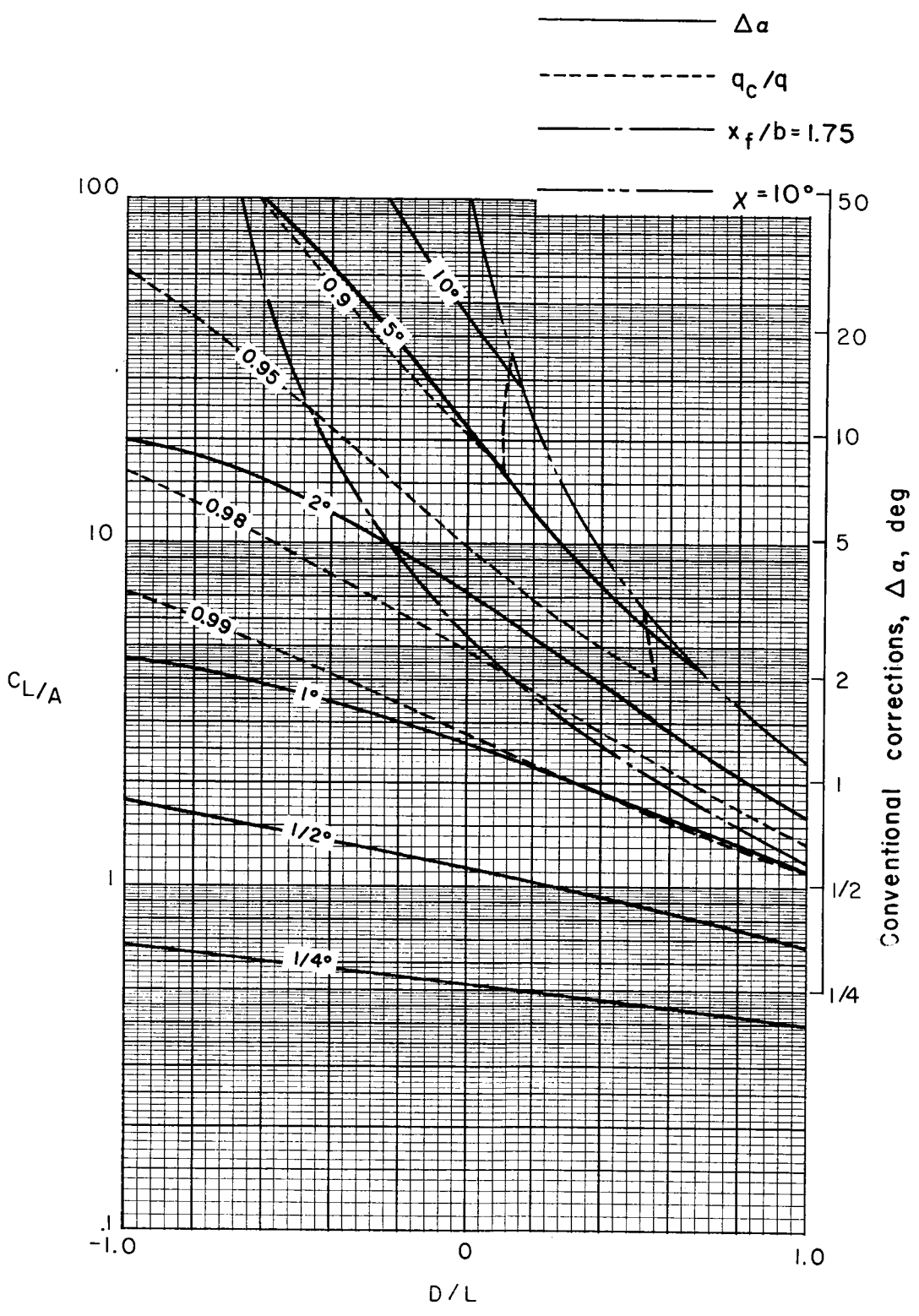


(a) σ = 1/4.

Figure 32.- Average corrections for a uniformly loaded wing centered in a closed rectangular tunnel. γ = 1.0; Λ = 0°.

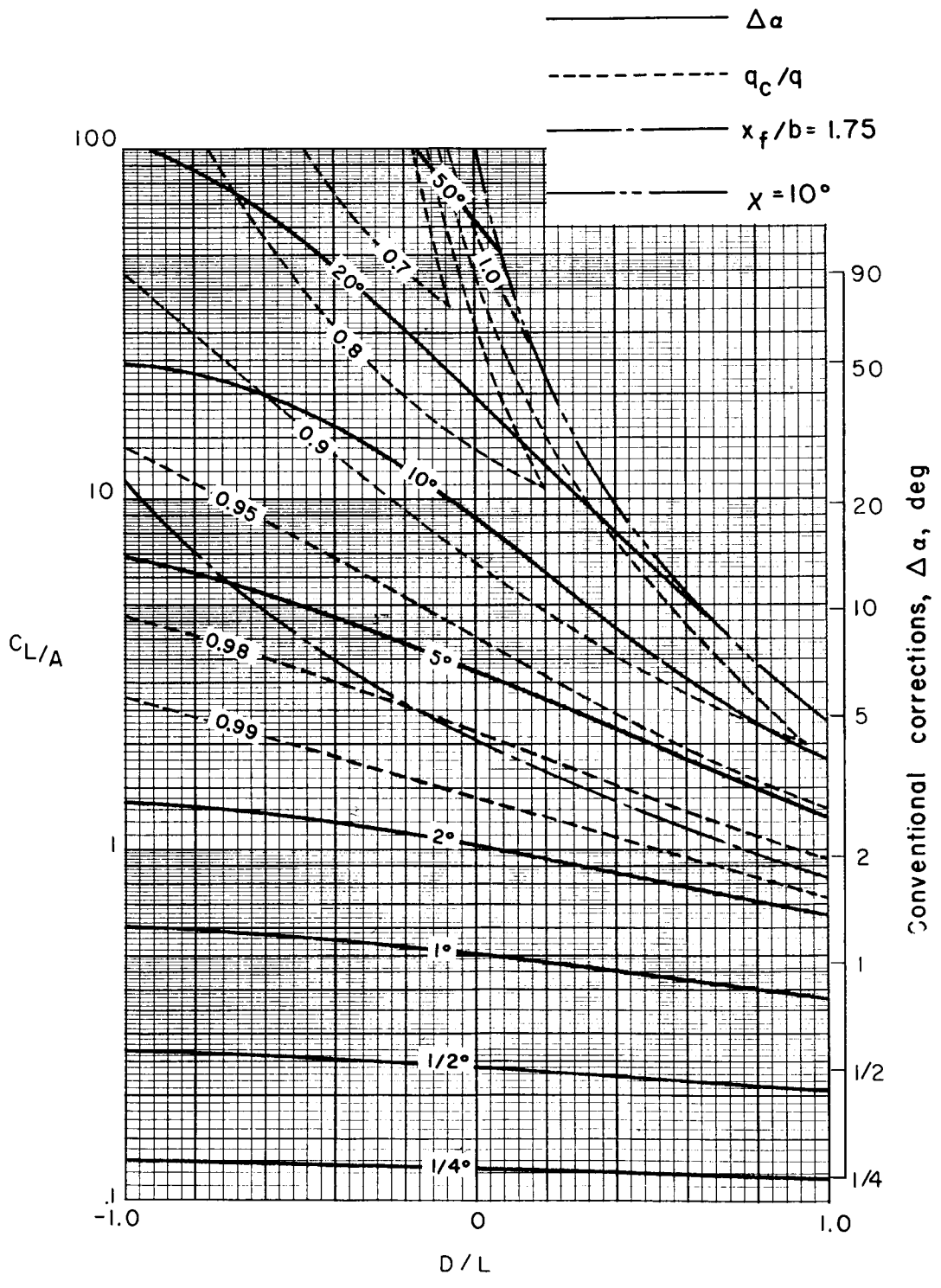


(b) σ = 1/2.

Figure 32.- Continued.

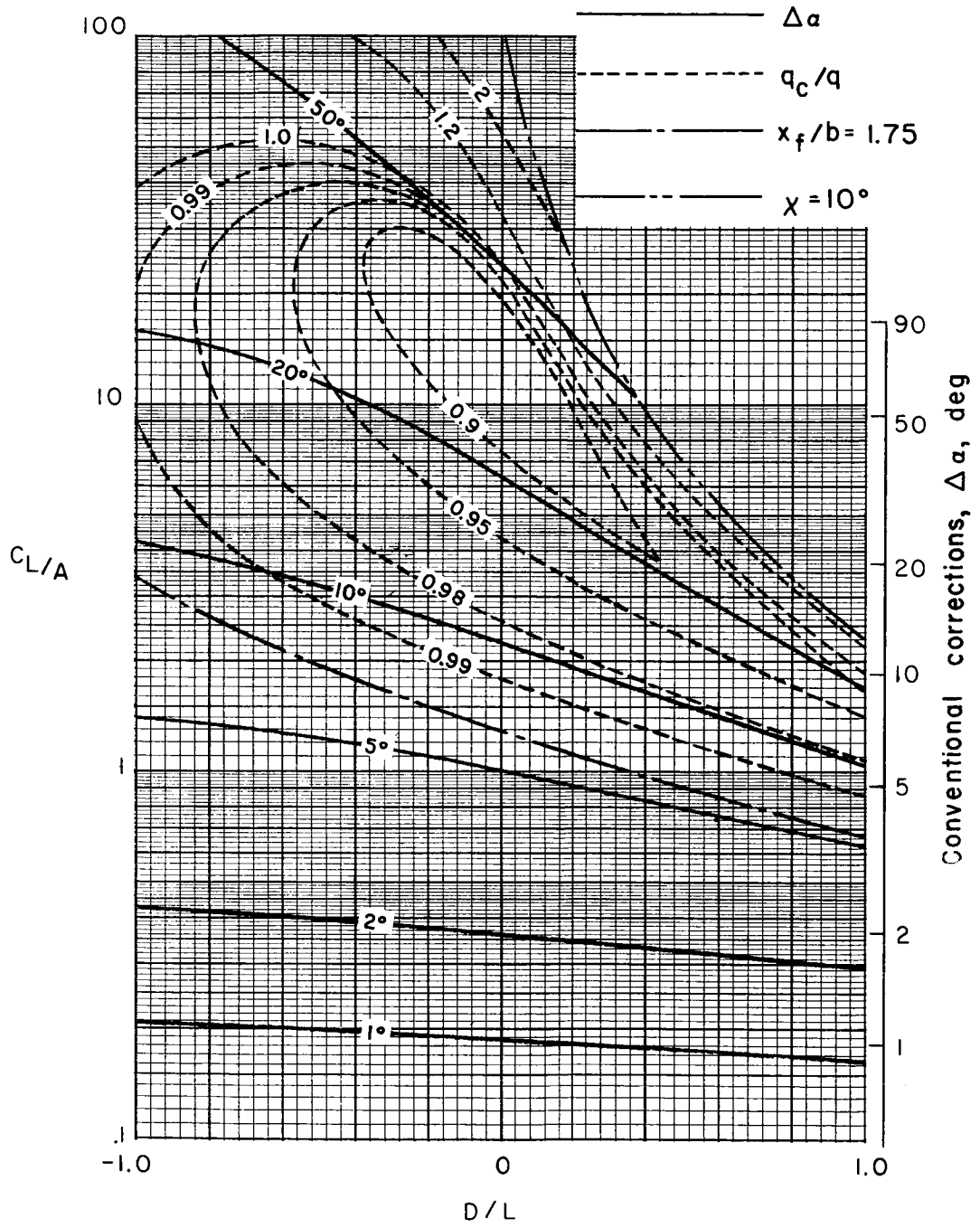


(c) σ = 3/4.

Figure 32.- Concluded.

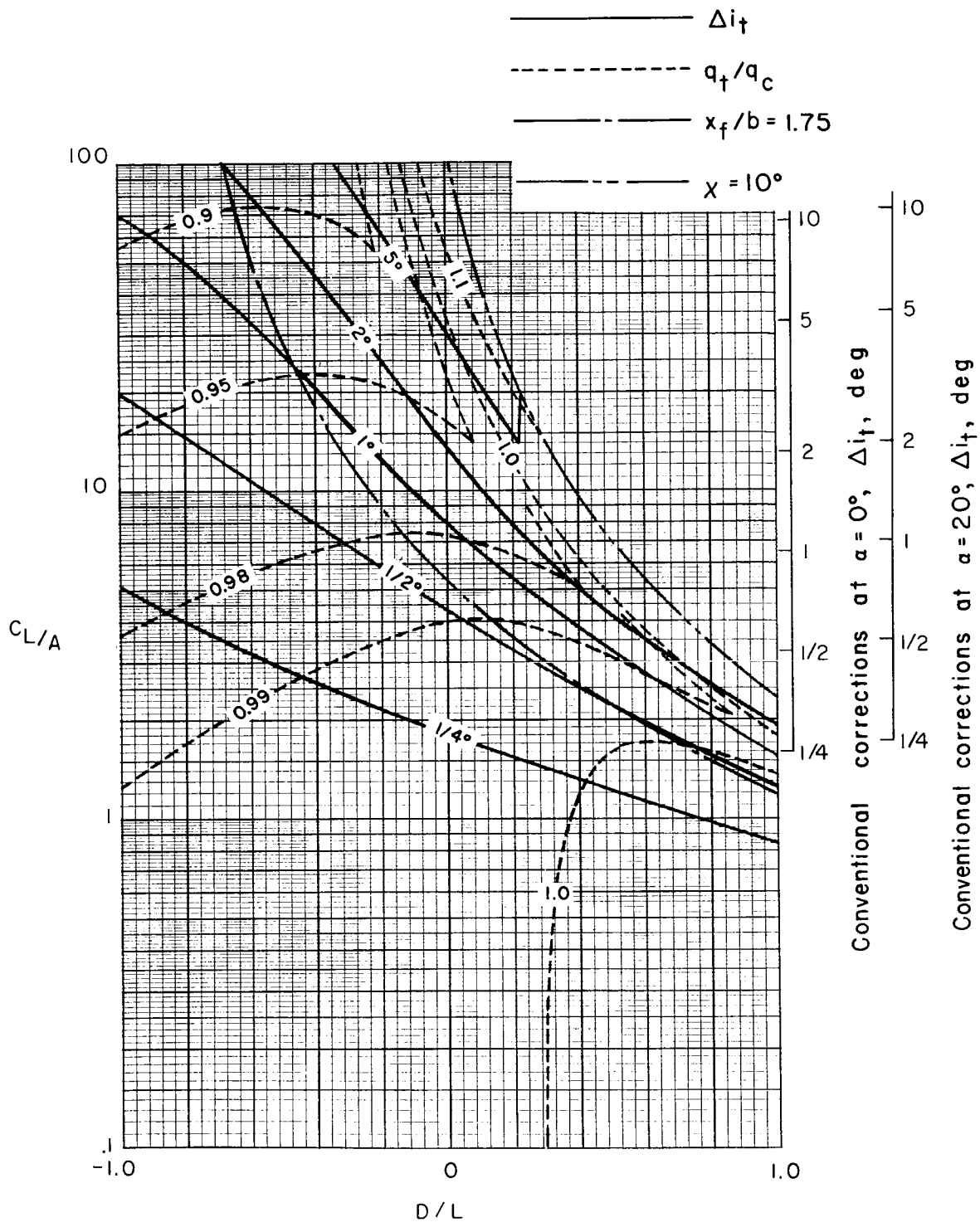


(a) $\sigma = 1/4$.

Figure 33.- Corrections at a zero-span tail behind a uniformly loaded wing centered in a closed rectangular tunnel. Tail length is three-fourths of wing span; tail height is zero; $\alpha = 20^0$; $\Lambda = 0^0$; $\gamma = 1.0$.

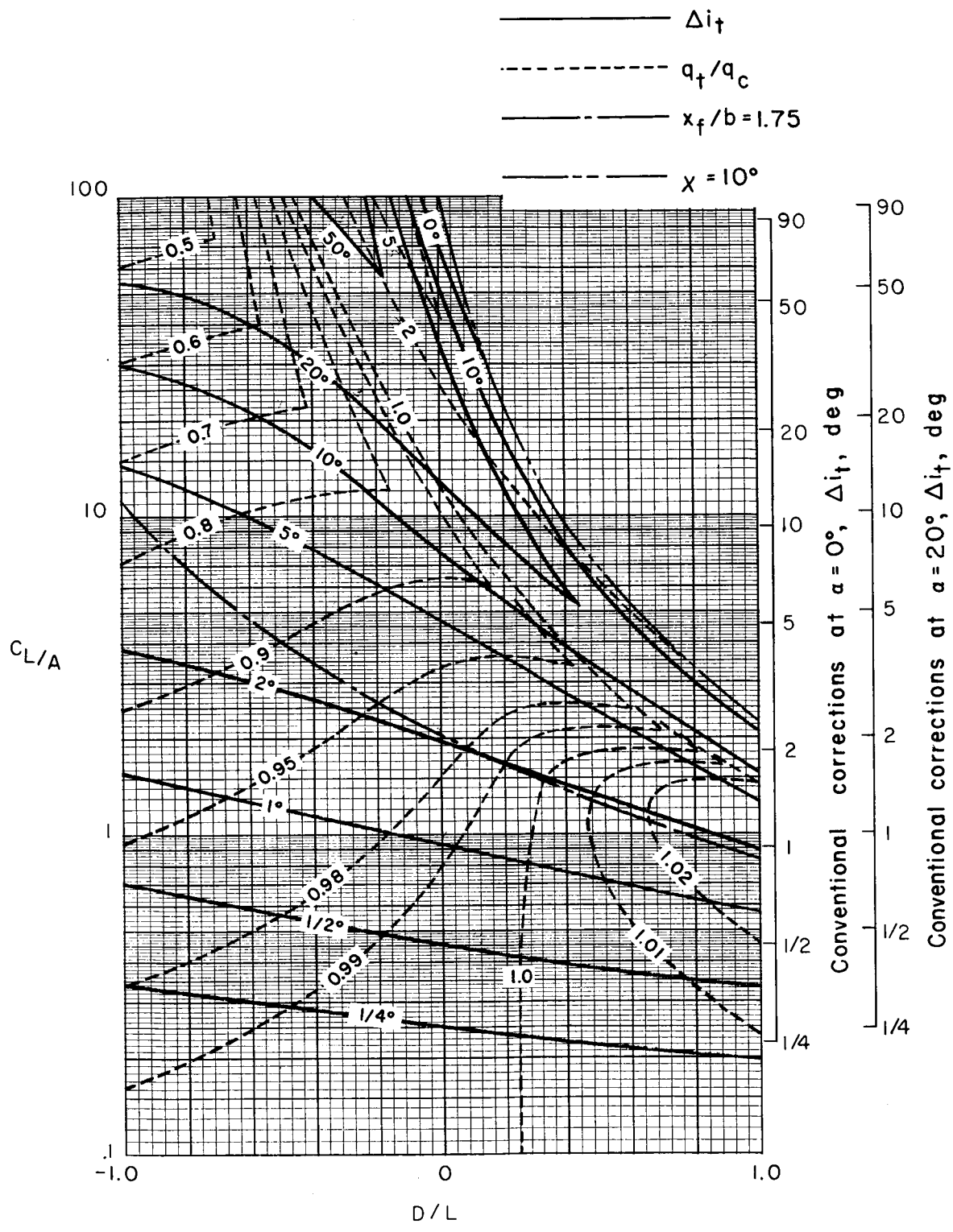


(b) $\sigma = 1/2$.

Figure 33.- Continued.

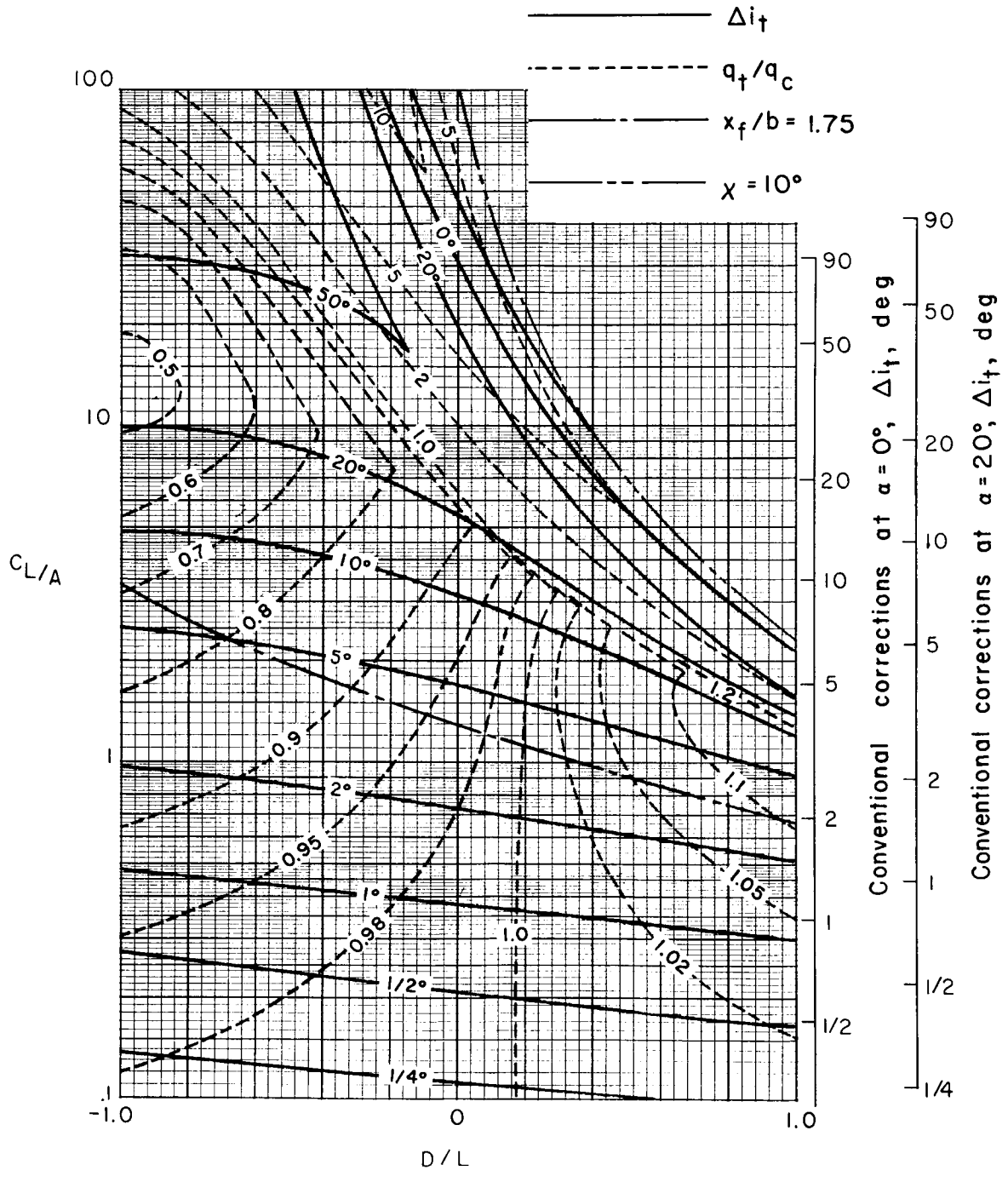


(c) $\sigma = 3/4$.

Figure 33.- Concluded.

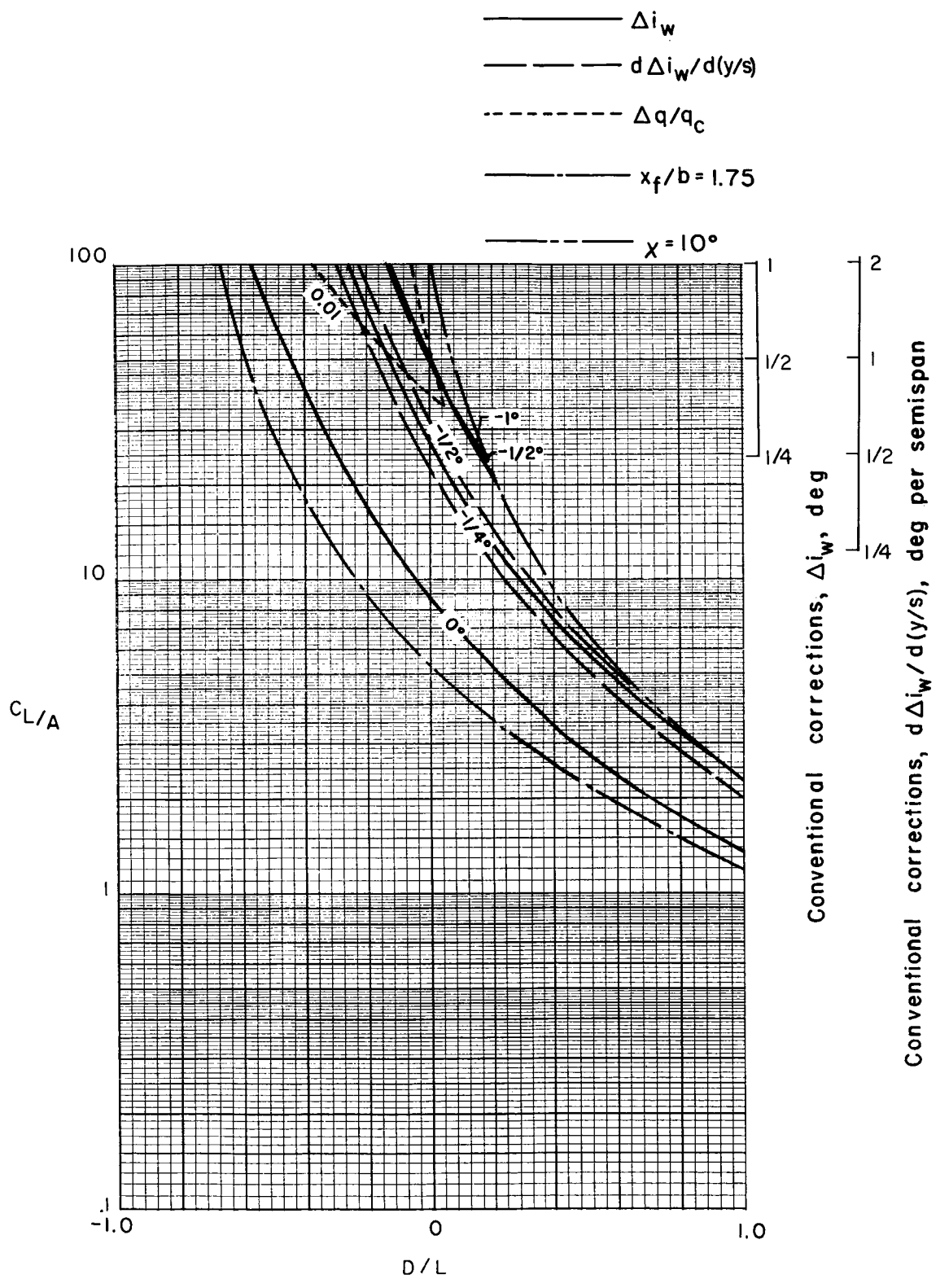


(a) $\sigma = 1/4$.

Figure 34.- Nonuniformity of corrections over a uniformly loaded wing centered in a closed rectangular tunnel. $\gamma = 1.0$; $\alpha = 0^0$; $\Lambda = 0^0$.

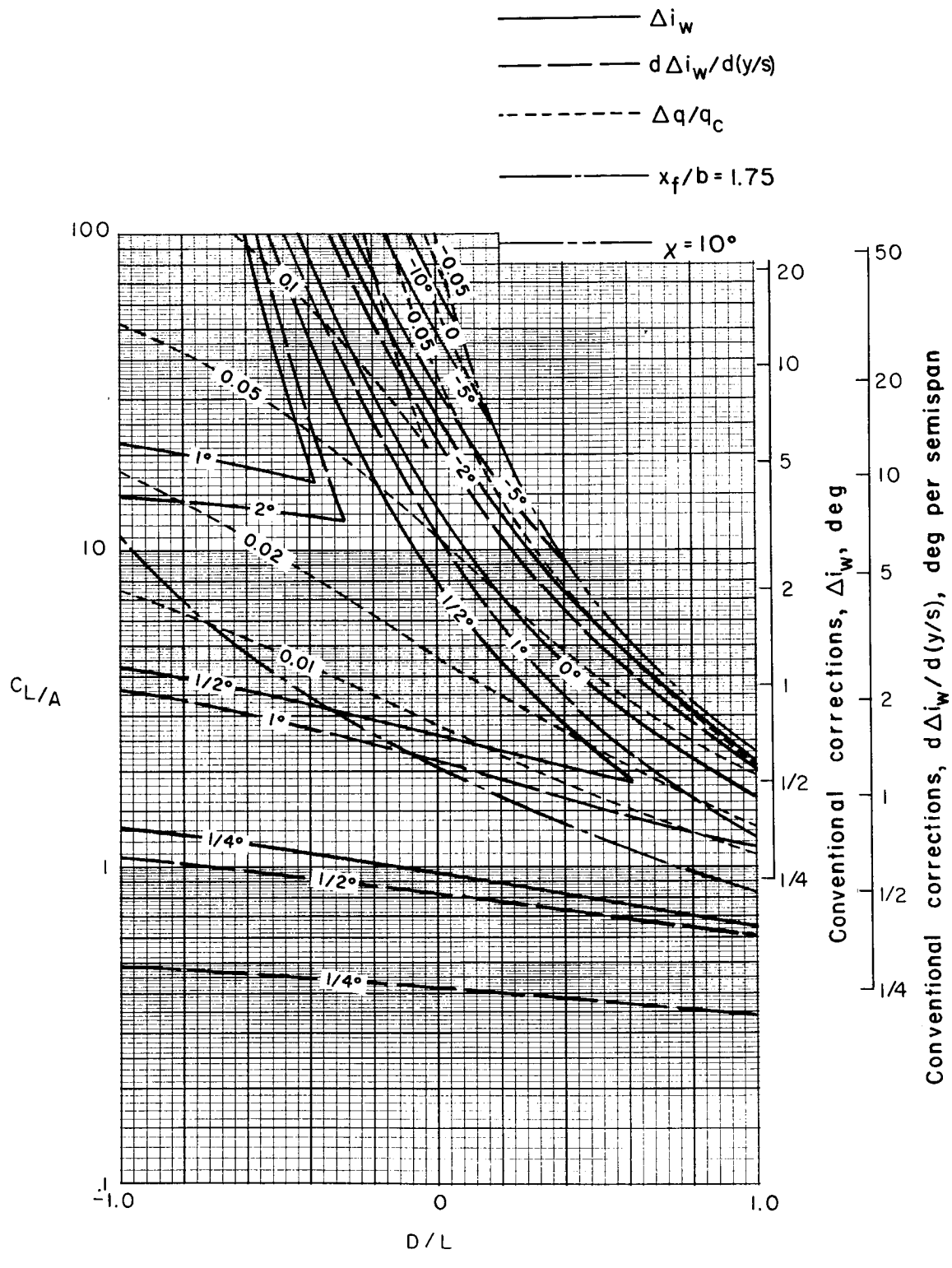


(b) $\sigma = 1/2$.

Figure 34.- Continued.

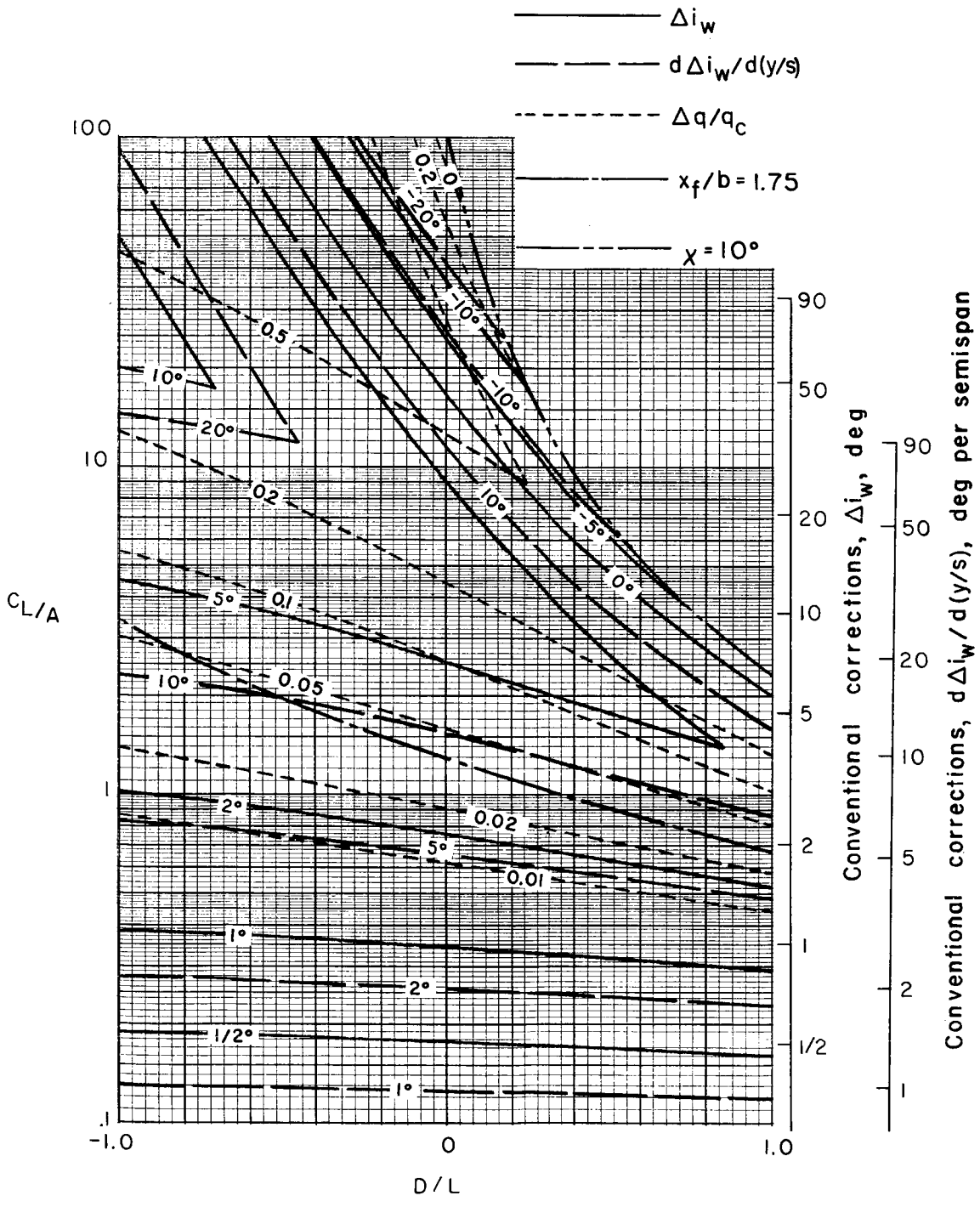


(c) $\sigma = 3/4$.

Figure 34.- Concluded.

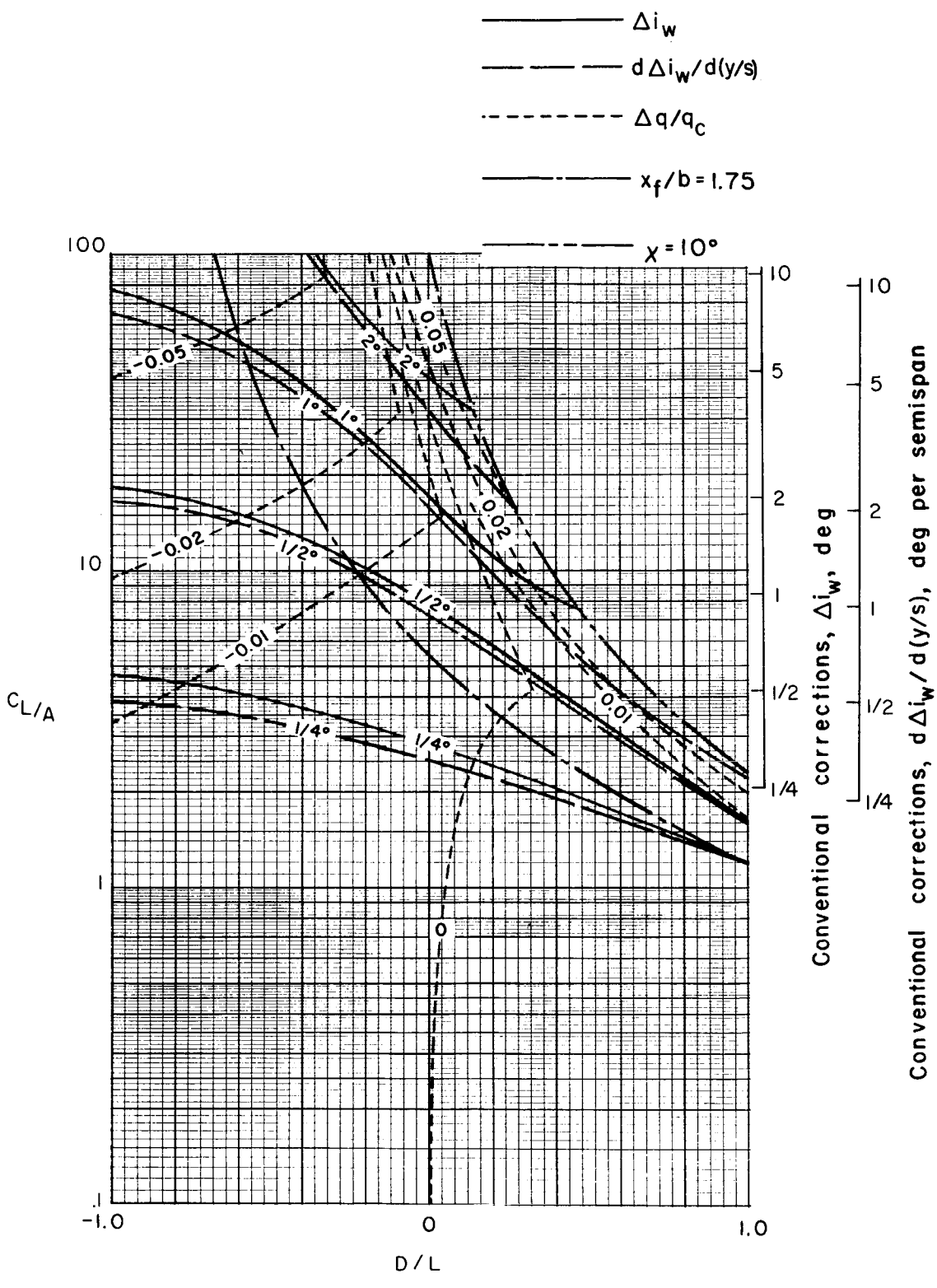


(a) $\sigma = 1/4$.

Figure 35.- Nonuniformity of corrections over a uniformly loaded wing centered in a closed rectangular tunnel. $\gamma = 1.0$; $\alpha = 0^0$; $\Lambda = 45^0$.

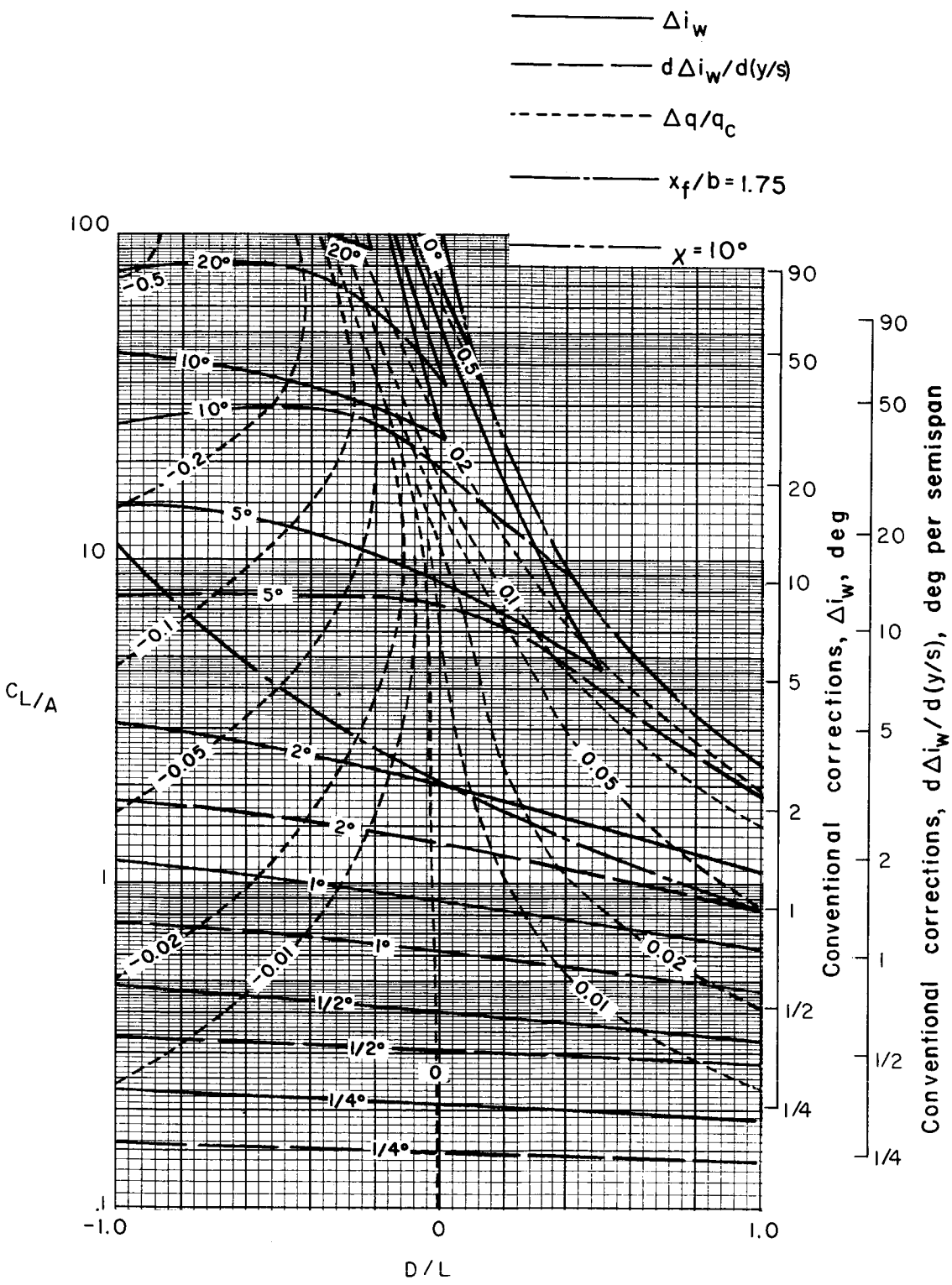


(b) $\sigma = 1/2$.

Figure 35.- Continued.

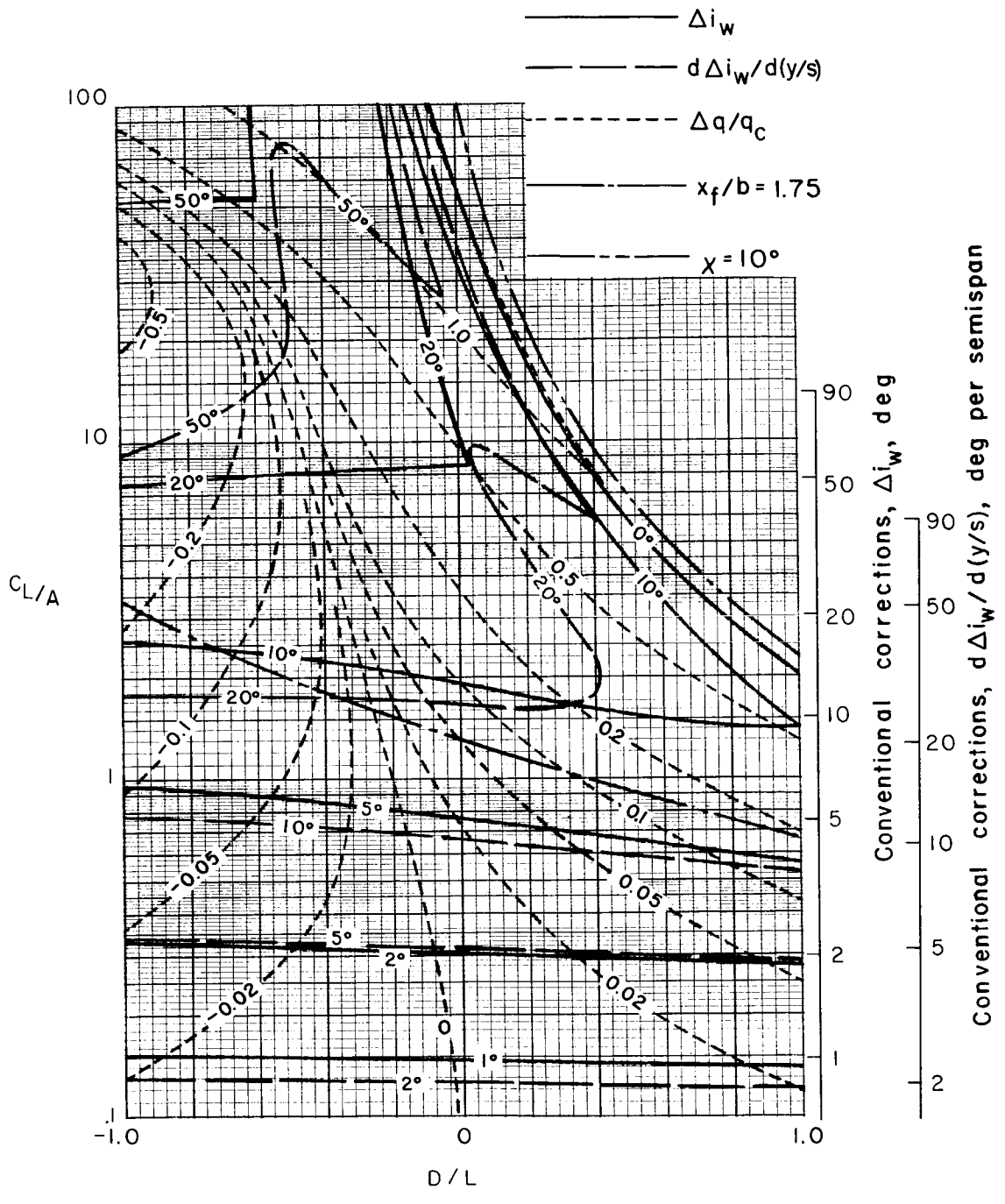


(c) $\sigma = 3/4$.

Figure 35.- Concluded.

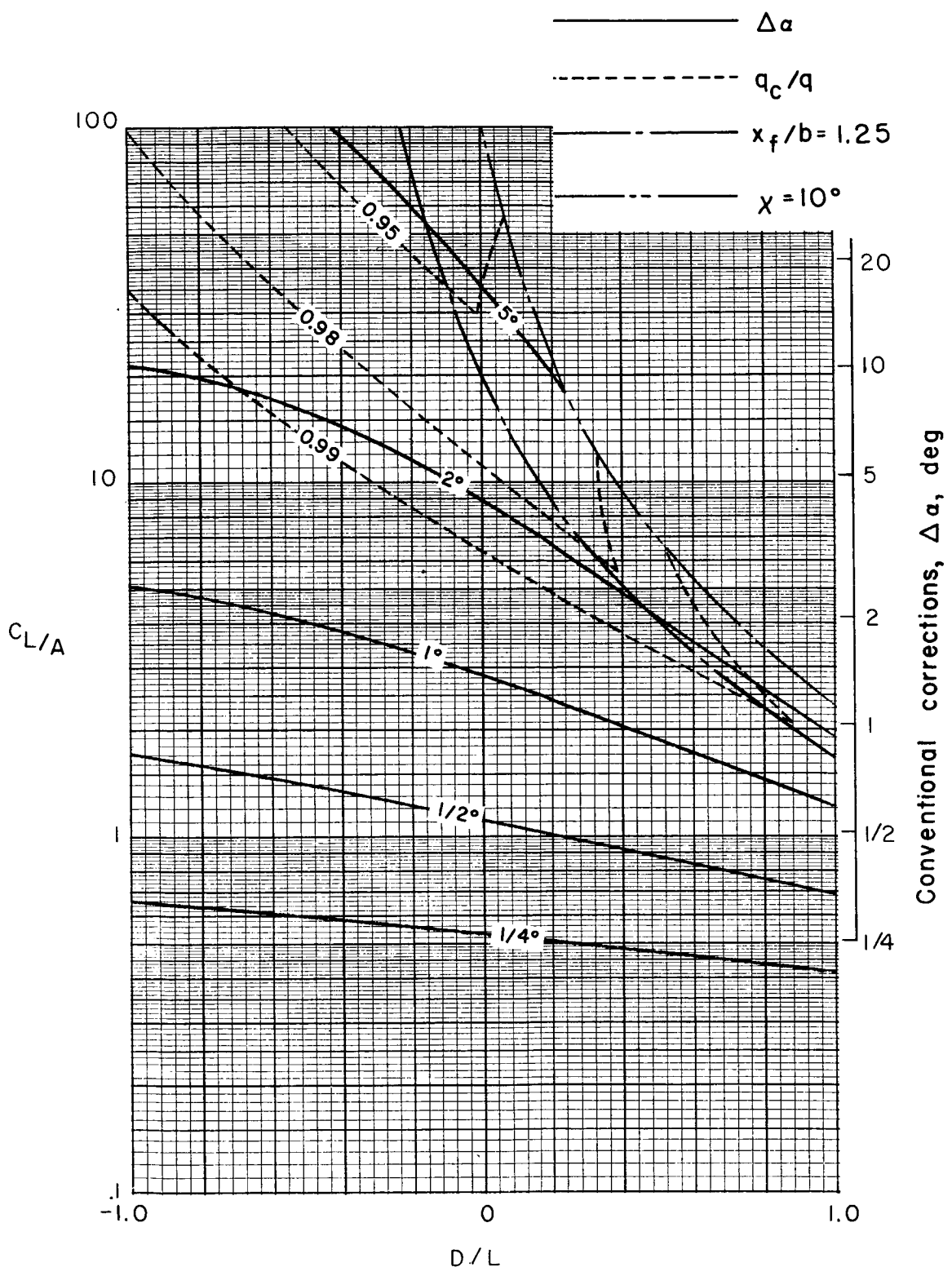


(a) σ = 1/4.

Figure 36.- Average corrections for a uniformly loaded wing centered in a closed rectangular tunnel. Λ = 0°; γ = 2/3.

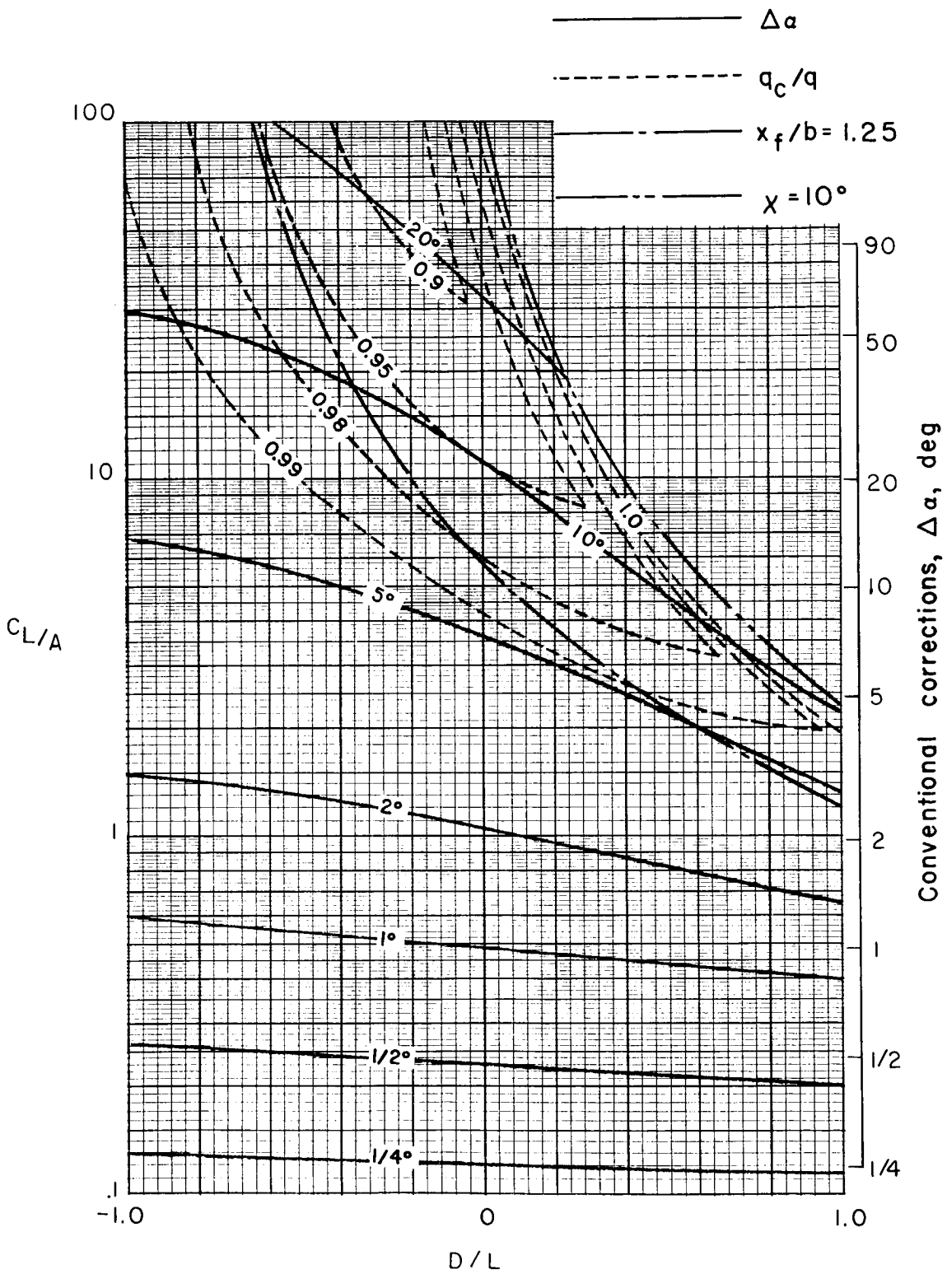


(b) σ = 1/2.

Figure 36.- Continued.

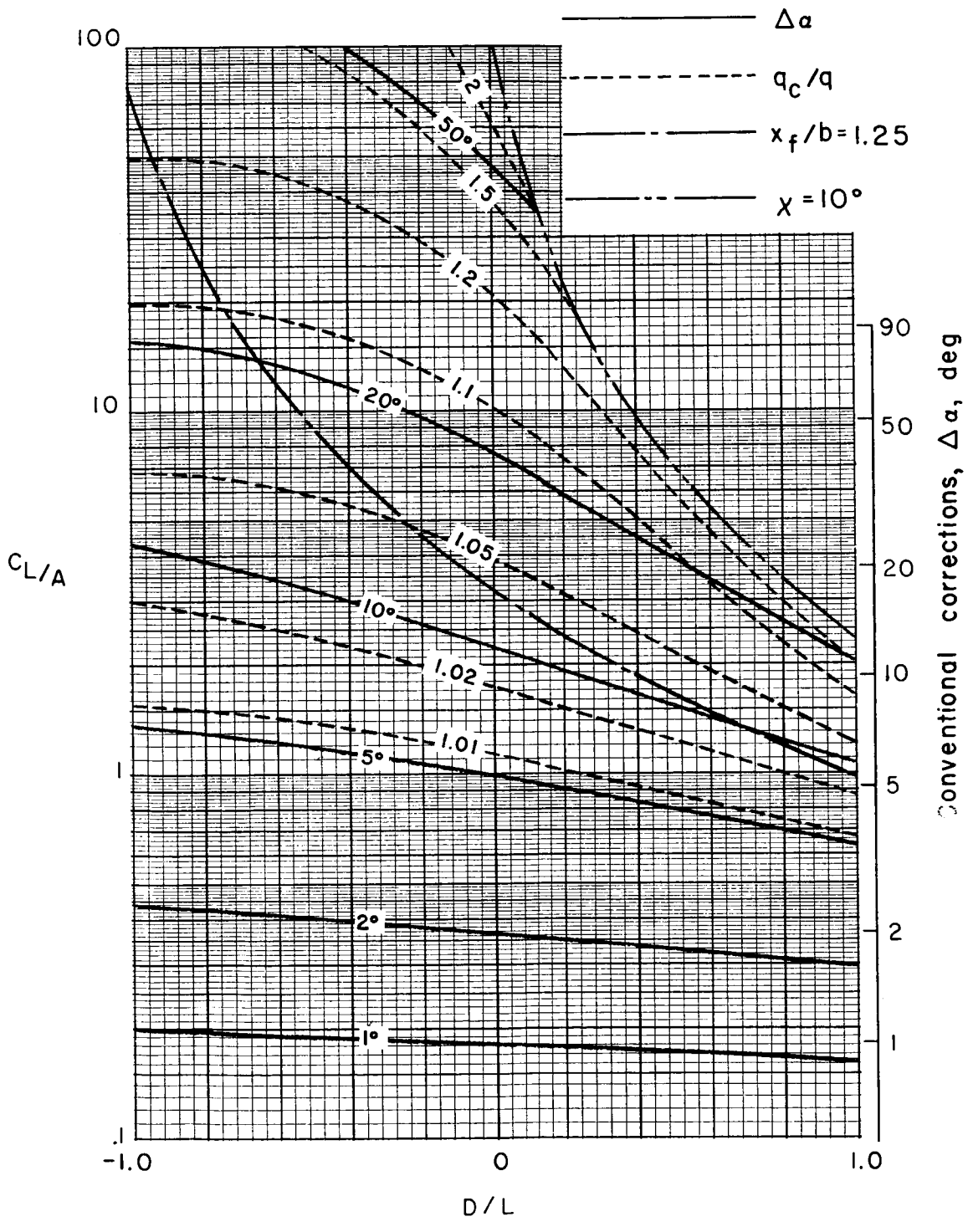


(c) σ = 3/4.

Figure 36.- Concluded.

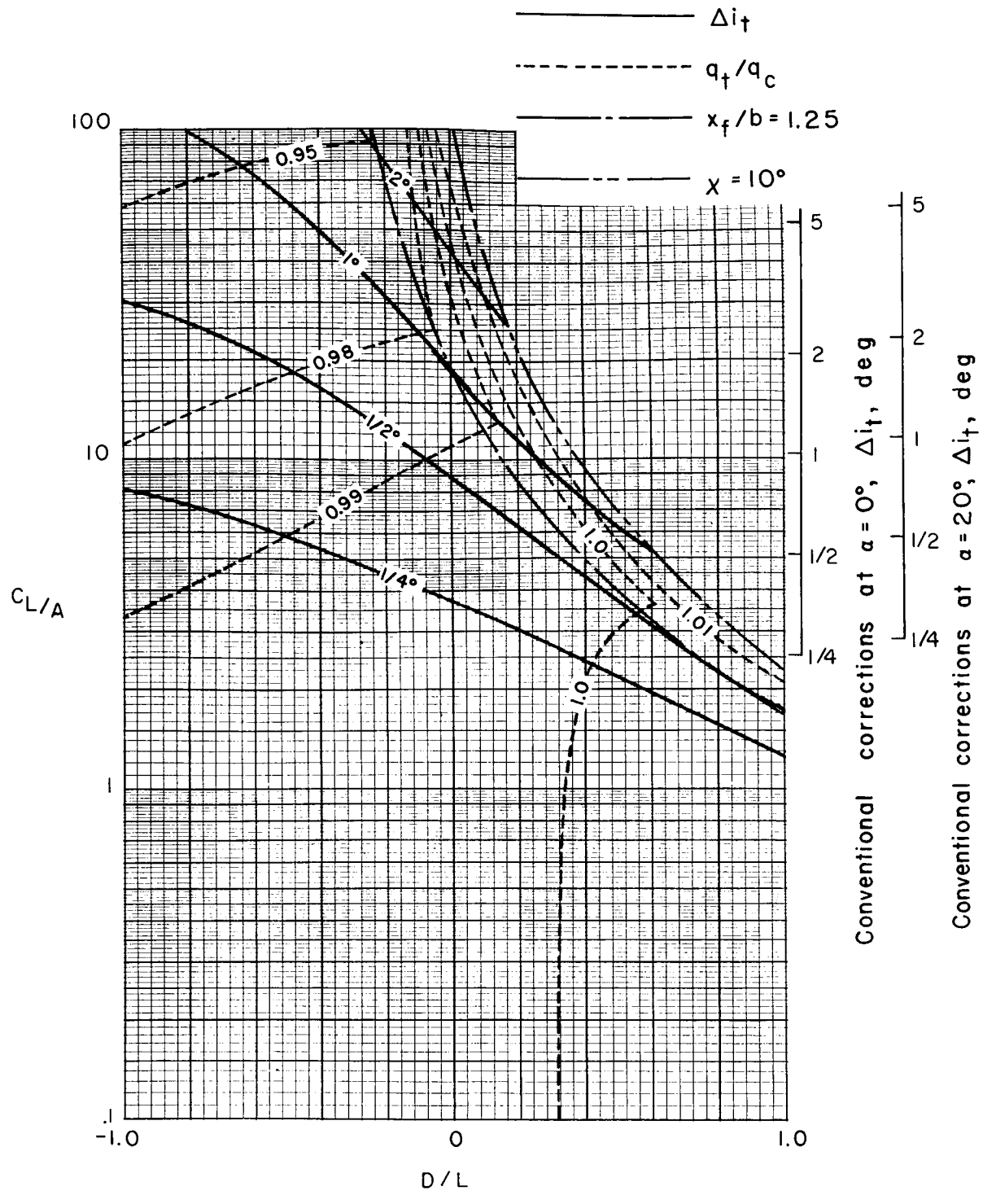


(a) $\sigma = 1/4$.

Figure 37.- Corrections at a zero-span tail behind a uniformly loaded wing centered in a closed rectangular tunnel. Tail length is three-fourths of wing span; tail height is zero; $\alpha = 20^0$; $\Lambda = 0^0$; $\gamma = 2/3$.

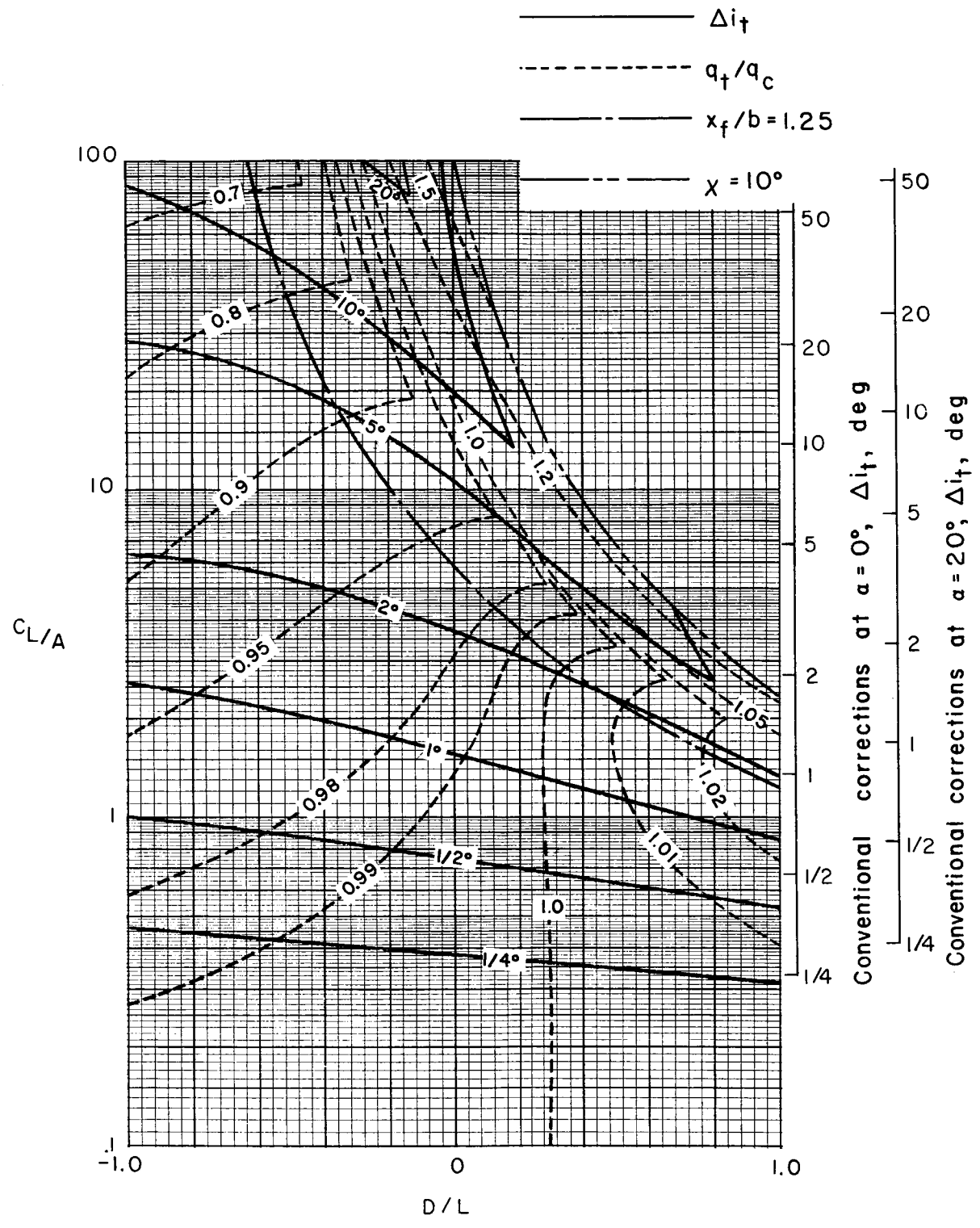


(b) $\sigma = 1/2$.

Figure 37.- Continued.

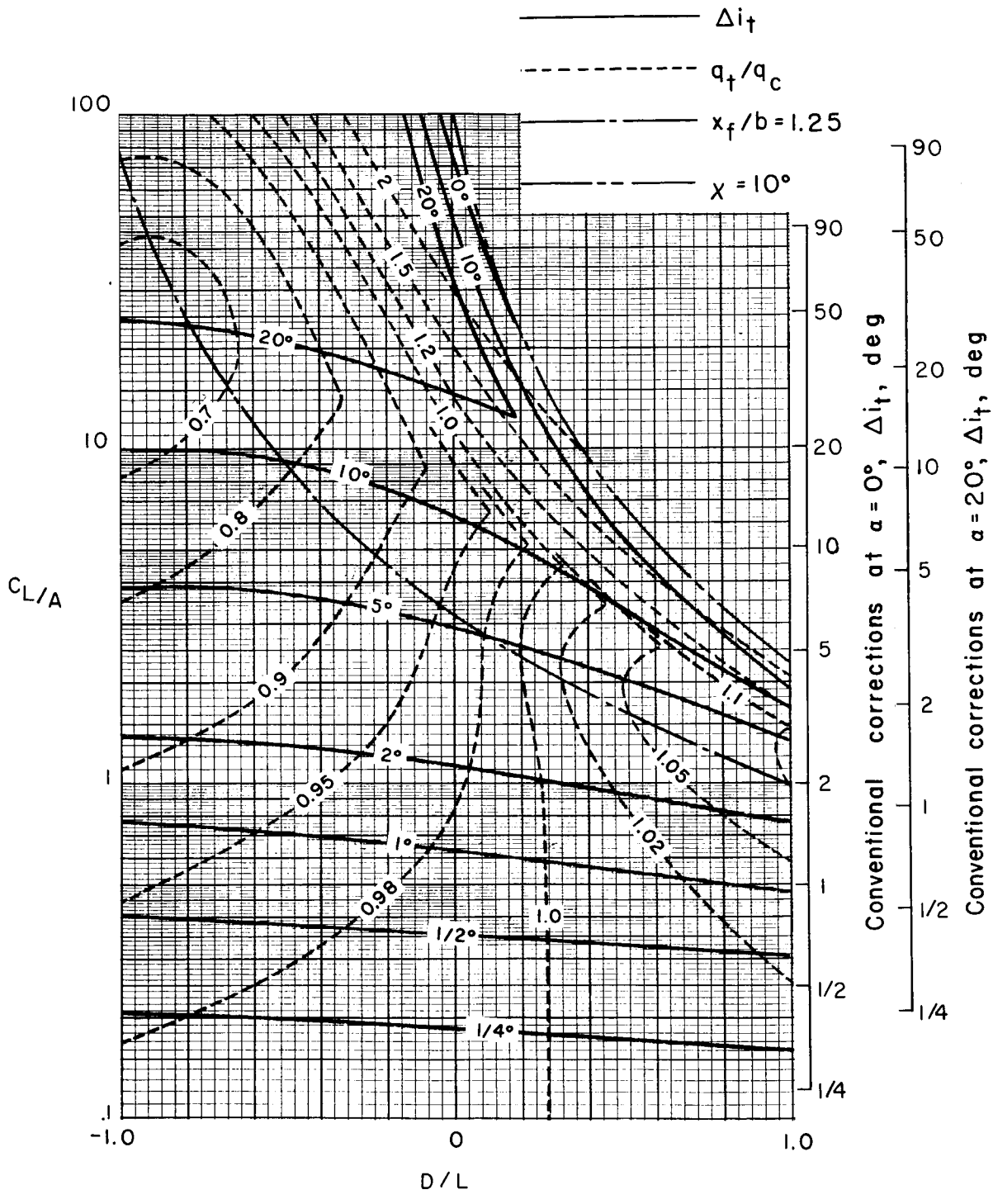


(c) $\sigma = 3/4$.

Figure 37.- Concluded.

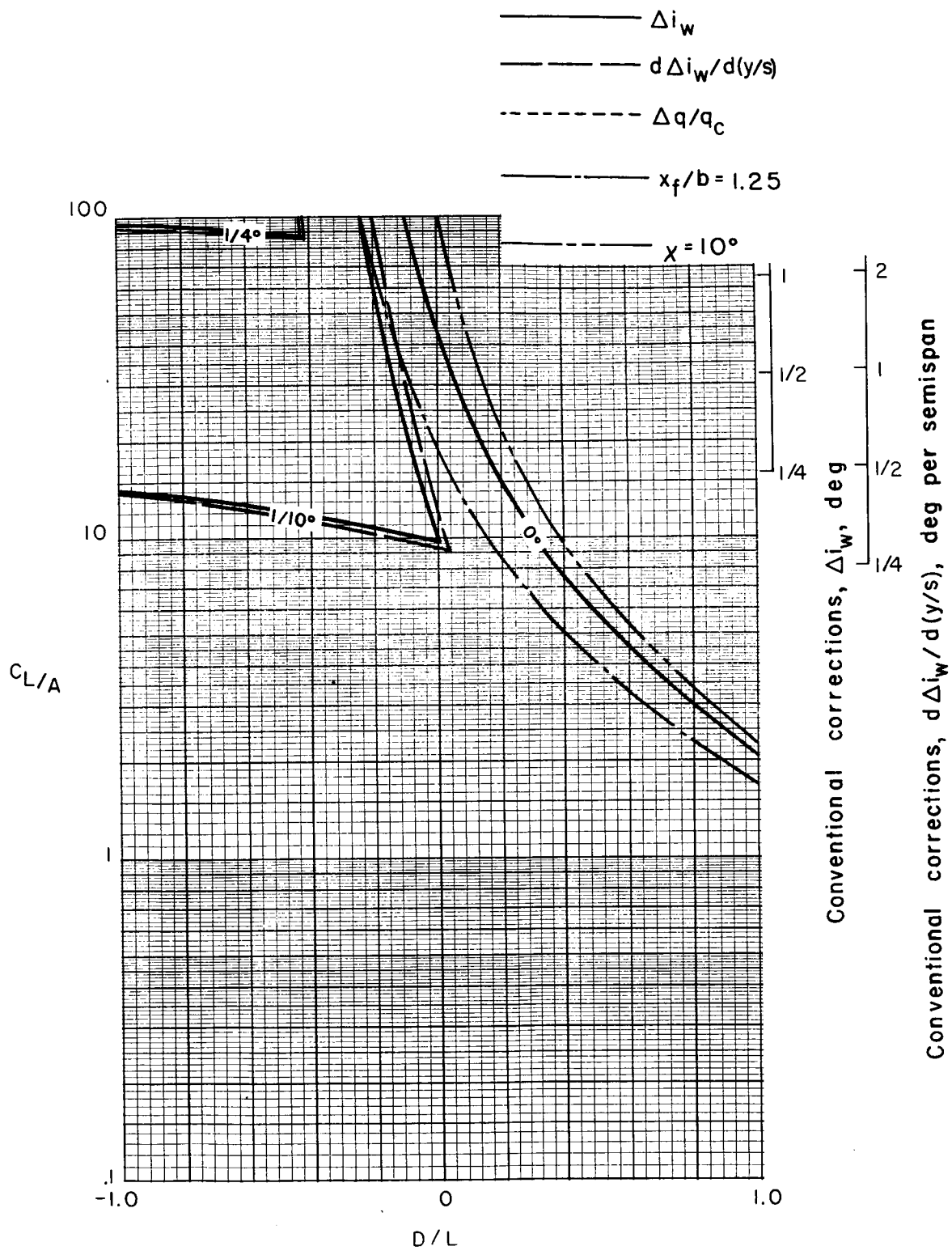


(a) σ = 1/4.

Figure 38.- Nonuniformity of corrections over a uniformly loaded wing centered in a closed rectangular tunnel. γ = 2/3; α = 0°; Λ = 0°.

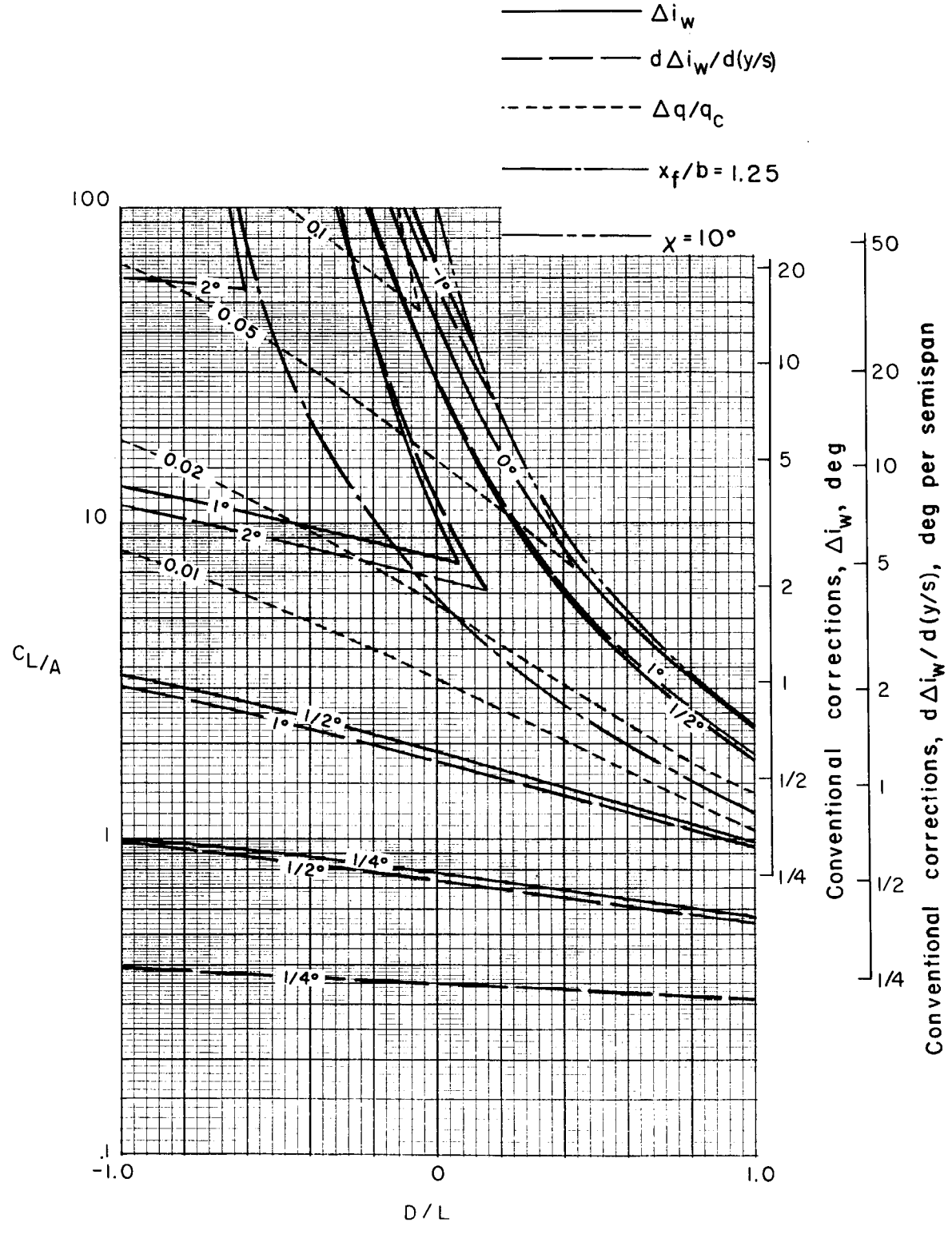


(b) $\sigma = 1/2$.

Figure 38.- Continued.

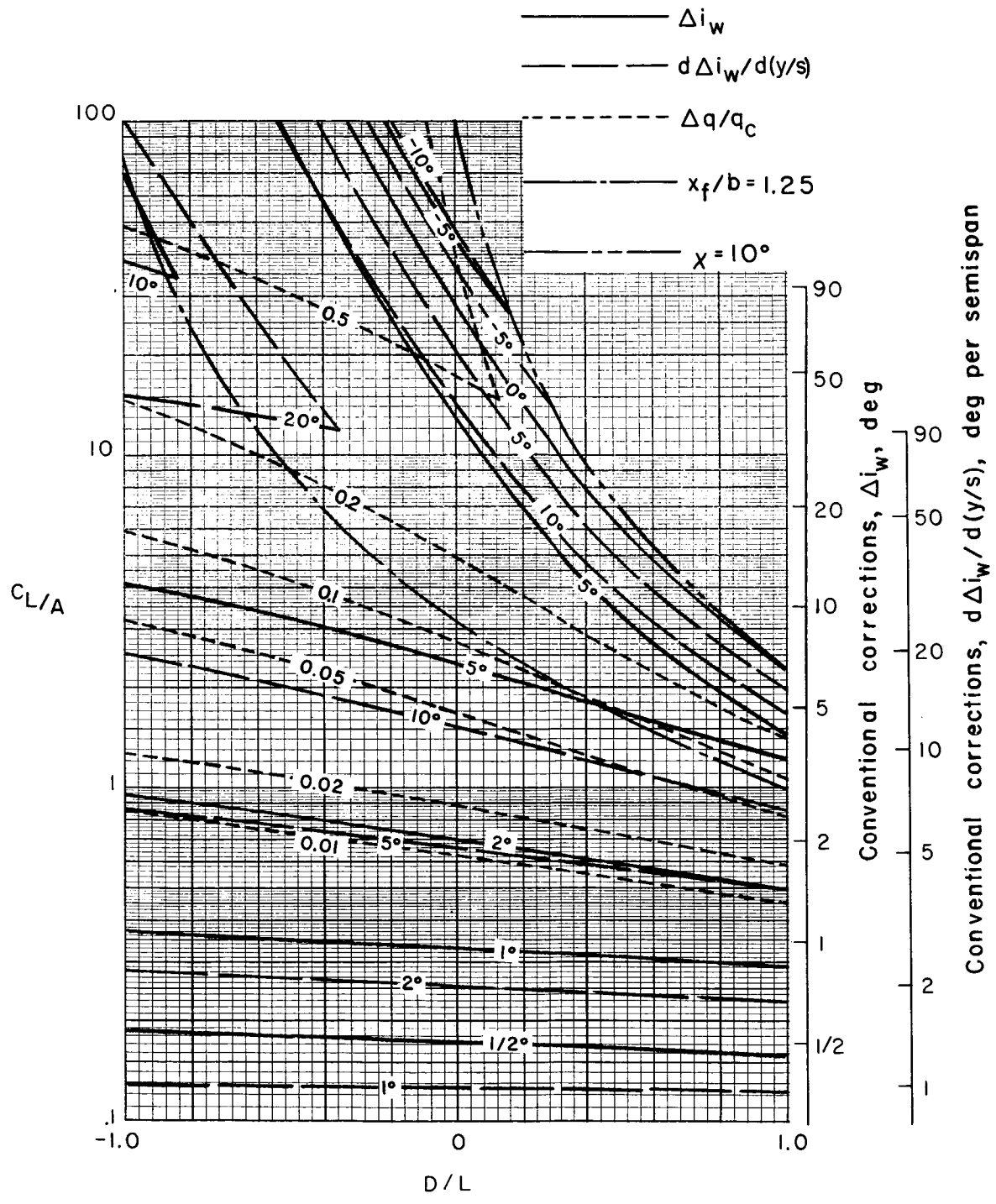


(c) $\sigma = 3/4$.

Figure 38.- Concluded.

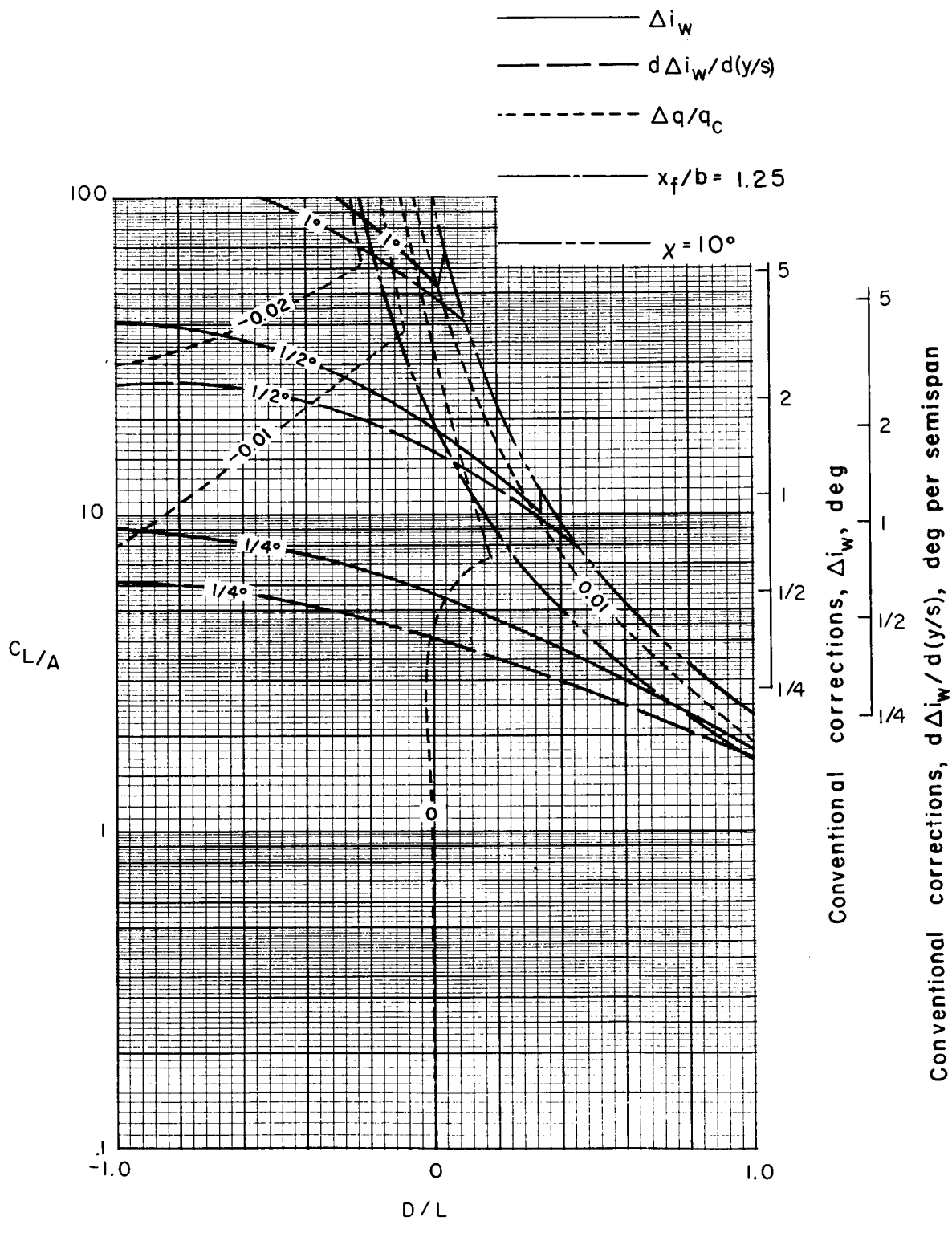


(a) $\sigma = 1/4$.

Figure 39.- Nonuniformity of corrections over a uniformly loaded wing centered in a closed rectangular tunnel. $\gamma = 2/3$; $\alpha = 0^0$; $\Lambda = 45^0$.

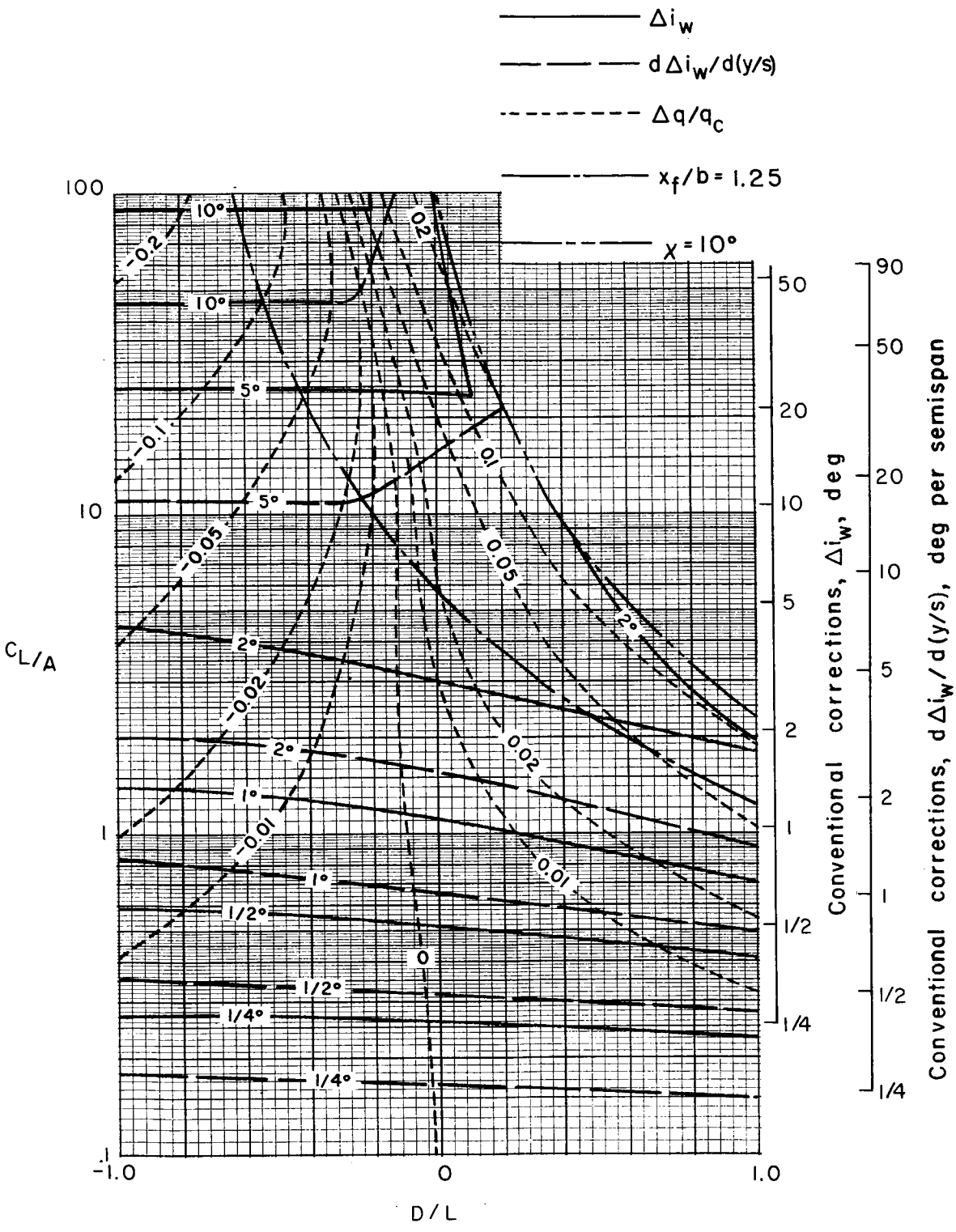


(b) $\sigma = 1/2$.

Figure 39.- Continued.

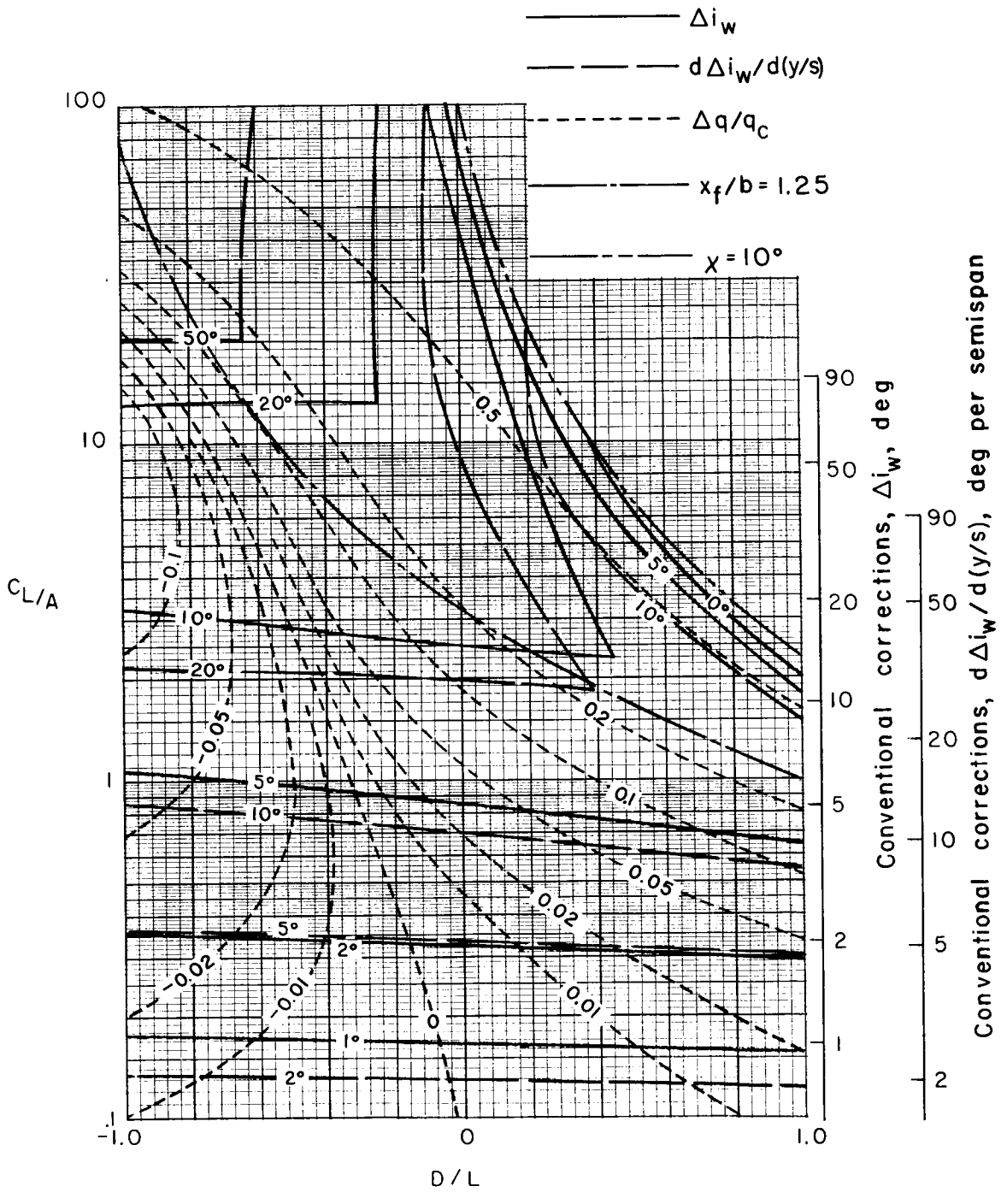


(c) $\sigma = 3/4$.

Figure 39.- Concluded.

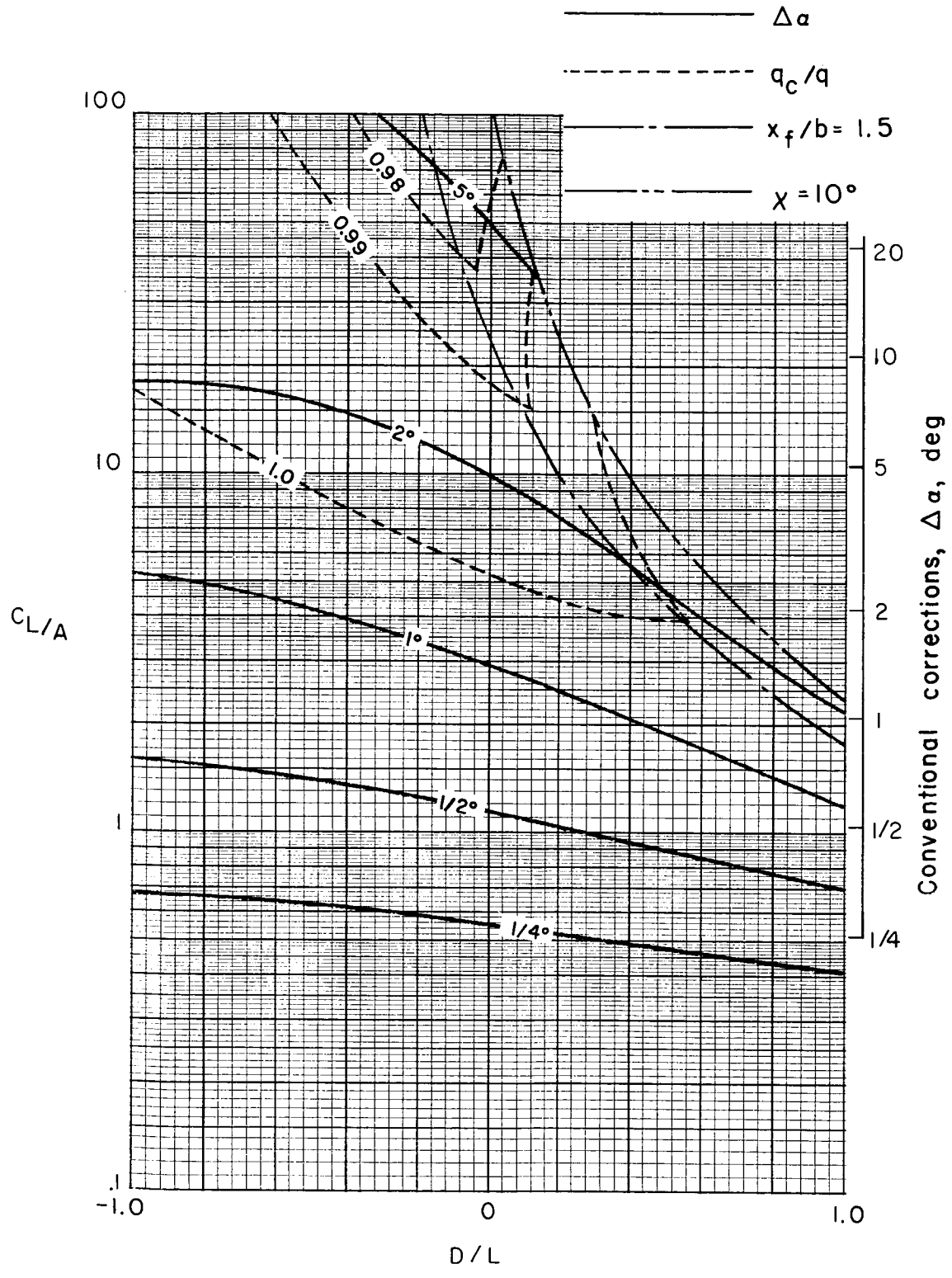


(a) σ = 1/4.

Figure 40.- Average corrections for a uniformly loaded wing centered in a closed rectangular tunnel. Λ = 0°; γ = 1/2.

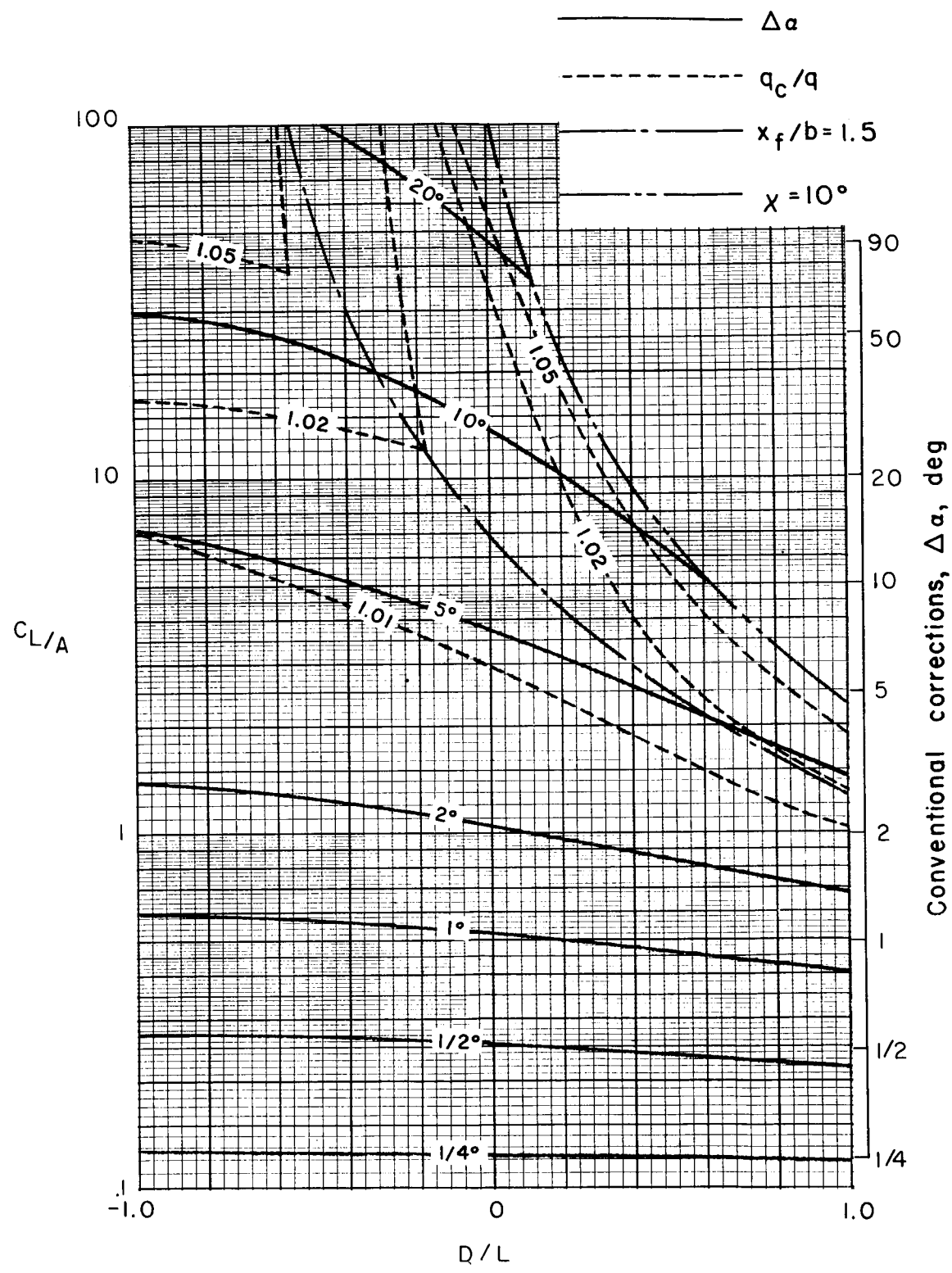


(b) σ = 1/2.

Figure 40.- Continued.

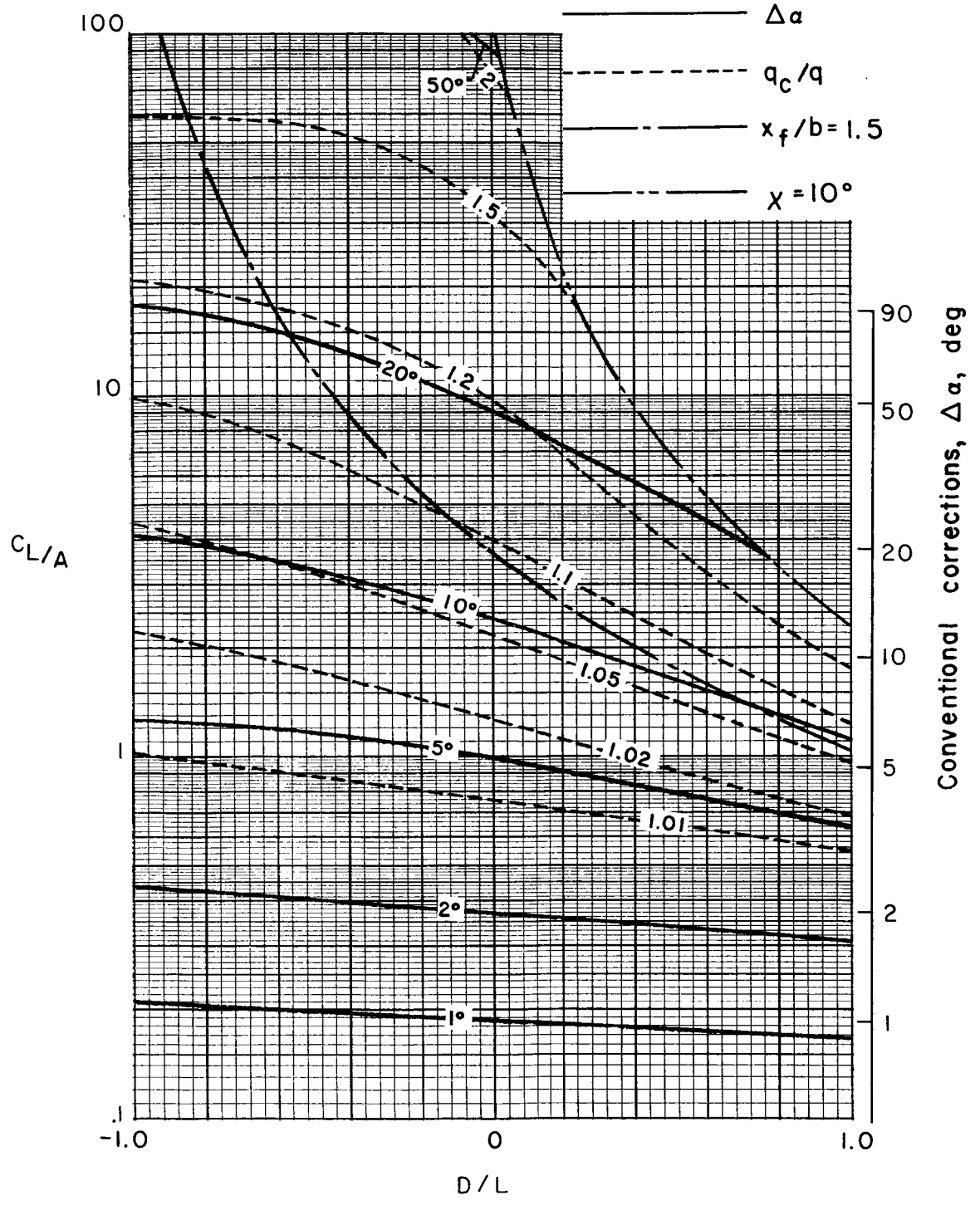


(c) σ = 3/4.

Figure 40.- Concluded.

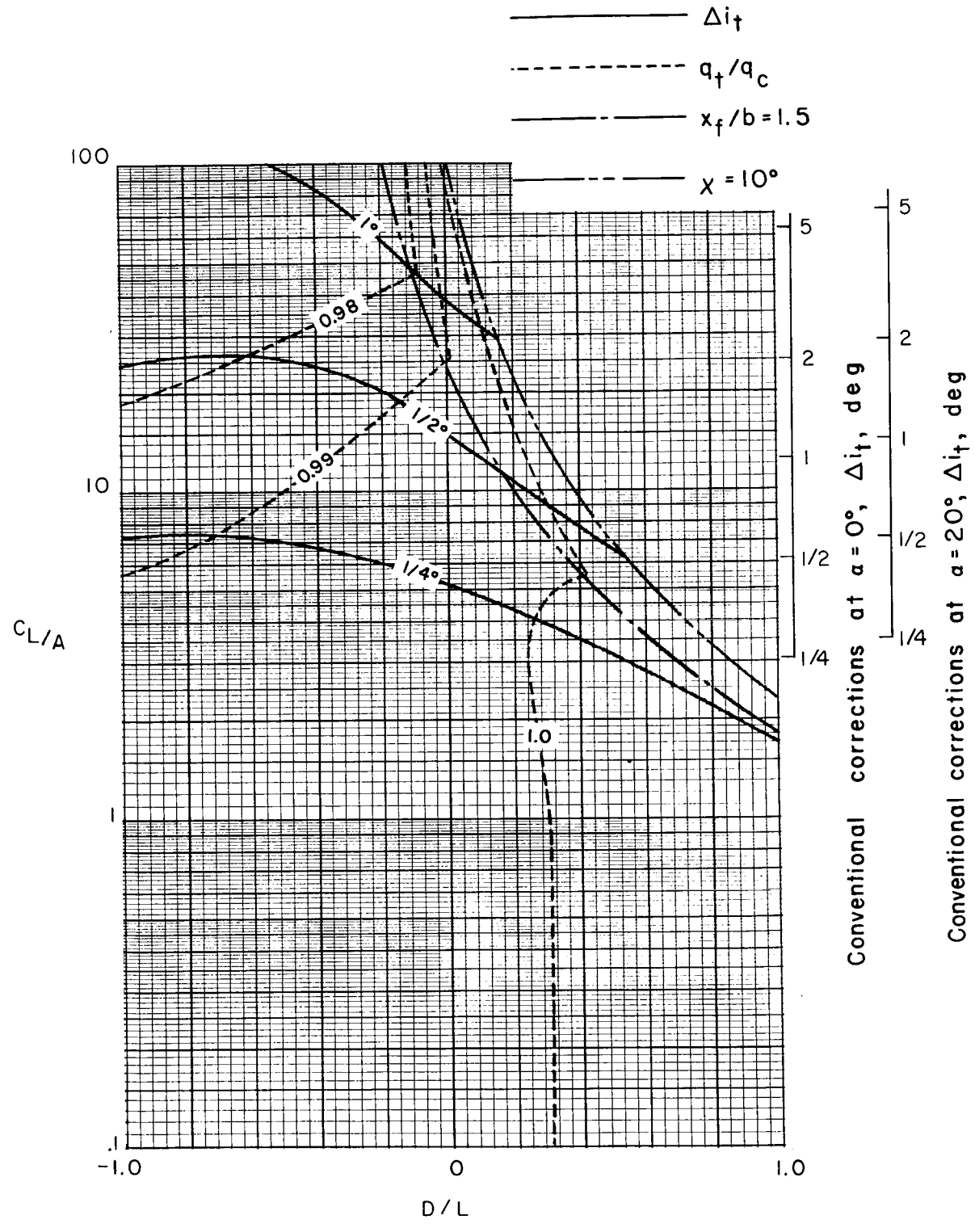


(a) σ = 1/4.

Figure 41.- Corrections at a zero-span tail behind a uniformly loaded wing centered in a closed rectangular tunnel. Tail length is three-fourths of wing span; tail height is zero; $\alpha = 20^0$; $\Lambda = 0^0$; $\gamma = 1/2$.

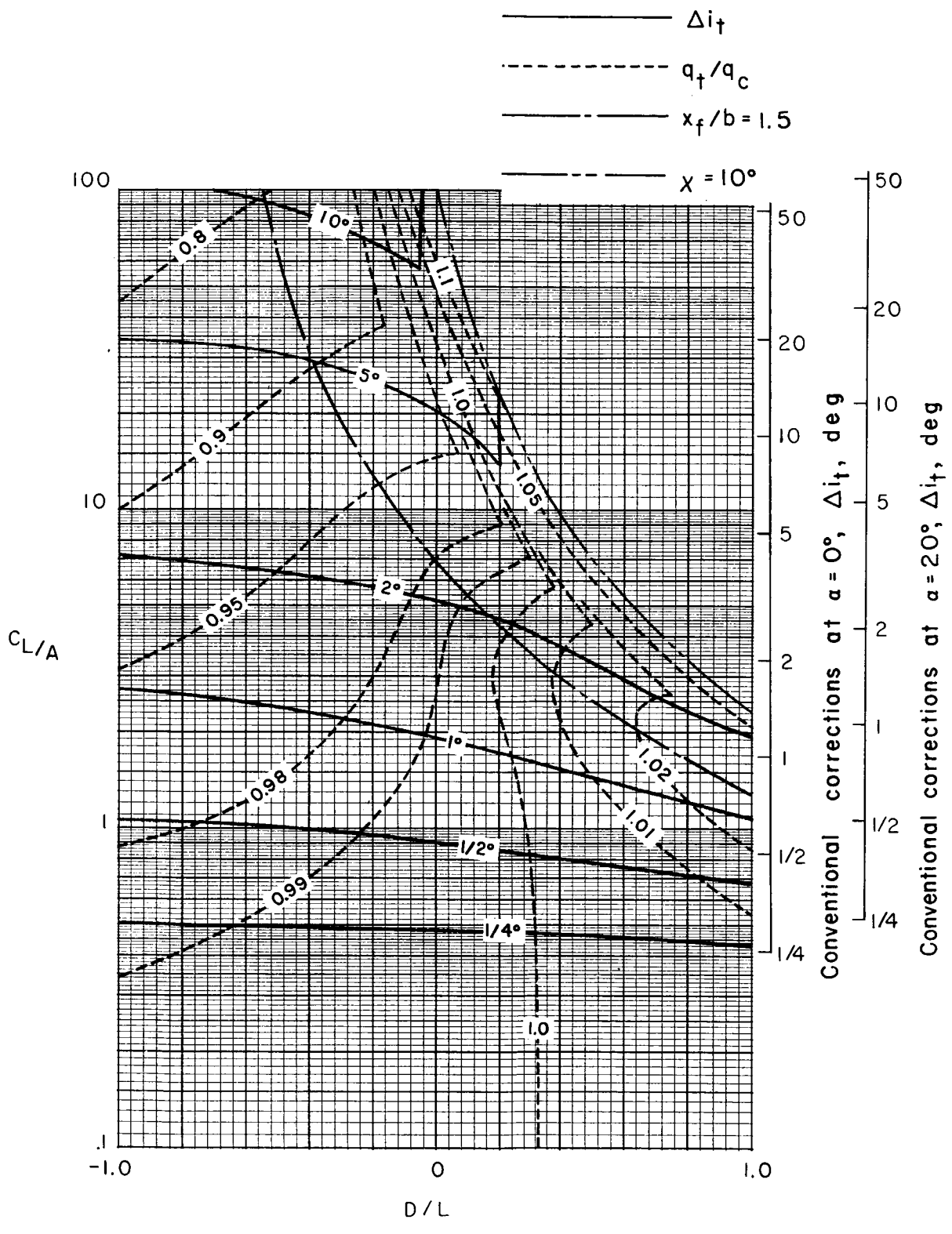


(b) $\sigma = 1/2$.

Figure 41.- Continued.

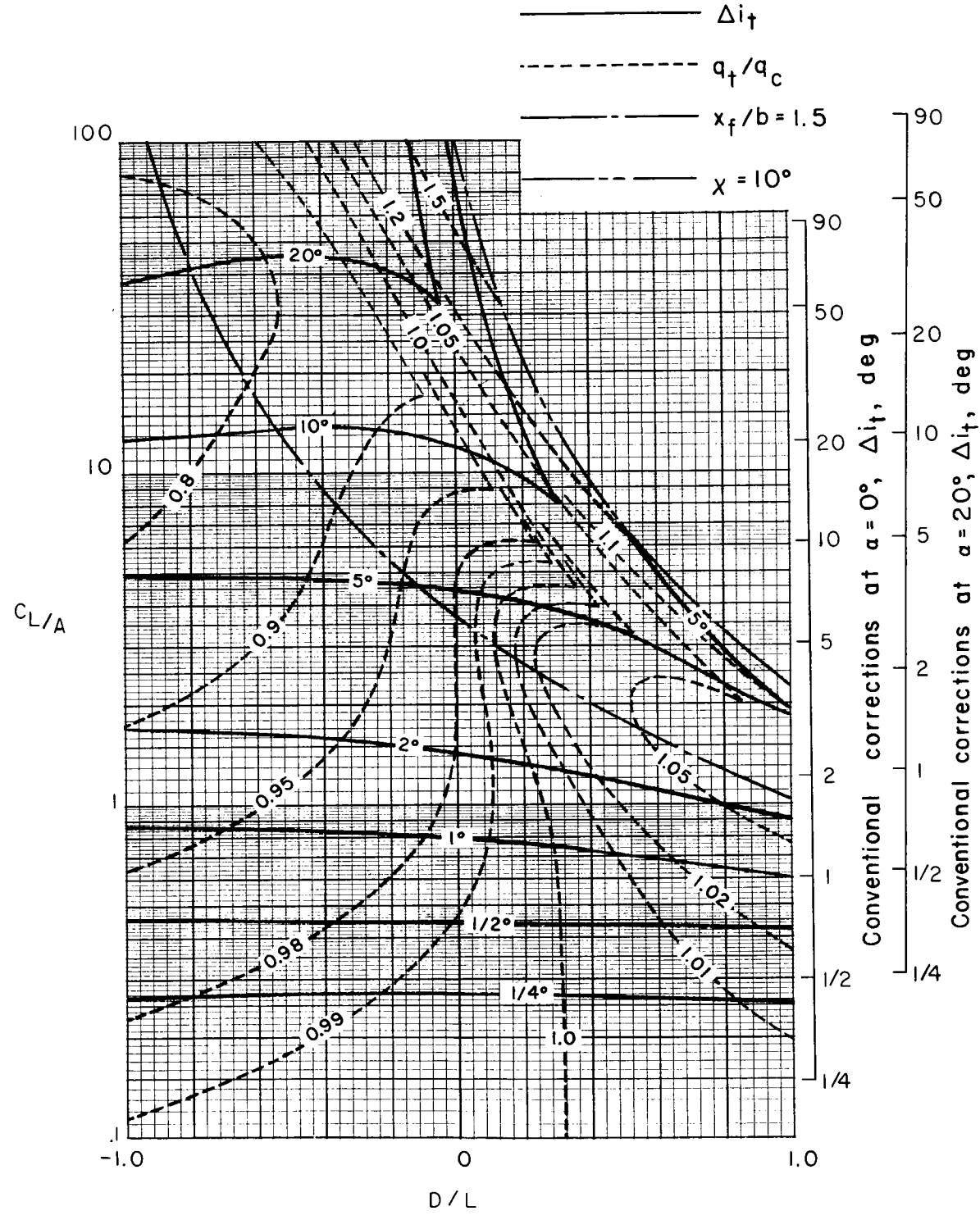


(c) $\sigma = 3/4$.

Figure 41.- Concluded.

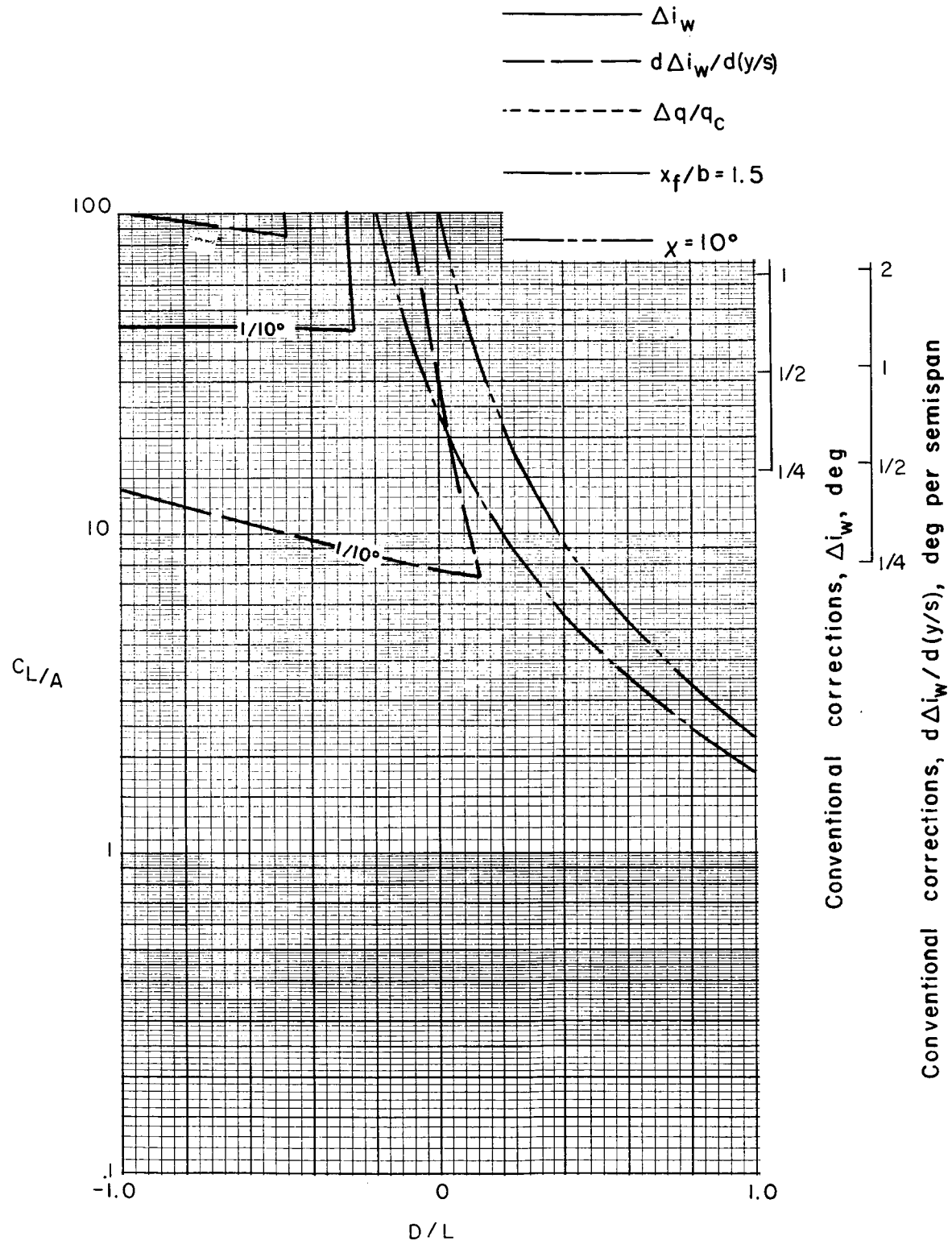


(a) $\sigma = 1/4$.

Figure 42.- Nonuniformity of corrections over a uniformly loaded wing centered in a closed rectangular tunnel. $\gamma = 1/2$; $\alpha = 0^0$; $\Lambda = 0^0$.

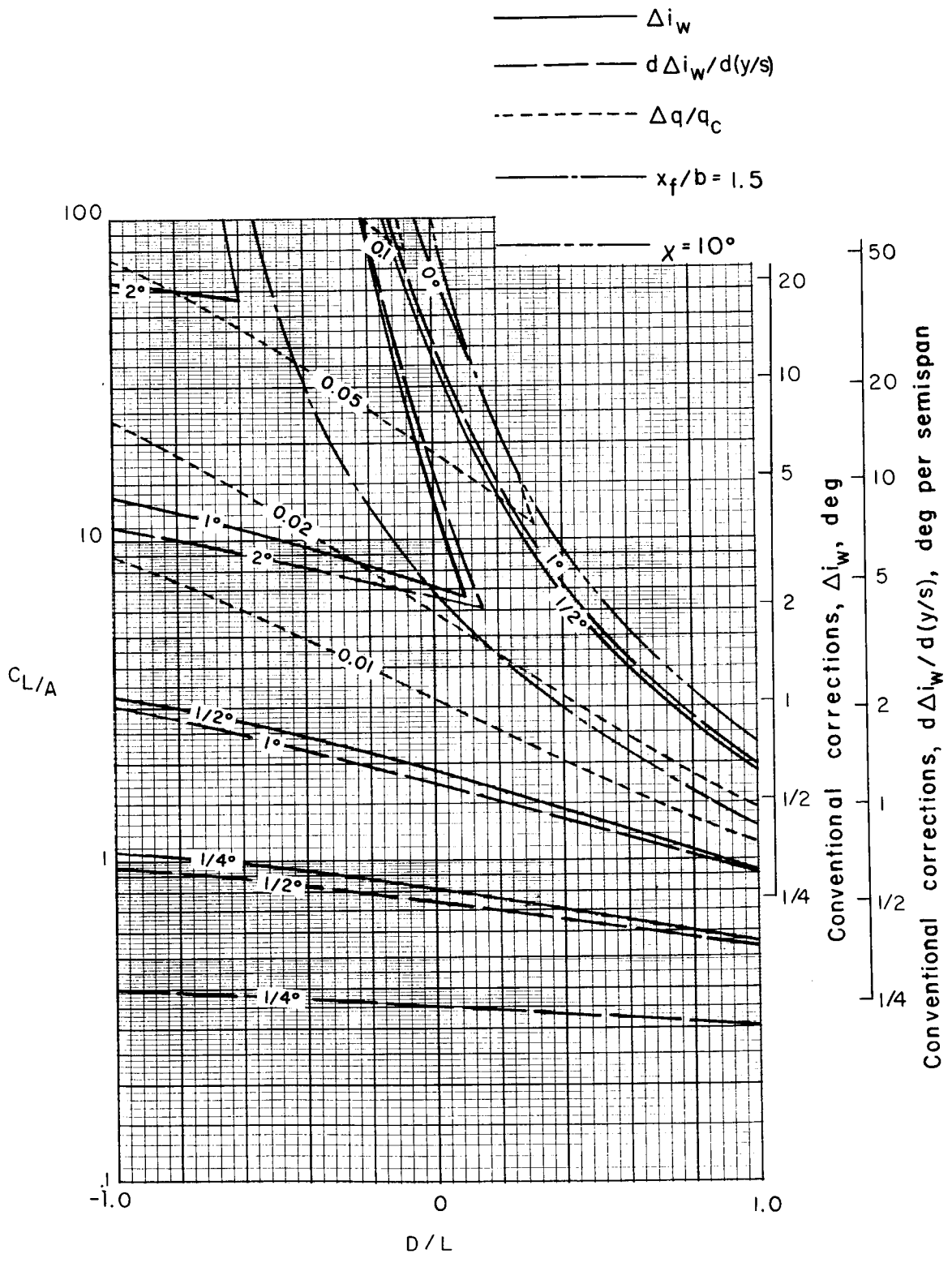


(b) $\sigma = 1/2$.

Figure 42.- Continued.

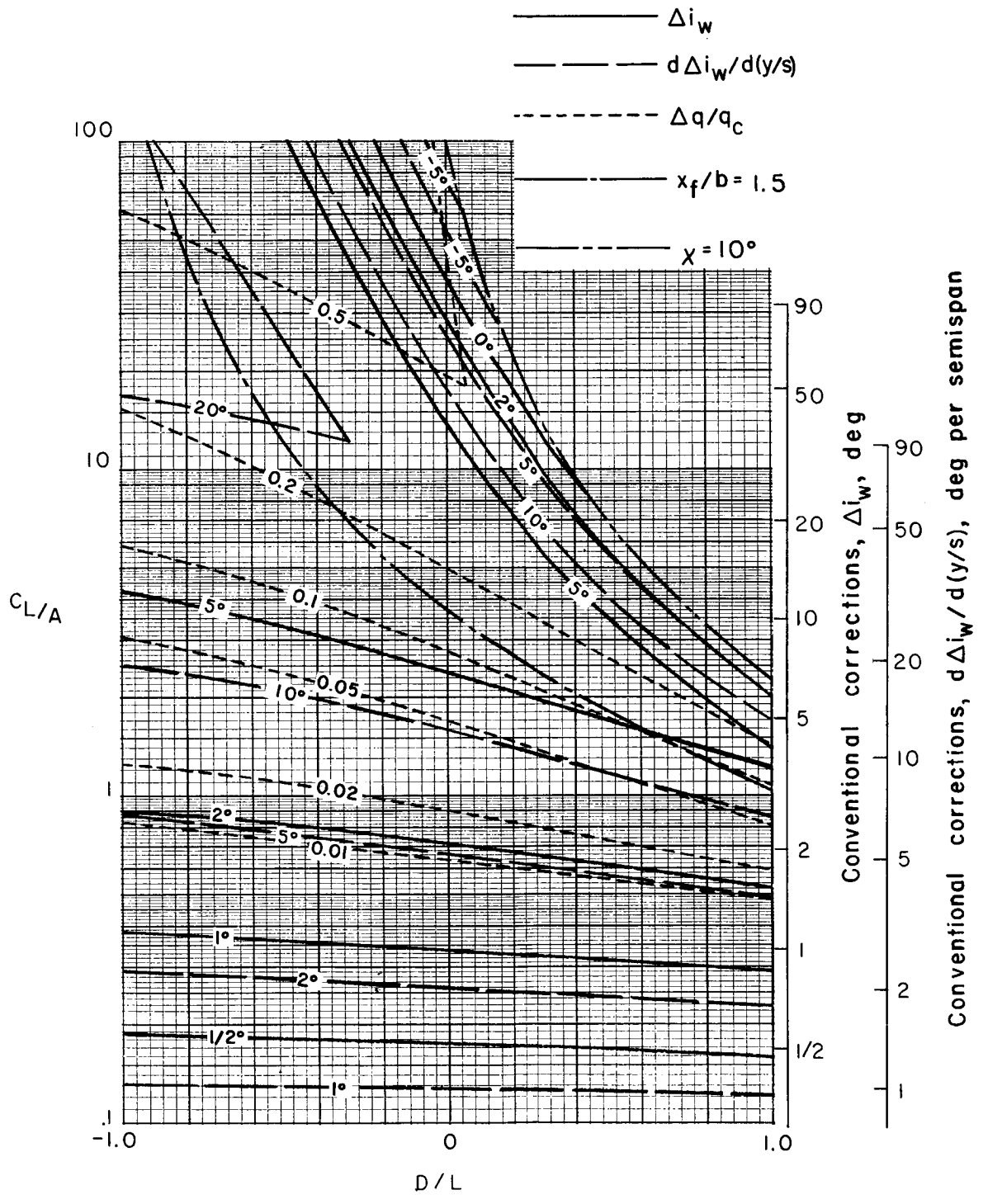


(c) $\sigma = 3/4$.

Figure 42.- Concluded.

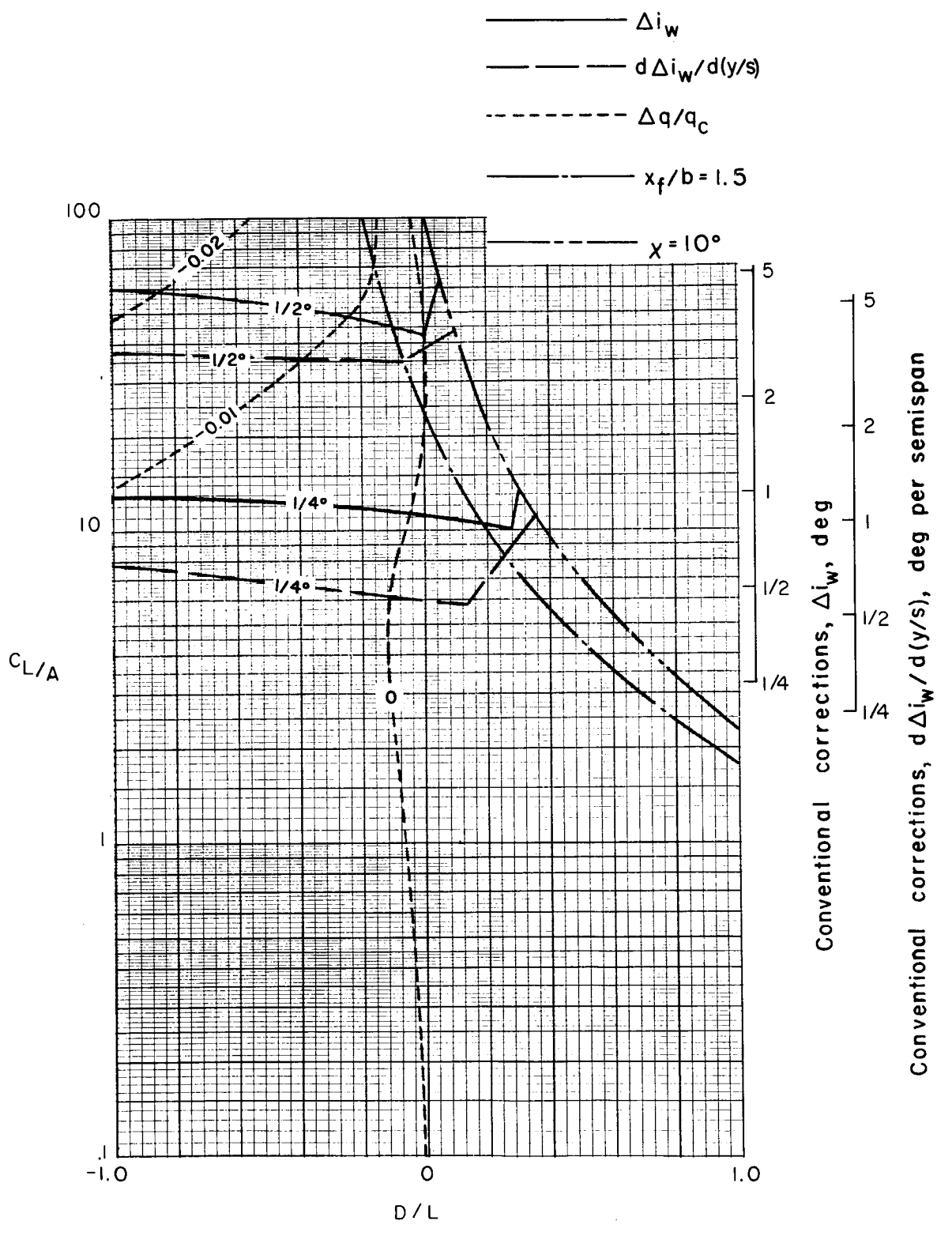


(a) $\sigma = 1/4$.

Figure 43.- Nonuniformity of corrections over a uniformly loaded wing centered in a closed rectangular tunnel. $\gamma = 1/2$; $\alpha = 0^0$; $\Lambda = 45^0$.

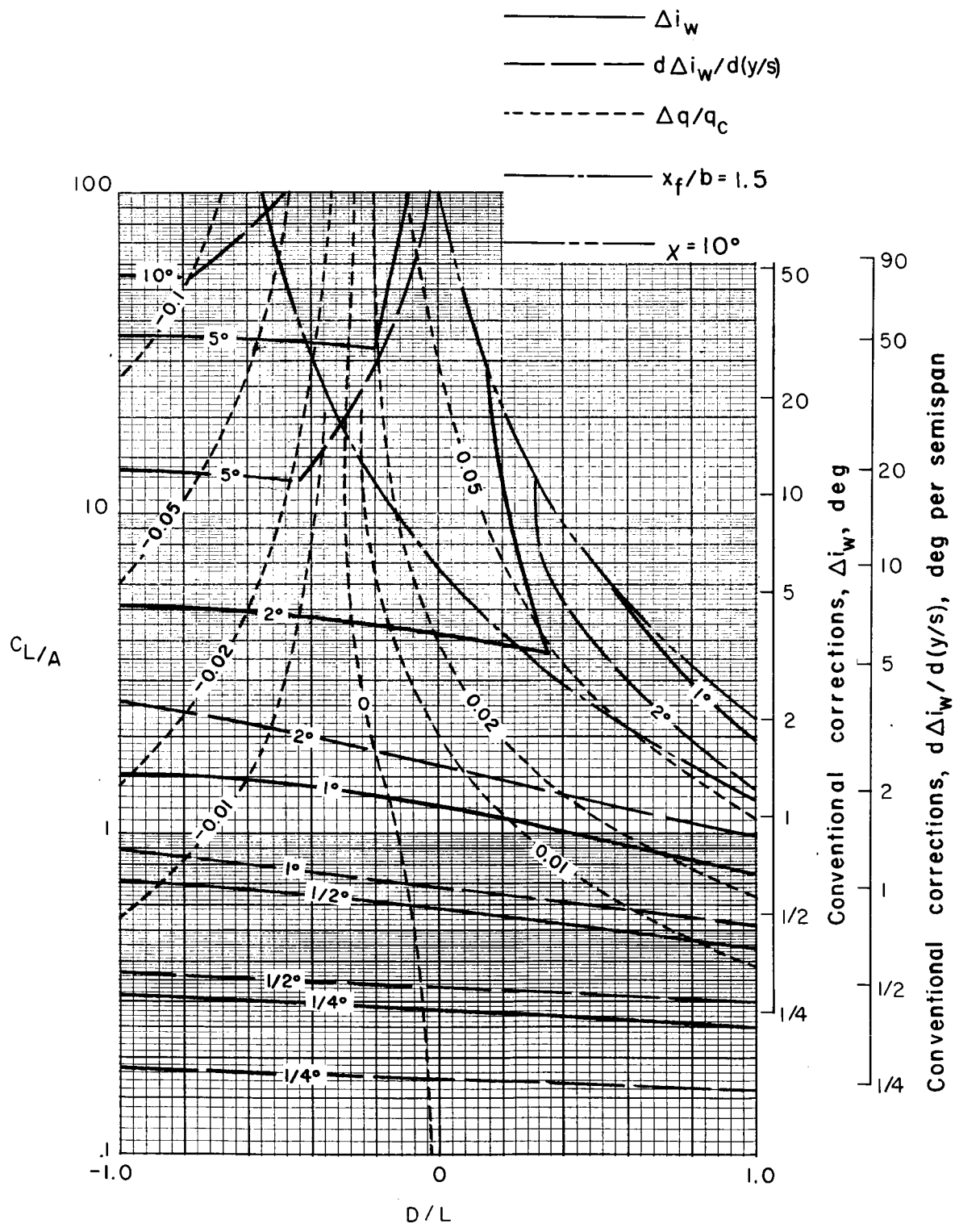


(b) $\sigma = 1/2$.

Figure 43.- Continued.

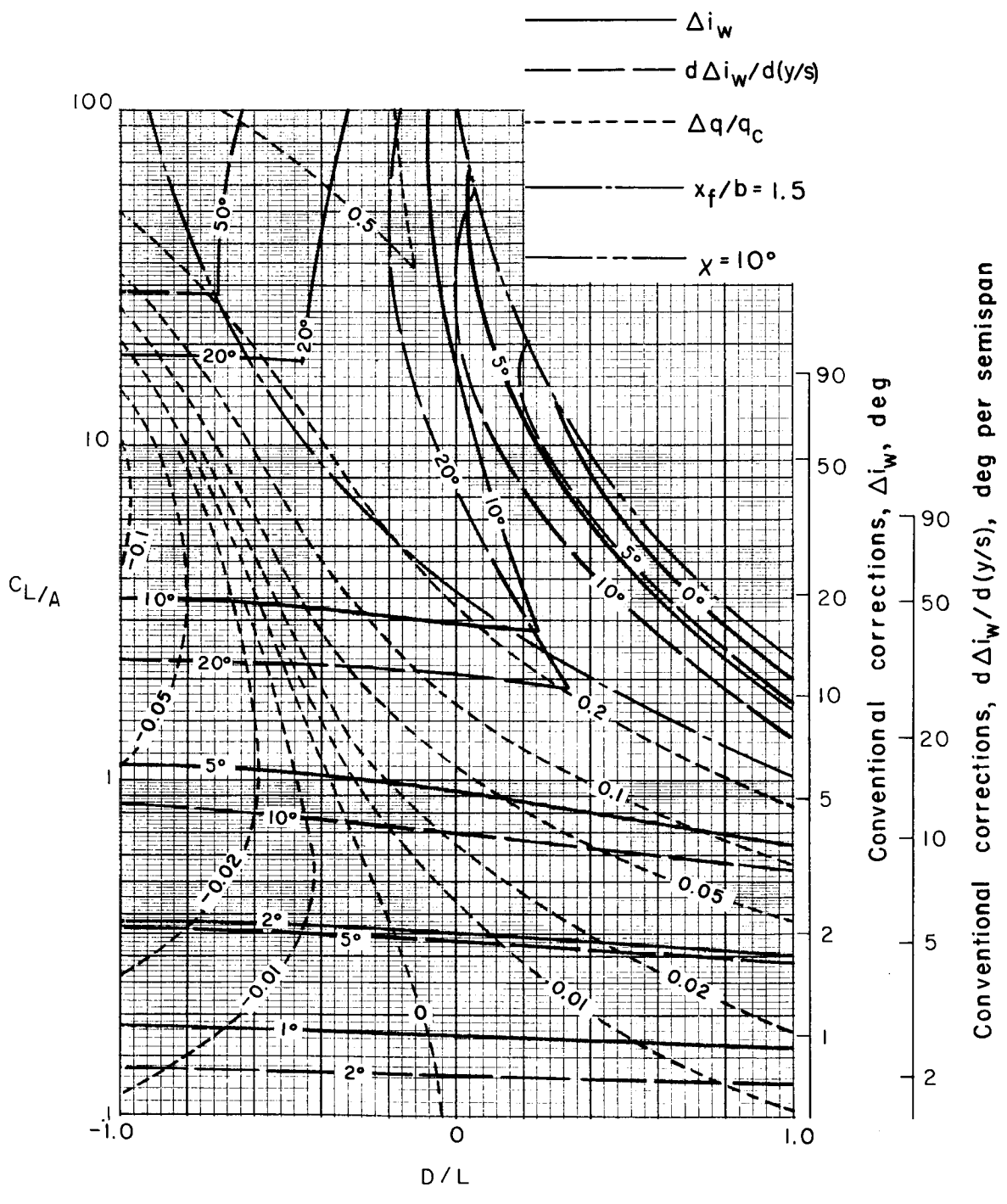


(c) $\sigma = 3/4$.

Figure 43.- Concluded.

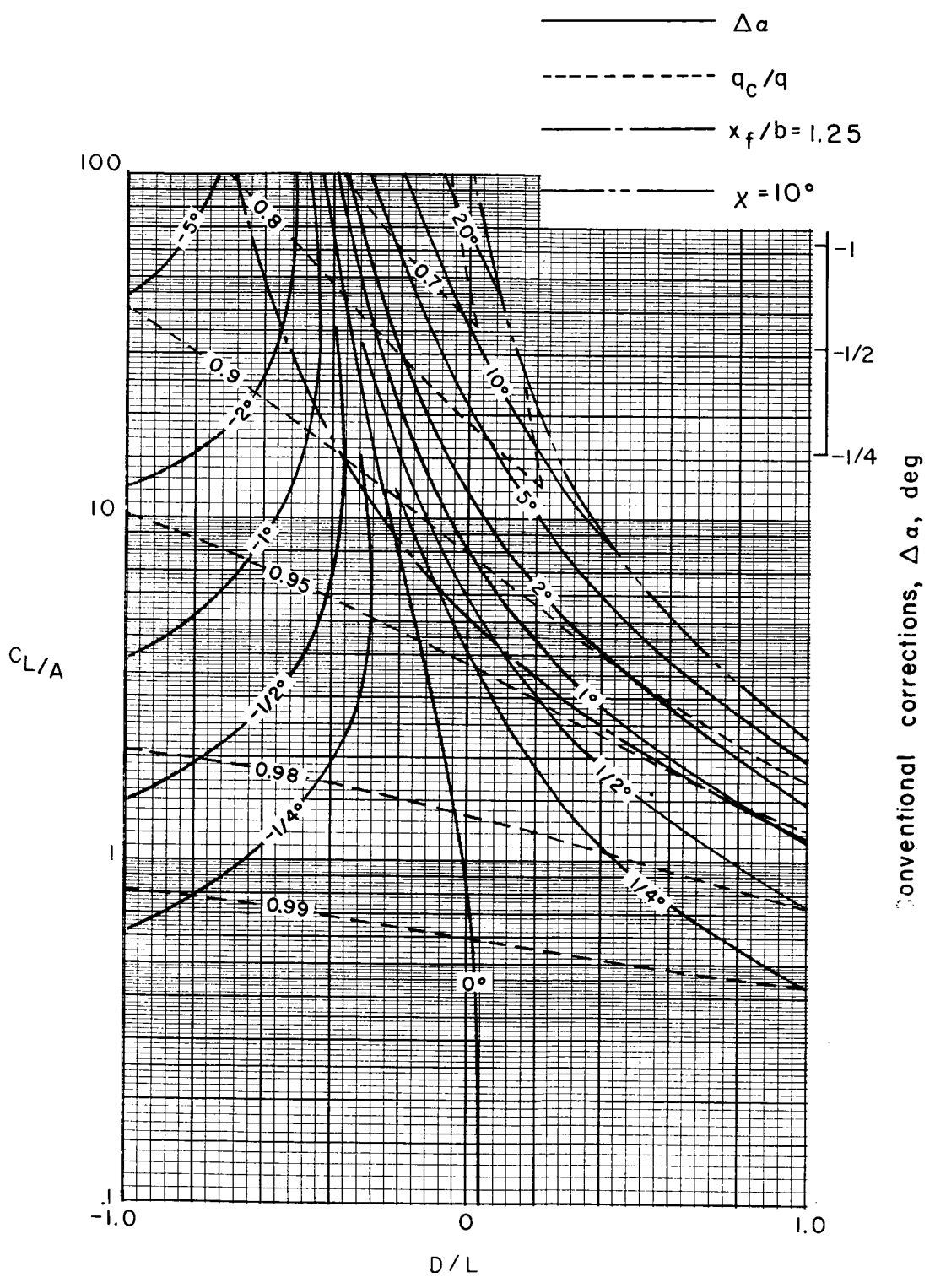


(a) σ = 1/6.

Figure 44.- Average corrections for a uniformly loaded wing centered in the Langley full-scale tunnel (9.1- by 18.3-m or 30- by 60-foot) with ground board. Λ = 0°.

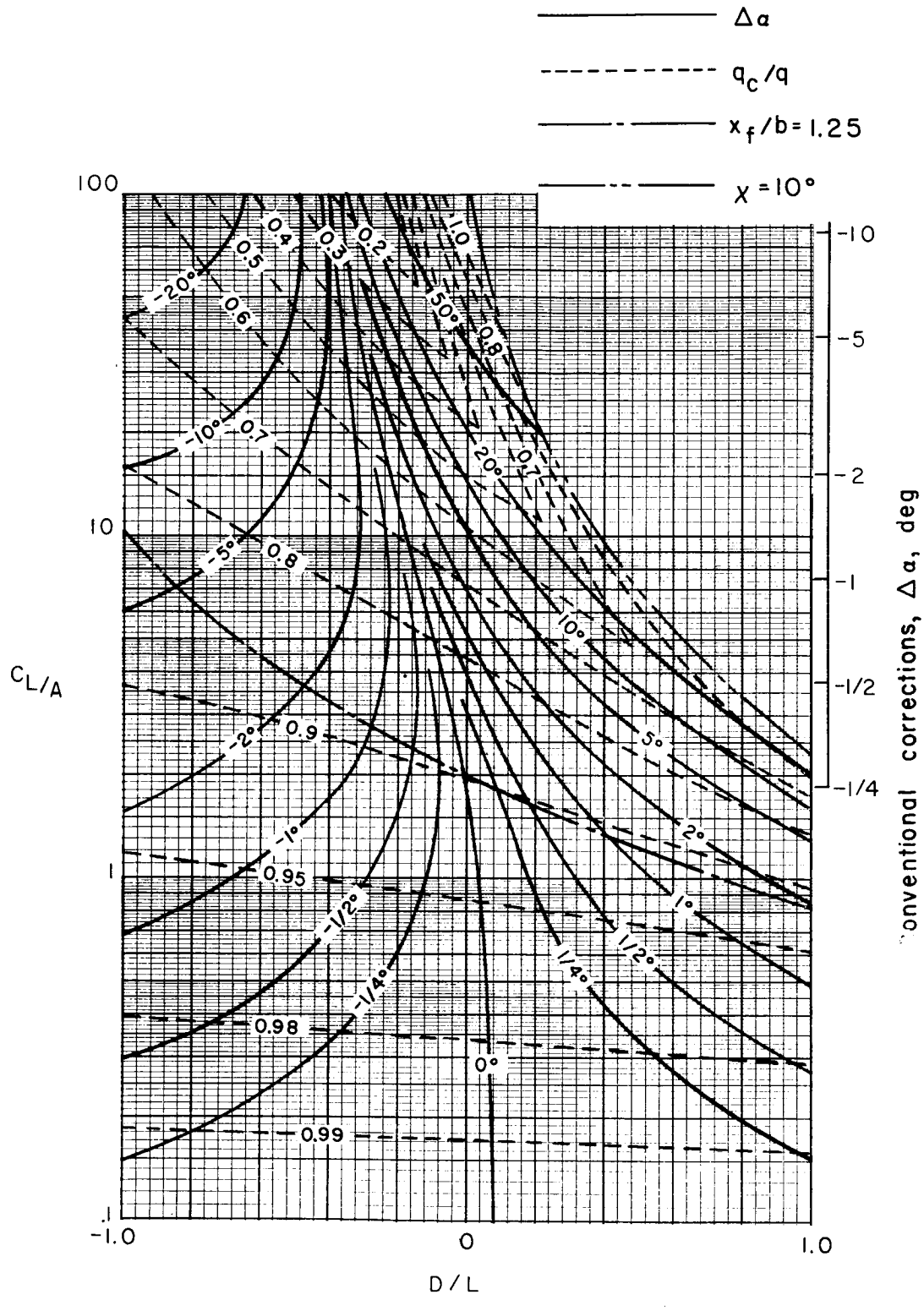


(b) σ = 1/3.

Figure 44.- Continued.

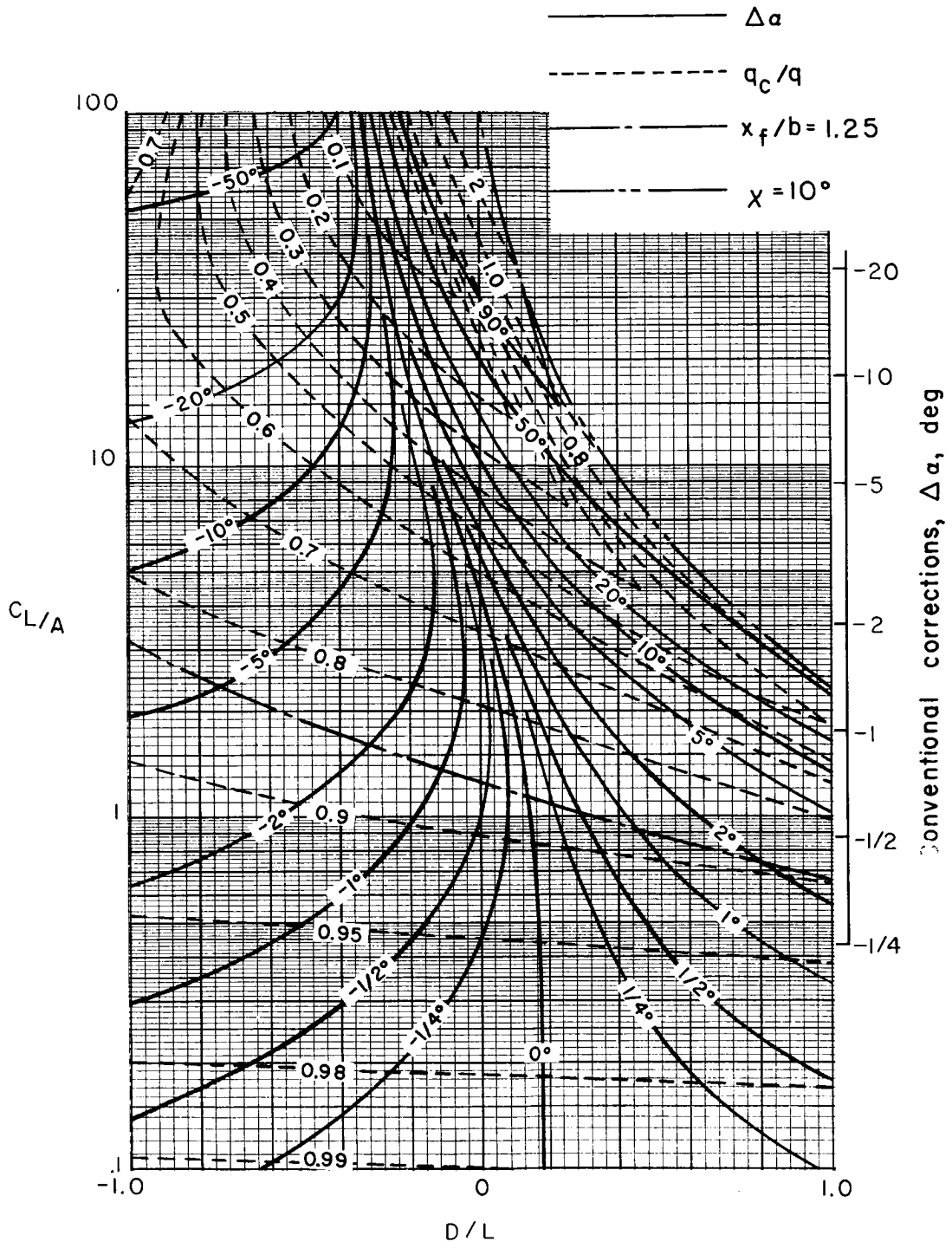


(c) σ = 1/2.

Figure 44.- Continued.

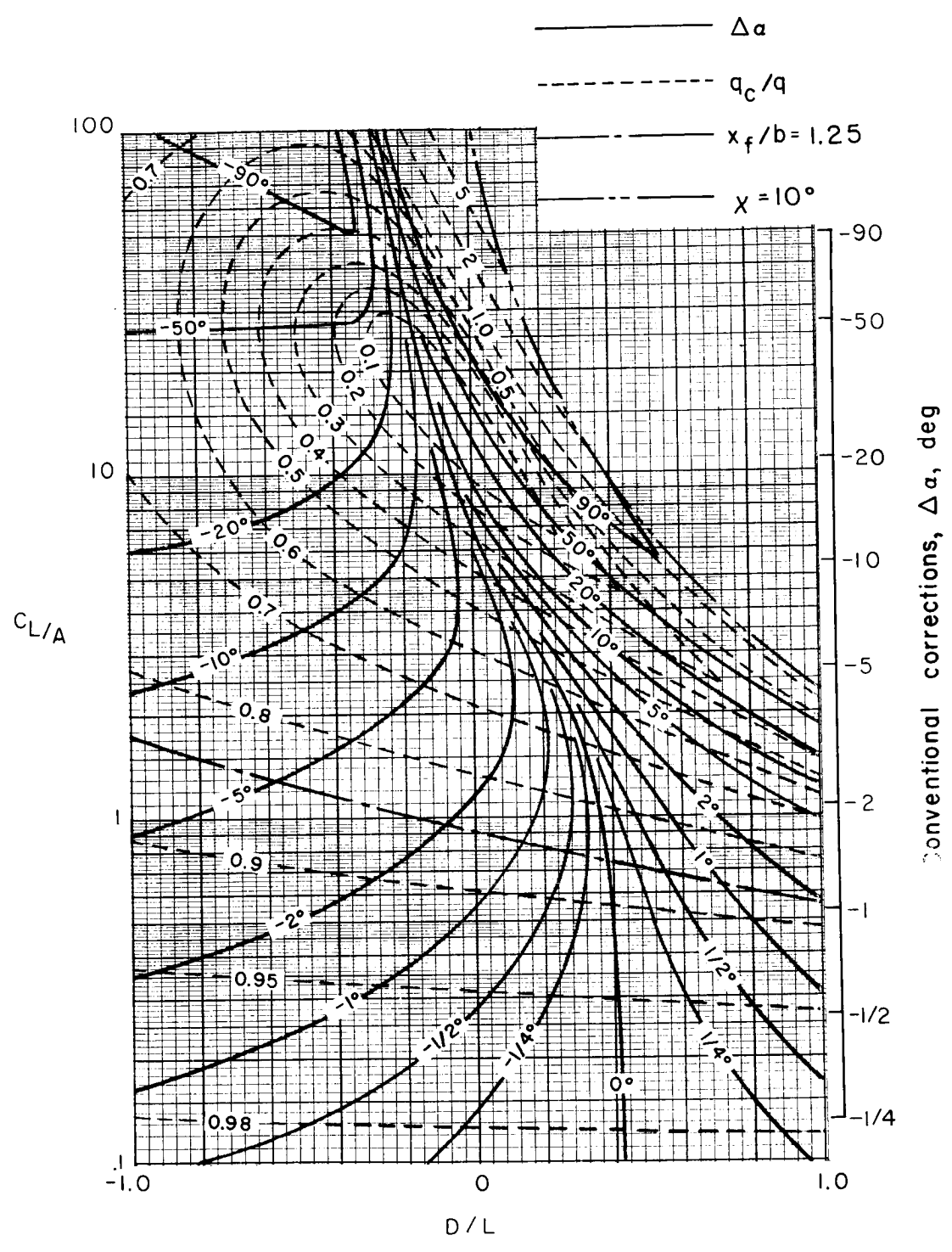


(d) σ = 2/3.

Figure 44.- Continued.

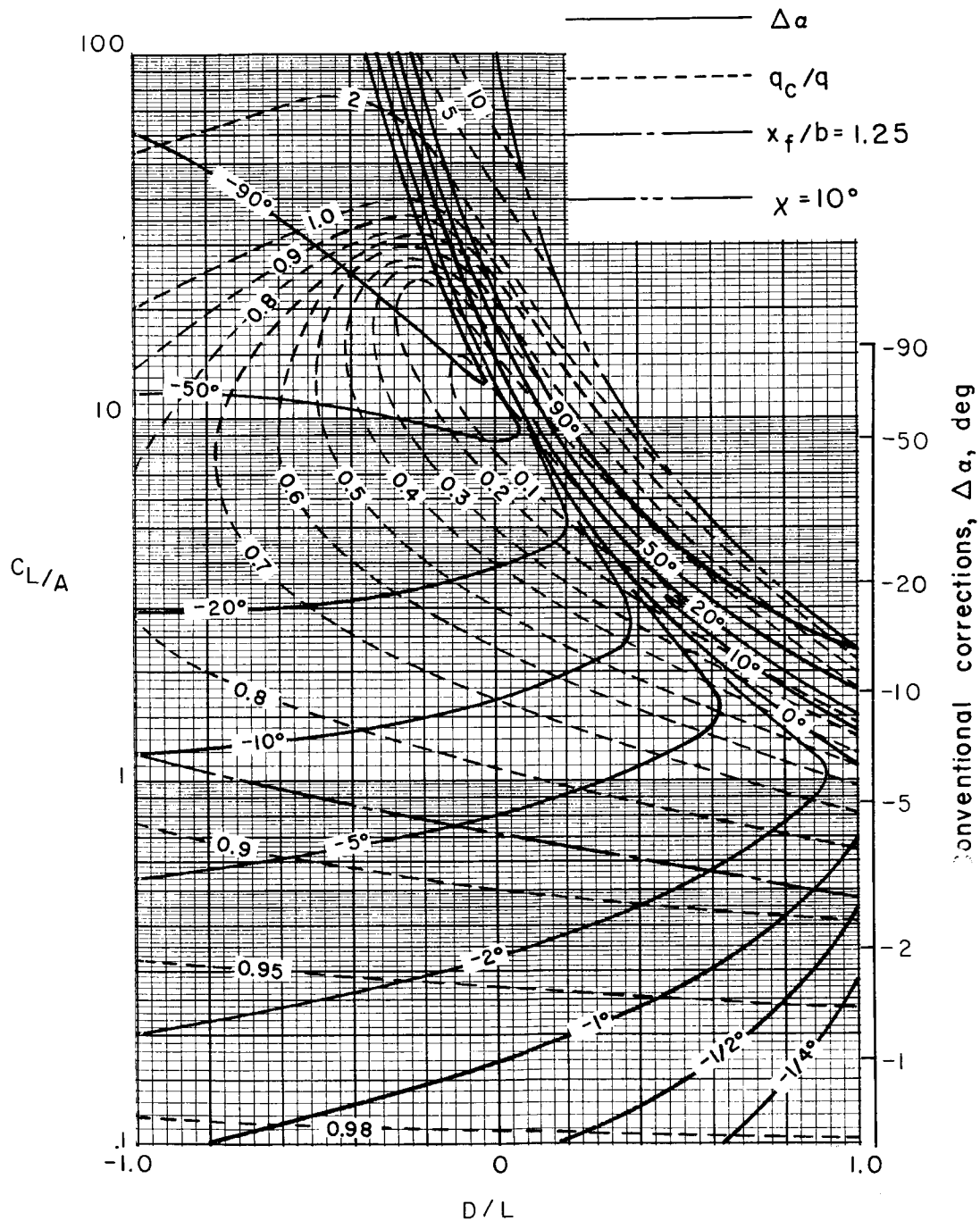


(e) σ = 5/6.

Figure 44.- Concluded.

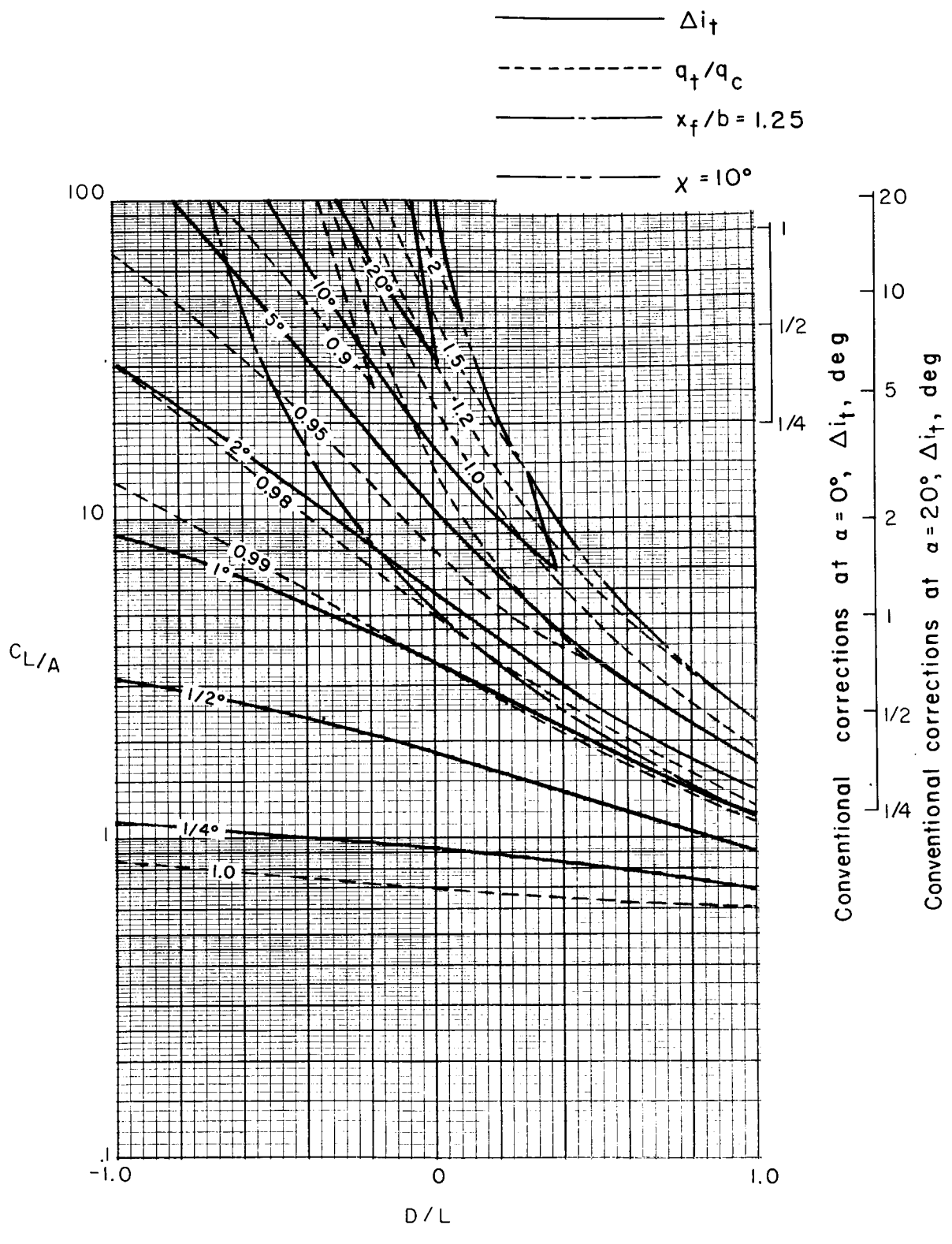


(a) $\sigma = 1/6$.

Figure 45.- Corrections at a zero-span tail behind a uniformly loaded wing centered in the Langley full-scale tunnel (9.1- by 18.3-m or 30- by 60-ft) with ground board. Tail length is three-fourths of wing span; tail height is zero; $\alpha = 20^0$; $\Lambda = 0^0$.

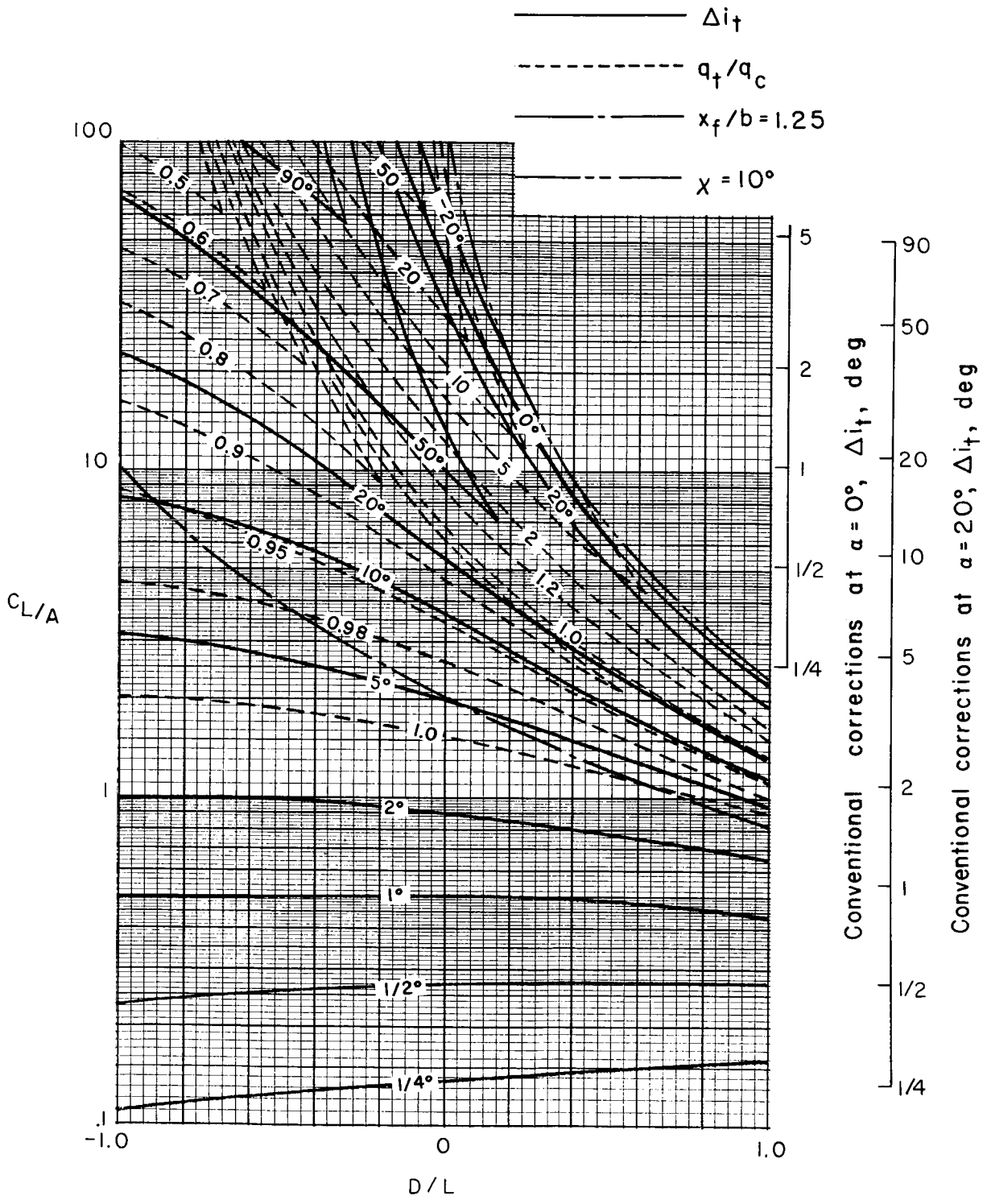


(b) $\sigma = 1/3$.

Figure 45.- Continued.

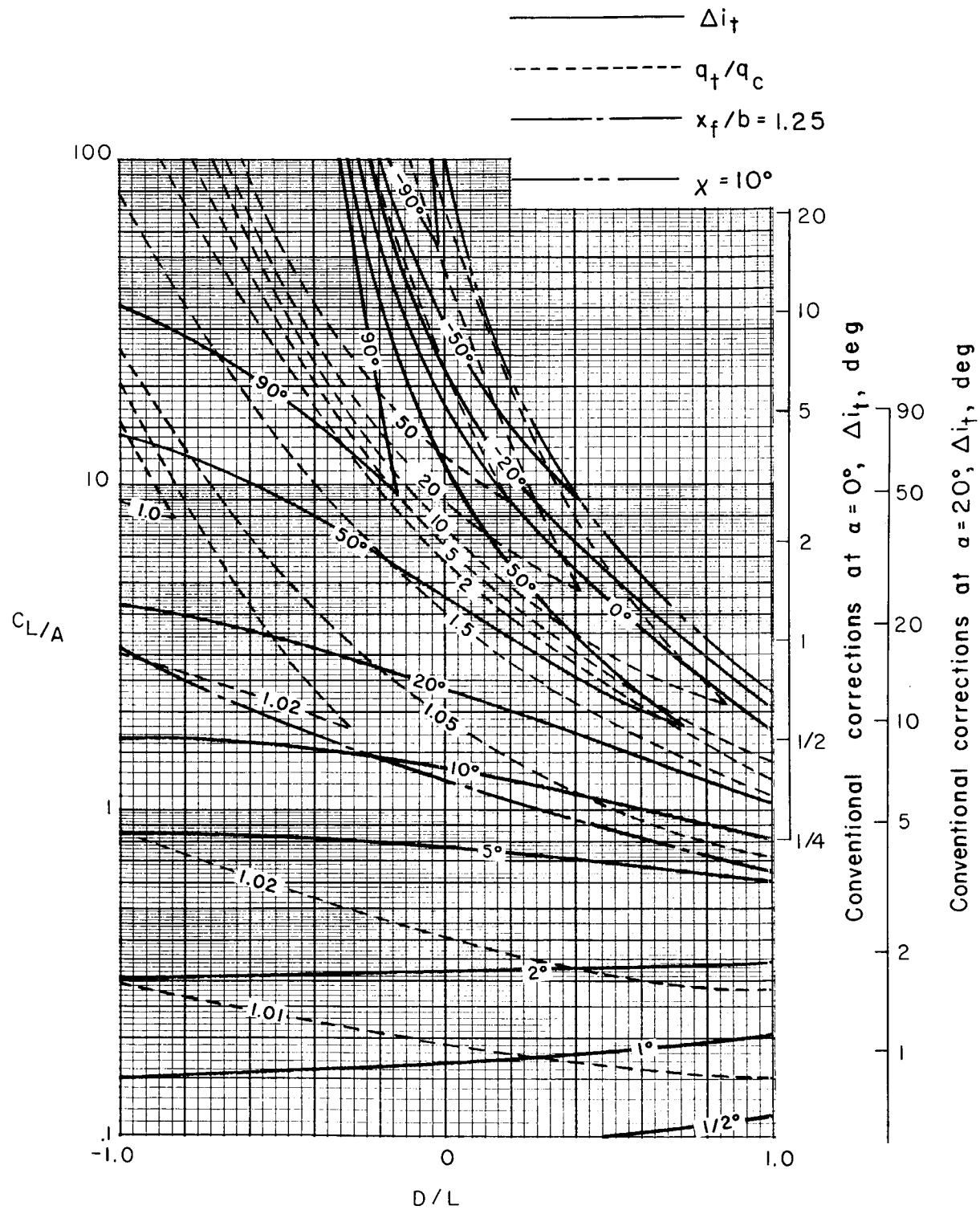


(c) $\sigma = 1/2$.

Figure 45.- Continued.

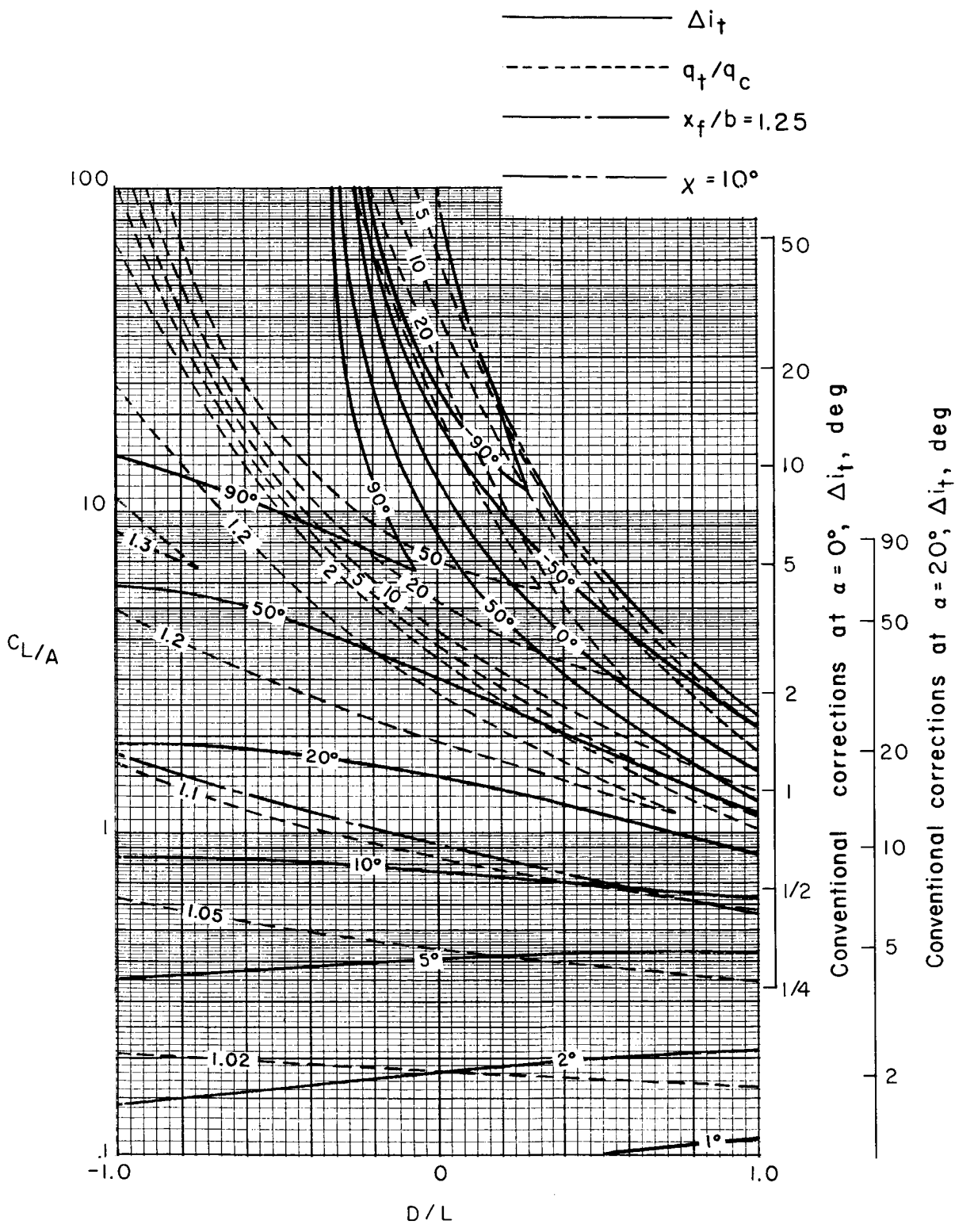


(d) $\sigma = 2/3$.

Figure 45.- Continued.

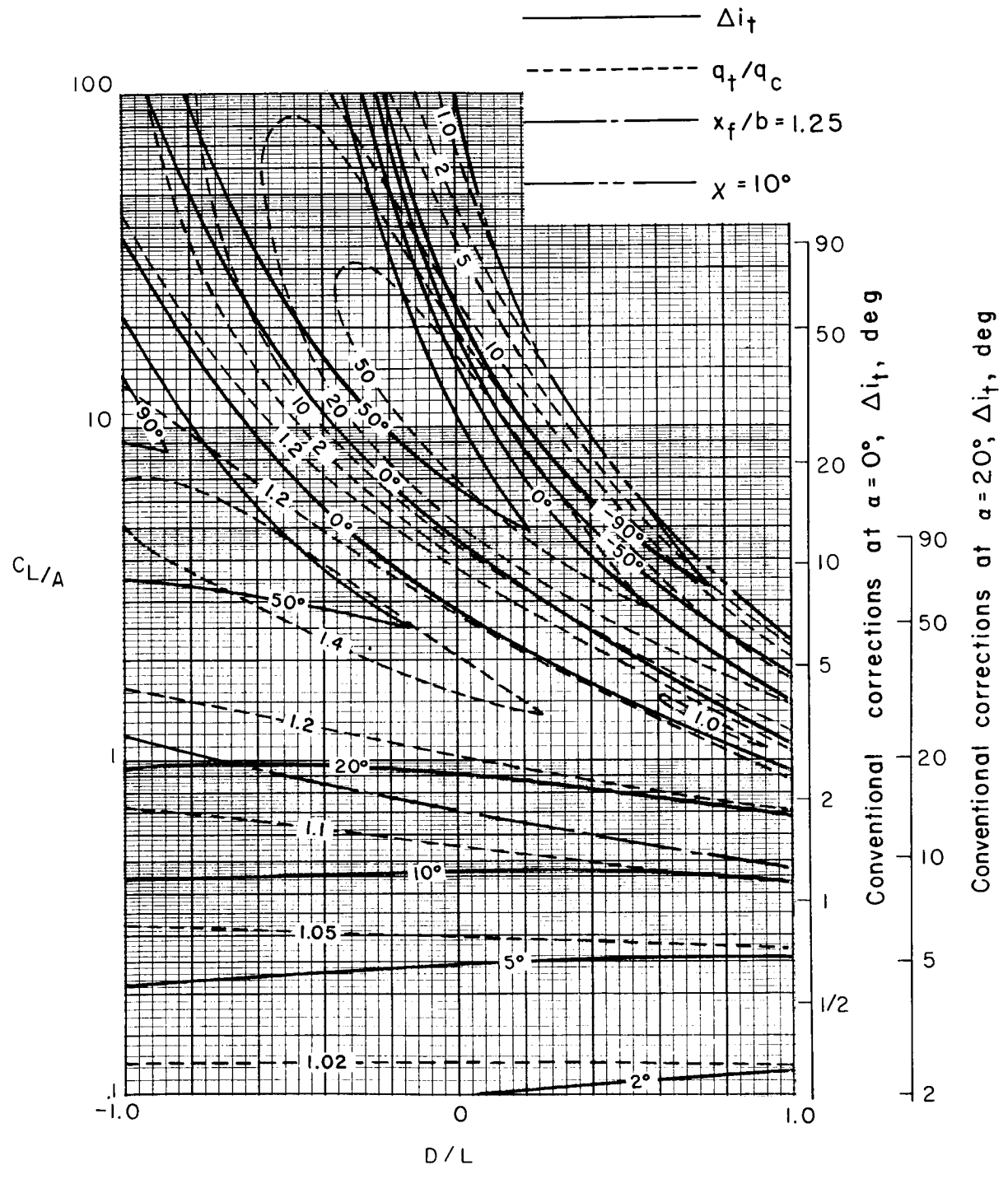


(e) $\sigma = 5/6$.

Figure 45.- Concluded.

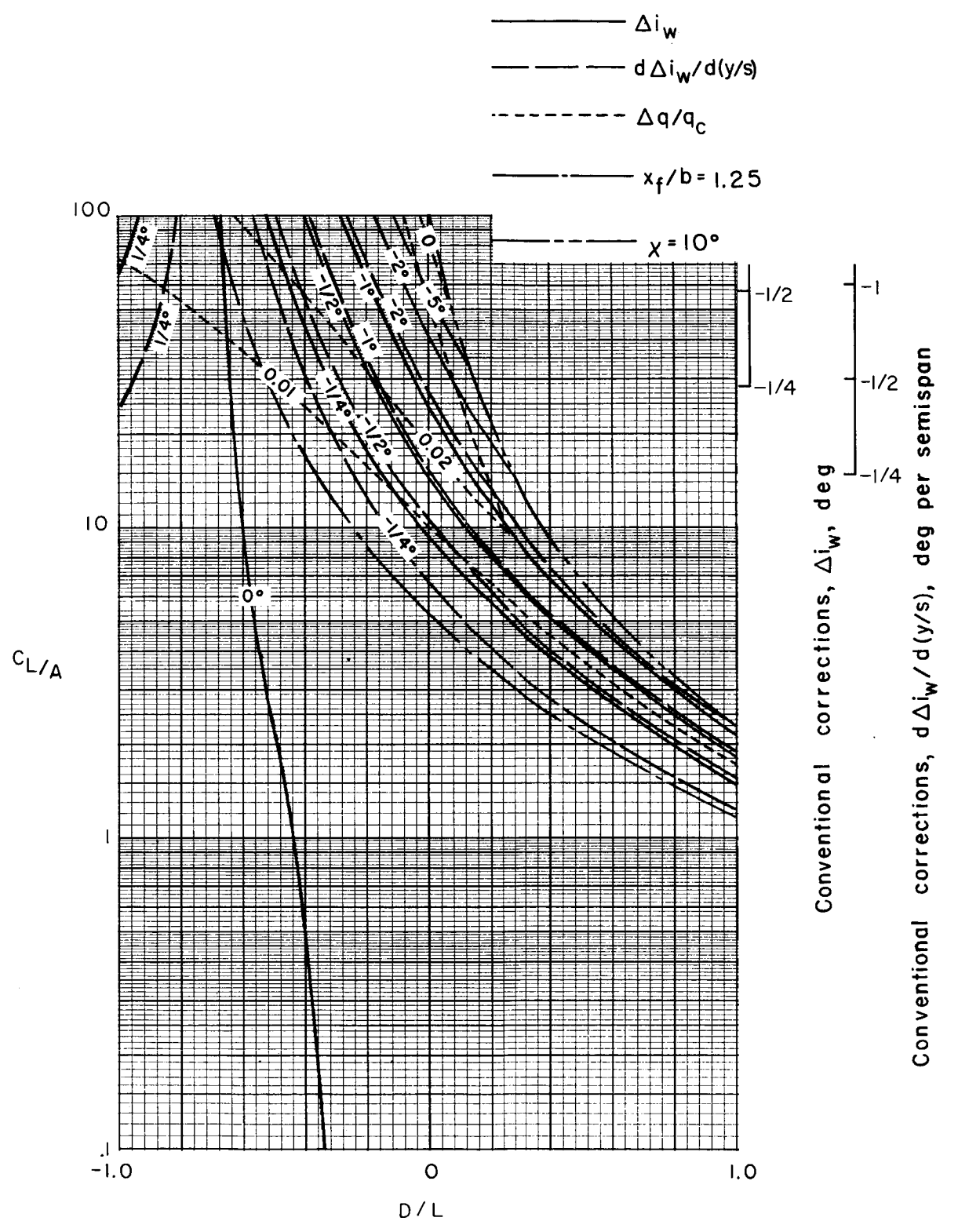


(a) $\sigma = 1/6$.

Figure 46.- Nonuniformity of corrections over a uniformly loaded wing centered in the Langley full-scale tunnel (9.3- by 18.3-m or 30- by 60-ft) with ground board. $\alpha = 0^o$; $\Lambda = 0^o$.

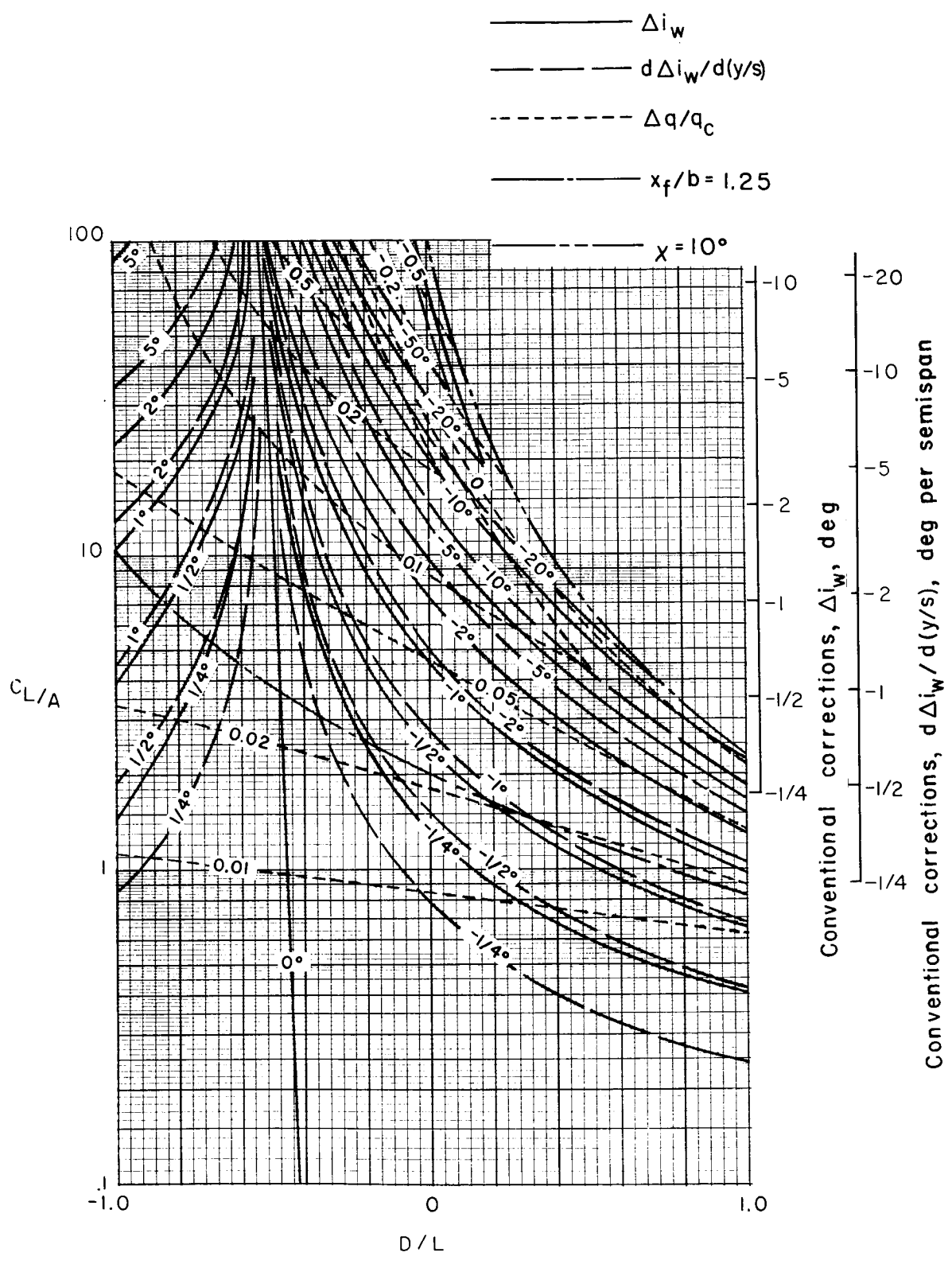


(b) $\sigma = 1/3$.

Figure 46.- Continued.

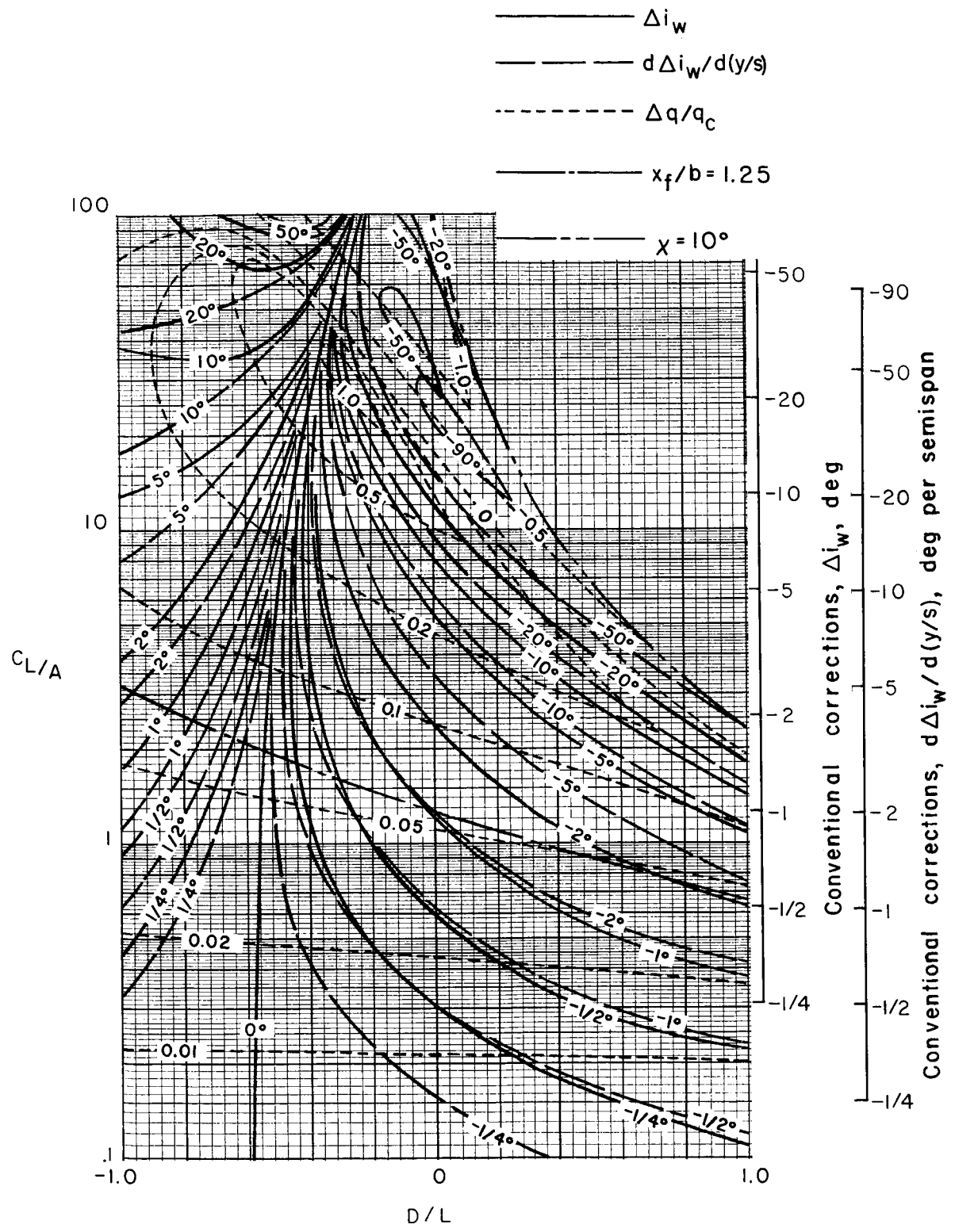


(c) $\sigma = 1/2$.

Figure 46.- Continued.

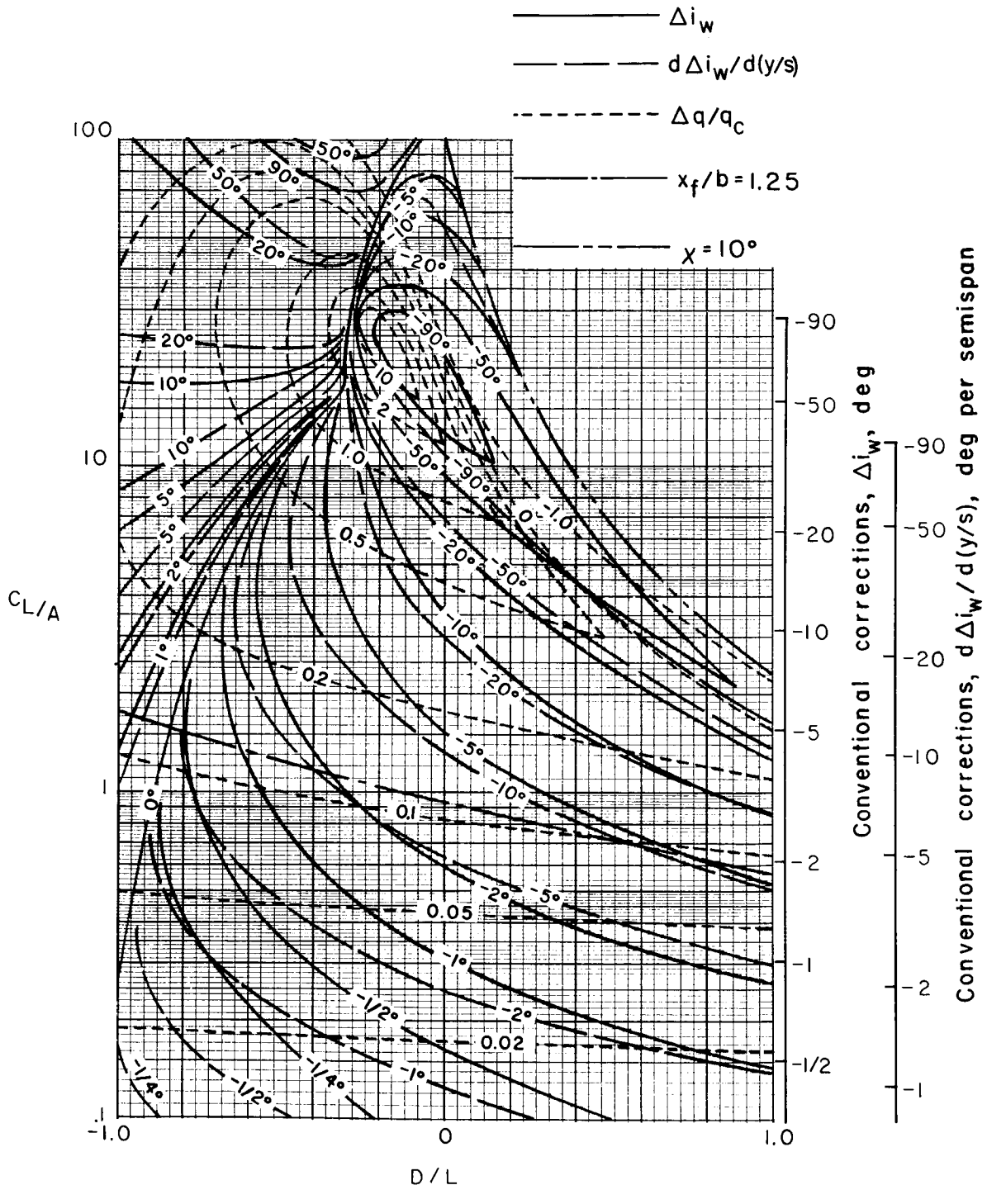


(d) $\sigma = 2/3$.

Figure 46.- Continued.

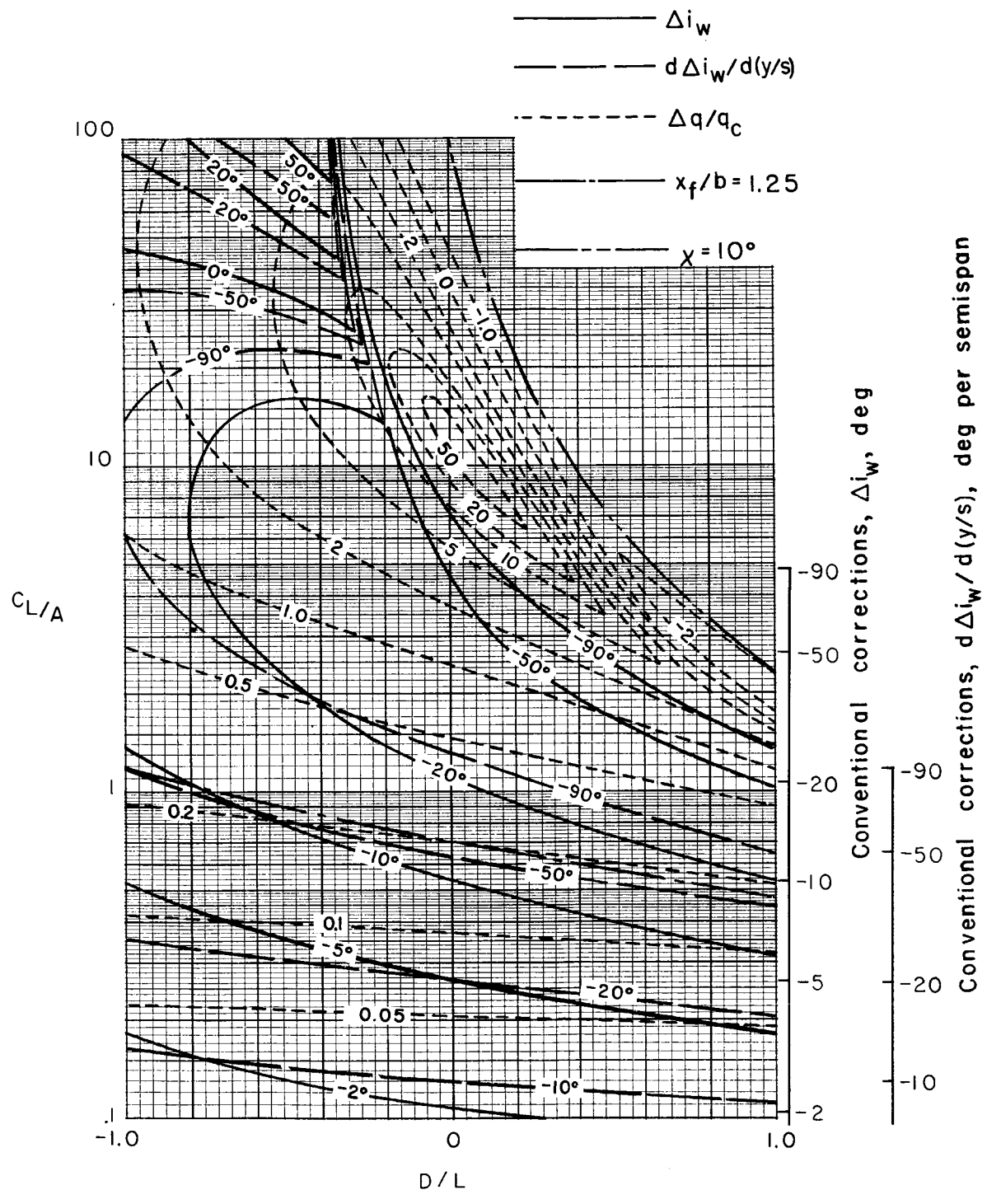


(e) $\sigma = 5/6$.

Figure 46.- Concluded.

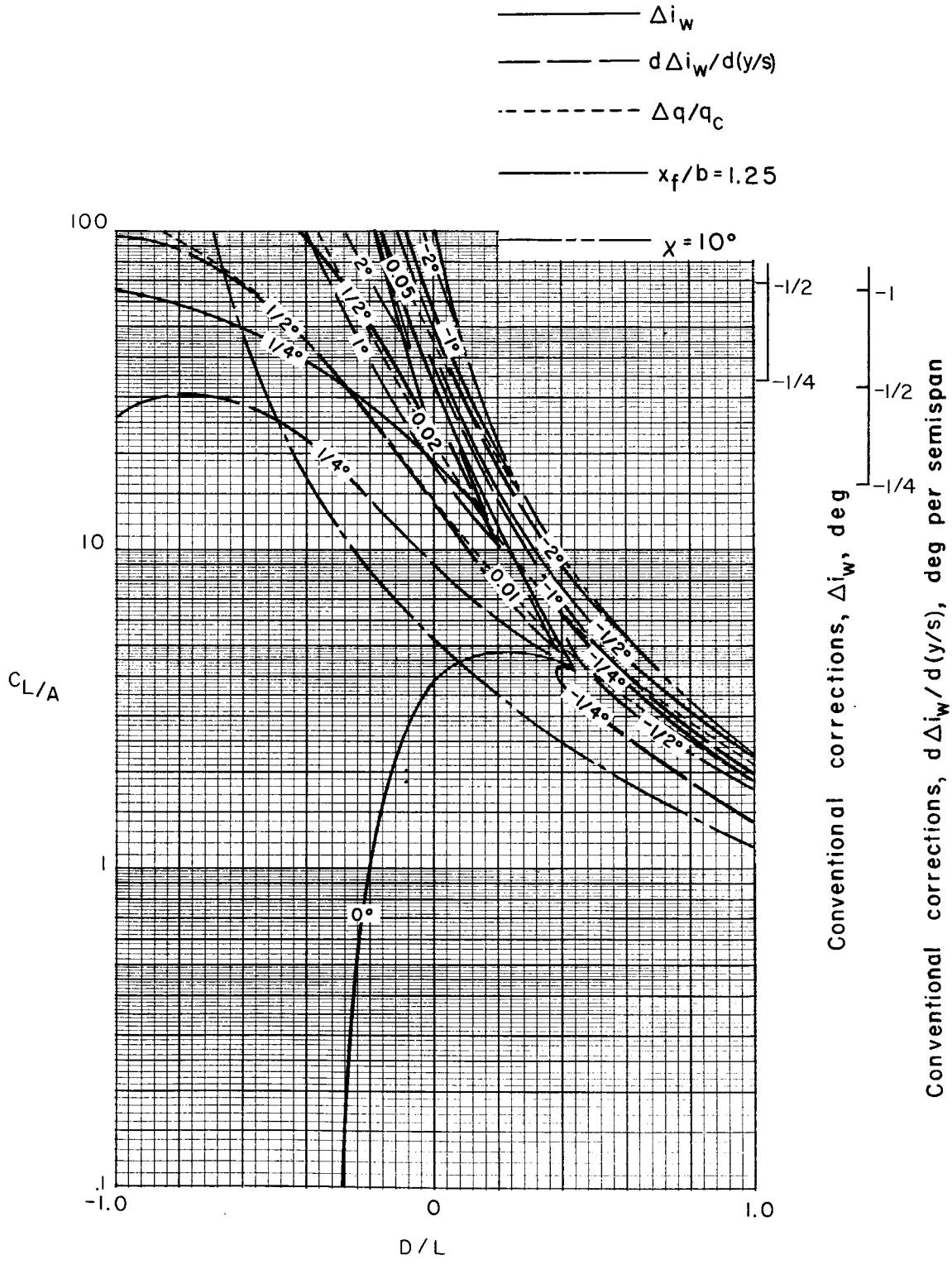


(a) $\sigma = 1/6$.

Figure 47.- Nonuniformity of corrections over a uniformly loaded wing centered in the Langley full-scale tunnel (9.1- by 18.3-m or 30- by 60-ft) with ground board. $\alpha = 0^0$; $\Lambda = 15^0$.

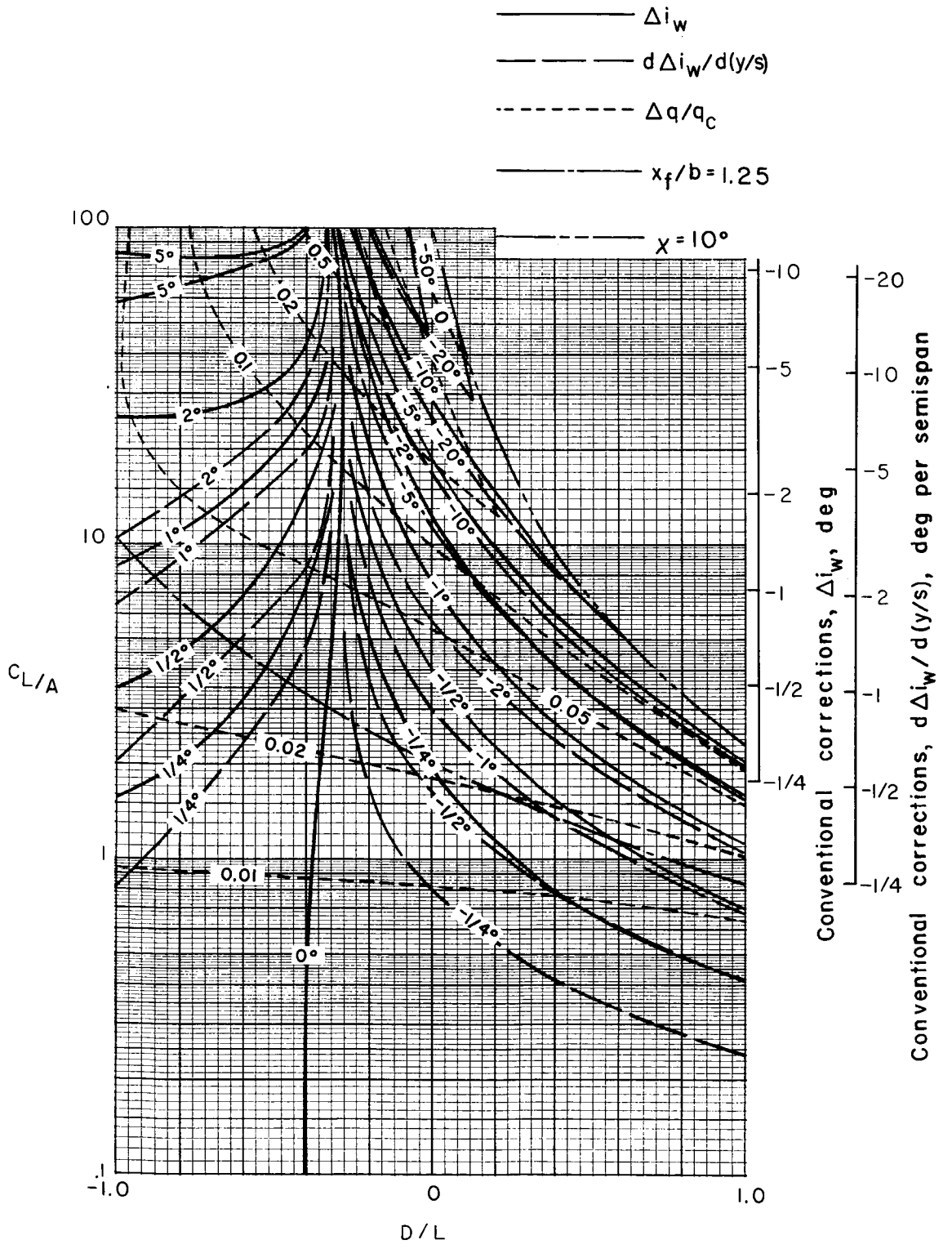


(b) $\sigma = 1/3$.

Figure 47.- Continued.

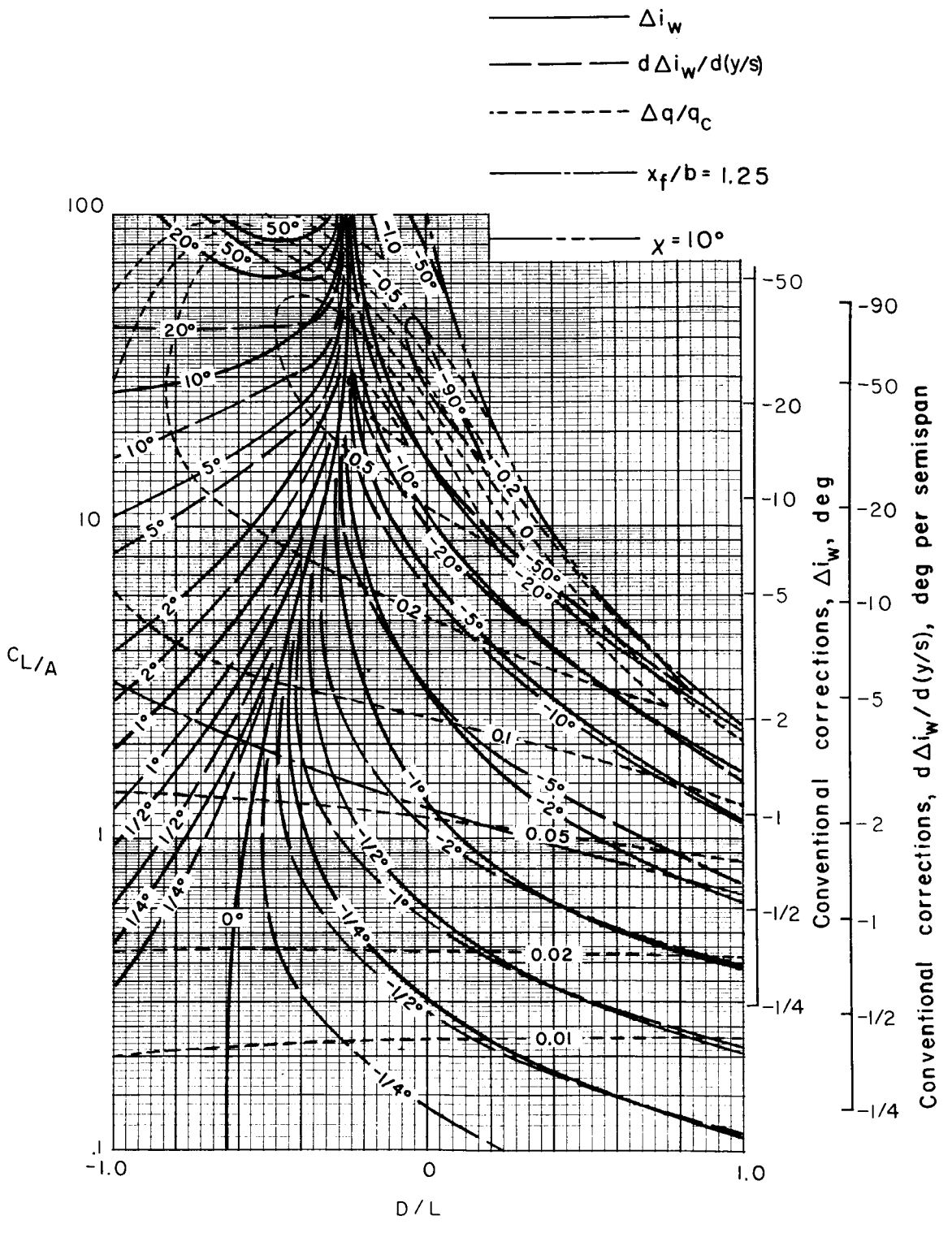


(c) $\sigma = 1/2$.

Figure 47.- Continued.

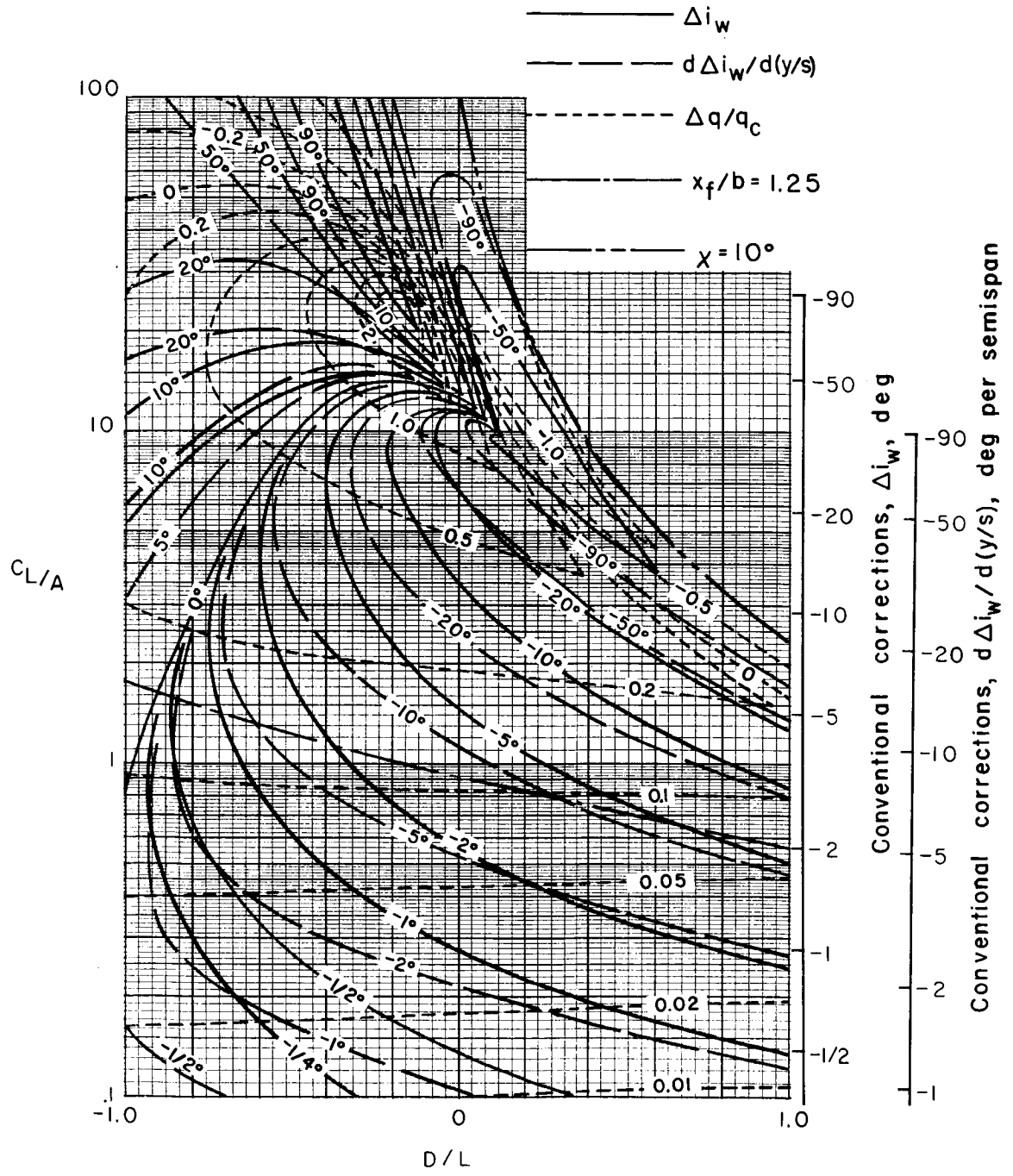


(d) $\sigma = 2/3$.

Figure 47.- Continued.

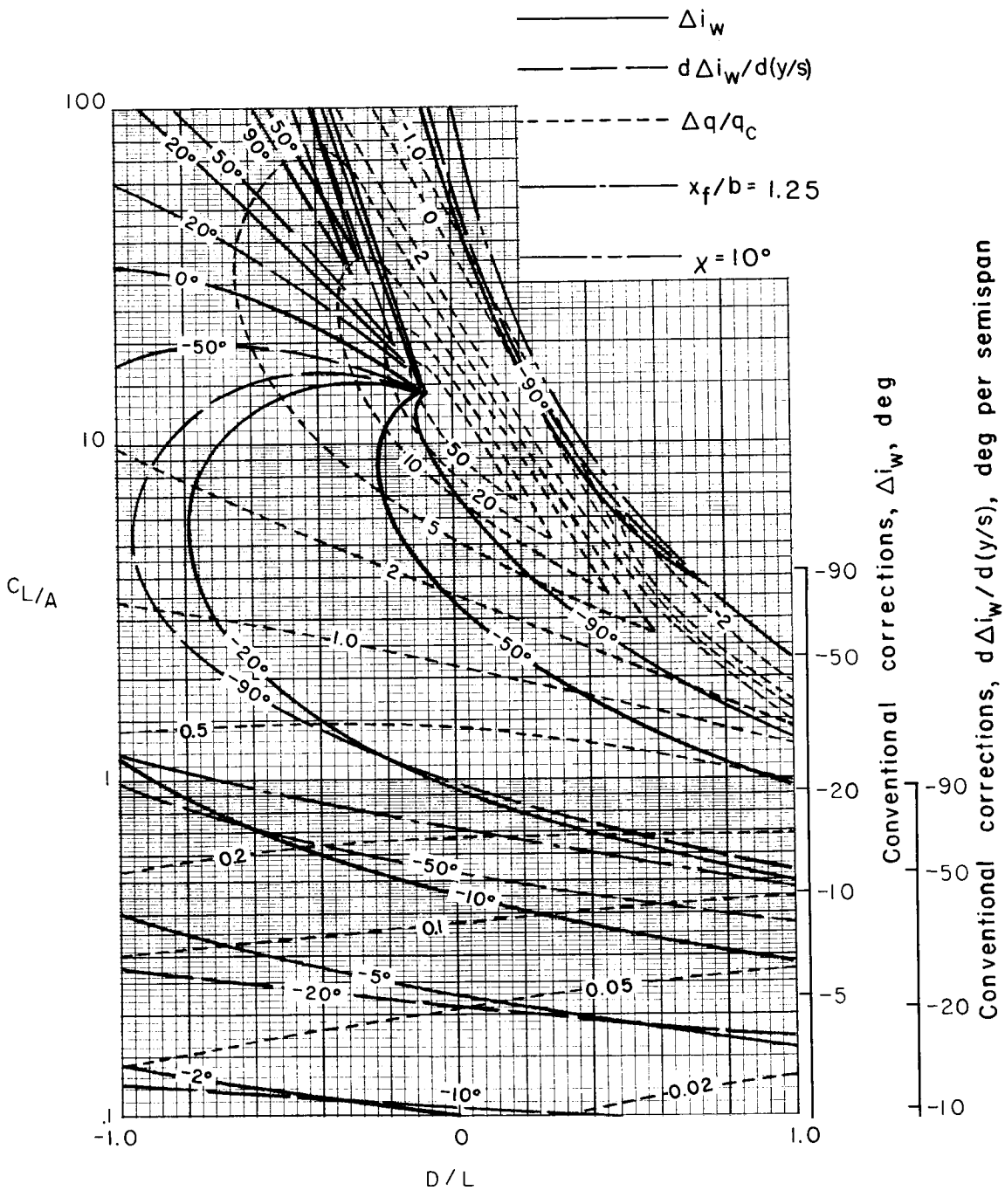


(e) $\sigma = 5/6$.

Figure 47.- Concluded.

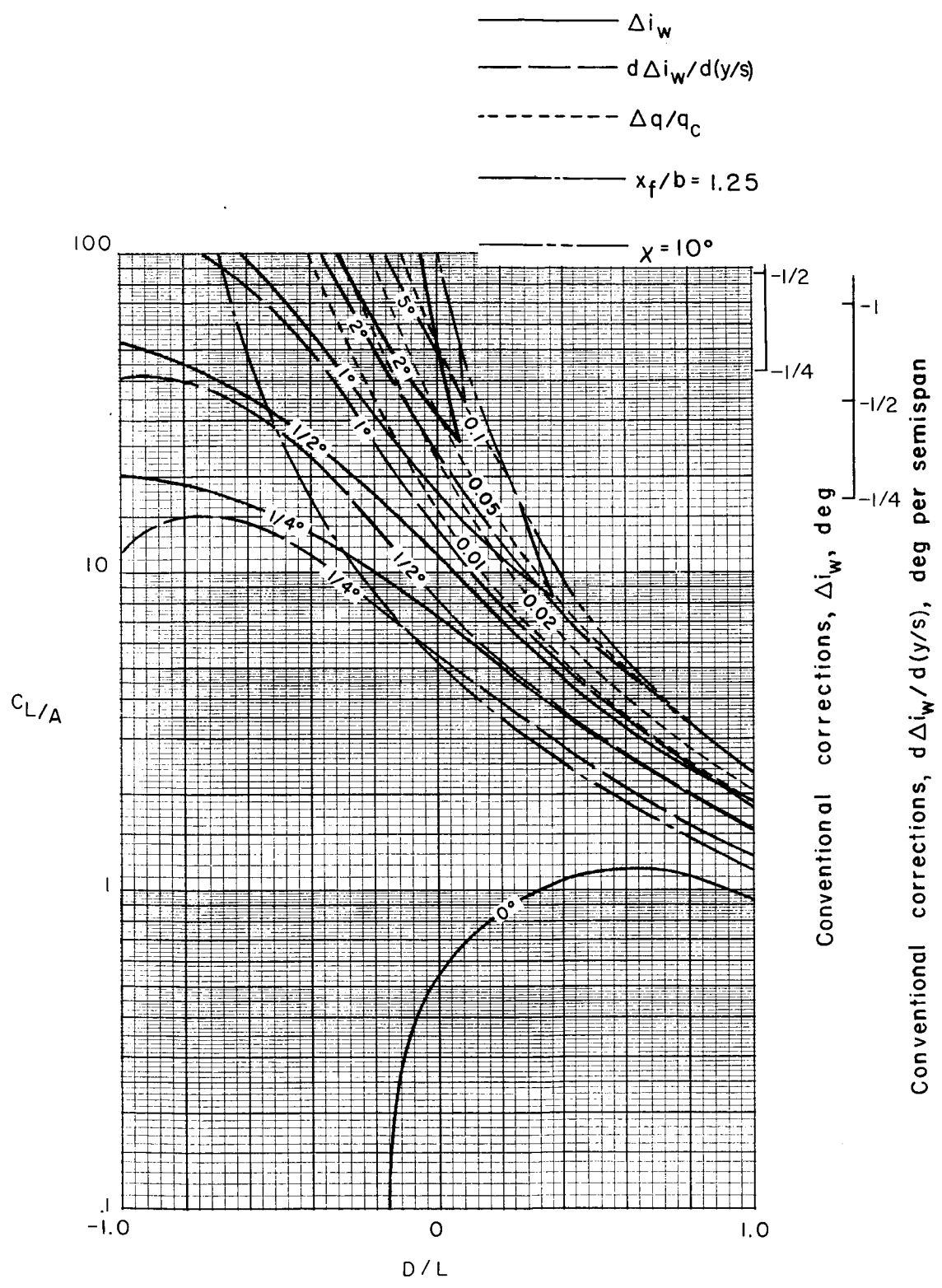


(a) $\sigma = 1/6$.

Figure 48.- Nonuniformity of corrections over a uniformly loaded wing centered in the Langley full-scale tunnel (9.1- by 18.3-m or 30- by 60 ft) with ground board. $\alpha = 0^0$; $A = 30^0$.

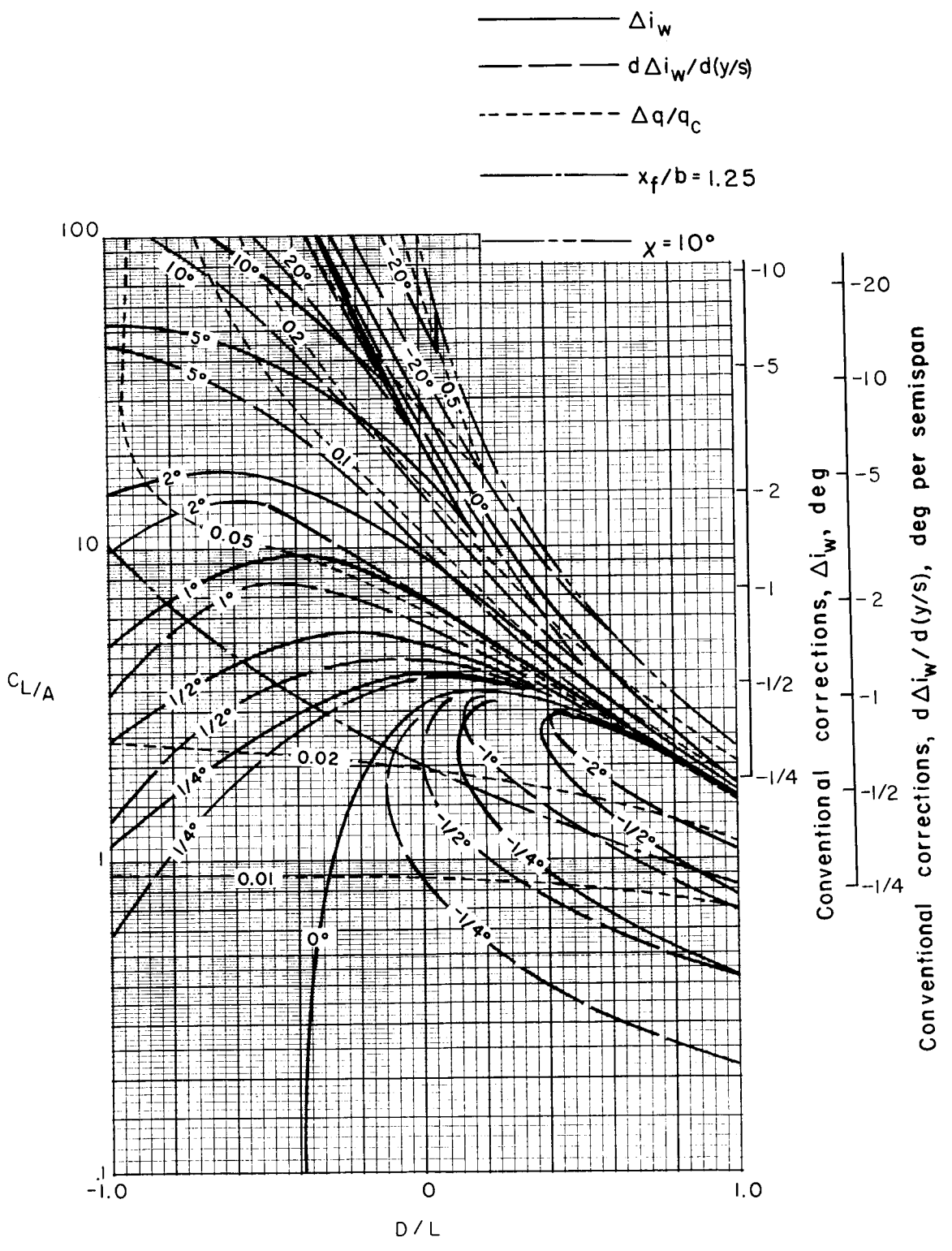


(b) $\sigma = 1/3$.

Figure 48.- Continued.

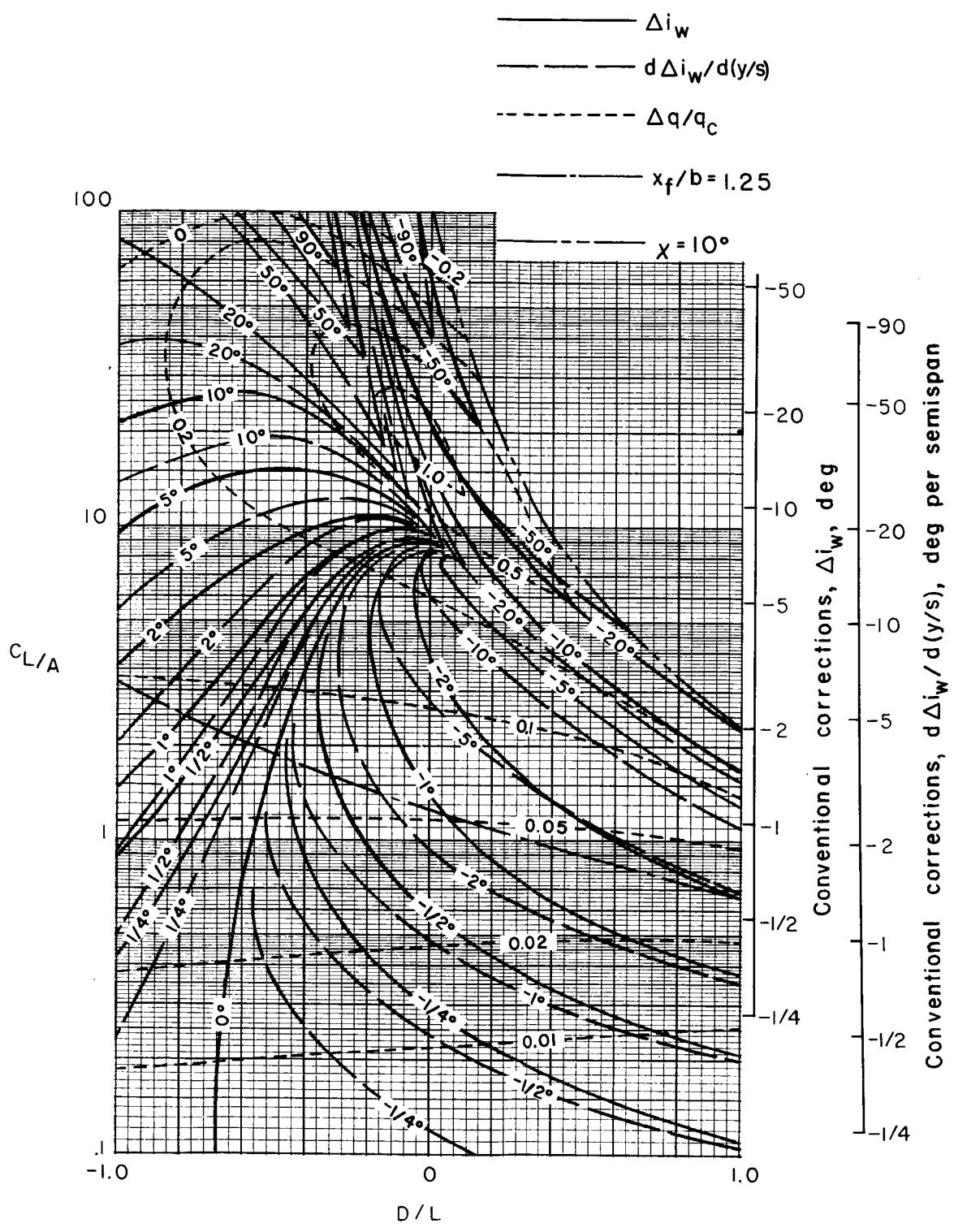


(c) $\sigma = 1/2$.

Figure 48.- Continued.

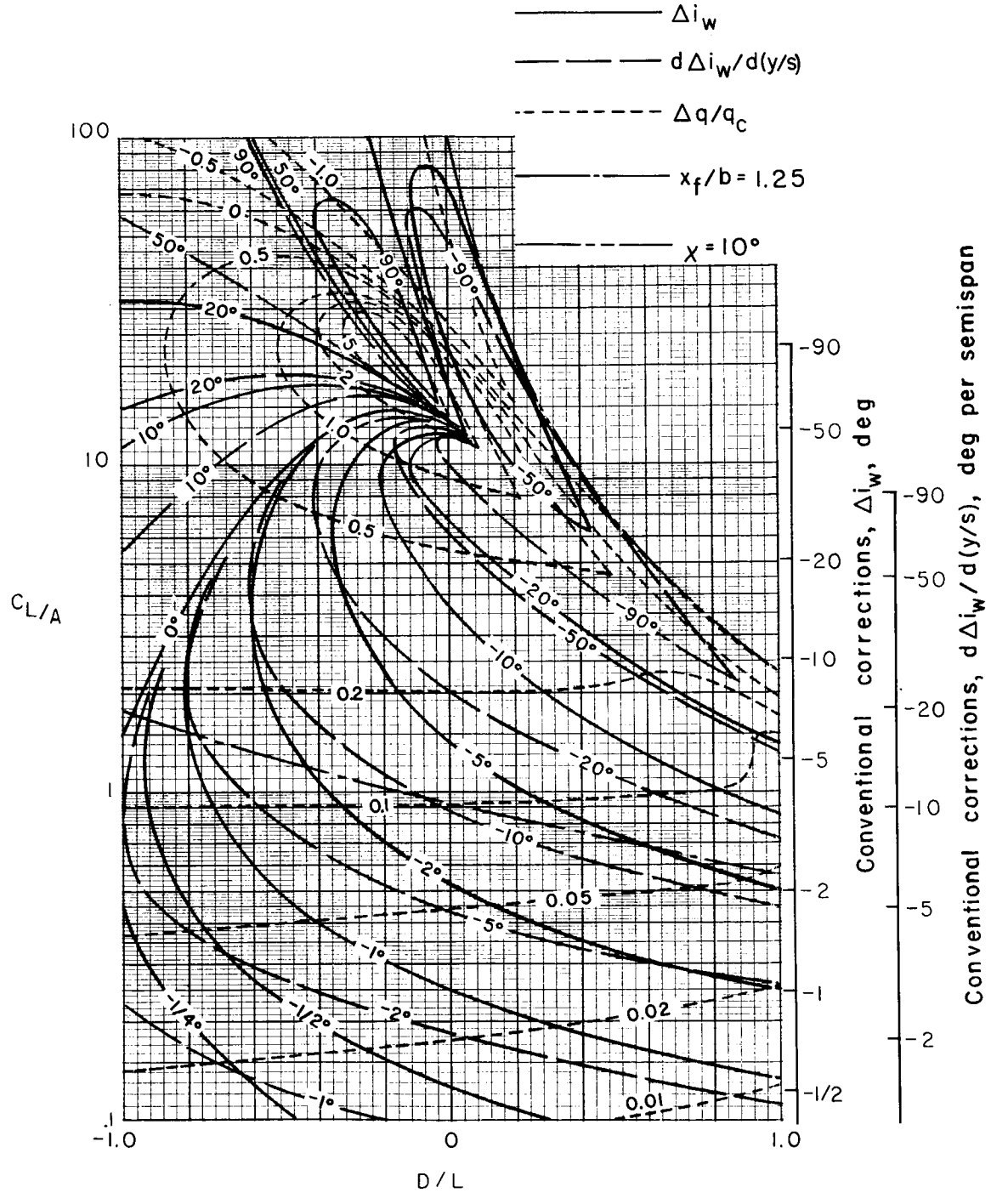


(d) $\sigma = 2/3$.

Figure 48.- Continued.

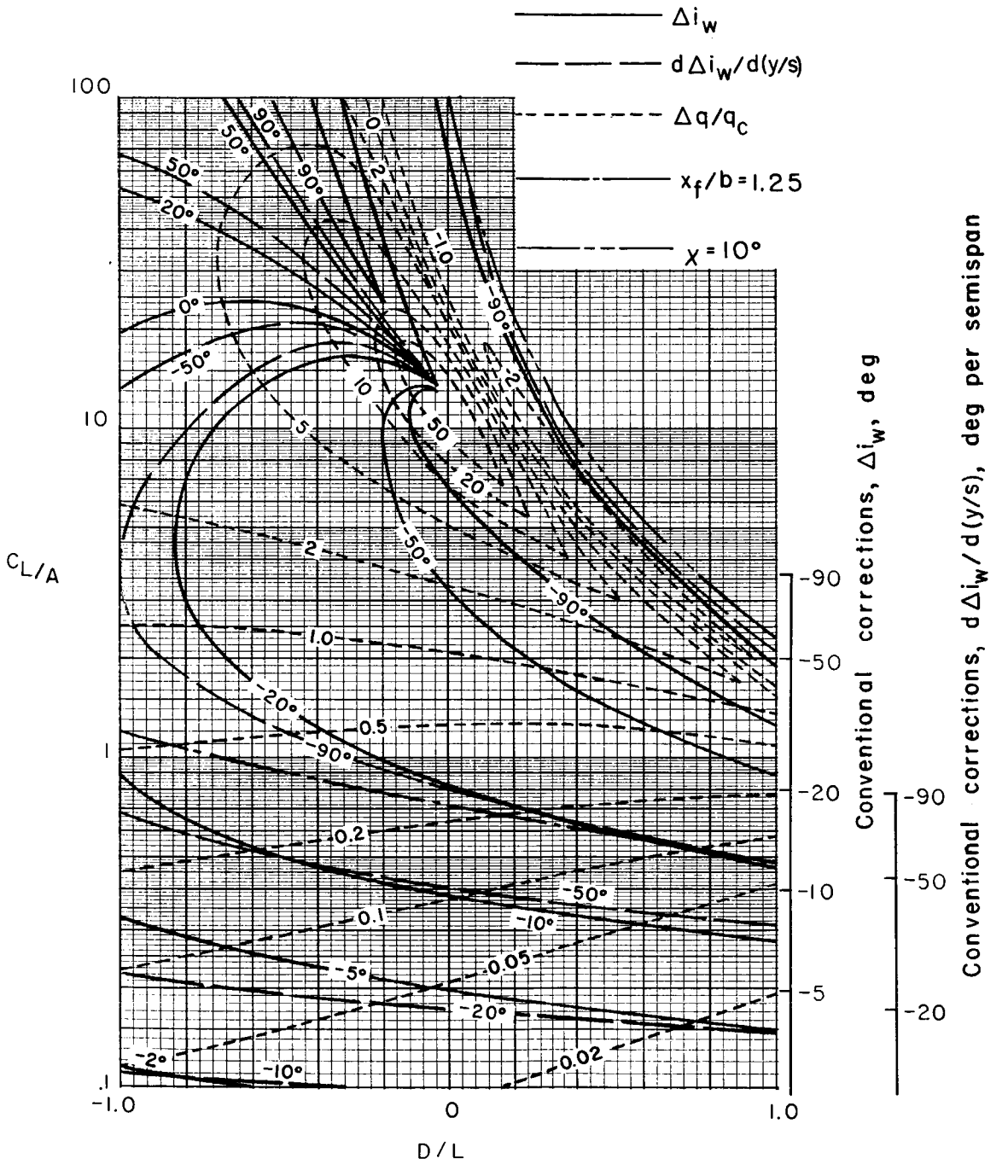


(e) $\sigma = 5/6$.

Figure 48.- Concluded.

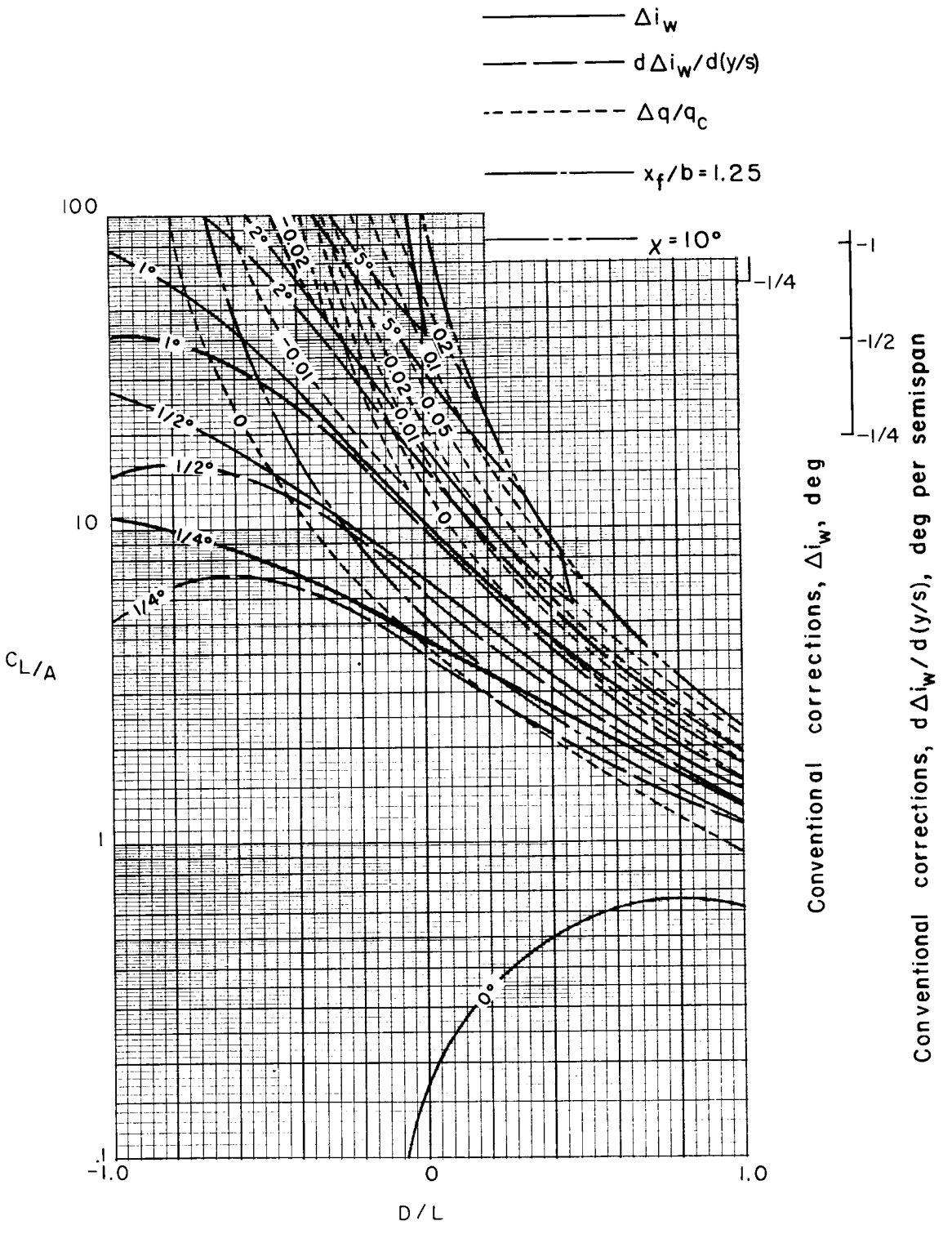


(a) $\sigma = 1/6$.

Figure 49.- Nonuniformity of corrections over a uniformly loaded wing centered in the Langley full-scale tunnel (9.1- by 18.3-m or 30- by 60-ft) with ground board. $\alpha = 0^0$; $\Lambda = 45^0$.

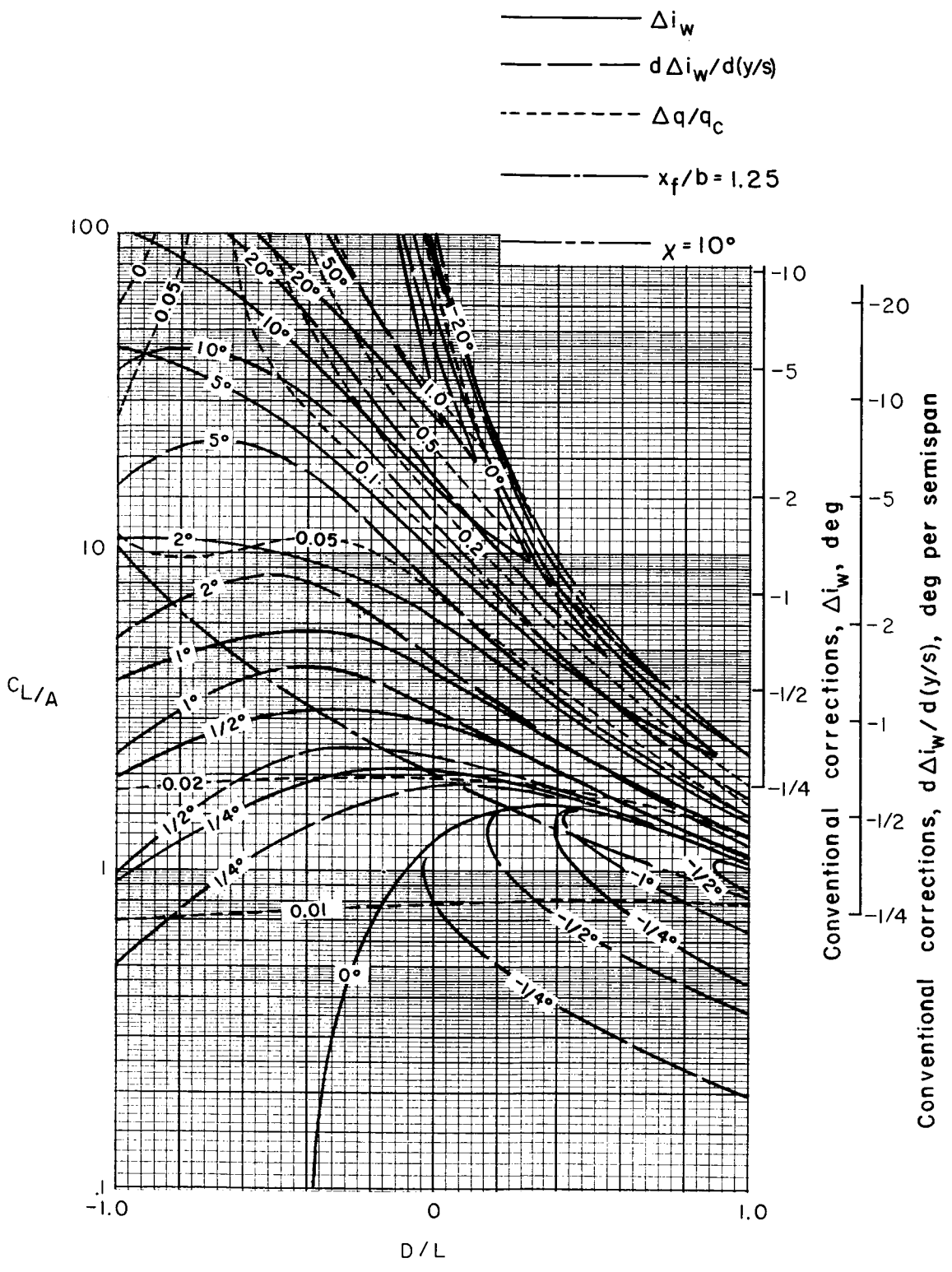


(b) $\sigma = 1/3$.

Figure 49.- Continued.

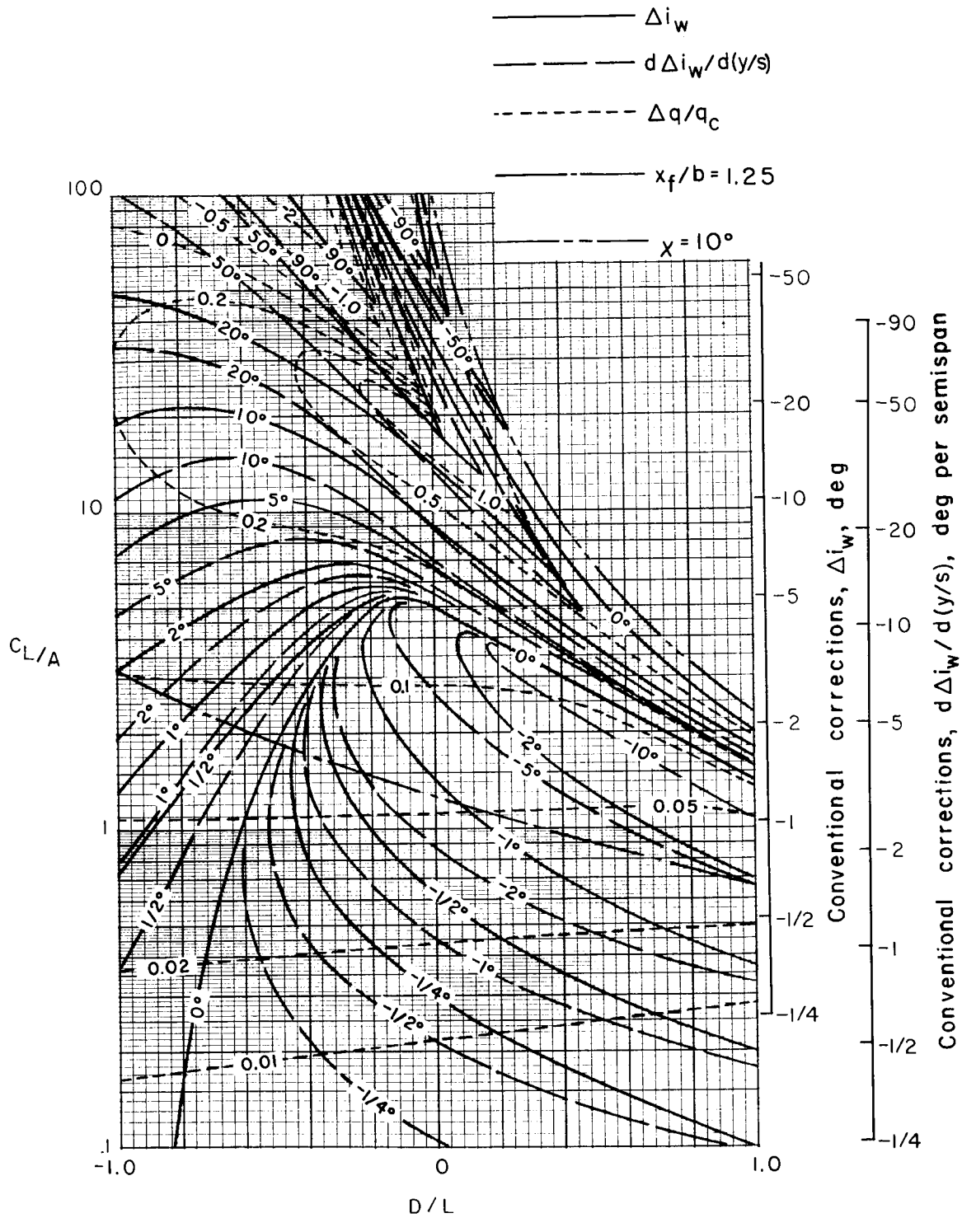


(c) $\sigma = 1/2$.

Figure 49.- Continued.

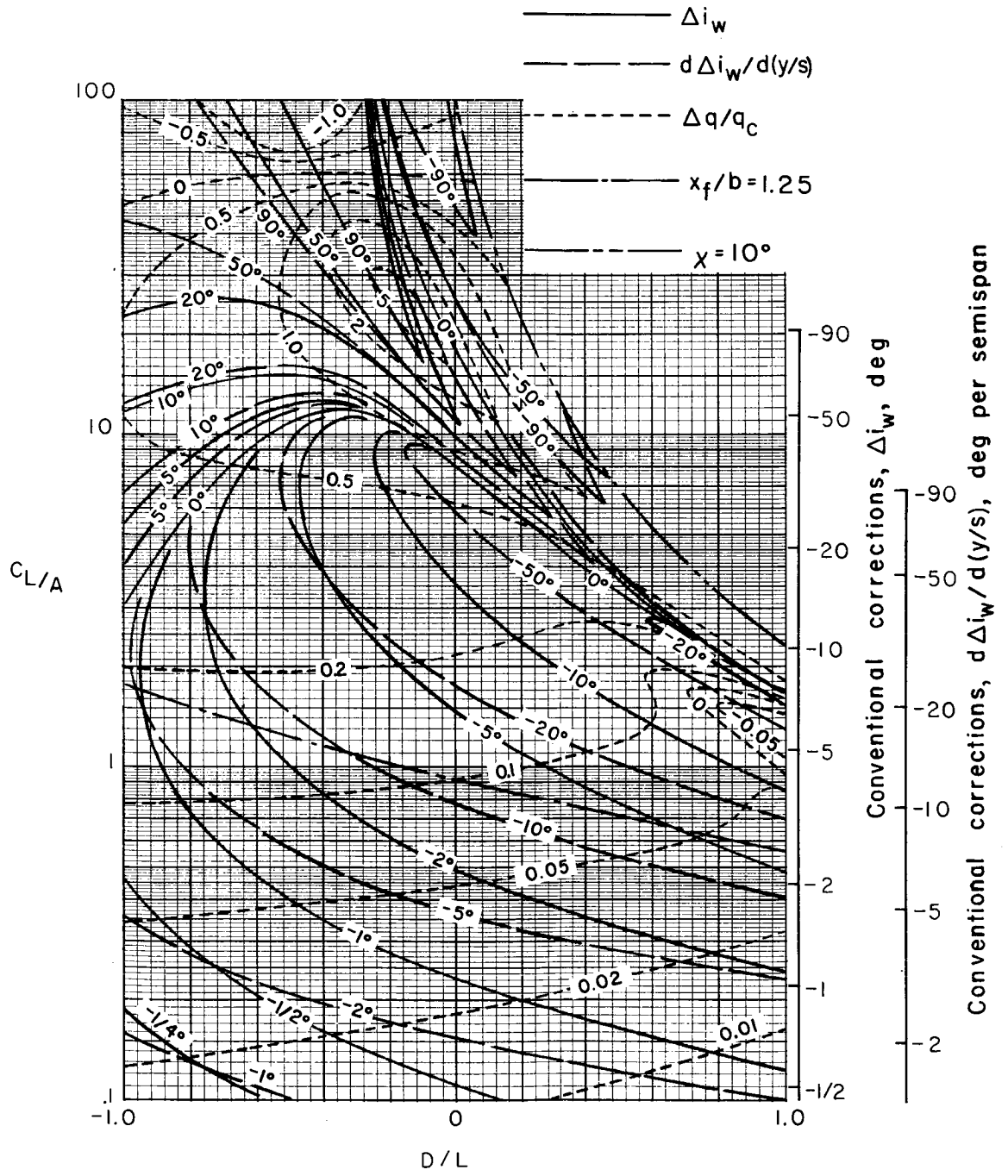


(d) $\sigma = 2/3$.

Figure 49.- Continued.

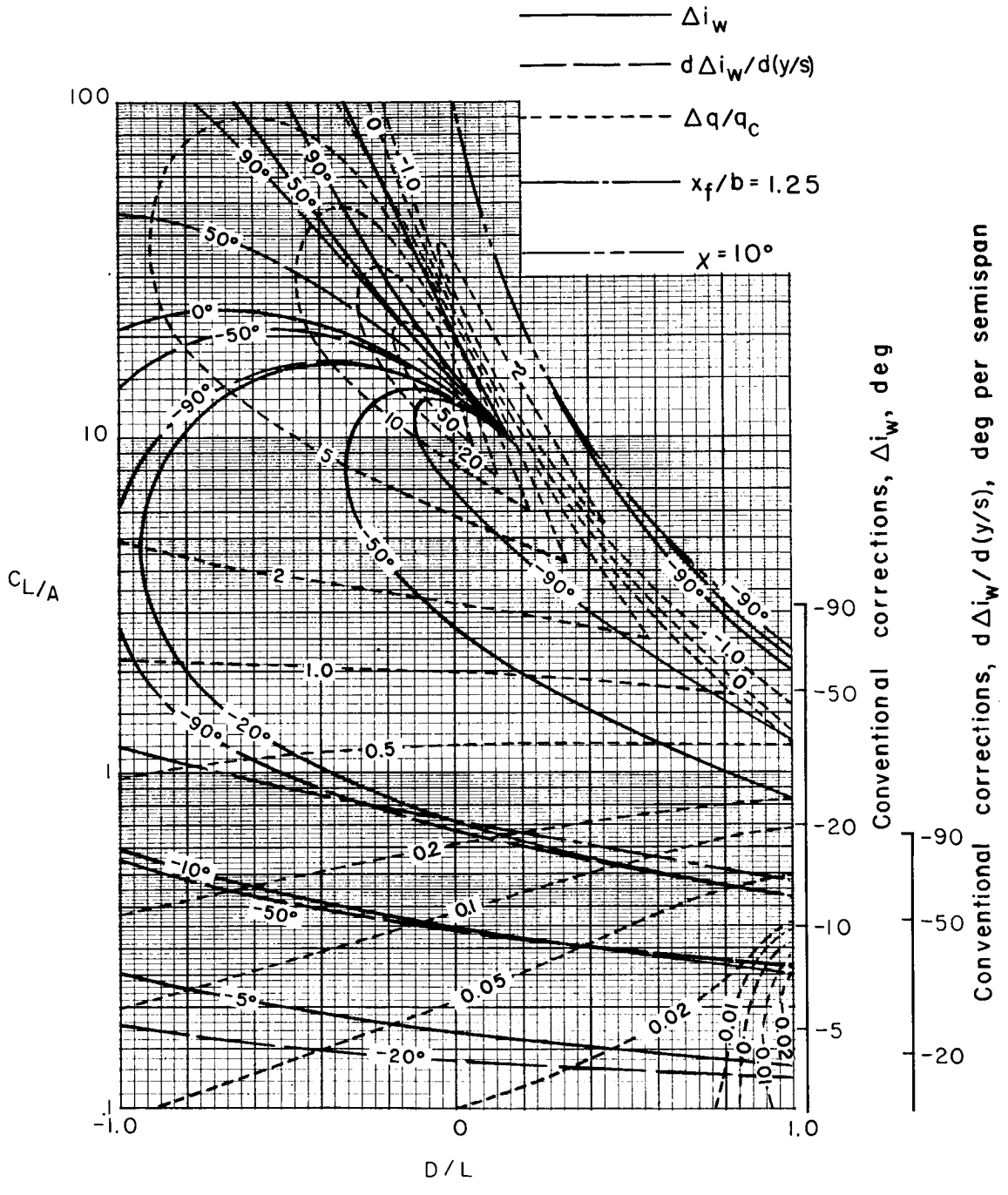


(e) $\sigma = 5/6$.

Figure 49.- Concluded.

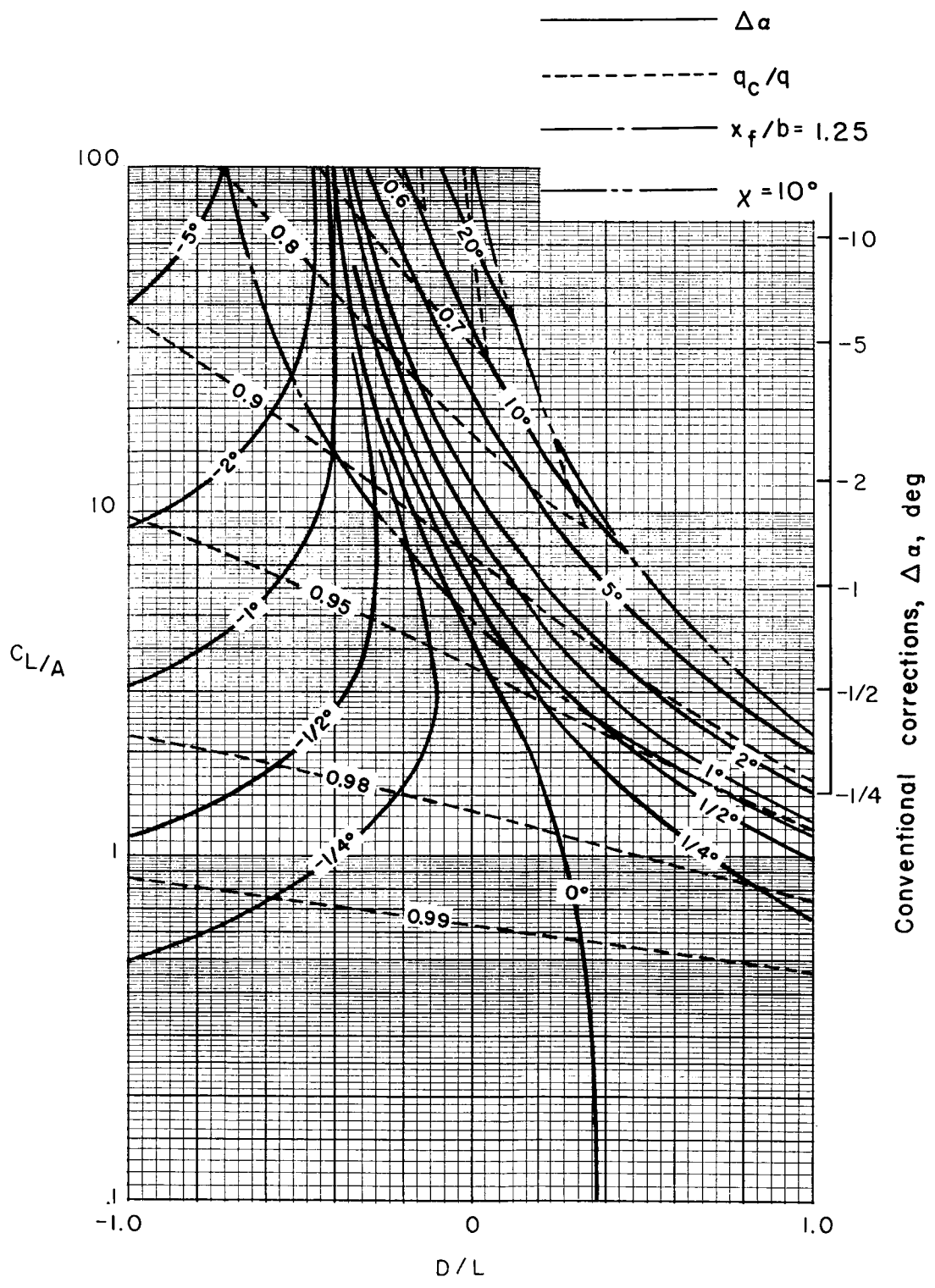


(a) σ = 1/4.

Figure 50.- Average corrections for a uniformly loaded wing centered in a rectangular tunnel closed on the bottom only. Λ = 0°; γ = 1.5.

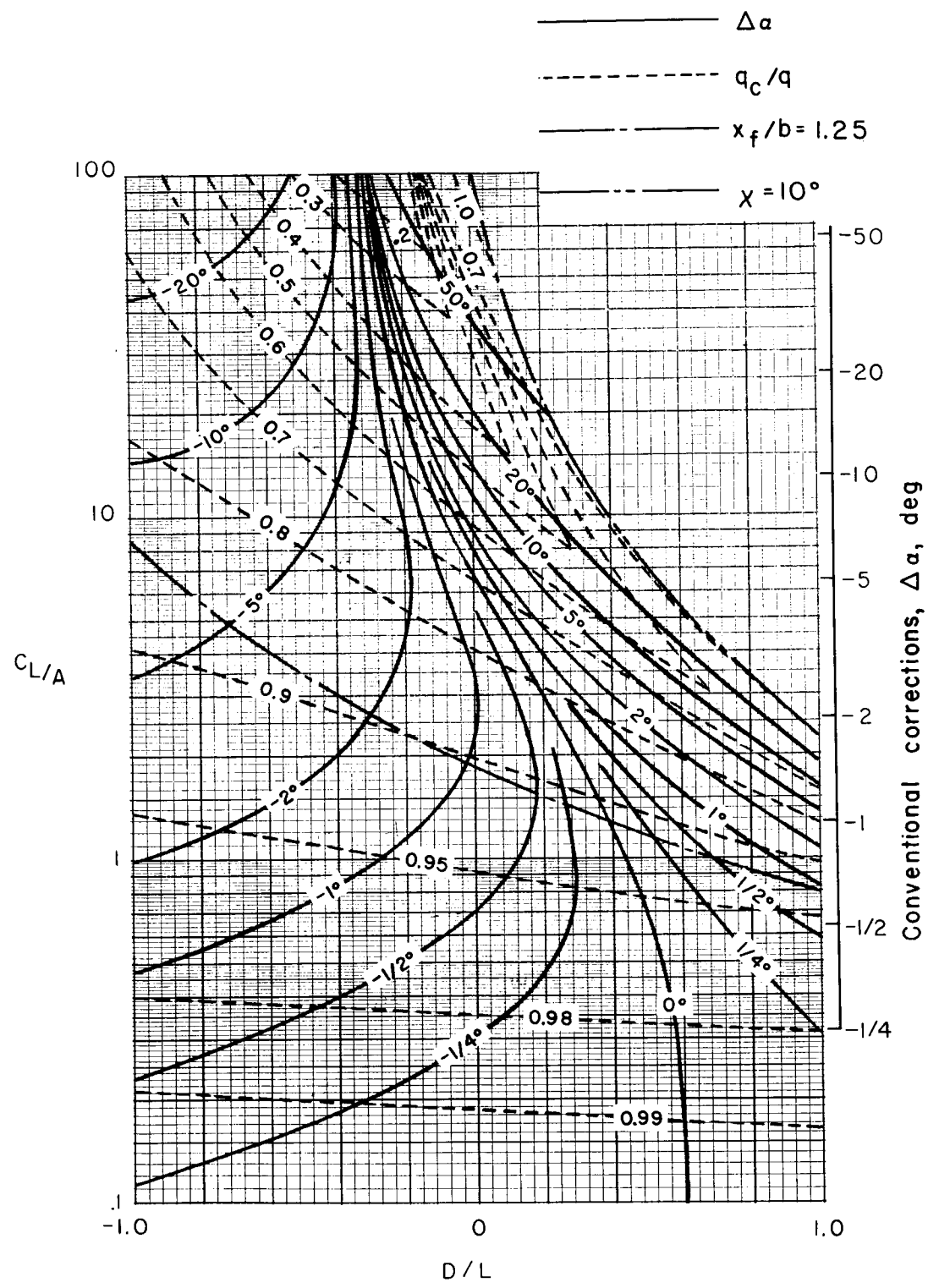


(b) σ = 1/2.

Figure 50.- Continued.

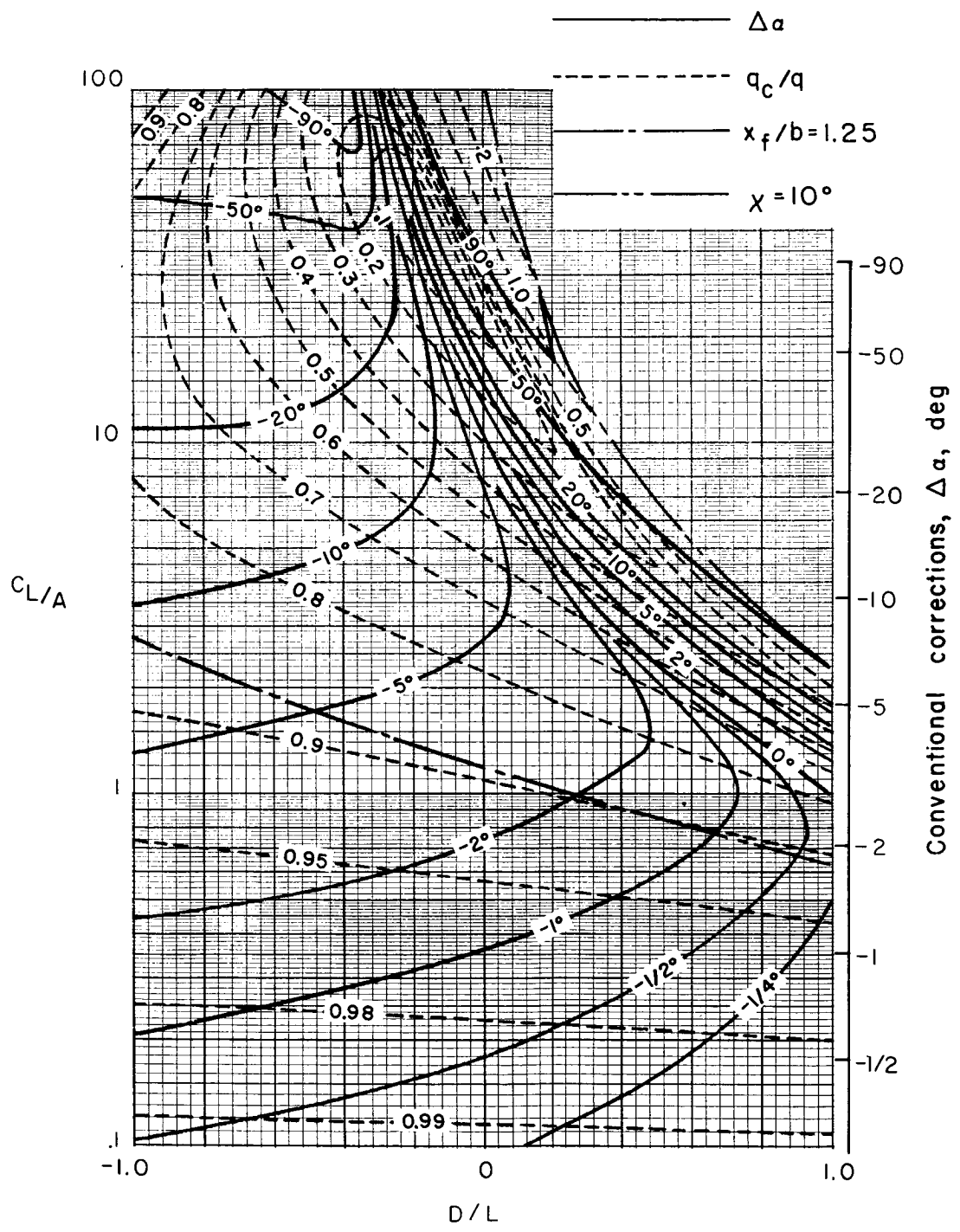


(c) σ = 3/4.

Figure 50.- Concluded.

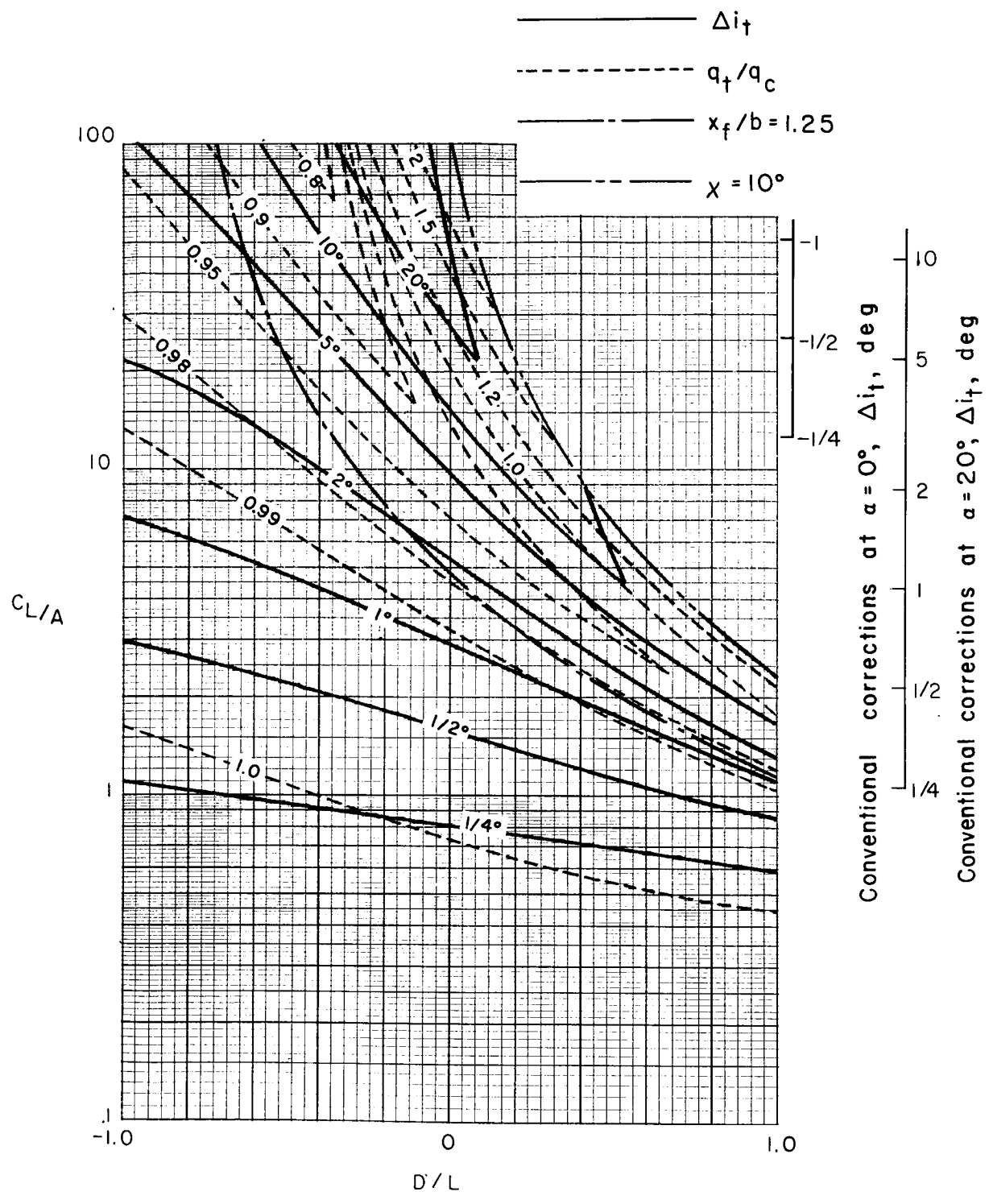


(a) $\sigma = 1/4$.

Figure 51.- Corrections at a zero-span tail behind a uniformly loaded wing centered in a rectangular tunnel closed on the bottom only. Tail length is three-fourths of wing span; tail height is zero; $\alpha = 20^0$; $\Lambda = 0^0$; $\gamma = 1.5$.

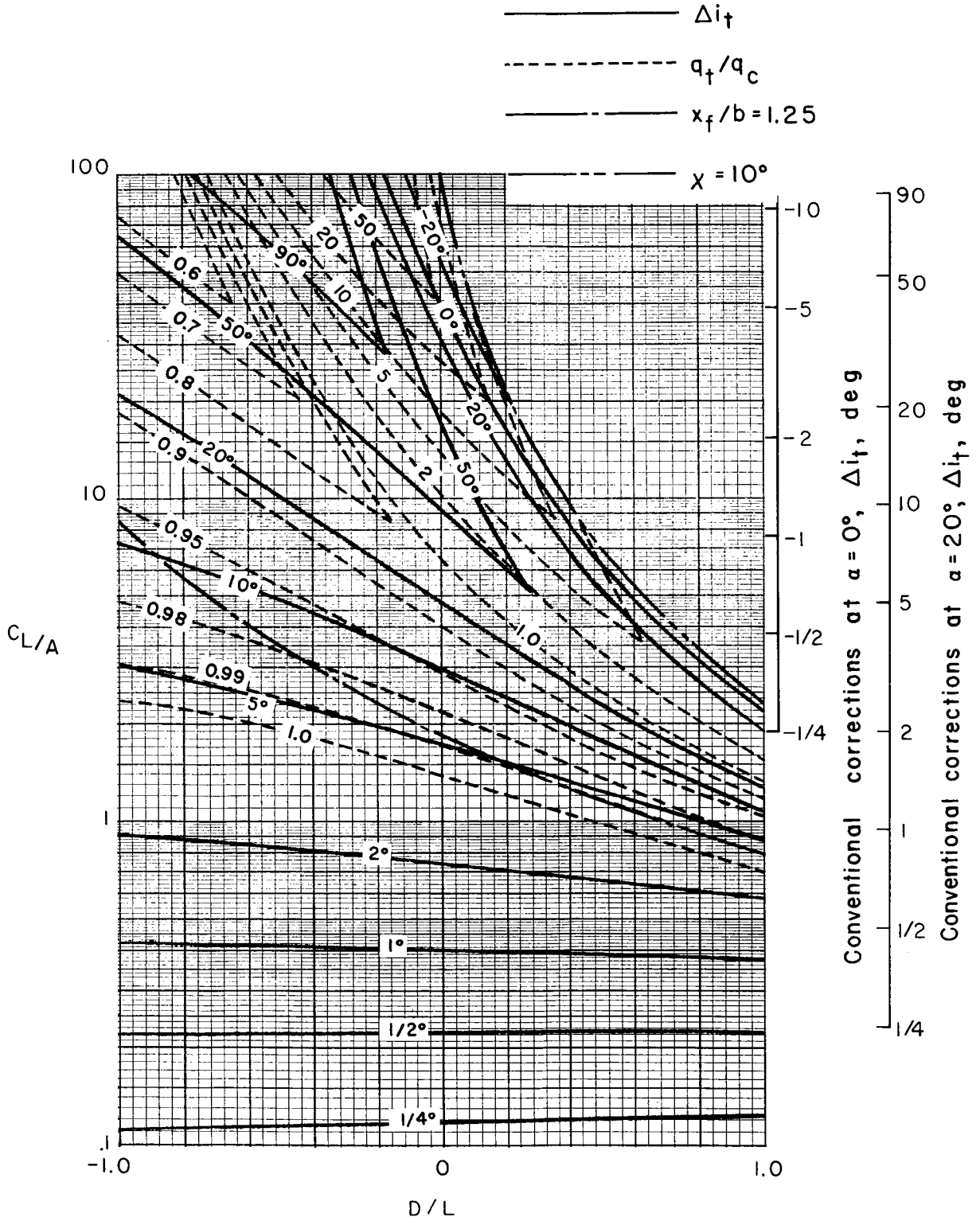


(b) σ = 1/2.

Figure 51.- Continued.

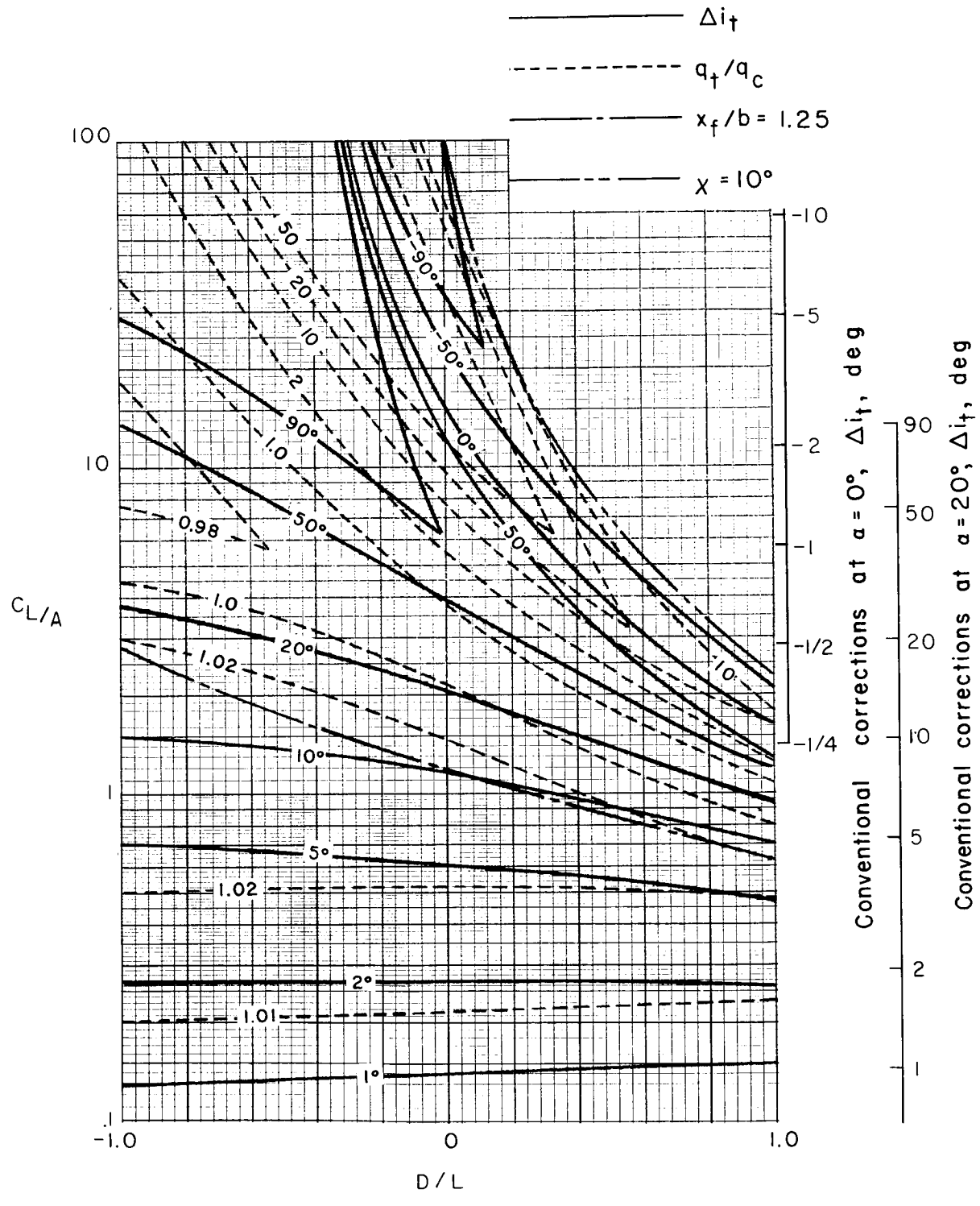


(c) $\sigma = 3/4$.

Figure 51.- Concluded.

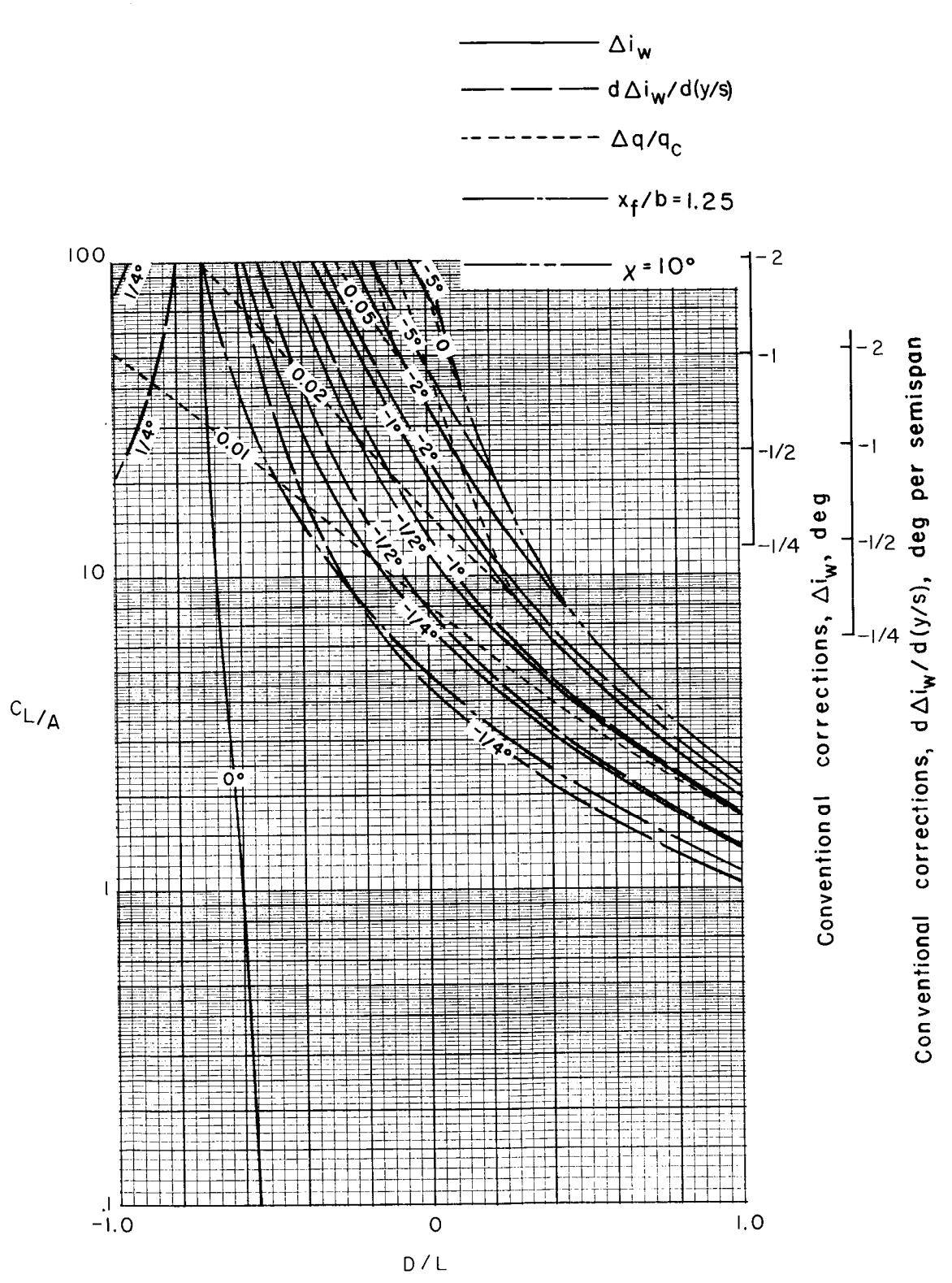


(a) $\sigma = 1/4$.

Figure 52.- Nonuniformity of corrections over a uniformly loaded wing centered in a rectangular tunnel closed only on the bottom. $\gamma = 1.5$; $\alpha = 0^0$; $\Lambda = 0^0$.

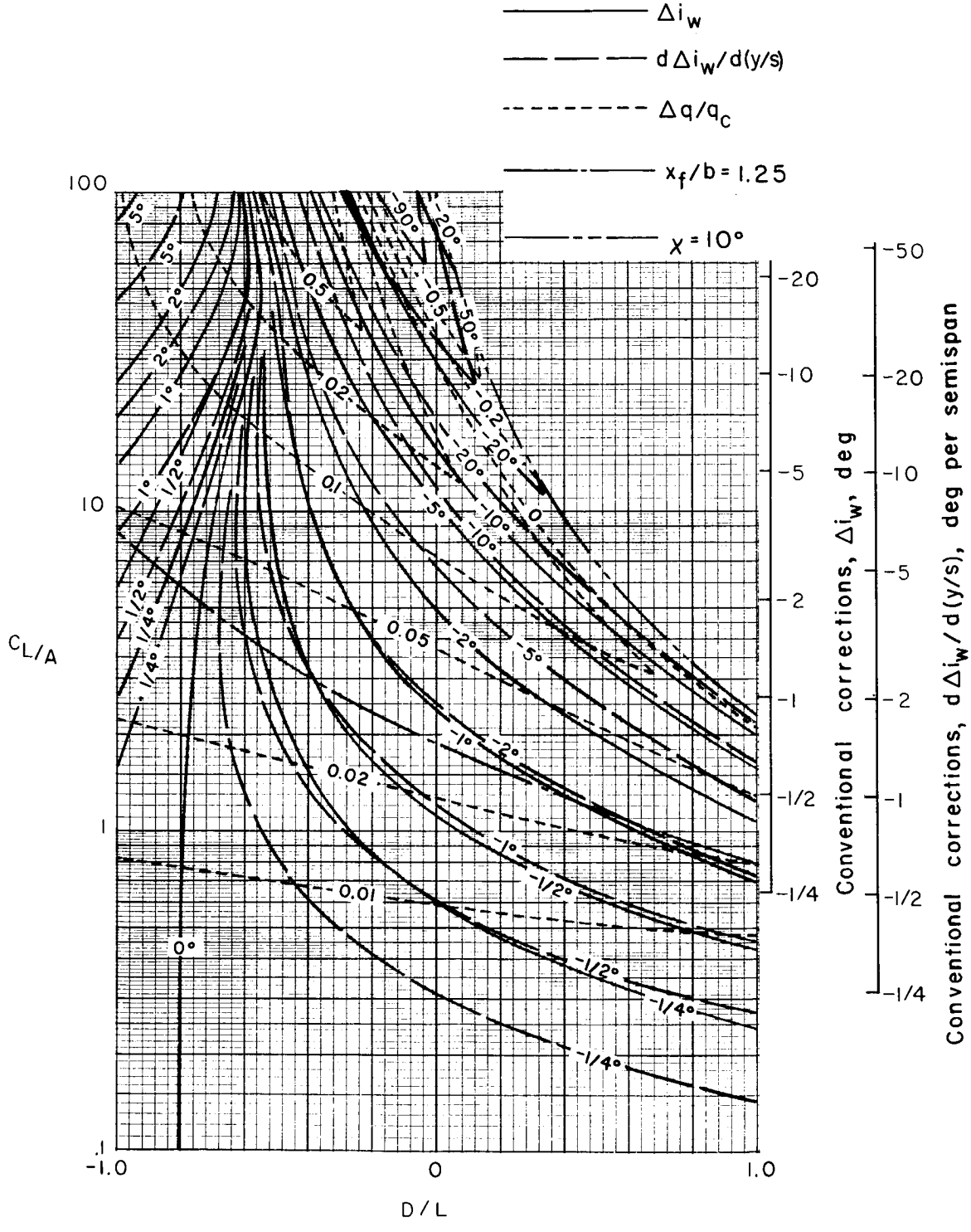


(b) $\sigma = 1/2$.

Figure 52.- Continued.

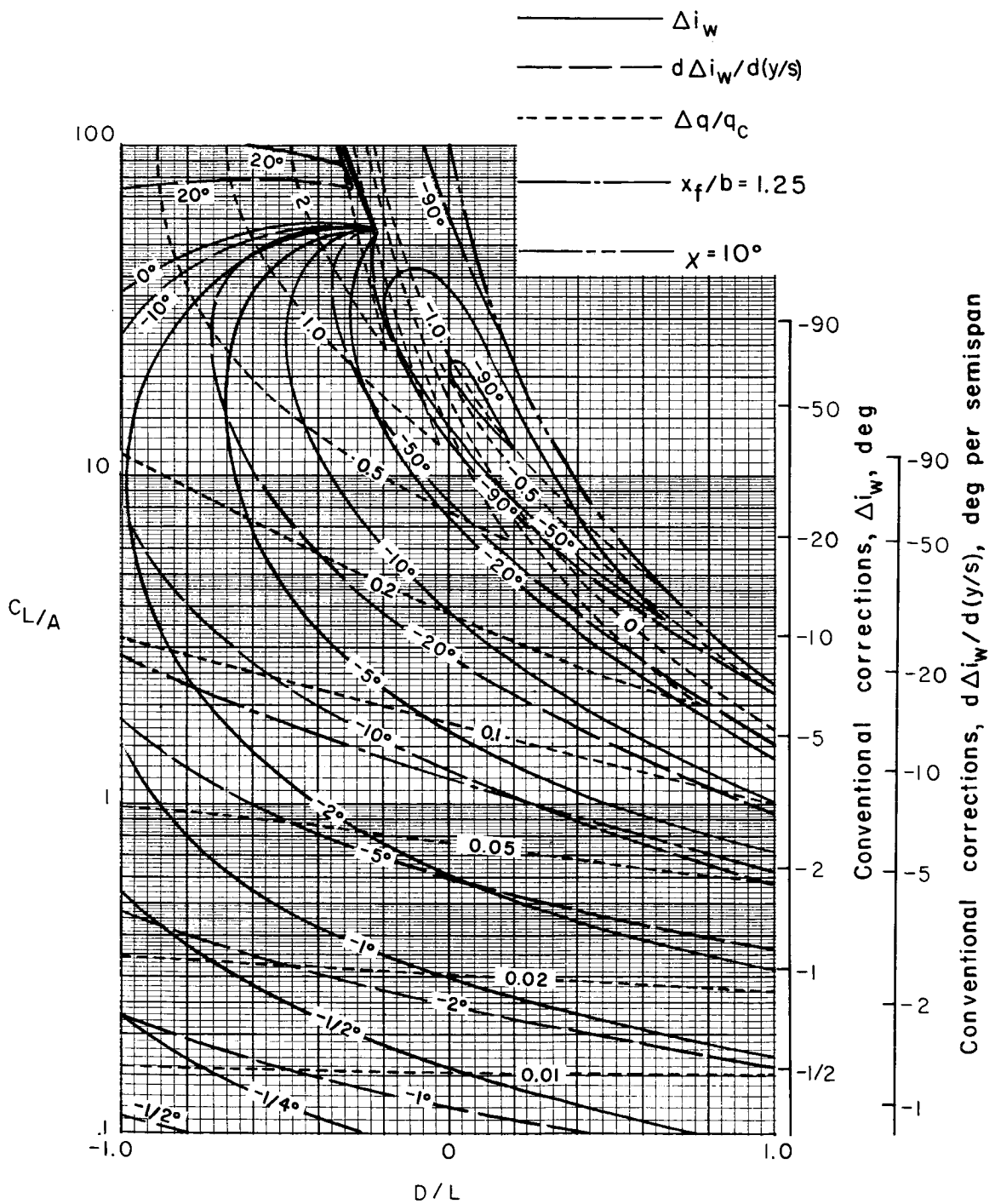


(c) $\sigma = 3/4$.

Figure 52.- Concluded.

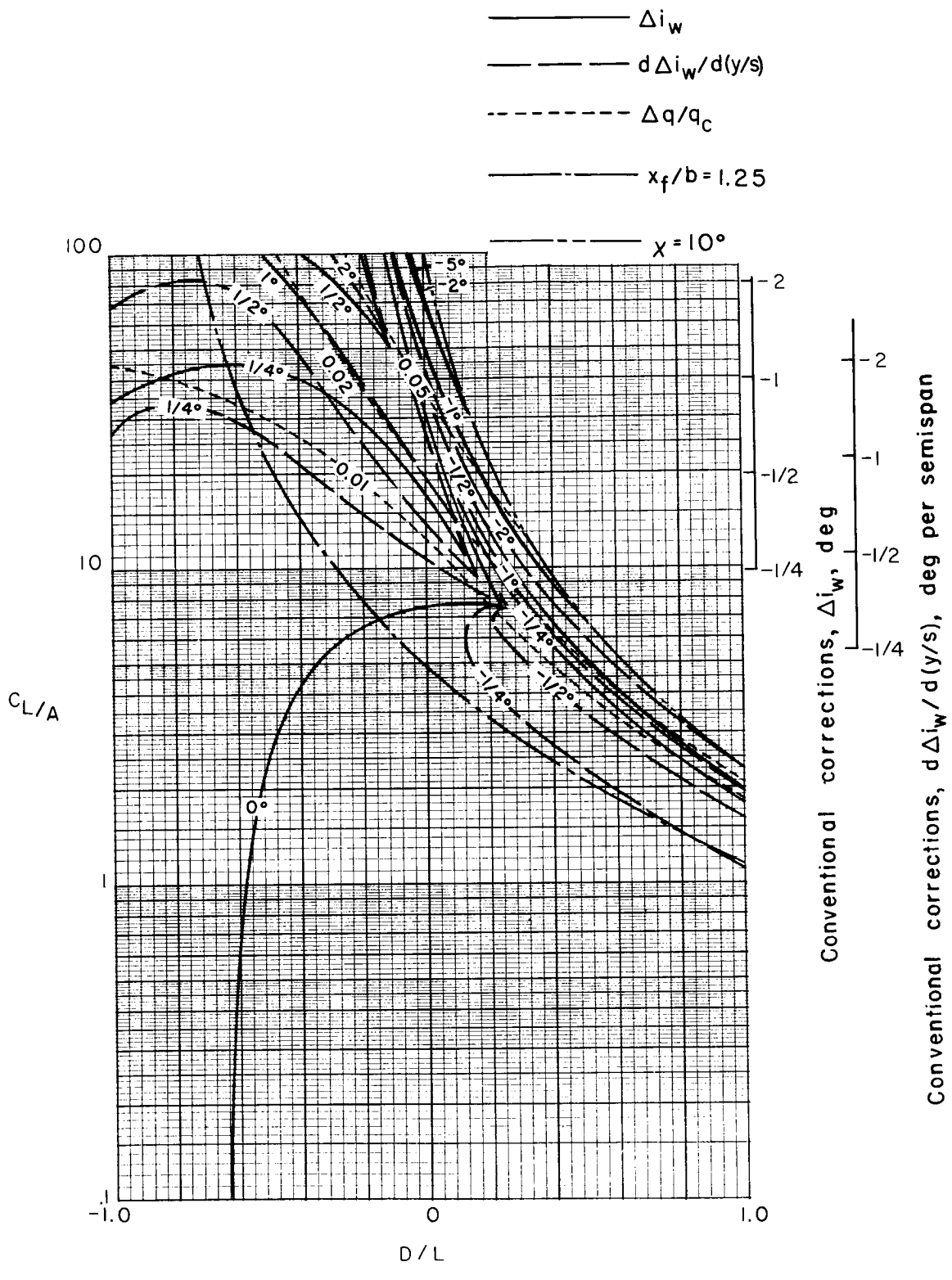


(a) $\sigma = 1/4$.

Figure 53.- Nonuniformity of corrections over a uniformly loaded wing centered in a rectangular tunnel closed only on the bottom. $\gamma = 1.5$; $\alpha = 0^0$; $\Lambda = 15^0$.

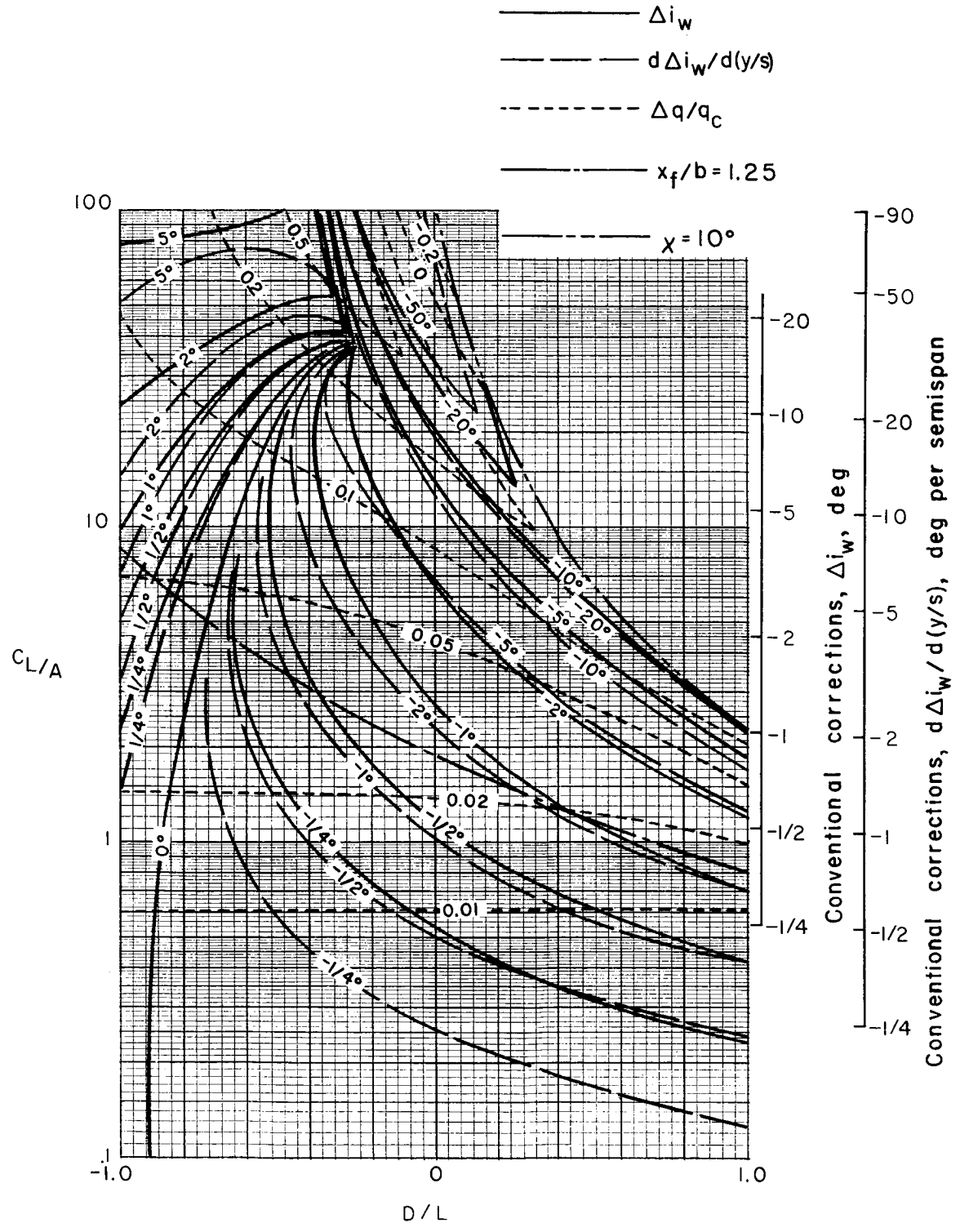


(b) $\sigma = 1/2$.

Figure 53. Continued.

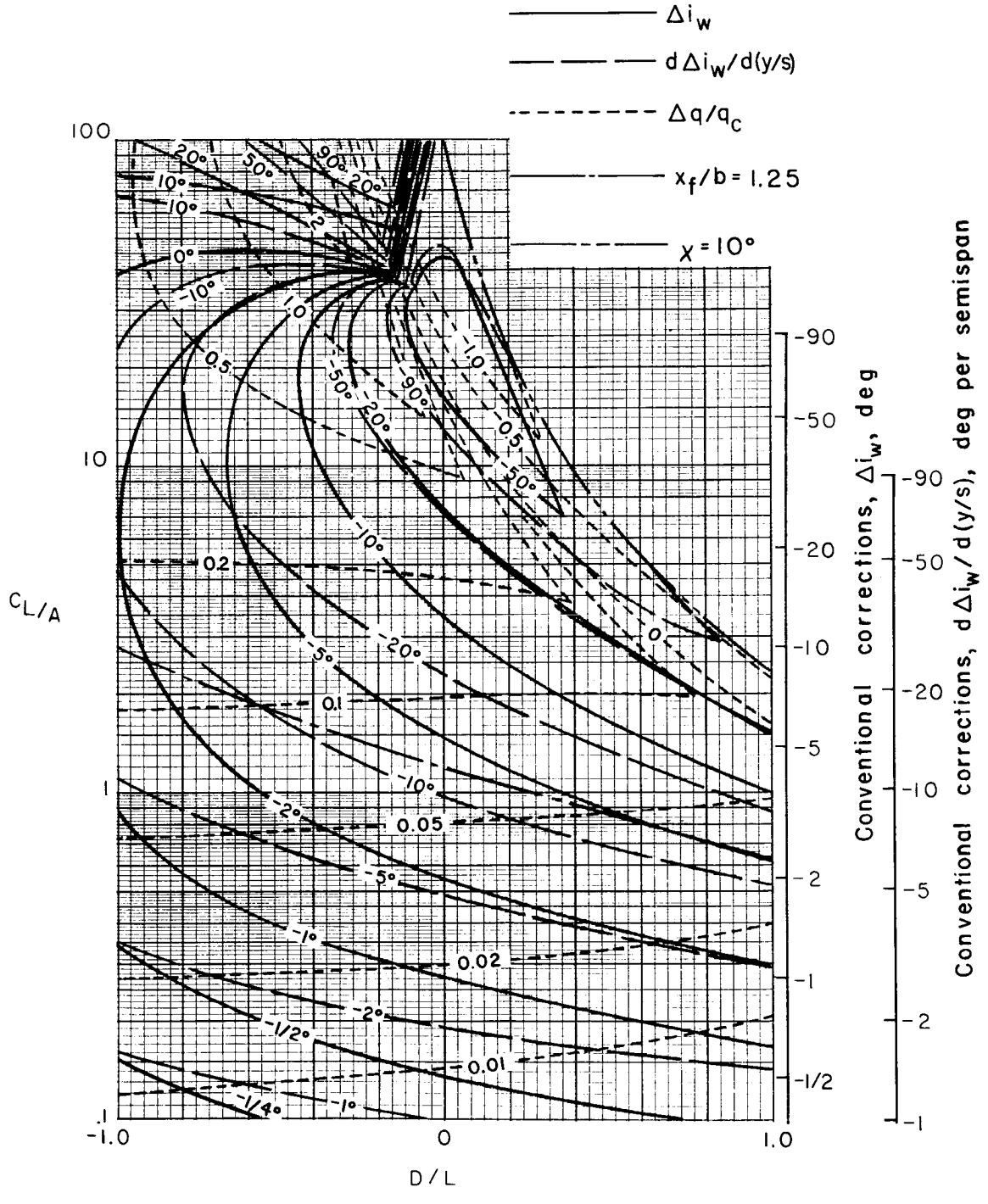


(c) $\sigma = 3/4$.

Figure 53.- Concluded.

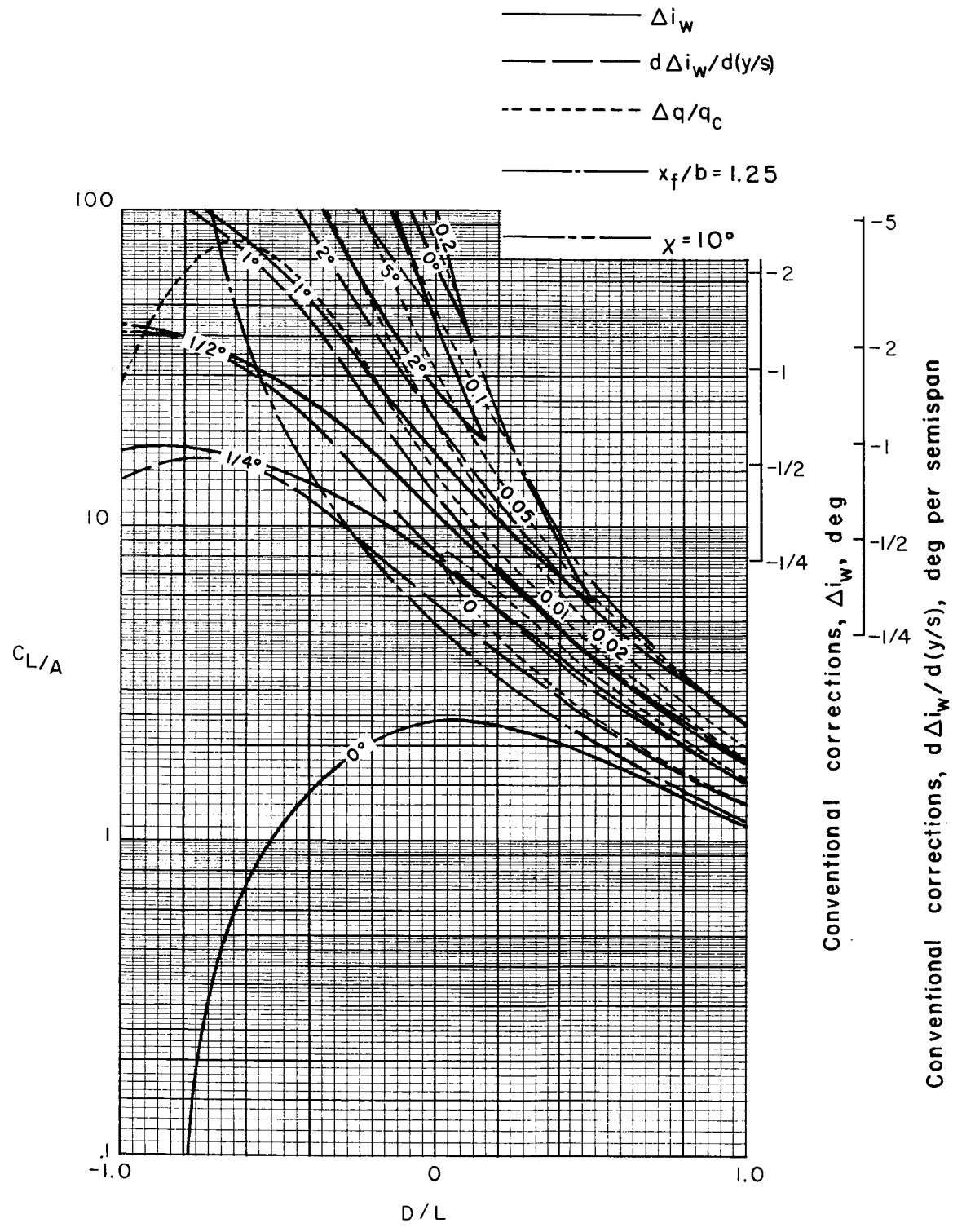


(a) $\sigma = 1/4$.

Figure 54.- Nonuniformity of corrections over a uniformly loaded wing centered in a rectangular tunnel closed only on the bottom. $\gamma = 1.5$; $\alpha = 0^0$; $\Lambda = 30^0$.

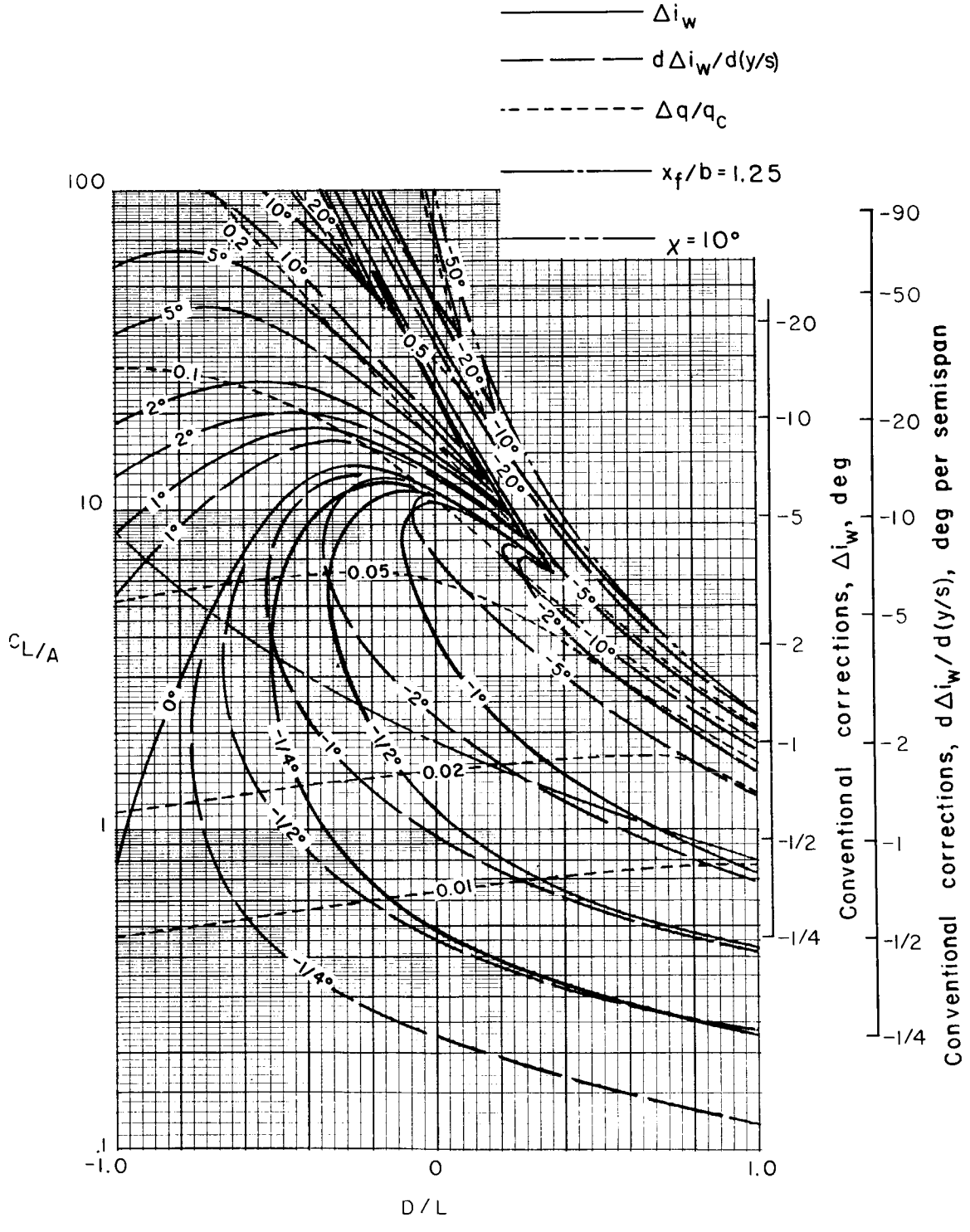


(b) $\sigma = 1/2$.

Figure 54.- Continued.

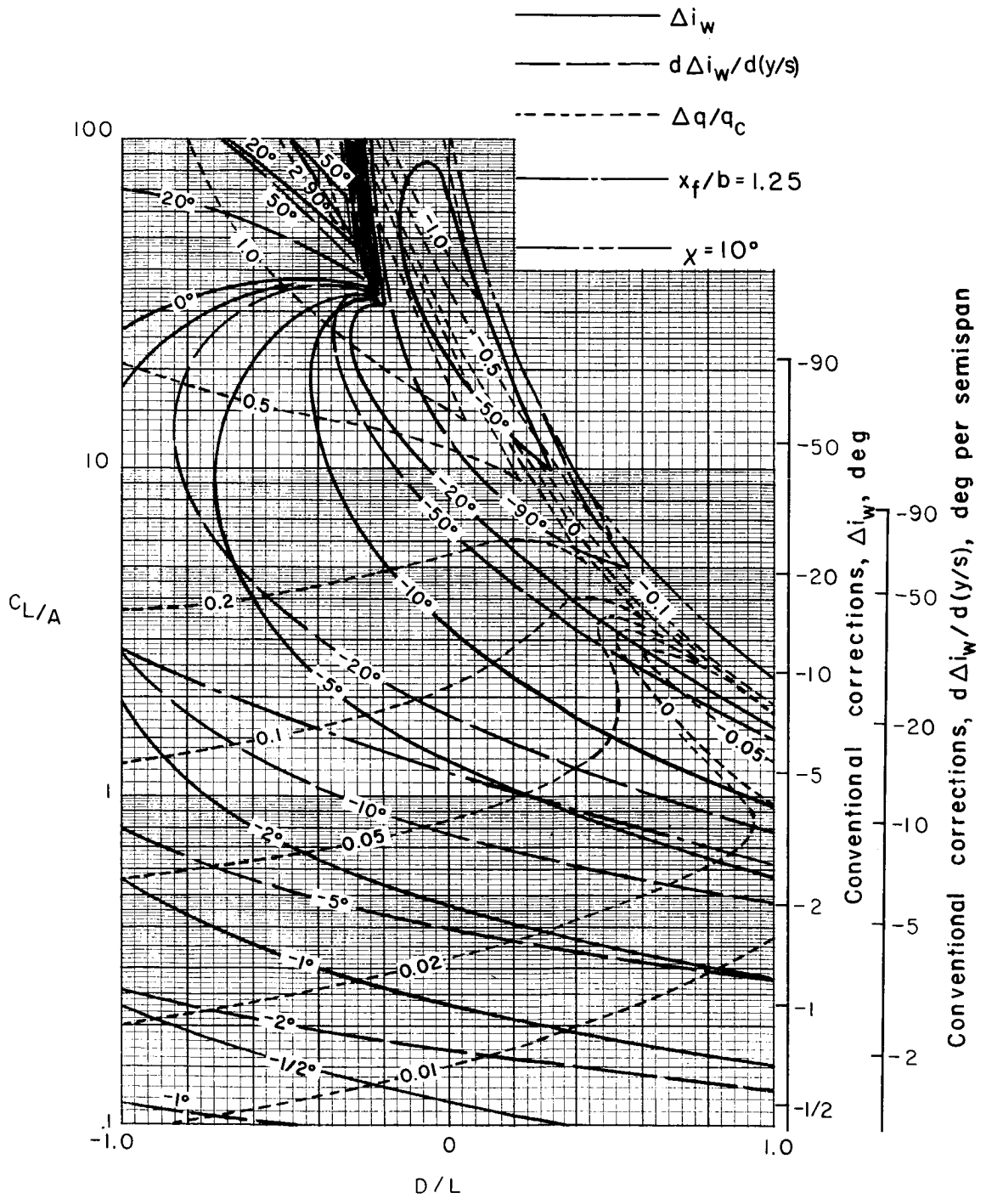


(c) $\sigma = 3/4$.

Figure 54.- Concluded.

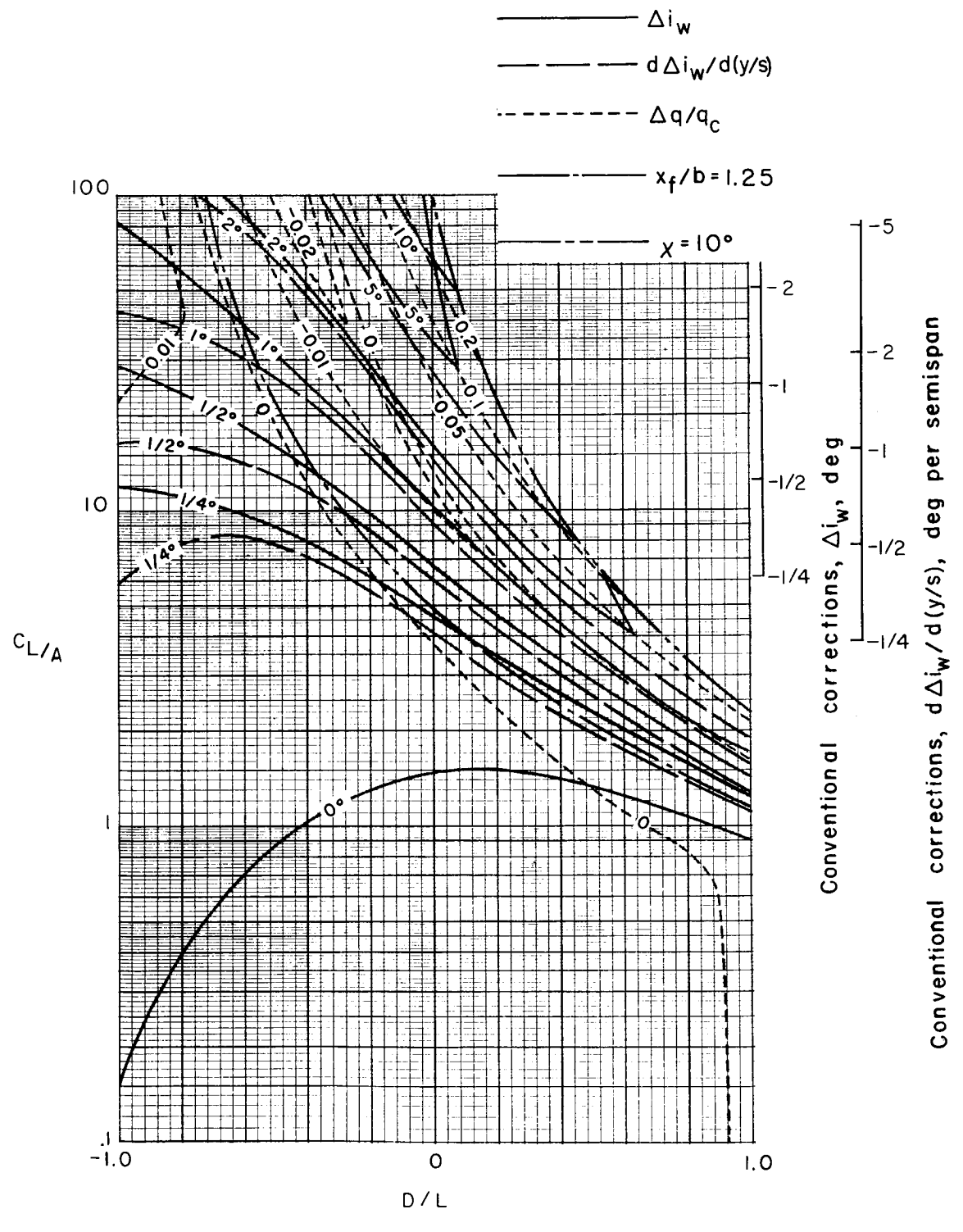


(a) $\sigma = 1/4$.

Figure 55.- Nonuniformity of corrections over a uniformly loaded wing centered in a rectangular tunnel closed only on the bottom. $\gamma = 1.5$; $\alpha = 0^0$; $\Lambda = 45^0$.

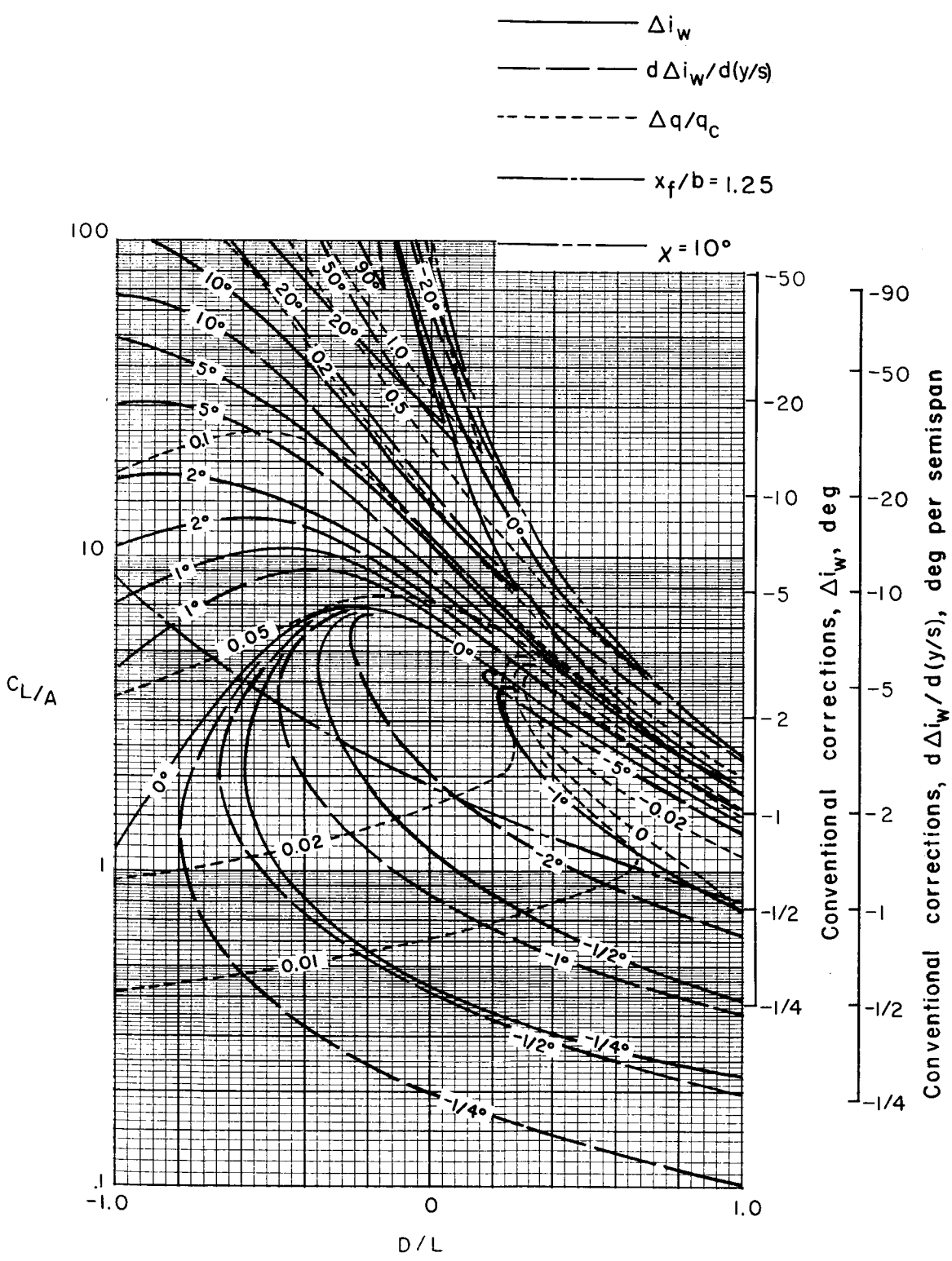


(b) $\sigma = 1/2$.

Figure 55.- Continued.

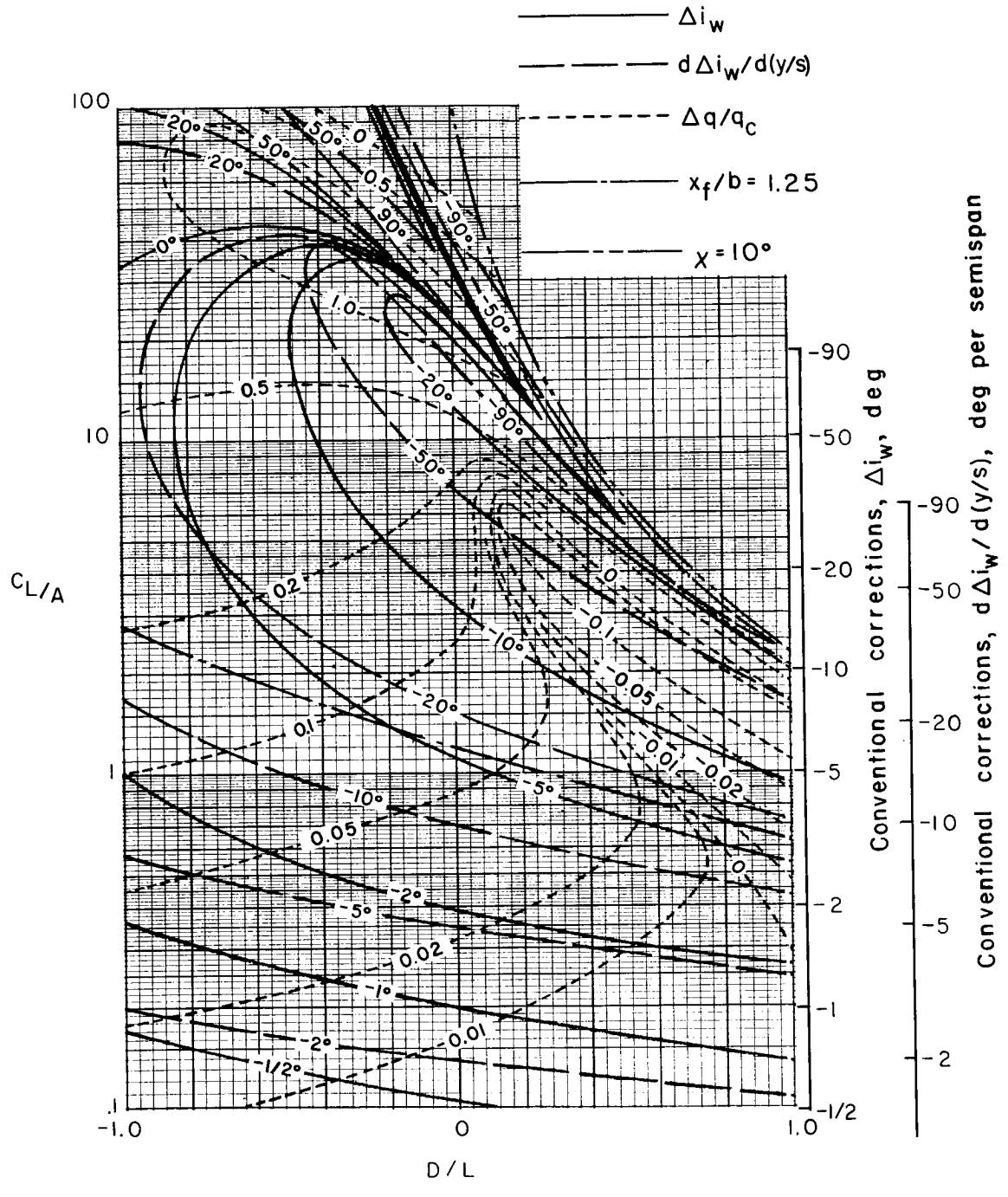


(c) $\sigma = 3/4$.

Figure 55.- Concluded.

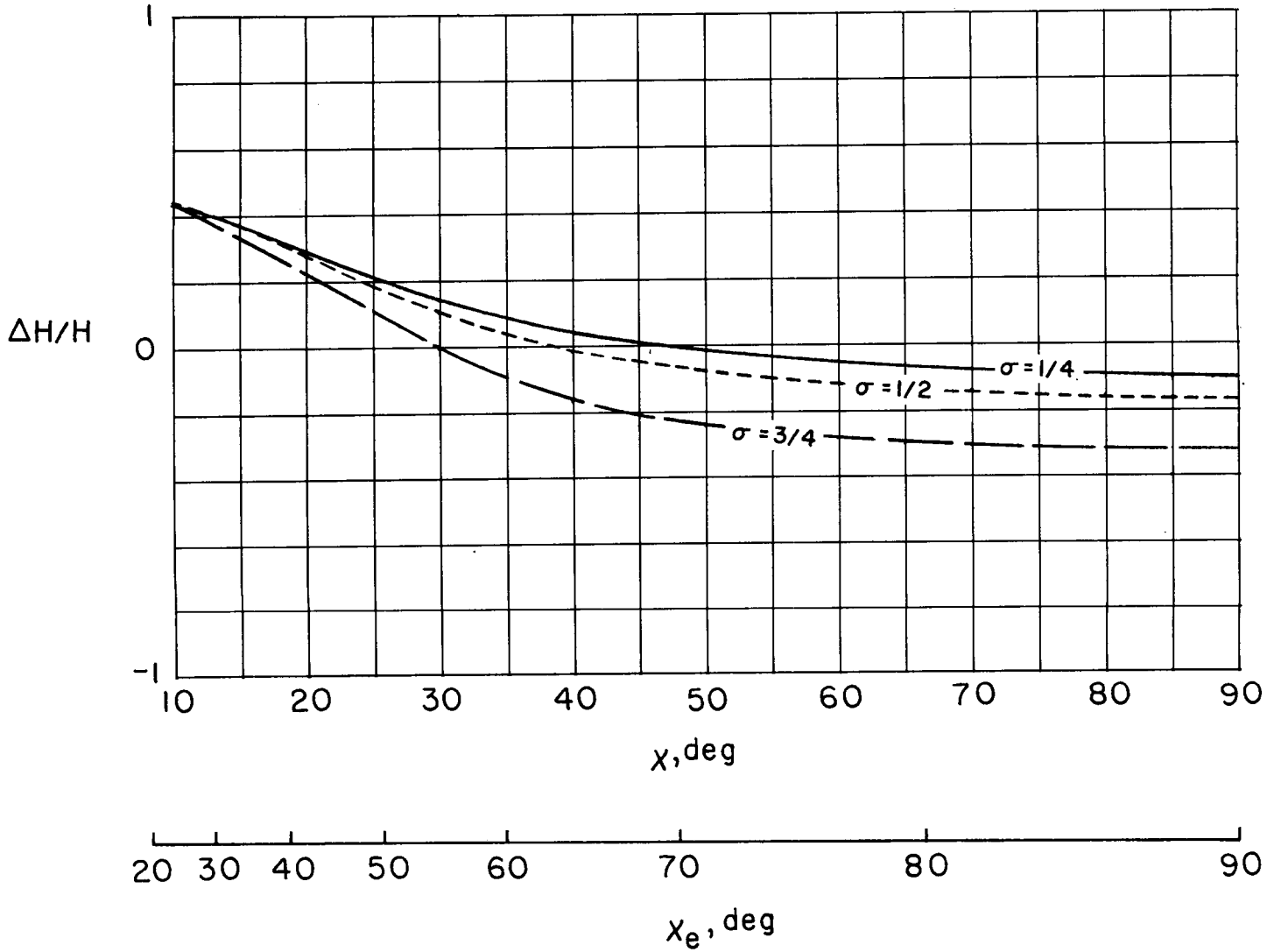


(a) $\Lambda = 0^{o}$.

Figure 56.- Schedule of model height for operation of a rectangular tunnel closed only on the bottom to maintain $\Delta w_L = 0$. $\gamma = 1.5$; $\alpha = 0^{o}$.

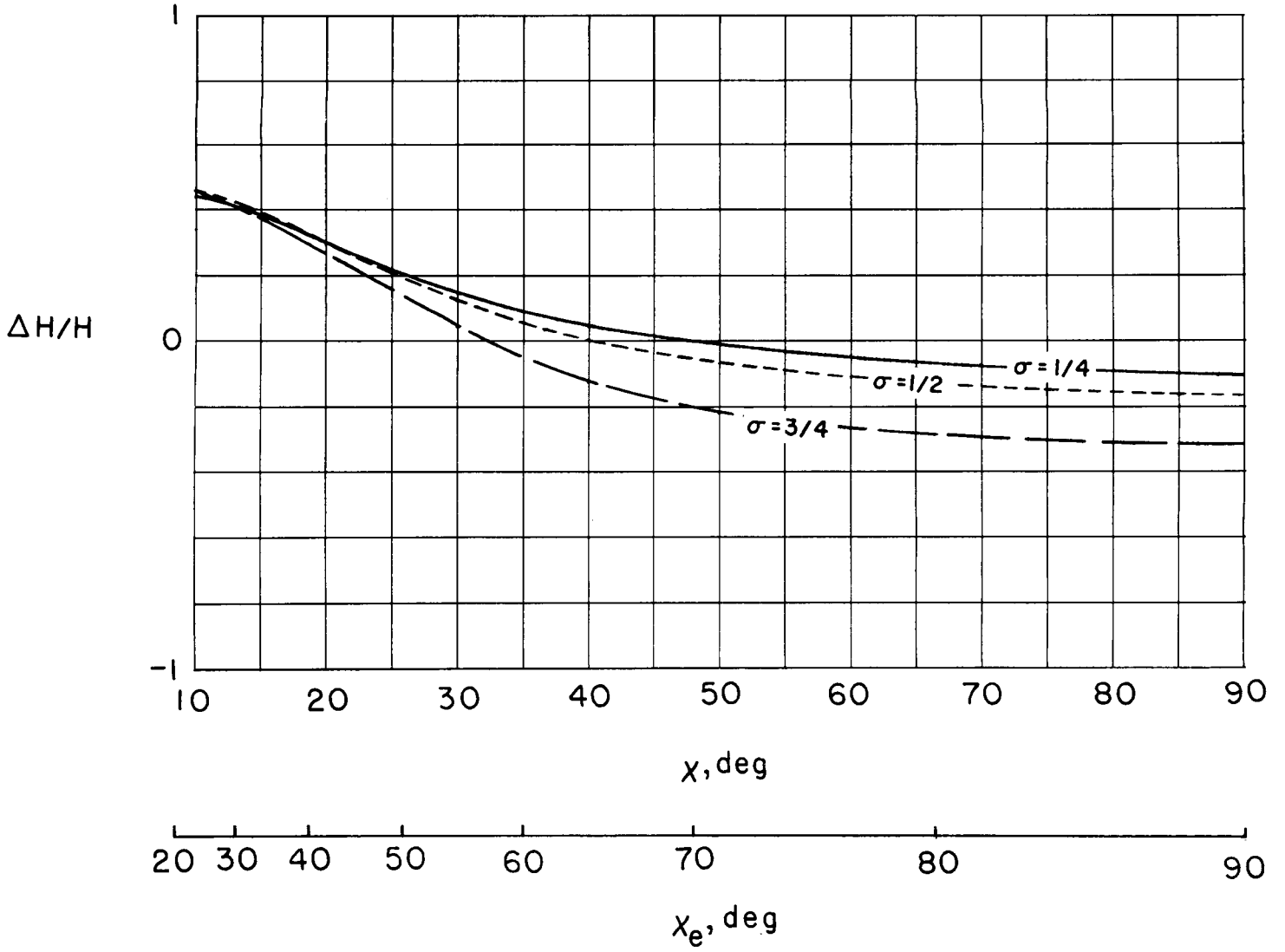


(b) $\Lambda = 45^0$.

Figure 56.- Concluded.

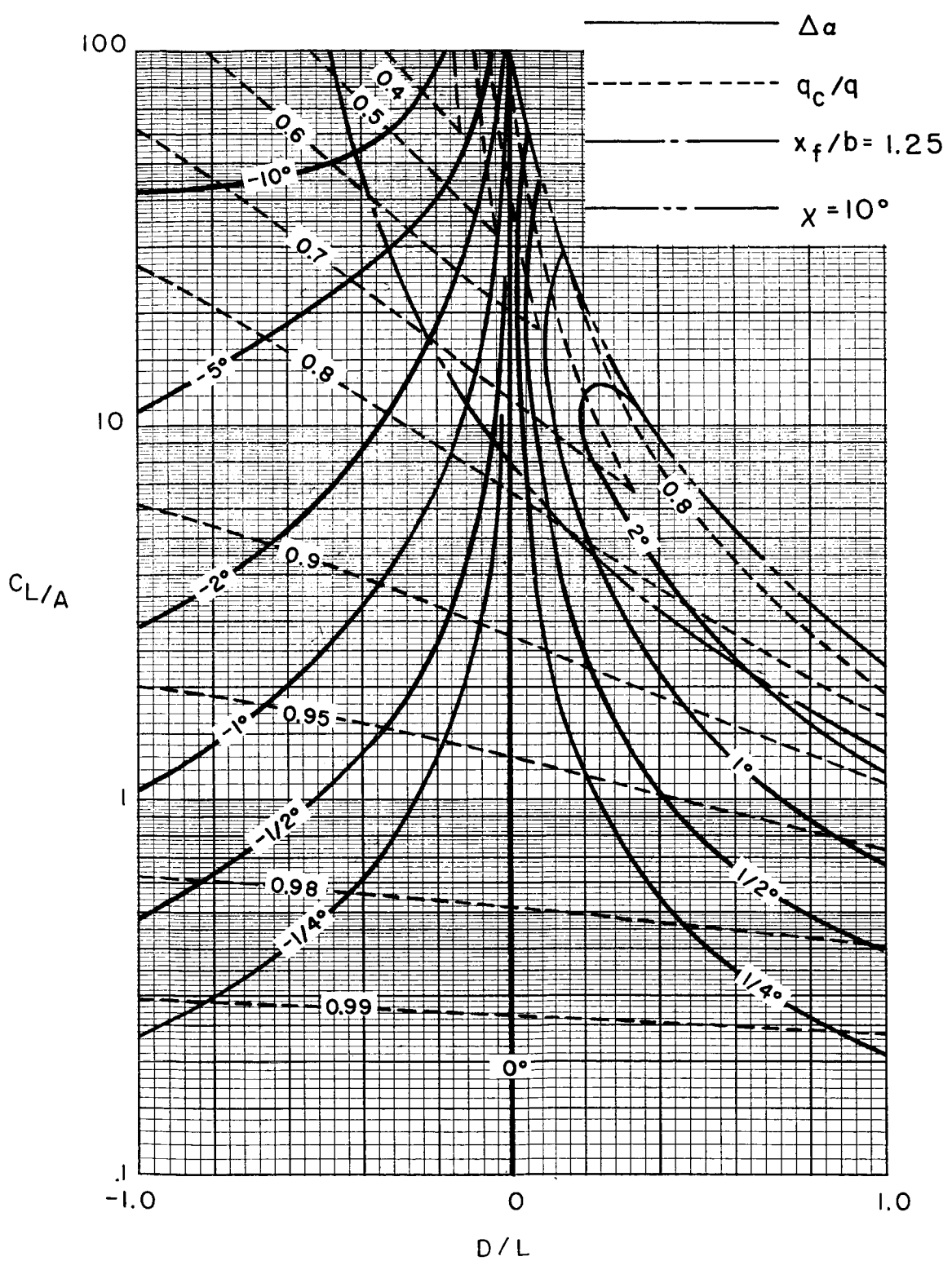


(a) $\sigma = 1/4$.

Figure 57.- Average corrections for a uniformly loaded wing in a rectangular tunnel closed only on the bottom when the model height is varied to maintain $\Delta w_L = 0$. $\Lambda = 0^0$; $\gamma = 1.5$.

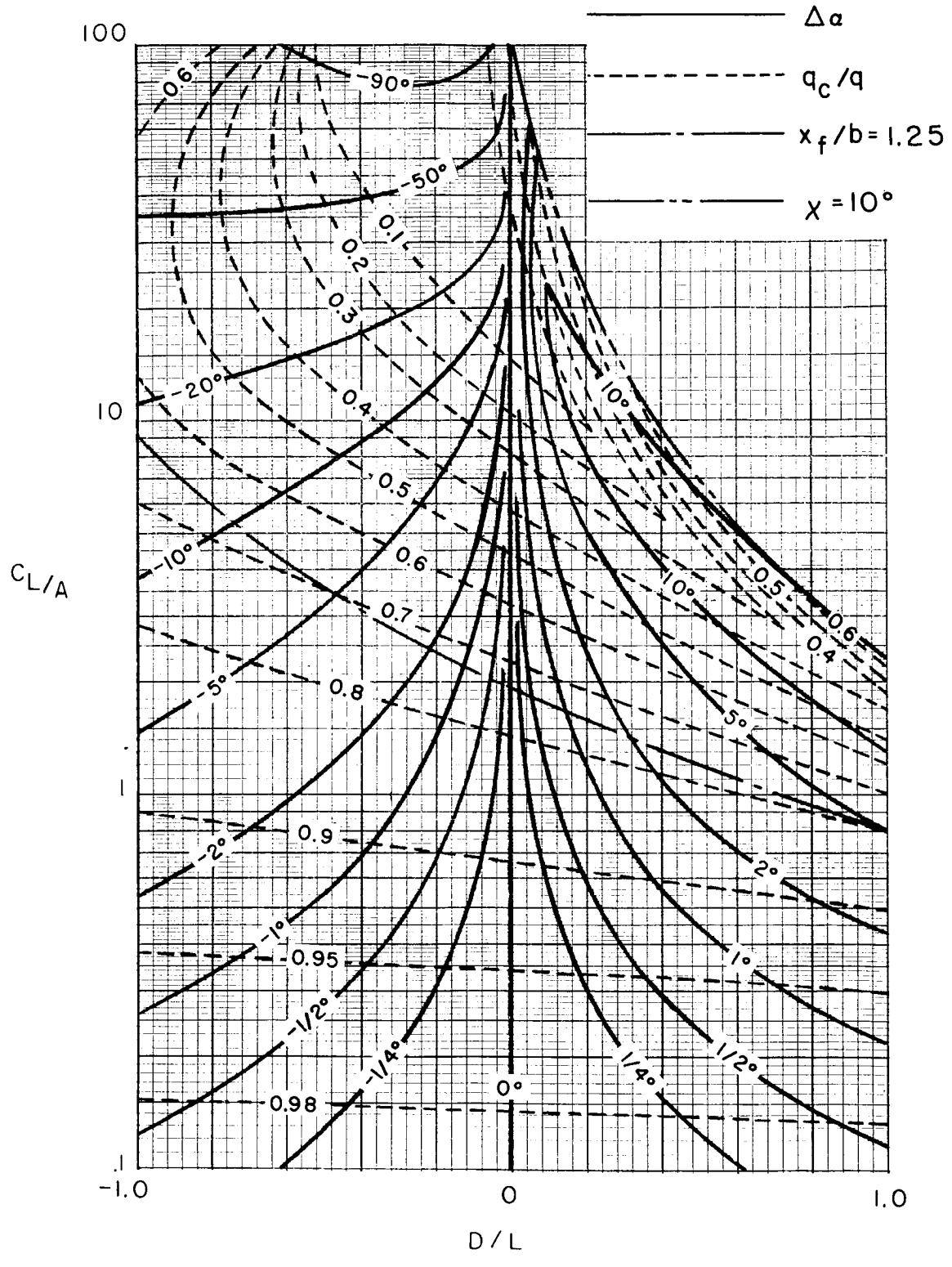


(b) σ = 1/2.

Figure 57.- Continued.

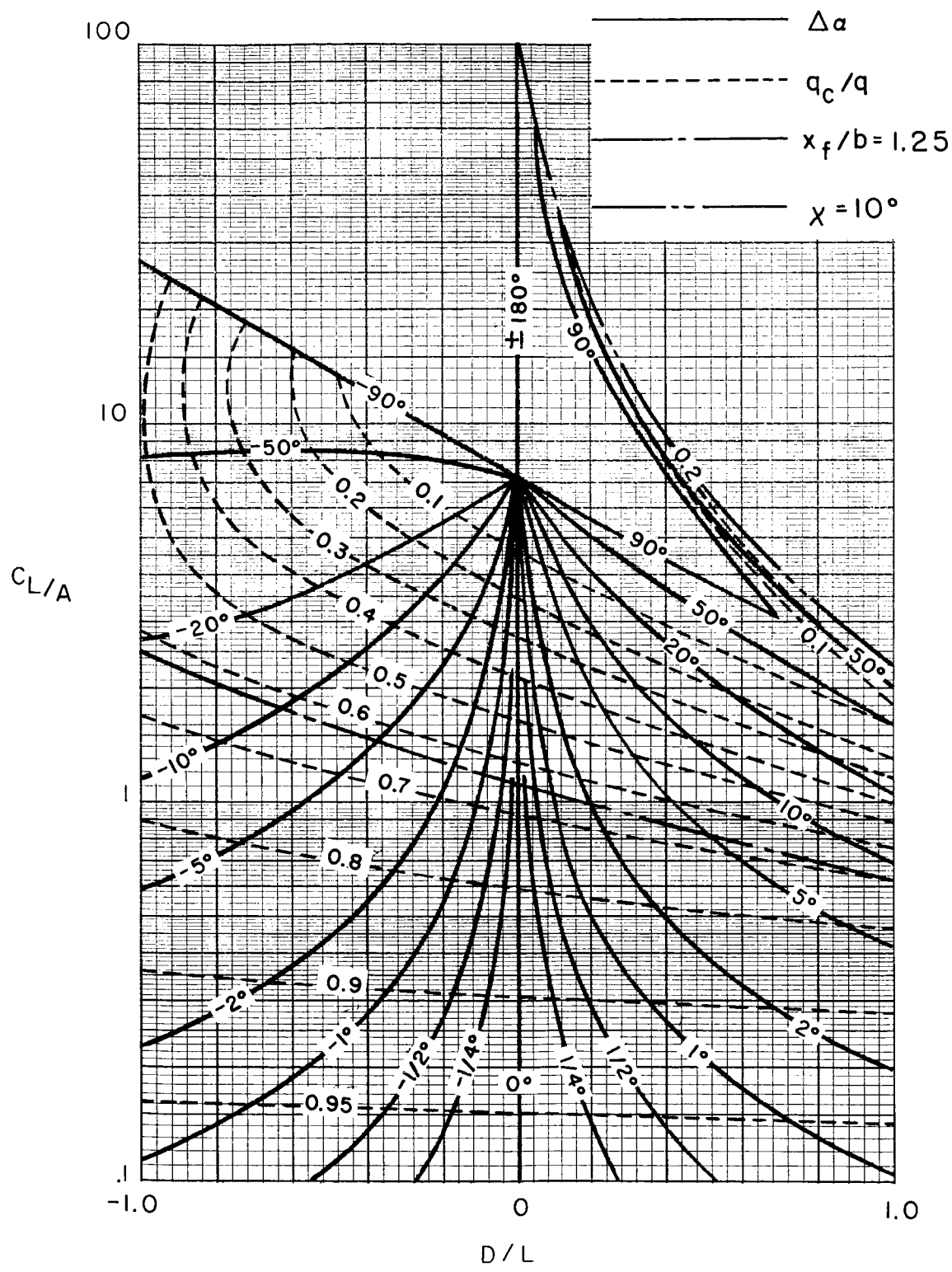


(c) σ = 3/4.

Figure 57.- Concluded.

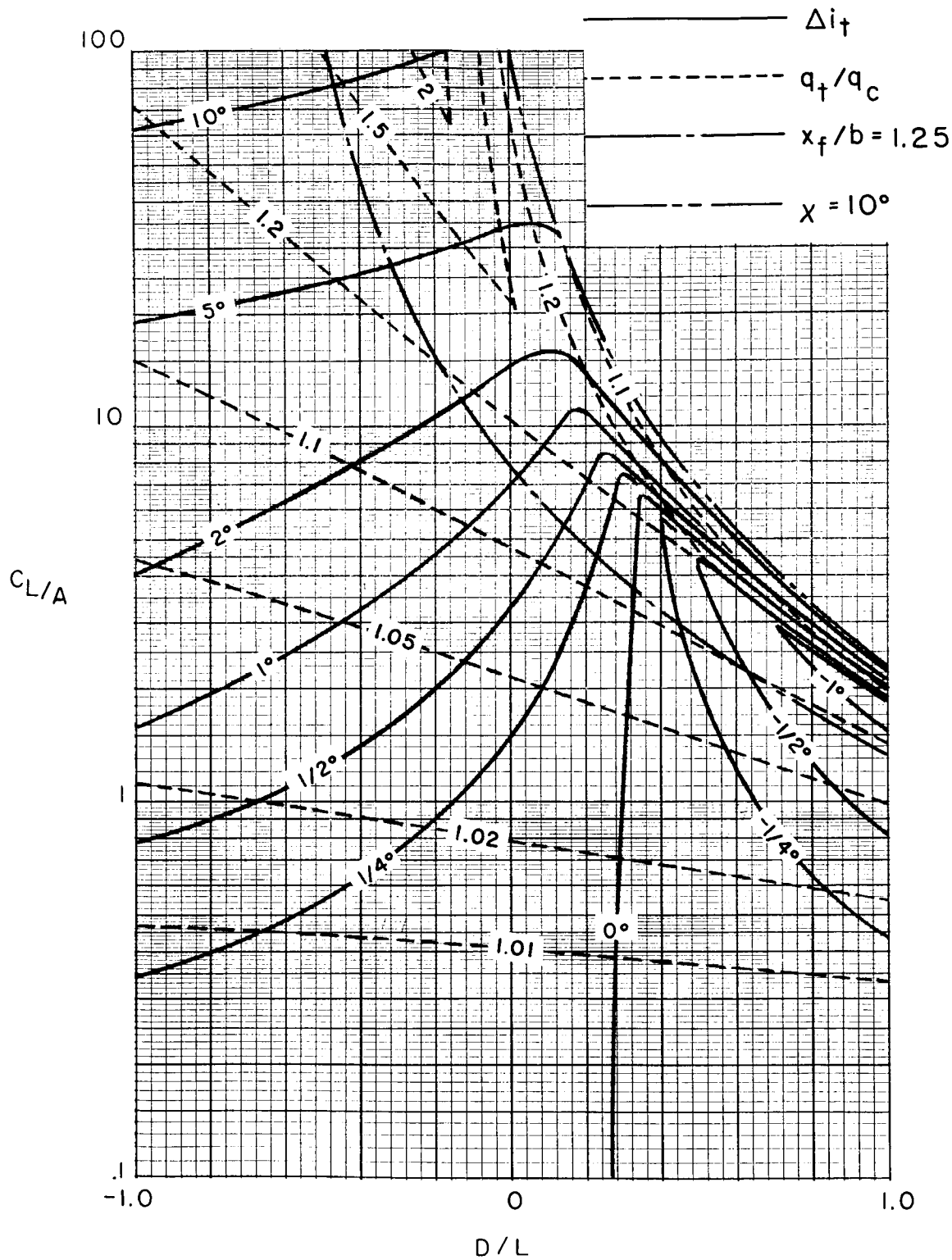


(a) $\sigma = 1/4$.

Figure 58.- Corrections at a zero-span tail behind a uniformly loaded wing in a rectangular tunnel closed only on the bottom when the model height is varied to maintain $\Delta w_L = 0$. Tail length is three-fourths of wing span; tail height is zero; $\alpha = 20^0$; $\Lambda = 0^0$; $\gamma = 1.5$.

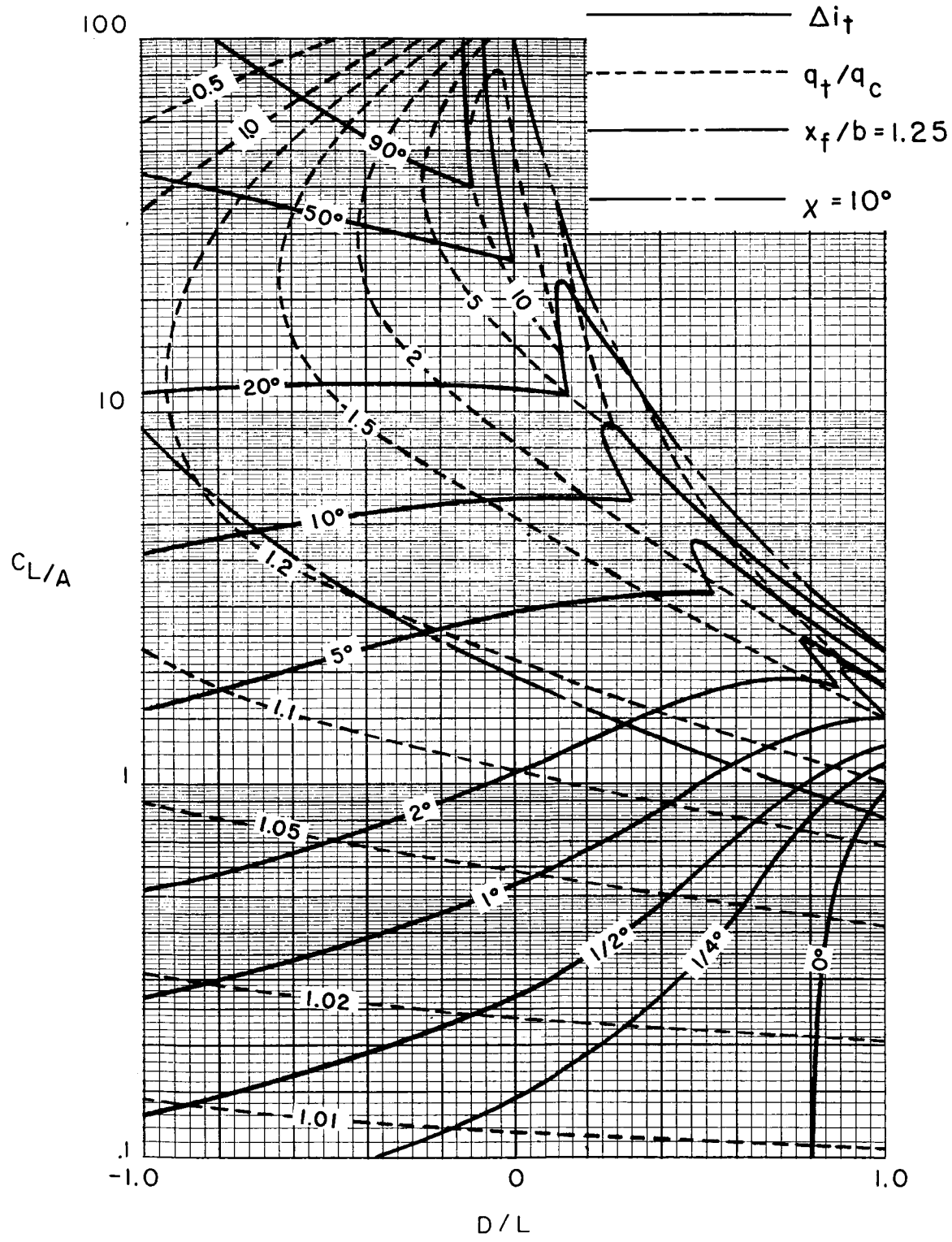


(b) $\sigma = 1/2$.

Figure 58.- Continued.

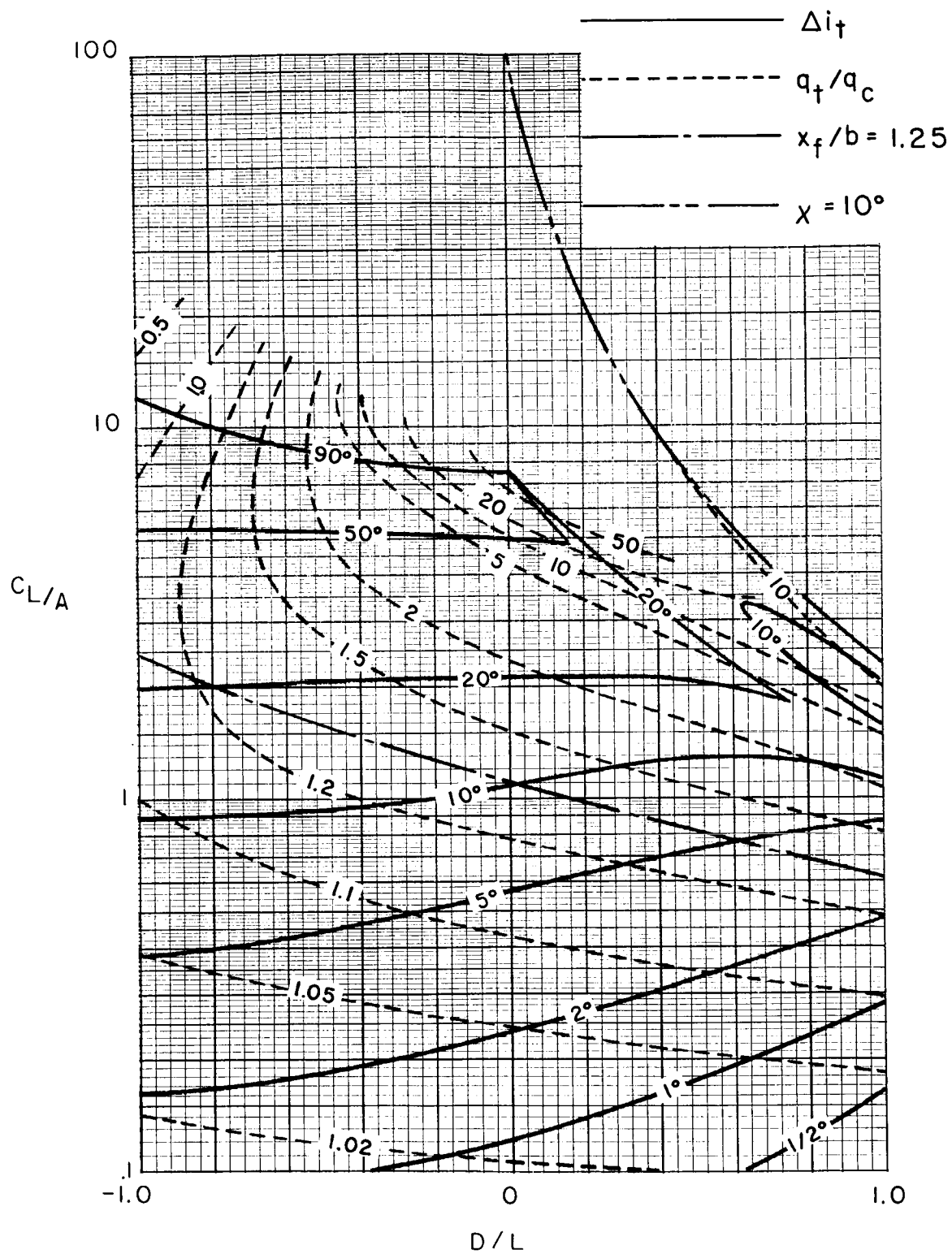


(c) $\sigma = 3/4$.

Figure 58.- Concluded.

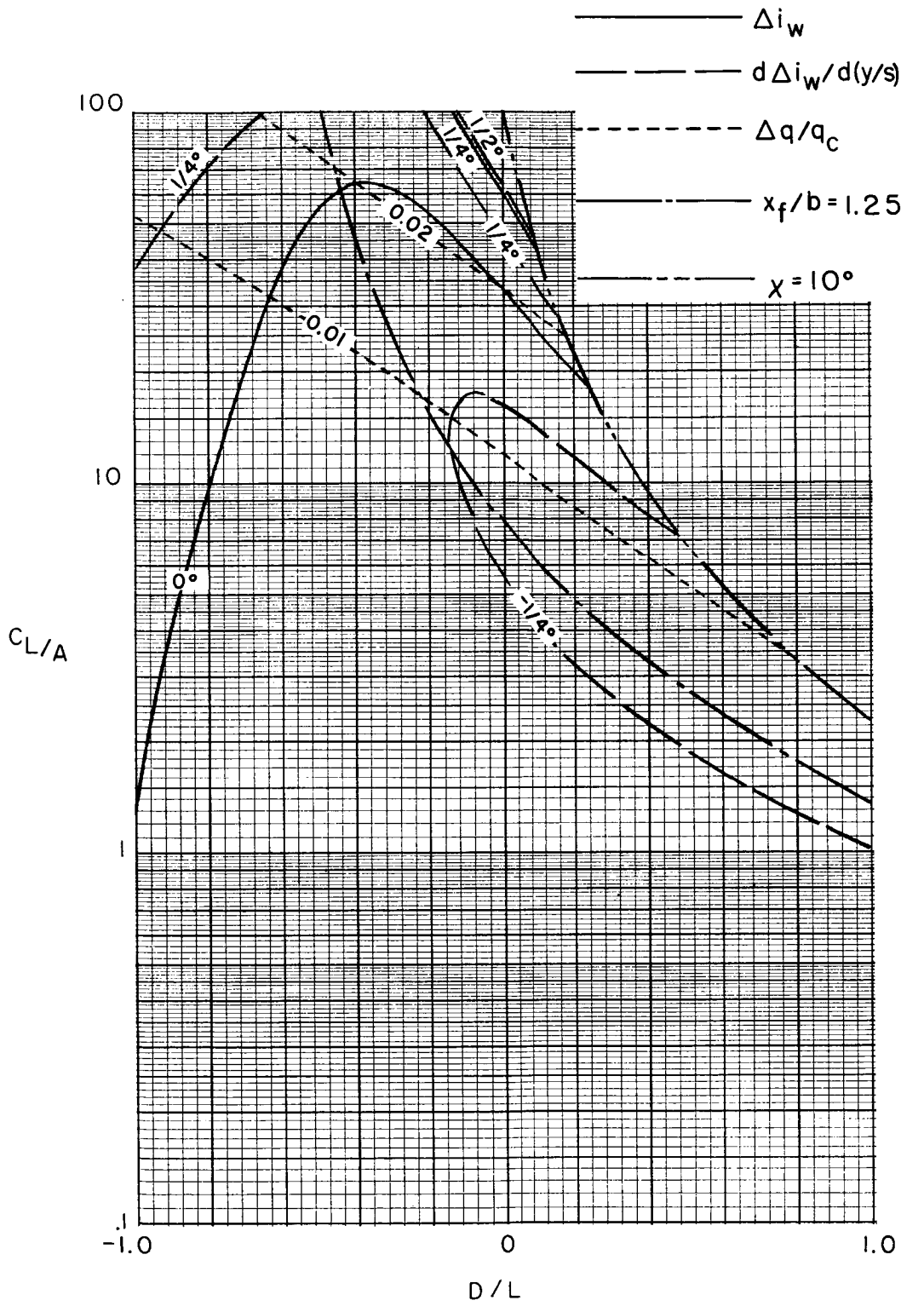


(a) $\sigma = 1/4$.

Figure 59.- Nonuniformity of corrections over a uniformly loaded wing in a rectangular tunnel closed only on the bottom when the model height is varied to maintain $\Delta w_L = 0$. $\gamma = 1.5$; $\alpha = 0^0$; $\Lambda = 0^0$.

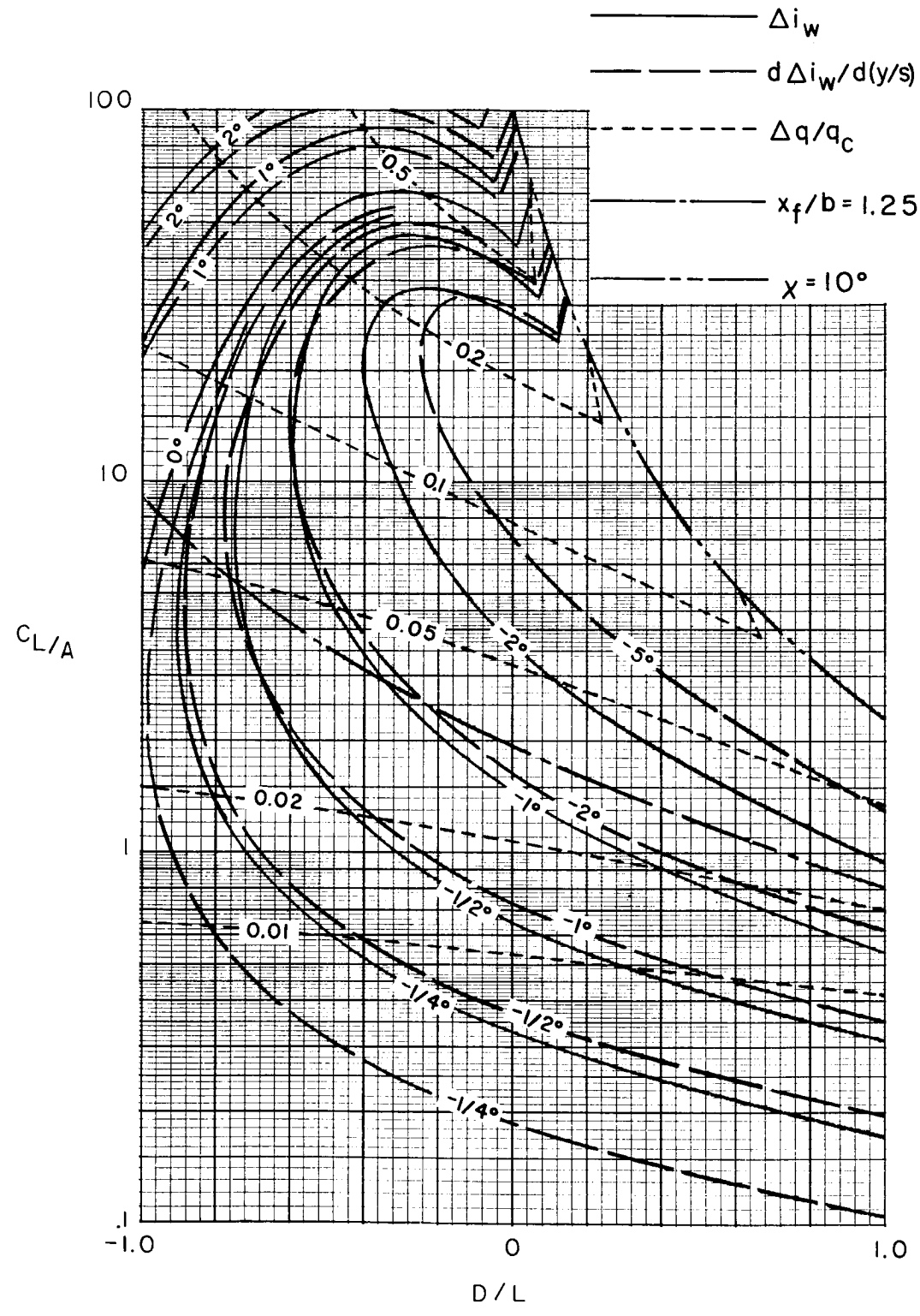


(b) $\sigma = 1/2$.

Figure 59.- Continued.

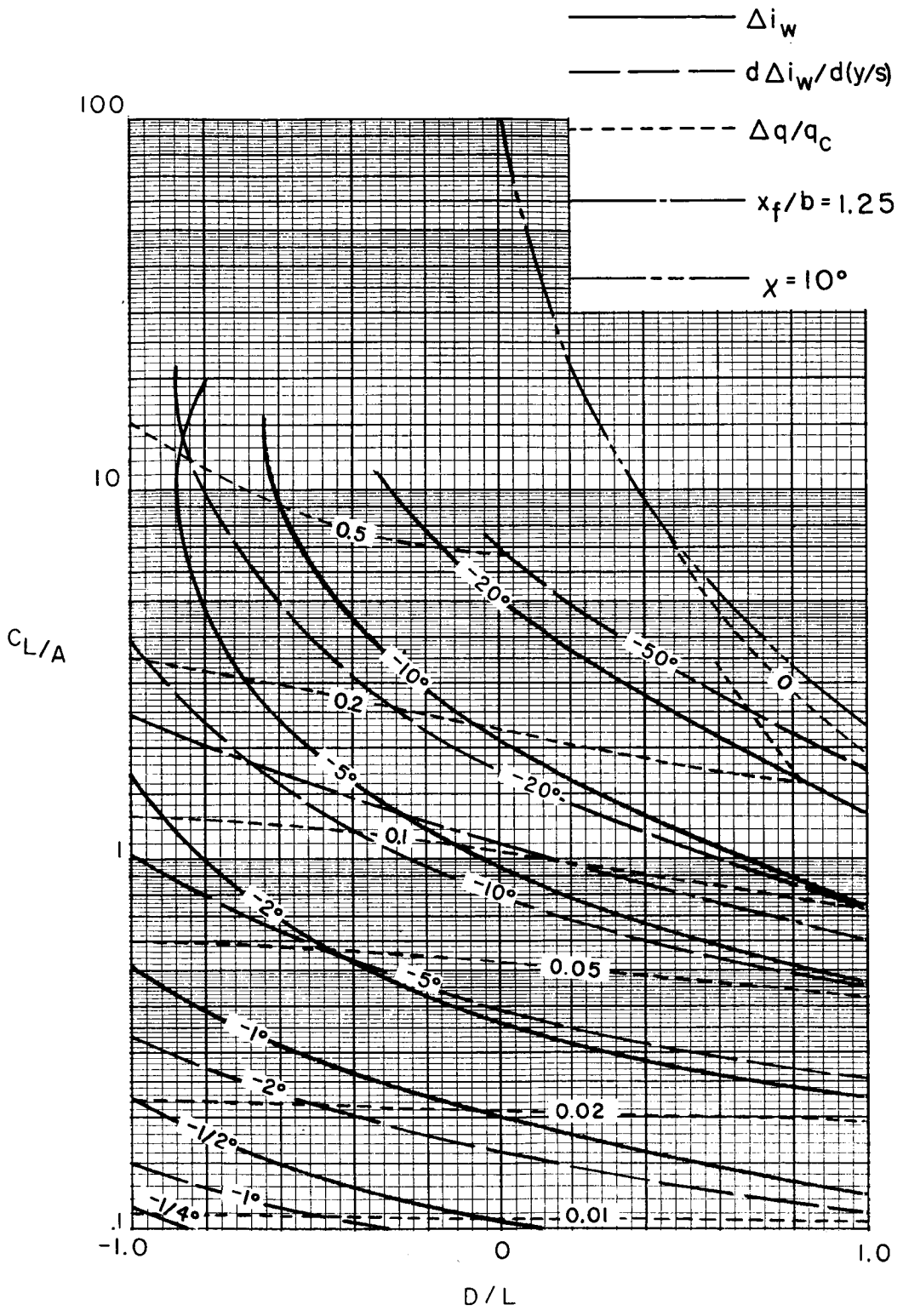


(c) $\sigma = 3/4$.

Figure 59.- Concluded.

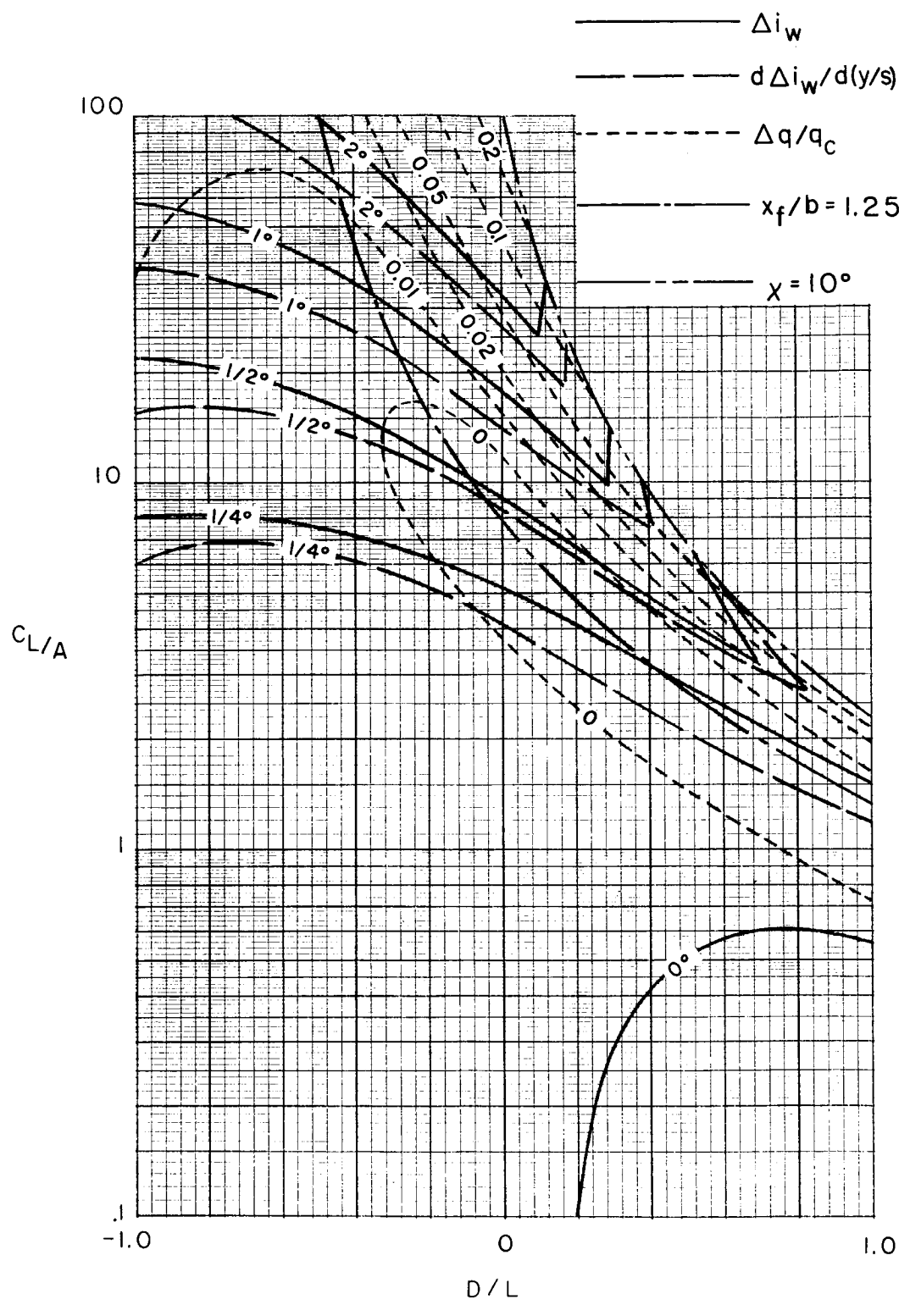


(a) $\sigma = 1/4$.

Figure 60.- Nonuniformity of corrections over a uniformly loaded wing in a rectangular tunnel closed only on the bottom when the model height is varied to maintain $\Delta w_L = 0$. $\gamma = 1.5$; $\alpha = 0^0$; $\Lambda = 45^0$.

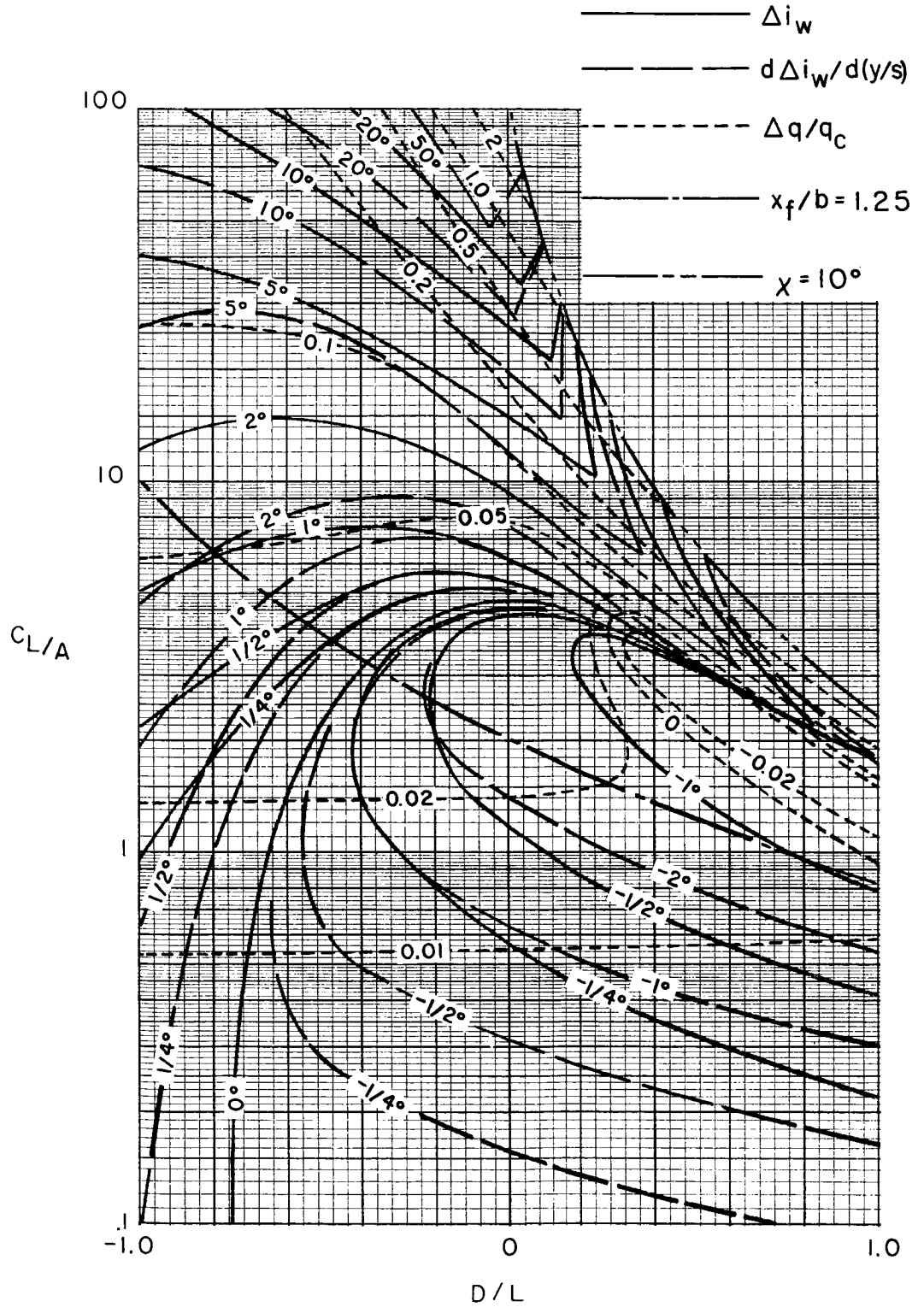


(b) $\sigma = 1/2$,

Figure 60.- Continued.

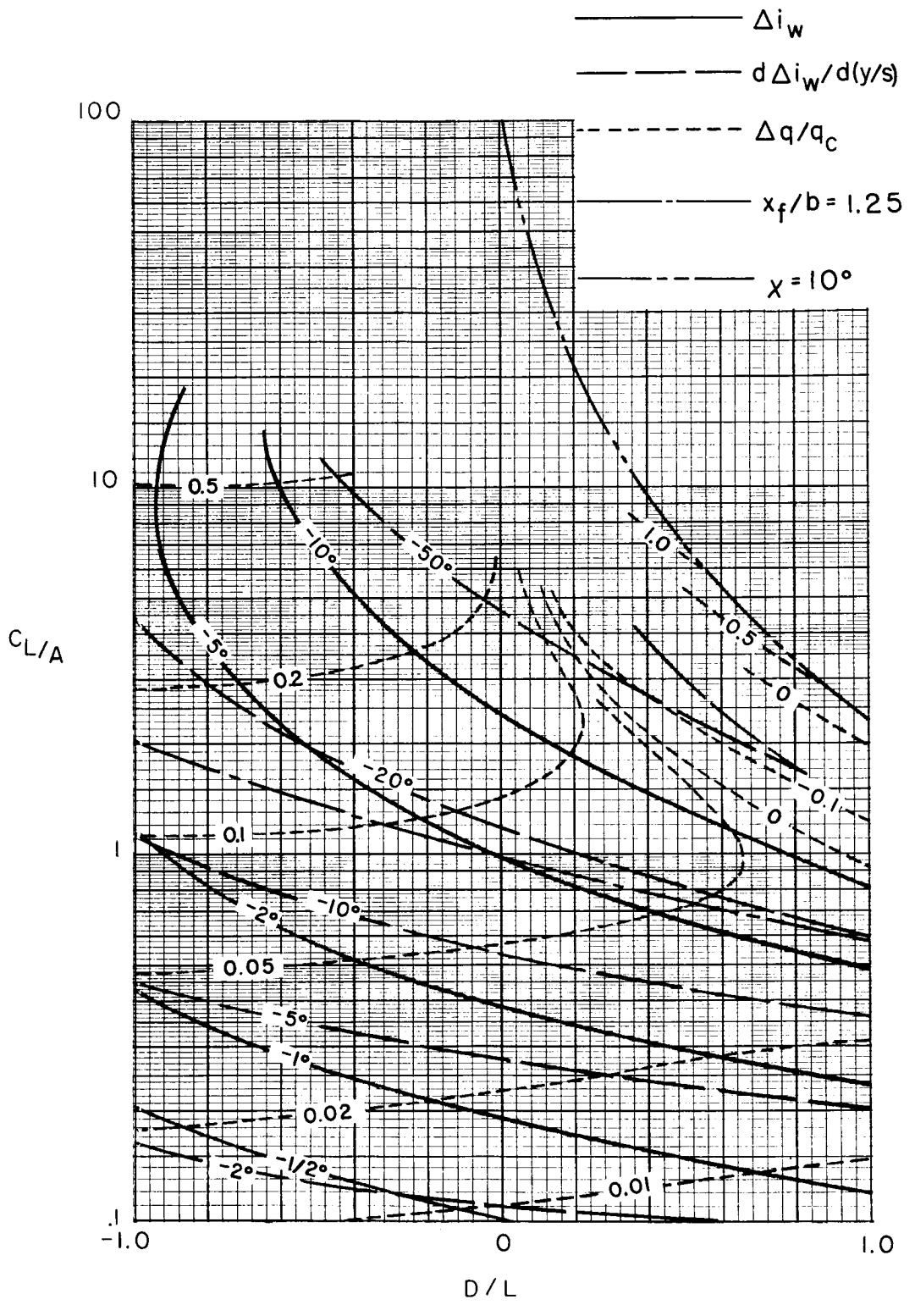


(c) $\sigma = 3/4$.

Figure 60.- Concluded.

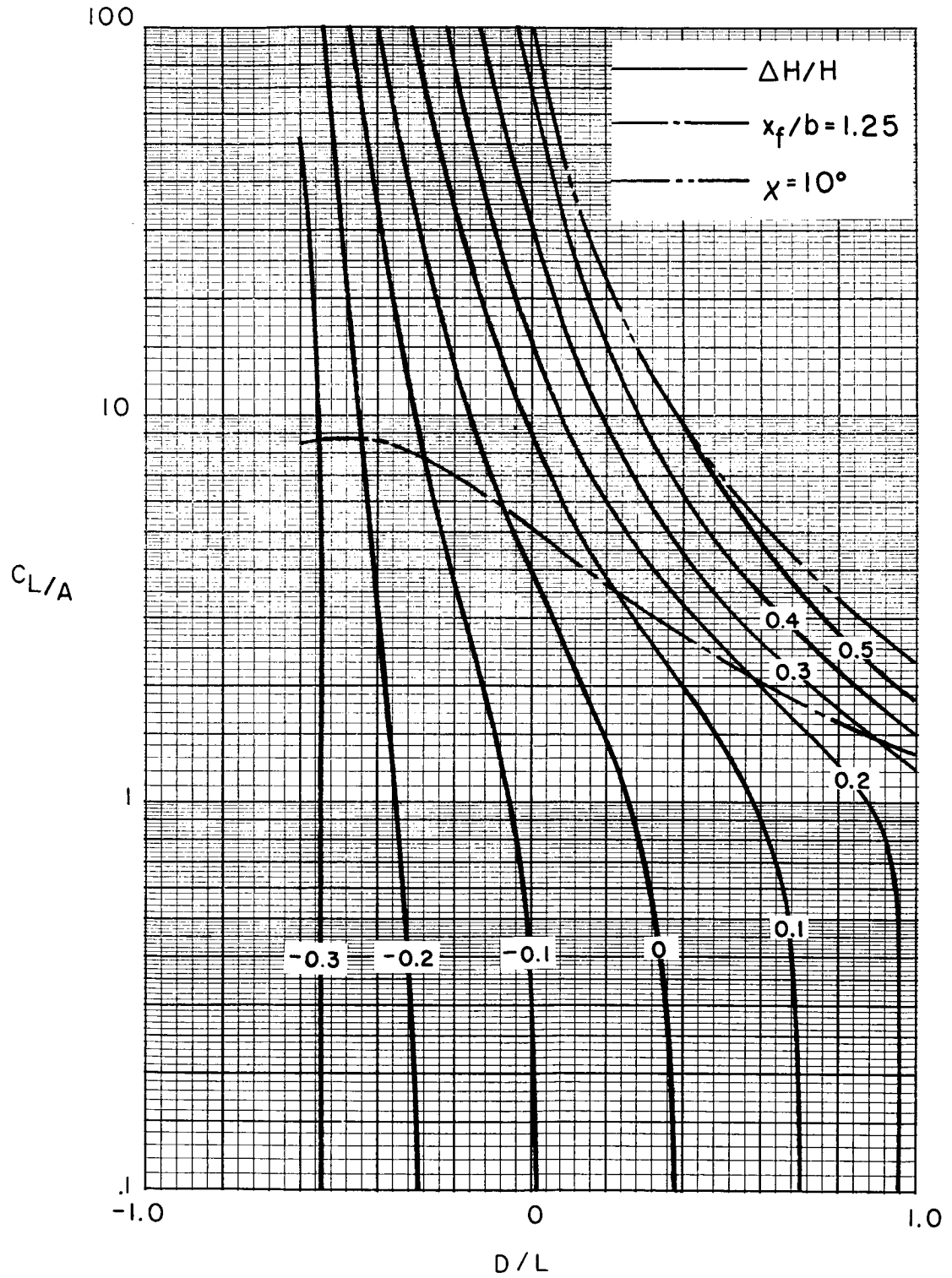


(a) $\sigma = 1/4$.

Figure 61.- Schedule of model height required to maintain $\Delta w = 0$ for a wing in a rectangular tunnel closed only on the bottom. $\Lambda = 0^0$; $\gamma = 1.5$.

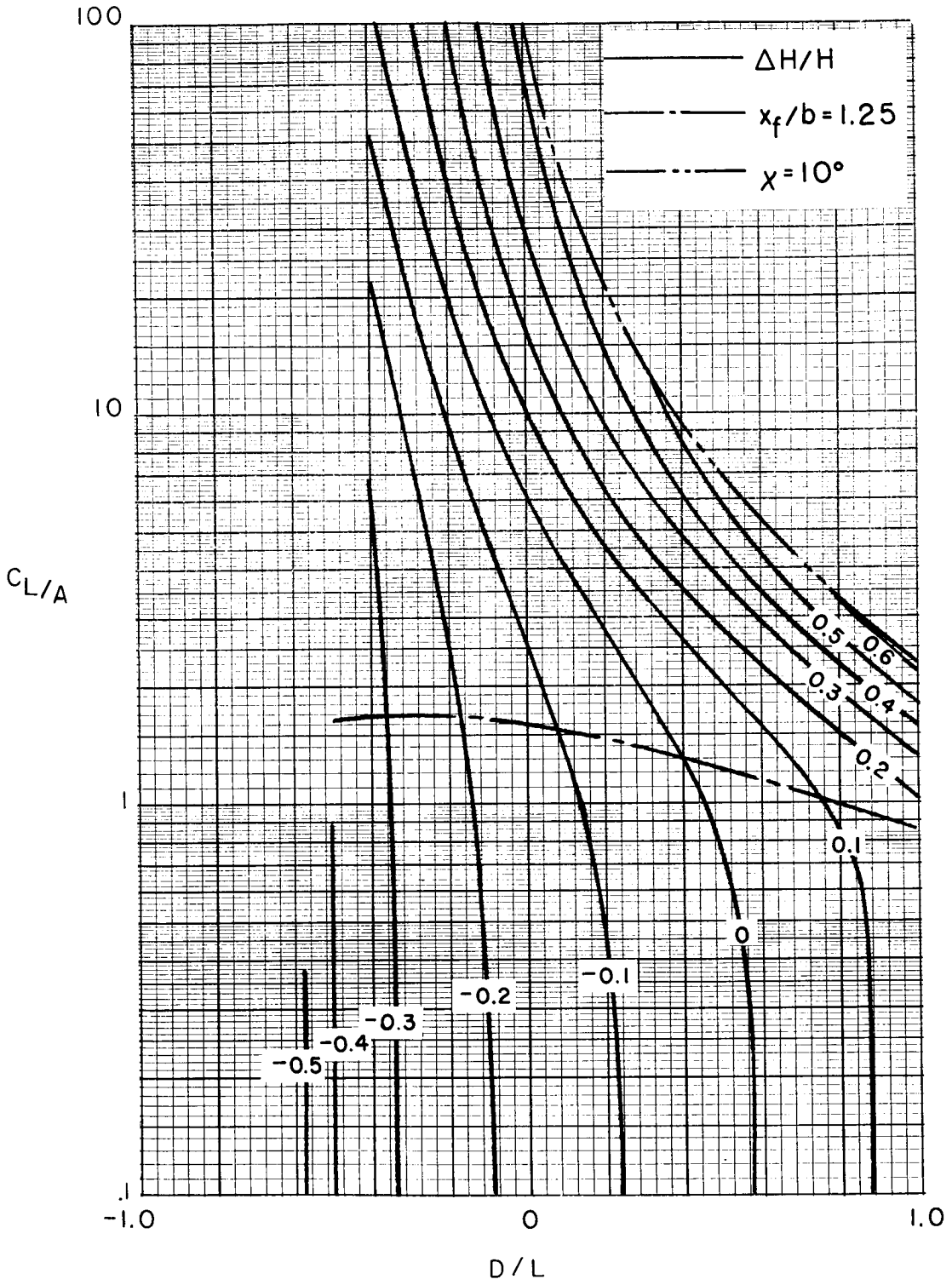


(b) $\sigma = 1/2$.

Figure 61.- Continued.

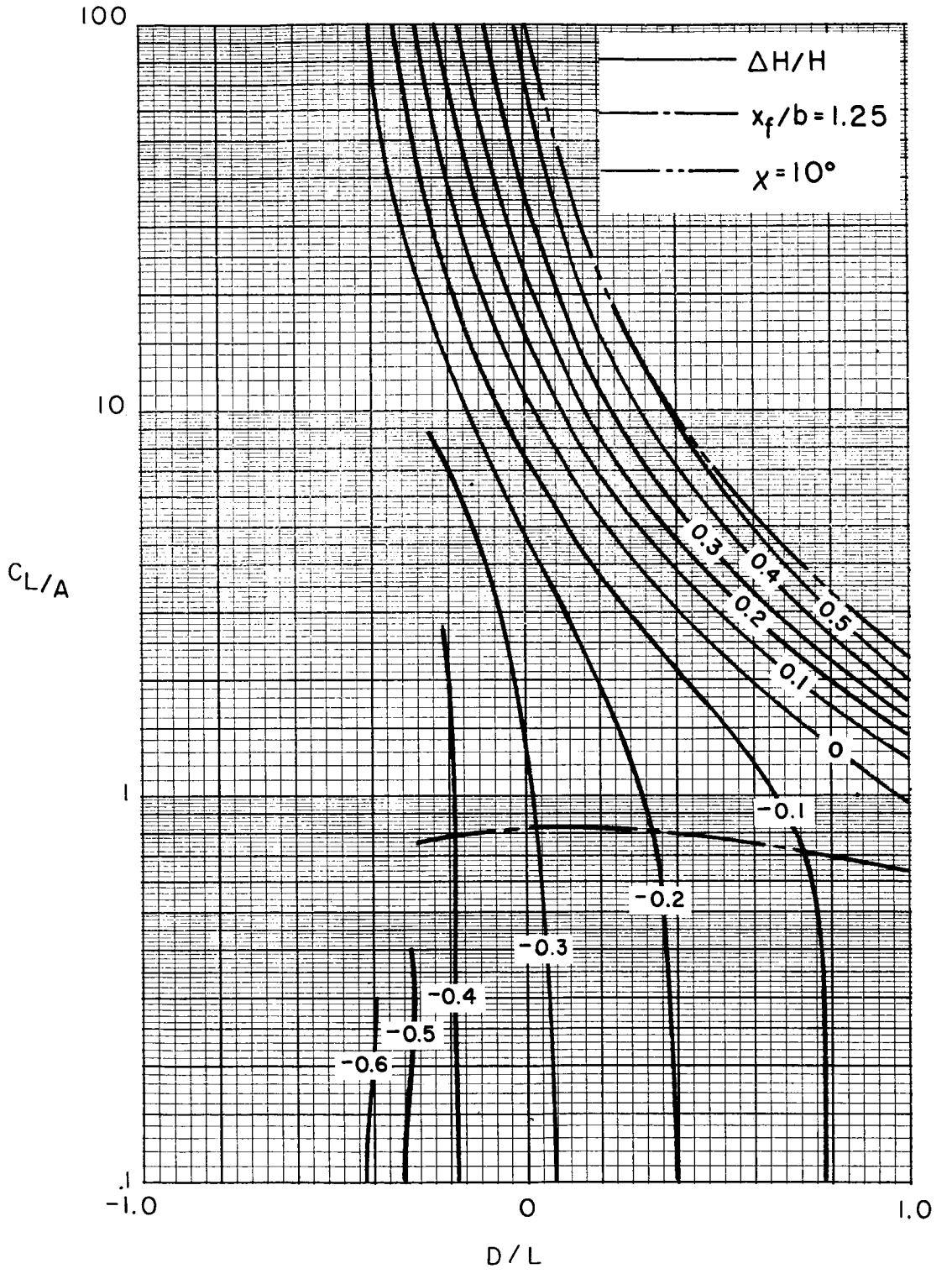


(c) $\sigma = 3/4$.

Figure 61.- Concluded.

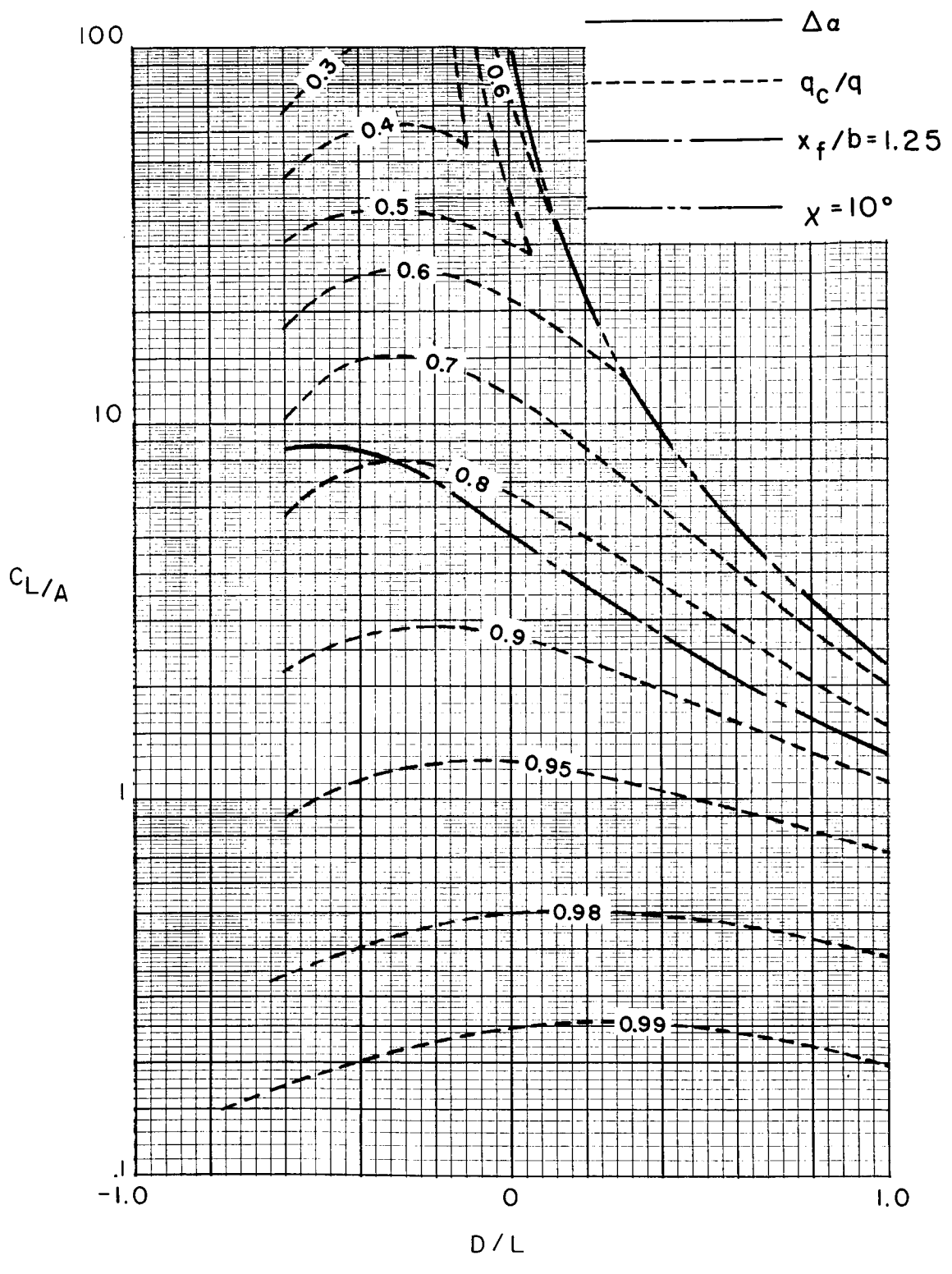


(a) σ = 1/4.

Figure 62.- Average corrections for a uniformly loaded wing in a rectangular tunnel closed only on the bottom when the model height is varied to maintain $\Delta w = 0$. $\Lambda = 0^0$; $\gamma = 1.5$.

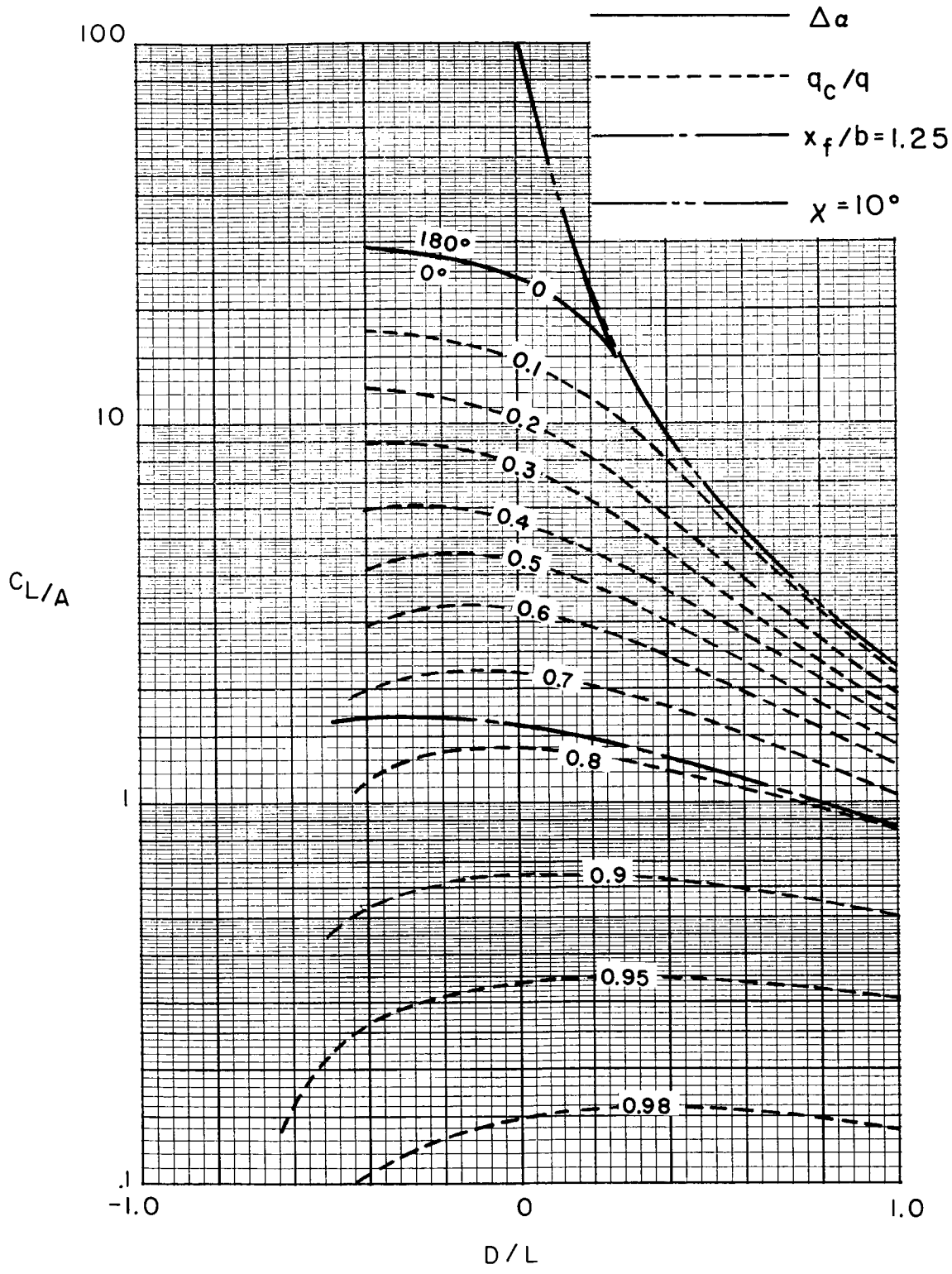


(b) σ = 1/2.

Figure 62.- Continued.

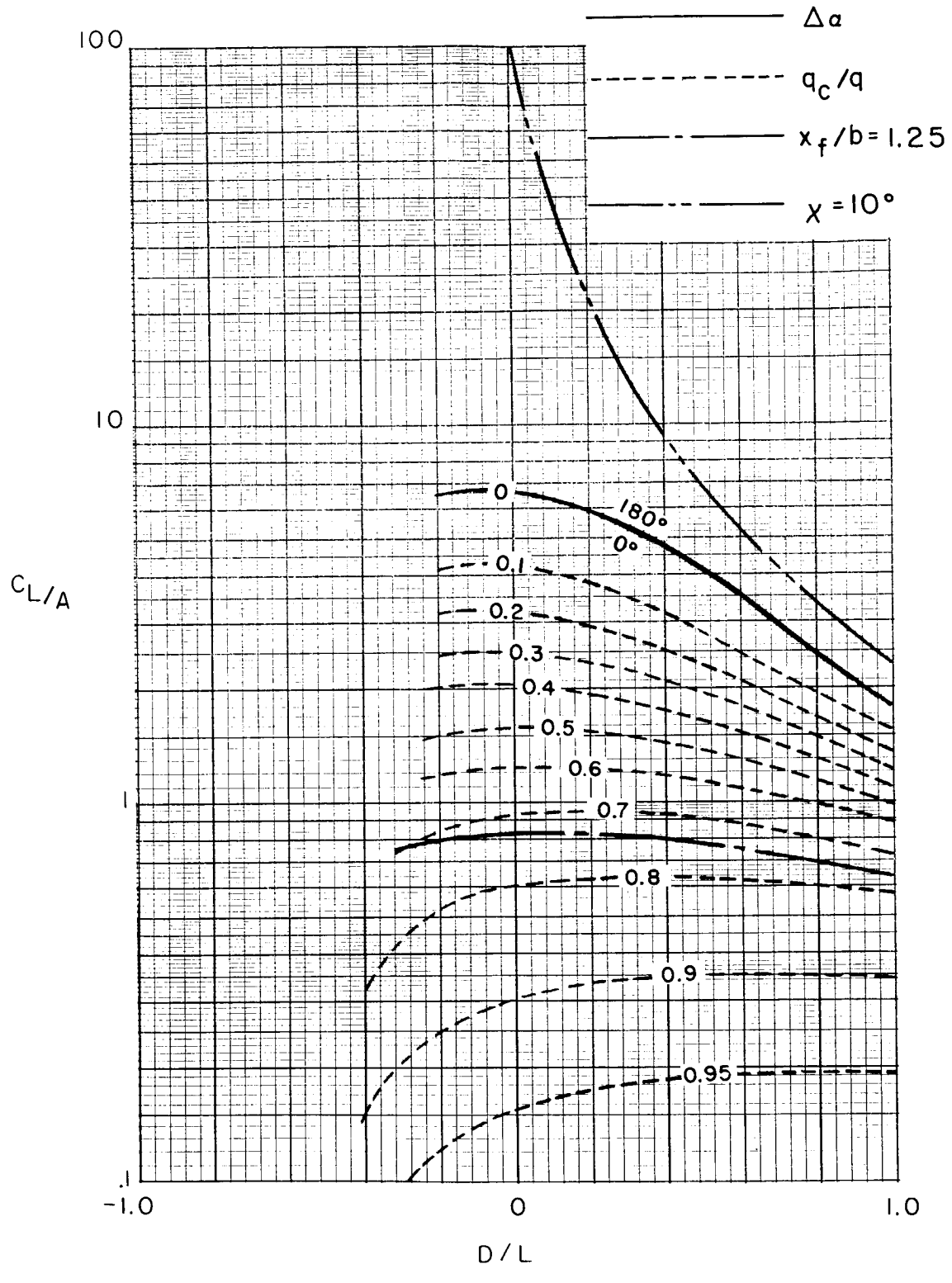


(c) σ = 3/4.

Figure 62.- Concluded.

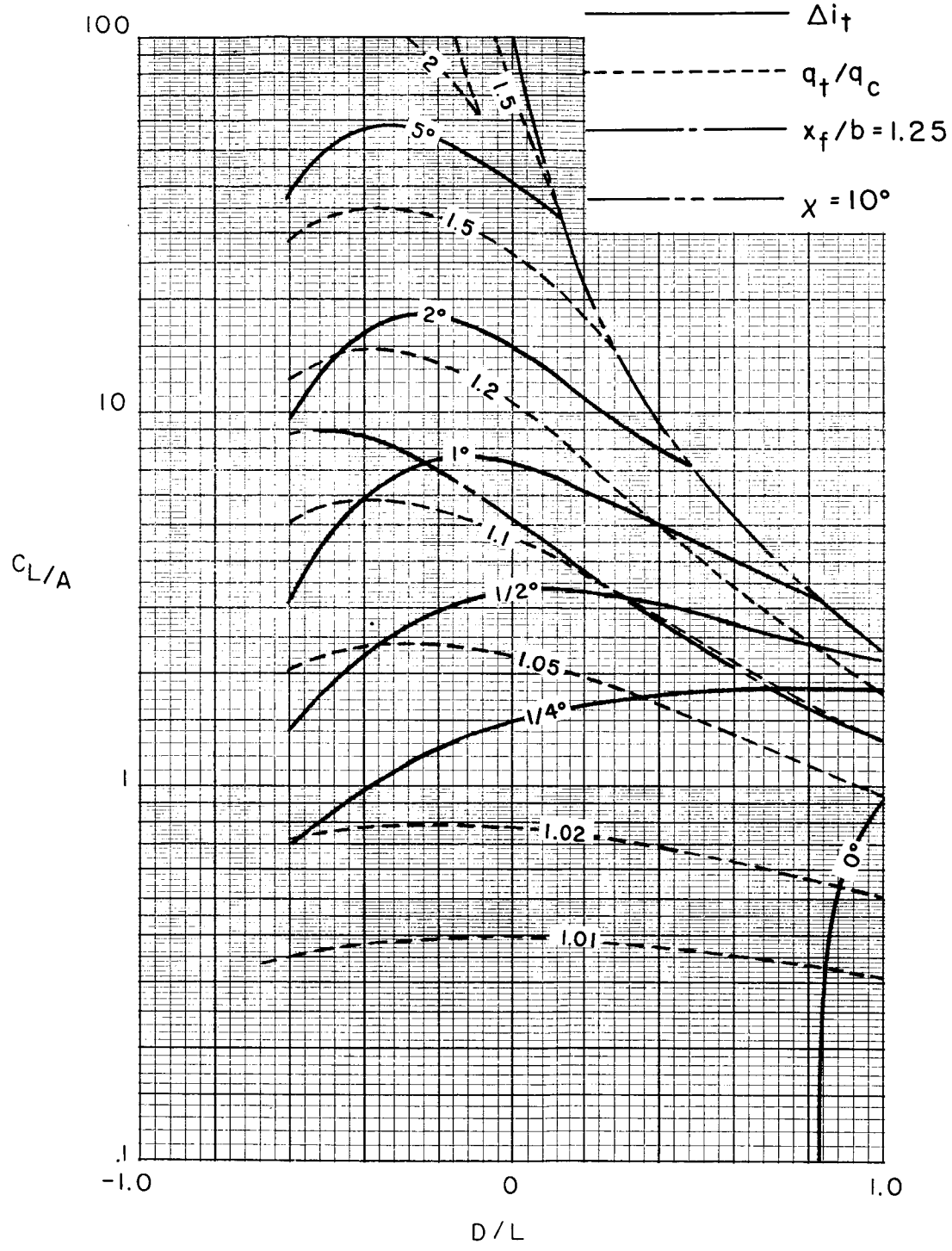


(a) $\sigma = 1/4$.

Figure 63.- Corrections at a zero-span tail behind a uniformly loaded wing in a rectangular tunnel closed only on the bottom when the model height is varied to maintain $\Delta w = 0$. Tail length is three-fourths of wing span; tail height is zero; $\alpha = 20^0$; $\Lambda = 0^0$; $\gamma = 1.5$.

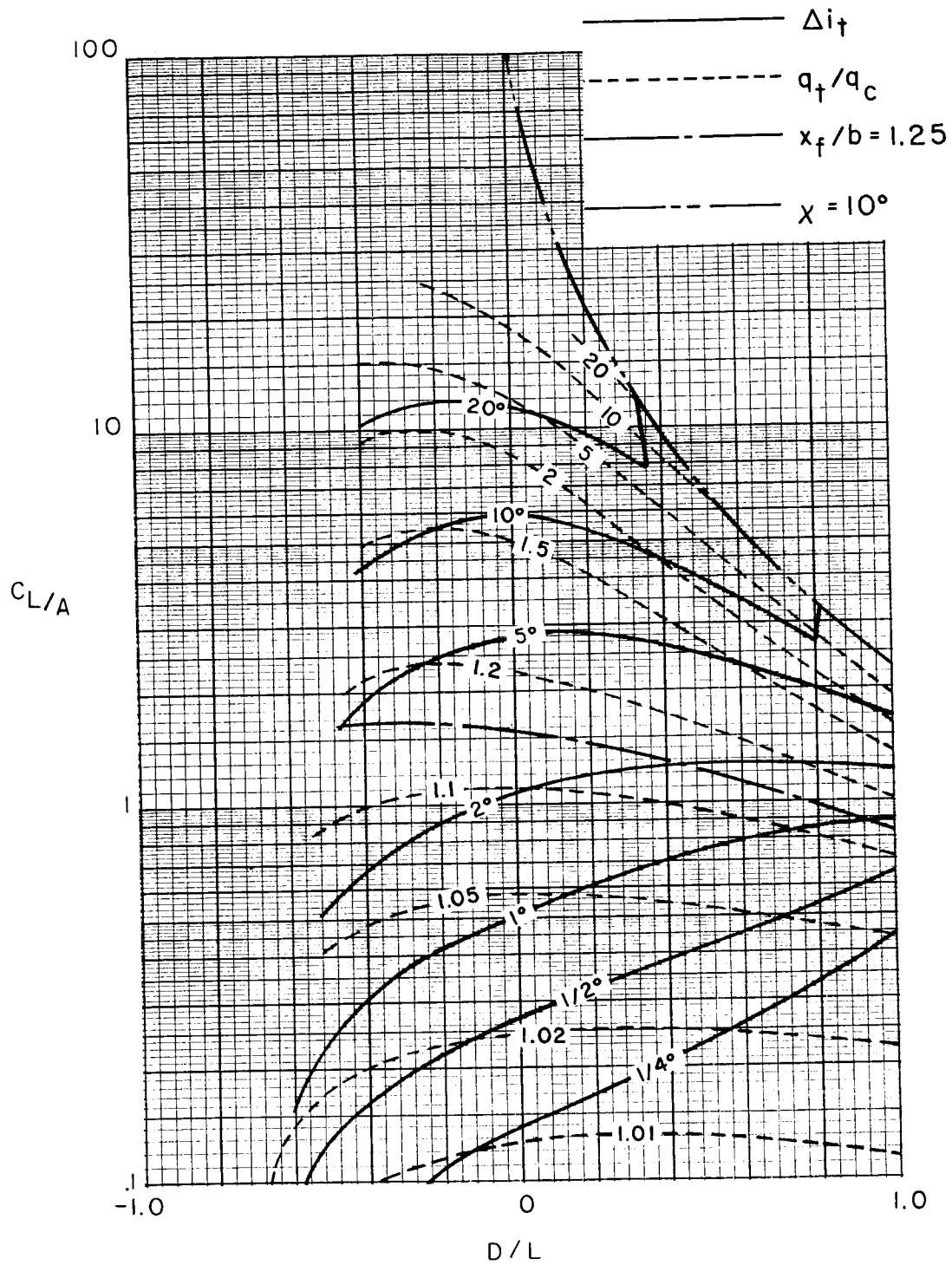


(b) $\sigma = 1/2$.

Figure 63.- Continued.

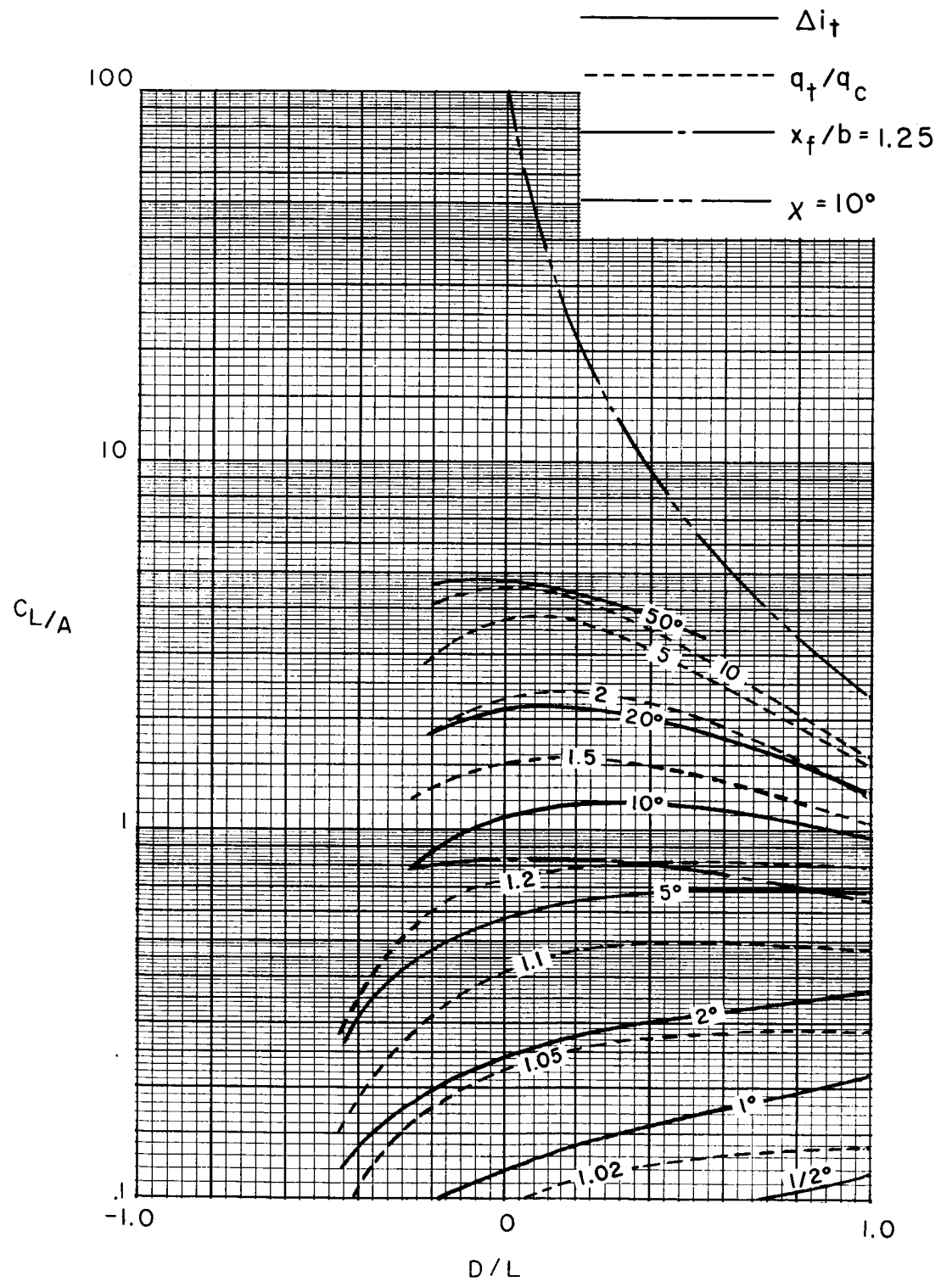


(c) $\sigma = 3/4$.

Figure 63.- Concluded.

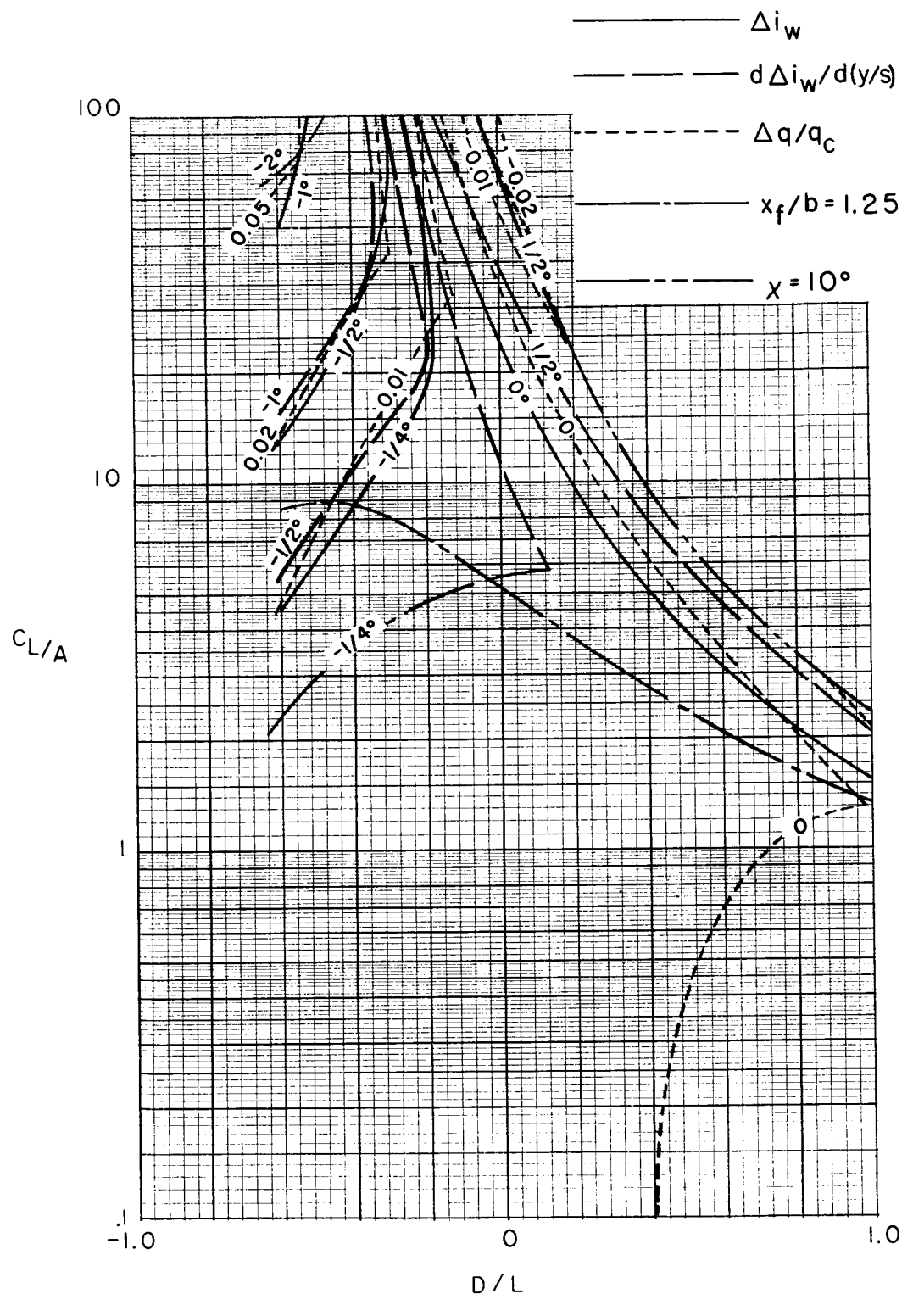


(a) $\sigma = 1/4$.

Figure 64.- Nonuniformity of corrections over a uniformly loaded wing in a rectangular tunnel closed only on the bottom when the model height is varied to maintain $\Delta w = 0$. $\gamma = 1.5$; $\alpha = 0^0$; $\Lambda = 0^0$.

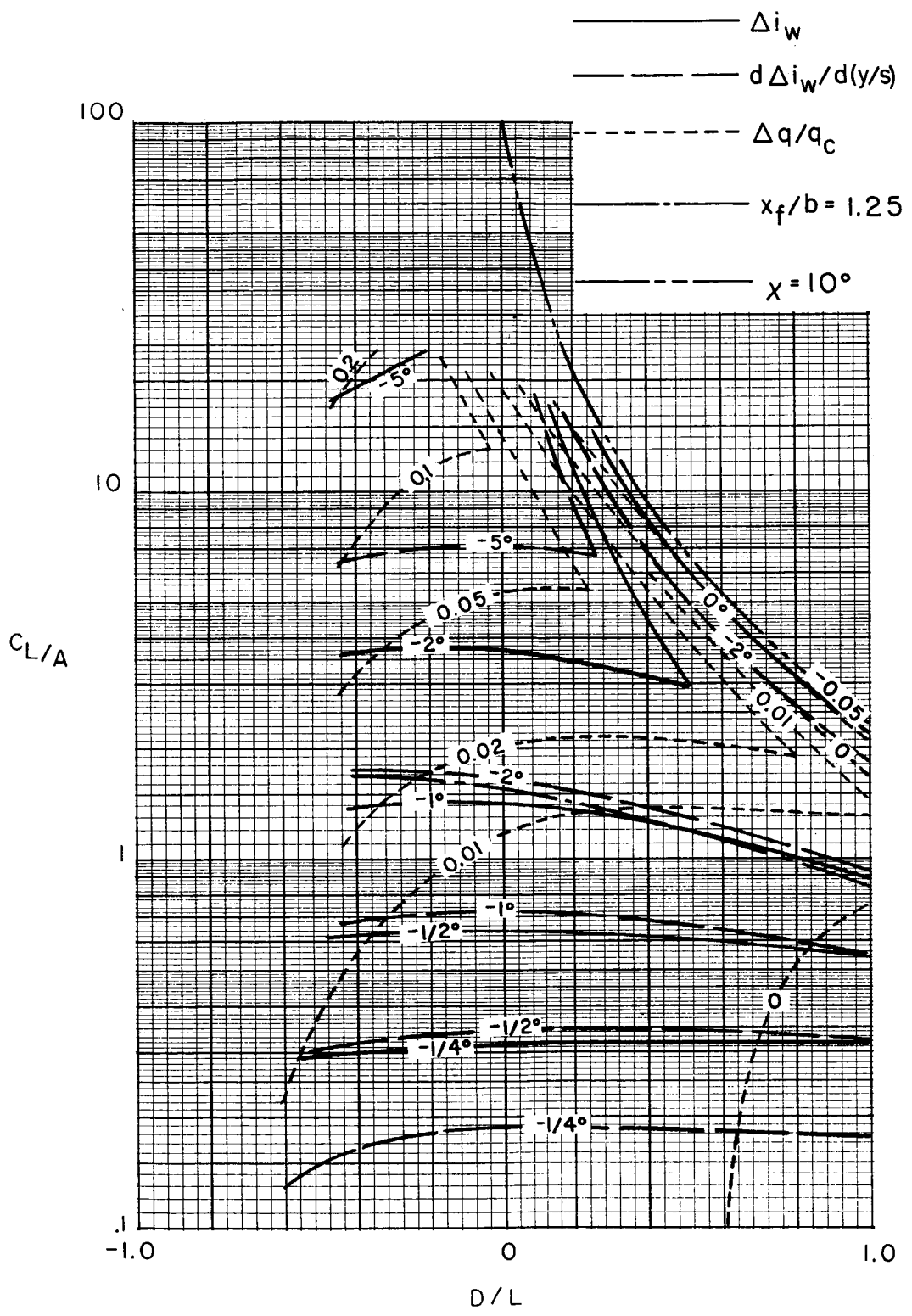


(b) $\sigma = 1/2$.

Figure 64.- Continued.

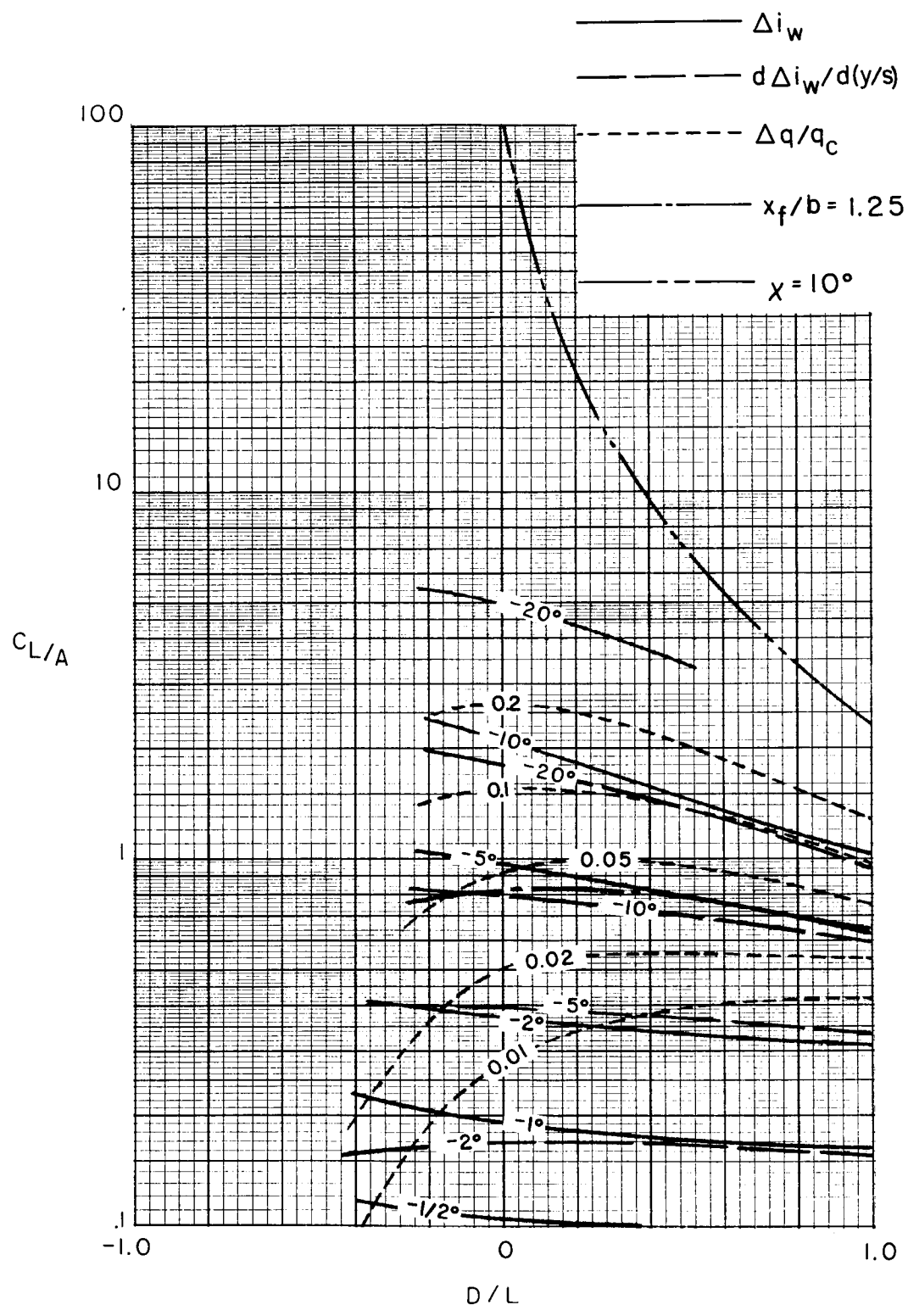


(c) $\sigma = 3/4$.

Figure 64.- Concluded.

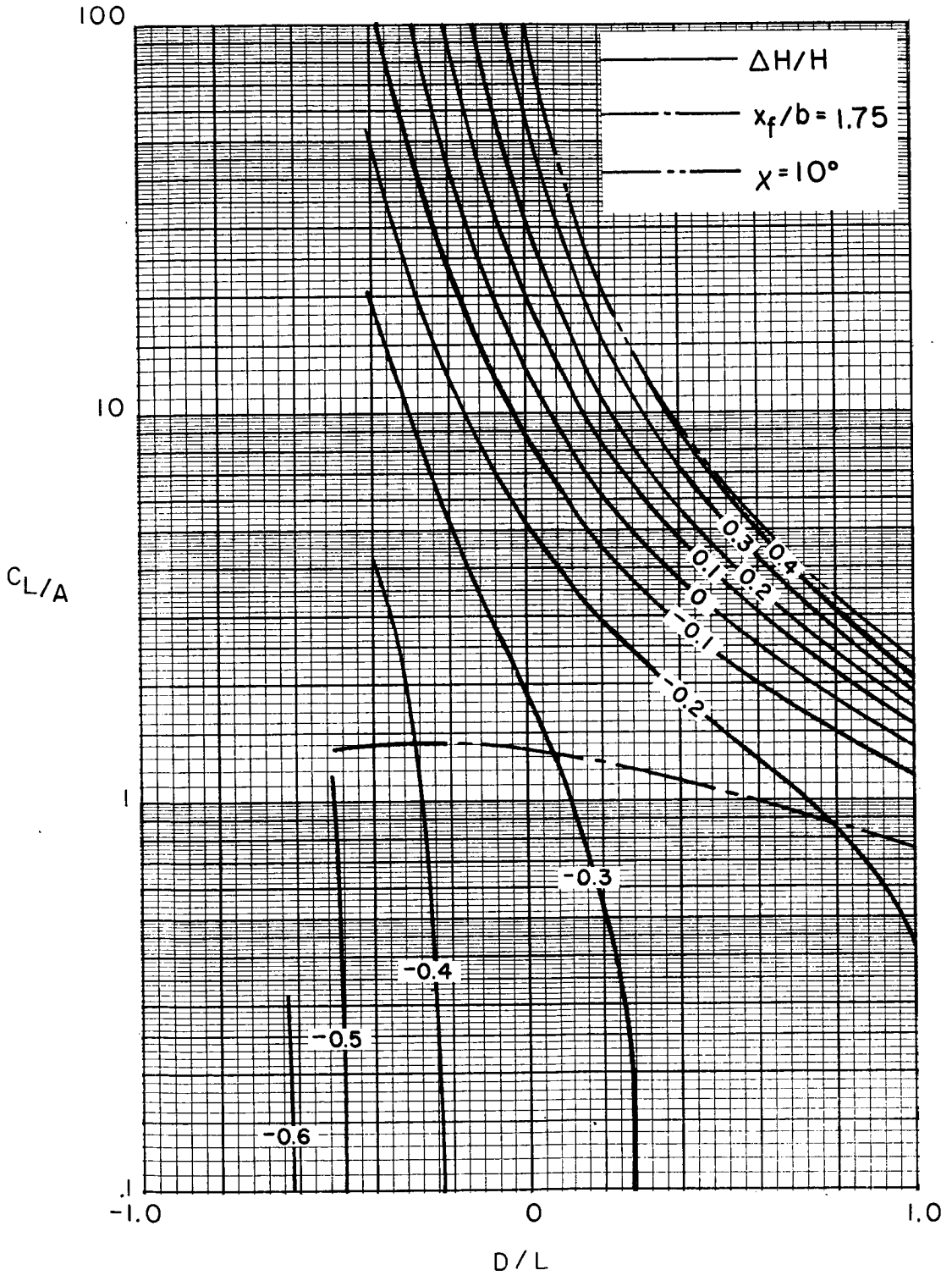


(a) $\gamma = 1$.

Figure 65.- Schedule of model height required to maintain $\Delta w = 0$ for a wing in a rectangular tunnel closed only on the bottom. $\Lambda = 0^0$; $\sigma = 0.5$.

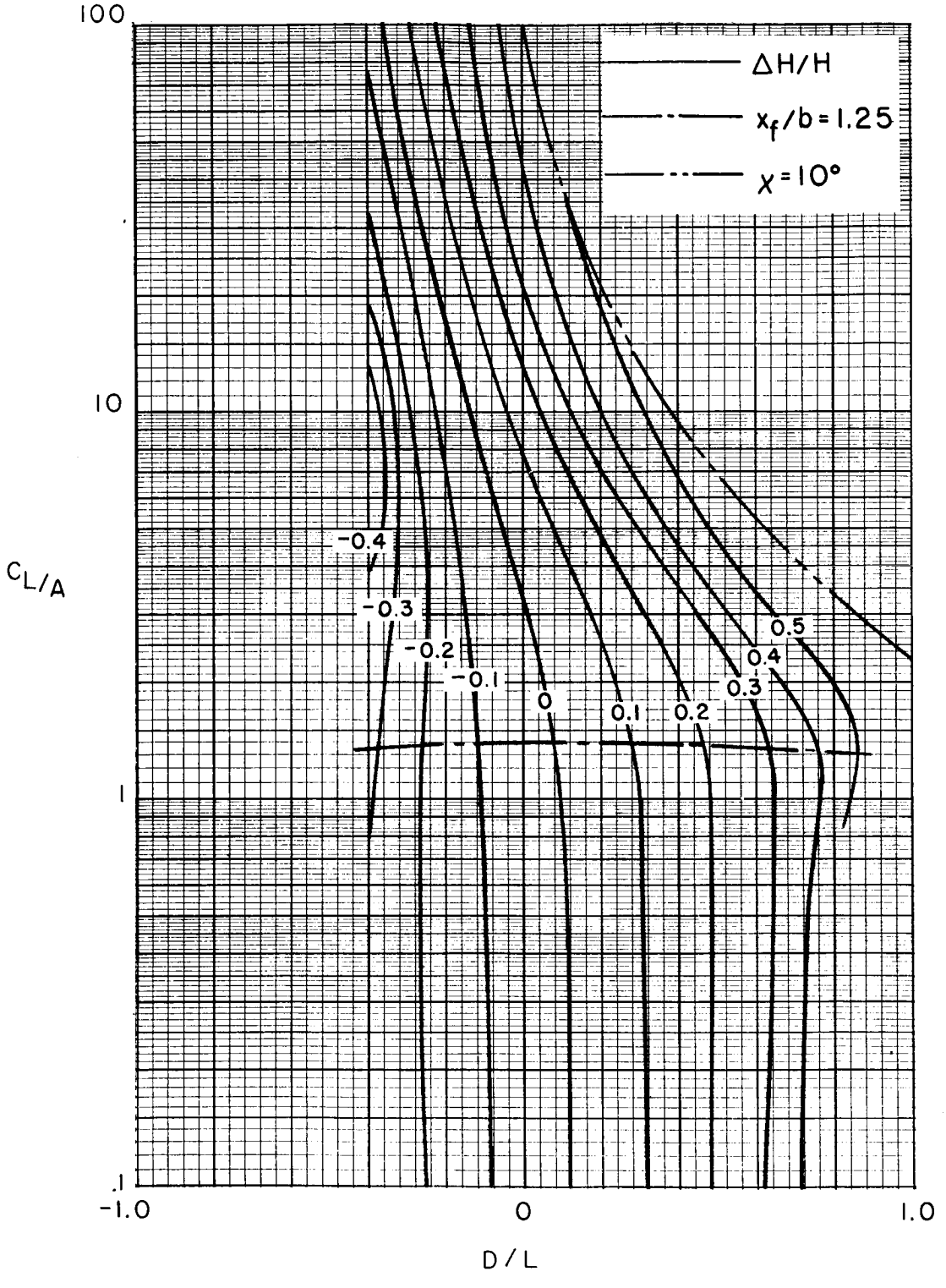


(b) $\gamma = 2$.

Figure 65.- Concluded.

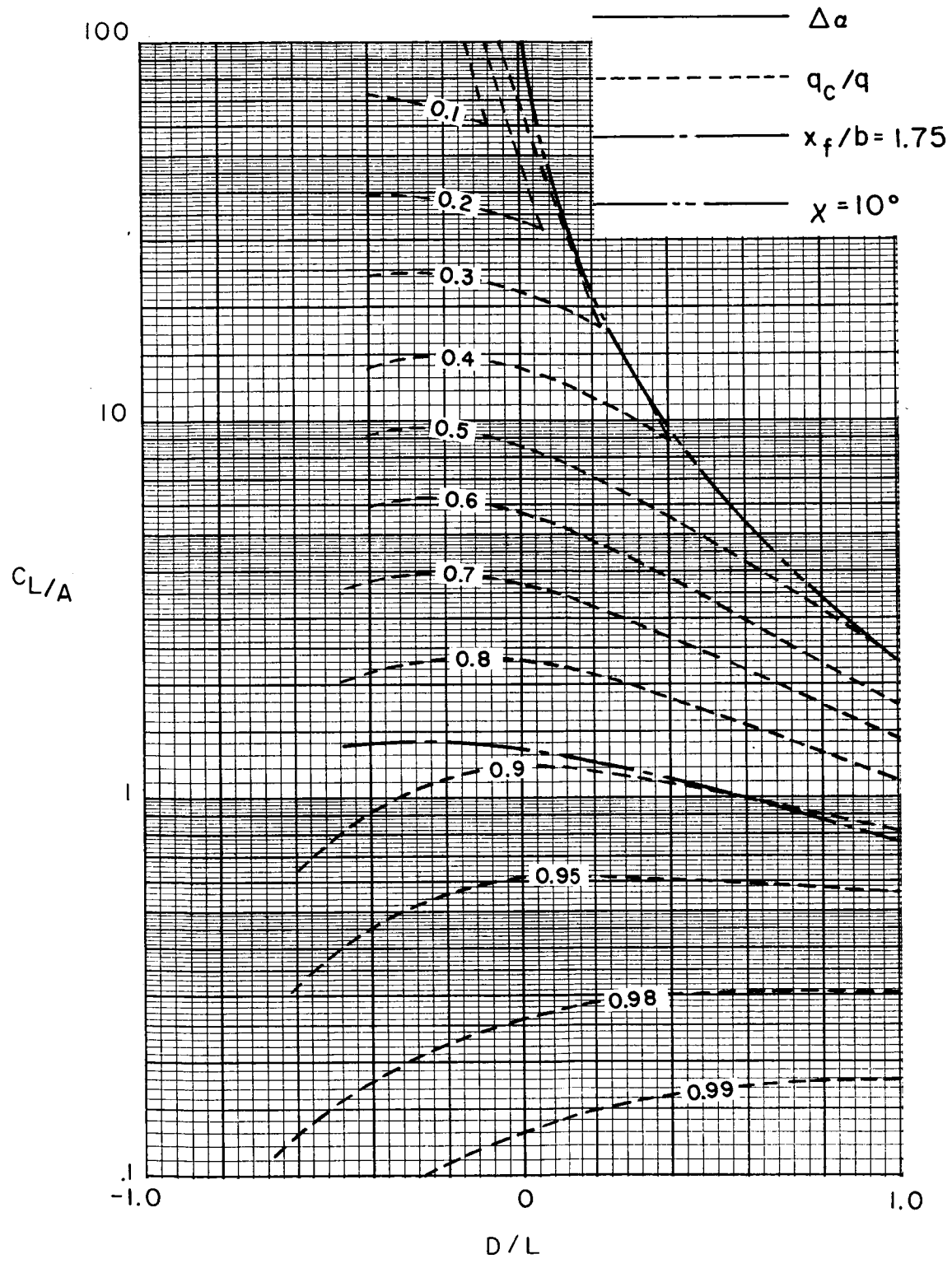


(a) $\gamma = 1$.

Figure 66.- Average corrections for a uniformly loaded wing in a rectangular tunnel closed only on the bottom when the model height is varied to maintain $\Delta w = 0$. $\Lambda = 0^0$; $\sigma = 0.5$.

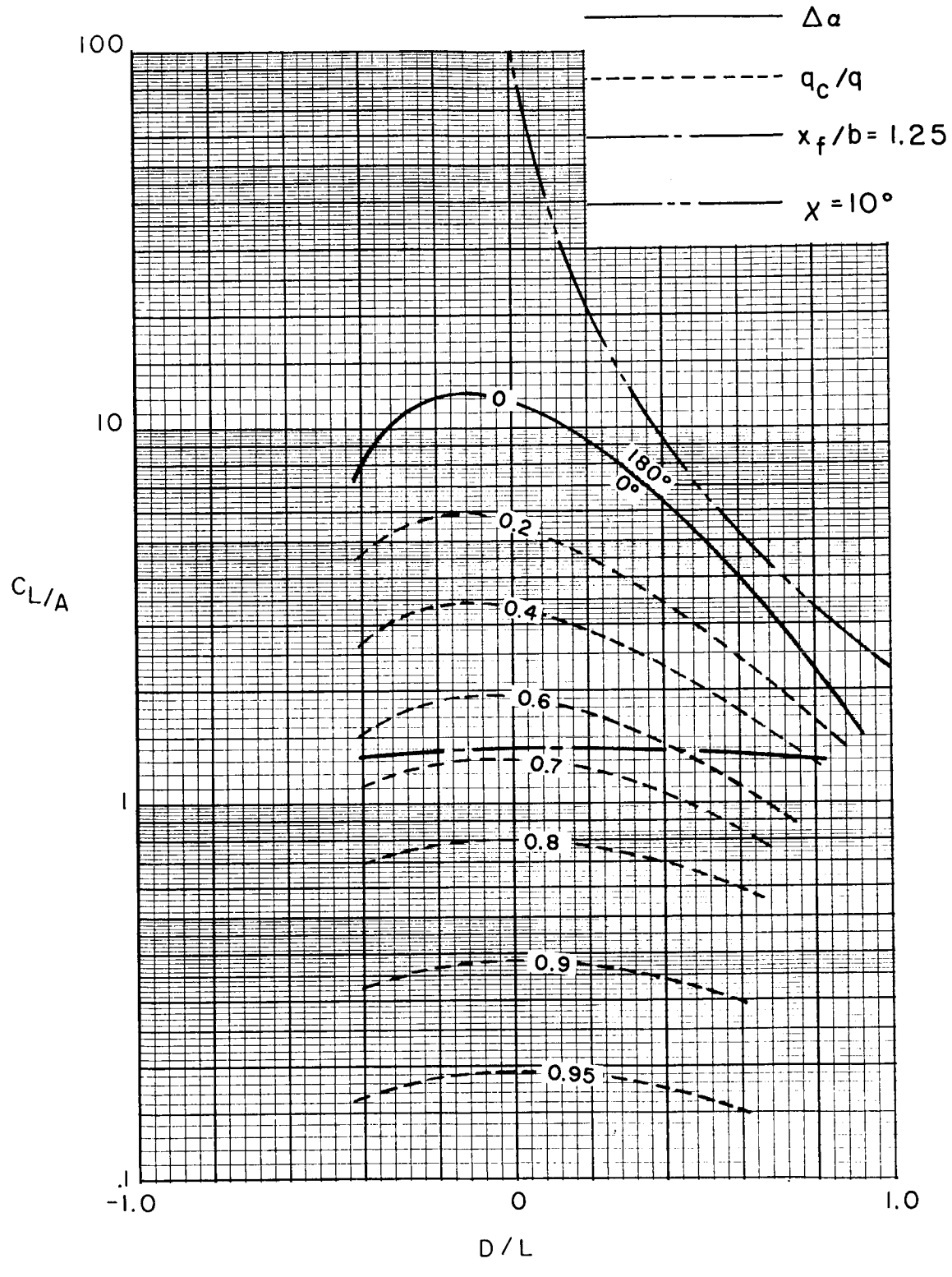


(b) $\gamma = 2$.

Figure 66.- Concluded.

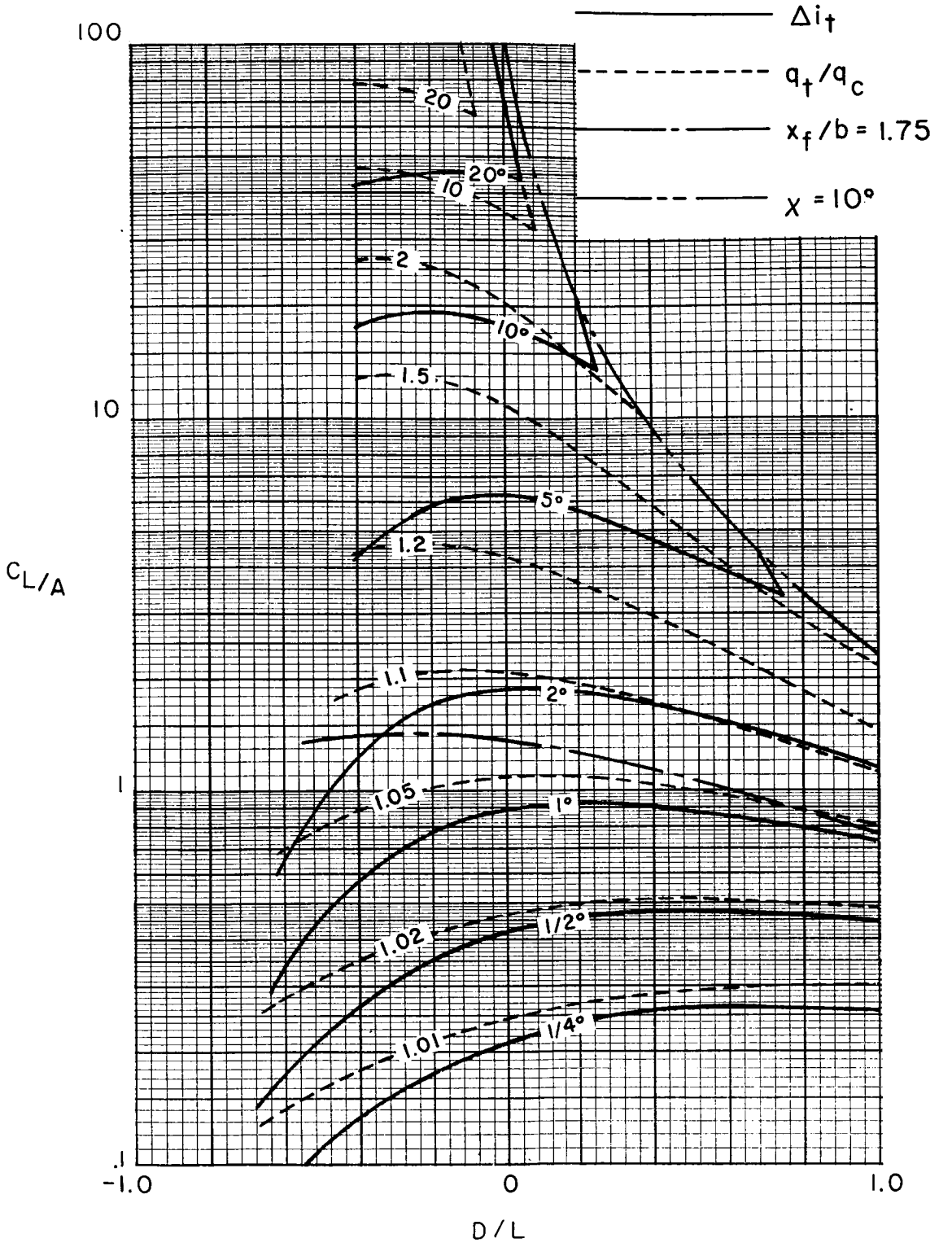


(a) $\gamma = 1$.

Figure 67.- Corrections at a zero-span tail behind a uniformly loaded wing in a rectangular tunnel closed only on the bottom when the model height is varied to maintain $\Delta w = 0$. Tail length is three-fourths of wing span; tail height is zero; $\alpha = 20^0$; $\Lambda = 0^0$; $\sigma = 0.5$.

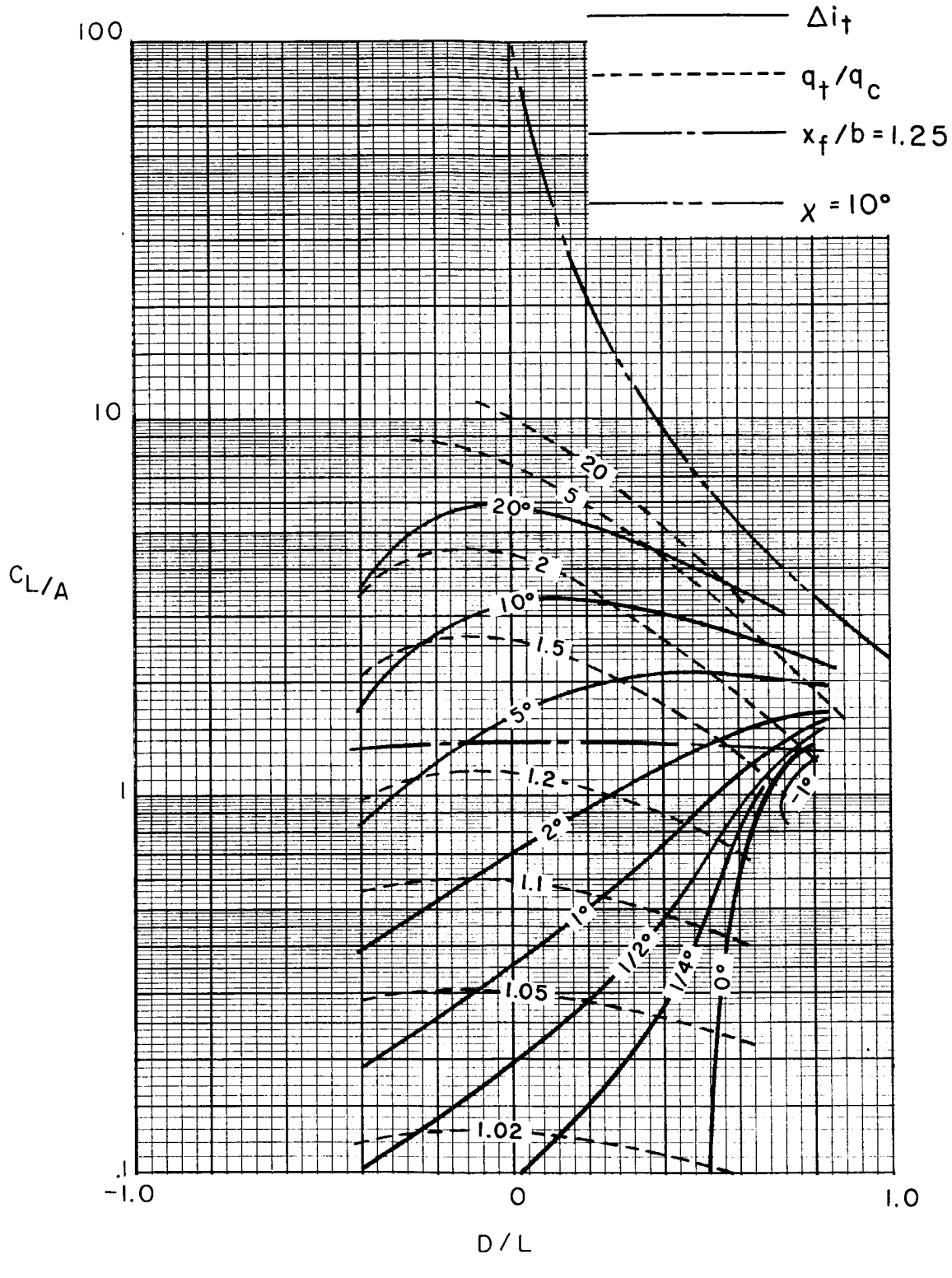


(b) $\gamma = 2$.

Figure 67.- Concluded.

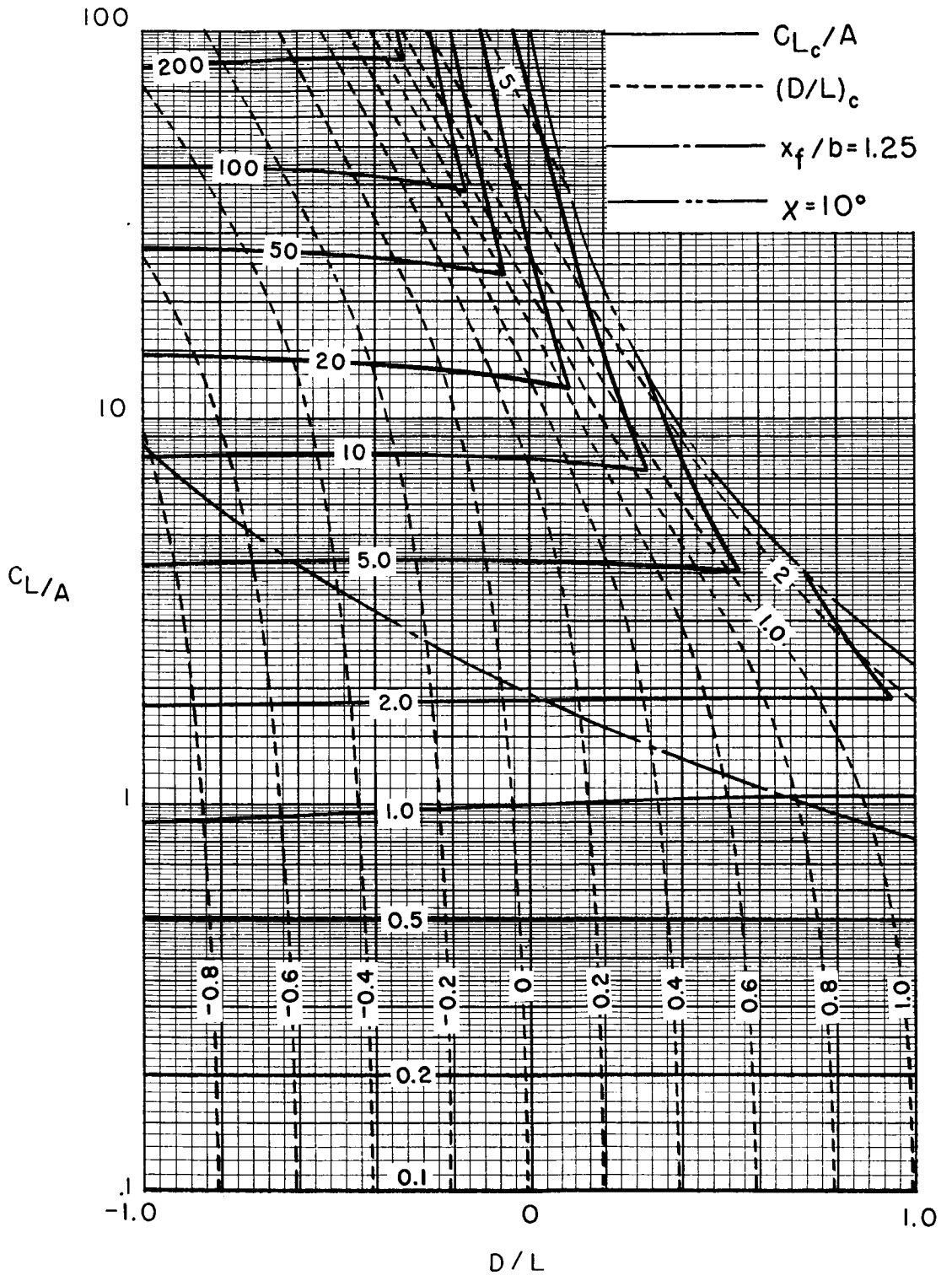


Figure 68.- Effect of average corrections on lift and drag in a closed rectangular tunnel when it is assumed that profile drag is zero. $\gamma = 1.5$; $\sigma = 0.5$.

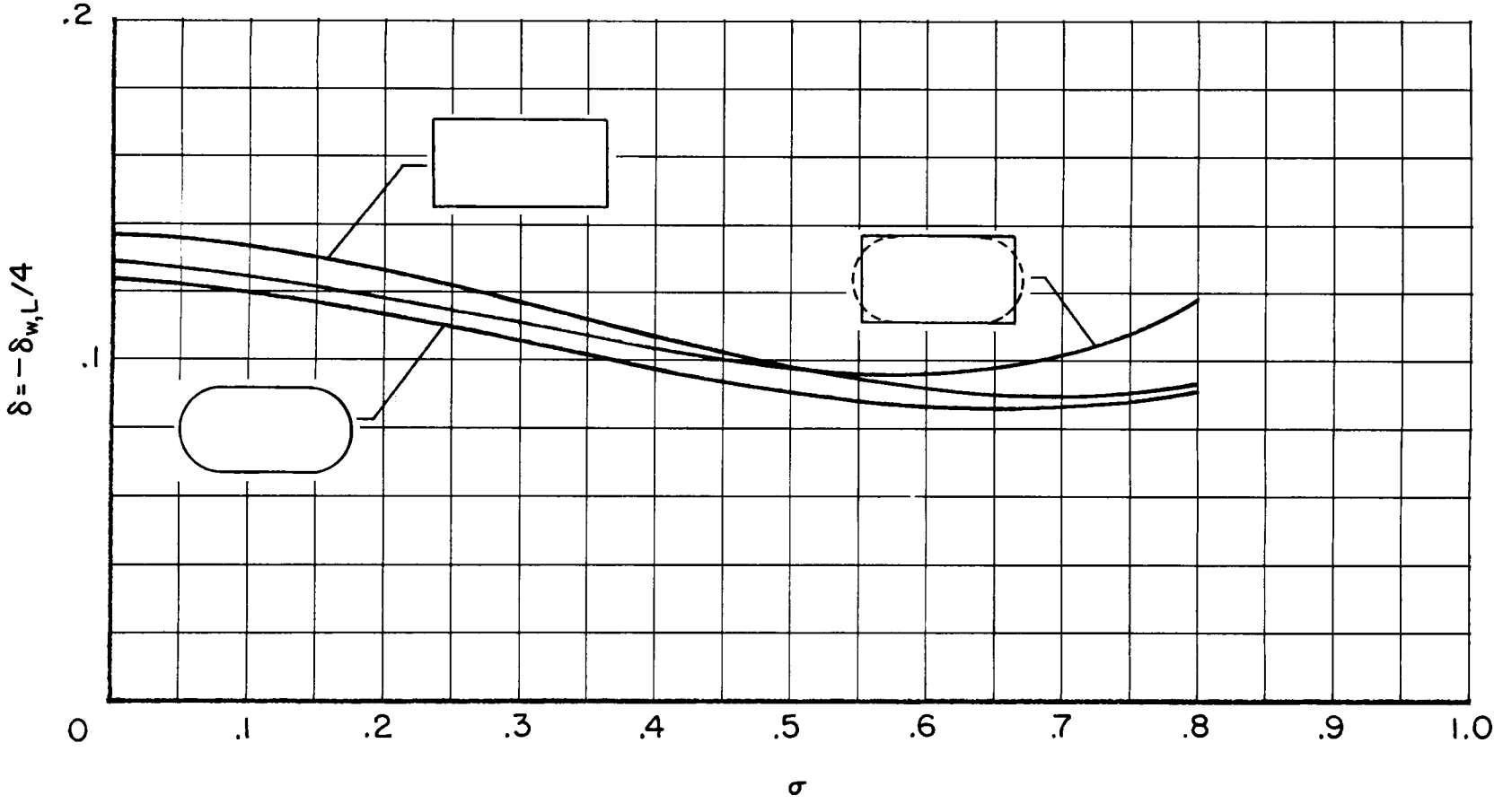


Figure 69.- Average interference factors calculated for a wind tunnel with semicircular ends by using different approximations to the tunnel cross section. $\chi = 90^0$; $\gamma = 2$.

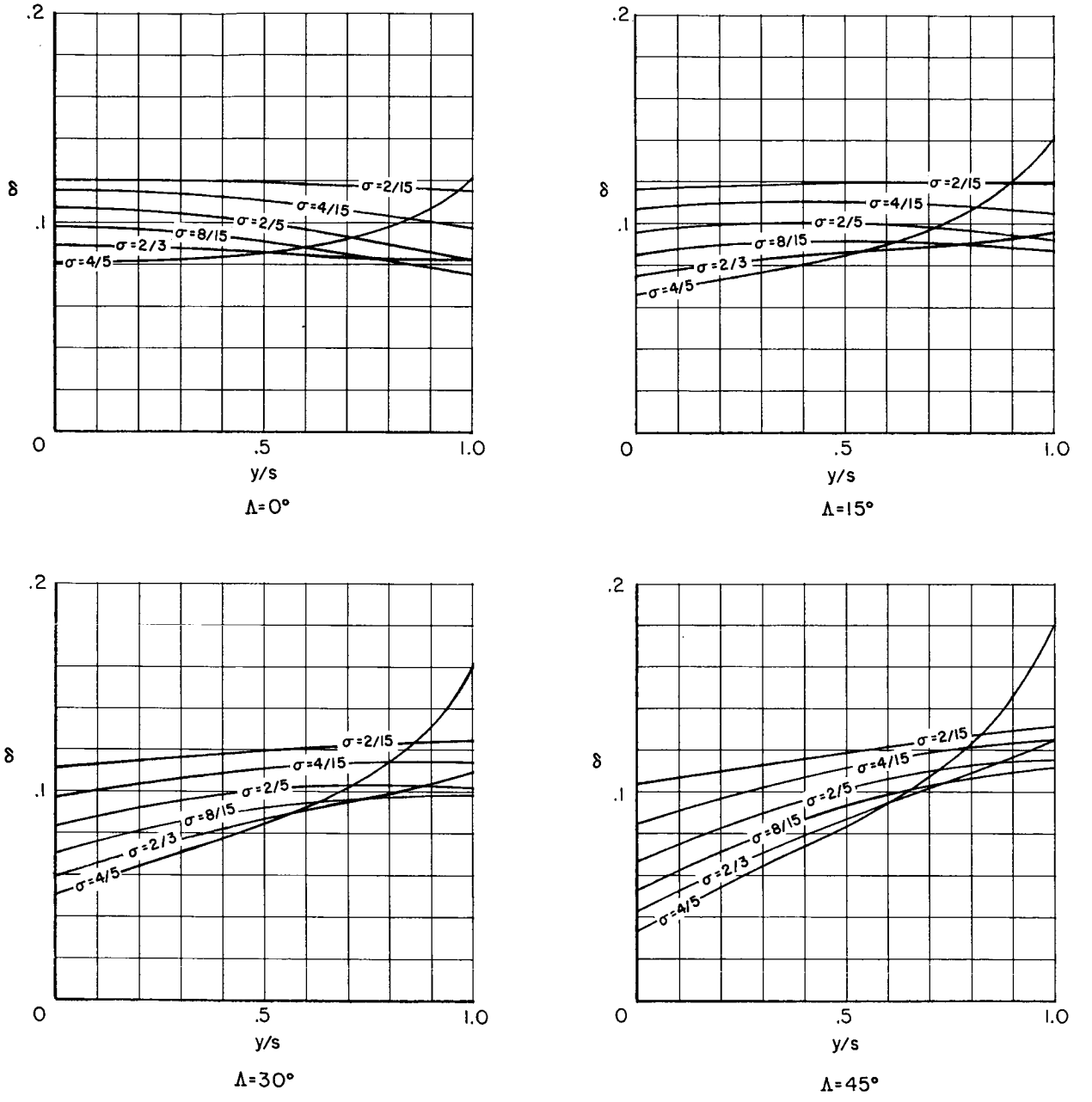


(a) Semicircular sides (ref. 31).

Figure 70.- Spanwise distribution of interference factors for a wind tunnel with semicircular ends as calculated by using different approximations to the tunnel cross section. $\chi = 90^{0}$; $\gamma = 2$.

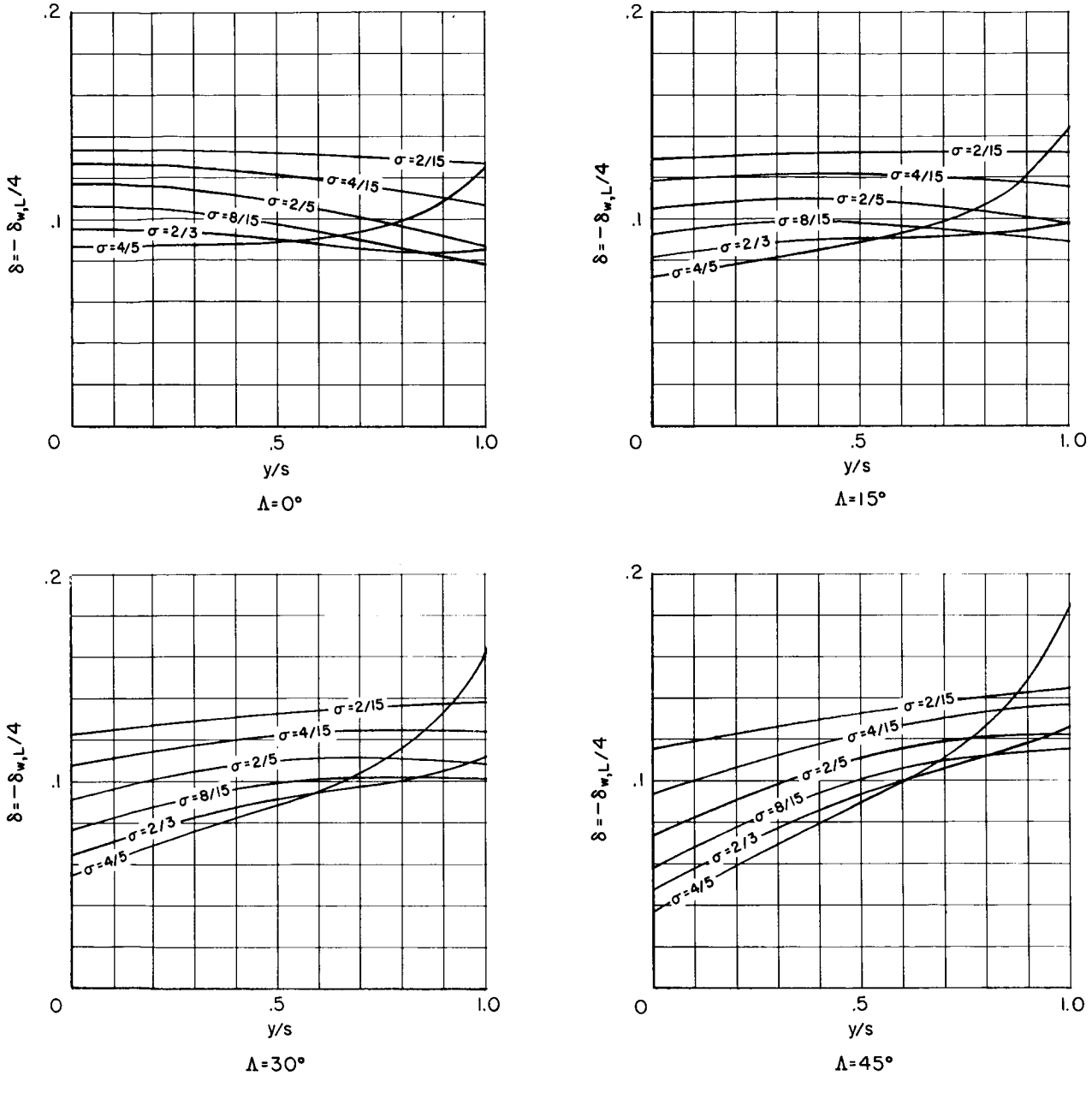


(b) Rectangular $\gamma = 2$.

Figure 70.- Continued.

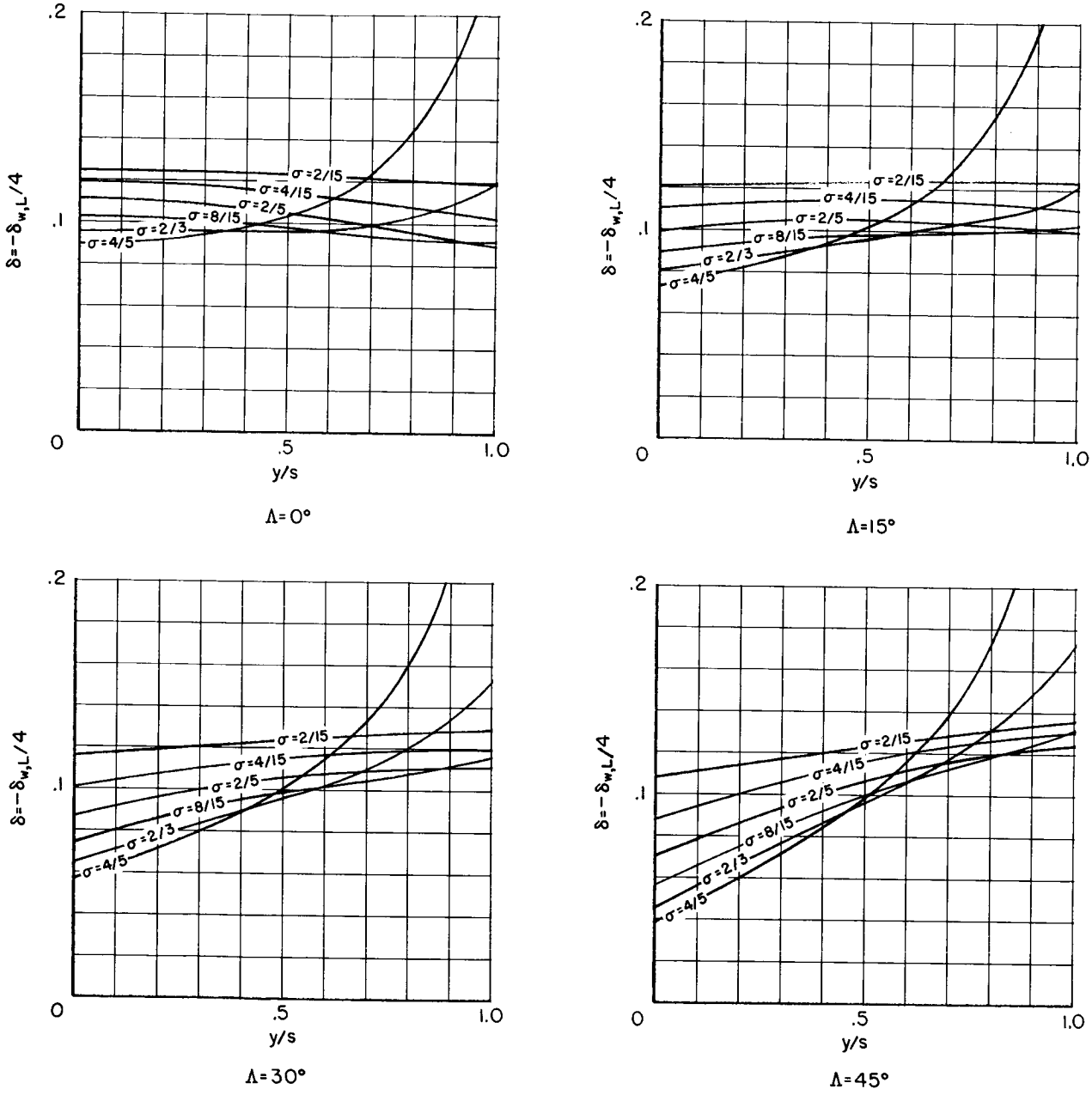


(c) Rectangular $\gamma = \frac{4+\pi}{4}$.

Figure 70.- Concluded.

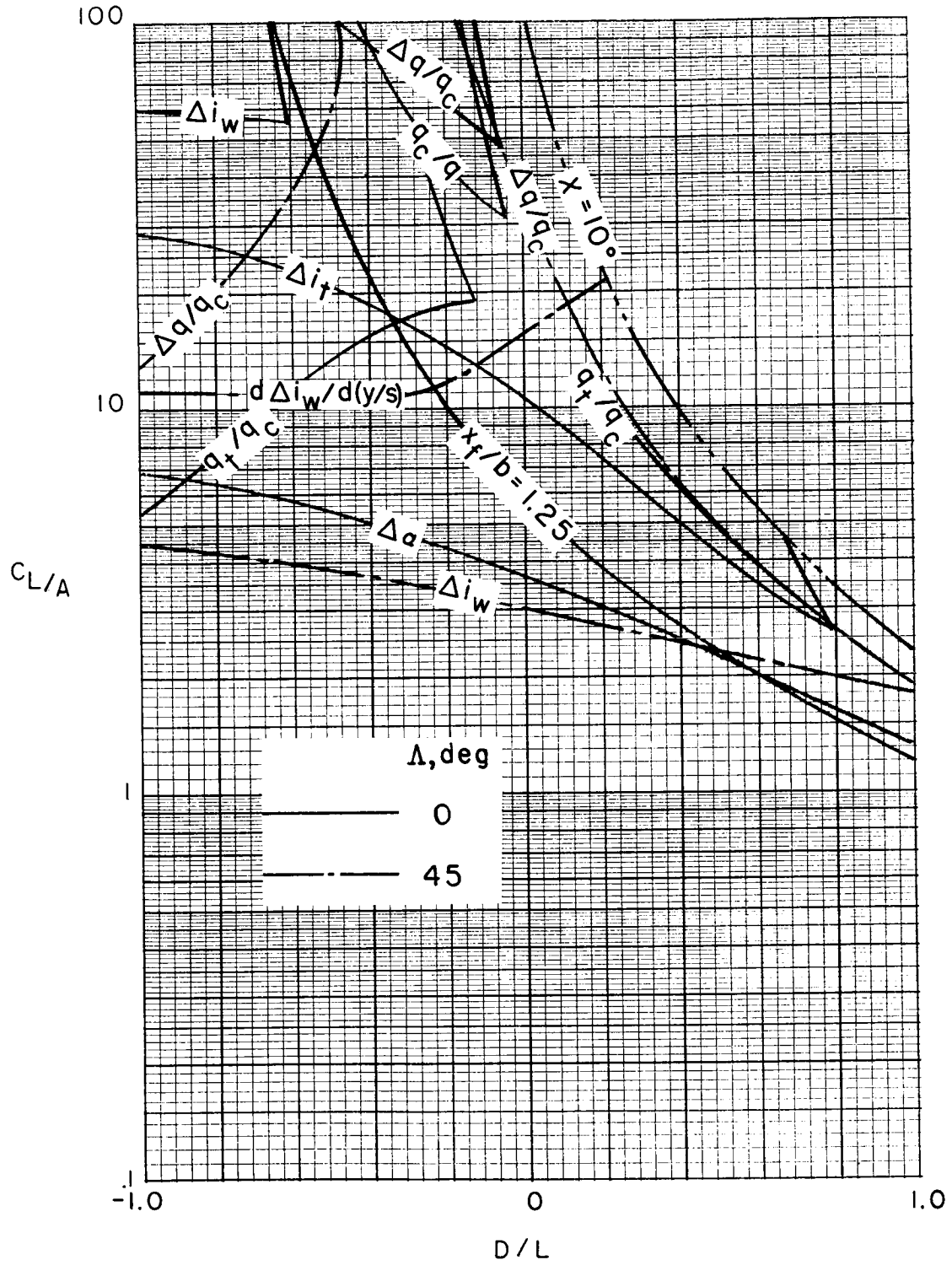


Figure 71.- Sample cross plot of limiting factors in a closed rectangular tunnel when the maximum practical corrections are applied. $\gamma = 2/3$; $\sigma = 1/2$. (See table II(a).)

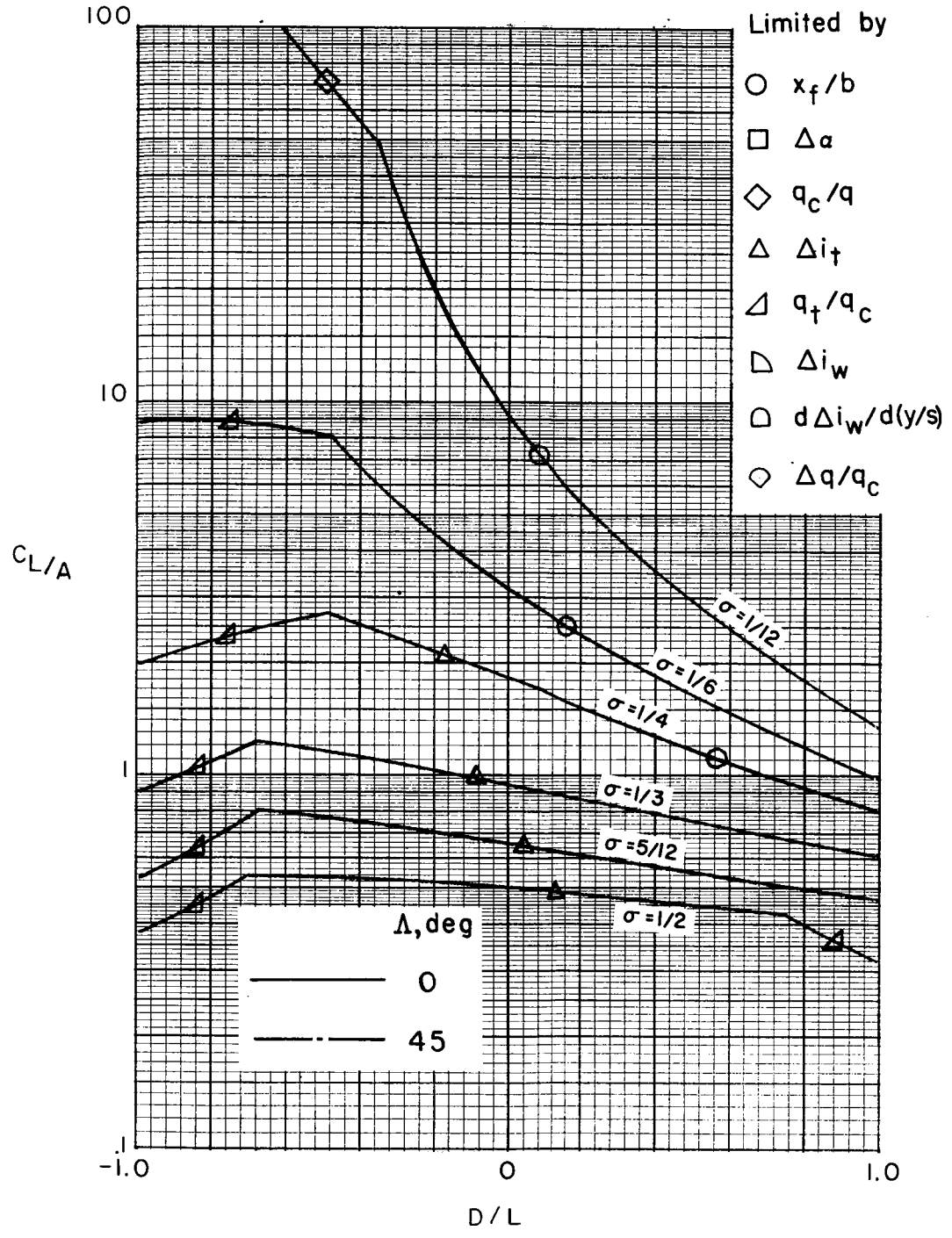


(a) $\gamma = 3$.

Figure 72.- Limits of testing in closed tunnels when applying the maximum practical corrections. (See table II(a).)

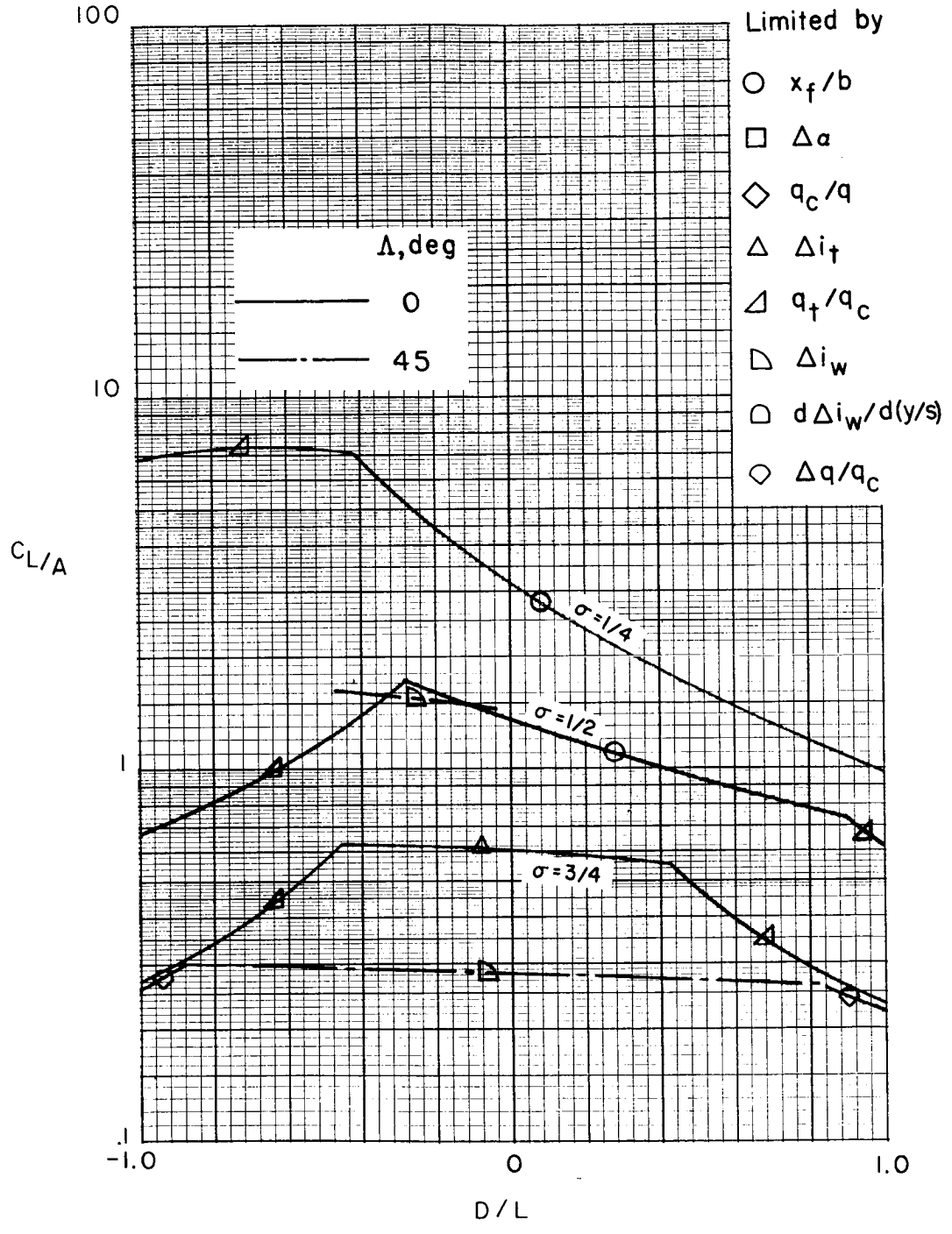


(b) $\gamma = 2$.

Figure 72.- Continued.

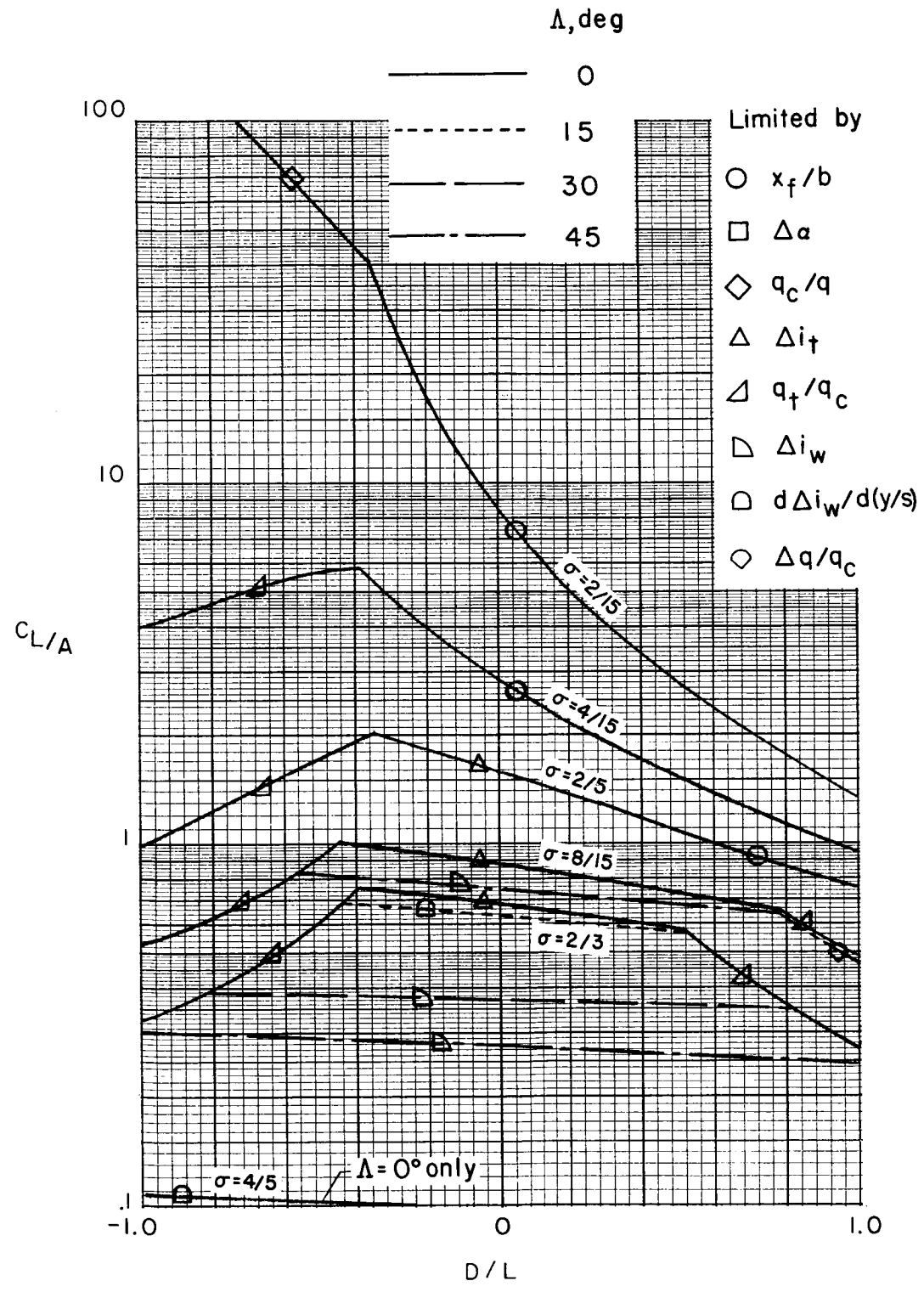


(c) $\gamma = 2$ with semicircular sides.

Figure 72.- Continued.

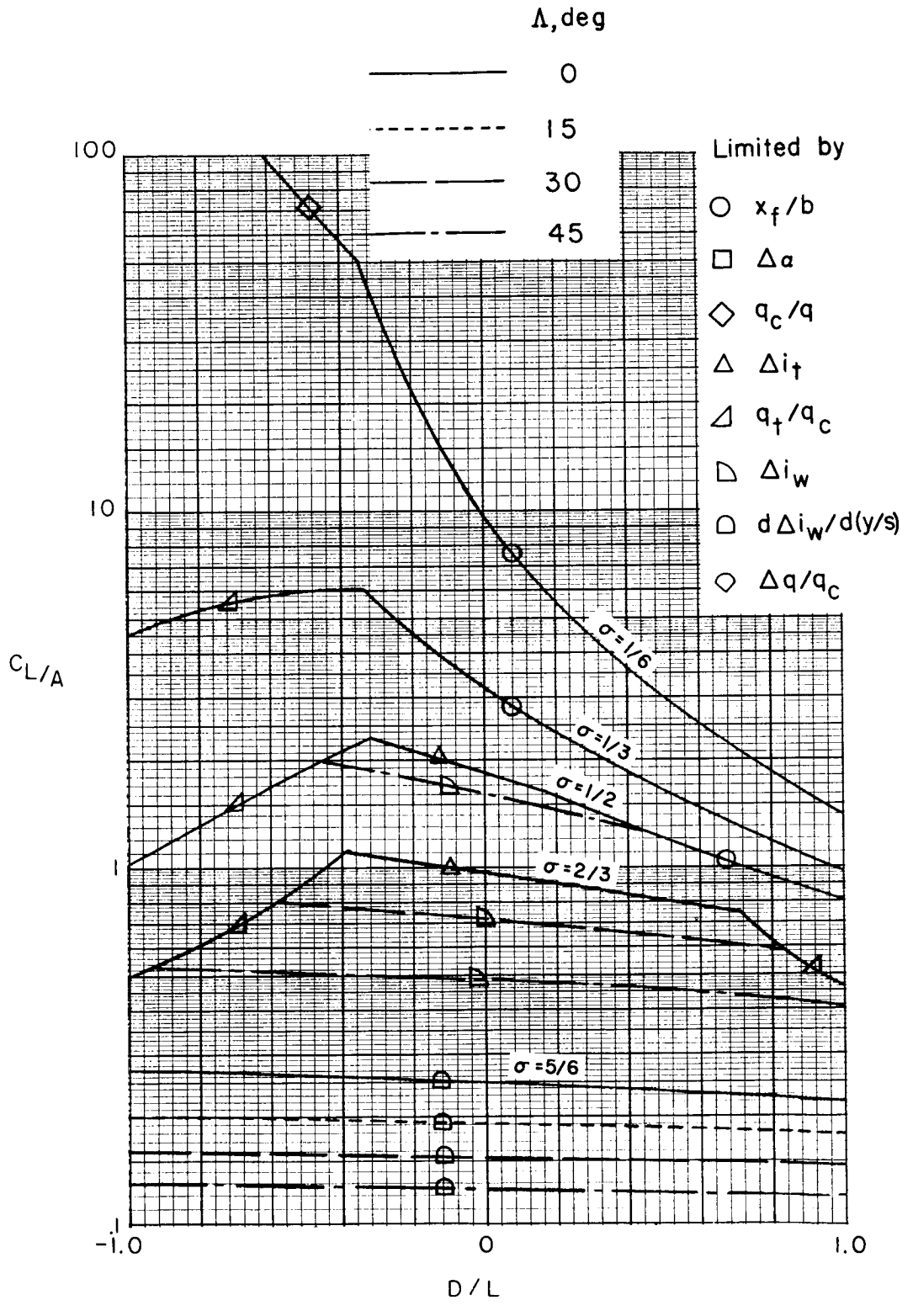


(d) $\gamma = 1.5$.

Figure 72.- Continued.

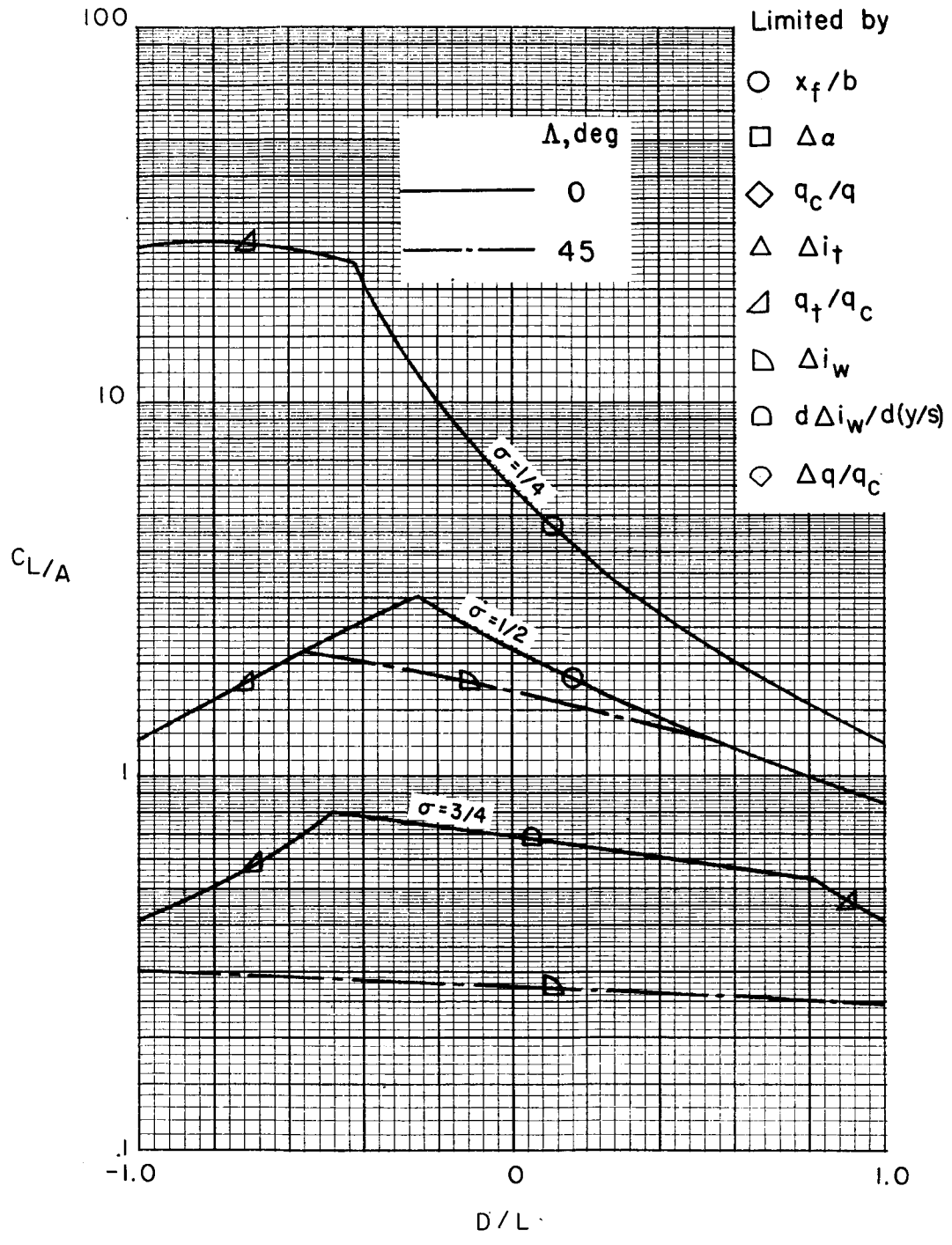


(e) $\gamma = 4/3$.

Figure 72.- Continued.

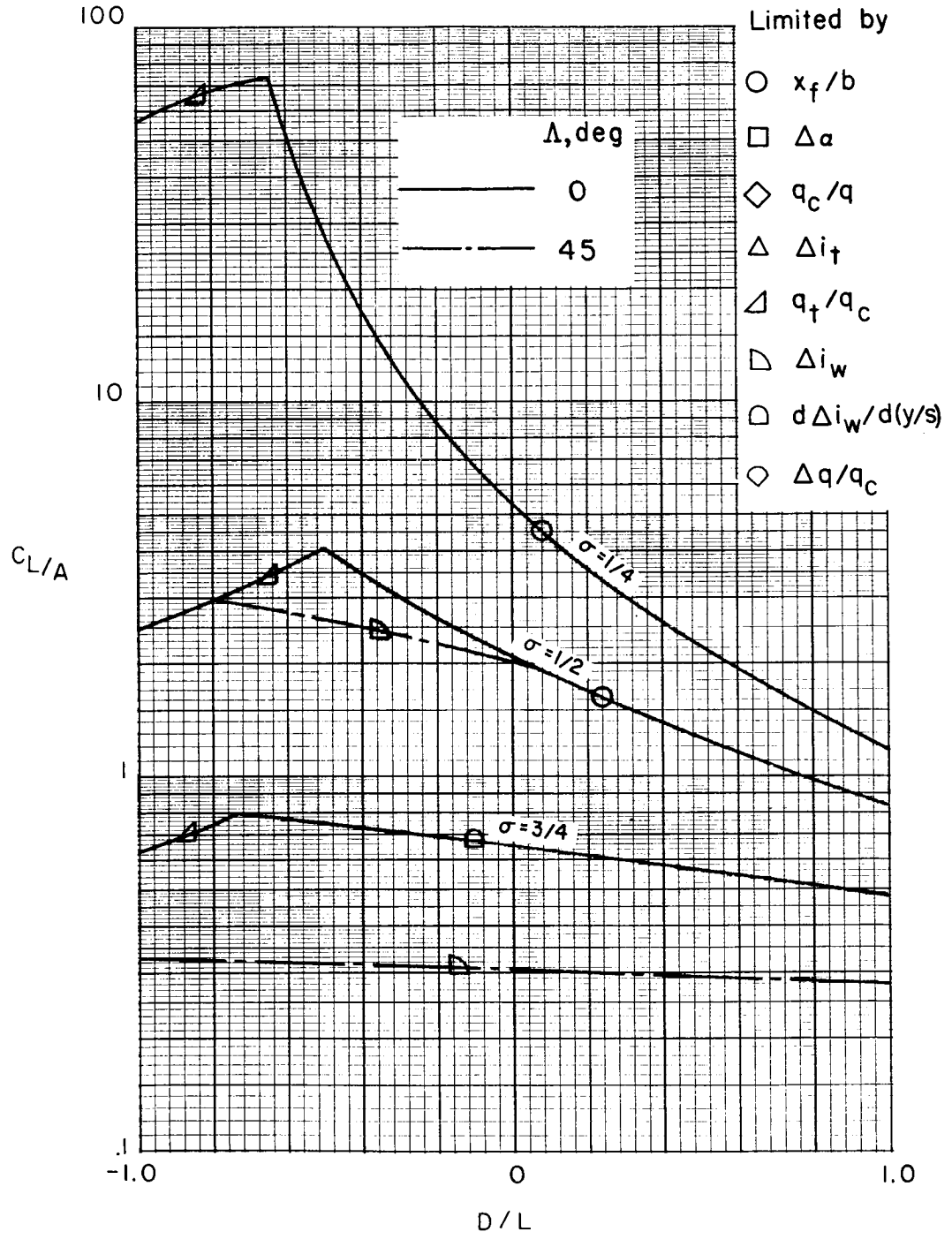


(f) $\gamma = 1$.

Figure 72.- Continued.

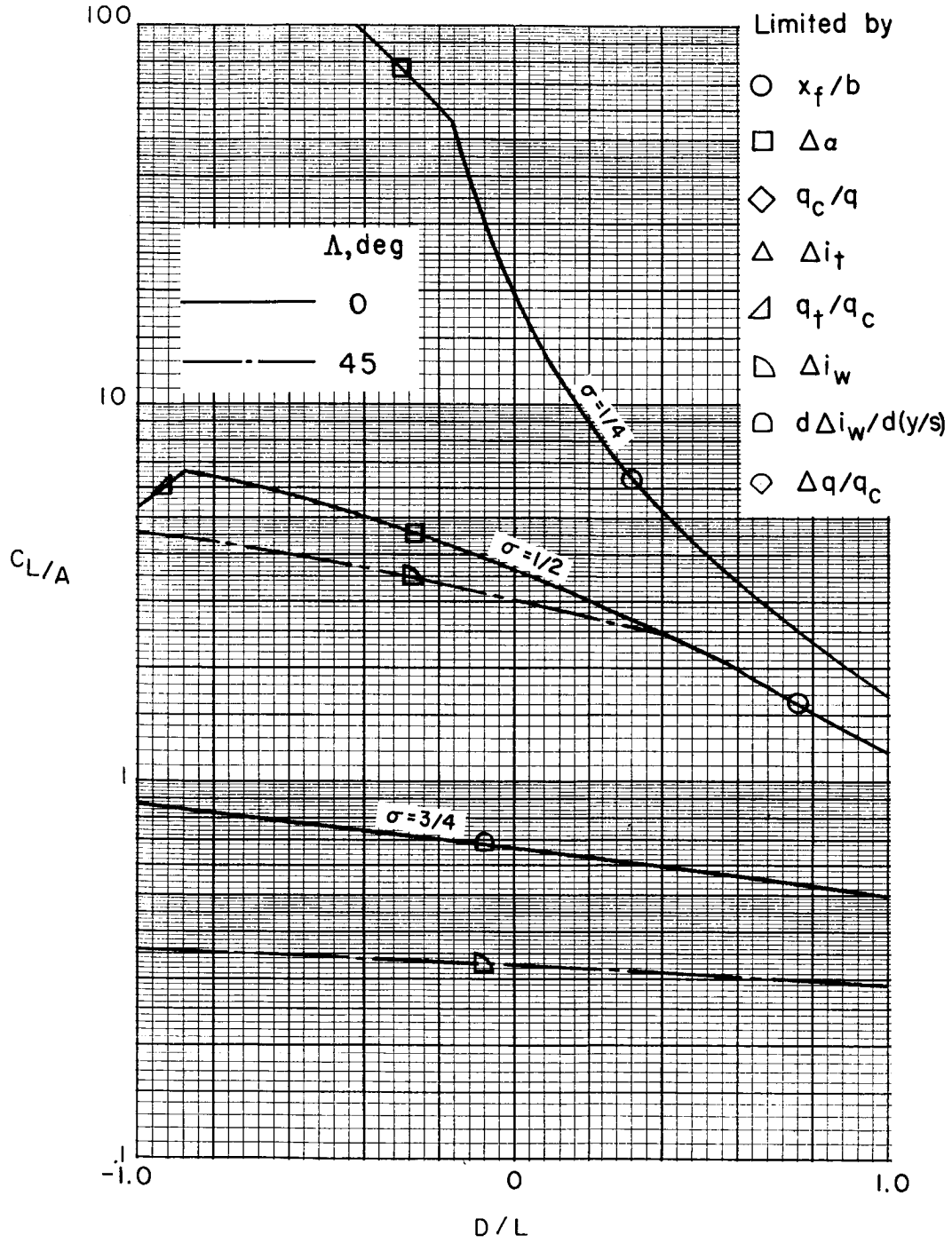


(g) $\gamma = 2/3$.

Figure 72.- Continued.

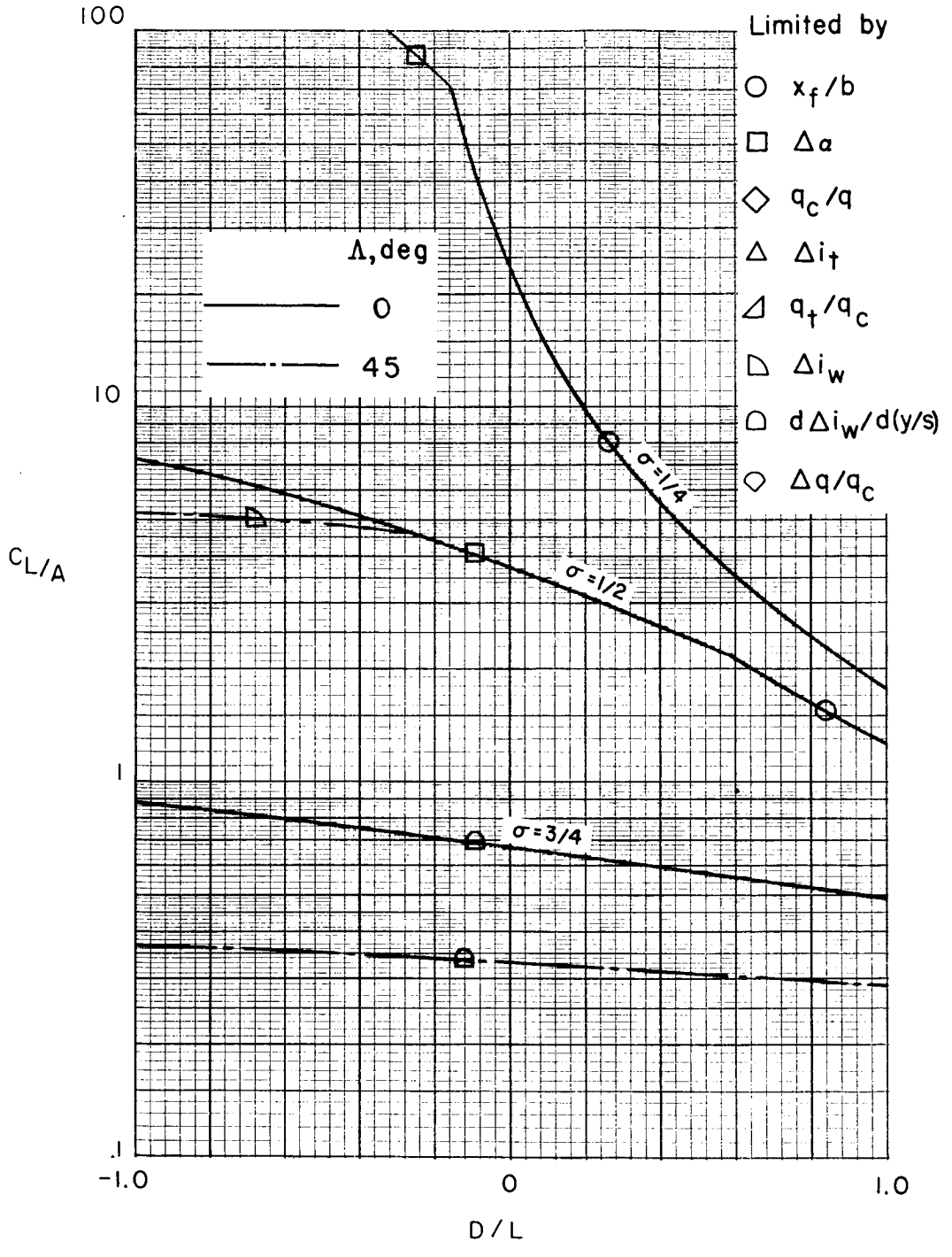


(h) $\gamma = 1/2$.

Figure 72.- Concluded.

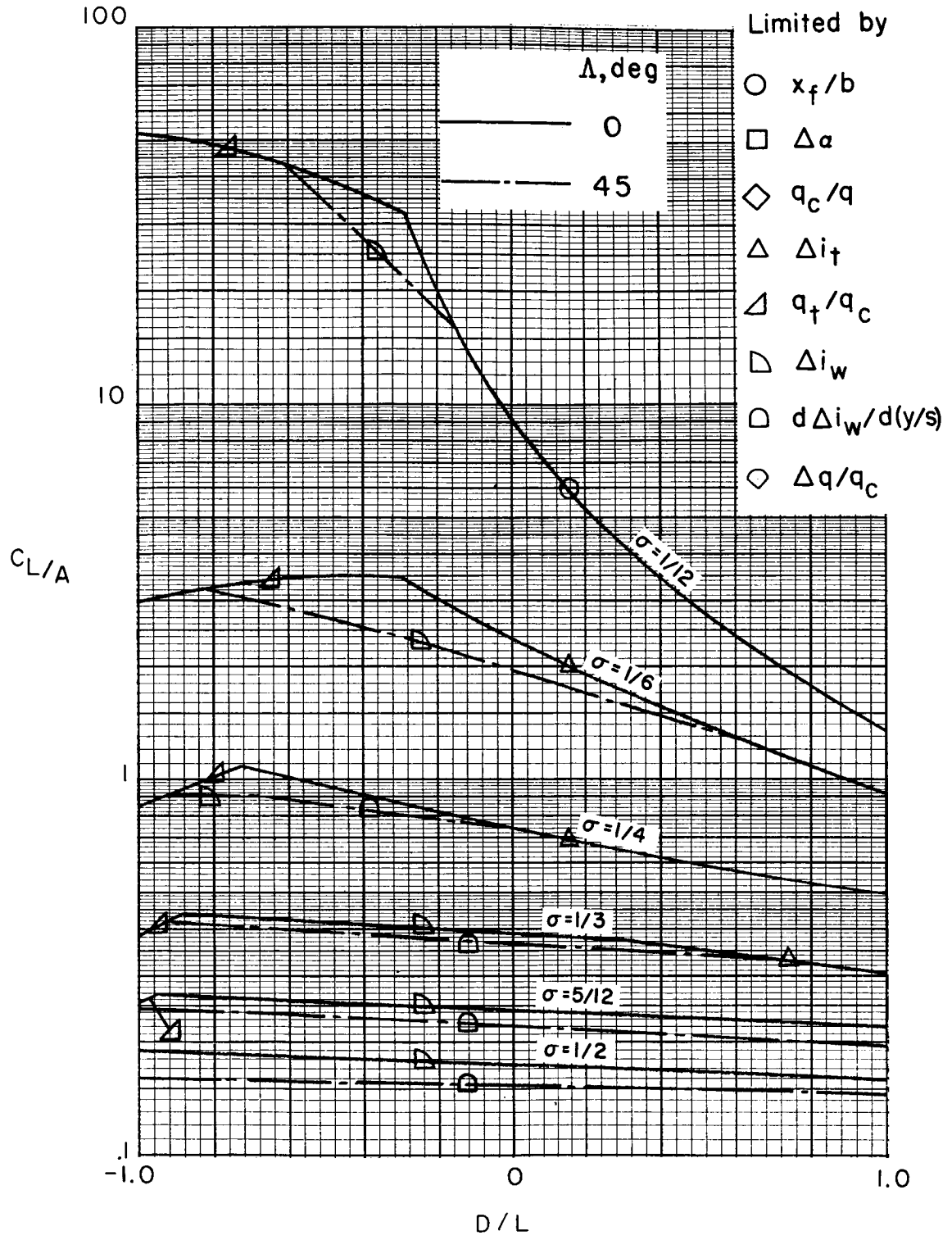


(a) $\gamma = 3$.

Figure 73.- Limits of testing in closed tunnels when applying moderate corrections. (See table II(b).)

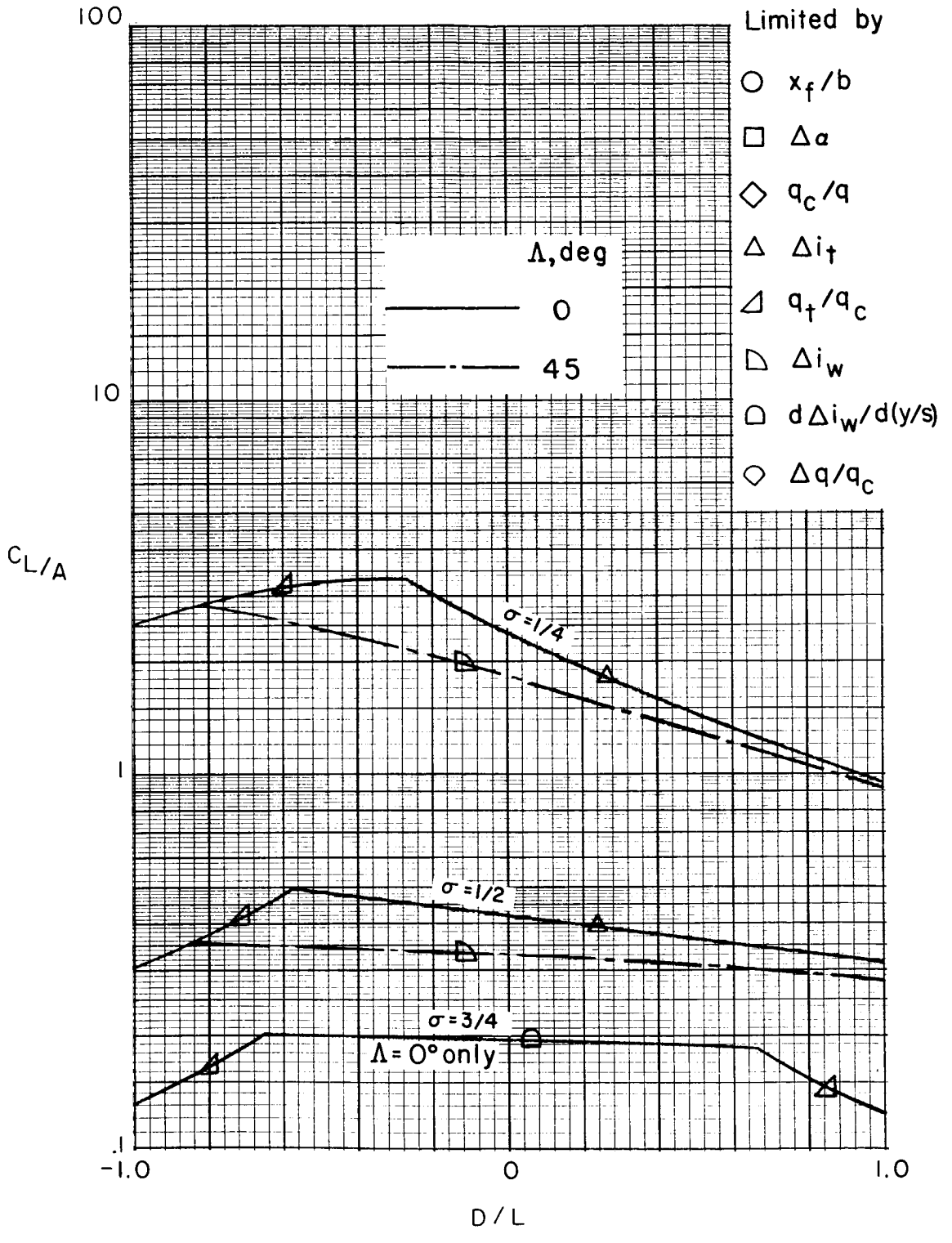


(b) $\gamma = 2$.

Figure 73.- Continued.

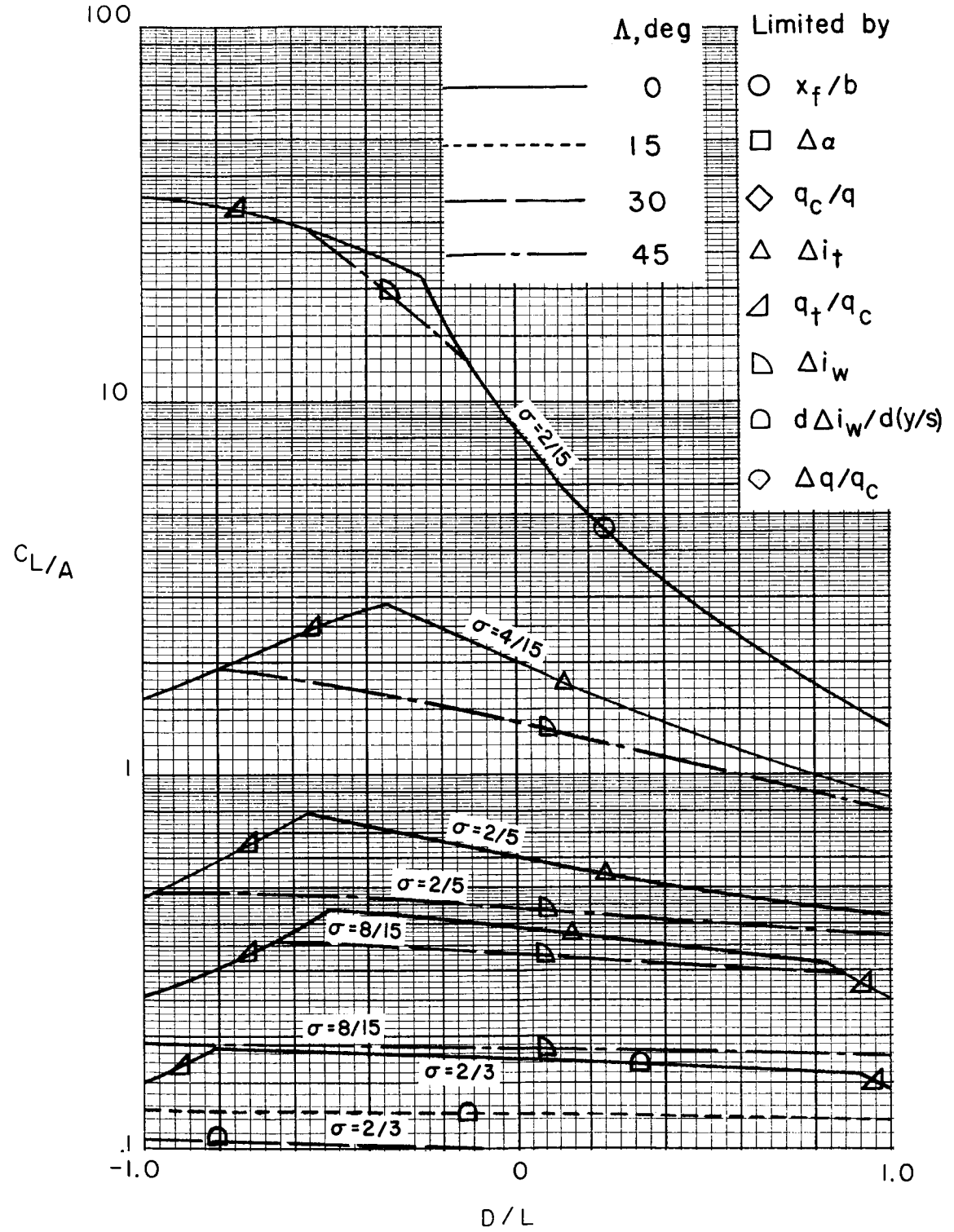


(c) $\gamma = 2$ with semicircular sides.

Figure 73.- Continued.

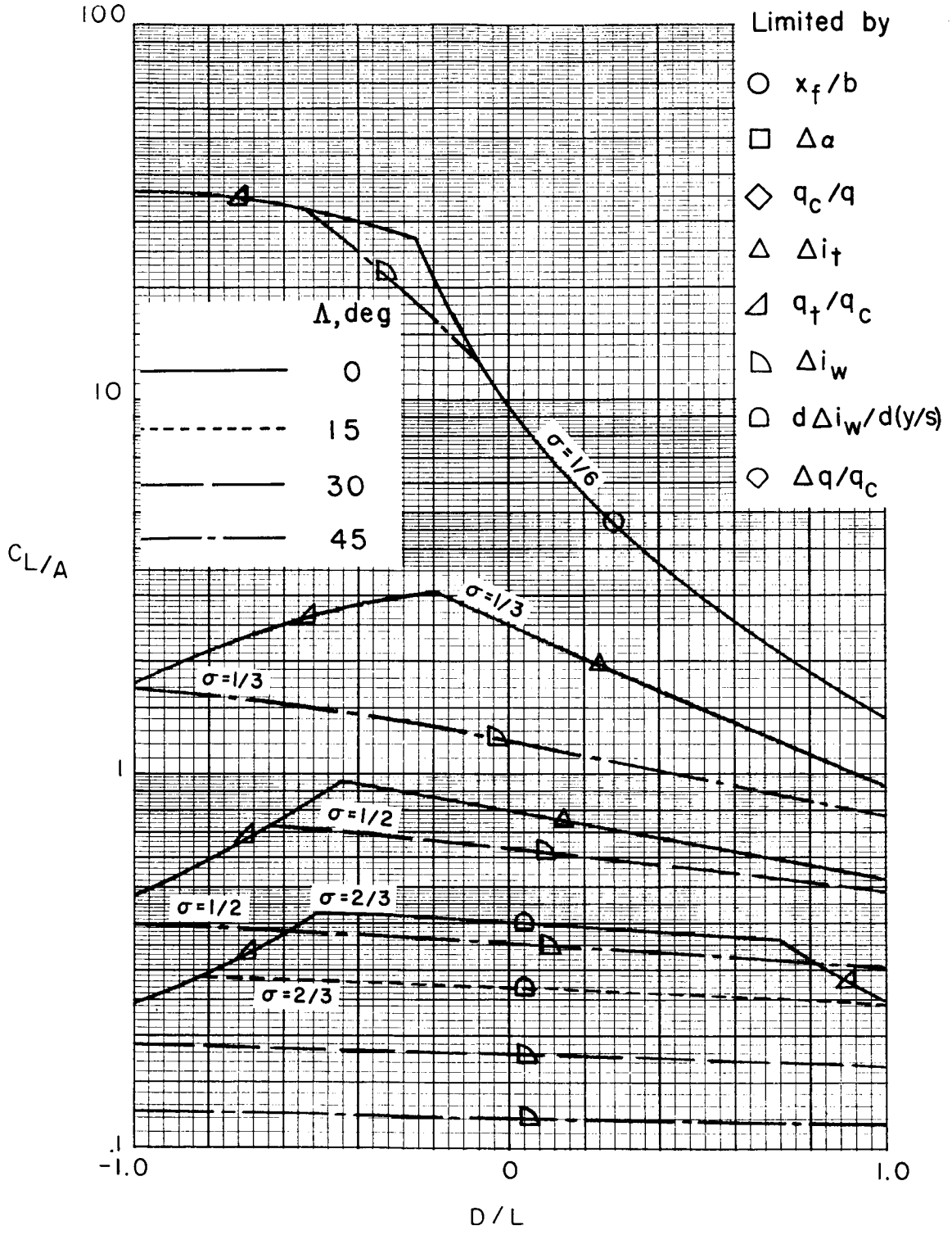


(d) $\gamma = 1.5$.

Figure 73.- Continued.

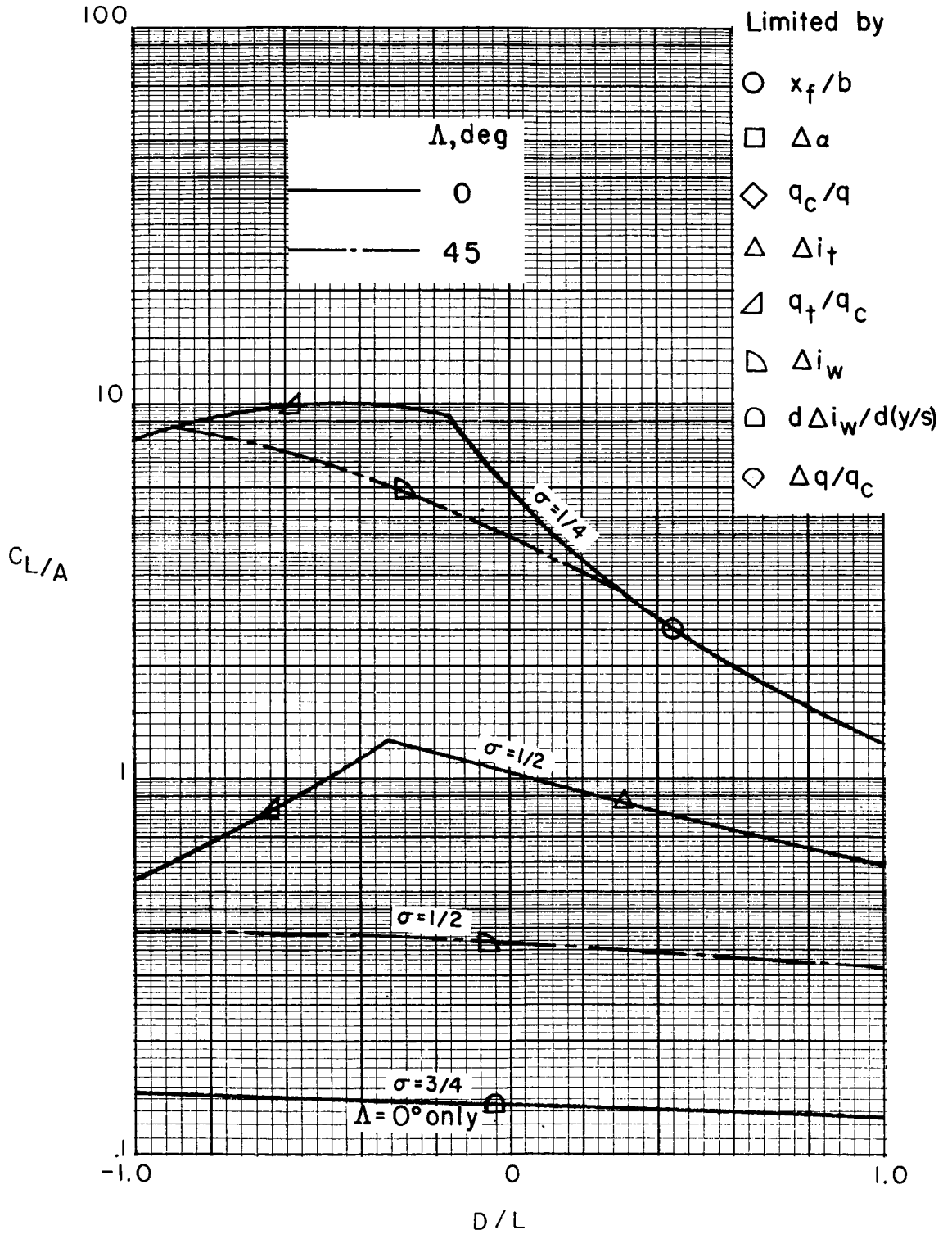


(e) $\gamma = 4/3$.

Figure 73.- Continued.

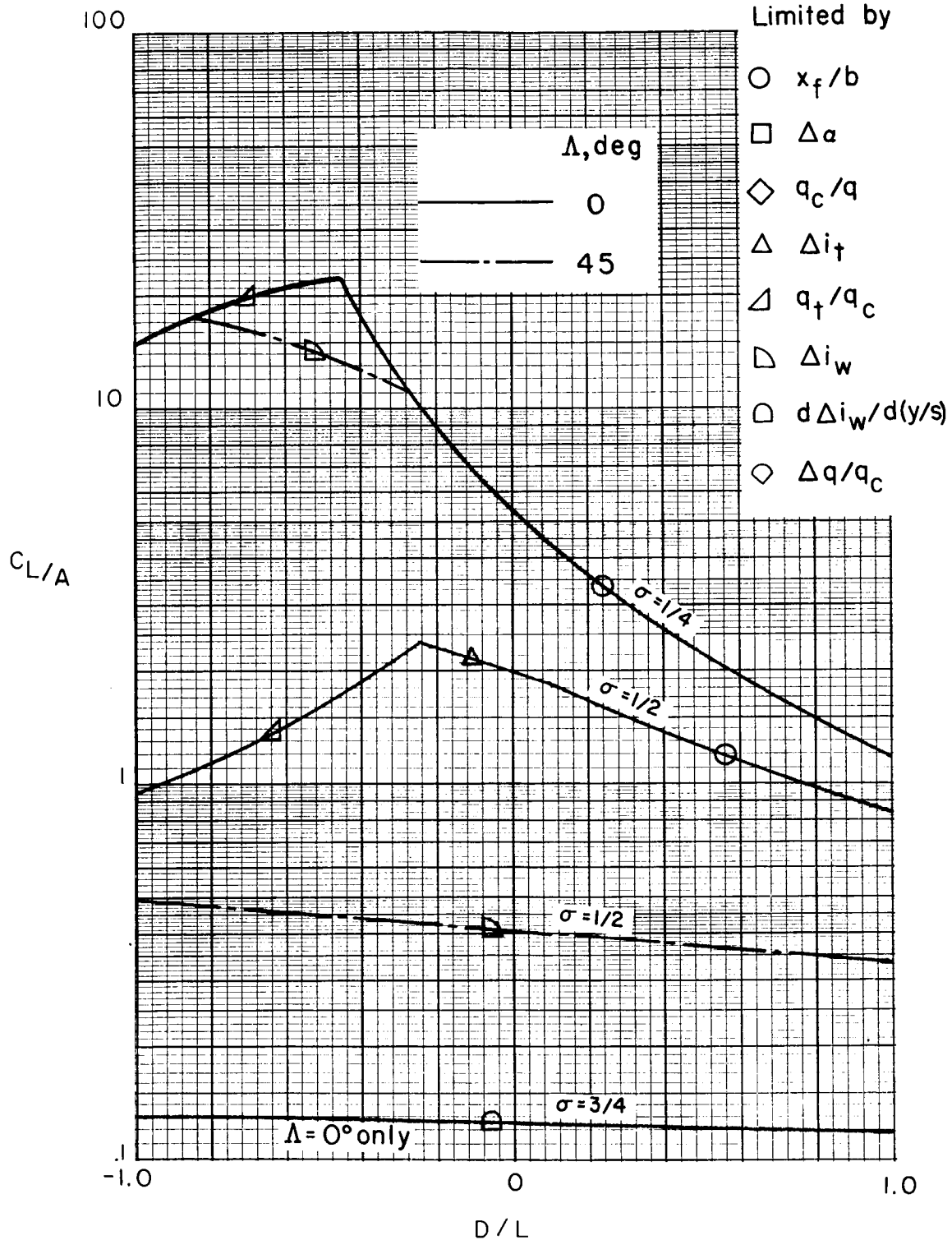


(f) $\gamma = 1$.

Figure 73.- Continued.

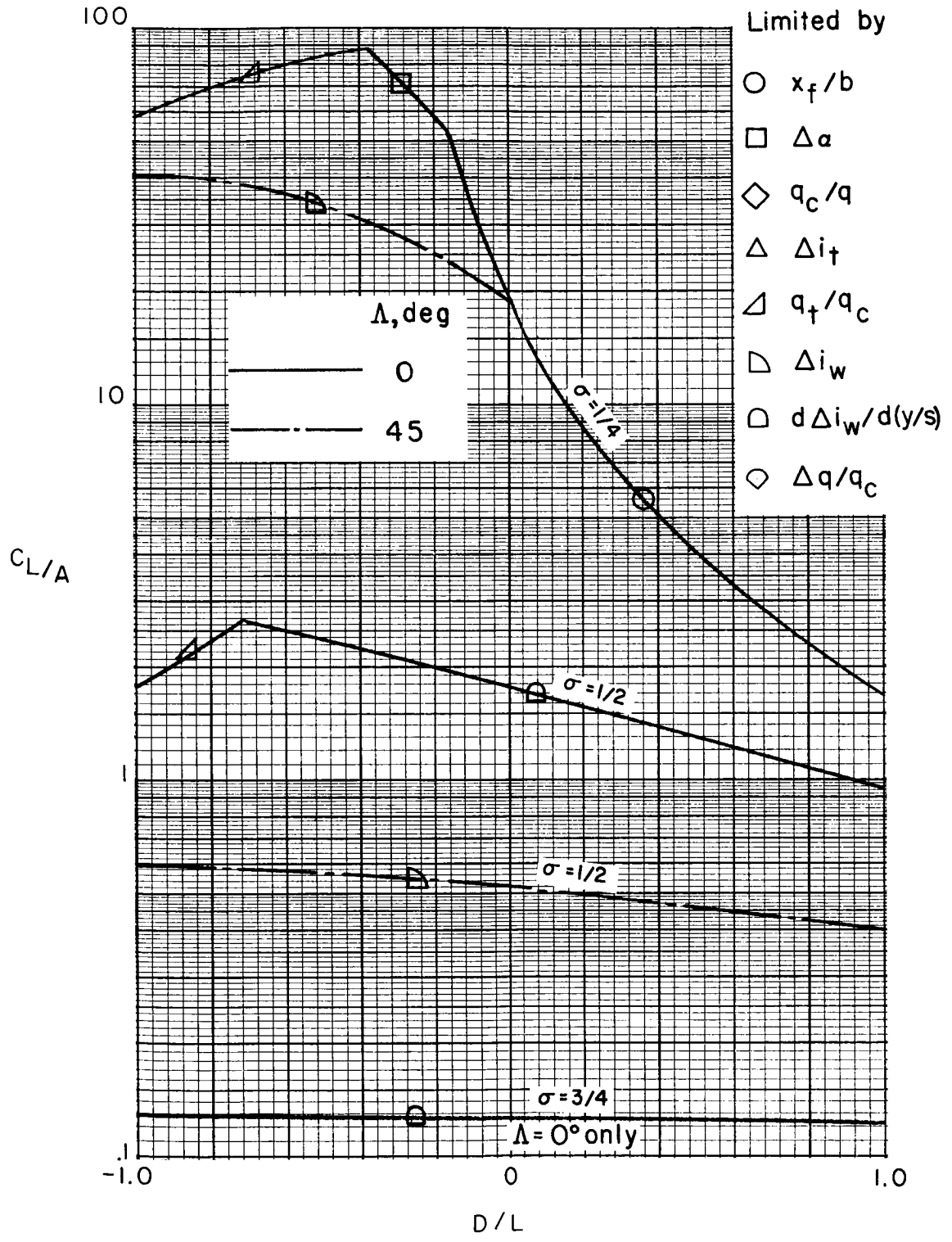


(g) $\gamma = 2/3$.

Figure 73.- Continued.

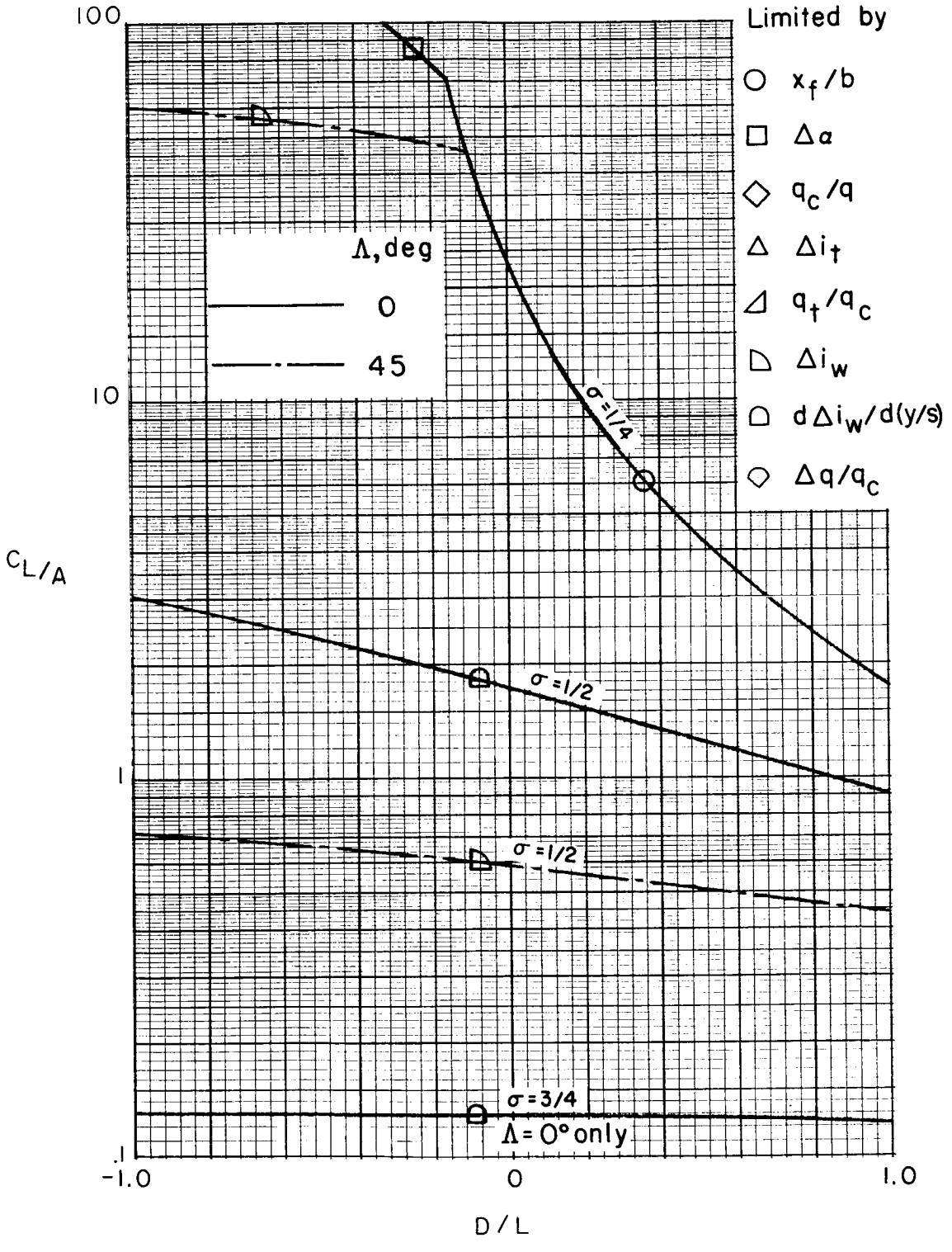


(h) $\gamma = 1/2$.

Figure 73.- Concluded.

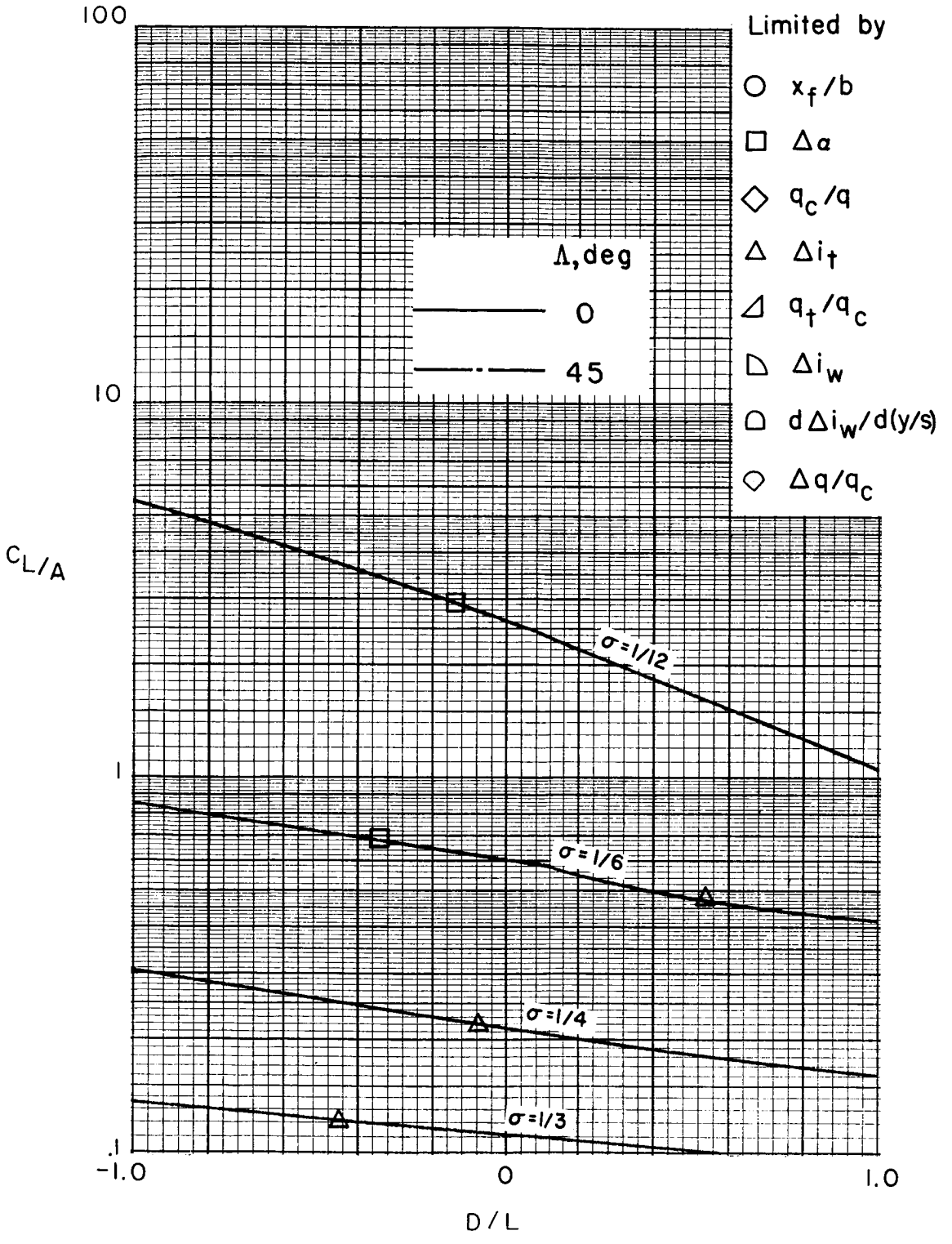


(a) $\gamma = 3$.

Figure 74. Limits of testing in closed tunnels when applying no corrections. (See table II(c).)

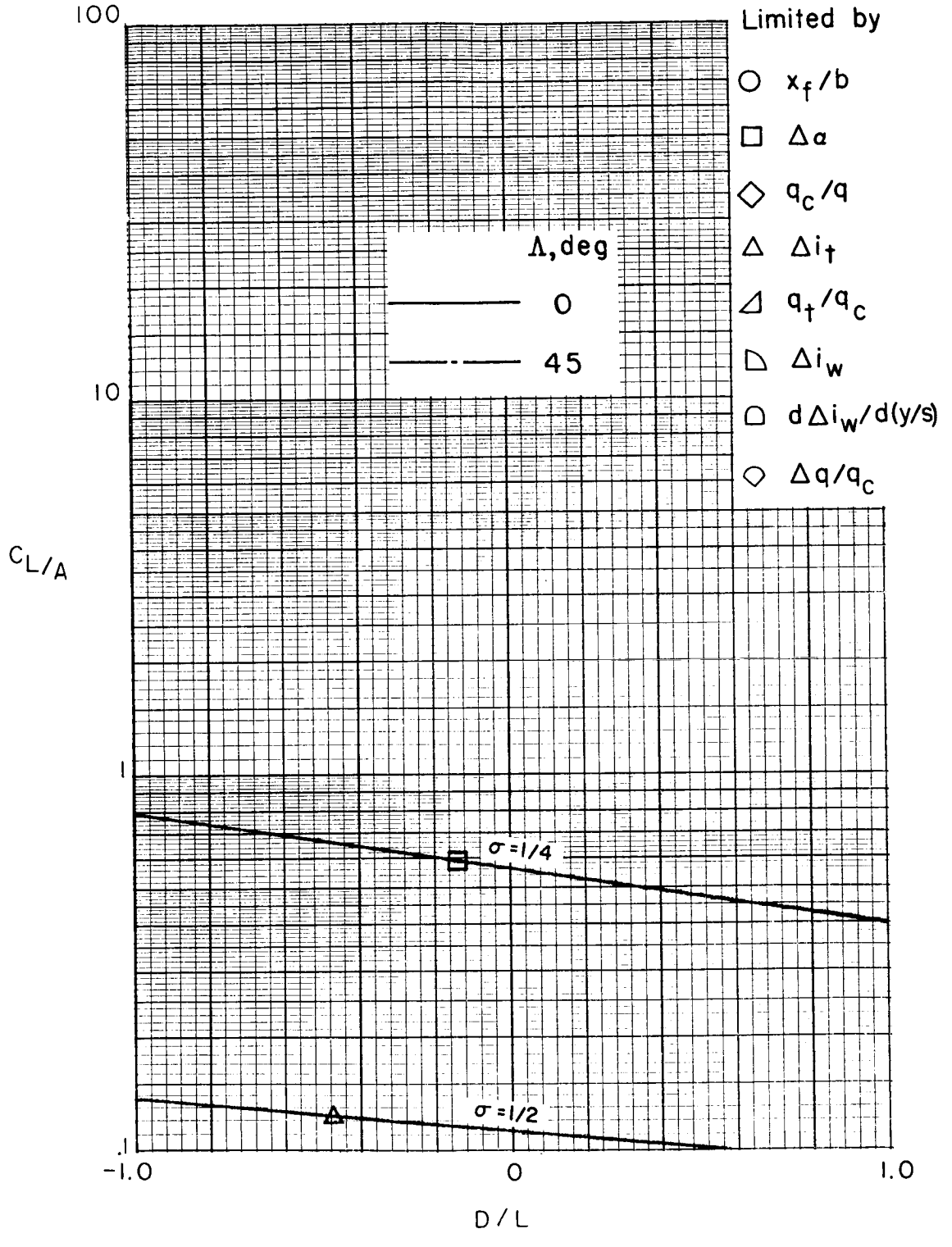


(b) $\gamma = 2$.

Figure 74.- Continued.

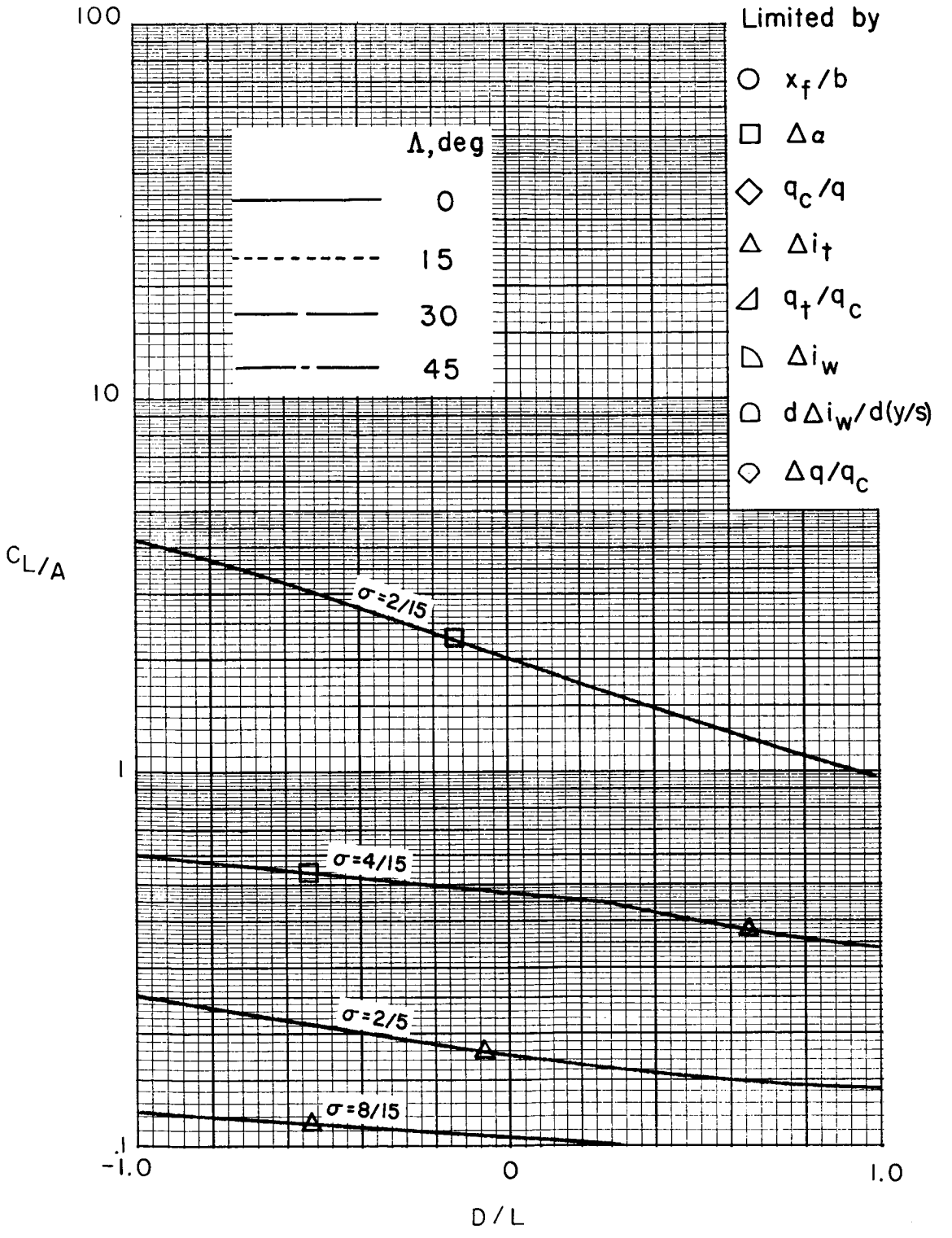


(c) $\gamma = 2$ with semicircular sides.

Figure 74.- Continued.

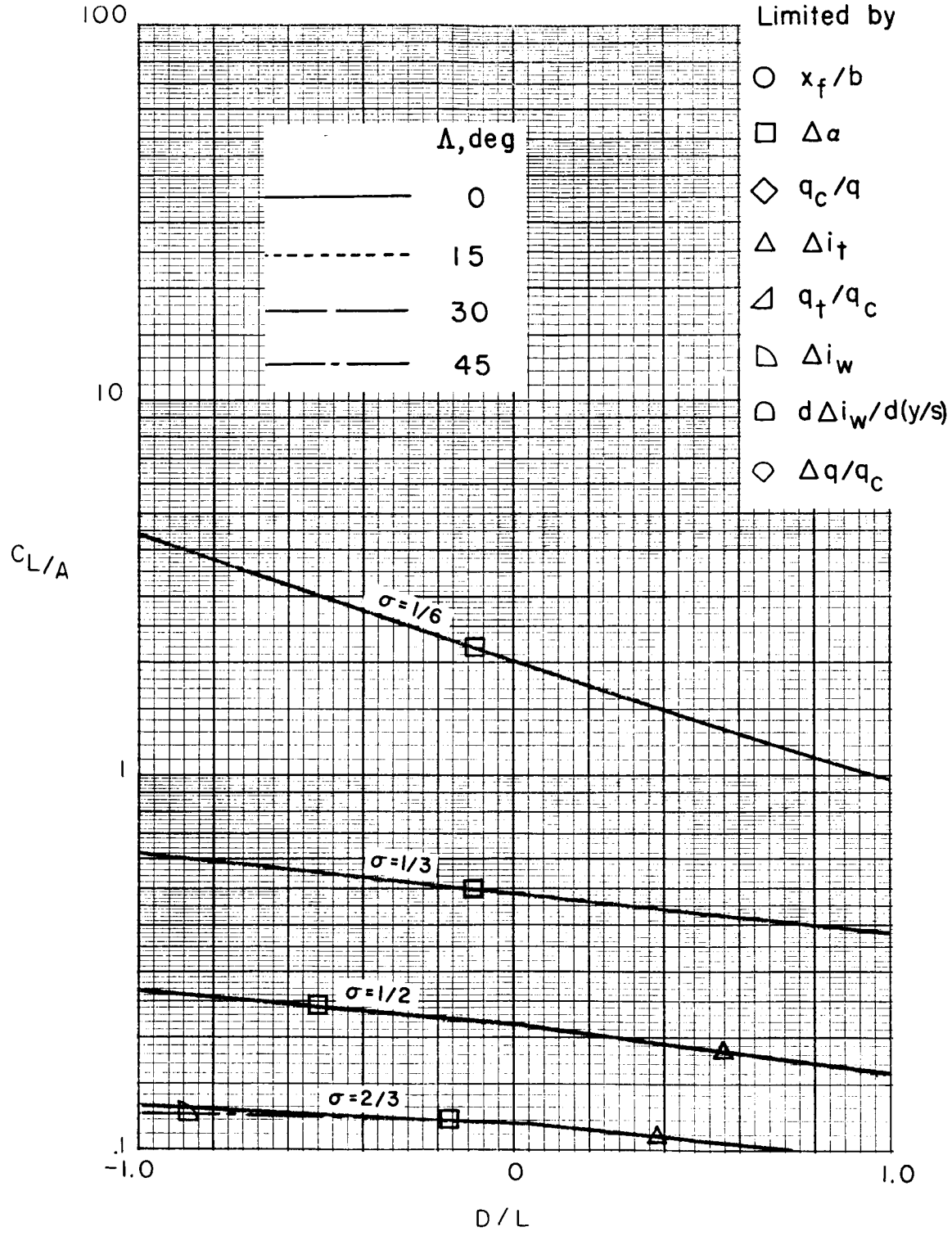


(d) $\gamma = 1.5$.

Figure 74.- Continued.

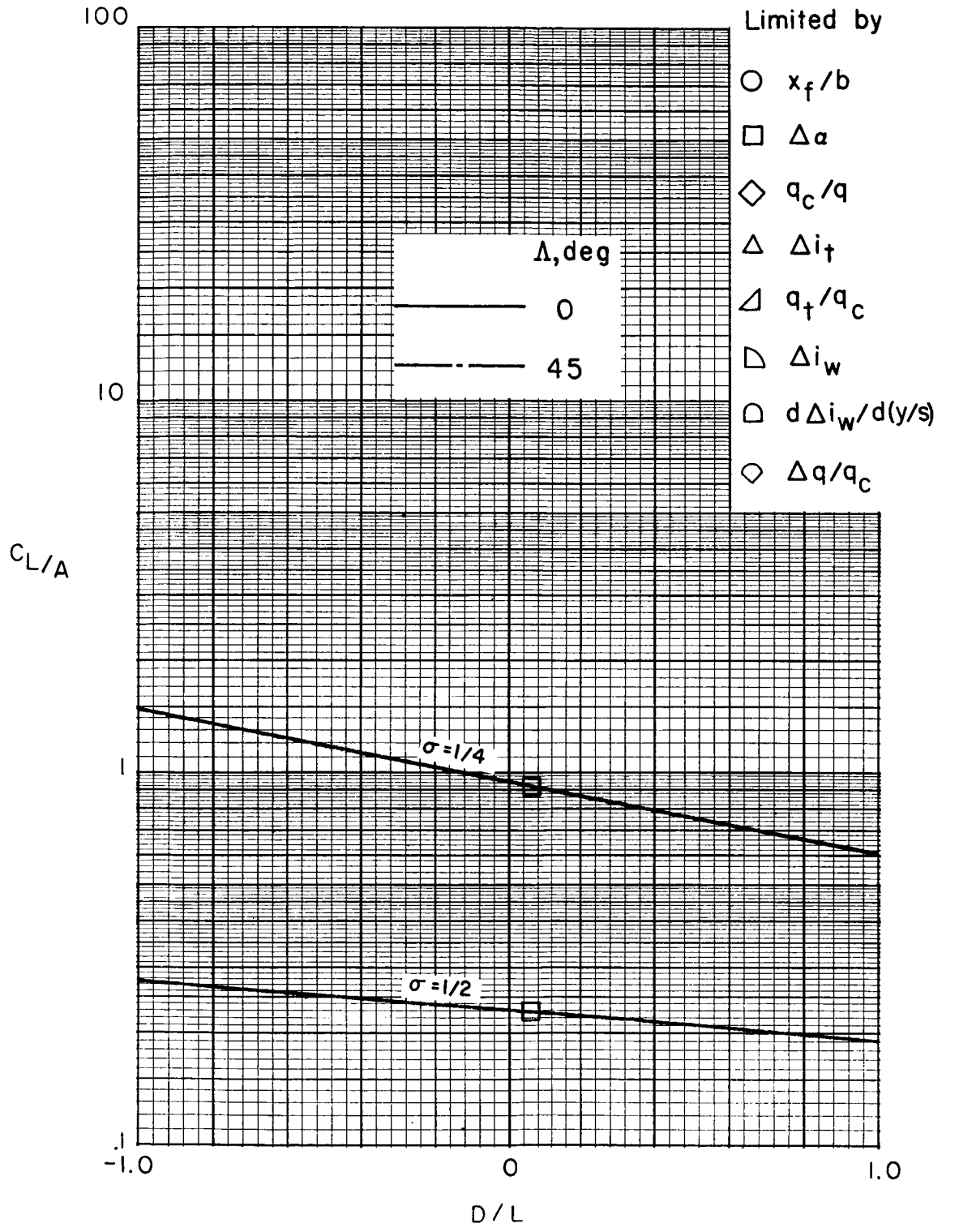


(e) $\gamma = 4/3$.

Figure 74.- Continued.

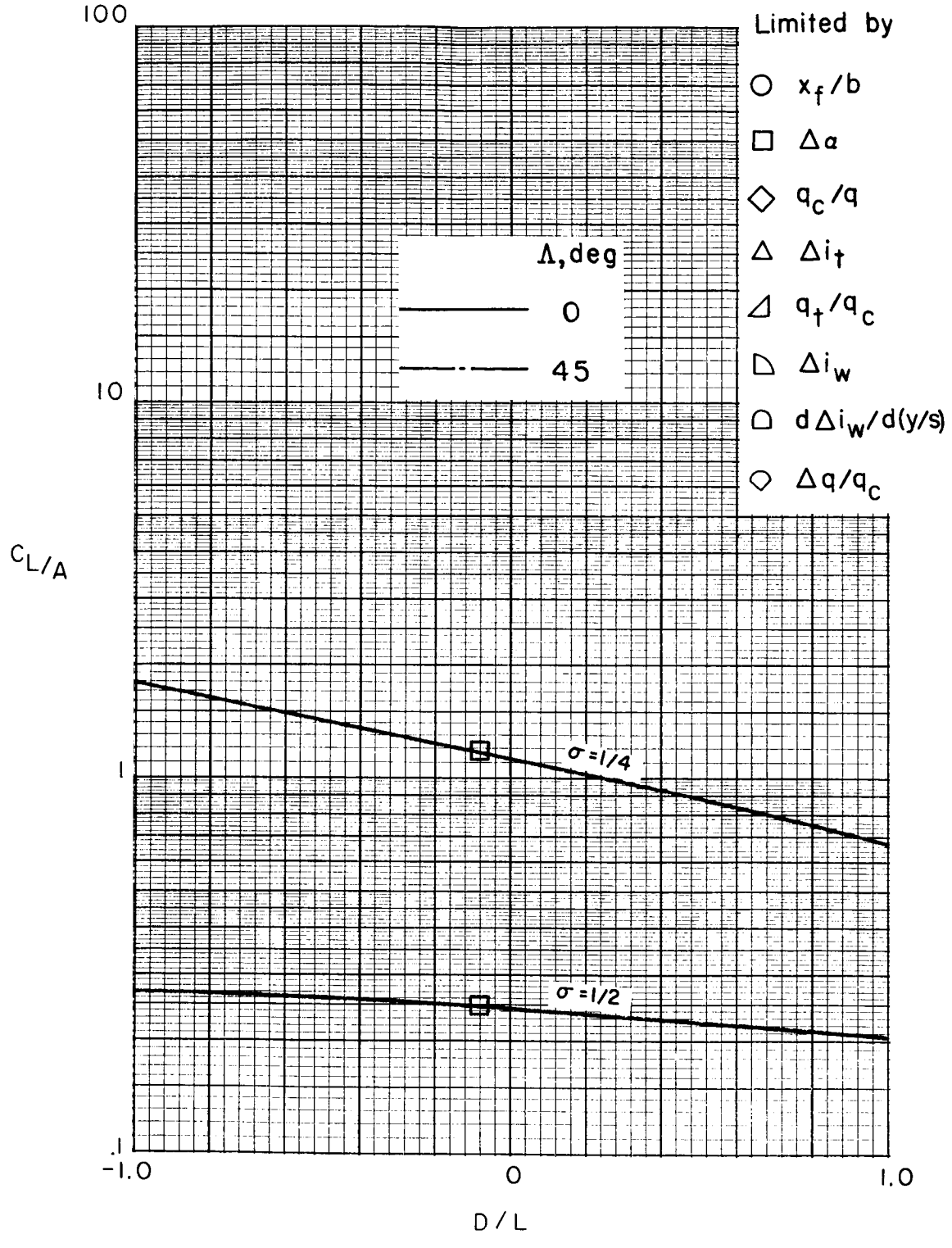


(f) $\gamma = 1$.

Figure 74.- Continued.

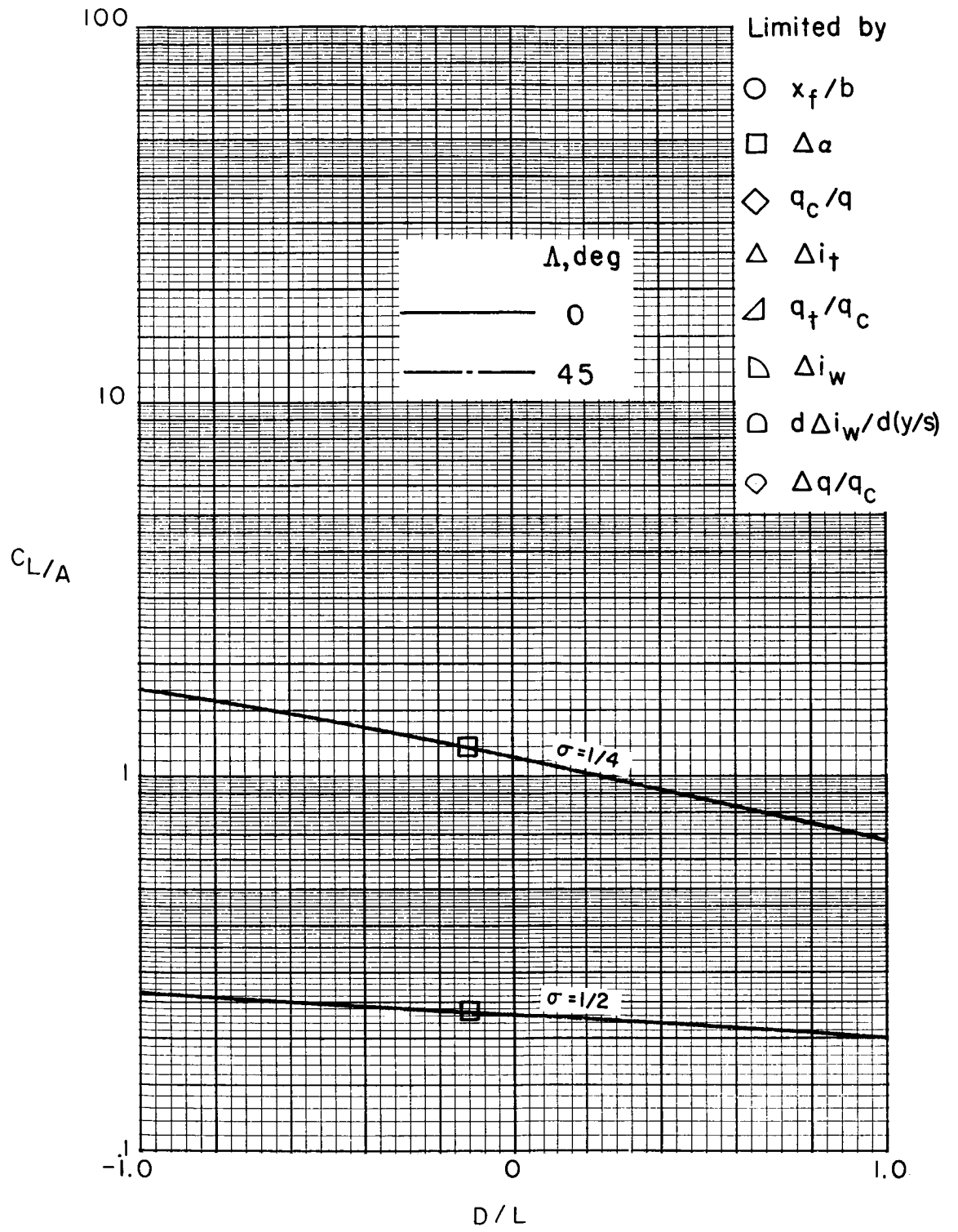


(g) $\gamma = 2/3$.

Figure 74.- Continued.

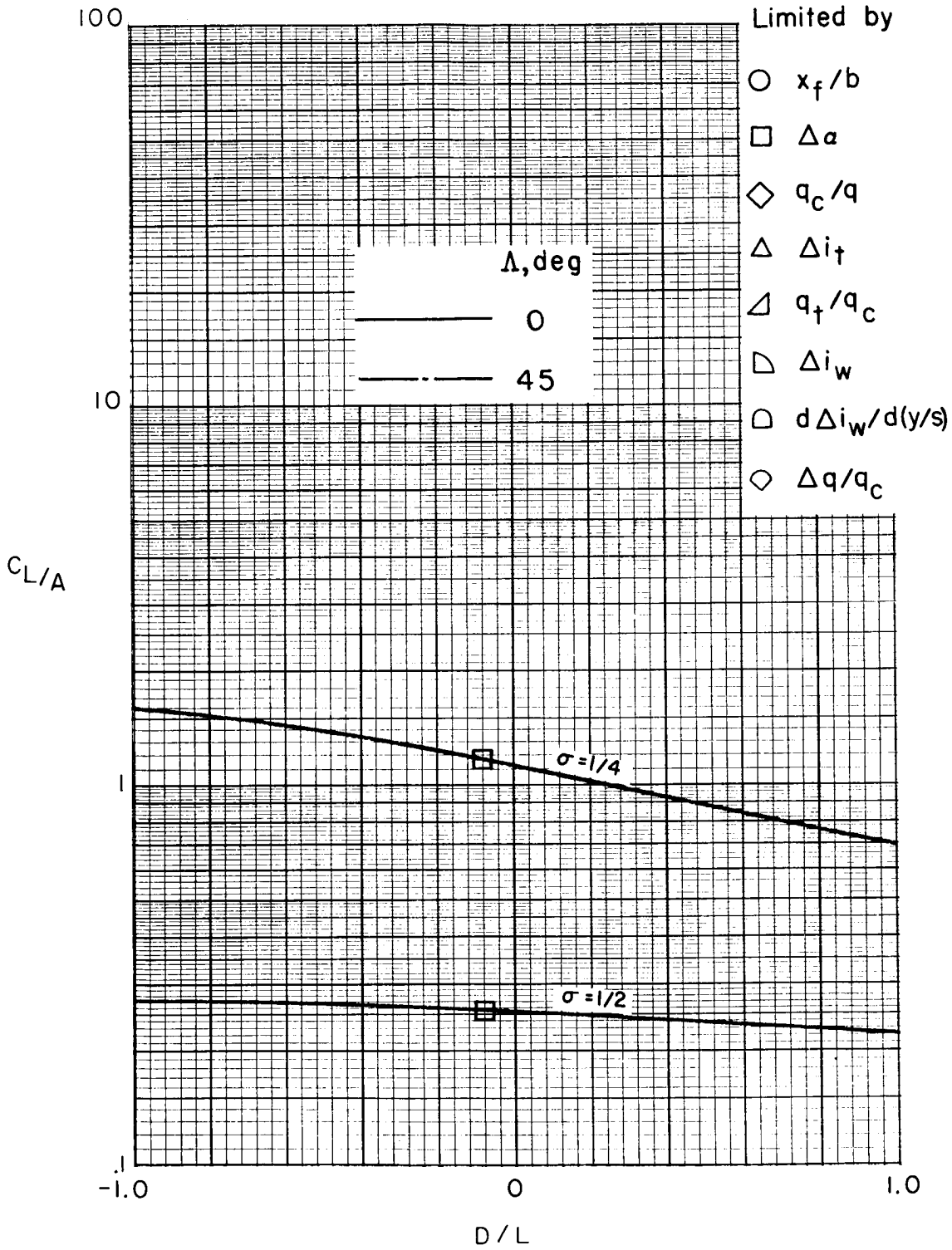


(h) $\gamma = 1/2$.

Figure 74.- Concluded.

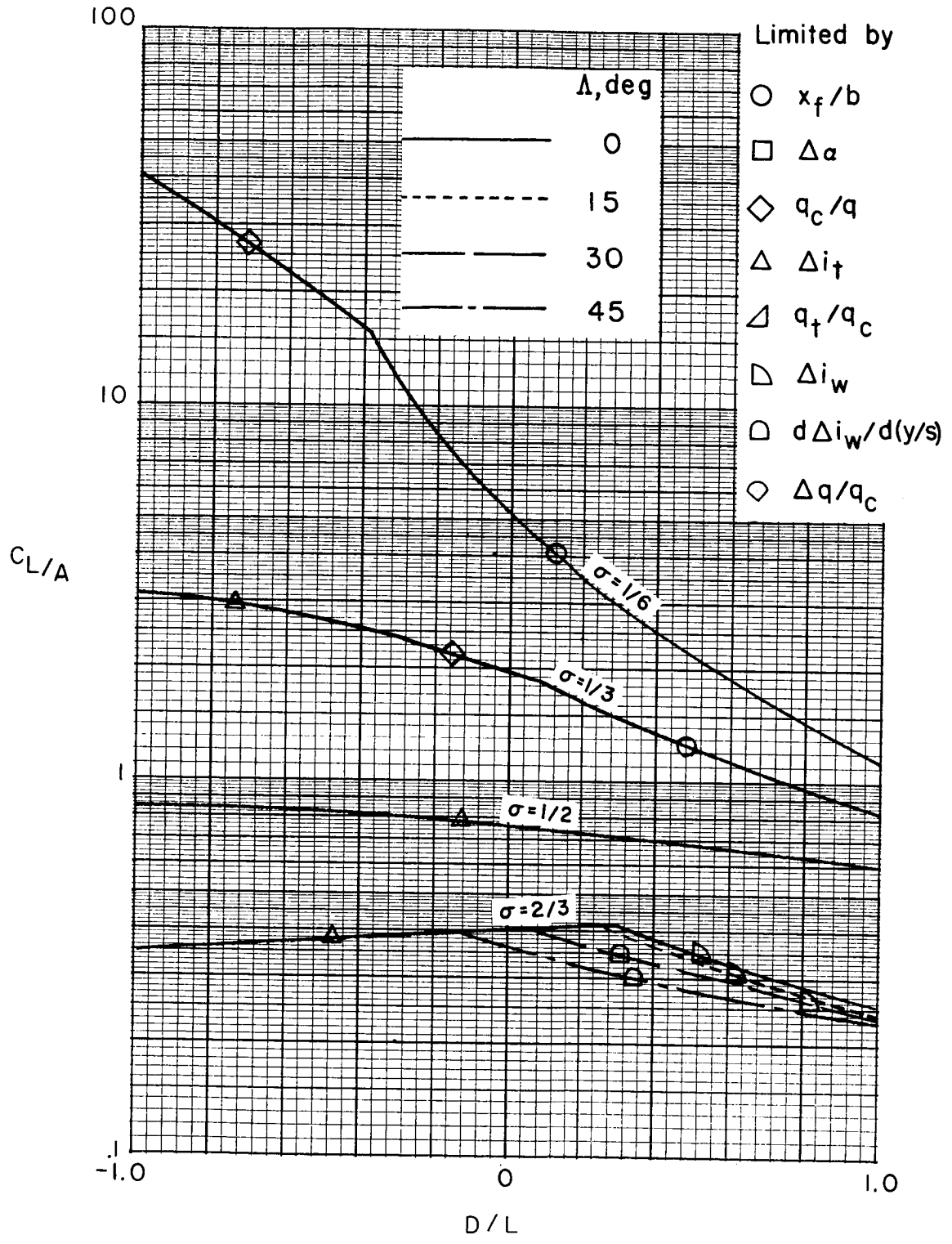


(a) Langley full-scale tunnel (9.1- by 18.3-m or 30- by 60-ft) with ground board.

Figure 75.- Limits of testing in tunnels closed only on the bottom when the maximum practical corrections are applied. (See table II(a).)

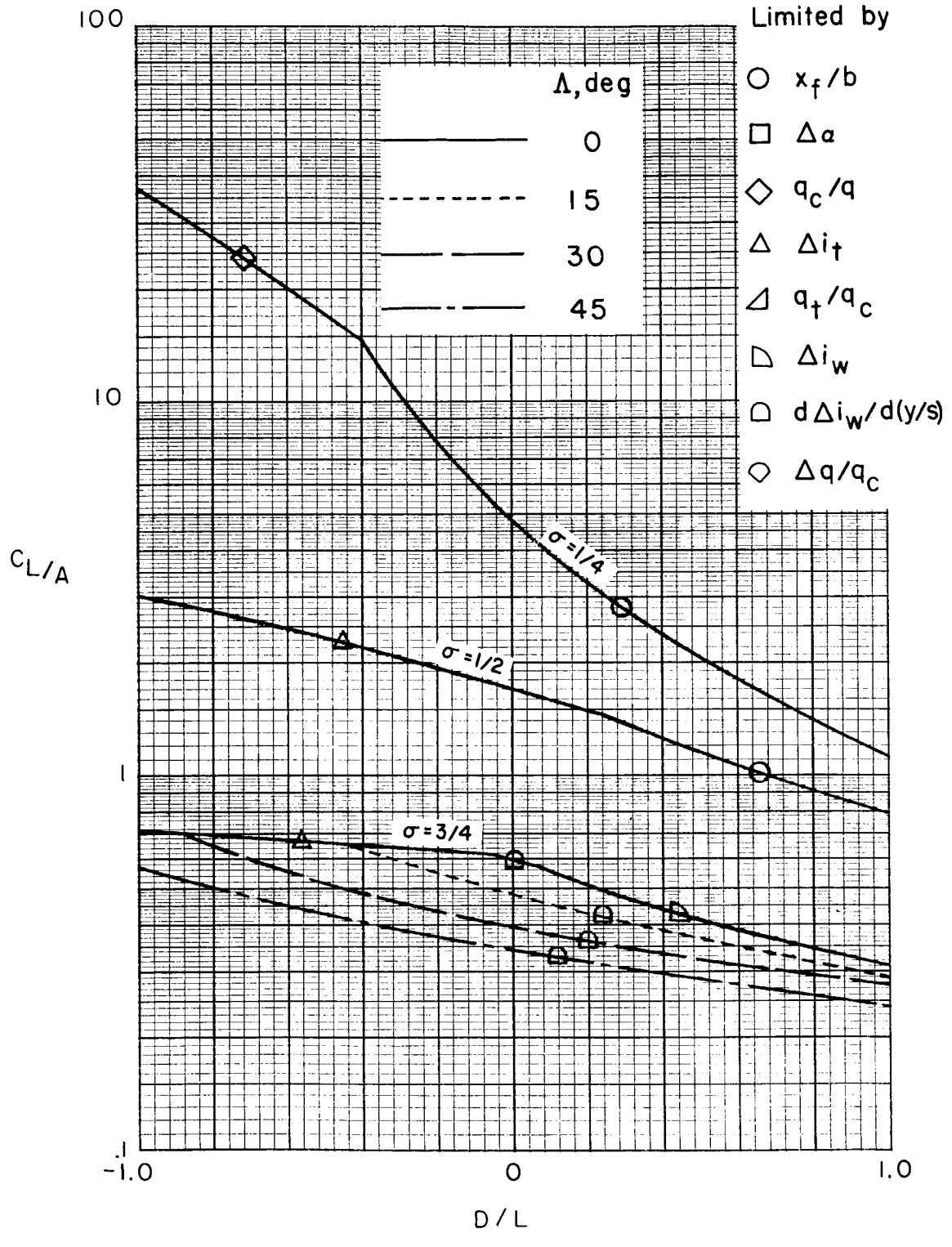


(b) $\gamma = 1.5$.

Figure 75.- Concluded.

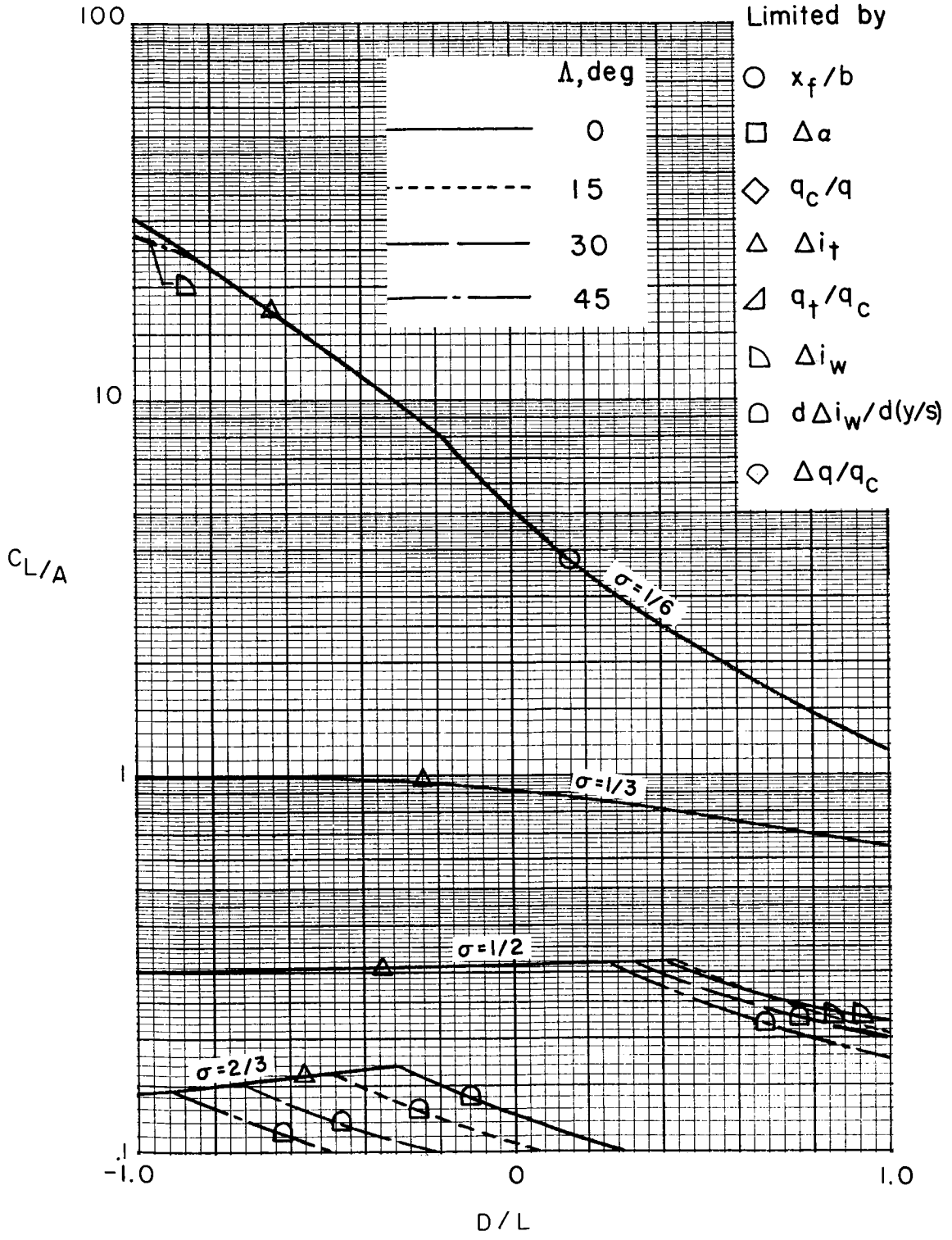


(a) Langley full-scale tunnel (9.1- by 18.3-m or 30- by 60-ft) with ground board.

Figure 76.- Limits of testing in tunnels closed only on the bottom when moderate corrections are applied. (See table II(b).)

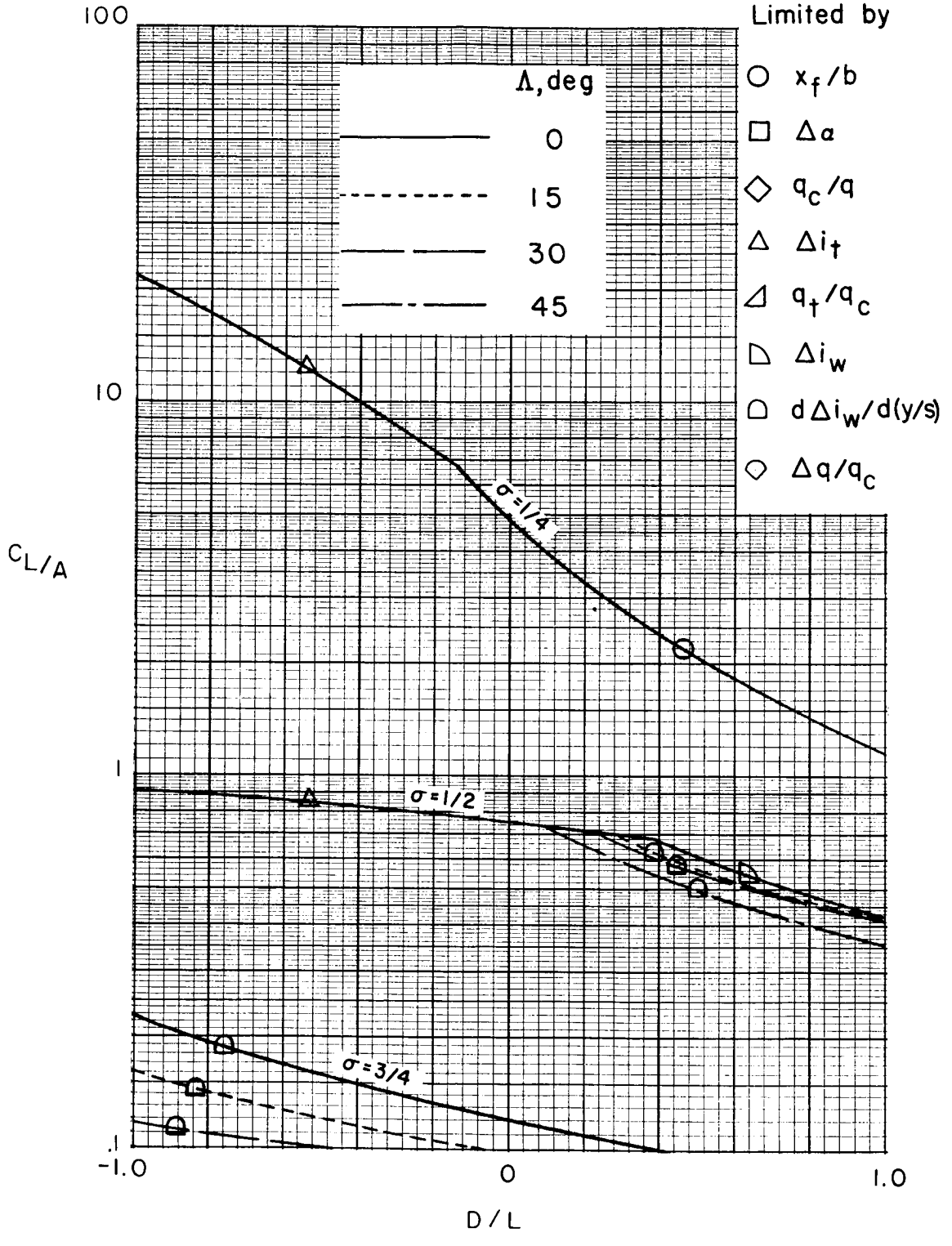


(b) $\gamma = 1.5$.

Figure 76.- Concluded.

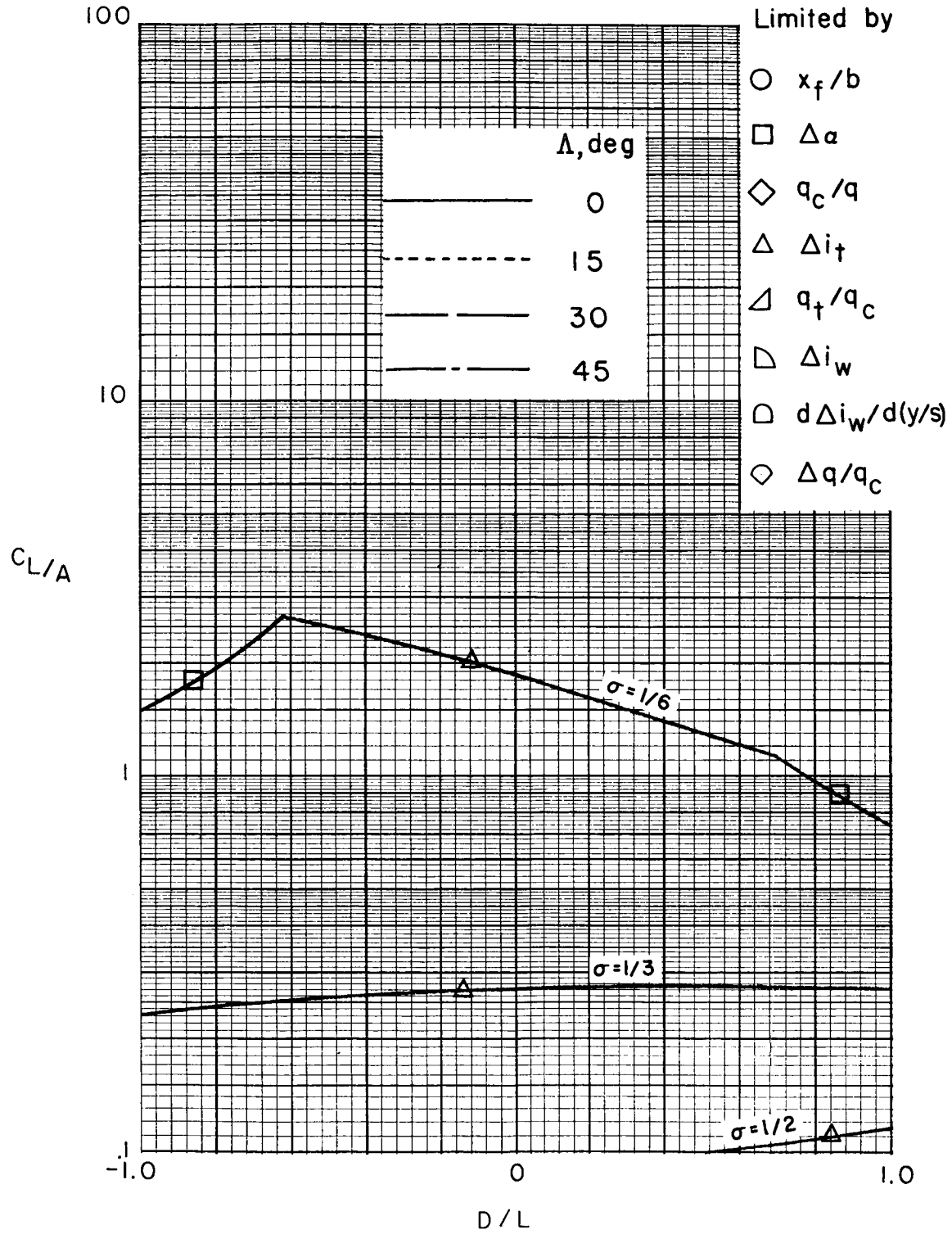


(a) Langley full-scale tunnel (9.1- by 18.3-m or 30- by 60-ft) with ground board.

Figure 77.- Limits of testing in tunnels closed only on the bottom when no corrections are applied. (See table II(c).)

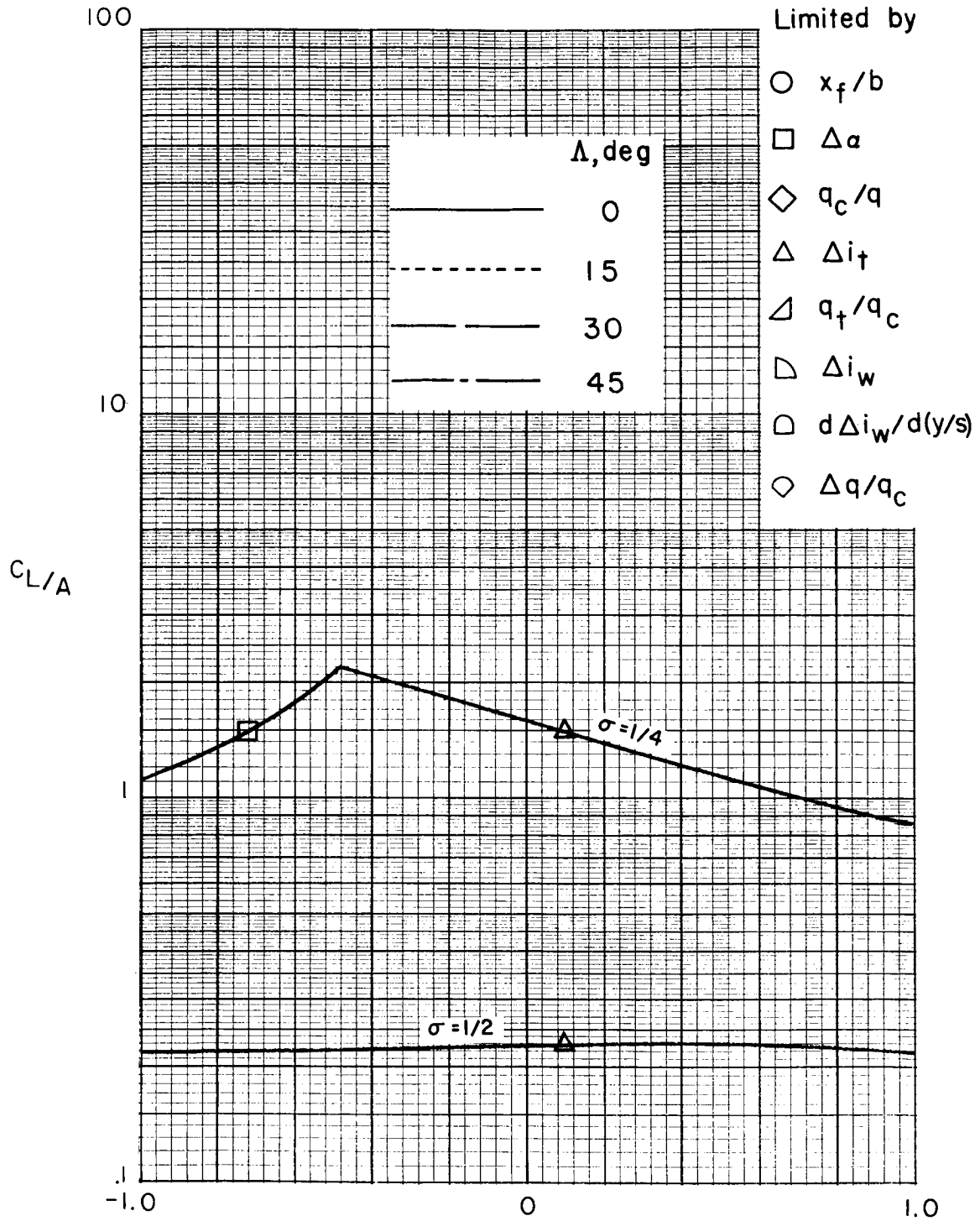


(b) $\gamma = 1.5$.

Figure 77.- Concluded.

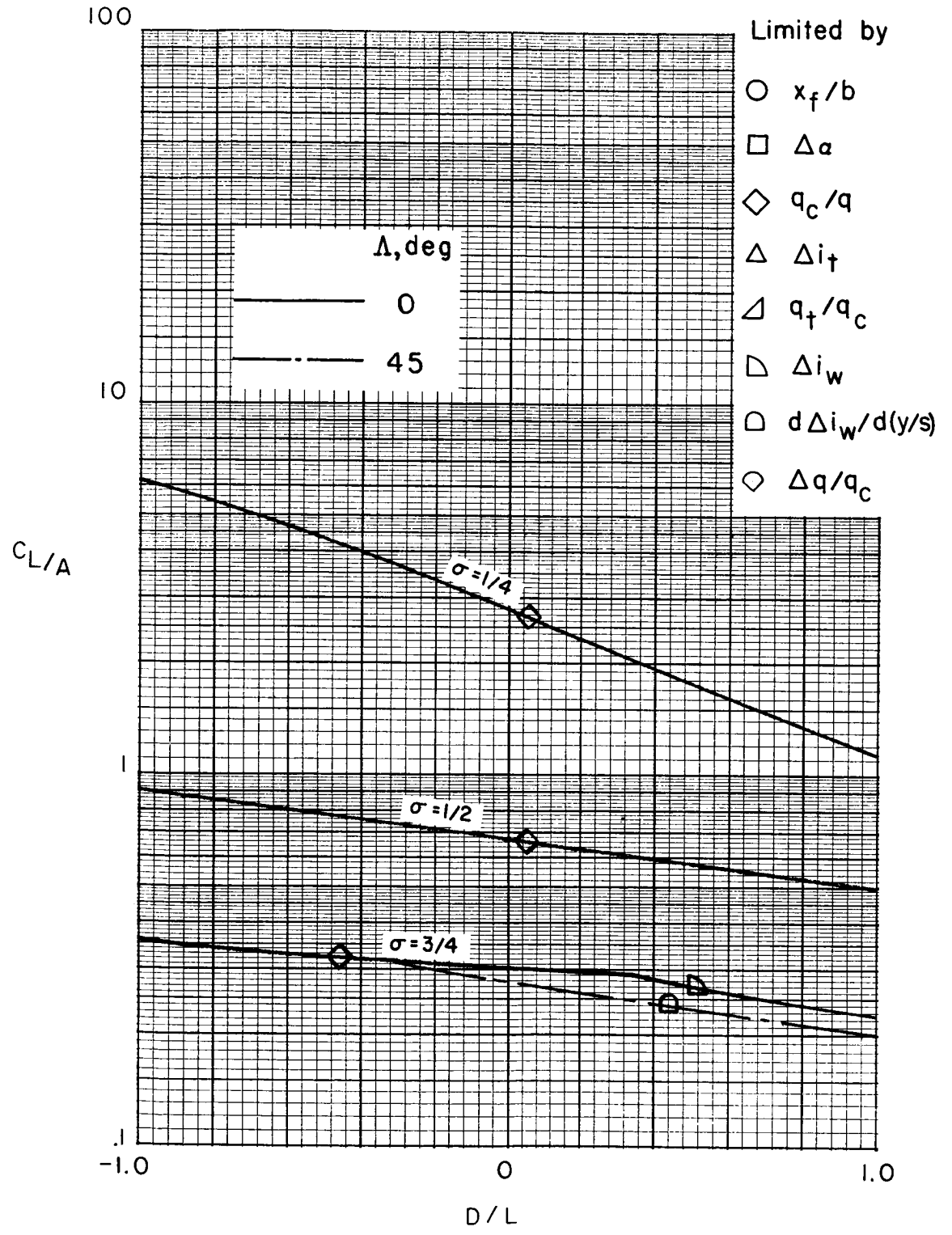


(a) Model height to maintain $\Delta w_L = 0$.

Figure 78.- Limits of testing in a closed-on-bottom-only tunnel with variable model height when the maximum practical corrections are applied. (See table II(a).) $\gamma = 1.5$.

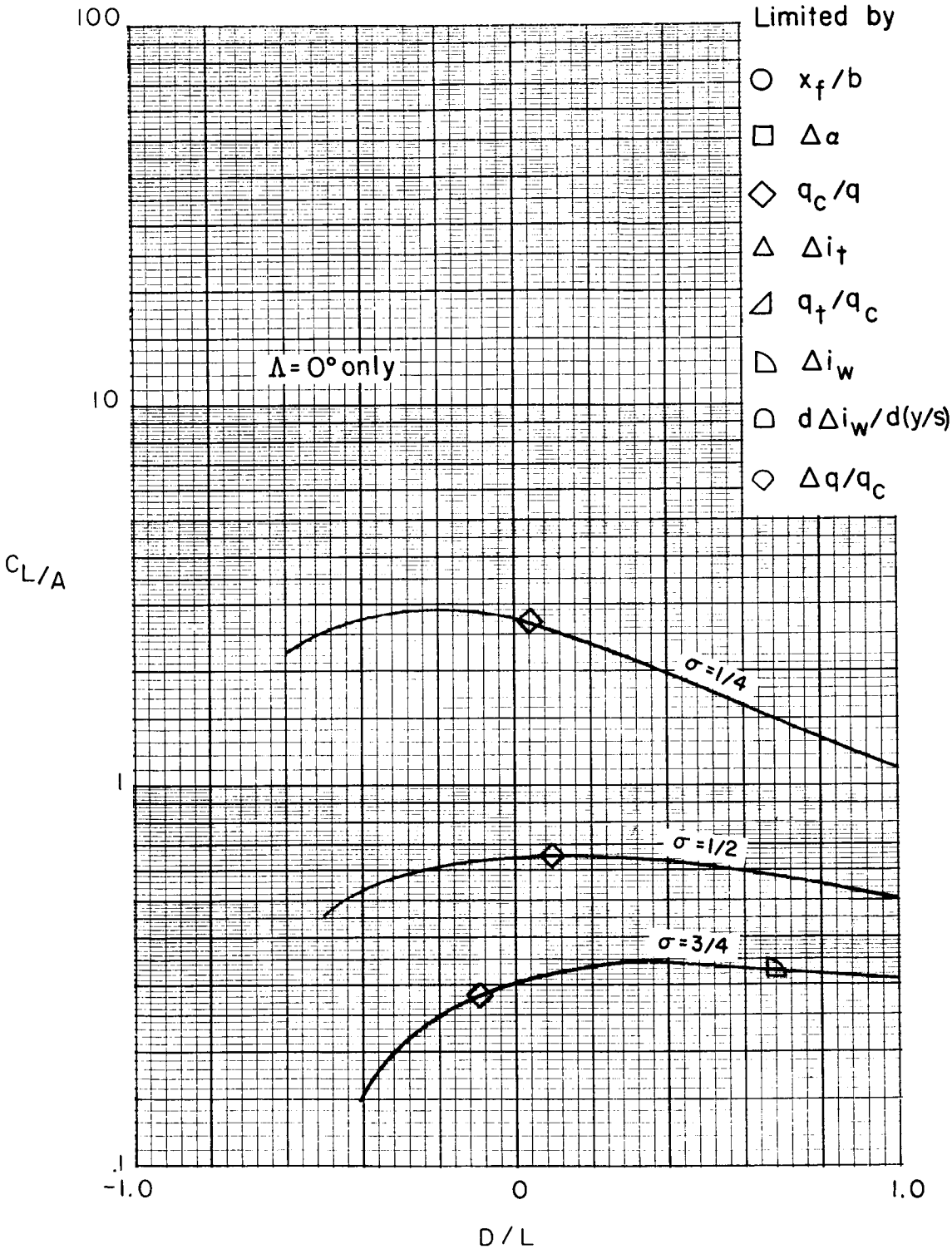


(b) Model height to maintain $\Delta w = 0$.

Figure 78.- Concluded.

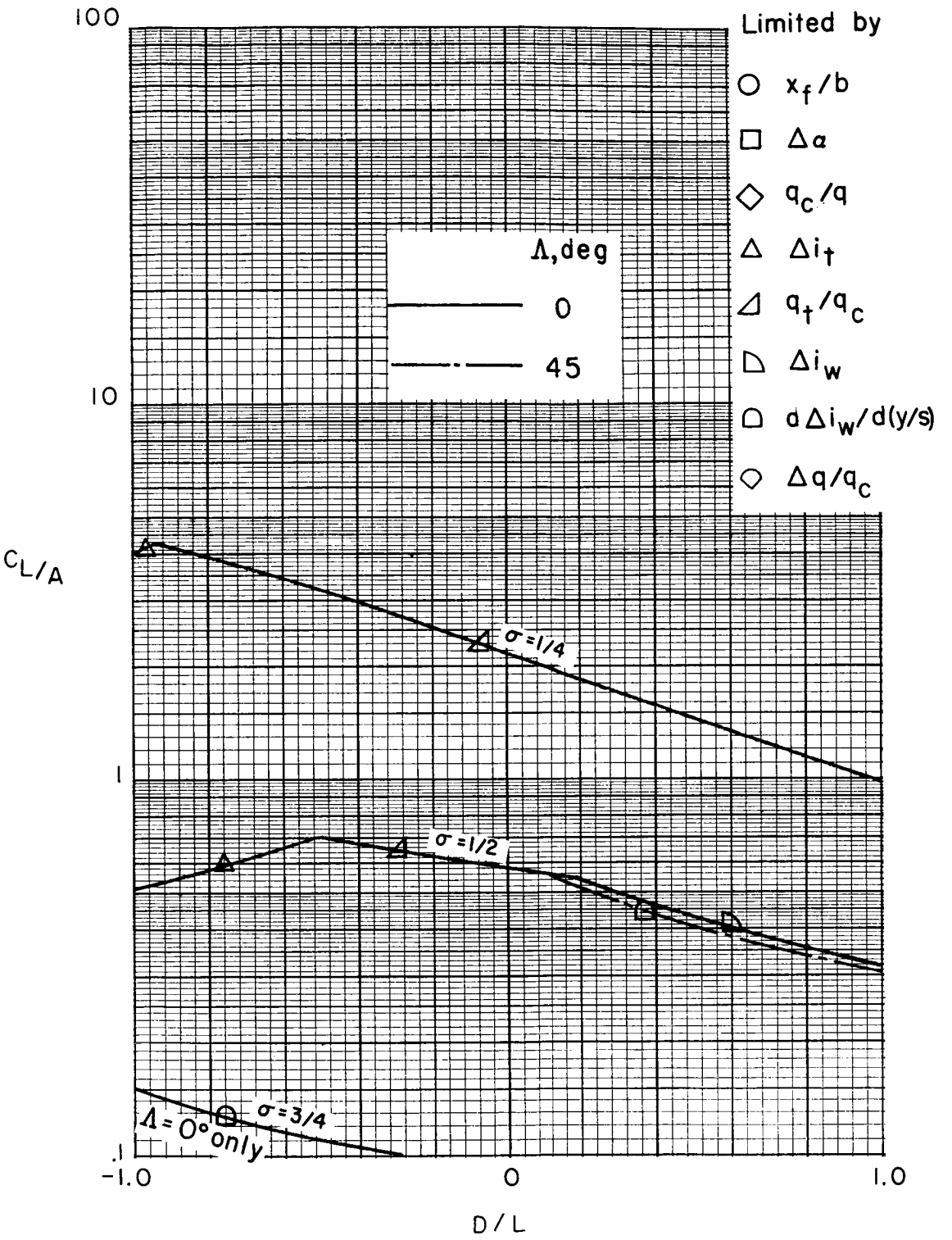


(a) Model height to maintain $\Delta w_L = 0$.

Figure 79.- Limits of testing in a closed-on-bottom-only tunnel with variable model height when moderate corrections are applied. (See table II(b).) $\gamma = 1.5$.

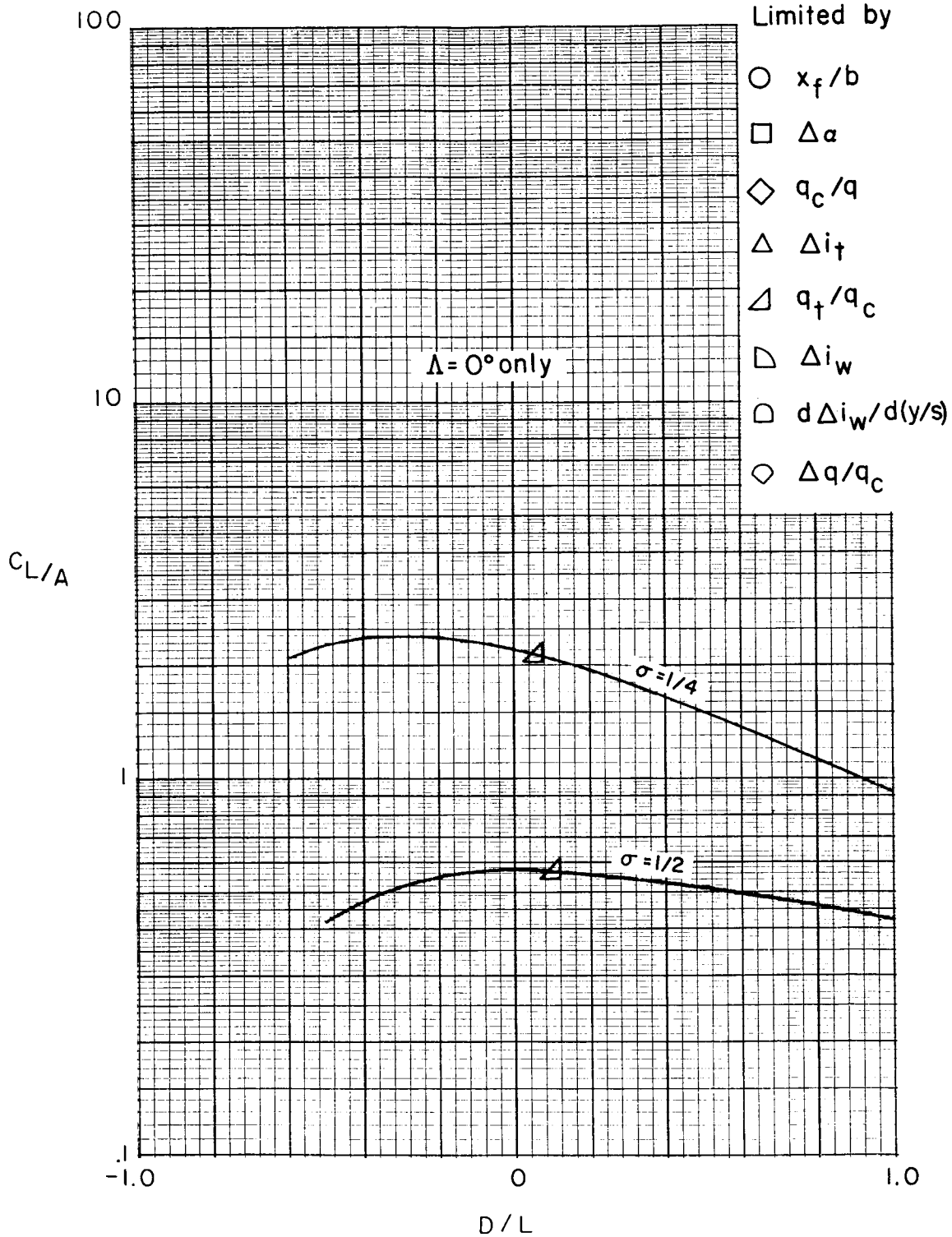


(b) Model height to maintain $\Delta w = 0$.

Figure 79.- Concluded.

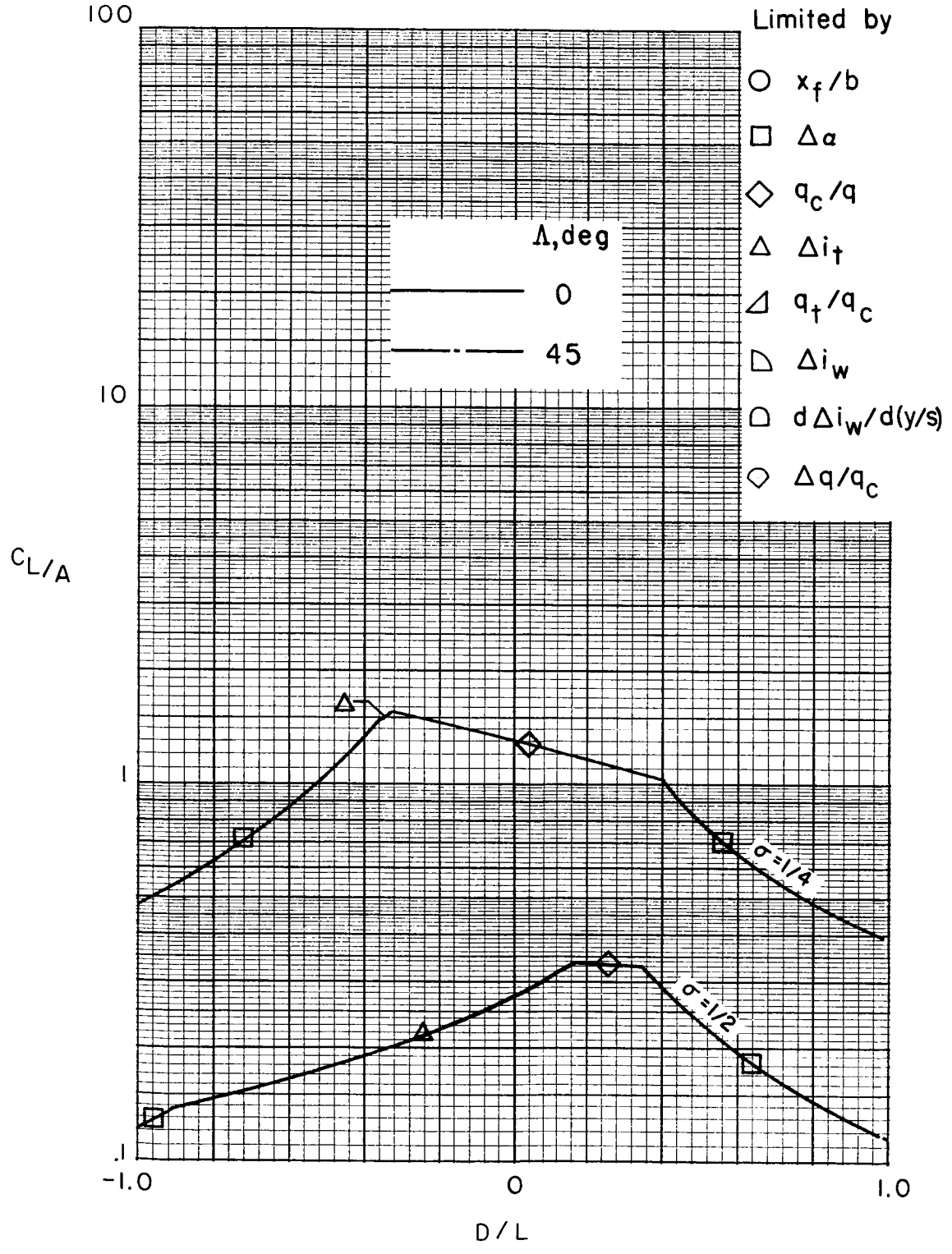


(a) Model height to maintain $\Delta w_L = 0$.

Figure 80.- Limits of testing in a closed-on-bottom-only tunnel with variable model height when no corrections are applied. (See table II(c).) $\gamma = 1.5$.

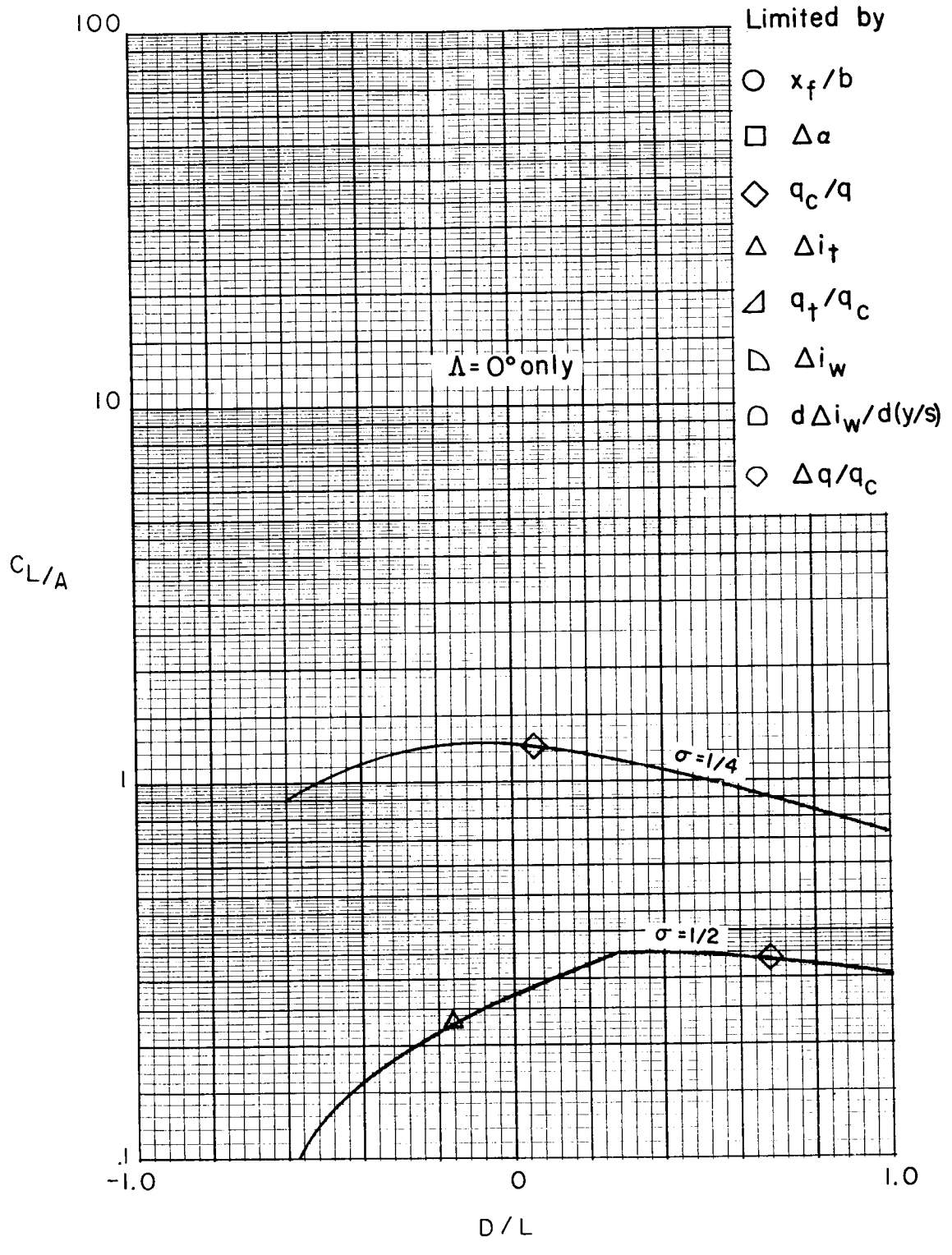


(b) Model height to maintain $\Delta w = 0$.

Figure 80.- Concluded.

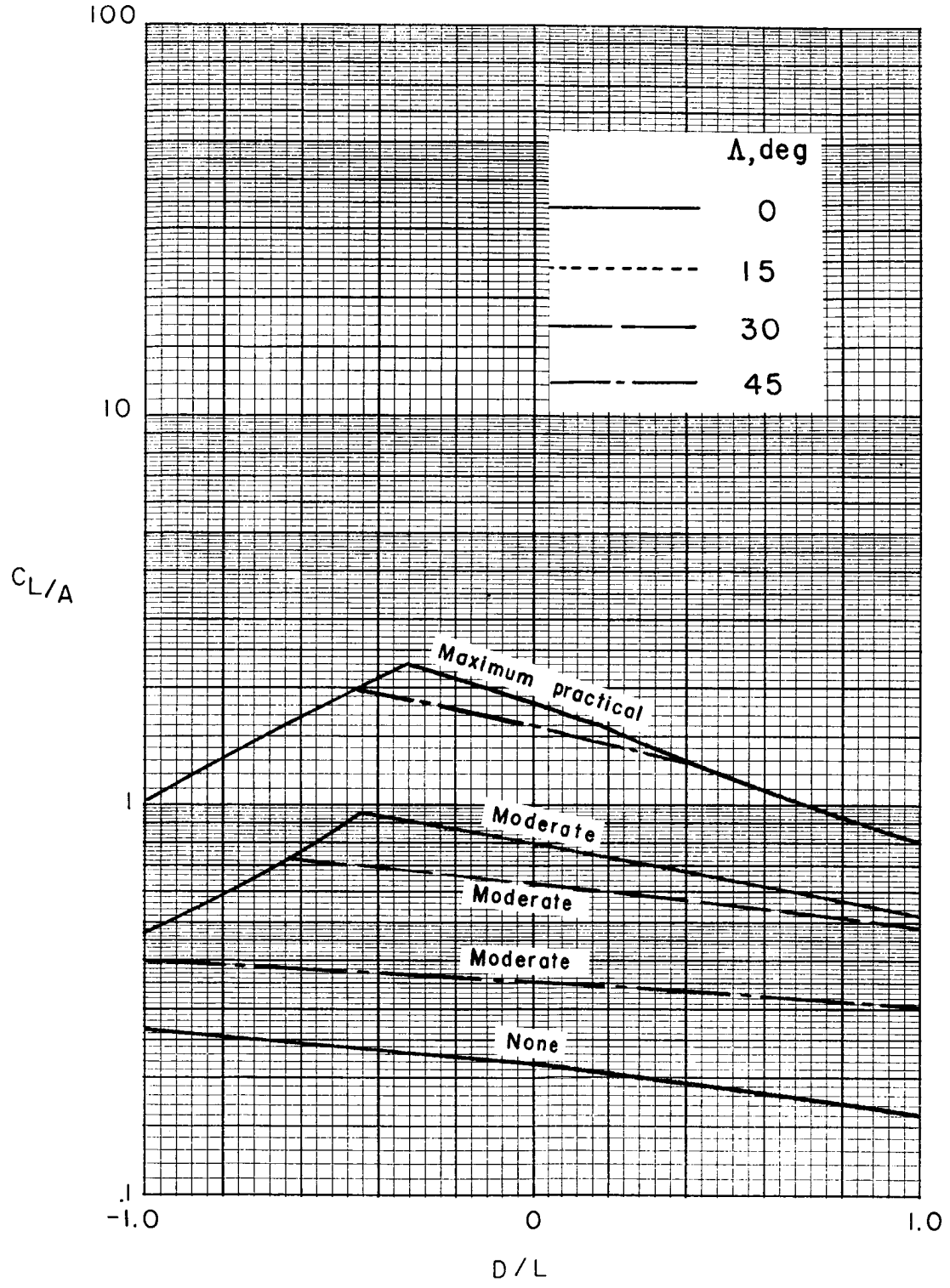


Figure 81.- Effects of corrections on testing limits in a closed rectangular tunnel. $\gamma = 1.5$; $\sigma = 1/2$.

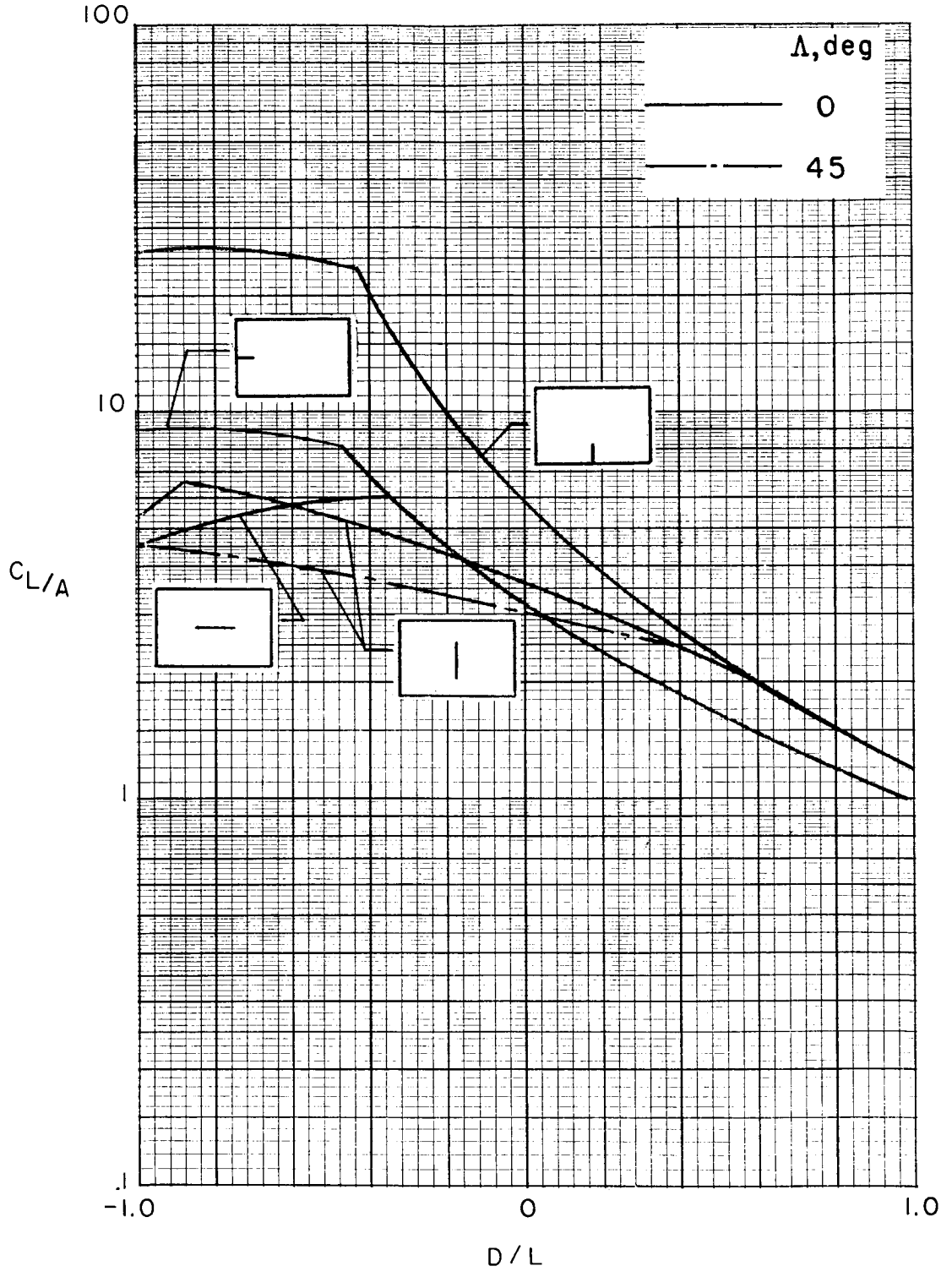


(a) Full span of 1 meter.

Figure 82.- Effect of model mounting on testing limits in a 2- by 3-meter closed tunnel when the maximum practical corrections are applied.

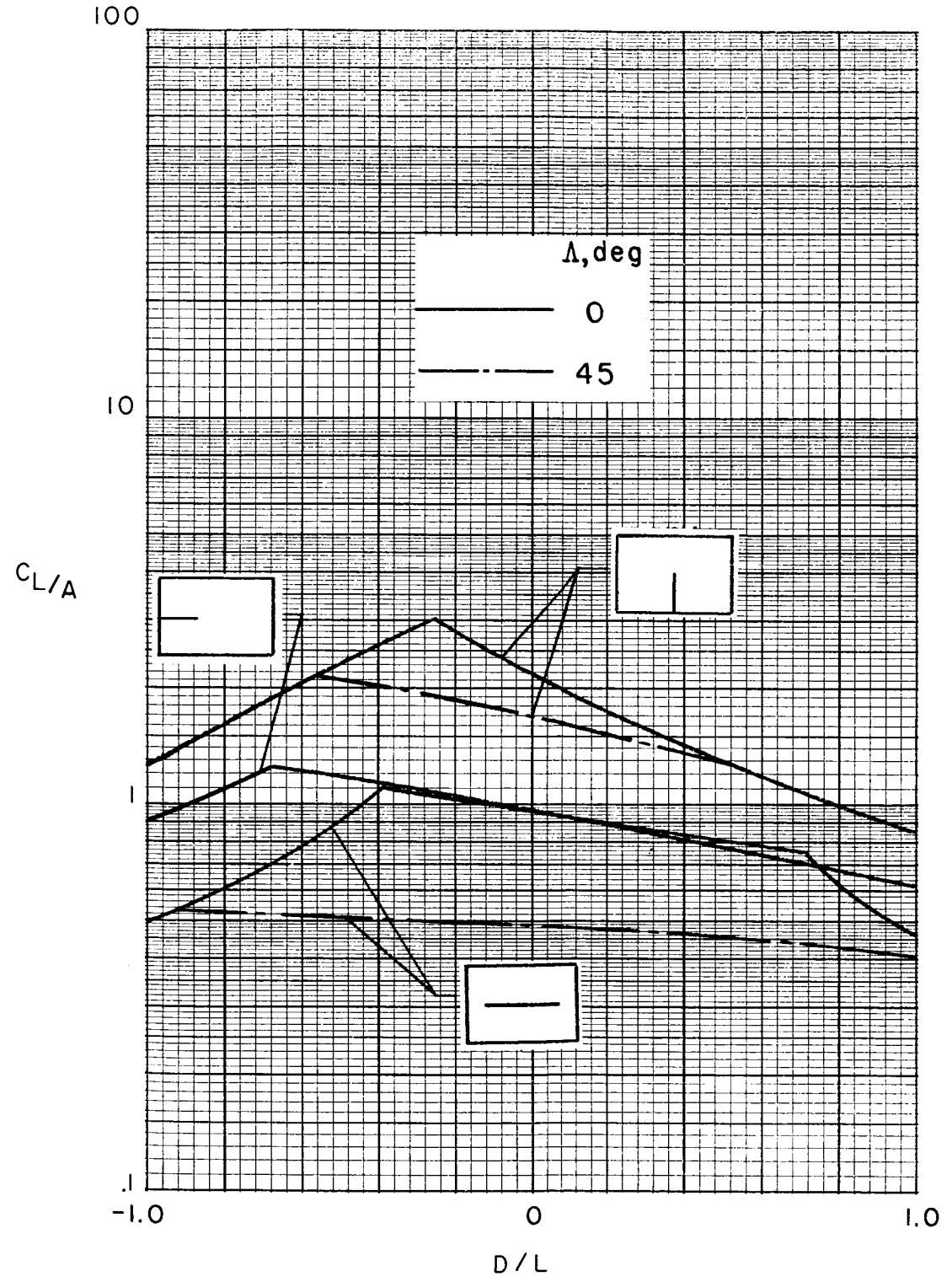


(b) Full span of 2 meters.

Figure 82.- Continued.

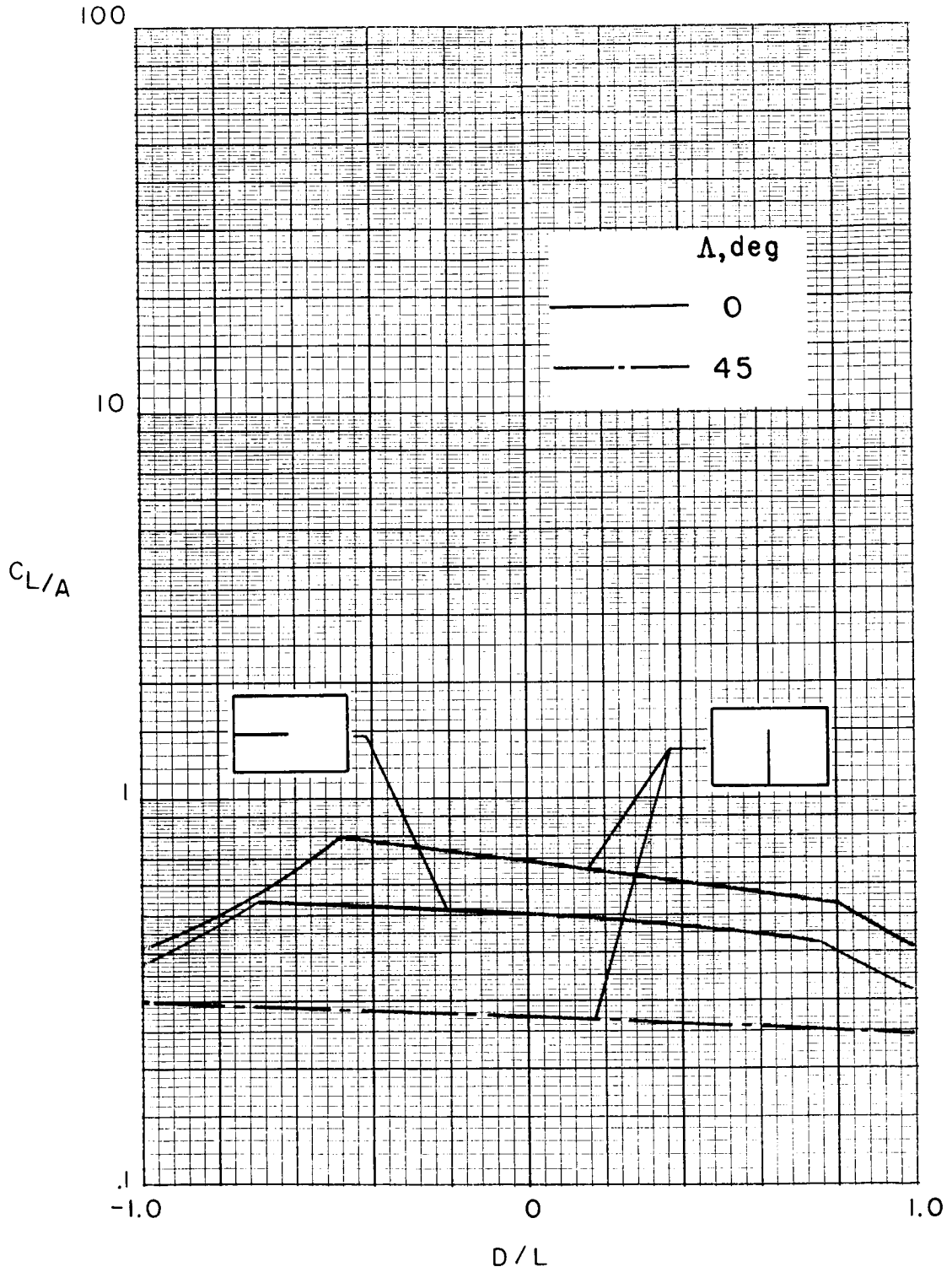


(c) Full span of 3 meters.

Figure 82.- Concluded.

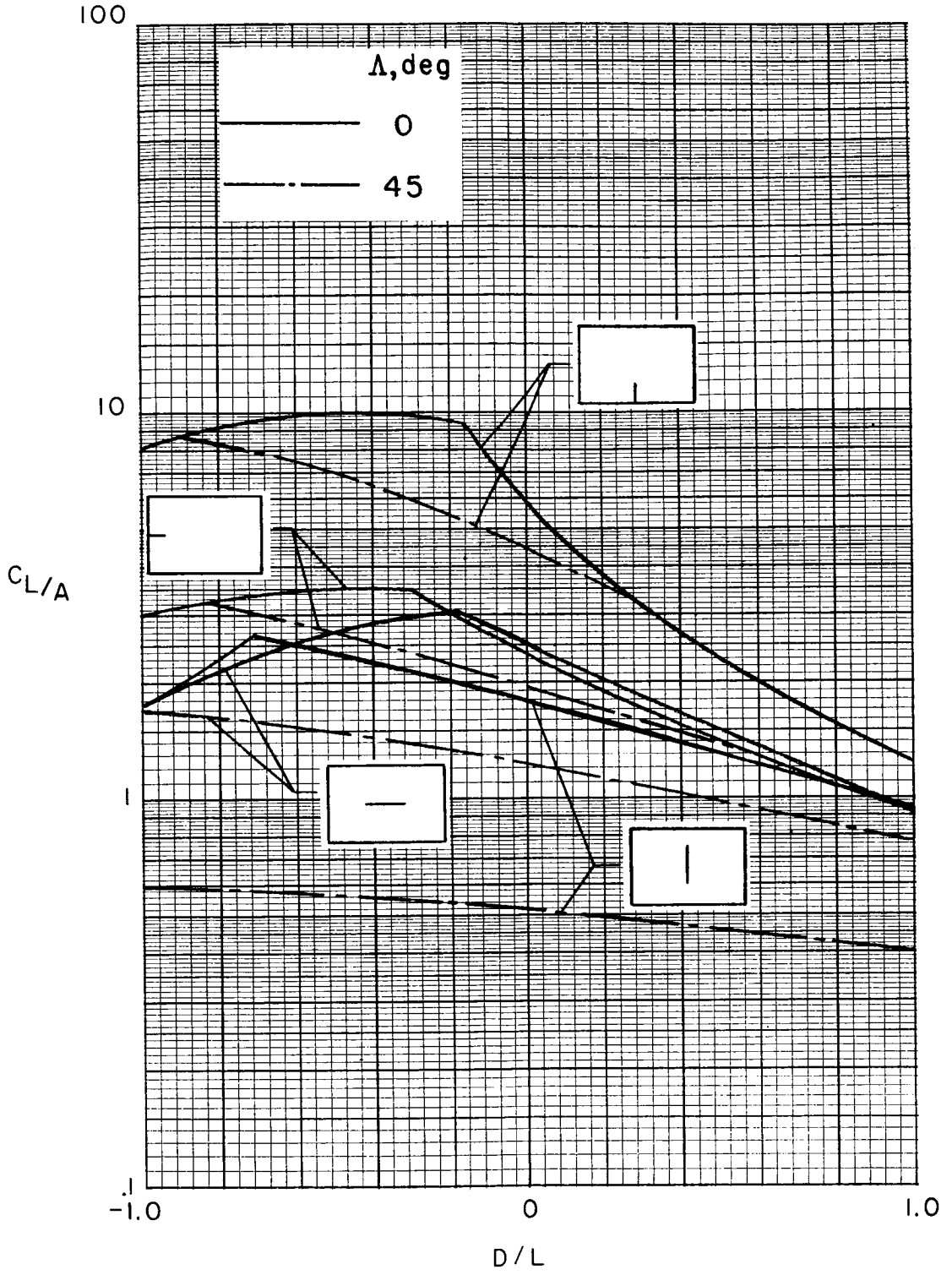


(a) Full span of 1 meter.

Figure 83.- Effect of model mounting on testing limits in a 2- by 3-meter closed tunnel when moderate corrections are applied.

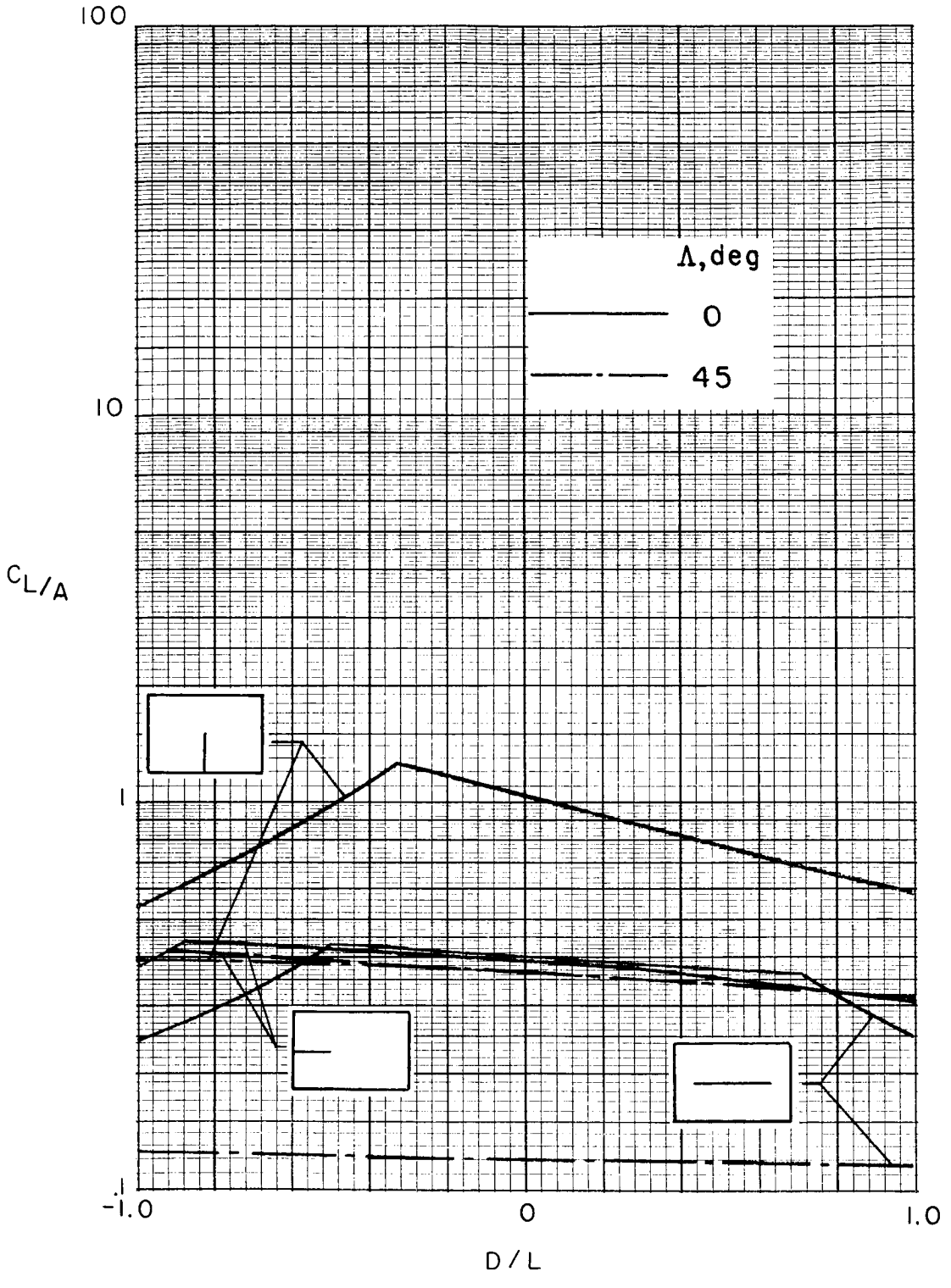


(b) Full span of 2 meters.

Figure 83.- Continued.

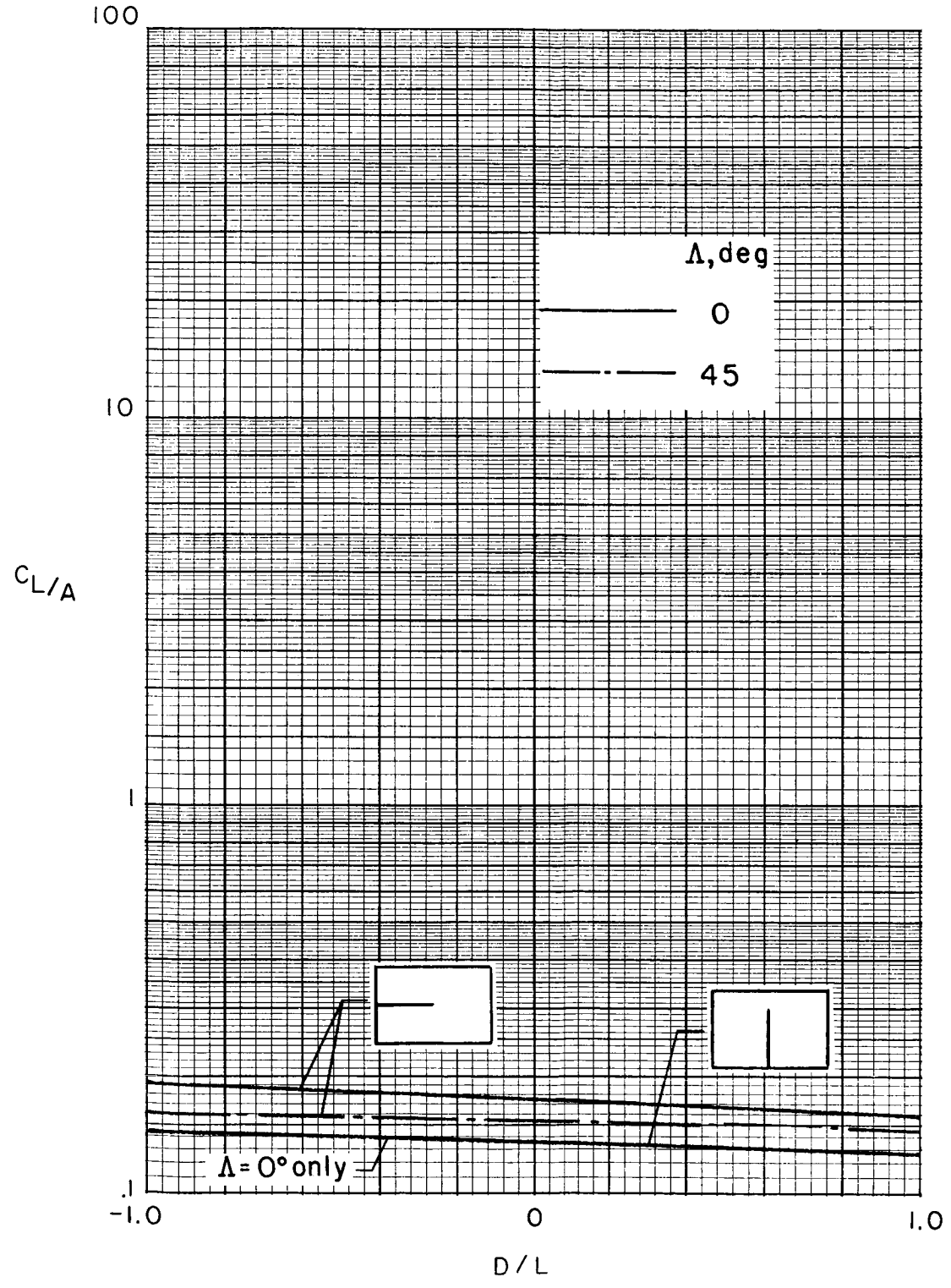


(c) Full span of 3 meters.

Figure 83.- Concluded.

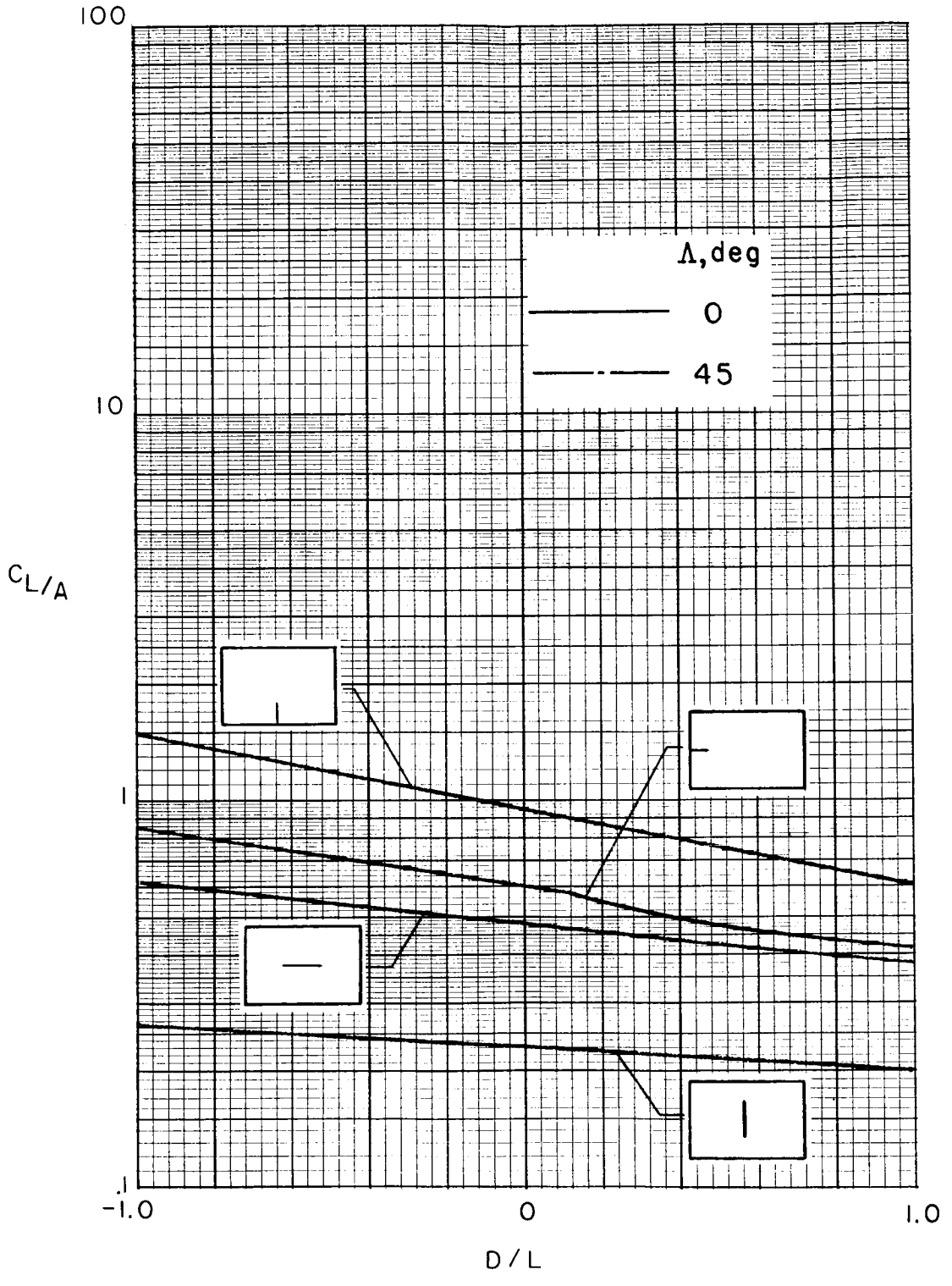


(a) Full span of 1 meter.

Figure 84.- Effect of model mounting on testing limits in a 2- by 3-meter closed tunnel when no corrections are applied.

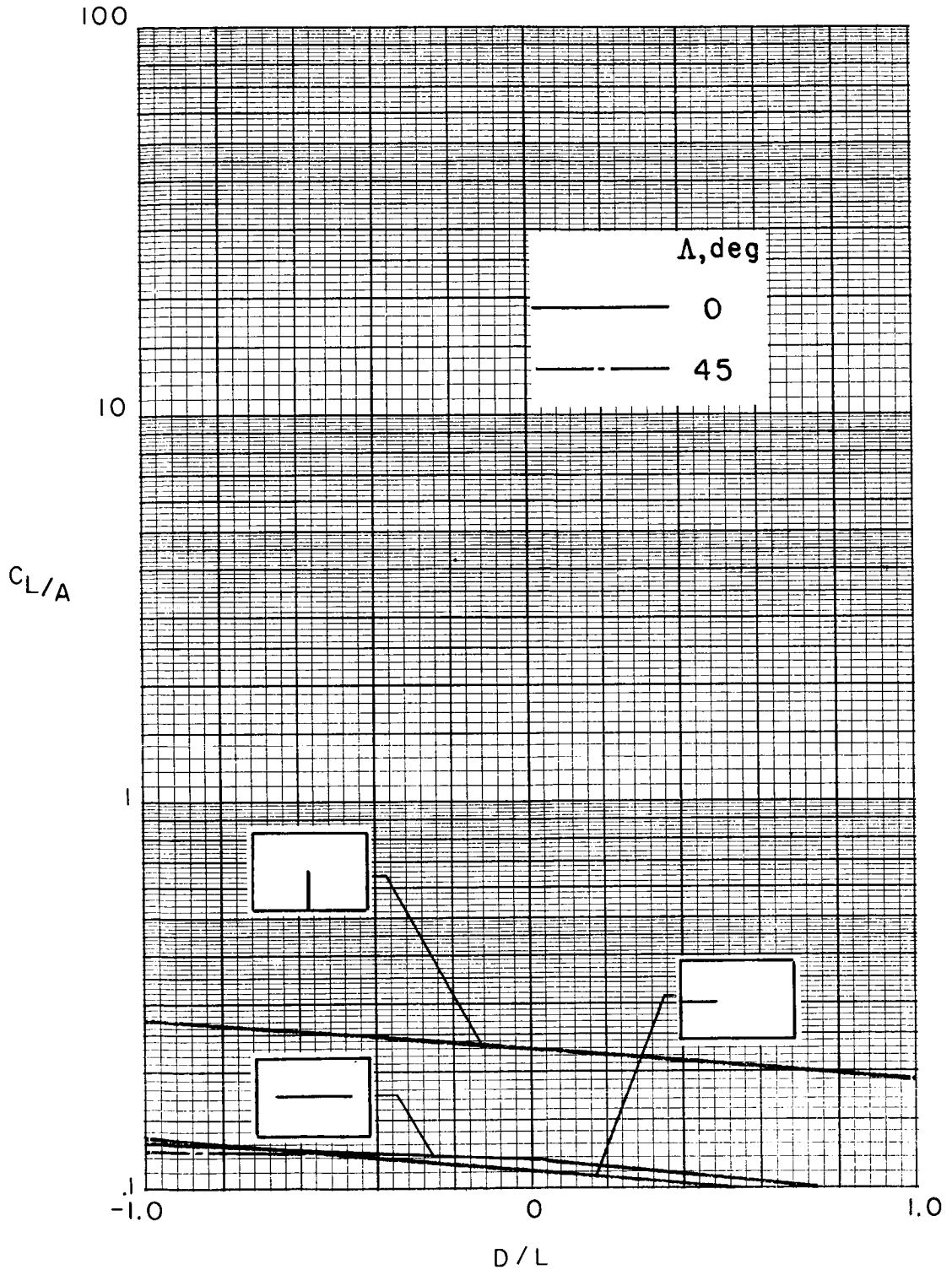


(b) Full span of 2 meters.

Figure 84.- Concluded.

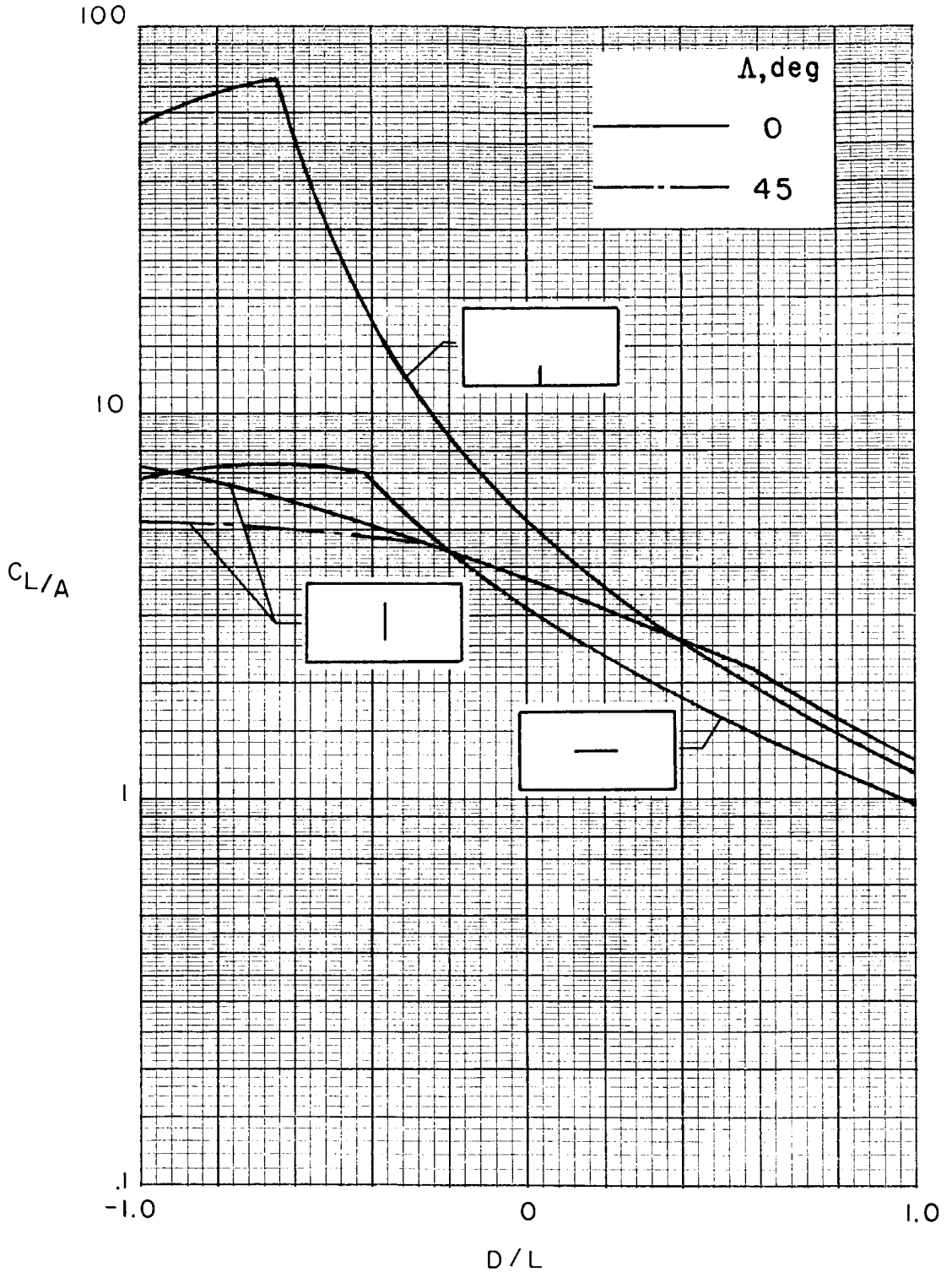


(a) Full span of 1 meter.

Figure 85.- Effect of model mounting on testing limits in a 2- by 4-meter closed tunnel when the maximum practical corrections are applied.

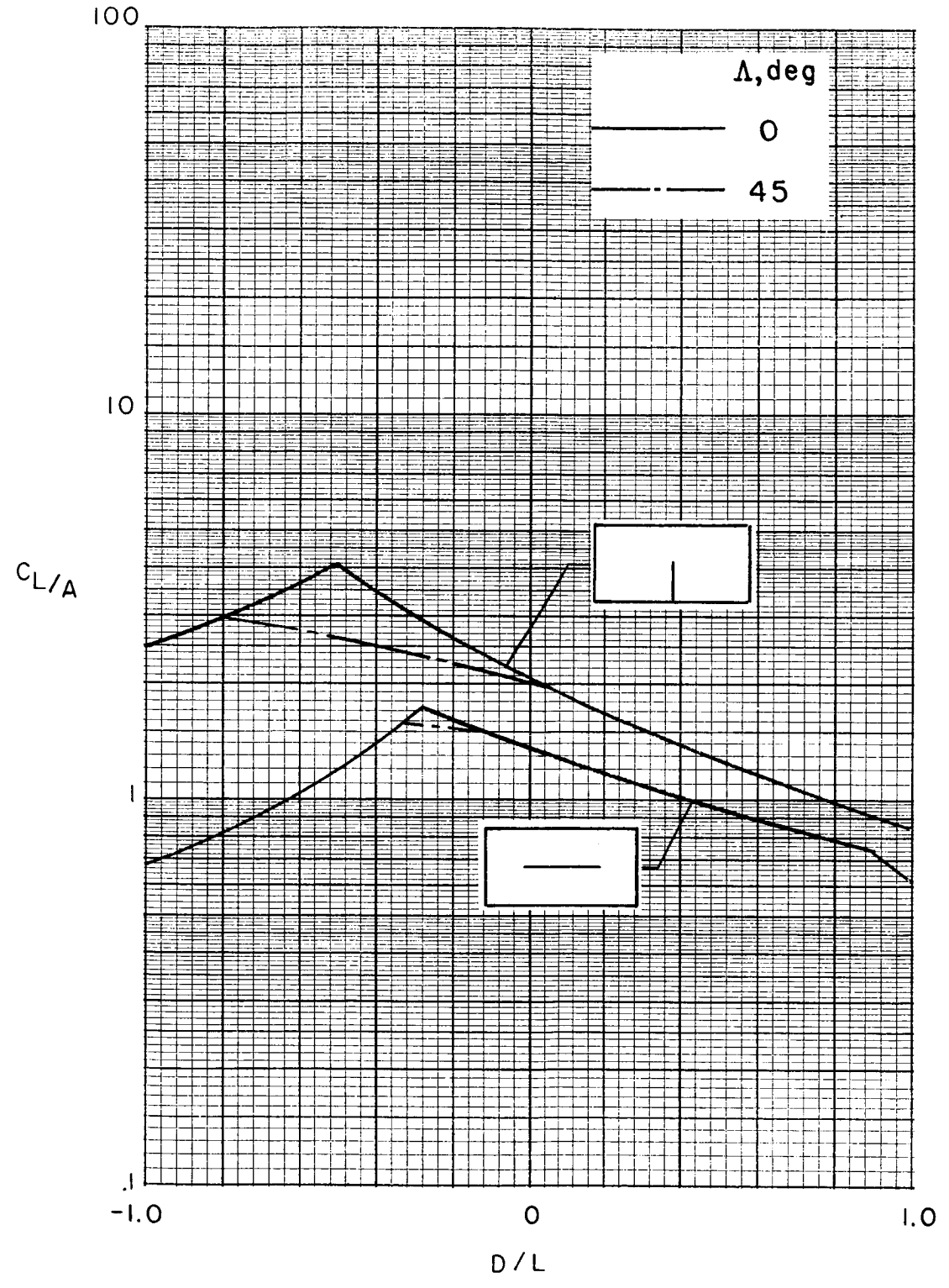


(b) Full span of 2 meters.

Figure 85.- Continued.

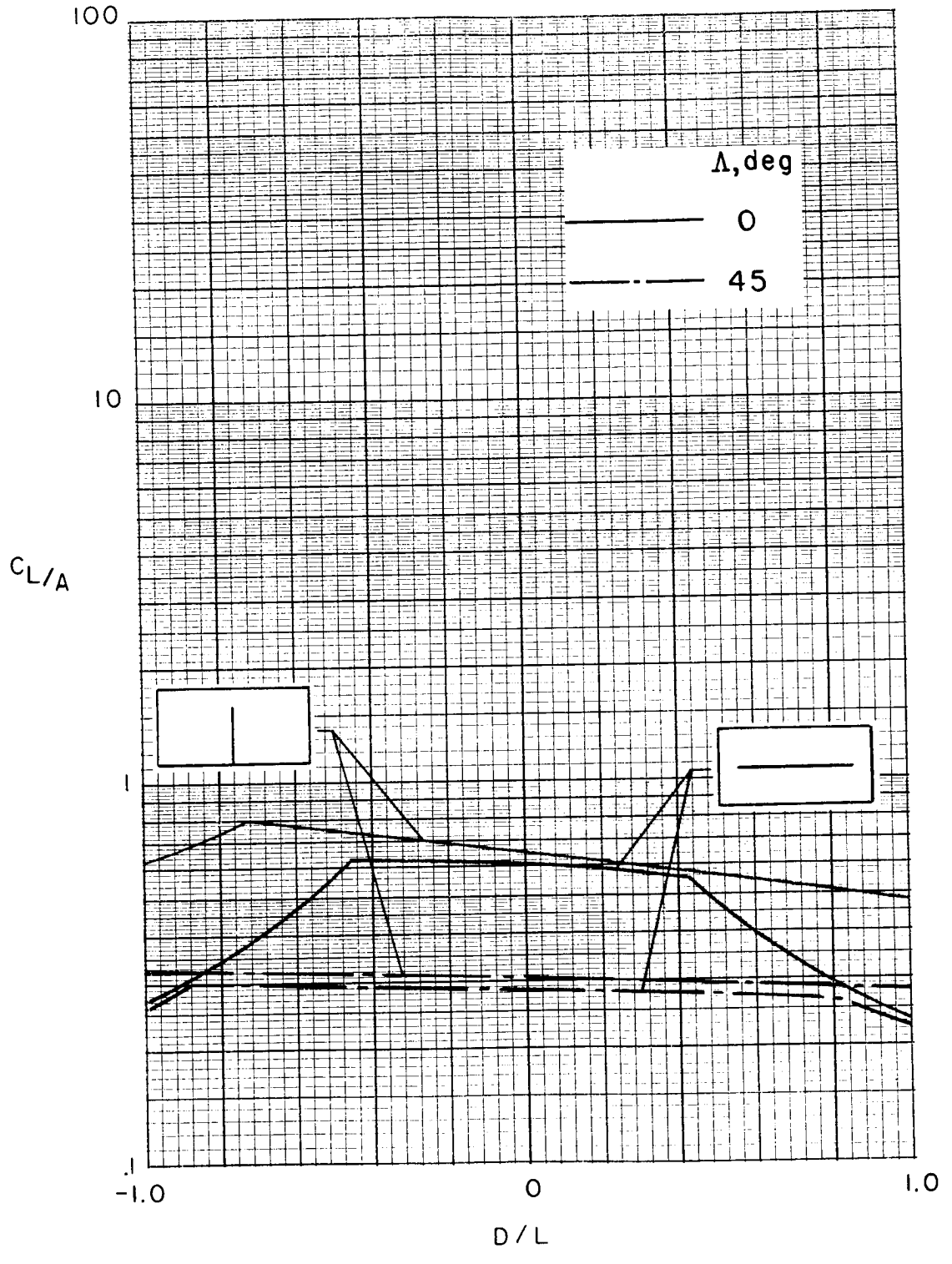


(c) Full span of 3 meters.

Figure 85.- Concluded.

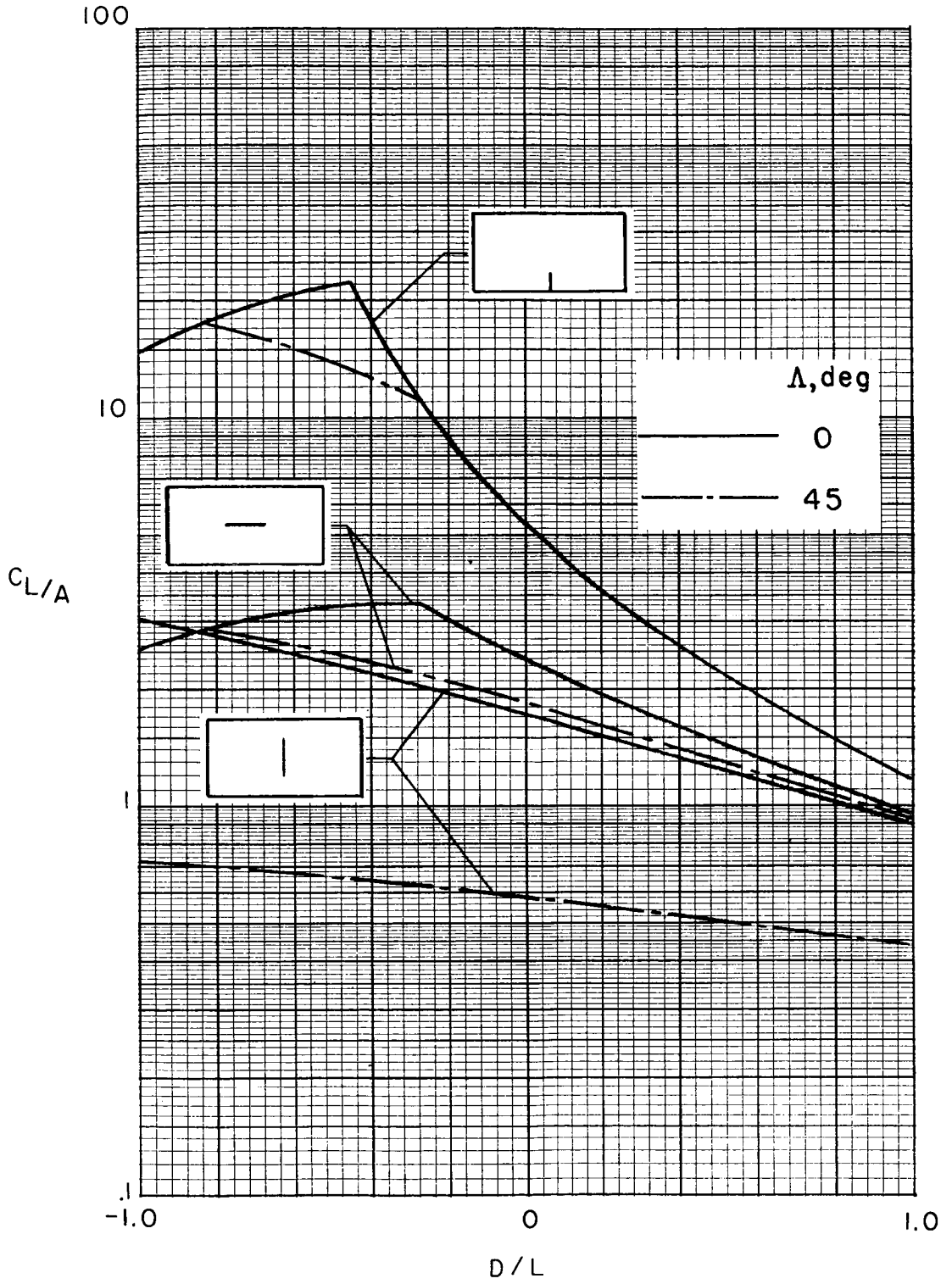


(a) Full span of 1 meter.

Figure 86.- Effect of model mounting on testing limits in a 2- by 4-meter closed tunnel when moderate corrections are applied.

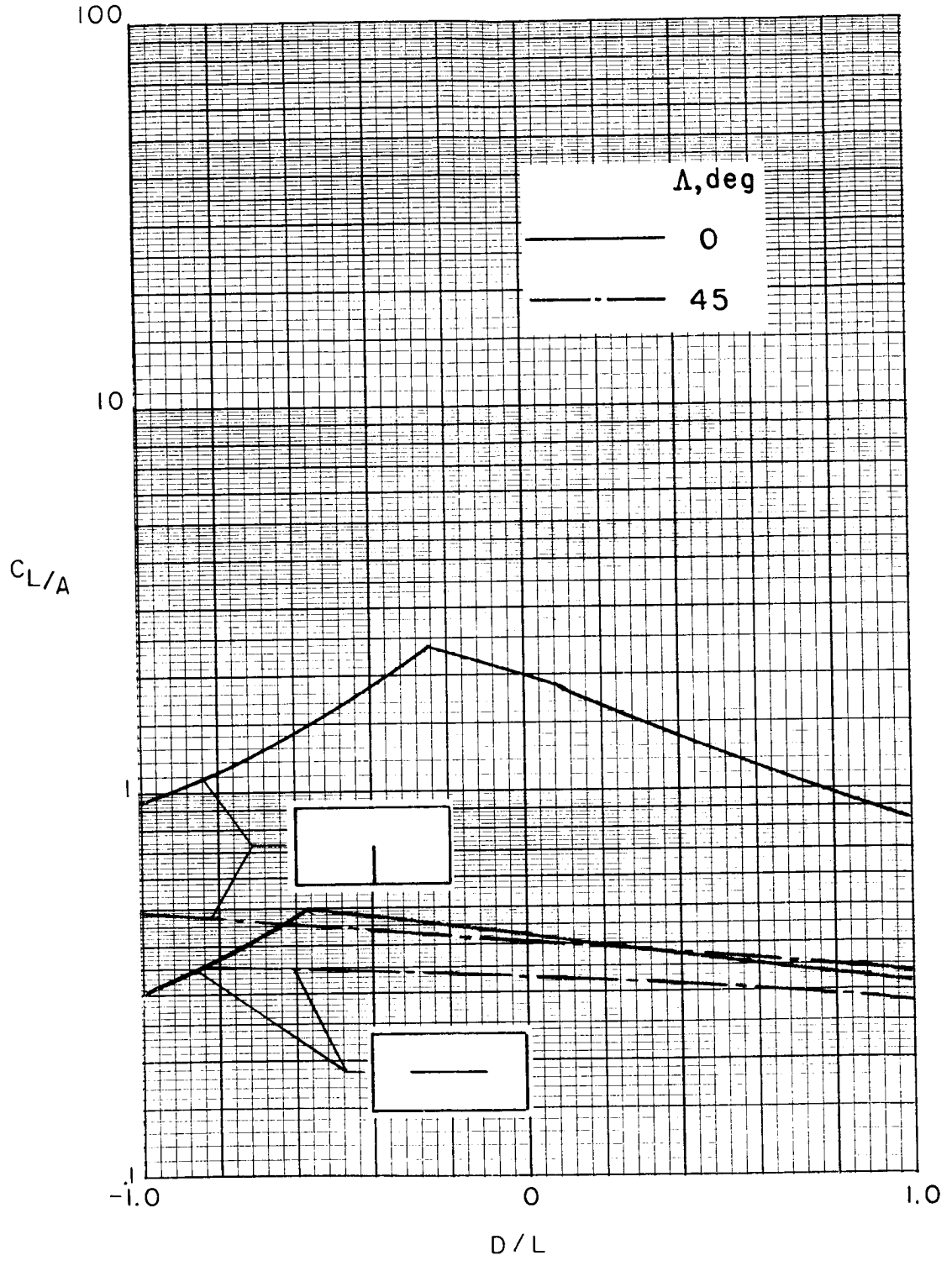


(b) Full span of 2 meters.

Figure 86.- Continued.

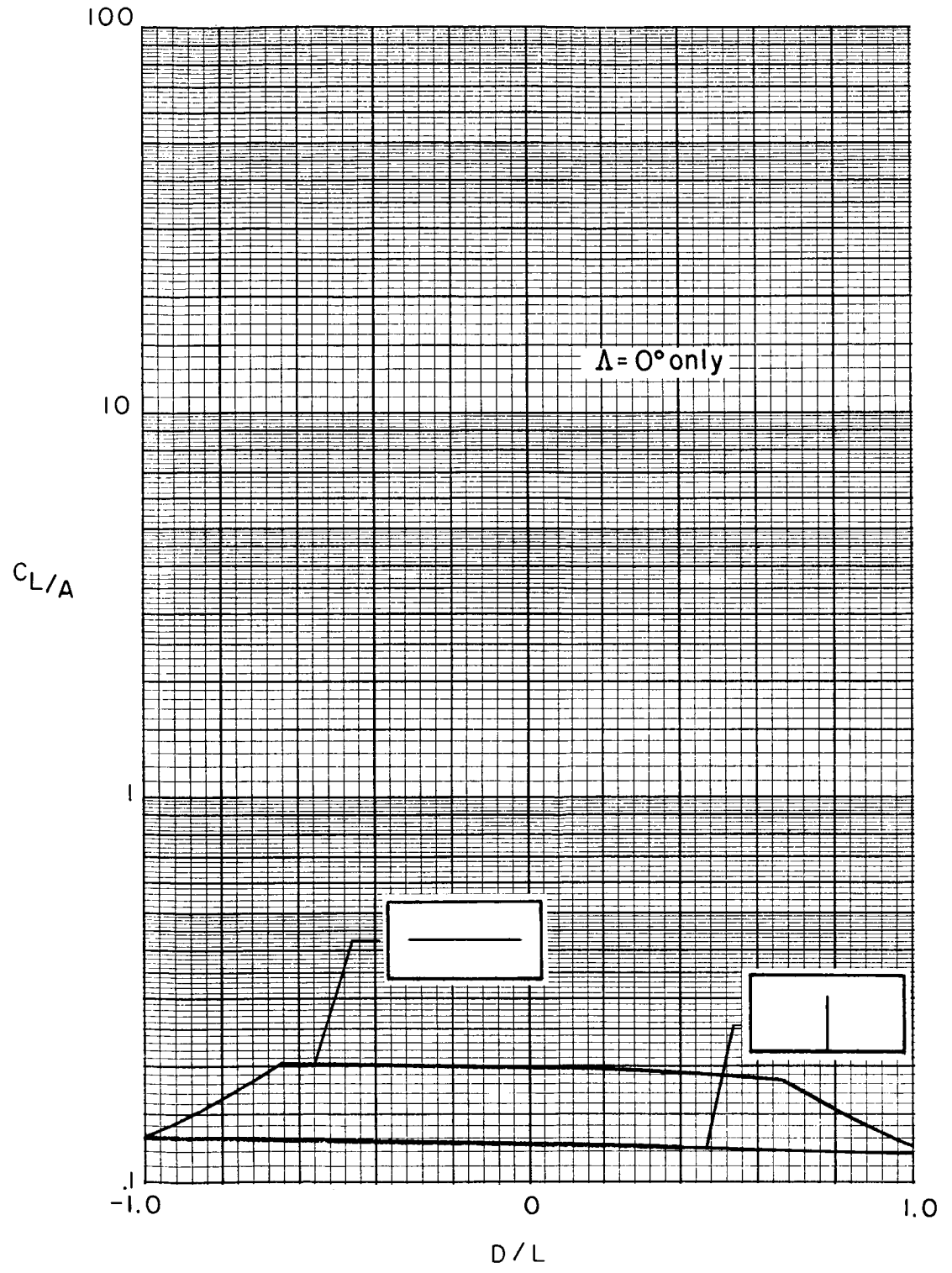


(c) Full span of 3 meters.

Figure 86.- Concluded.

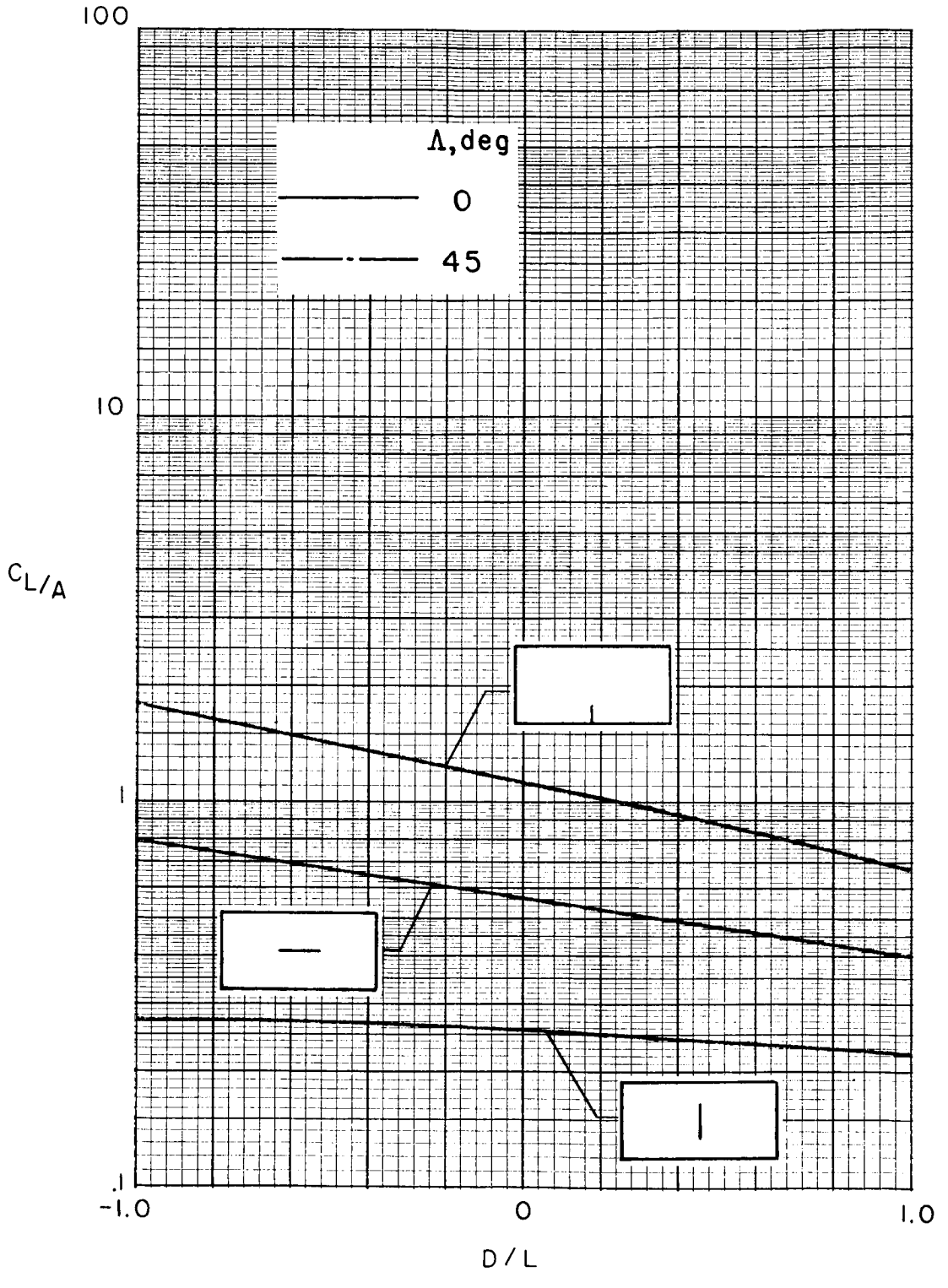


(a) Full span of 1 meter.

Figure 87.- Effect of model mounting on testing limits in a 2- by 4-meter closed tunnel when no corrections are applied.

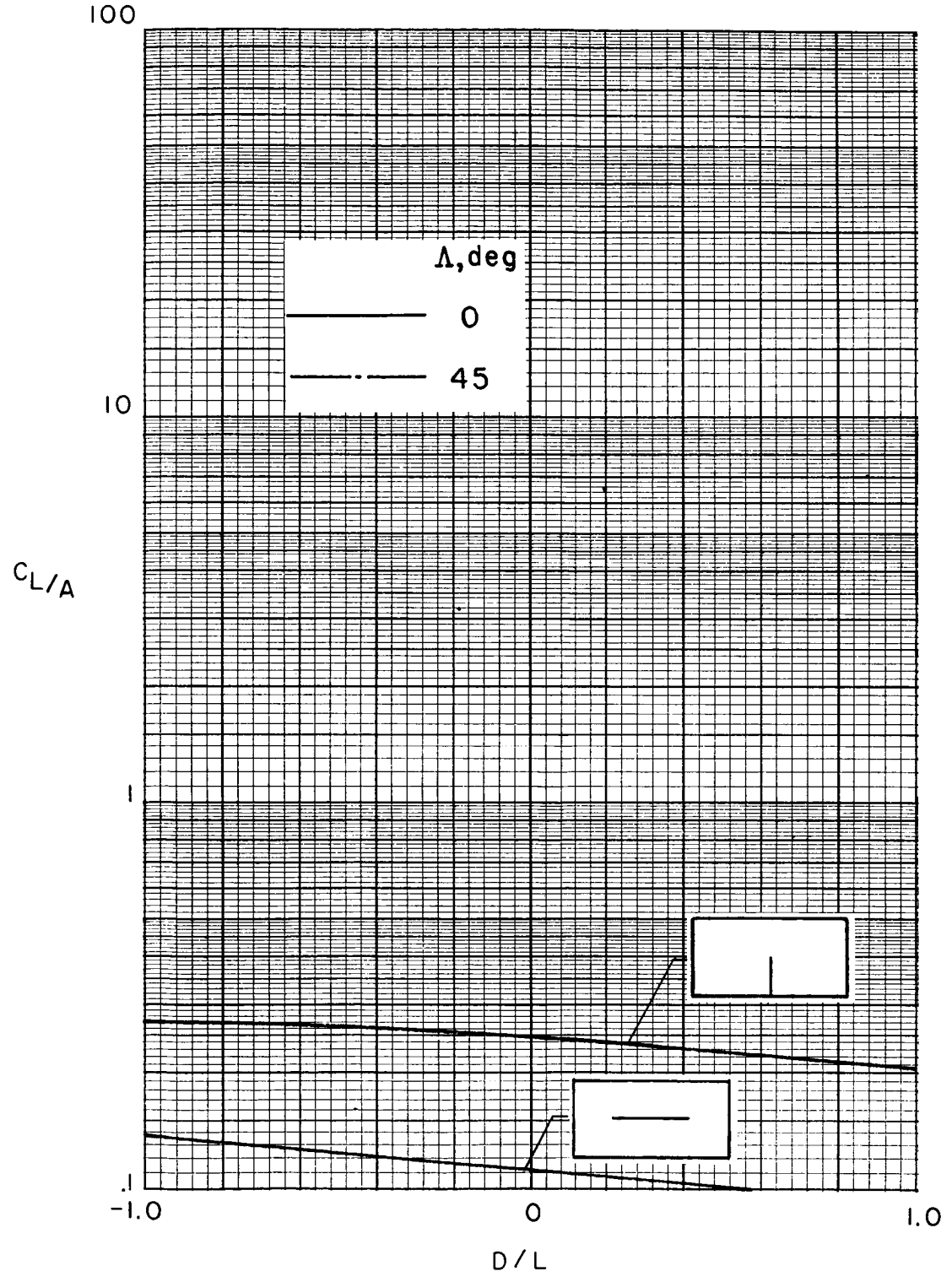


(b) Full span of 2 meters.

Figure 87.- Concluded.

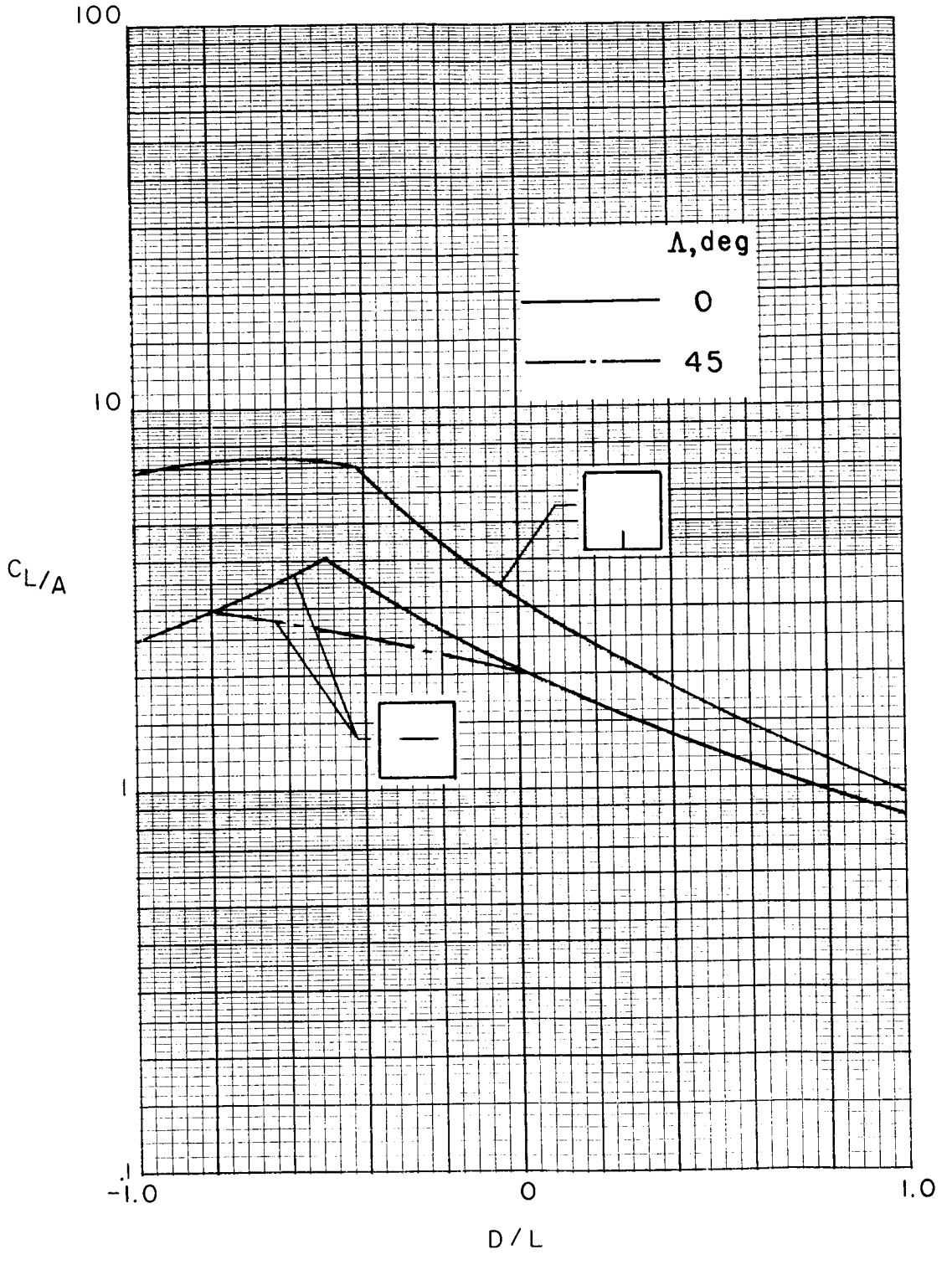


(a) With maximum practical corrections.

Figure 88.- Effect of model mounting on testing limits for a wing with full span of 1 meter in a 2- by 2-meter closed tunnel.

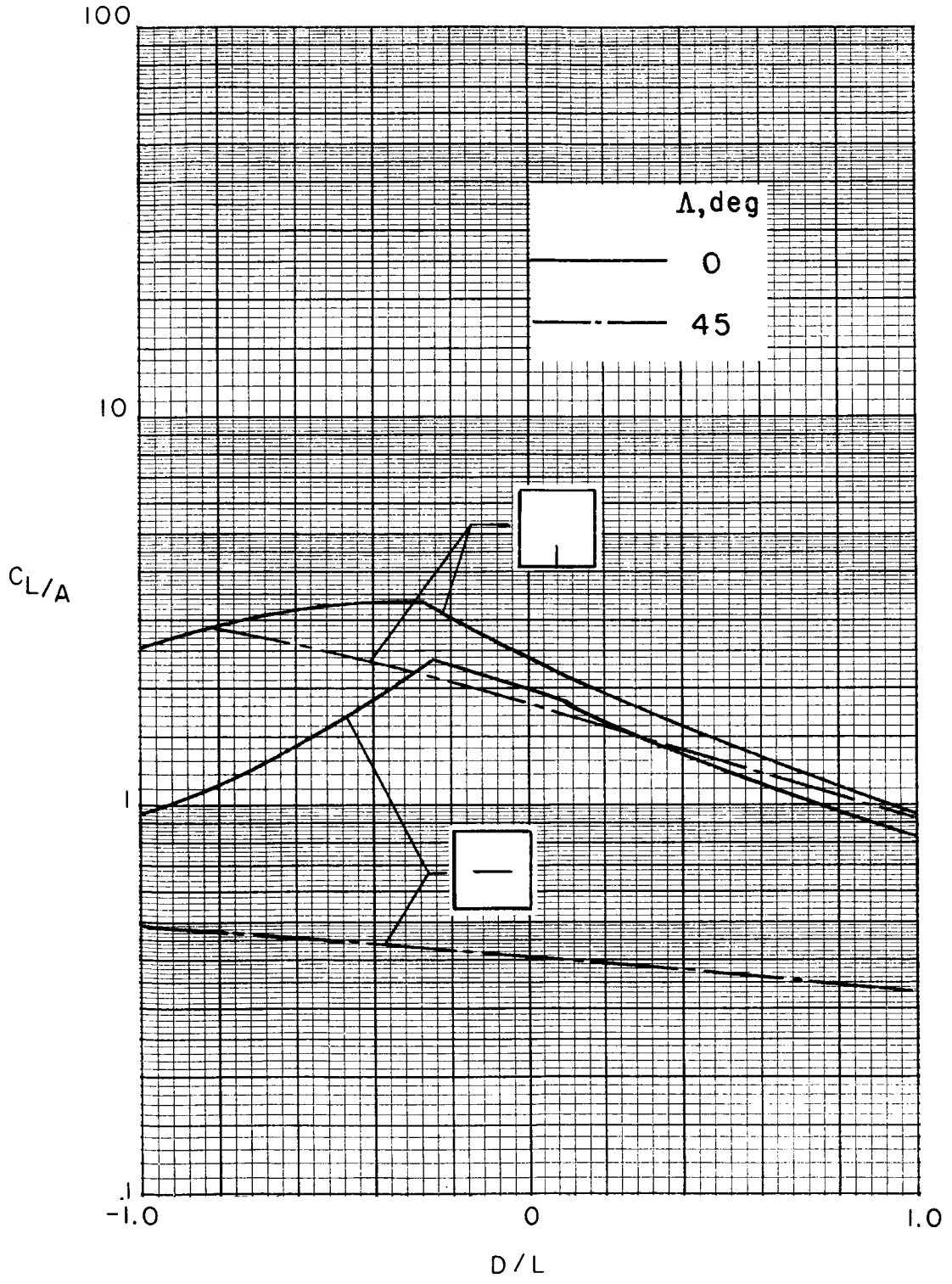


(b) With moderate corrections.

Figure 88.- Continued.

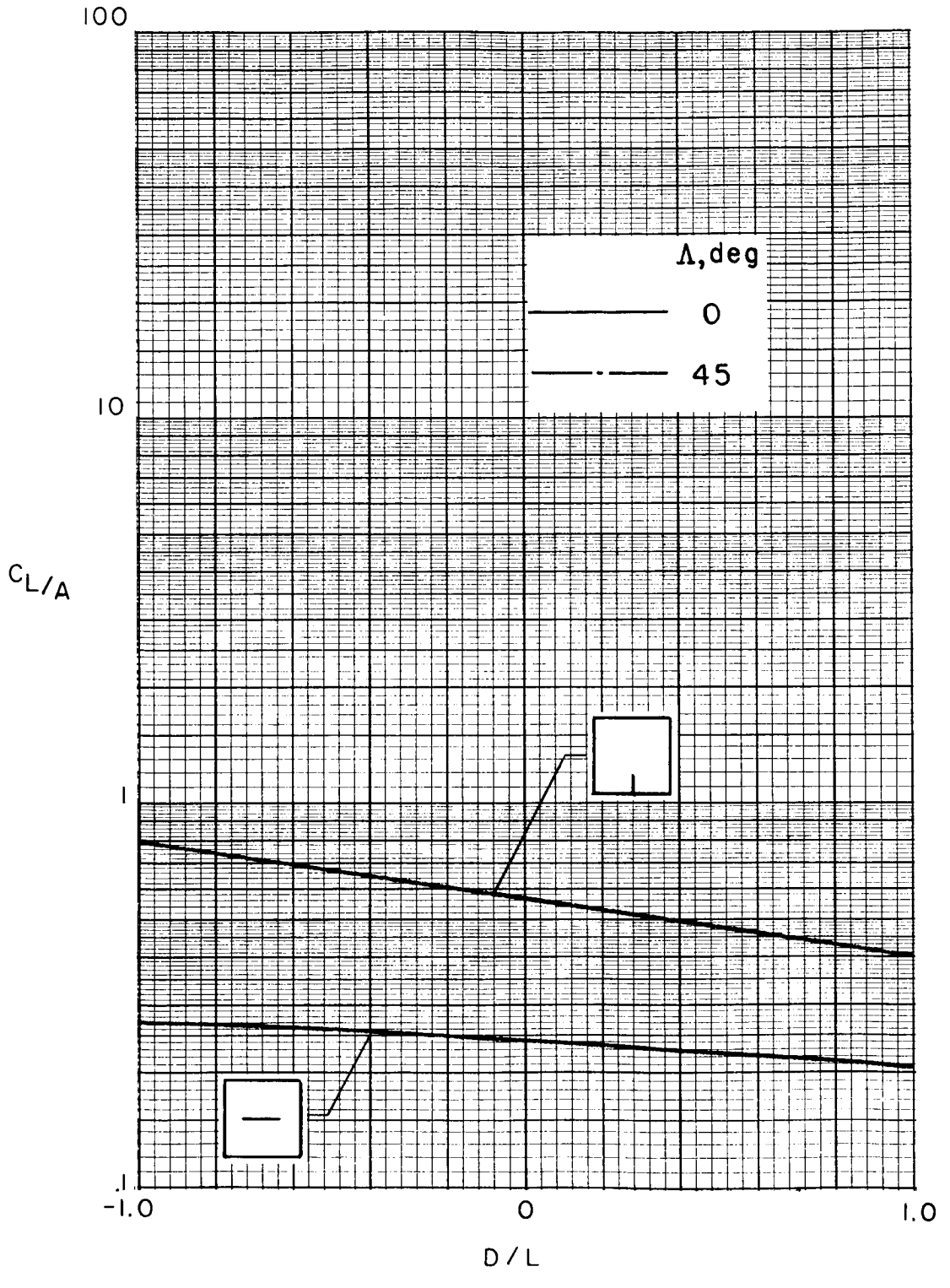


(c) With no corrections.

Figure 88.- Concluded.

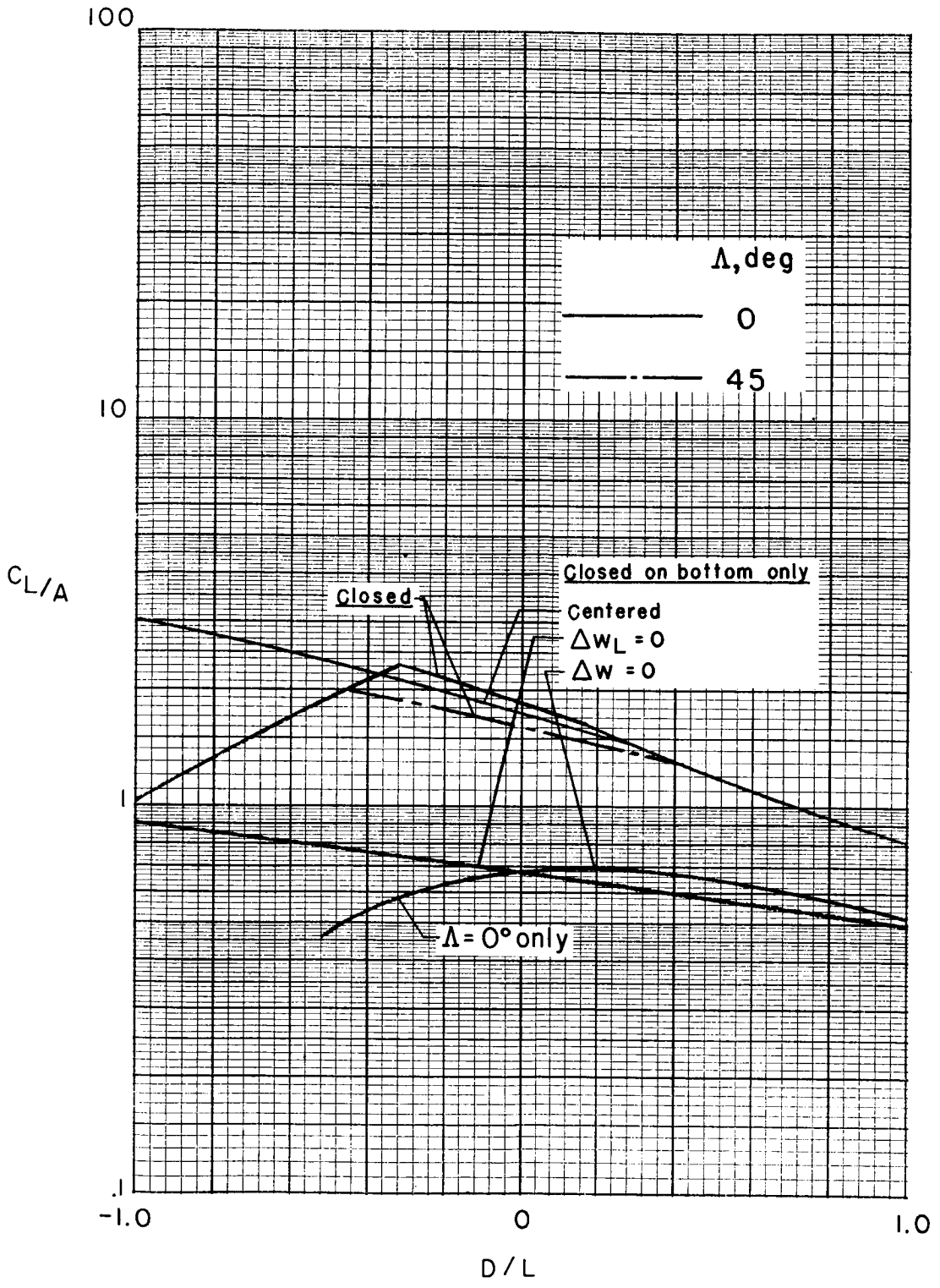


(a) With maximum practical corrections.

Figure 89.- Effect of various modes of operation on testing limits in the Langley V/STOL tunnel ($\gamma$ = 1.5). $\sigma$ = 1/2.

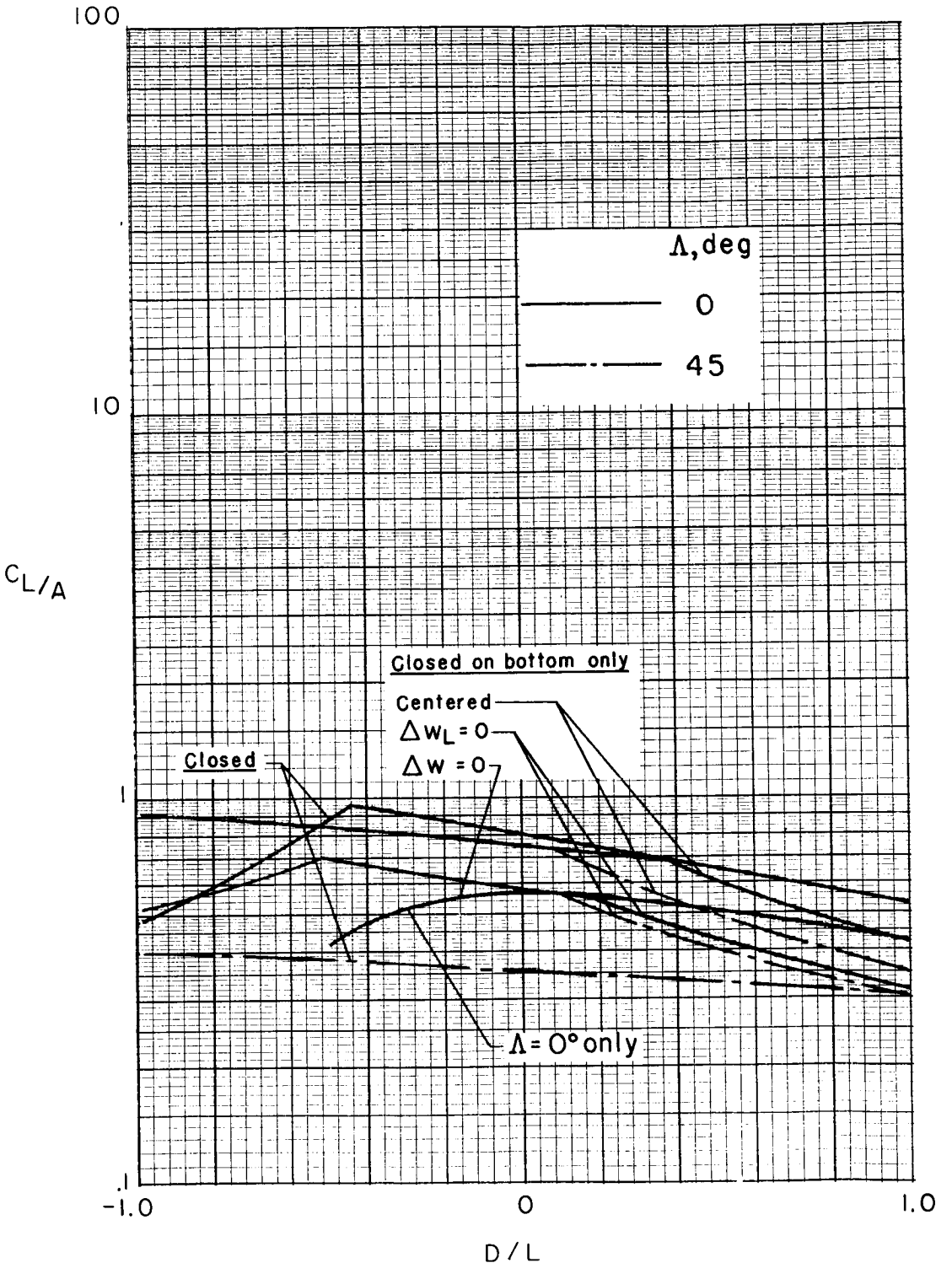


(b) With moderate corrections.

Figure 89.- Continued.

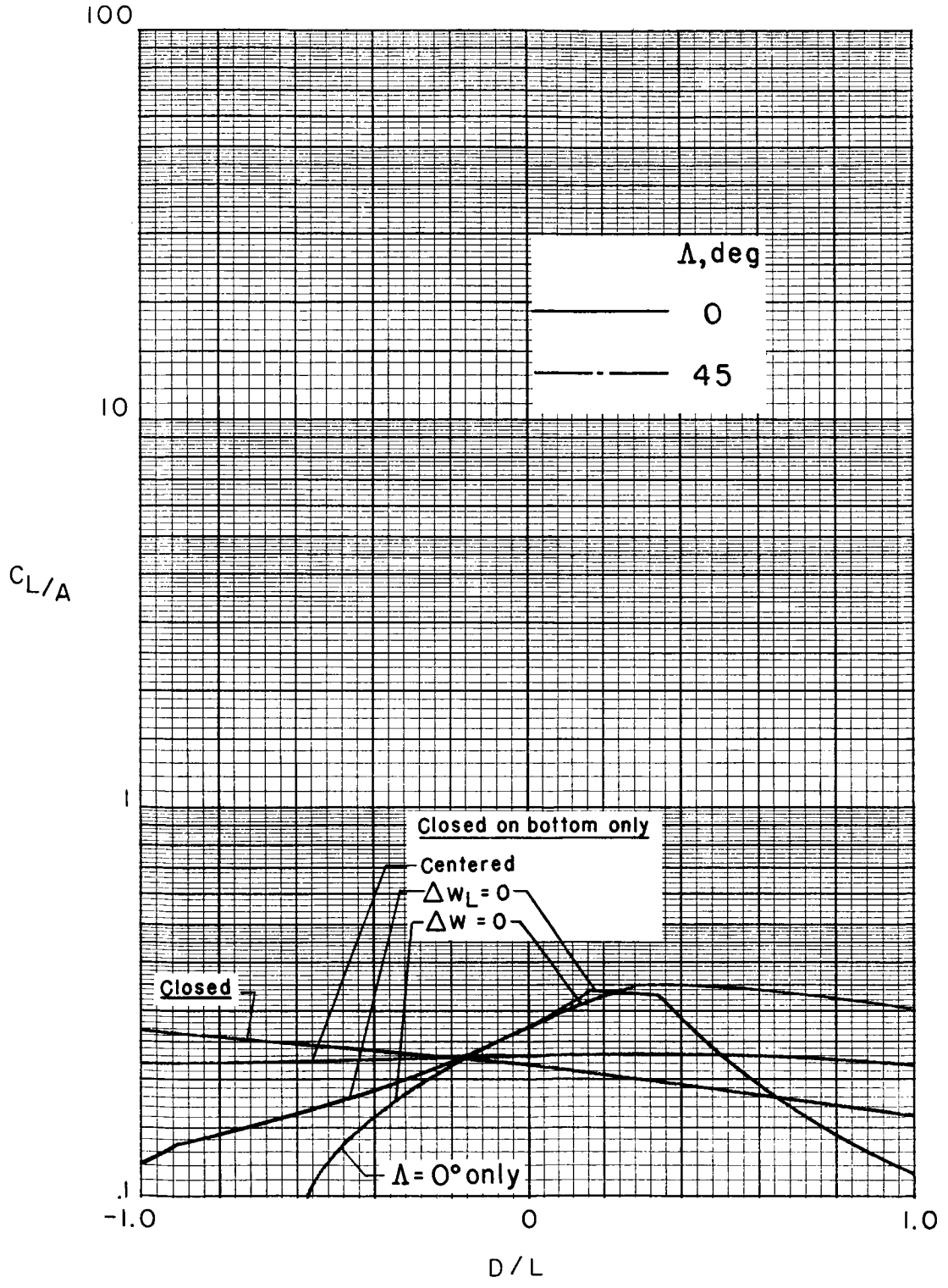


(c) With no corrections.

Figure 89.- Concluded.

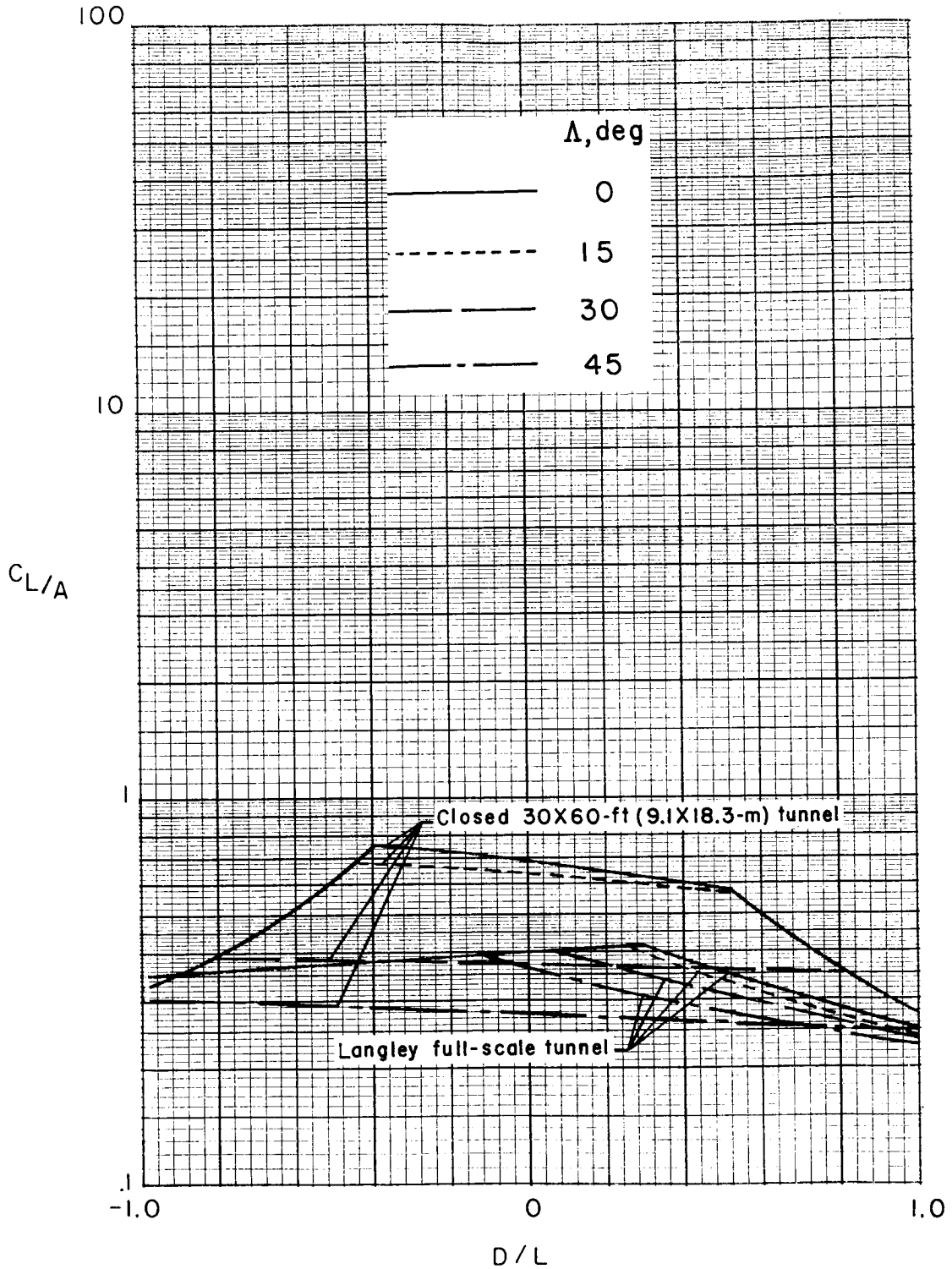


Figure 90.- Comparison between Langley full-scale tunnel with ground board and a closed 9.1- by 18.3-m (30- by 60-ft) tunnel with semicircular sides when using the maximum practical corrections. $\sigma = 2/3$.

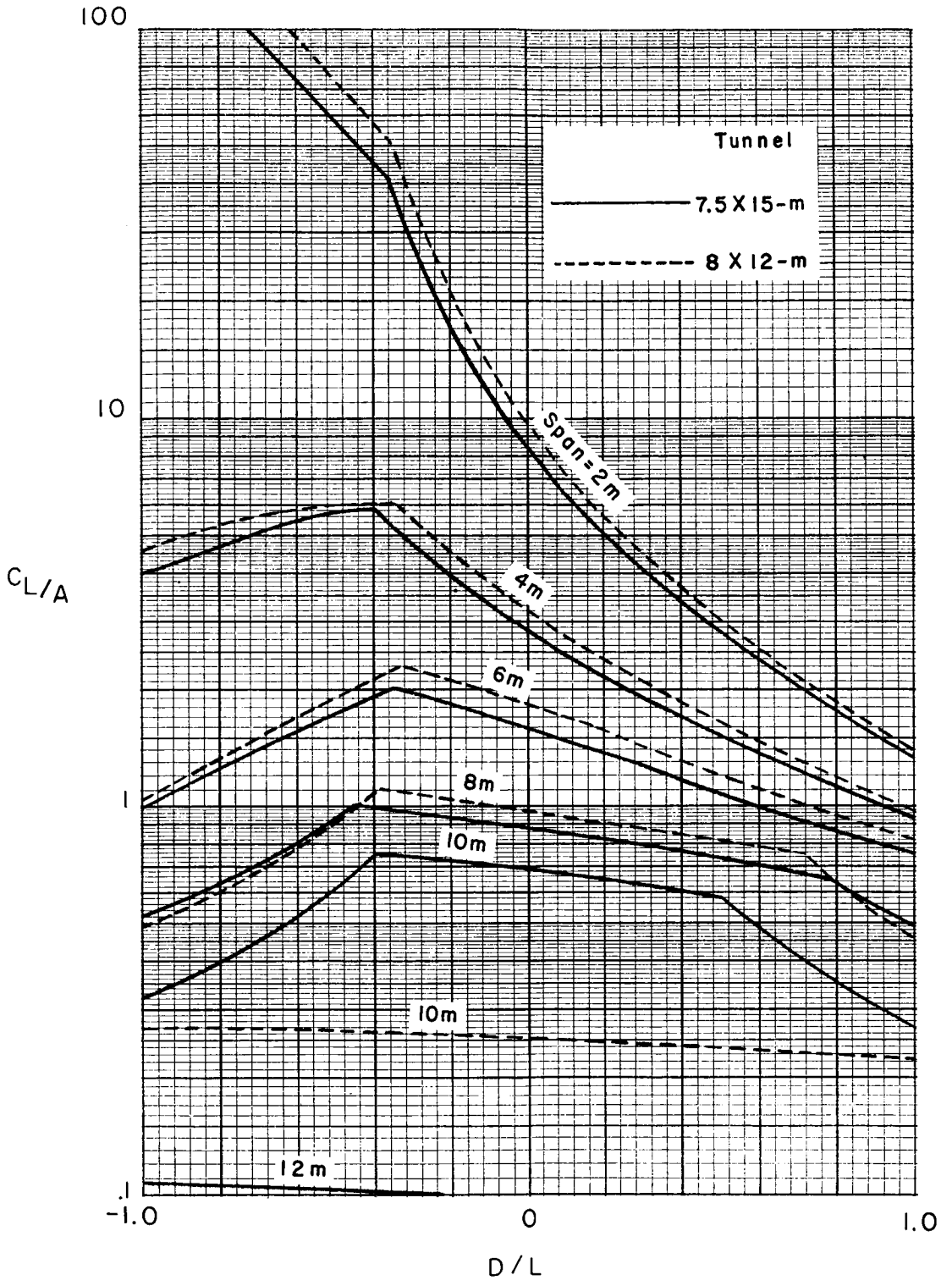


(a) $\Lambda = 0^0$.

Figure 91.- Comparison between closed 7.5- by 15-m tunnel with semicircular sides and a rectangular 8- by 12-m tunnel when maximum corrections are applied. (See table II(a).)

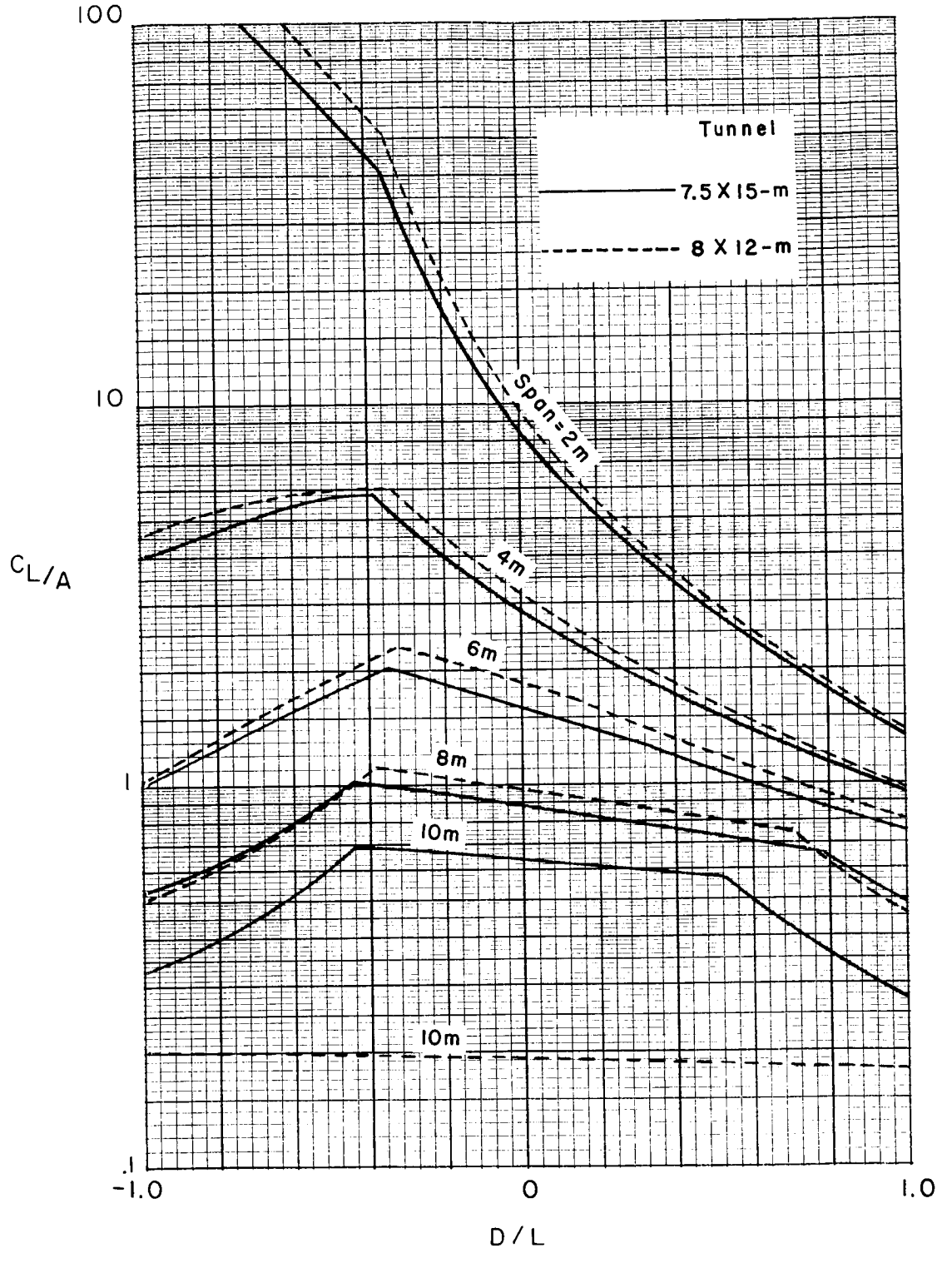


(b) $\Lambda = 15^{0}$.

Figure 91.- Continued.

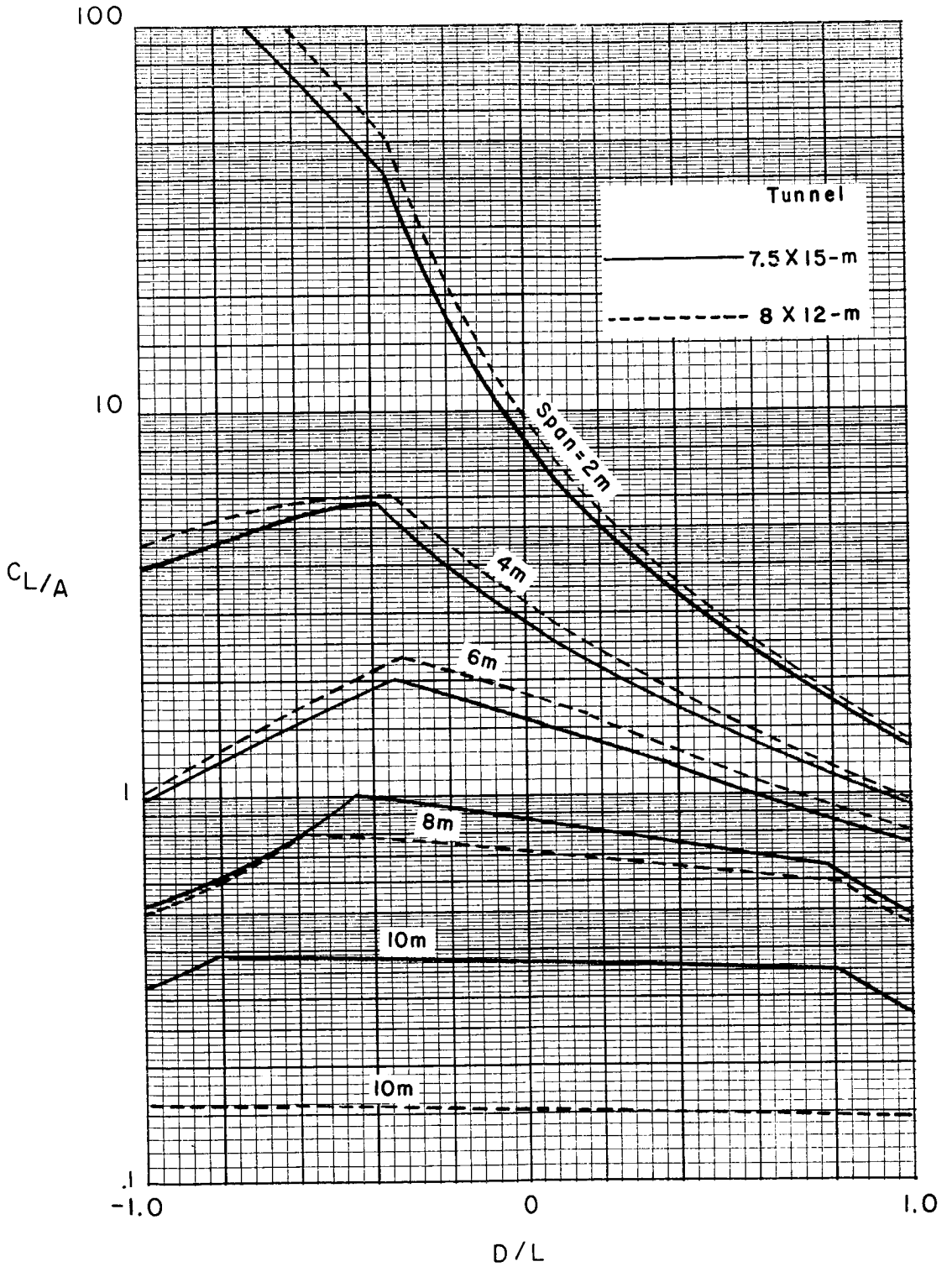


(c) $\Lambda = 30^{0}$.

Figure 91.- Continued.

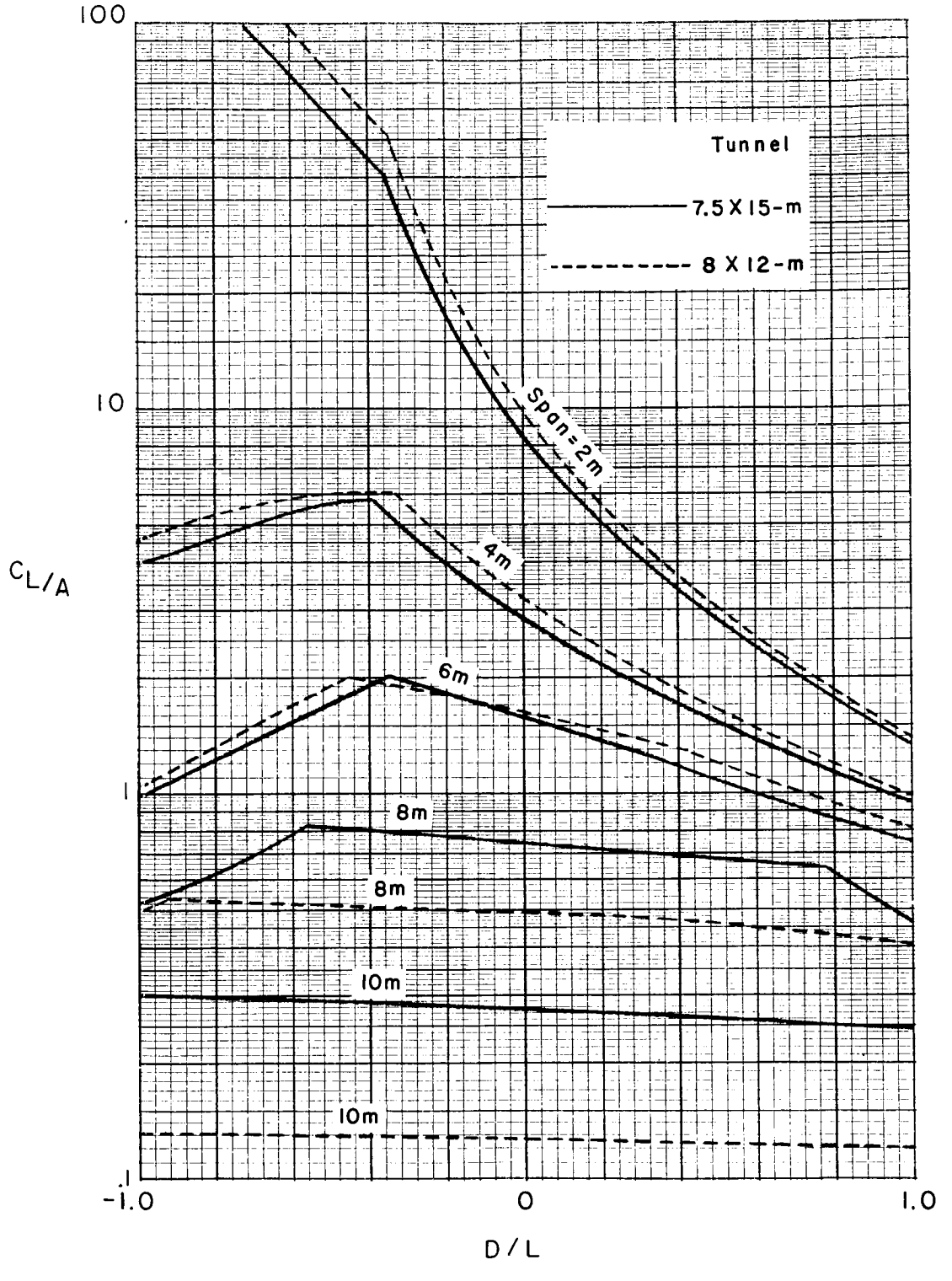


(d) $\Lambda = 45^{0}$.

Figure 91.- Concluded.

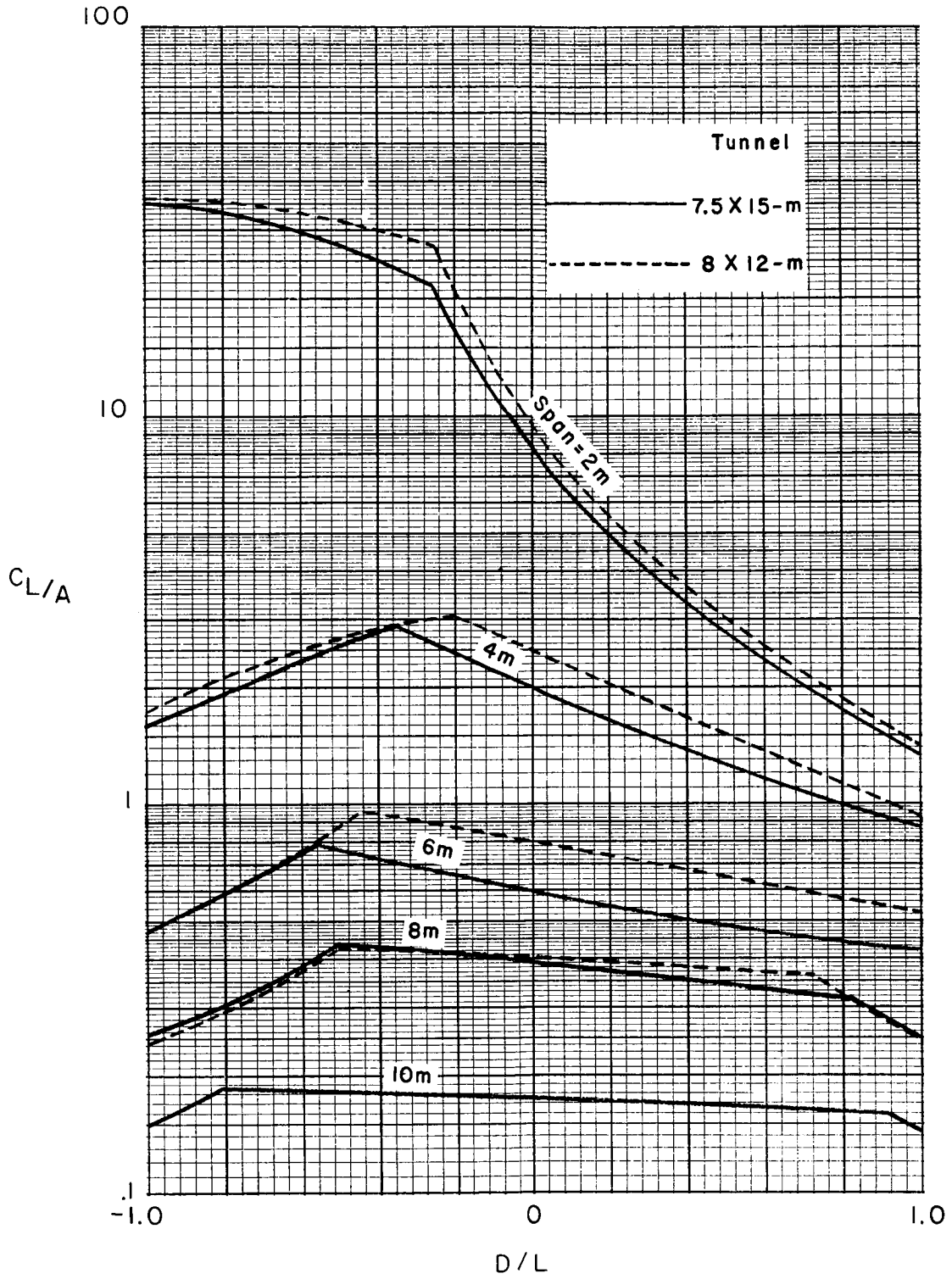


(a) $\Lambda = 0^0$.

Figure 92.- Comparison of limits in a rectangular 8- by 12-m tunnel and a 7.5- by 15-m tunnel with semicircular sides when moderate corrections are applied. (See table II(a).)

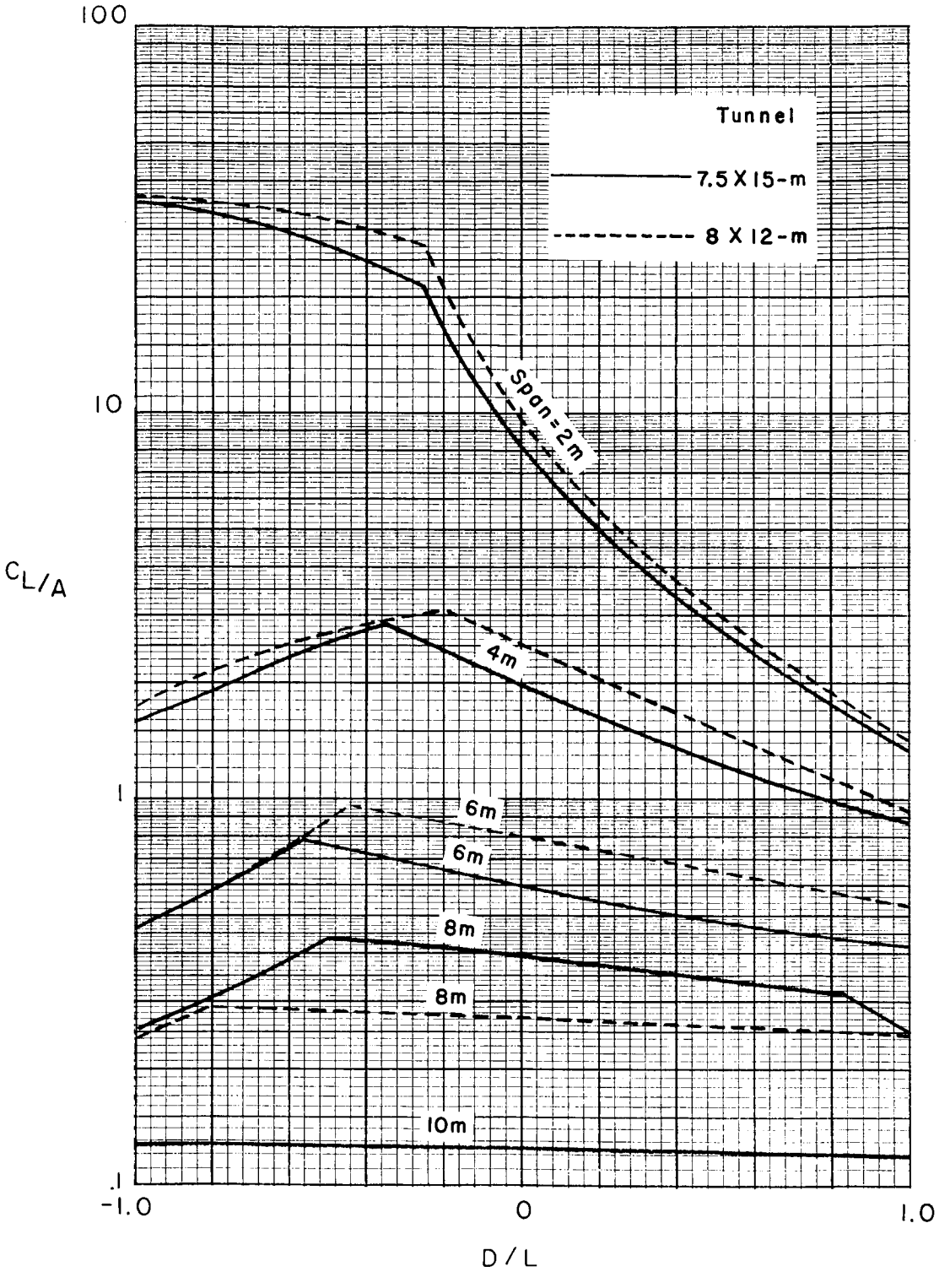


(b) $\Lambda = 15^{0}$.

Figure 92.- Continued.

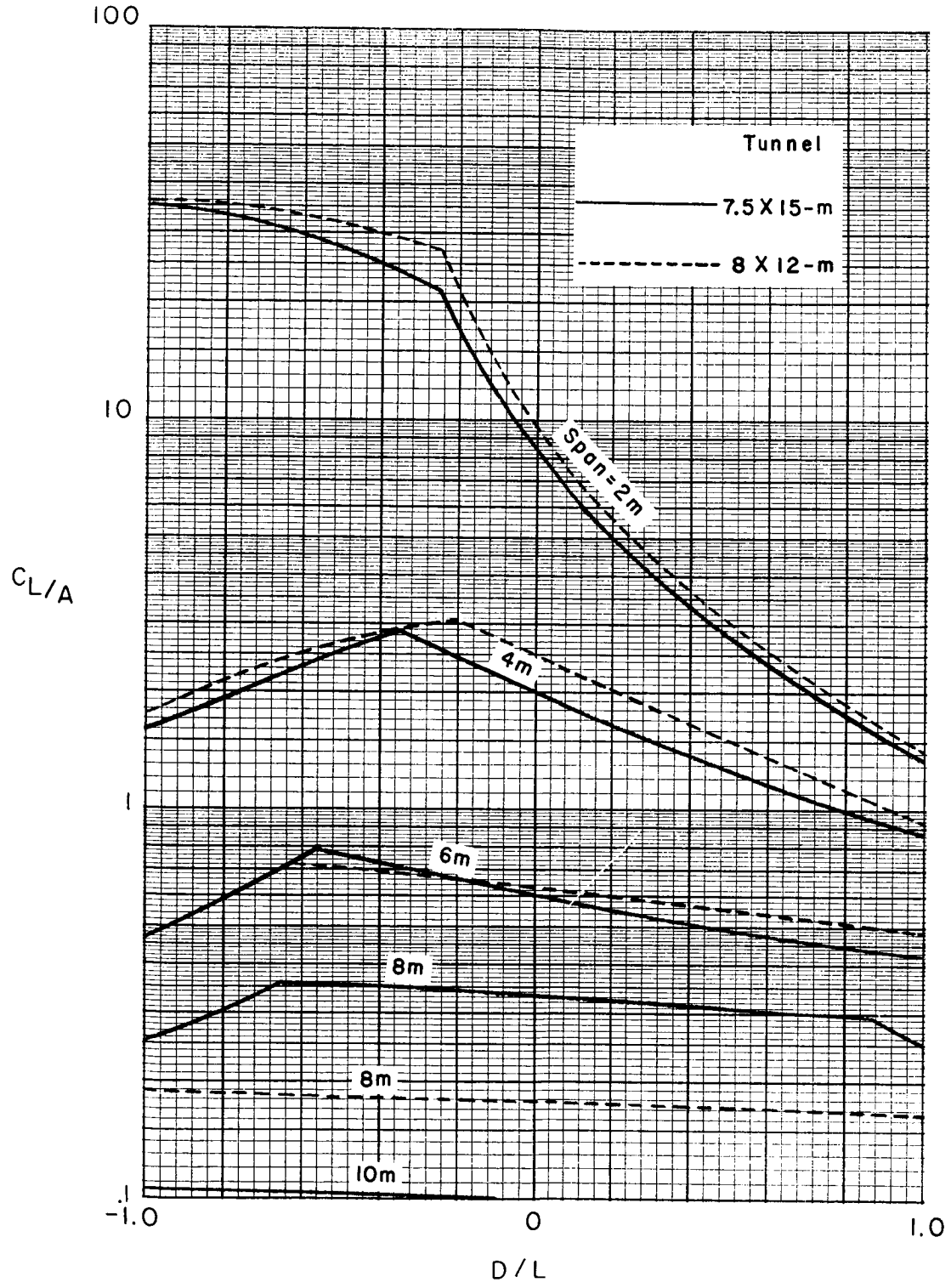


(c) $\Lambda = 30^{0}$.

Figure 92.- Continued.

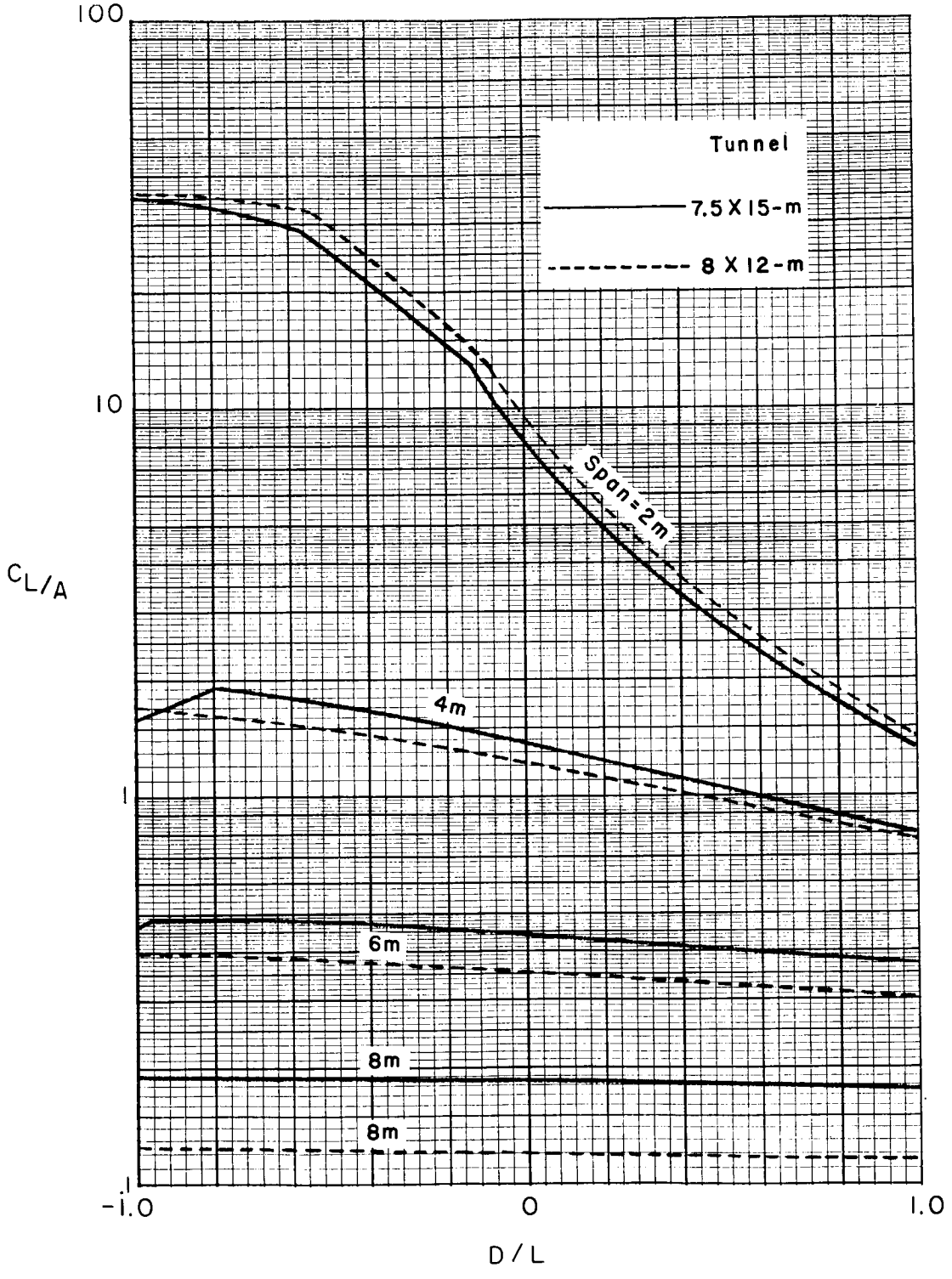


(d) $\Lambda = 45^{o}$.

Figure 92.- Concluded.

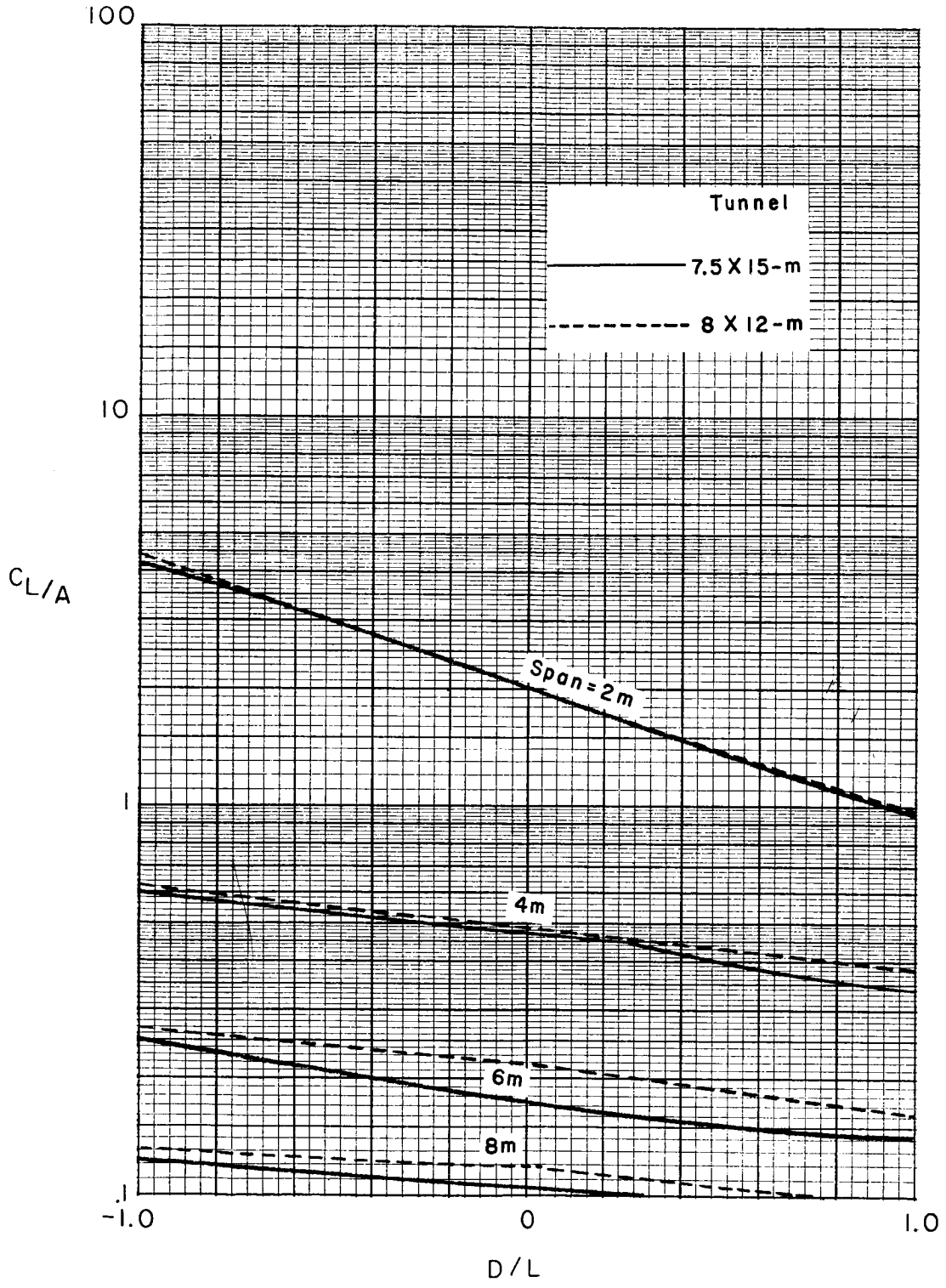


Figure 93.- Comparison of testing limits in a rectangular 8- by 12-m tunnel and a 7.5- by 15-m tunnel with semicircular sides when no corrections are applied. $0 \leq \Lambda < 30$. (See table II(c).)